EXTENDED SURFACE FLUIDIZED BED HEAT TRANSFER

by

GORDON ANTHONY ATKINSON, M.Sc.,C.Eng.,M.I.Mech.E.

A thesis submitted for the degree of
DOCTOR OF PHILOSOPHY
of
THE UNIVERSITY OF ASTON IN BIRMINGHAM

Faculty of Engineering
Department of Mechanical Engineering

Head of Department : Professor A.J.Ede
Supervisor : Professor D.E.Elliott

OCTOBER 1974

SUMMARY

Experimental data and theoretical calculation on the heat transfer performance of extended surface submerged in shallow air fluidized beds - less than 150 mm, are presented. Energy transferrence from the bed material was effected by water cooled tubes passing through the fins.

The extended surface tested was either manufactured from square or radial copper fins silver soldered to a circular basic tube or commercially supplied, being of the crimped or extruded helical fin type.

Performances are compared, for a wide range of geometric variables, bed configurations and fluidized materials, with plain and oval tubes operating under similar experimental conditions. A statistical analysis of all results, using a regression technique, has shown the relative importance of each significant variable. The bed to surface heat transfer coefficients are higher than those reported in earlier published work using finned tubes in much deeper beds and the heat transfer to the whole of the extended surface is at least as good as that previously reported for un-finned tubes.

The improved performance is attributed partly to the absence of large bubbles in shallow beds and it is suggested that the improved circulation of the solids when constrained in the narrow passages between adjacent fins may be a contributory factor.

Flow visualisation studies between a perspex extended surface and a fluidized bed using air at ambient temperatures, have demonstrated the effect of too small a fin spacing.

Fin material and the bonding to the basic tube are more important in the optimisation of performance than in conventional convective applications because of the very much larger heat fluxes involved. A theoretical model of heat flow for a radial fin surface, provides data concerning the maximum heat transfer and minimum metal required to fulfil a given heat exchange duty. Results plotted in a series of charts aim at assisting the designer of shallow fluidized beds.

ACKNOWLEDGEMENTS

The experimental work for this thesis was carried out in a research laboratory at the Department of Mechanical and Production Engineering of the City of Birmingham Polytechnic.

The author would like to thank Mr J.P. Bertinat, the former Head of Department, for providing the research facilities and acting as an external supervisor.

Thanks are also due to the staff of the Thermodynamics Laboratory, in particular Mr J. Holland for assistance in the manufacture of the research rig and the production of a variety of extended surface tubes.

Finally, the author is indebted to Dr. A.Watson, who acted as external supervisor during the last few months of the work, Dr.J.Aston for his valuable comments on the statistical analysis content of the results and Professor D.E.Elliott for his support and encouragement throughout the research period.

INDEX

LIST OF FIGURES

LIST OF TABLES

NOMENCLATURE

Symbol	Definition	Units
a	Mesh size of square grid - numerical technique	mm
A	Total extended surface area ($A_1 + A_2$)	m^2
A_b	Bed plan sectional area	m^2
A_E	Effective surface area ($A_1 + E_F A_2$)	m^2
A_i	Basic tube inside surface area	m^2
A_o	Basic tube outside surface area	m^2
A_R	Area ratio $(A_1 + A_2)/A_o$	
A_x	Oval tube cross-sectional area	m^2
A_1	Primary surface area	m^2
A_2	Secondary surface area	m^2
b	Spacing between adjacent fins	mm
c_p	Specific heat at constant pressure of coolant	kJ/kg K
d_e	Equivalent oval tube diameter	mm
d_i	Basic tube inside diameter	mm
d_o	Basic tube outside diameter	mm
$\bar{d}_p$	Mean fluidized particle diameter	μm
D	Radial or square fin outside dimension	mm
D	Oval tube major outside dimension	mm
E_F	Fin efficiency	
E_{FFECT}	Fin effectiveness factor	
G	Mass flow rate of fluidizing gas per bed sectional area	kg/s m^2
h	Position of surface above distributor - plain and oval tube from surface centre line - extended surface from lower fin edge	mm
h_i	Basic tube inside surface heat transfer coefficient	kW/m^2 K
h_M	Bed to metal heat transfer coefficient	kW/m^2 K
h_o	Bed to outside surface heat transfer coefficient	kW/m^2 K
h_{op}	Plain tube bed to surface heat transfer coefficient	kW/m^2 K
H	Static height of bed material	mm
H_a	Pressure difference across air orifice plate	mm H_2O
H_w	Pressure difference across water circulation orifice plate	mm H_2O

Symbol	Definition	Units
I_0	Modified Bessel function of first kind and zeroth order	
I_1	Modified Bessel function of first kind and first order	
k	Thermal conductivity of surface material	kW/m K
k_p	Thermal conductivity of particle material	W/m K
k_w	Thermal conductivity of water	kW/m K
K_0	Modified Bessel function of second kind and zeroth order	
K_1	Modified Bessel function of second kind and first order	
I	Fin height of radial extended surface	mm
L	Finned length or plain surface length exposed to the bed	mm
m	Term used in conduction equation	mm^{-1}
$\dot{m}$	Feed water mass flow rate	kg/s
$\dot{M}$	Circulation water mass flow rate	kg/s
n	Total number of fins of extended surface	
N	Number of fins per metre length of tube	
P_a	Air gauge pressure at orifice plate	mm Hg
P_{at}	Absolute barometric pressure	mm Hg
Q	Rate of heat transfer to total surface	kW
Q_1	Rate of heat transfer to primary surface	kW
Q_2	Rate of heat transfer to secondary surface	kW
r	Fin radius at which fin temperature is T	mm
r_e	Fin radius at tip position	mm
r_o	Fin radius at root position	mm
t	Fin thickness	mm
t	Statistical quantity	
t_r	Residence time of particle at surface	ms
T	Radial fin temperature at radius r	^oC
T	Oval tube thickness	mm
T_a	Air temperature at orifice plate	^oC
T_{at}	Atmospheric temperature	^oC
T_b	Fluidized bed temperature	^oC
$\bar{T}_f$	Mean fin temperature	^oC
T_{RF}	Fin root temperature	^oC

Symbol	Definition	Units
T_i	Basic tube inside surface temperature	^oC
T_m	Experimental average surface metal temperature	^oC
T_o	Basic tube outside surface temperature	^oC
T_w	Mean water temperature	^oC
T_{wi}	Feed water inlet temperature or water inlet temperature to surface	^oC
T_{wo}	Feed water outlet temperature or water outlet temperature from surface	^oC
T_x	Water temperature at inlet to surface	^oC
u	Mean coolant velocity through basic tube	m/s
u_f	Superficial fluidizing velocity	m/s
u_{mf}	Minimum superficial fluidizing velocity	m/s
U	Overall heat transfer coefficient	kW/m^2 K
$\dot{V}_a$	Volumetric air flow rate at 15°C and 760 mm Hg absolute conditions	m^3/s
V_{FIN}	Volume occupied by metal of fins	m^3
$\dot{V}_g$	Volumetric gas flow rate at 15°C and 760 mm Hg absolute conditions	m^3/s
V_1	Volume occupied by extended surface in bed	m^3
V_2	Volume occupied by metal of extended surface	m^3
W	Square fin outside dimension or oval tube minor outside dimension	mm
W	Power required to drive circulating pump	kW
X	Effective basic tube length exposed to the bed	mm
α	Thermal diffusivity of particle material	m^2/s
Θ	Bed to fin temperature difference	K
Θ_o	Bed to fin root temperature difference	K
μ	Dynamic viscosity of coolant	kg/m s
ρ	Density of coolant	kg/m^3

Dimensionless Groups

Nu Nusselt Number : $\frac{h_i d_i}{k_w}$ Re Reynolds Number : $\frac{\rho u d_i}{\mu}$

ϕ Parameter in conduction efficiency expressions : $(r_e - r_o)m$ η Temperature difference ratio : $\frac{T_b - \bar{T}_f}{T_b - T_o}$

CHAPTER I
INTRODUCTION

1.1 The Concept of Fluidization

Fluidization is a generic term for the processes whereby a liquid-like behaviour can be induced in a mass of solid particles. Such processes generally involve an upward flow of fluid, through a bed of solid particles, at a rate dependant upon the type of fluidization required.

Initially the close packed mass of particles rests upon a distributor plate designed to disperse the fluid over the cross-sectional area of the particle bed. At low rates of flow, the rising fluid can diffuse through the interstices of the packed solids without disturbing the packing arrangement. As the flow rate is increased however, the drag forces on the particles reach a sufficient level to cause separation of the particles as the fluid forces its way through the bed. The presence of a fluid film between many of the particles reduces the ability of the bed to withstand an applied shear force and the bed begins to exhibit the characteristics of a liquid: disturbance of the bed surface causes ripple propagation and objects dropped onto the bed surface float or sink according to their density. At this stage of fluidization the bed has a well defined surface and only slow mixing of the particulate matter takes place. The fluid velocity required to induce this stage of fluidization is termed the critical or minimum fluidizing velocity for the system. Over a range of fluid velocities above the minimum for fluidization, important changes in the nature of the fluidized bed takes place.

With increasing fluid velocity, expansion of the bed volume increases and motion within the bed becomes more turbulent. A bubble mechanism of fluid flow completely changes the appearance of the bed surface from the quiescent, well defined nature initially observed, to a diffuse region of scattered particles. The fluid distributor at the base of the bed can exert a very strong influence on the structure of the whole bed. Ideally it should be porous with a fine texture so that the fluid is introduced through a multitude of small injection points. The

bubbles of fluid form at the distributor surface and grow by coalescence as they rise through the bed at a faster rate than the average or superficial fluidizing velocity. Particles in the bed are caught in the wake of these bubbles and dragged to the surface of the bed. Here they are only subject to the superficial fluidizing velocity and gradually sink once more until affected by another fluid bubble. Thus during this dense phase of fluidization, there is a rapid mixing and circulation of particles within the bed.

Eventually the average fluid velocity through the bed approaches the free fall velocity of the various particles and a disperse phase of fluidization is encountered. In this phase the separation of particles by the fluid is considerable and elutriation of the bed material is increasingly significant. Ultimately the superficial fluid velocity exceeds the free fall velocity of the particles and the bed is destroyed by entrainment of the particles in the fluid stream.

1.2 Heat Transfer Applications

Although the technique of fluidization was appreciated at the beginning of the century it was only during the second world war that it was first put to practical use by the chemical engineering industry for the catalytic cracking of petroleum. The vigorous mixing of particles within the bed and the intimate contact between the solid particles and the fluidizing medium, were recognized to have considerable advantages in promoting rapid chemical reactions. For a reactive bed in which the heat is generated within the bed or an inert bed which is pre-heated by the fluidizing medium, the mixing characteristics give rise to high heat and mass transfer between the solid particles and fluid, and high heat transfer coefficients to surfaces immersed in the bed. Such fluidized systems are used in dehydration of solutions (or suspensions) and of wet granular materials, heat treatment of metal parts, and heating and cooling of gases and powdered granular solids. During the last ten years, there has been a considerable amount of research and development effort on the efficient combustion of solid, liquid and gaseous fuels. The Central Electricity Generating Board and the National Coal Board have all carried out experimental work burning solids of

pulverised coal in fluidized beds with a view to the development of large-scale industrial fluidized bed boilers suitable for power station operation.

The technology could easily be applied to domestic and small to medium-scale industrial boilers for total energy situations and such applications will prove beneficial by reducing overall operating costs. Elliott[1*], 1971, reviewed these applications for possible use in total energy systems. Pressurized combustion of fluidized beds is interesting in that it can be used for combined power cycle operation; the steam generated in the fluidized bed boiler is used for operating a steam turbine and the energy in the gases from the bed is recovered in a gas turbine. In the field of normal heat exchange waste heat recovery systems from gas turbine and internal combustion engine exhausts are being investigated.

The degree of success of the aforementioned fluidized bed technology applications depend largely upon the heat transfer rates that can be obtained. Studies of heat exchangers transferring energy between a liquid or vapour and a gas, through a metallic wall have shown that the main resistance to heat flow occurs on the gas side of the wall. Thus the thermal performance of such a heat exchanger may be improved by including additional heat transfer surface on the gas-side of the system in the form of fins or spines. In fluidized bed systems where the bed to basic tube heat transfer coefficients are three to ten times that of an equivalent forced convection system, the controlling resistance to heat flow remains on the bed side for water/steam flow through the basic tube. This improvement is only obtained at the expense of the relatively high pressure drop necessary to pass the gas through the fluidized bed . Extended surface in fluidized bed systems is therefore an attractive proposition provided the pressure drop can be reduced. However, because of thermal gradients that exist in the fin material, the increase in performance will not be directly proportional to the amount of surface added.

---

* Subscripts refer to references coded to the Bibliography.

1.3 Purpose of Research Work

Owing to the need for the controlled addition or extraction of considerable amounts of thermal energy during the progress of many chemical reactions, much work has already been carried out on the mechanism of heat transfer in deep fluidized beds; greater than 150 mm. Many workers have investigated heat transfer rates obtained with various combinations of bed material and fluidizing medium. The results of these investigations, which will be reviewed in subsequent chapters, are widely reported in the technical journals and many correlations have been published which attempt to account for the observed results in terms of the numerous parameters affecting heat transfer. These correlations are not exact even within the limited range of conditions from which they were derived. Thus considerable errors can arise from attempts to utilize these correlations over the whole range of fluidized bed heat transfer applications. Hence, even though there is considerable knowledge concerning the general behaviour of fluidized systems, very little information has been published on extended surface fluidized bed heat transfer.

For systems in which it is desired to transfer heat from the fluidizing gases and solids to a tube bundle, the pressure drop could be reduced by operating with fine particles of solids in shallow fluidized beds, less than 150mm, with their correspondingly low fluidization velocity. In this case the surface area of the fluidized bed to pass a given gas volume will have to be large and thus incur high capital costs for the distributor and the bed containment. It is therefore very important to optimise both geometry and arrangement of the surface in order to reduce this problem.

Experimental data and theoretical calculation of the heat transfer performance of a variety of extended surface configurations submerged in shallow gas fluidized beds will be presented. To date no research work on extended surface in shallow gas fluidized bed systems has been reported. Various bed materials will be used, the fluidizing medium being the products of combustion resulting from a weak mixture of air/propane gas. The pre-heated bed material temperatures will be limited to less than 350°C by the influence of the extended surfaces which are water cooled. Such an arrangement could be employed in heat recovery or boiler systems.

Fin geometry and materials are very much more important in the optimisation of such heat transfer applications than in conventional convective systems because of the very much higher heat fluxes involved and this is emphasised by theoretical studies of fin conduction efficiency. The particular type of extended surface governs whether an analytical or numerical solution to the fin conduction theory is used. For radial fins of rectangular profile attached to a basic tube the equation for the temperature distribution in the fin will be derived and a solution for fin efficiency presented. This concept of fin efficiency will be used to reduce the actual geometric area of fin surface which is not at uniform temperature, to an equivalent area at one definite temperature, namely, that existing on the tube wall at the point of attachment of the fin. This makes it possible to treat all the heating surface as if it were part of the plain tube and one-hundred percent efficient. The performance of such extended surface will be compared with experimental results from plain basic tubes tested under similar conditions by means of an "effectiveness factor".

The theoretical model of heat flow in the fins of a fluidized bed heat exchanger has been extended to give data concerning the minimum amount of metal needed to fulfil a given heat exchange duty. This allows the cost effectiveness of such extended surfaces to be established in order to promote the applications of this new technology.

Finally, the sensitivity of finned tube assemblies to the overall geometry of the fluidized bed is investigated.

CHAPTER II

A REVIEW OF FLUIDIZED BED HEAT TRANSFER

2.1 The Mechanism of Bed to Surface Heat Transfer

2.1.1 Introduction

The general behaviour of a bed as it begins to fluidize is well known. The way in which the heat transfer coefficient of a surface, immersed in the particles, changes on gradual transition from a fixed bed to develop fluidization is illustrated in figure 2.1. After the minimum fluidizing velocity is reached the heat transfer coefficient increases rapidly over a comparatively narrow range - the rising branch of the curve. The rise is of one to two orders of magnitude for gas systems. The heat transfer coefficient then increases more slowly to the "plateau" maximum and then reduces slightly - the falling branch of the curve.

The most significant contributions, from the published literature, which have attempted to explain the mechanism of bed to surface heat transfer, are reviewed in the following section.

2.1.2. Physical Models of Heat Transfer

Because the bubbling gas fluidized bed looks so very like a boiling liquid, many workers felt that heat transfer between the bed and a surface immersed in it must be limited by that which corresponds to the limiting laminar film as in conventional convective systems. Thus Leva, Weintrub and Grummer[2], 1949, for example, who appreciated that the core of a well fluidized bed was isothermal and so of negligible thermal resistance, suggested that the rate of heat transfer between the bed and a surface was dependant on the thickness of the boundary layer at the heat transfer surface, the thickness of this layer being a function mainly of the gas kinematic viscosity and the vertical particle velocity near the surface. They suggested that the particles acted as turbulence promoters to erode away the film and reduce its thickness. Levenspiel and Walton[3], 1954, suggested that the gasfilm was broken whenever a particle touched the surface. Many other similar models have been proposed. In a later paper, Wen and Leva[4], 1956, reviewed the work of Leva[2] et al, 1949, concluding that the controlling factor is heat conduction through

a laminar boundary layer, noting that a maximum occurred in the heat transfer coefficient - fluidizing velocity curve. They attributed this to the counteractive effects of two processes;

(i) an increase in the coefficient due to increased particle motion and "scouring action" with an increase in the gas flow rate, and

(ii) a reduction in solid concentration at high gas flow rates leading to a reduction in the number of particles impinging on a given surface area and thus a reduction in heat transfer coefficient.

Mickley and Trilling[5], 1949, were the first to appreciate the implications of the true unsteady nature of the process. The dominating factor with gas fluidized systems is the much greater ability of the circulating solids to transfer heat because particle volumetric heat capacities are of the order of one thousand times higher than those of atmospheric gases. for example, although they had previously been associated with a model of the heat transfer process based on gas convection, Ziegler and Brazelton[6], 1964, showed that 80 - 95% of the heat transferred in a fluidized bed was transported by solids convection. The solids act as a local source or sink of heat. Thermal equilibrium is quickly established between the gas and the particles because of the very large exposed surface area of the small particles. The interstitial flowing gas quickly follows the temperature of the surrounding particles - not the reverse as Dow and Jakob[7], 1951, earlier seemed to think. Particles in the bulk of the bed exchange heat with each other through the gas phase but usually stay in the bulk of the bed long enough to come to the same temperatures as their neighbours. Then some of them, at the bed temperatures, are swept into close proximity with the heat exchange surface under the natural circulation currents occurring within the bed. Initially, when the particles first arrive close to the heat transfer surface, there is a high local temperature gradient between them and the surface and most of the heat transfer takes place by conduction through the thin gas film between the particles and the surface, rather than by direct conduction at the particle/surface contact points. However, this gas conduction is not the limiting factor and the residence time of particles near the surface is of prime

importance since their heat capacity is small. The longer the particles reside there, the more nearly their temperature approaches that of the surface with consequent reduction in the local temperature gradient and the effective rate of heat transfer. If the particles become immobile at the surface it becomes a heat insulator. Accordingly, highest rates of heat transfer and highest heat transfer coefficients are to be expected under conditions in which there is most rapid exchange between particles in the bulk of the bed and those at the surface.

It should be stressed that under good operating conditions, the bulk of the bed is isothermal and the temperature gradient is concentrated at the heat transfer surface. Heat is being transferred through the bulk of the bed by solids convection. To make a comparable contribution one thousand times the atmospheric volume of gas would have to flow between the bulk of the bed and the transfer surface.

Solids convection is a key factor. As Rowe et al[8], 1965, have shown the rising bubbles are responsible for the particle mixing. The distributor will obviously have an important bearing on the bubbling patterns developing within the bed and so will any internals within the bed.

Mickley and Fairbanks[9], 1955, developed a mathematical model of the mechanism of bed to surface heat transfer which has just been described. Their supposition was that heat transfer from bed to surface is by contact with small groups or "packets" of particles and gas. These packets are assumed to have the properties of the bulk of the bed. They included the influence of particle motion by a "stirring factor" which was ill defined, and used several different fluidizing gases to test the influence of gas properties. They concluded that the main influences on heat transfer were the properties of the "packets", particularly their thermal conductivities.

In a later study, Mickley, Fairbanks and Hawthorne[10], 1961, attempted to measure the packet residence times experimentally by immersing an electrically heated strip heater of small heat capacity within the bulk of the bed. Because of the heaters low

heat capacity, its resistance varied with change in the rate of heat transfer between it and the bed. From the profile of the strip temperature fluctuations with time they deduced packet residence times under the conditions of their experiments. Henwood[11], 1969, has made some similar measurements of local heat transfer coefficients within and adjacent to a rising bubble in a two-dimensional bed. In both of these experiments, the small surface was positioned in the direct path of rising bubbles so at times it exchanged heat with the gas and the transfer rate was low. At other times it was being contacted by fresh solids which were drawn rapidly past it. Particle residence time waslow and heat transfer coefficients correspondingly high. Much lower localbed wall heat transfer coefficients were observed in their experiments by Drinkenburg, Huige and Rietema[12], 1966, . The bubbles passed up the wall surface only comparatively rarely and heat was being exchanged with particles moving more slowly down the wall in the "stick-slip" flow that they described. The transfer rate was correspondingly lower because of the longer particle residence time at the transfer surface. Such differences in various investigators results reflect the differences in the solids flow patterns at different positions within the bed.

In work done at the University of Birmingham[13], between 1963 and 1970, Botterill and his co-workers have shown that the Mickley and Fairbanks[9], 1955, assumption that particles and gas phase can be considered as a medium of uniform properties ; those of the bed at the point of fluidization, clearly does not hold in the region close to the heat transfer surface and for short residence times. In a simple model Botterill[14], 1963, analysed the unsteady state conduction between a surface of infinite heat capacity and a cylindrical solid particle immersed in a gas. From the calculated temperature distribution isotherms could be drawn through the system for different particle residence times. Significant heat transfer only occurs through regions of very close particle to surface approach. On the assumption of cubical packing of particles close to the surface, an overall heat transfer coefficient was estimated for a system of known particle residence time. Gabor[15], 1970, has extended the type of unsteady-state

conduction calculation, outlined above, to consider the transfer of heat from a string of particles in depth into the bed giving similar results to those of Botterill[14], 1963. In view of the uncertainties about the particle orientation - most particles are irregular in shape, and the packing of the particles close to a surface, there seems little value in expending effort in developing further complicated models which are expensive in computing time.

A model which contains the basic features of the lower temperature bed - to - surface heat transfer process (where radiant heat transfer may be neglected) has been described by Yoshida, Kunii and Levenspiel[32], 1969. This involves the supply of heat to an emulsion phase by a random renewal mechanism and its subsequent transfer through the emulsion phase to the heat transfer surface. Here the emulsion phase would correspond to those downflowing particles close to a surface, which, if it is the containing wall of the bed, are only occasionally directly disturbed by rising bubbles. The problem remains, however, that the relevant parameters (the thermal properties of the emulsion phase which are very sensitive to the particle packing; the emulsion thickness; the renewal rate) are not known nor do we appreciate how they are likely to change with change in design detail of the bed and immersed surfaces or with change in the bed material. Thus the principal present value of the model must lie in using it to fit given experimental results for the interpretation of what is happening there rather than as a means for the prediction of what will happen in quite different circumstances.

The initial rapid rise of heat transfer coefficient in figure 2.1 is attributed, therefore, to increase solids circulation following the onset of fluidization, whilst the plateau region is the result of an interaction between competing processes; the increasing fluidizing velocity intensifies particle circulation which improves heat transfer, but the greater bubble activity reduces the number of particles in contact with the surface which has the opposite effect. In most cases, the heat exchanger would be designed to operate in the plateau region, which fortunately is relatively flat over a wide range of fluidizing velocities.

It is clear from this brief literature survey that the magnitude of bed to surface heat transfer coefficient is dependent on particle circulation and especially on the frequency of particle exchange between the bulk of the bed and the vicinity of the heat transfer surface. In extreme cases of very short residence times particle thermal properties are of importance. Although the heat transfer coefficient is not amenable to calculation, factors which might also be expected to influence it include fluidizing velocity, particle size, thermal properties of the gas, distributor design and geometrical arrangement and position of the heat transfer surface in the bed.

2.2 Extended Surface Heat Transfer

2.2.1 Introduction

From the previous section it is apparent that for good heat exchange the surface needs to be brought into contact as rapidly as possible with fresh particles from regions of the bed away from the surface. Therefore, a defluidized region of the bed near the upper and lower portion of a horizontal tube would be detrimental to good heat transfer. Experimental evidence for this comes from the work of Vreedenberg[16,17,18], 1952, 1958 and 1960, while Sinclair, Wright and Thomas[19], 1964, have found that a flat plate is best arranged vertically in a fluidized bed - rather than at any other angle to the vertical, in order to optimize heat transfer from bed to the plate. Therefore, it would suggest that for the best thermal performance an extended surface should have fins mounted vertically in the bed, on one or a series of small diameter horizontal basic tubes.

2.2.2 Relevant Published Papers

The first published information on extended surfaces in fluidized beds was given by Petrie, Freeby and Buckham[20], 1968. They were concerned with the development and operation of a radioactive waste calcination process. The processing rate was controlled by the rate of energy addition to the bed of radioactive material. Extended surface with continuous helically wound fins on a basic tube as well as plain tubes, were arranged in horizontal bundles and located in the lower regions of a series of deep beds, the static height being approximately 900 mm. Bed

sizes rangedfrom 300 mm to 1200 mm diameter and the energy was transferred to the air fluidized bed material electrically or by circulating hot liquid metal or steam through the tubes of each bundle. Bed temperatures were maintained at about 400°C. Heat transfer coefficients were measured under a range of fluidizing velocities and compared for a 19 mm diameter plain tube and two sizes of extended surface. The fins were 0.4 mm thick and were either 197 fins/m or 433 fins/m in number, attached to a 19 mm diameter basic tube. The fin height was constant at 10.3 mm. The effect of tube bundle spacing was not investigated and from the limited range of tubing tested a correlating equation was established.

Without any particular application in mind, Bartel, Genetti and Grimmett[27], 1970, measured coefficients for heat transfer from an electrically heated horizontal surface, to a bed material of spherical glass particles fluidized by air. The surfaces tested were a plain tube and a serrated carbon steel, discontinuous finned tube. The experimental variables were particle diameter, fin height, fin thickness and fluidizing velocity. Temperatures to a maximum of 100°C were recorded in a 300 mm diameter bed. The surfaces were positioned 200 mm above a perforated steel distributor plate, the static bed height being 560 mm. A "fin effectiveness factor" was defined to relate the heat transfer coefficients of the finned tubes with those of the bare tube. Finally, a mathematical model was used to correlate all of the experimental heat transfer data into one equation containing all the experimental variables. The work of Bartel, et al[27], 1970, was extended by Genetti, Schmall and Grimmett[28], 1970, using the same research equipment, who studied the effect of tube orientation on their defined heat transfer coefficients. For the horizontal position a comparison was made between copper - clad and carbon steel wound finned tube.

Investigations on heat transfer at longitudinally and discontinuous radial and square finned tubes in the horizontal position, were carried out by Natusch and Blenke[23], 1972. Again, glass beads were fluidized with air at a static bed height of 500 mm in a steel container of 305 mm diameter, the distributor being a plastic grid. The tubes were positioned 250 mm above the

distributor and electrically heated by an internal fire - element. Bed temperatures were limited to about 100°C. In addition to the variables investigated by Bartel, et al[27], 1970, the fin spacing was varied between 2 mm and 10 mm for the radial finned extended surface. The copper basic tube diameter was 25 mm and the copper fins varied in height from 7.5 mm to 37.5 mm for a series of fin thicknesses 0.5 mm, 1 mm and 2 mm. The effect of finned tube geometry variation, which influences the heat transfer coefficient between bed and surface was compared. The need for positioning fins vertically in the bed, which was mentioned in the introduction to this section, is apparent from the results of the authors longitudinally finned tubes.

In a Russian paper, Khasanov et al[31], 1972, investigated the heat transfer between a bundle of 20 mm diameter vertical tubes each with three longitudinal fins 20 mm in height and 1 mm thick. The bed diameter was 300 mm and the dispersed material quartz sand and silica gell, to a static height of 300 mm. The lower edge of the duralamin tube was 100 mm from a perforated plate distributor through which atmospheric air was blown. The bed temperature was not specified, but from the size of the electrical heating element it is estimated that the bed temperature was in the region of 50°C to 100°C. Curves of heat transfer coefficient versus superficial fluidizing velocity are presented.

Bartel and Genetti[29], 1973, have extended their work of 1970 by studying the effect of the same horizontal plain and discontinuous serrated finned tubes, in tube bundle formation, in a rectangular bed 394 mm by 207 mm. The pitch and spacing of the seven tubes were varied, the lowest tube being positioned some 350 mm above the distributor. For variables of particle diameter, fin height and fluidizing velocity as well as tube position heat transfer coefficients between tube and bed, based on the total surface area subjected to the bed material, are presented and discussed. Finally the results are correlated by a single equation.

An interesting paper by Hager and Thomson[30], 1973, on the bubble behaviour around immersed tubes in a fluidized bed has recently been presented in the literature. X - ray and flow visualization experiments are reported for bare and finned tubes

at various orientation angles. The extended surface used was of both the discontinuous serrated and radial type, the latter being identical to that presented in this dissertation. The radial finned tube used for flow visualization only, was produced by 275 fins/m of thickness 1.4 mm and height 2.5 mm on a basic tube diameter of 7.6 mm. The bed which was rectangular 318 mm by 150 mm containing small glass beads, was fluidized by atmospheric air, the maximum temperature being 30°C. Evidence is presented which indicates that under certain conditions the bubbles will flow along or adhere to the tube surface. This effect is a function of both the orientation angle and the roughness of the tube surfaces. Studies of the defluidized cap above horizontal immersed tubes indicate that significant particle interchange between the cap and the emulsion is occurring at flow rates much lower than previously expected.

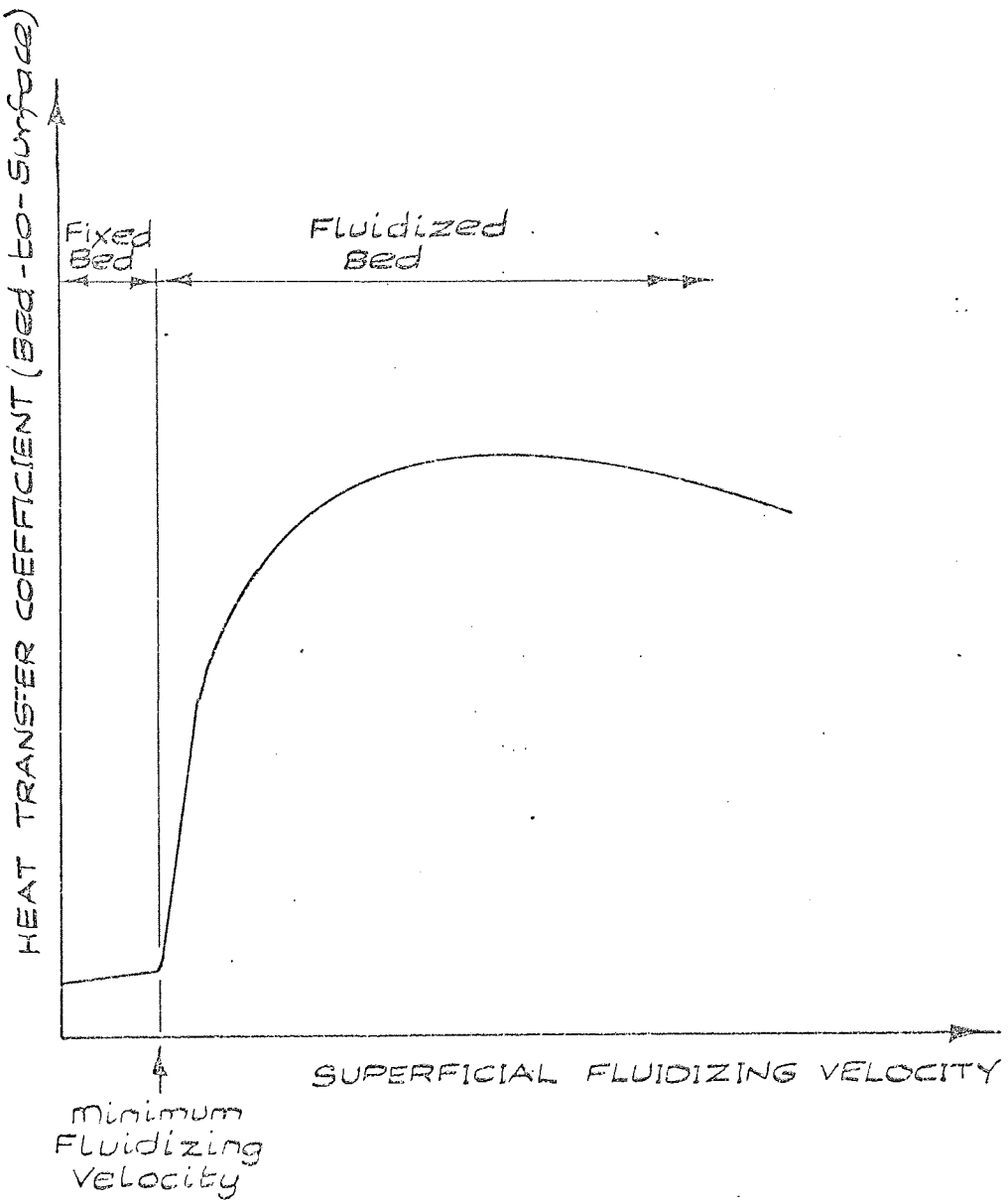

Figure 2.1 Influence of Gas Velocity on Bed-to-Surface Heat Transfer Coefficient

CHAPTER III

THEORETICAL CONSIDERATIONS

3.1 Introduction

In this chapter the theory associated with the particular type of extended surface will be derived together with that for the plain and oval tube. Equations will be developed enabling the general level of performance of such surfaces to be determined from experimental results.

3.2 Assumptions of Fin Conduction Theory

Before deriving the necessary equations several general assumptions of a physical nature are necessarily involved. They are:

(i) The heat flow and temperature distribution throughout the fin are independent of time.

(ii) The fin material is homogeneous and isotropic.

(iii) There are no heat sources in the fin itself.

(iv) The heat flow to the fin surface at any point is directly proportional to the temperature difference between the surrounding bed material and the surface at that point.

(v) The thermal conductivity of the fin is constant.

(vi) The temperature of the bed material is constant.

(vii) The temparature at the base of the fin is uniform.

(viii) The fin thickness is so small compared to its height that temperature gradients normal to the surface may be neglected.

Particular assumptions will be discussed when the relevant equations are derived.

3.3 Radial Fin of Rectangular Section

3.3.1 Bed to Extended Surface Heat Transfer Coefficient

Considering a section of extended surface as shown in figure 3.1 and assuming h_o remains constant at the basic tube primary surface, then

$$Q_1 = h_o A_1 (T_b - T_o) \qquad (3.1)$$

It is also assumed that the bed particle temperature remains the same, between adjacent fins and the bulk of the bed*.

---

* This assumption will be discussed in Chapter IX.

Also, assuming the heat transfer coefficient at the fin tip and flanks to remain constant* and equivalent to that at the basic tube

$$Q_2 = h_o A_2 (T_b - \bar{T}_f) \tag{3.2}$$

The total heat transfer to the extended surface is

$$Q = Q_1 + Q_2$$

$$Q = h_o A_1 (T_b - T_o) + h_o A_2 (T_b - \bar{T}_f) \tag{3.3}$$

Defining the dimensionless temperature ratio η by

$$\eta = \frac{T_b - \bar{T}_f}{T_b - T_o} \tag{3.4}$$

then,

$$Q = h_o (A_1 + \eta A_2)(T_b - T_o)$$

$$Q = h_o A_E (T_b - T_o) \tag{3.5}$$

where

$$A_E = A_1 + \eta A_2 \tag{3.6}$$

Assuming the root fin and primary tube surface temperature to be equal i.e. $T_{RF} = T_o$, then the conduction through the basic tube is radial only, and

$$Q = \frac{4\pi k \; L (T_o - T_i)}{\ln \left(\frac{A_o}{A_i} \right)} \tag{3.7}$$

On the assumption that the heat transfer coefficient and temperature at the inside basic tube wall remain constant, then

$$Q = h_i A_i (T_i - T_w) \tag{3.8}$$

Basing the overall heat transfer coefficient on the basic tube surface area

$$Q = U A_o (T_b - T_w) \tag{3.9}$$

Combining equations (3.5),(3.7),(3.8) and (3.9) and rearranging the heat transfer coefficient between bed and metal of the extended surface is given by

$$h_o = \frac{1}{\frac{A_E}{U A_o} - \frac{A_E \ln \left(\frac{A_o}{A_i} \right)}{4\pi k L} - \frac{A_E}{h_i A_i}} \tag{3.10}$$

* This assumption will be discussed in Chapter IX

Hence, providing the variables on the right hand side of equation (3.10) can be established, then the bed to metal heat transfer coefficient may be determined.

3.3.2 Definition of Fin Efficiency

Defining the fin efficiency E_F as the ratio of the actual heat transferred from the bed to the fin, to that which would be transferred if all the fin were at the root temperature T_{RF}. This implies that the fin material has an infinite thermal conductivity, from which

$$E_F = \frac{h_o A_2 (T_b - \bar{T}_f)}{h_o A_2 (T_b - T_{RF})} = \frac{T_b - \bar{T}_f}{T_b - T_{RF}} \qquad (3.11)$$

As indicated previously it has already been assumed that the primary tube surface and root fin temperatures are the same. Hence

$$E_F = \eta = \frac{T_b - \bar{T}_f}{T_b - T_o} \qquad (3.12)$$

and from equation (3.6)

$$A_E = A_1 + E_F A_2 \qquad (3.13)$$

This assumption is not strictly correct in practice, Sparrow and Hennecke[21], 1970, indicating a temperature depression at the root of the fin i.e. T_{RF} less than T_o. The effect of material thermal conductivity can also affect the difference as suggested by Klett and McCulloch[22], 1972. It is also pointed out by Natusch and Blenke[23], 1972, for this type of extended surface in a fluidised bed application, that the smaller the fin spacing and the greater the material thermal conductivity the better the assumption becomes.

The fin efficiency is influenced by the fin material, fin height and fin thickness, as well as the bed to metal heat transfer coefficient. An exact solution is possible from the fin conduction differential equation, which establishes the temperature profile through the fin material using suitable boundary conditions.

3.3.3 Fin TemperatureProfile

Consider a differential element of fin thickness t and length dr as shown in figure 3.1 . The element conducts radially heat Q_r and $Q_{(r+dr)}$ and gains energy at the fin flanks from the bed Q_b. The steady state heat energy balance for the element is

$$Q_{(r+dr)} + Q_b = Q_r \qquad (3.14)$$

Using Fourier's basic equation of conduction, equation (3.14) becomes

$$k.2\pi(r+dr).t\frac{\partial}{\partial r}\left[T+\frac{\partial T}{\partial r}.dr\right]+2(2\pi r\,dr)h_o(T_b-T)$$

$$= k.2\pi r.t.\frac{\partial T}{\partial r}$$

from which

$$\frac{\partial^2 T}{\partial r^2}+\frac{1}{r}.\frac{\partial T}{\partial r}+m^2(T_b-T)$$

where

$$m^2=\frac{2h_o}{k\,t}$$

Let $\theta = T_b - T$, then $\frac{\partial T}{\partial r}=-\frac{\partial \theta}{\partial r}$ and $\frac{\partial^2 T}{\partial r^2}=-\frac{\partial^2 \theta}{\partial r^2}$ and since T is only a function of r we may write

$$\frac{d^2\theta}{dr^2}+\frac{1}{r}.\frac{d\theta}{dr}-m^2\theta=0 \qquad (3.15)$$

The general solution to this conduction equation is

$$\theta = C_1 I_o(mr)+C_2K_o(mr) \qquad (3.16)$$

where C_1 and C_2 are arbitrary constants to be evaluated from the boundary conditions imposed.

This solution is readily available in the literature, the most notable being due to Harper and Brown[24], 1922, and Gardner[25], 1945, both of whom analysed a series of different extended surface configurations. The particular solution to equation(3.16) is simplified by neglecting the heat flow through the fin tip. This was the case with both Harper and Brown and Gardner's analyses, although Harper and Brown suggested that this could be accounted for by an approximation. In fluidized bed applications where the heat flux is large compared with that for conventional forced convection systems, this assumption is no longer generally valid except in cases of small fin thickness and fin height and high material thermal conductivity. It was therefore decided to impose a general boundary condition of heat transfer into the fins at the tip position even though the analysis is complicated.

Hence, when $r = r_o$ $\theta = \theta_o$ and when

$$r = r_e \quad -k\left(\frac{d\theta}{dr}\right) = h_o\theta$$

Now $$\left(\frac{d\theta}{dr}\right)_{r=r_e} = m\left[C_1 I_1(mr_e) - C_2 K_1(mr_e)\right]$$

Hence $$\theta_o = C_1 I_o(mr_o) + C_2 K_o(mr_o) \qquad (3.17)$$

and $$-\frac{km}{h_o}\left[C_1 I_1(mr_e) - C_2 K_1(mr_e)\right] = C_1 I_o(mr_e) + C_2 K_o(mr_e) \qquad (3.18)$$

From equations (3.17) and (3.18) the constants can be determined.

$$C_1 = \frac{\theta_o}{\gamma K_o(mr_o) + I_o(mr_o)}.$$

where $$\gamma = \frac{\frac{h_o}{km}\cdot I_o(mr_e) + I_1(mr_e)}{K_1(mr_e) - \frac{h_o}{km}\cdot K_o(mr_e)}$$

and $$C_2 = \frac{\theta_o\gamma}{\gamma K_o(mr_o) + I_o(mr_o)}$$

$$\therefore \quad \frac{\theta}{\theta_o} = \frac{T_b - T}{T_b - T_o} = \frac{I_o(mr) + \gamma K_o(mr)}{\gamma K_o(mr_o) + I_o(mr_o)} = f\left(\frac{r}{r_o}; \frac{r_e}{r_o}; mt; \phi\right) \qquad (3.19)$$

where $mr = mr_o\left(\frac{r}{r_o}\right)$ and $\phi = m(r_e - r_o)$

Equation (3.19) therefore defines the temperature profile through the fin material. A computer programme was developed to show the variation of these dimensionless parameters under experimental conditions, the results being discussed in Chapter IX.

3.3.4 Evaluation of Fin Efficiency

From a knowledge of the temperature profile it is possible to develop an expression for the fin efficiency in terms of the physical conditions.

Now the actual heat transferred by each fin is that entering the root of the fin, namely

$$-k.2\pi r_o t\left(\frac{d\theta}{dr}\right)_{r=r_o}$$

and the amount if the fin were subject to a constant temperature difference between bed and metal of θ_o

$$h_o\theta_o\left[2\pi(r_e^2 - r_o^2) + 2\pi r_e t\right]$$

Hence $$E_F = \frac{-k.2\pi r_o t\left(\frac{d\theta}{dr}\right)_{r=r_o}}{h_o\theta_o\left[2\pi(r_e^2 - r_o^2) + 2\pi r_e t\right]}$$

which when expressed in dimensionless parameters is given by

$$E_F = \frac{2}{\frac{r_e}{r_o}(\phi + mt) + \phi}\left[\frac{\gamma K_1(mr_o) - I_1(mr_o)}{I_o(mr_o) + \gamma K_o(mr_o)}\right] \qquad (3.20)$$

$$E_F = f\left(\frac{r_e}{r_o}; mt; \phi\right)$$

The variation of fin efficiency for a range of different operating conditions is represented in figures 8.86 and 8.87.

It is apparent from equation (3.10) that in order to solve for h_o an iterative solution is required, the heat transfer coefficient appearing implicitly on both sides of the equation. With the advent of the high speed computer this computation is made easy.

3.3.5 Basic Tube Surface to Water Heat Transfer Coefficient

It is found experimentally that for the case of fully developed turbulent flow in a long tube, with Re greater than 10,000 and for fluids whose Prandtl number, Pr, are in the range from about 0.5 upwards, heat transfer coefficients are given, within good accuracy, by the Dittus - Boelter equation recommended by McAdams[26]

$$Nu = 0.023 Re^{0.8} Pr^{0.4} \qquad (3.21)$$

The heat transfer coefficient, h_i, in the Nusselt number is a mean value. It is equivalent to that obtained by the average heat flux divided by the logarithmic mean temperature difference between tube wall and the water. The physical properties of water u, c_p and k_w are evaluated at the mean water temperature; that is arithmetic mean of the inlet and outlet water temperatures.

Empirical equations for water properties as a function of the mean water temperature are given in Appendix A3.

Rearranging equation (3.21) gives

$$h_i = 0.023 \frac{k_w}{d_i} \left[\frac{\rho u d_i}{\mu}\right]^{0.8} \left[\frac{c_p \mu}{k_w}\right]^{0.4} \qquad (3.22)$$

Thus from equation (3.22) h_i may be determined.

3.4 Square Fin of Rectangular Section

3.4.1 Bed to Extended Surface Heat Transfer Coefficient

In the case of square fins it is difficult to define an effective area A_E, particularly when the primary tube surface is assymetrically disposed about the fin flank. This is shown in figure 3.2. To alleviate this problem the heat transfer

coefficient between the bed and the metal can be determined by

$$h_M = \frac{Q}{(A_1+A_2)(T_b-\bar{T}_f)} \qquad (3.23)$$

where $\bar{T}_f$ is a measure of the mean metal temperature, being determined by suitable positioning of several thermocouples throughout the fin cross-section.

For the square fin with a central basic tube an analytical solution can be established, for conduction heat transfer, in a similar fashion to that previously derived for the radial fin. The solution is very complex and does not warrant a theoretical analysis. However, the value of h_M obtained from equation (3.23) can be used to estimate the temperature distribution in the fin using a numerical technique. From the analysis a comparison of temperature profiles can be made on the assumption of a constant heat transfer coefficient over the whole fin surface.

3.5 Spine of Rectangular Section

An overall heat transfer coefficient can be determined using equation (3.9) rearranged

$$U = \frac{Q}{A_o(T_b-T_w)} \qquad (3.24)$$

Owing to the complexity of the surface no bed to metal heat transfer coefficient is derived.

3.6 Performance of Oval Tube

Figure 3.3 gives the geometry and nomenclature of the section. It is only necessary to consider the steady state conduction through the tube wall. Then, using the overall U and inside h_i heat transfer coefficients determined from equations (3.24) and (3.22) respectively an expression for the bed to metal heat transfer coefficient can be deduced. In equation (3.22) an equivalent tube diameter is required, namely

$$d_i = d_e = \frac{4A_xL}{A_i} \qquad (3.25)$$

Assuming the temperature at the inside and outside walls of the tube to remain constant then steady state conduction is in a radial direction only and is divided into two components. Therefore

$$Q = 2\pi kL(T_o-T_i)\left[\frac{4\alpha}{360\ln\left(\frac{R}{R-T}\right)} + \frac{4\beta}{360\ln\left(\frac{r}{r-T}\right)}\right]$$

$$Q = \frac{\pi k L}{45}(T_o - T_i)\left[\frac{\alpha}{\ln\left(\frac{R}{R-T}\right)} + \frac{\beta}{\ln\left(\frac{T}{T-T}\right)}\right] \qquad (3.26)$$

where

$$\alpha = \frac{180}{\pi}.\tan^{-1}\left[\frac{\frac{D}{2}-R}{T-\frac{W}{2}}\right] \qquad (3.27)$$

and

$$\beta = 90 - \alpha \qquad (3.28)$$

Hence combining equations (3.8),(3.9) and (3.26) and rearranging

$$h_o = \frac{1}{\frac{1}{U} - \frac{45 A_o}{\pi k L\left[\frac{\alpha}{\ln\left(\frac{R}{R-T}\right)} + \frac{\beta}{\ln\left(\frac{T}{T-T}\right)}\right]} - \frac{A_o}{h_i A_i}} \qquad (3.29)$$

3.7 General Performance

The experimental variables required to establish the general level of performance of both plain and oval tube and extended surface may be determined as follows. Determine the heat transfer rate by establishing the energy extracted by the cooling water from the system. From figure 3.4 which shows a simplified schematic diagram of the water circuit Q may be determined. Assuming heat transfer between the system and atmosphere is negligible compared with the heat transfer between the system and the fluidised bed a simple energy balance is possible. The effects of this assumption will be discussed later. Considering heat and work transfers across the system boundary, then under steady conditions

$$Q = \dot{m} C_p (T_{wo} - T_{wi}) - W \qquad (3.30)$$

Thus, since the pump work W, the feed water flow rate $\dot{m}$ and the feed water temperatures T_{wo} and T_{wi} can be found by experiment, the heat transfer rate between bed and extended surface, Q, can be determined.

By employing this type of circulatory water system the water flow rate within the boundary can be high thereby reducing the temperature difference across the extended surface to a low value. Also

$$Q = (\dot{m} + \dot{M}) C_p (T_{wo} - T_x) \qquad (3.31)$$

and

$$T_w = \frac{T_{wo} + T_x}{2} = T_{wo} - \left(\frac{T_{wo} - T_x}{2}\right) \qquad (3.32)$$

From equations (3.31) and (3.32)

$$T_w = T_{wo} - \frac{Q}{2c_p(\dot{m}+\dot{M})} \qquad (3.33)$$

Thus an overall heat transfer coefficient can be established from equation (3.24).

For plain tubes

$$Q = h_{op} A_o (T_b - T_o) \qquad (3.34)$$

Therefore, combining equations (3.7),(3.8), (3.9) and (3.34) and rearranging the heat transfer coefficient between bed and basic tube surface is given by

$$h_o = h_{op} = \frac{1}{\frac{1}{U} - \frac{A_o \ln\left(\frac{A_o}{A_i}\right)}{4\pi k L} - \frac{A_o}{h_i A_i}} \qquad (3.35)$$

3.8 Extended Surface Fin Effectiveness

In order to compare the performance of extended surface to that of plain tube under similar conditions, it is useful to define an "effectiveness factor". The total heat transferred between the bed and the extended surface may be expressed as

$$Q = h_{op}(A_1 + A_2) \cdot E_{FFECT} \cdot (T_b - T_o) \qquad (3.36)$$

where h_{op} is the heat transfer coefficient between bed and basic tube surface corresponding to the same superficial fluidizing velocity experienced by the extended surface. The total surface area subjected to the bed material is given by the primary plus secondary areas ($A_1 + A_2$).

E_{FFECT} is the "effectiveness factor" which accounts for the individual fin efficiency as well as the variation in bed to metal heat transfer coefficients between extended surface and the plain tube.

From equations (3.5) and (3.13)

$$Q = h_o(A_1 + E_F A_2)(T_b - T_o) \qquad (3.37)$$

Combining equations (3.36) and (3.37) and rearranging

$$E_{FFECT} = \frac{h_o(A_1 + E_F A_2)}{h_{op}(A_1 + A_2)} \qquad (3.38)$$

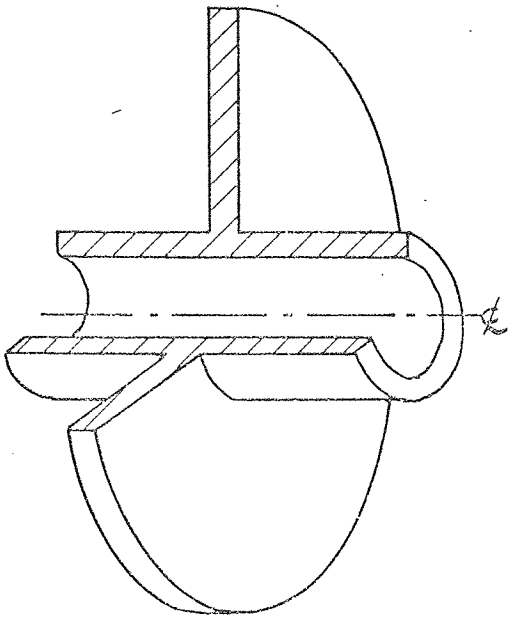

(A) Single Radial Fin

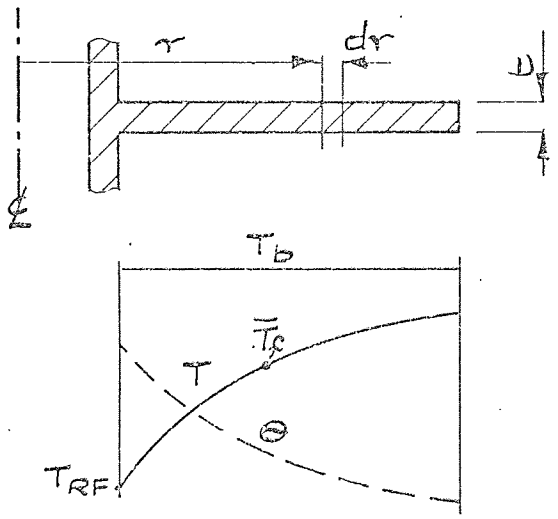

(B) Fin Element and Temperature Distribution

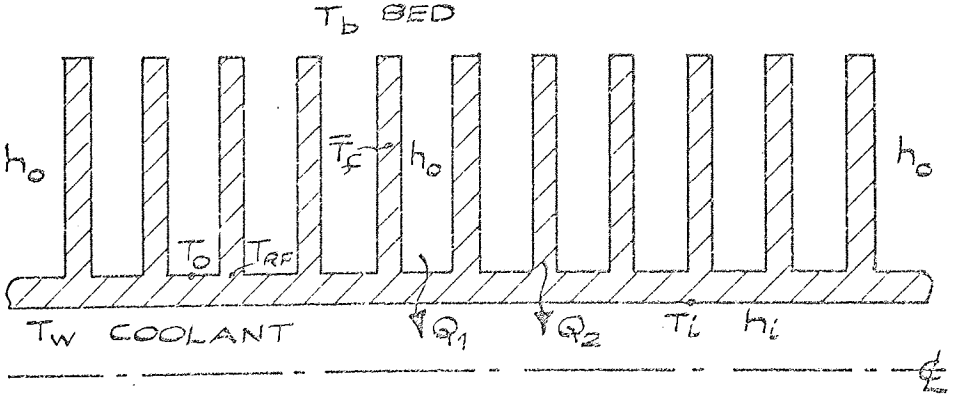

(C) Extended Surface

Figure 3.1 Radial Fin of Rectangular Section

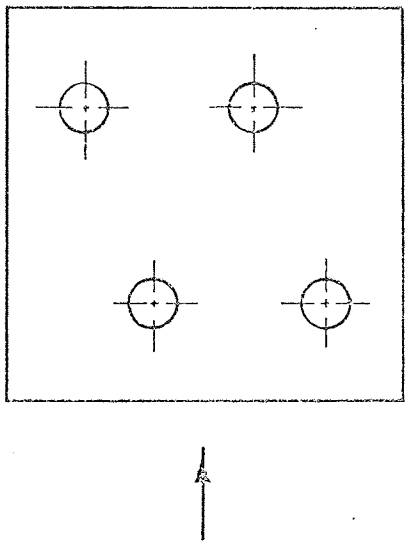

(A) Single Square Fin with Asymetric Basic Tubes

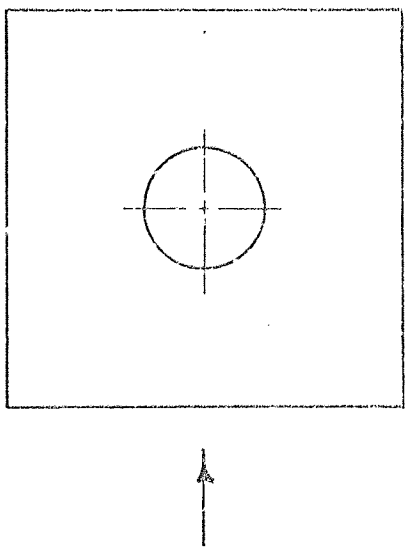

(B) Single Square Fin with Central Basic Tube

Figure 3.2 Square Fin of Rectangular Section

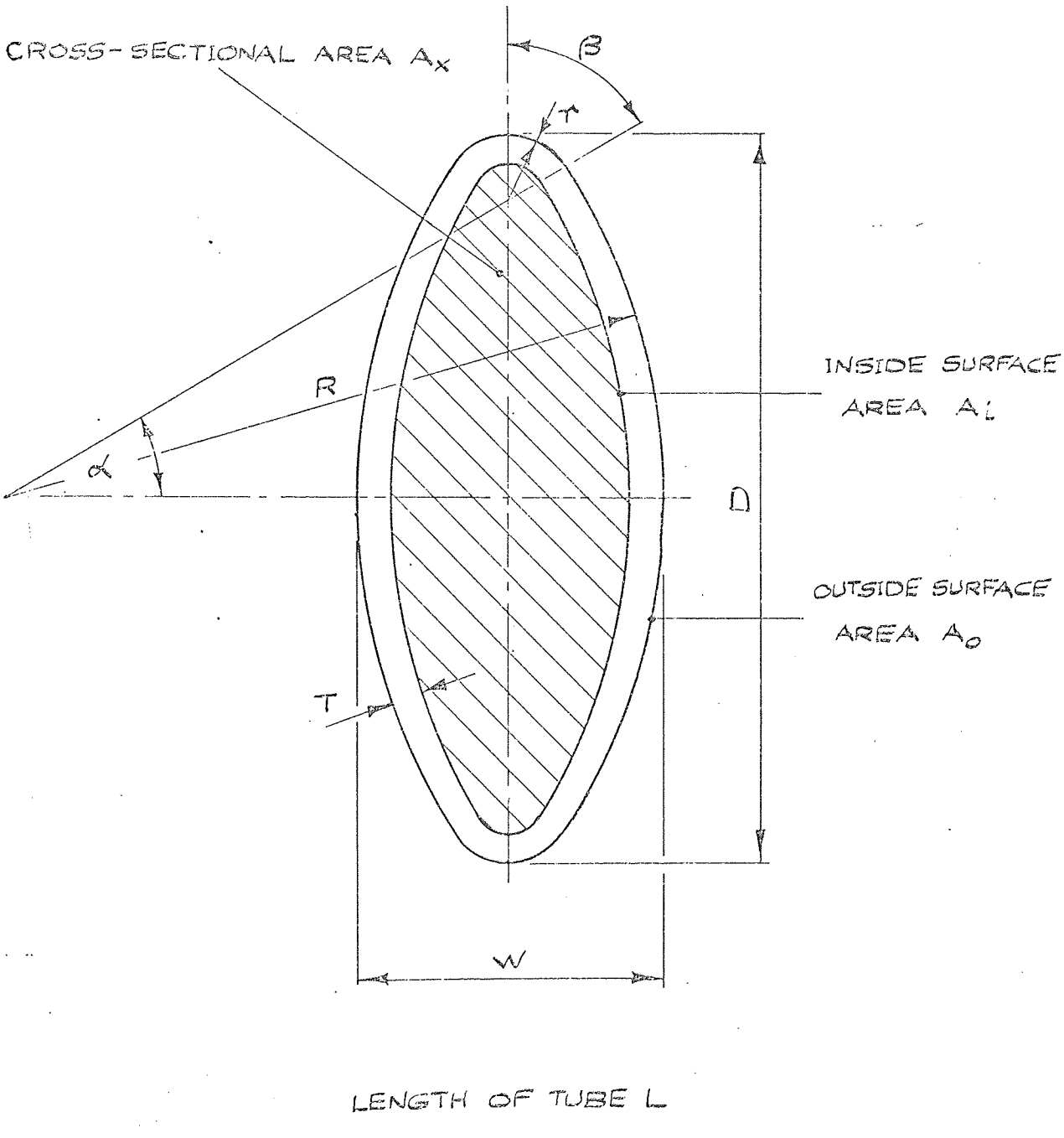

Figure 3.3 Oval Tube Geometry and Nomenclature

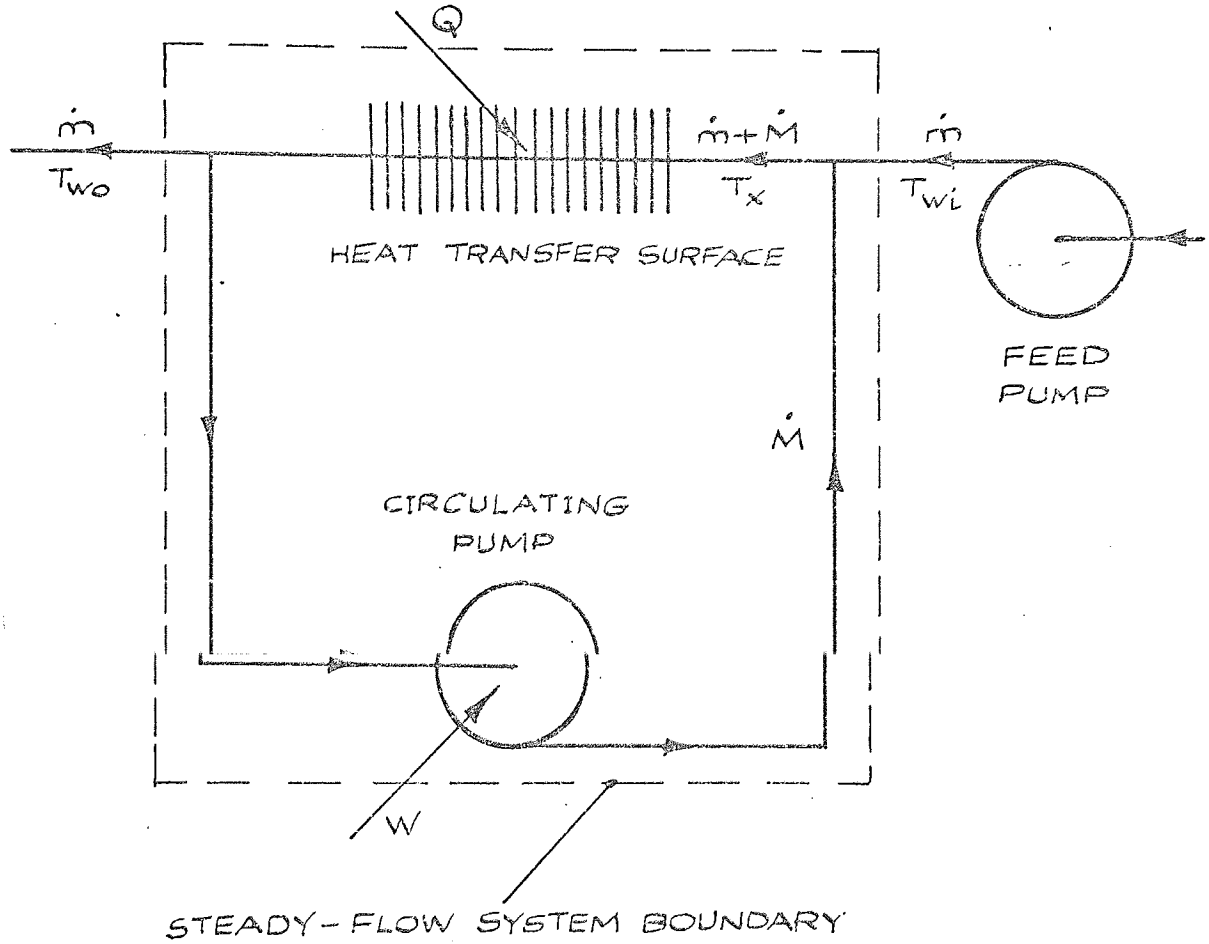

Figure 3.4 Schematic Diagram of Water System

CHAPTER IV

A THEORETICAL ANALYSIS OF EXTENDED SURFACE WITH RADIAL FINS OF RECTANGULAR SECTION

4.1 Introduction

Extended surface with radial fins of rectangular section are manufactured for use in a variety of natural and forced convection and/or radiation applications. Surfaces produced range from tubes with integral fins to tubes with mechanically attached fins, the fins being of the continuous helical type. Wright[33,34], 1967 and 1969, gives excellent reviews on the manufacture of this form of extended surface. Since this tubing is readily available at a reasonable cost, it would suggest that a theoretical appraisal should be considered, in order to establish the necessary geometric configuration of such surfaces for fluidized bed applications.

Previous theoretical investigations have been restricted to the analysis of a single radial fin. Equations relating the optimum dimensions to the heat transfer and thermal properties of the fin and the heat transfer coefficient between the surrounding fluid and the fin have been derived. Brown[35], 1965, computed results covering a wide range of conditions and presented them graphically in the form of dimensionless parameters. To do justice to such an analysis, one must consider the influence of individual fins which provide the complete extended surface. The optimisation for maximum heat transfer or minimum cost is related to fin spacing as well as the individual fin geometry.

The performance analysis of complete extended surface is not really warranted for conventional forced convection gas systems, since the heat transfer coefficients between surroundings and surface are of a low magnitude. This is one of the reasons why manufacturers' who produce the majority of this type of tubing for gas applications are not too concerned about such a detailed analysis. The practicalities are such that for liquid applications where the heat transfer coefficient is very high, the surface produced for gas systems is used even though it may be very inefficient.

In fluidized bed applications where the heat transfer coefficients are up to an order of magnitude greater than forced

convection gas applications, the optimisation of extended surface geometry is very important. Such an analysis is essential to the understanding of extended surface fluidized bed heat transfer. The theoretical work that follows is original.

The optimisation of heat transfer and heat transfer per volume of extended surface material are established for a variety of constant conditions. The heat transfer per volume of metal is essentially an extended surface cost factor, since for the majority of materials considered - copper, aluminium, aluminium-brass and stainless steel, the manufacturing cost is a small proportion of the raw material cost for large quantities of tubing. A third factor, the heat transfer per volume occupied by the extended surface is important to a designer when deciding the layout of the tubing in the bed volume. This is not covered in great detail in the analysis, but it is appreciated to be an important consideration. It was pointed out in Chapter I that if the bed plan area is large containment costs will be high. This would be the case if a large amount of tubing was required for a high energy transferrence, since reducing bed costs by providing tube bundle arrangements will affect the overall system pressure drops. Experimental work will establish values for the heat transfer coefficients using a variety of surface geometries.

The combination of theoretical and experimental studies will enable a complete performance assessment to be made for the typical surface required to fulfil a given heat transfer duty.

4.2 Nomenclature and Geometry ofSurface

The extended surface geometry and characteristic dimensions are shown in figure 4.1. A discontinuous radial fin surface is indicated - that is one with plain annular washers attached to a central basic tube. This simplification to a manufactured surface, where the fins are continuous along the entire length, is acceptable providing the helix angle is small. The basic equations necessary for the theoretical analysis are derived from figure 4.1 and from the expressions given in section 3.3 of Chapter III, and presented in Appendix A4.

4.3 Performance Curves

4.3.1 Maximum Heat Transfer

For a range of constant $k, h_o, h_i, d_o, d_i, (T_b - T_w)$ and V_2 values the heat transfer rate may be expressed as a function of fin thickness for a particular number of fins. The form of the equation can be deduced from the equations given in Appendix A4. Figure 4.2 shows this variation, for a family of N points. At particular values of t a maximum heat transfer is observed, the value progressively decreasing for increasing values of N. The problem is one of establishing the variation in the locus of maximum points for a variation in the constant values. The variables may be reduced by considering fixed h_i and $(T_b - T_w)$ values. If h_i is maintained at a high value then its influence on the curves is negligible. Also, $(T_b - T_w)$ only affects the magnitude of the heat transfer and may be regarded as a scale factor. Thus for a series of k values - a measure of the extended surface material, h_o values - established from experimental work, basic tube size d_i and d_o and metal volume V_2, the analysis can be completed. Under certain conditions it is possible that no maximum Q values occur. It will be appreciated that the problem is complex and requires a computer to effect a solution. Furthermore, with the use of a graph plotter the tedious work associated with the plotting of each curve is eliminated.

4.3.2 Maximum Heat Transfer per Metal Volume

In this case for a range of k, h_o, h_i, d_o, d_i, t and $(T_b - T_w)$ values the heat transfer per volume of metal may be expressed as a function of the number of fins for a particular fin height. Figure 4.3 shows this variation for a family of l curves. At particular values of N a maximum heat transfer per metal volume is observed, increasing for decreasing values of l. Again using a range of physical values it is possible to determine the locus of maximum points and show the effect of a change in the constant values.

4.4 Sample Results

Computer programmes developed to derive the performance curves of figures 4.2 and 4.3 are given in Appendix A4 together with a set of line-printer output using a series of typical values. A sample of graph plotter output is contained in a pocket inside the rear cover of the thesis. Results derived from a wide range of conditions are presented in Chapter VIII.

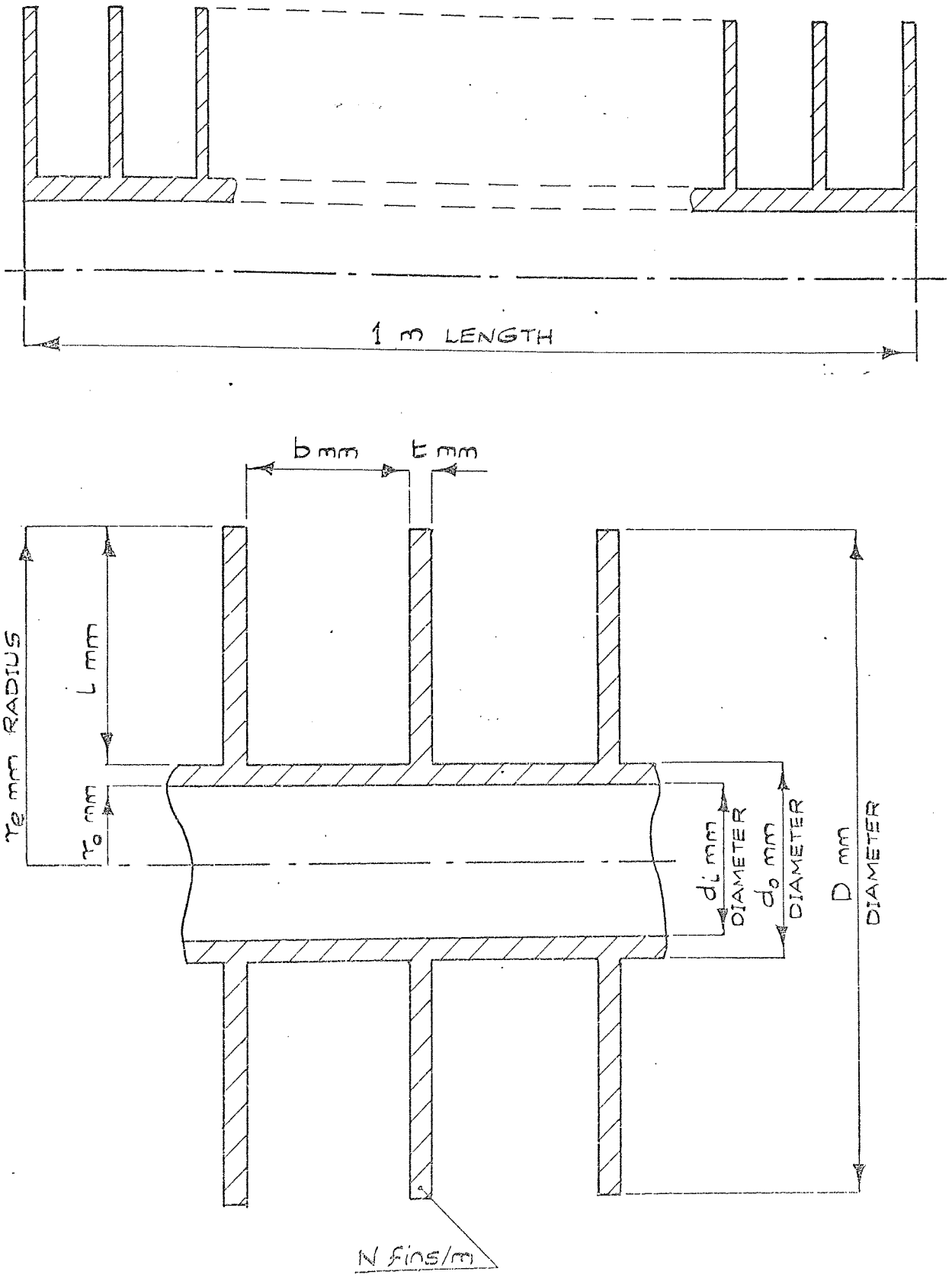

Figure 4.1 Nomenclature and Geometry of Surface

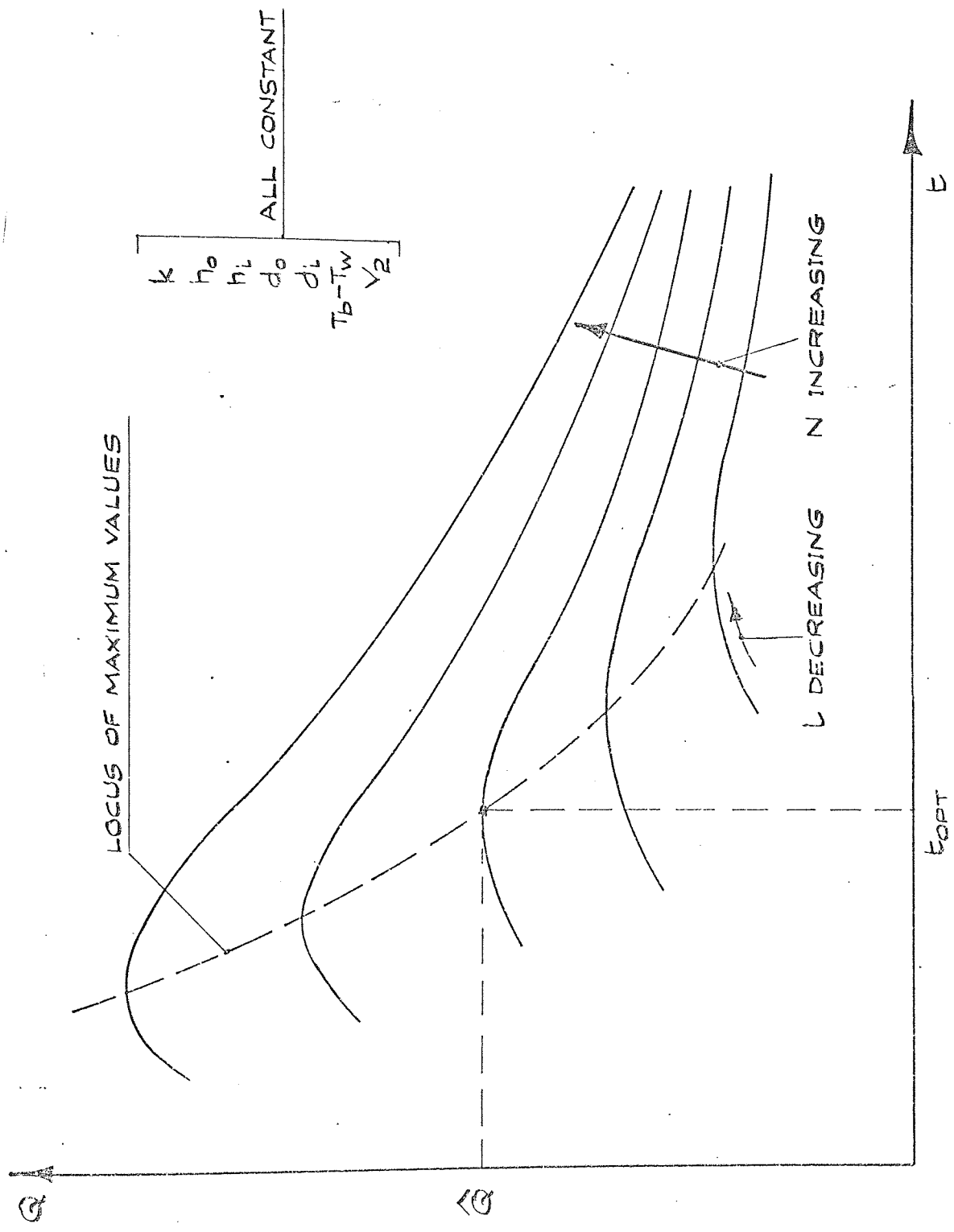

Figure 4.2 Maximum Heat Transfer

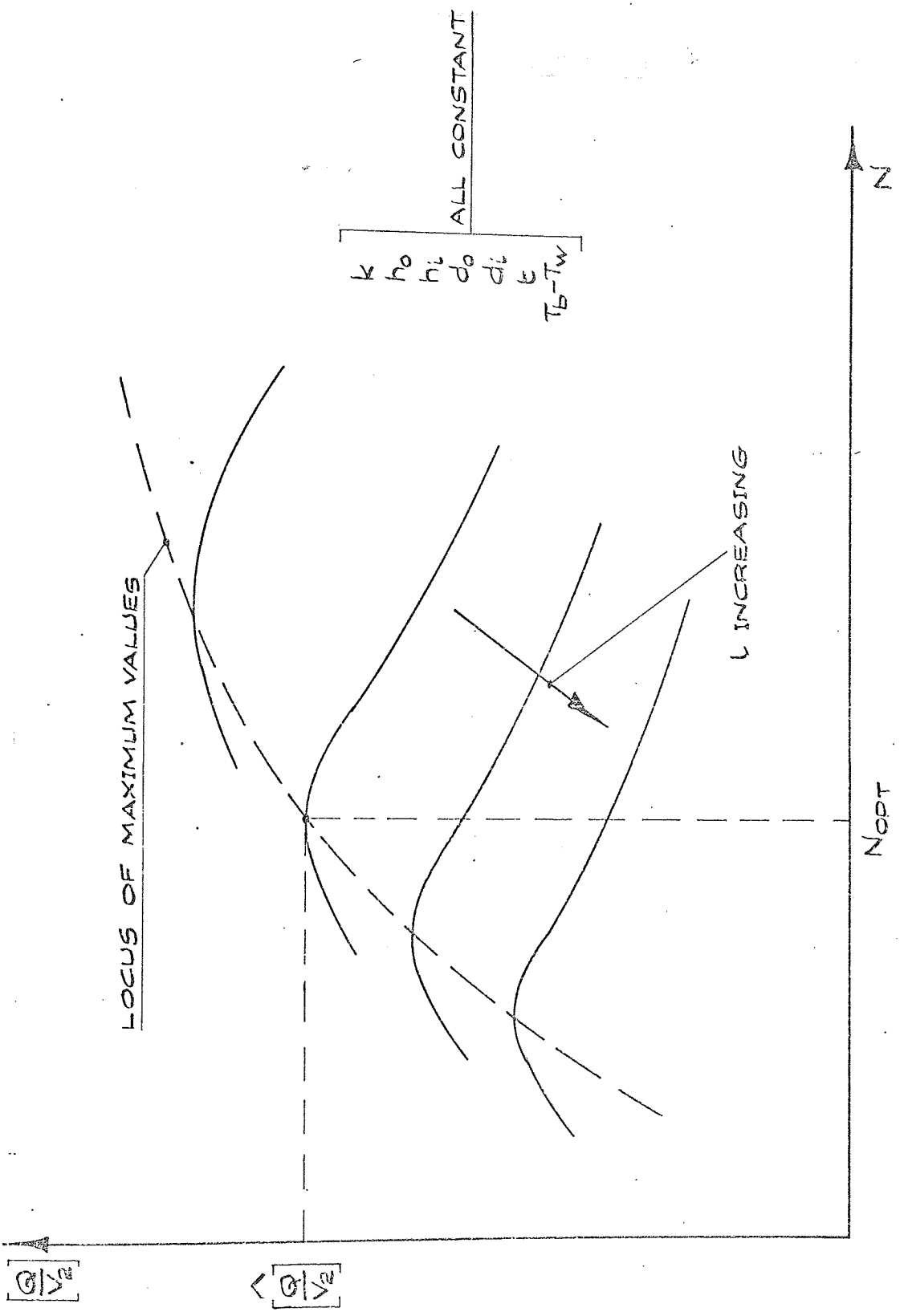

Figure 4.3 Maximum Heat Transfer per Metal Volume

CHAPTER V

THE EXPERIMENTAL EQUIPMENT

5.1 Introduction

The test equipment used for this investigation was initially designed as a general purpose installation, to enable work to be carried out covering all aspects of fluidized bed heat transfer. To provide for this flexibility the insulation was designed to withstand high temperatures as a result of proposed combustion within the bed. Two fans supplying the fluidizing air were connected in series thereby allowing tests to be conducted in deep beds where increased overall system pressure drops are prevalent. However, the research was limited to the use of heat transfer surface in shallow fluidized beds at low material temperatures and as a consequence the complete test facility was not utilized. The deep bed sections catered for in the initial design served as a "cowl" to prevent elutriation of the bed material into the research room. Later, smaller rectangular shaped beds were designed with thinner insulation, the lower material temperature level depending on the rate of extraction of energy from the bed by the water coolant passing through the basic tube. A general photograph of the experimental equipment is shown in figure 5.1.

In order to rationalize information pertaining to items of experimental equipment, a coded reference is introduced and presented in section 5.8 of the chapter.

5.2 The Heat Transfer Surface

Surfaces used for the experimental work ranged from plain and oval tube to extended surface produced with radial or square fins and spines of a rectangular section, attached to a basic tube. Both fin and basic tube materials were the same, namely copper, aluminium-brass or mild steel. To enable each tube to be classified the designation given in figure 5.2 was used. The complete range, indicating the individual sections, is summarised in figure 5.3.

The extended surfaces were either manufactured in the University or Polytechnic workshops or supplied by a number of industrial concerns. Among the firms were Yorkshire Imperial Metal Industries, The British Steel Corporation and Serck Heat

Transfer. Figures 5.4, 5.5 and 5.6 are photographs of all the heat transfer surface tested. In the case of the extended surfaces manufactured in the workshops, the individual fins were silver soldered to the basic tube and equi-spaced over a length of approximately 220 mm. The finned tubes were therefore of the discontinuous type as opposed to the surfaces supplied, which were of the continuous helical type.

In order to determine bed-to-metal heat transfer coefficients for certain heat exchanger elements it was necessary to obtain various metal temperatures. This was achieved by using stainless steel sheathed, chromel-alumel thermocouples[1E], 1.02 mm diameter and 1.5 m in length. The thermocouple hot junctions were inserted in holes drilled to different depths in a number of fin edges. Each hole size was such that the thermocouple sheath was a force fit in the fin material, thereby ensuring metal to metal contact. The relative positioning of these thermocouples in the fins of each extended surface are shown in the relevant section of Chapter VII.

5.3 Fluidized Bed Material

Three bed materials were used - namely; zircon sand, supplied by R. Hostombe Ltd.[2E], silica sand, supplied by Buckland Sand and Silica Co. Ltd.[3E], and steel shot, supplied by Bradley and Foster Ltd.[4E]. The majority of the tests were conducted using zircon sand as this was a small diameter, dense particle material which fluidized well and was ideally suited to such heat transfer applications. Each material was sieved using sieves calibrated to B.S.410 [39], the results being given in Appendix A5, which also includes relevant thermal and physical properties of the materials. The concept of a mean particle diameter is also discussed and determined from the sieve analyses.

5.4 Fluidized Bed Configuration and Construction

During the course of the experimental work three different configurations / bed size were used - namely:

(i) Circular - 534 mm diameter - designated Mk 1

(ii) Rectangular - 102 mm by 305 mm - designated Mk 2

(iii) Rectangular - 127 mm by 305 mm - designated Mk 3

The photographs in figure 5.7 show the Mk 1 and Mk 3 versions. It has already been mentioned in the introduction to this chapter, that the initial bed construction - Mk 1, was designed to withstand high temperatures. The considerable thickness of insulation provided, was a result of the intended use of the vessel for fluidized bed combustion studies. As a consequence a refractory lining[5E] and a lightweight thermal insulation[6E] were cast in situ, the refractory being designed to withstand 1000°C. A sectional elevation is shown in figure 5.8. Features worthy of note are the porous ceramic tile distributor plate and the cone shaped baffle plate in the plenum chamber, which together ensured an evenly dispersed fluid flow across the horizontal cross-section of the plan bed area. The distributor plate was formed from two 610 mm by 305 mm rectangular ceramic porous tiles manufactured by Doulton Industrial Products[7E]. The tiles were formed by a brick saw and cemented together using an industrial ceramic cement[8E].

In order to establish the effect of bed size and configuration on the experimental results, Mk 2 and Mk 3 beds were produced. By extending the hot gas inlet pipe shown in figure 5.8 in a vertical direction and providing a transition piece between the pipe and the bed plan section as shown in figure 5.9, the new beds could be supported across the lower section of the old bed. Triton Kaowool[9E] was used to thermally insulate the additional components. The final arrangement may be noted from figure 5.7. Furthermore, since bed temperatures were limited to less than 350°C for the subsequent tests, only a thin refractory lining[5E] was required, this being cast in situ as the Mk 1 bed version. For both rectangular beds the distributor plate was formed from one 305 mm by 305 mm square ceramic porous tile of the same grade as the tiles used for the Mk 1 bed.

Bed temperatures were recorded by using stainless steel sheathed, chromel-alumel thermocouples[1E], 3.18 mm diameter and 1.0 m in length inserted into holes drilled through the bed casing and insulation lining. For each bed three thermocouples were used and positioned as indicated in figure 5.10.

Provision was made for positioning the heat transfer surface up to approximately 100 mm above the distributor for both Mk 2 and

Mk 3 versions. This was achieved by machining the end sealing plates in a tenon arrangement of "Sindanyo" insulation material. The end cover plates and gaskets were slotted to allow for this movement. Positioning of the surfaces in the Mk 1 bed was achieved by clamping the vertical coolant supply tubes and/or support rod by small grub screws located in the top support plate. Figure 5.11 shows photographs of an extended surface in the Mk 1 bed and a plain tube in the Mk 3 bed.

5.5 Gas and Air Flow Systems

Figure 5.12 shows the arrangement of the gas and air systems which permitted close control of the relative flow rate of air and propane gas necessary for regulating the combustion temperature. A centrifugal fan[10E] provided the air supply to the system, the flow rate and therefore superficial fluidizing velocity being controlled by a gate valve "A". The gas was supplied from a propane liquid petroleum gas cylinder and controlled by the operation of two needle valves[11E] "B" and "C". Non-return valve[11E] "D" was installed for safety. The mixture of air and gas was ignited by a diesel engine glow plug, the power being supplied by two 1.5 V knife cells, situated downstream of a propane burner[12E]. A view port fixed adjacent to the glow plug enabled the burner flame to be observed.

The products of combustion on leaving the bed were extracted through a canopy by means of a bifurcated fan[13E] to the atmosphere outside the building. A general view of the rig and extraction system is shown in figure 5.13.

5.6 Water Flow System

The arrangement of the water flow system was designed to allow either a circulatory or a once through flow of cooling water to the heat exchanger element and is illustrated in figure 5.14.

Water from the mains is fed to a header tank by means of a standard ball float control valve and this tank forms the supply for a centrifugal feed pump[14E] as shown. The feed pump supplies cold water straight through the heat exchanger to drain via control valve "A". By utilizing a circulating pump[15E] this flow rate may be supplemented. Use of the circulation system enables the flow rate of water through the heat exchanger to be maintained at a high level,

thereby minimising the temperature difference across the heat exchanger in the fluidized bed. The feed water flow rate may then be adjusted to provide a reasonable overall temperature difference ($T_{wo} - T_{wi}$) and reduce experimental error. An added advantage of a high inside heat transfer coefficient is also achieved, by maintaining a high water flow rate through the basic tube of the surface. Valve "G" controls a sample of feed water for inlet water temperature measurement. At very high water flow rates there was a danger of cavitation occurring in the circulating pump impeller. The fitting of a 50 mm diameter by 400 mm long copper pipe before the eye of the pump allowed the flow velocity to be reduced. This formed the basis of an air/vapour trap, the top outlet being returned to the header tank by plastic tubing.

5.7 Experimental Instrumentation

5.7.1 Temperature Measurements

Thermocouples used for measurement of extended surface and fluidized bed temperatures were connected via chromel-alumel compensating leads to a Leeds and Northrup, twenty-four point Speedomax recorder[16E]. The recorder provided a continuous record of the thermocouple outputs on a moving chart having a calibrated temperature scale. A range card and variable chart speed facility complemented the instrumentation.

To avoid overheating of the inlet baffle plate of the Mk 1 bed and the extension pipe and transition pieces of the Mk 2 and Mk 3 beds, an approximate indication of the preheated air temperature was obtained by means of a 3.18 mm diameter, stainless steel sheathed thermocouple[1E]. The output from this thermocouple, positioned after the last inlet pipe elbow, was monitored by means of a digital voltmeter[17E].

The air flow temperature downstream of the fan was sensed by a five-point sampling grid arranged across the pipe diameter, each thermocouple hot junction being positioned at an equivalent area point. The 40 S.W.G. chromel-alumel wires were connected to a battery powered temperature indicator[18E].

Water temperatures at inlet and outlet to the apparatus were measured by laboratory calibrated mercury-in-glass thermometers. The inlet thermometer was supported in a "tee" section of the pipework by a rubber bung and wire and the outlet thermometer was freely supported by a retort stand at the drain position.

5.7.2 Flow and Pressure Measurements

The air flow rate was measured by an orifice plate constructed in brass according to B.S. 1042[40]. The upstream pressure was given by a mercury manometer [19E] and the orifice pressure difference recorded on a differential sloping water manometer[20E]. A laboratory scaled rotameter[21E] indicated the gas flow rate, the instrument calibration pressure of 1 bar gauge being recorded by means of a mercury manometer[19E].

To enable the correct air/gas mixture to be set prior to ignition, the mixture pressure was sensed before entry to the fluidized bed by means of a second sloping water manometer on the orifice pressure difference instrument[20E].

Water feed pump flow rates were recorded by laboratory scaled rotameters[21E] at inlet to the system. The circulating pump flow rate was determined from an orifice plate constructed in brass according to B.S.1042[40], and positioned downstream of the pump. The pressure difference was measured by a specially manufactured inverted U-tube vertical manometer.

The complete range of instrumentation used during the experimental work is shown by the photographs of figures 5.15 and 5.16. Instrument calibration factors are included in the equations given in Appendix A3.

5.8 Experimental Equipment References

1E. British Insulated Callender Cables mineral insulated stainless steel sheathed thermocouples, cable references 0.125SS1/25K and 0.040SS1/7K, Prescot, Lancashire.

2E. C.R.Z. grade zircon sand, R.Hostombe Ltd.,Regent Street, Sheffield, Lancashire.

3E. 50FG grade silica sand, Buckland Sand and Silica Co. Ltd., Reigate, Surrey.

4E. S70 grade steel shot, Bradley and Foster Ltd., Darlaston, Staffordshire.

5E. KS-4 grade castable refactory lining, A.P.Green Refactories Ltd., Slough, Buckinghamshire.

6E. Plicasto Airlite grade lightweight thermal insulation, Plibrico Co. Ltd., London.

7E. Pyrolith Aerox Filter Media G.14 tiles, Doulton Industrial Products, Stone, Staffordshire.

8E. Autostic ceramic and industrial cement, Carlton Brown and Partners, Elford, Staffordshire.

9E. Triton Kaowool 64 kg/m^3 blanket density, Morgan Ceramic Fibres Ltd., Wirral, Cheshire.

10E. Centrifugal fan 1100 mm water gauge at 7.07 m^3/min produced by Alldays and Peacocks Co.Ltd., Birmingham. Driven by 5.6 kW, 3 phase 440 V Crompton Parkinson Motor.

11E. Simplifix Couplings Ltd., Maidenhead, Berkshire, needle valves type D71/162/162, non-return valve D61/16/16.

12E. Bullfinch (Gas Equipment) Ltd., Burners List number 1270 for large Mk 1 bed, List number 1260 for small Mk 2 and Mk 3 beds, Birmingham.

13E. Keith Blackman HT Bifurcated fan code number 12BX43, London.

14E. James Bereford and Sons Ltd., PV-100 plastic centrifugal pump, driven by 3 phase 440 V, 0.56 kW motor, Birmingham.

15E. Worthington Simpson PAA3845C plastic centrifugal pump, driven by 240 V, 50 Hz, 0.46 kW motor, Birmingham.

16E. Speedomax W, 240 V, 50 Hz, multipoint recorder, serial number WM-71-01923-1-1. Twenty four points, each response time 1.2 s, for chromel-alumel thermocouples. Range cards 0-250°C and 0-500°C, with a variable chart speed. Leeds and Northrup Ltd., Birmingham.

17E. Digital Voltmeter LM1604/05, 240 V 50 Hz, serial number 200043. Range used 100 mV - sensitivity 10 uV. The Solartron Electronic Group Ltd., Farnborough, Hampshire.

18E. Spembly Multitemp Type 6610 CA thermocouple temperature indicator - twelve points powered by four Mallory RM - 12R batteries, each with a $1^{\circ}C$ resolution. Sittingbourne, Kent.

19E. Airflow Developments Slim Jim Type industrial manometers 0 - 380 mm Hg air pressure, 0 - 760 mm Hg gas pressure range, High Wycombe, Buckinghamshire.

20E. Airflow Developments Mk 4 Bench Mounted Test Set, instrument number M12882. Variable range 0 - 500 mm H_2O long tube and 0 - 250 mm H_2O short tube. High Wycombe, Buckinghamshire.

21E. Rotameters, laboratory type 100 for gas flow, serial number R841209/H, water flow serial numbers R841210/N and R841211/N. GEC - Elliott Process Instruments Ltd., Croydon, Surrey.

Missing page(s) from the bound copy

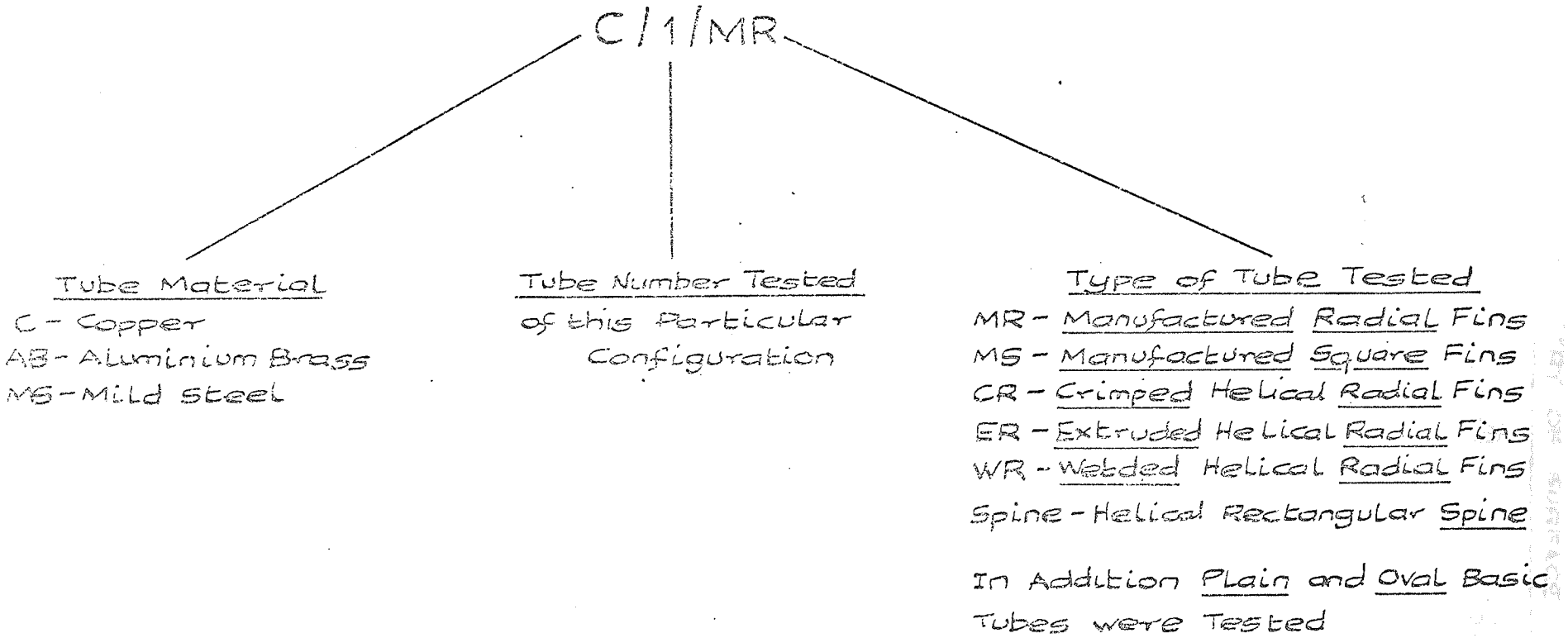

Figure 5.2 Heat Transfer Surface Designation

DESIGNATION	GEOMETRY OF SURFACE
C/1/MS	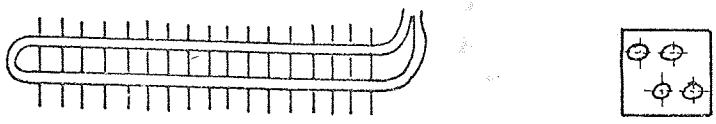
C/2/MS	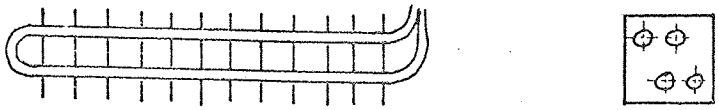
C/3/MS	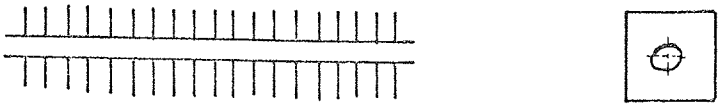
C/1/MR C/2/MR C/3/MR C/4/MR	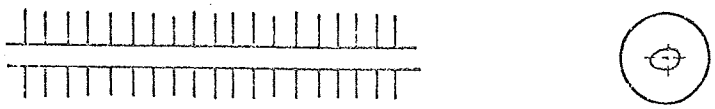 Manufactured in University and Polytechnic workshops, material being supplied by Yorkshire Imperial Metal Industries
C/1/ER C/2/ER C/3/ER C/4/ER C/5/ER C/6/ER C/7/ER	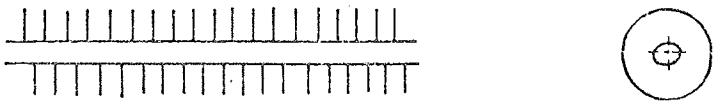 Supplied by Yorkshire Imperial Metal
MS/1/ER MS/2/ER MS/1/WR MS/2/WR	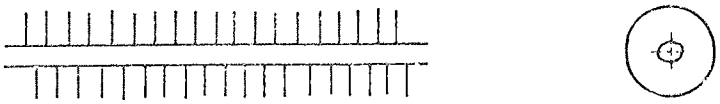 Supplied by British Steel Corporation
C/1/CR C/2/CR C/3/CR C/4/CR C/5/CR	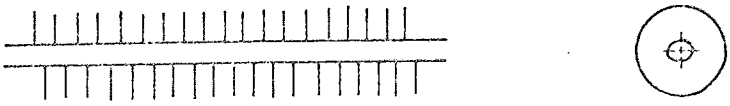 Supplied by Serck Heat Transfer
MS/1/Spine	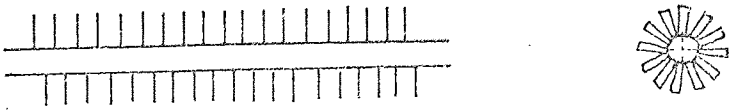 Supplied by British Steel Corporation

In addition to the extended surfaces, one oval tube and four plain tubes were tested.

Figure 5.3 Experimental Heat Transfer Surfaces

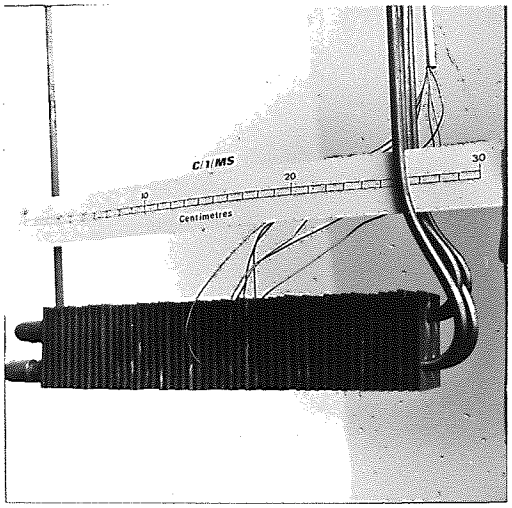

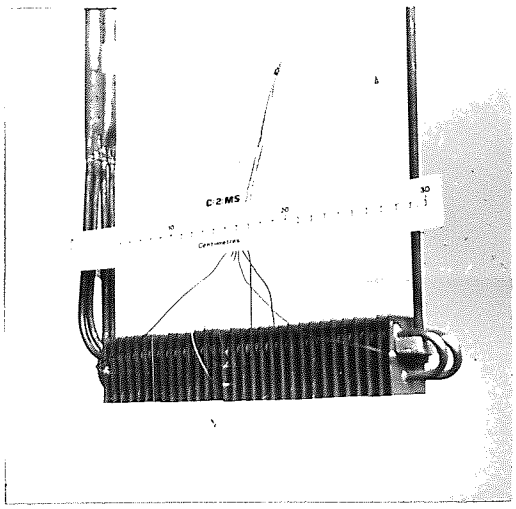

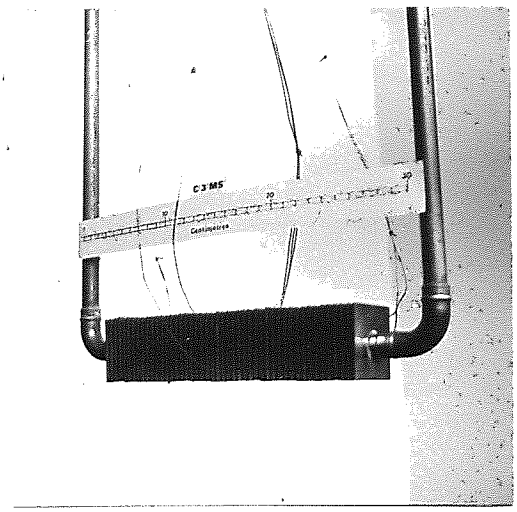

Figure 5.4 Manufactured Square Finned Surfaces

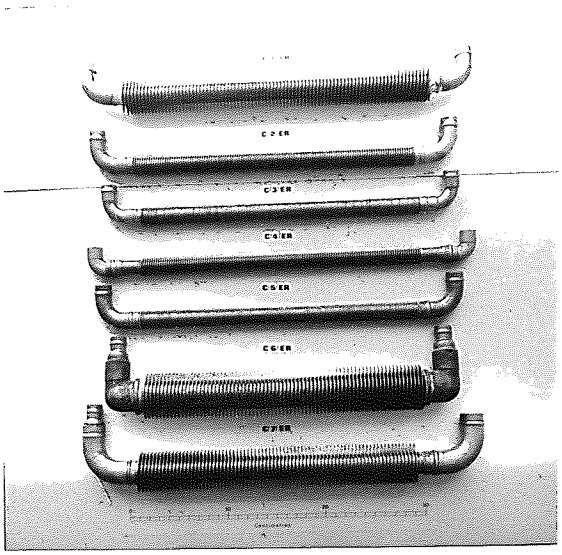

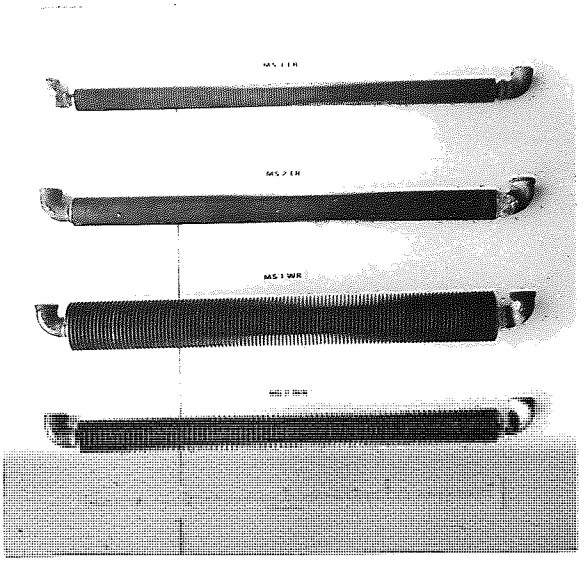

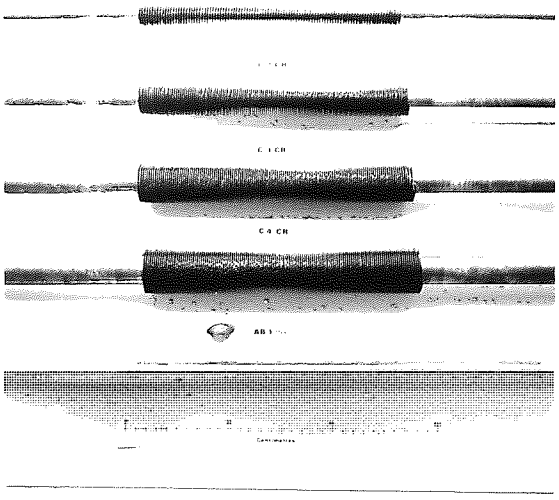

Figure 5.5 Commercially Produced Extended Surface

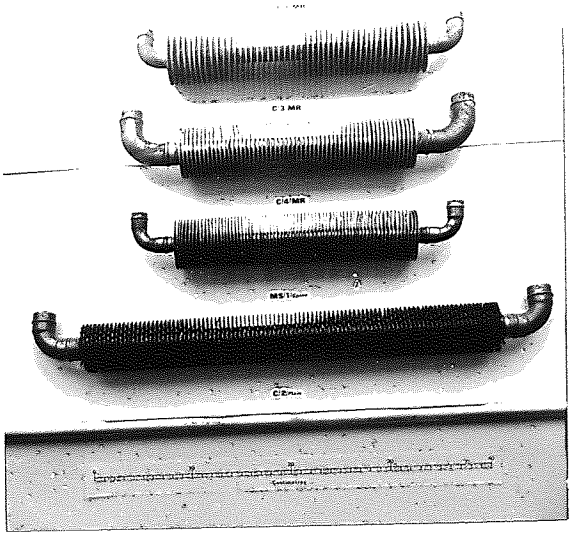

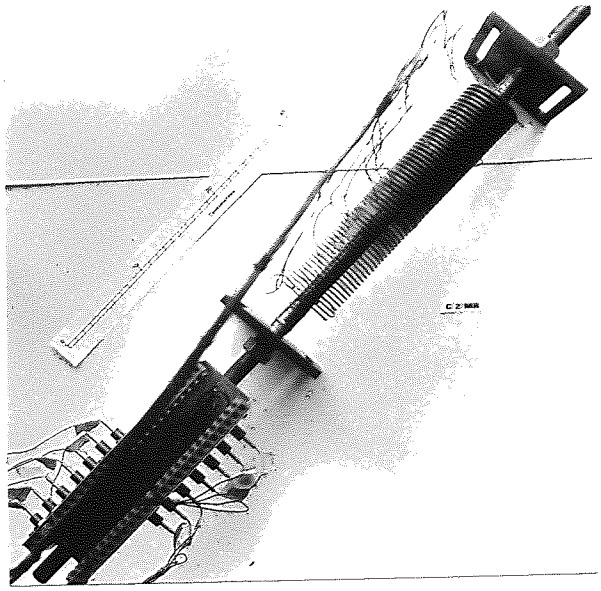

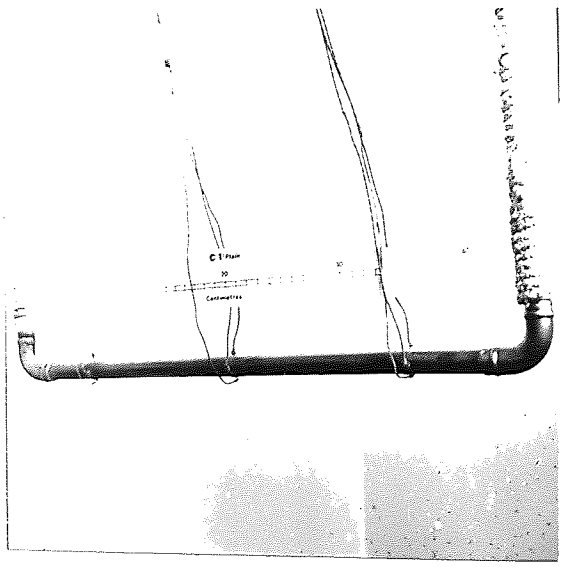

Figure 5.6 Manufactured Radial Fin, Spine and Plain Tube Surfaces

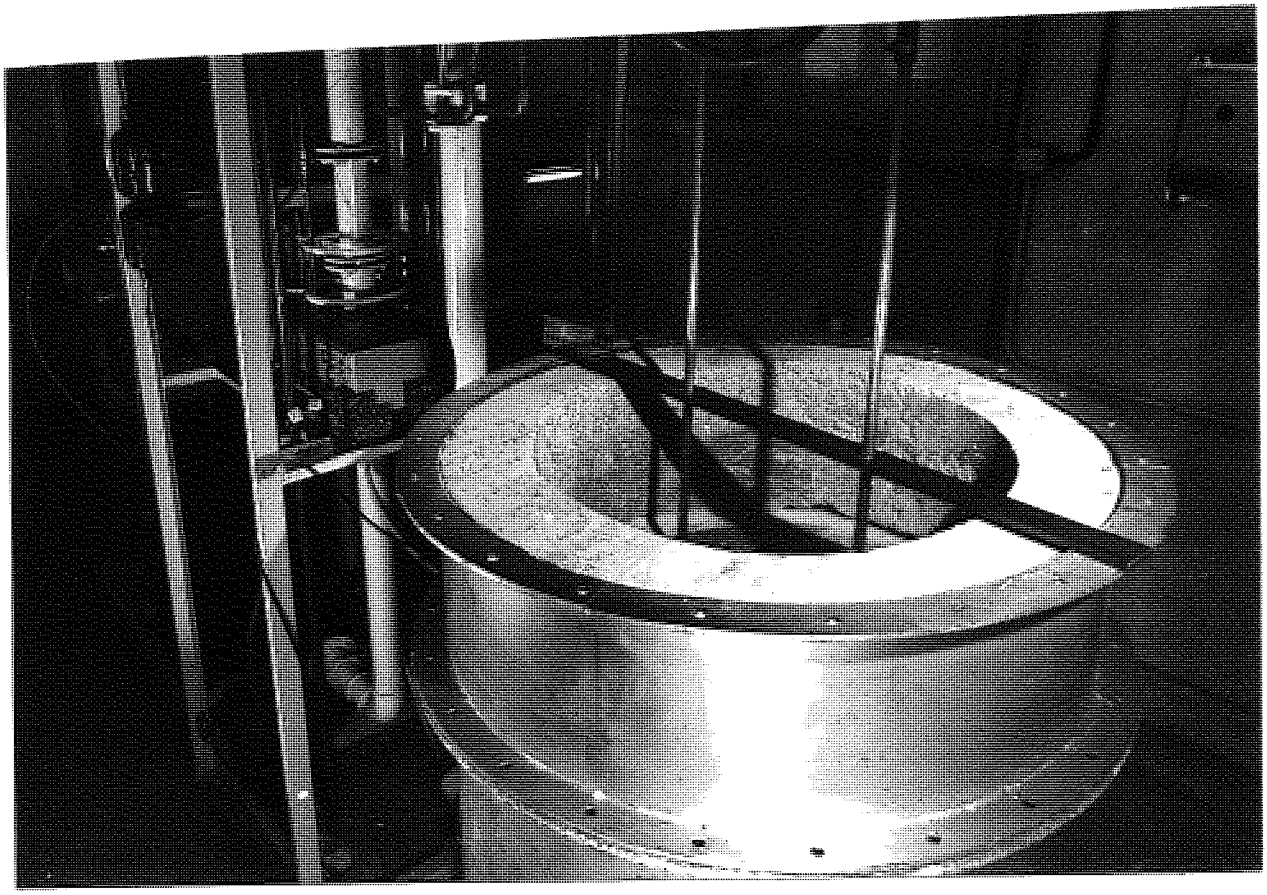

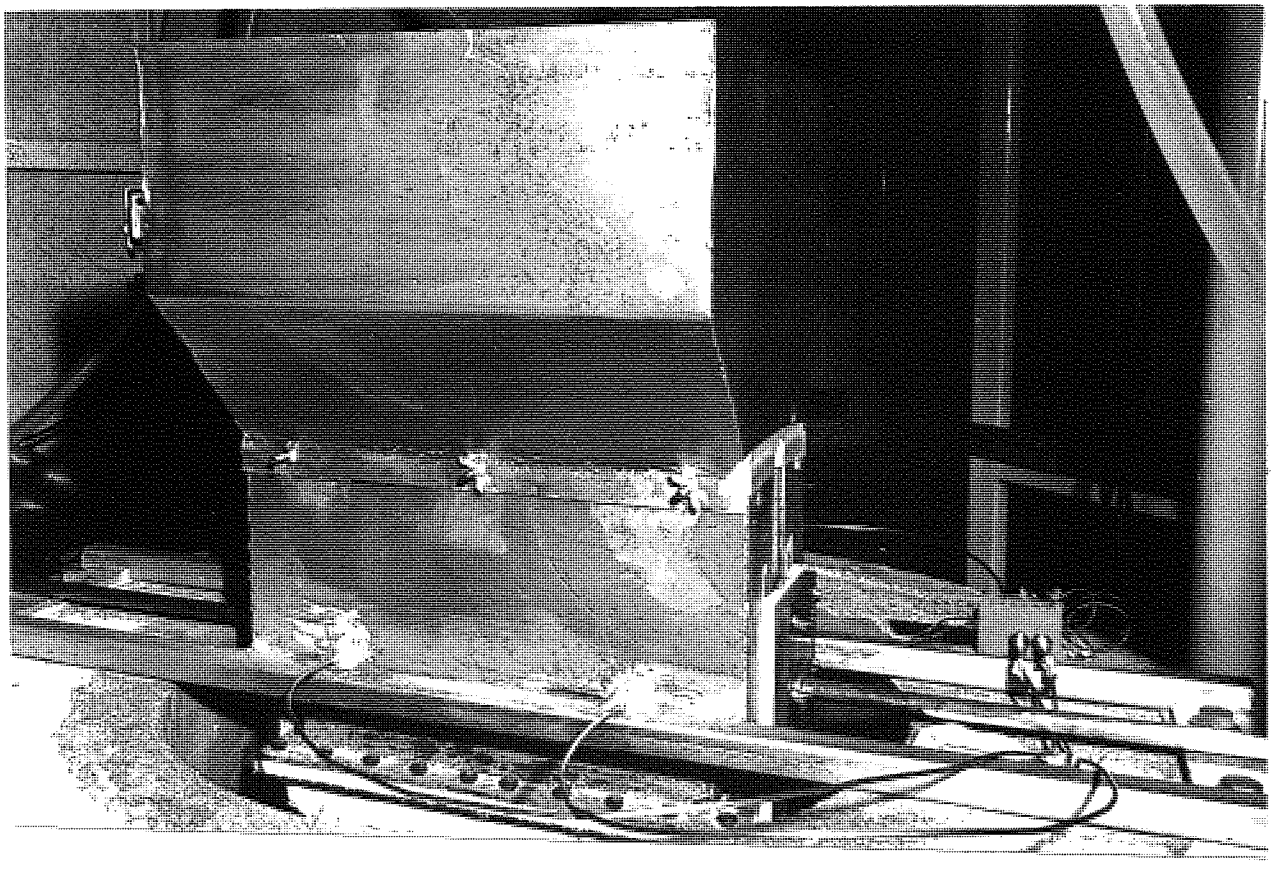

Figure 5.7 Mk 1 and Mk 2 Fluidized Beds

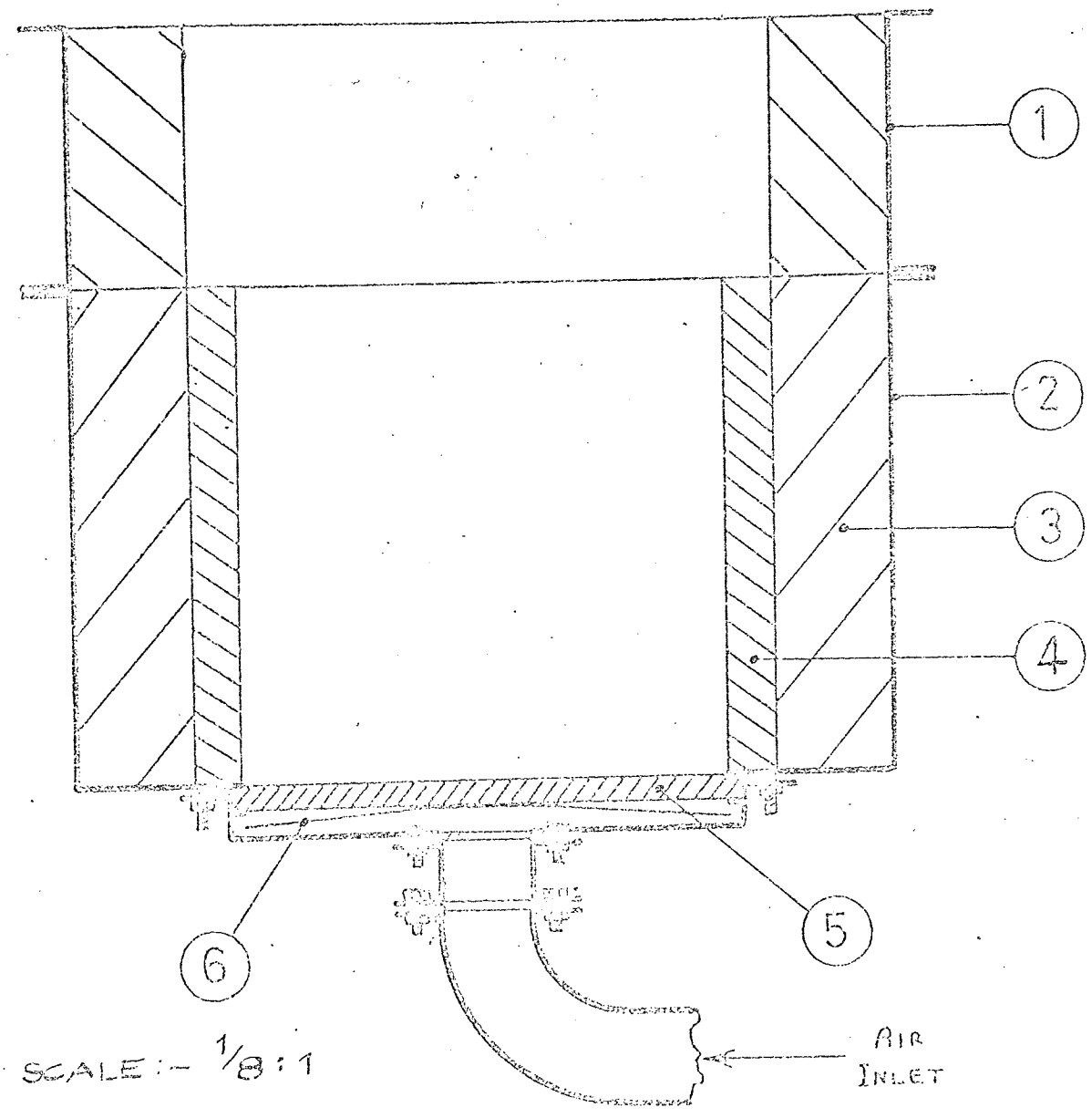

1. Removable Extension
2. Fabricated Steel Shell
3. Lightweight Thermal Insulation
4. Cast Refractory Lining
5. Porous Ceramic Tile Distributor Plate
6. Steel Baffle Plate

Figure 5.8 Sectional Elevation of Mk 1 Bed

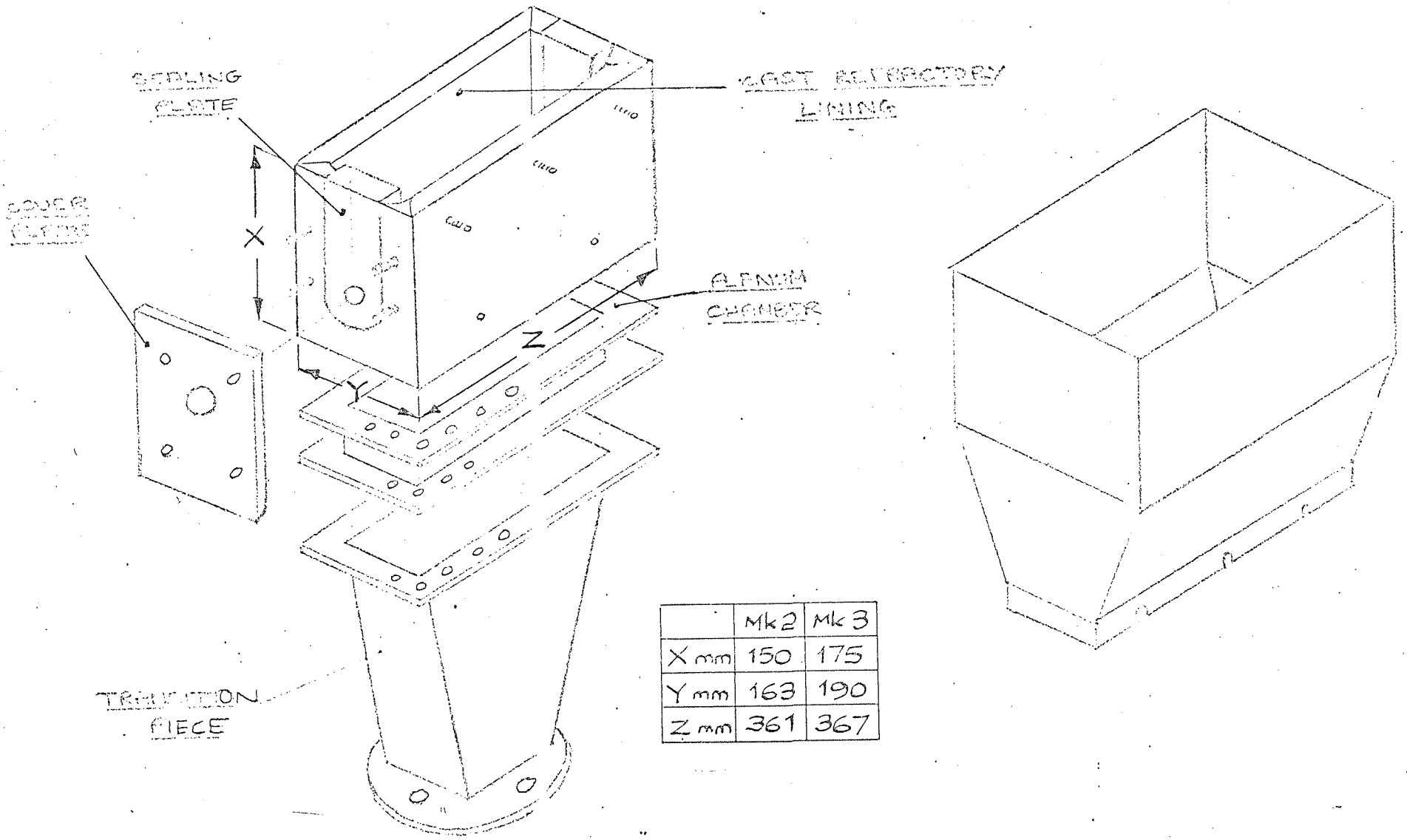

	Mk 2	Mk 3
X mm	150	175
Y mm	163	190
Z mm	361	367

Figure 5.9 Exploded View of Mk 2 and Mk 3 Fluidized Beds

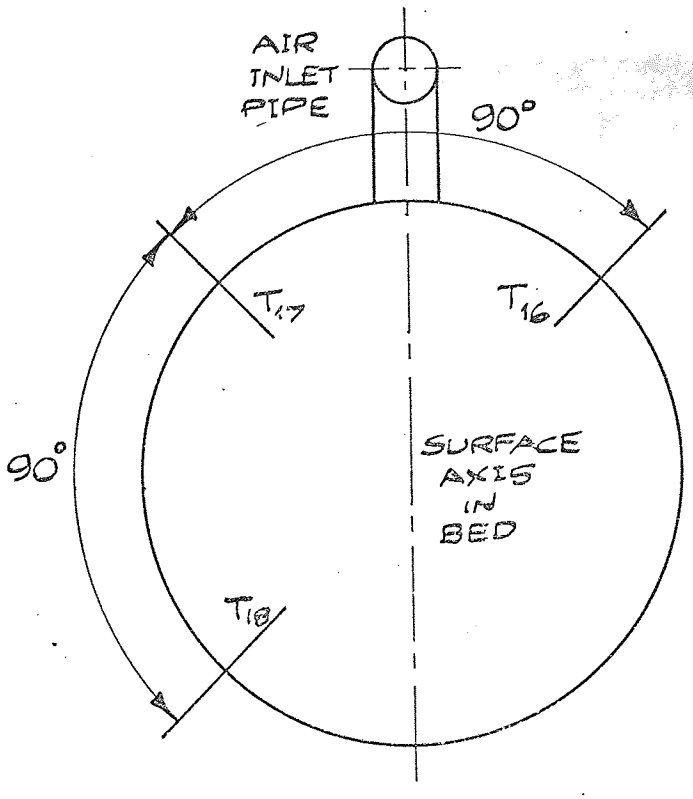

Circular Bed - Mk 1 - 534 mm diameter

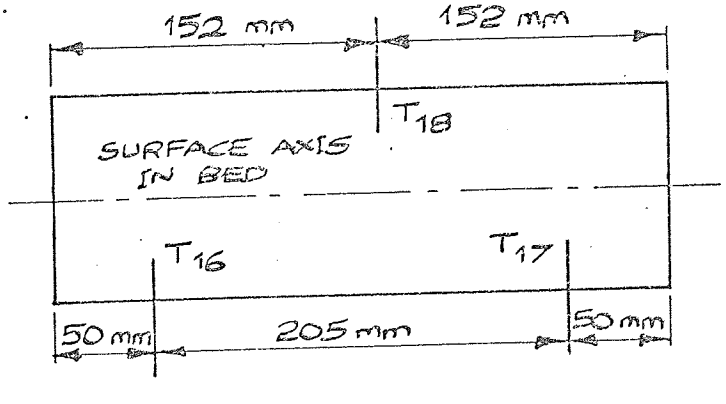

Rectangular Bed - Mk 2 - 102 mm x 305 mm

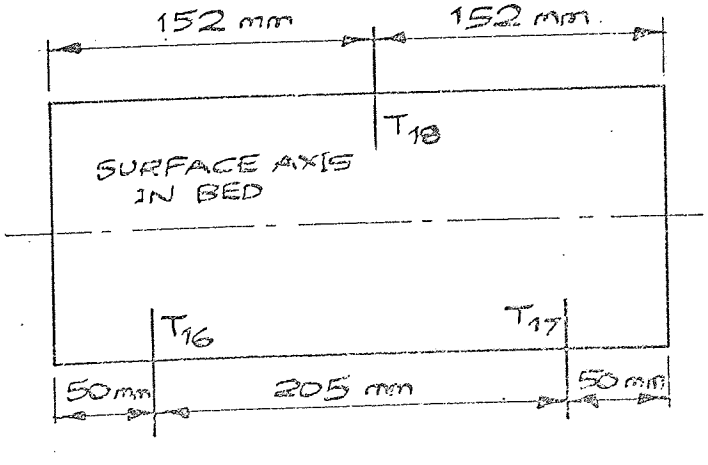

Rectangular Bed - Mk 3 - 127 mm x 305 mm

Figure 5.10 Bed Thermocouple Positions - Plan Views

Figure 5.11 Surface Location in Mk 1 and Mk 3 Bed

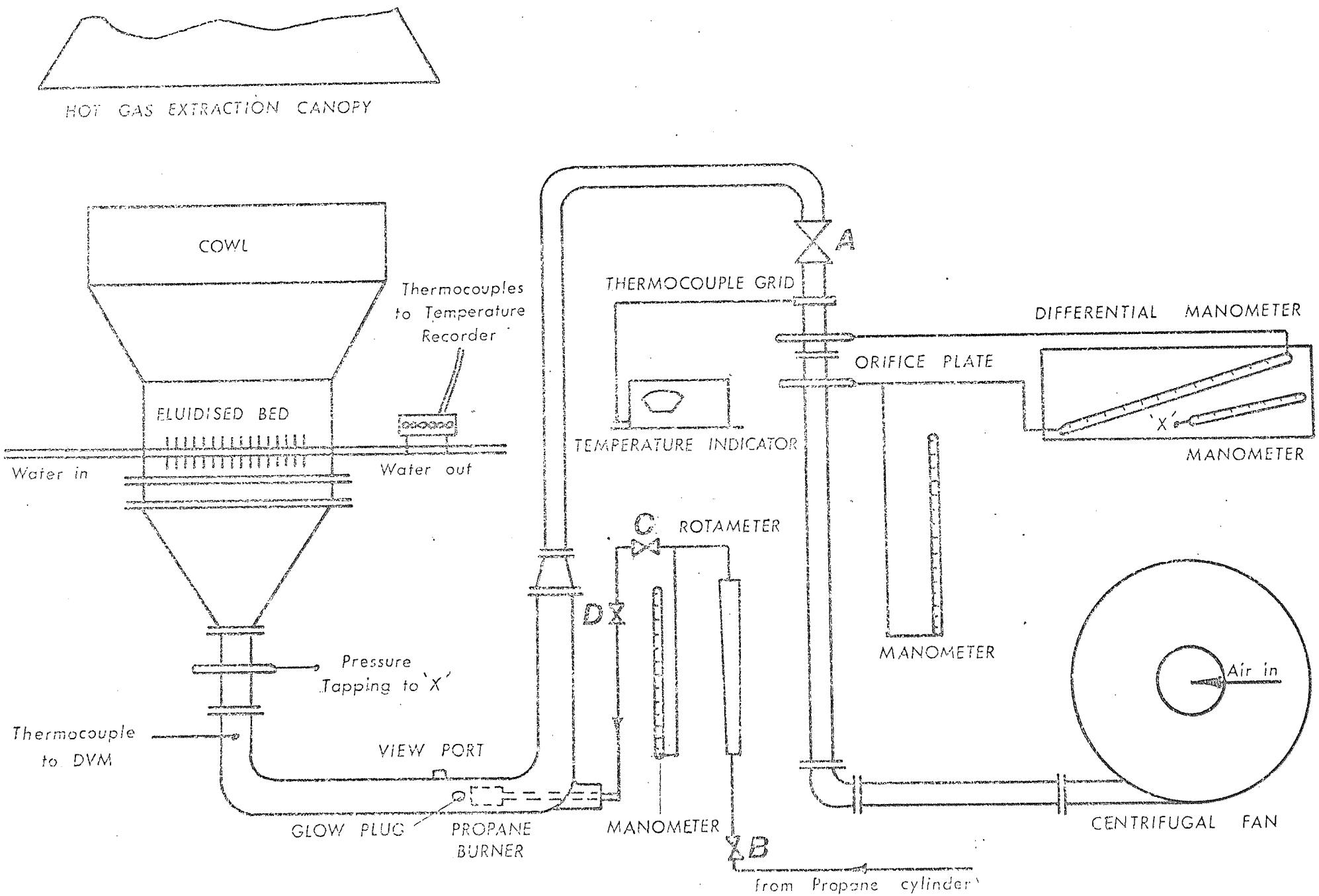

Figure 5.12 Schematic Arrangement of Experimental Equipment

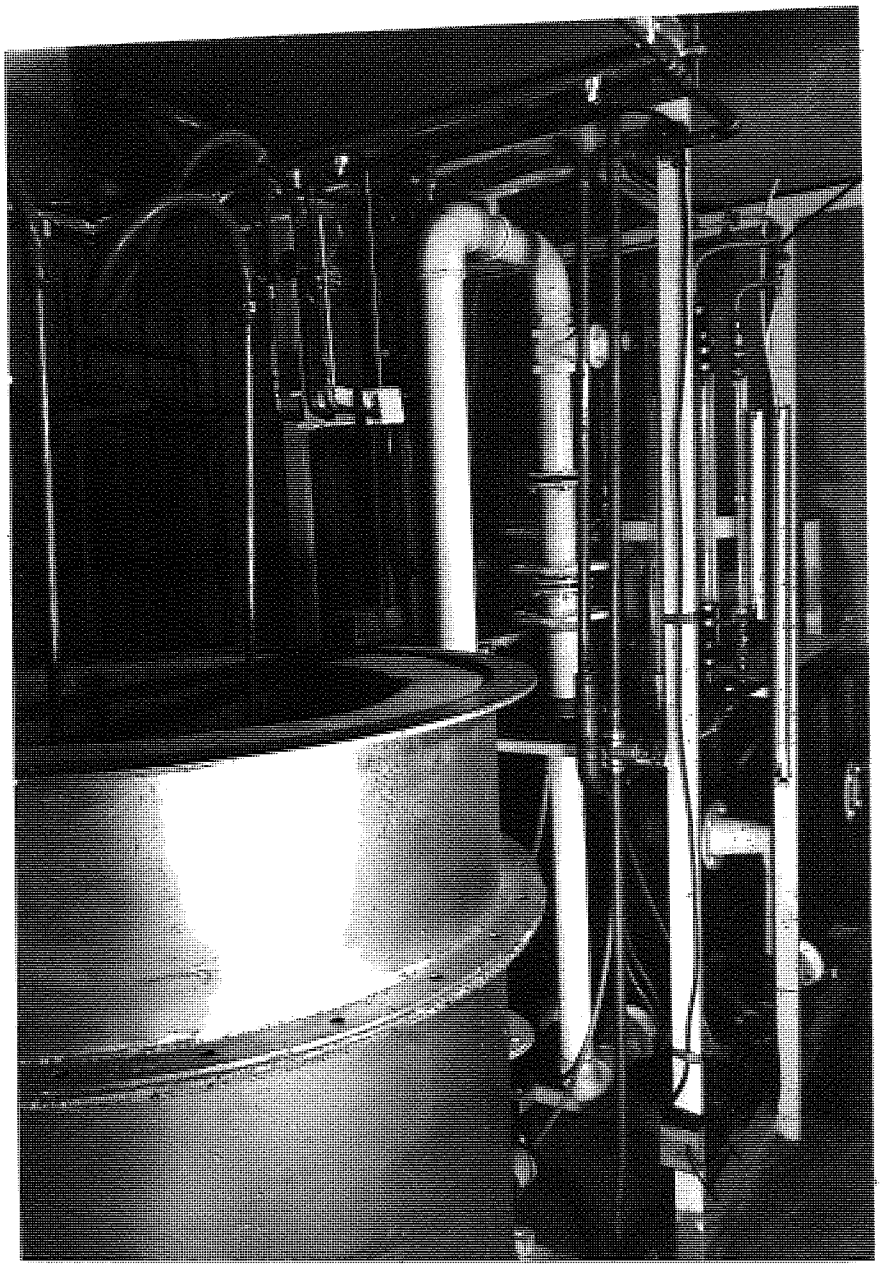

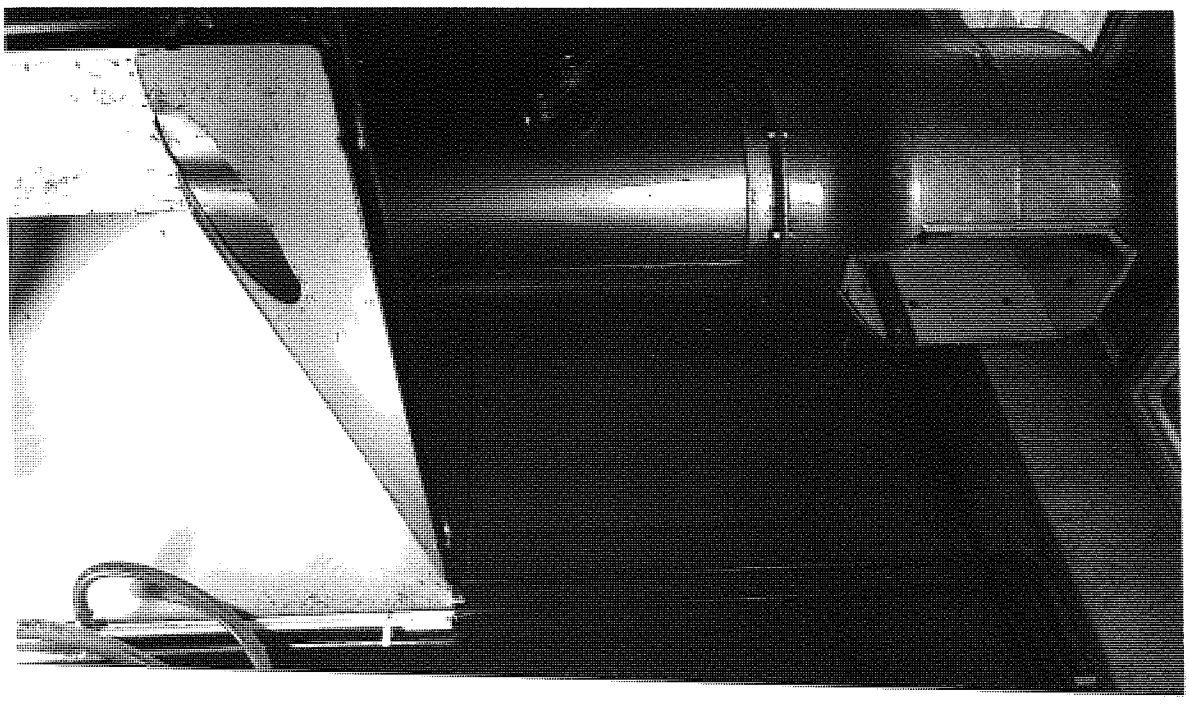

Figure 5.13 Equipment, Extraction Canopy and Fan

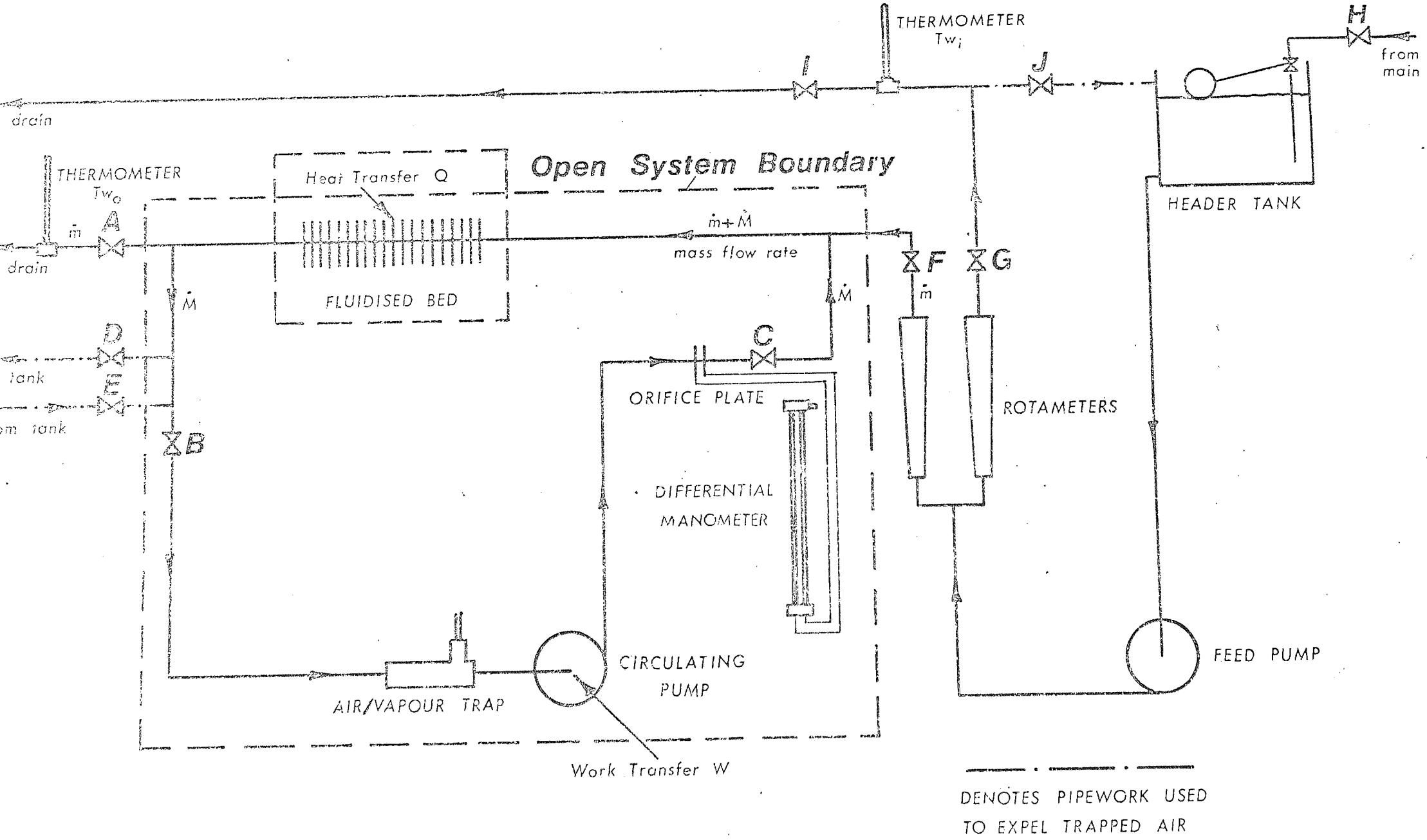

Figure 5.14 Schematic Diagram of Water Circuit

Figure 5.15 Experimental Instrumentation

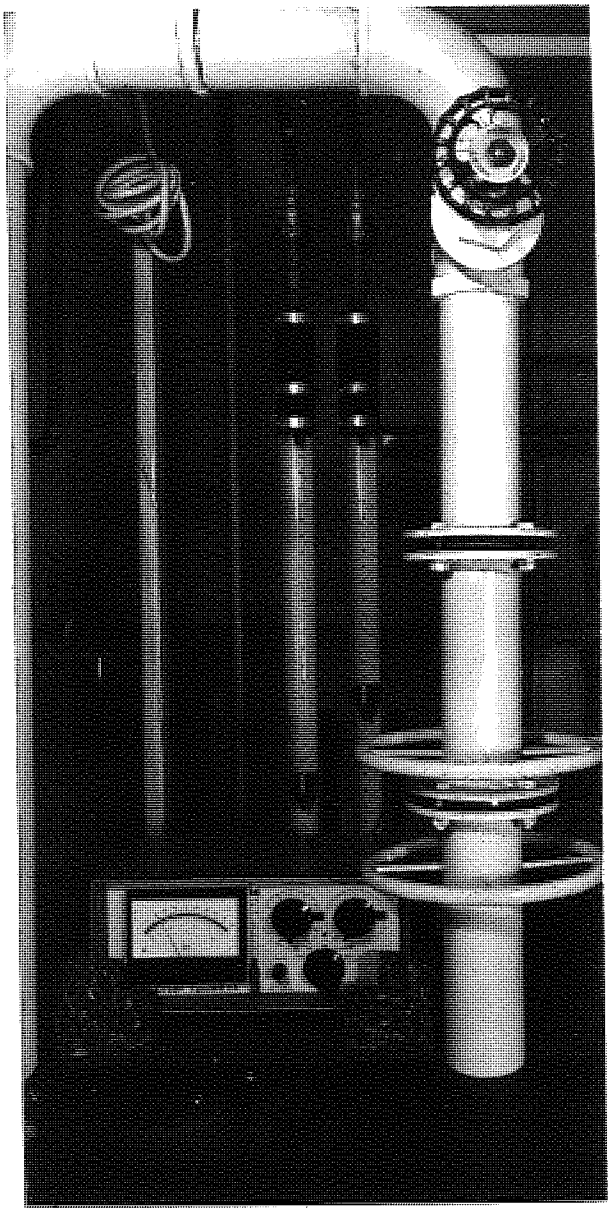

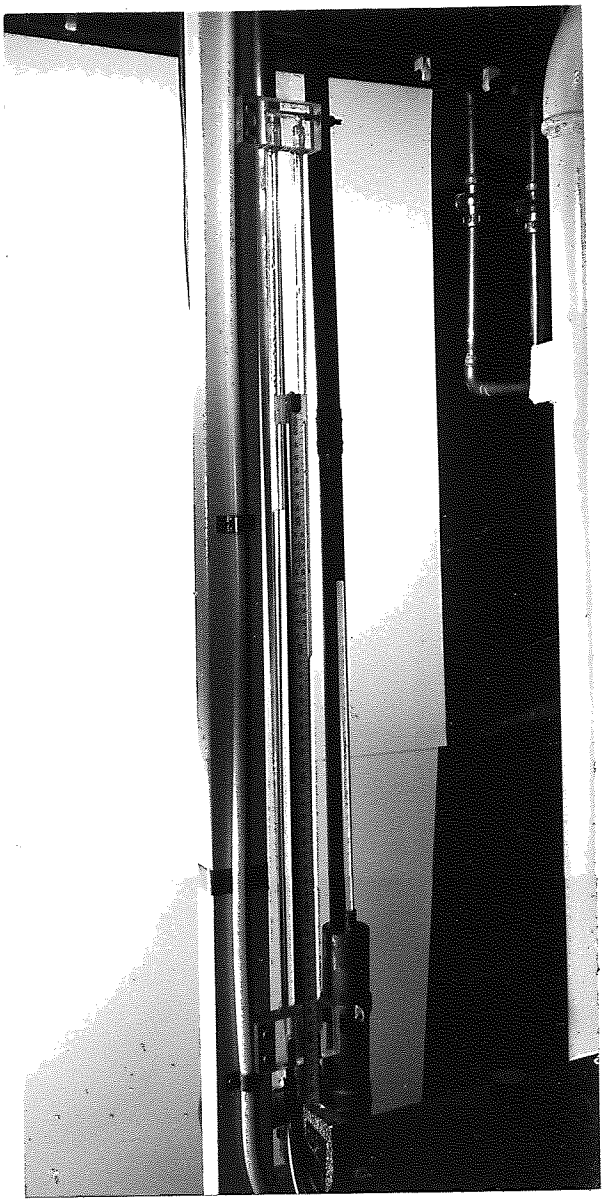

(A) (B)

(A) Air Flow : Orifice Plate and Thermocouple Grid
Water Flow : Rotameters

(B) Water Flow : Manometer

(C) Air Flow : Manometer

(D) Gas Flow : Manometer and Rotameters

(E) Temperature Recorder and D.V.M.

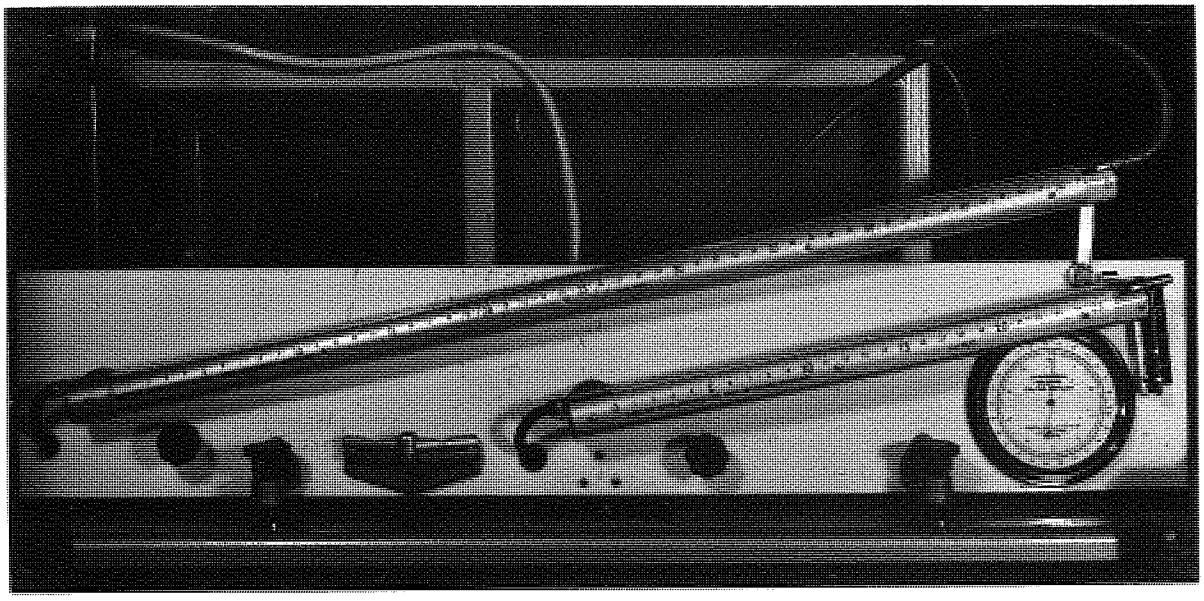

(C)

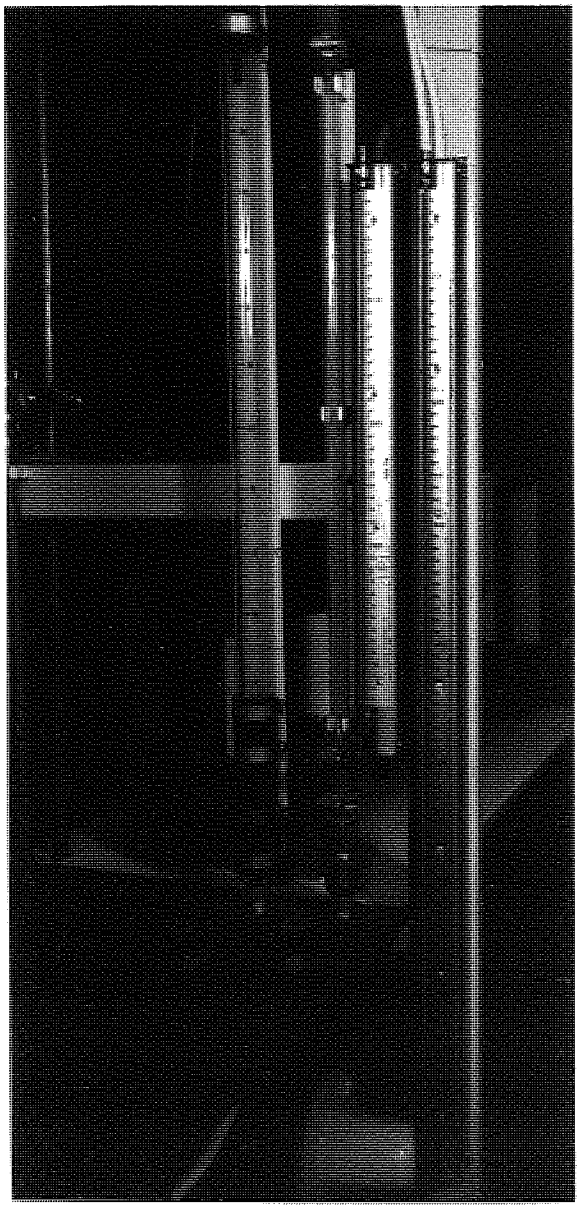

(D)

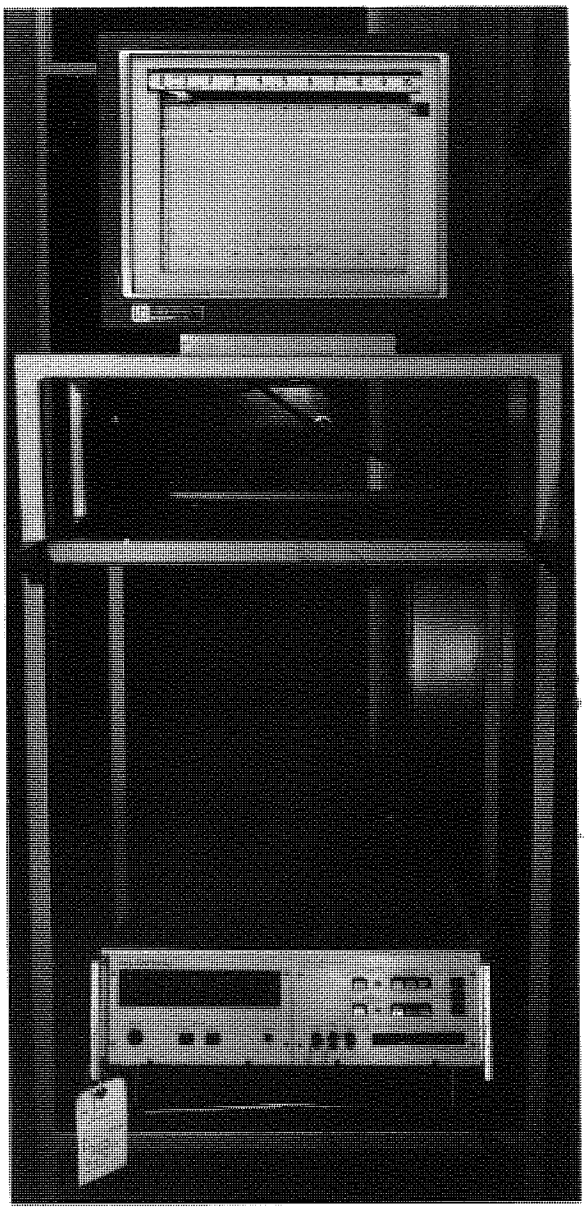

(E)

CHAPTER VI

FLOW VISUALISATION BETWEEN A FLUIDIZED BED AND AN EXTENDED SURFACE

6.1 Introduction

In the last decade a number of investigators have attempted to study the nature of the two-phase flow in fluidized beds. Of particular interest are the phenomena associated with the passage of voids or bubbles through the bed. In this context the work of Rowe[44], 1962, and Davidson and Harrison[43], 1963, has been very successful in advancing the understanding of flow patterns within and around the bubbles. This is of great importance in fluidized bed heat transfer since the particle movement results from the bubble behaviour. More recently Rowe and Everett[45], 1972, have reported their observations of bubble behaviour in the vicinity of objects immersed in two- and three-dimensional beds using X-ray techniques. Hager and Thomson[30], 1973, presented information from X-ray and flow visualisation studies on plain and finned tubes in both two- and three-dimensional beds. However, their flow visualisation experiments were conducted in two-dimensional beds of 20 mm thickness, the bubble behaviour around their immersed objects being observed externally through the transparent bed sides. The bed was illuminated externally using photographic flood lamps.

Without having access to a suitable X-ray facility to study the particle/bubble motion around an extended surface, a flow visualisation technique was developed. The most desirable way to observe the flow behaviour between adjacent fins, is by viewing directly across the fin flanks. With a two-dimensional bed one of the external wall faces can act as a fin flank but the flow patterns observed will not be truly representative of that occurring in a three-dimensional bed. By manufacturing a suitable extended surface model with a simple optical system and internal lighting source an attempt was made to investigate the motion of bubbles and particles between adjacent fins when immersed in a three-dimensional bed.

6.2 Design and Construction of the Equipment

6.2.1 The Bed and Plenum Chamber

The flow visualisation studies were carried out in a circular

bed configuration whose diameter was identical to that used in the heat transfer studies - namely 534 mm diameter. Furthermore, the distributor plate was formed from two 610 mm by 305 mm rectangular ceramic porous tiles manufactured by Doulton Industrial Products of the same grade as used in the Mk 1 bed. The bed was constructed from clear P.V.C. sheeting 1.5 mm in thickness and clear Perspex sheeting 9 mm in thickness. The P.V.C. was used for the cylindrical shaped components and the Perspex for the more rigid parts, such as flanges. A general arrangement drawing of the bed and plenum chamber is shown in figure 6.1, together with the dimensions, and a photograph in figure 6.2. The individual component parts were fabricated together using "Durapipe" cement adhesive for the P.V.C. and acrylic tensol cement for the Perspex. A general purpose "Bostik" adhesive was used to seal the P.V.C. and Perspex sections. The plenum chamber was designed to allow the air to be distributed evenly across the whole face of the ceramic tile. This was achieved by use of a cone shaped baffle plate which was adjustable in both height and angle.

6.2.2 Air Supply to the Bed

A four stage turbo-blower manufactured by William Allday and Co. Ltd. rated to give 18 l/s at a pressure of 1.9 m water gauge, supplied the air. Air flow rate was determined at inlet to the blower by an orifice plate 44.4 mm diameter in a 63.5 mm diameter pipe. The orifice plate conformed to B.S. 1042 using D and D/2 pressure tappings and the atmospheric air relative humidity was noted by an Edney Paper Hygrometer. Air flow rate was controlled by means of a throttle valve situated downstream of the blower and flexible plastic hose connected the valve outlet to the plenum chamber inlet pipe. Figure 6.3 shows the complete installation.

6.2.3 The Extended Surface Model

As indicated in the introduction to this section the most effective way of obtaining the particle/bubble motion was by viewing from inside one of the extended surface fins across the space to the adjacent fin. With actual surface fins in the order of 50 mm by 50 mm by 1.5 mm thick the problem of providing lighting and visionary equipment into one of the fins was very difficult. To avoid the problems of miniaturisation a large scale model of extended surface C/3/MS was produced. It was necessary to have the equipment combined

in the fins, as its existence elsewhere in the bed would have affected the flow patterns. The model is shown in figure 6.4 and consisted of six 76 mm by 76 mm by 6 mm thick fins with variable fin spacing of 3, 6 and 9 mm on a central basic tube 17 mm in diameter. Of the two central fins, one was hollow and housed a number of miniature electric light bulbs providing the illumination. Since sands have a high expansion ratio when fluidized the voidage fraction is high and the transmission of light across the fin spacing gap to the adjacent fin is excellent. The second adjacent fin was therefore produced as a hollow section and extended above the level of the fluidized material to form a periscope whereby the transmitted light could be reflected and the flow patterns observed by the naked eye.

6.2.4 The Optical System

The basic periscope which is shown in figure 6.5 was constructed of 1.5 mm thick Perspex being simply an extension of a central fin to a height of 600 mm. The box section created was open at the top. As the reflective properties of the clear Perspex were unsuitable for use as a periscope body, the inside of the section was painted with a matt black cellulose paint, with the exception of a 76 mm section at the bottom of one face, which acted as the viewing area. This treatment proved to be most effective in reducing internal reflections of light in the periscope.

The periscope required two mirrors. The top mirror presented no problems since it was mounted outside the box section ; a piece of commercial mirror glass being utilised and mounted on perspex supports. The bottom mirror, needed to be small enough to be placed inside the 6 mm box section, while being accurately aligned at 45 degrees to the section and to be traversed up and down at least 76 mm. The alignment was an important consideration since the reflective area was small compared with the reflective distance. Initially a piece of mirror glass was used but due to its thickness its effective area was reduced when mounted at 45 degrees, making it unsuitable. Attempts were made to produce a mirror by silver plating a small strip of 28 S.W.G. copper sheet. The main problem was to produce a thick enough coating to allow for subsequent polishing. Also the silver coating tended to tarnish rapidly over a period of a few hours, leaving the surface a mottled black. This method was therefore abandoned. The mirror was finally

produced from a piece of 28 S.W.G. stainless steel which was mounted on a perspex block and successively polished to a 1 μm surface finish using a diamond grinding wheel. During this process the perspex block was mounted accurately at 45 degrees. The mirror block was then attached to the end of two 16 S.W.G. steel wires which were passed through the top mirror support of the periscope. These wires allowed the raising and lowering of the bottom observation mirror externally from the bed.

The fin flank opposite to the face of the periscope was illuminated so that the activity of the particles and bubbles could be observed through the periscope by the transmitted light. Since this section of the model was also a box section 76 mm by 76 mm by 6 mm thick, it was necessary to use very small electric bulbs for illumination. The only bulbs available for this purpose were 6.5 V, 1 W, L.E.S. pilot bulbs. Initially eight of these bulbs were mounted on a rosette of perspex. The bulbs were placed inside the box section and a polished stainless steel backing plate was provided to reflect as much light as possible in the desired direction. The secondary surface was mounted on a 17 mm P.V.C. tube, the electrical conductors being passed through the end of the tube, which was sealed with a modelling clay. The other end of the tube was butted to the periscope face with perspex cement. A further length of tube was then butted to the back of the periscope fin and two further perspex fins were pushed over each protruding end. The fins with the exception of the periscope were free to slide along the tube thereby providing a variable fin spacing.

The optical arrangement, built into the extended surface, was lowered into the fluidized bed and held in position by two clamping screws attached to a perspex plate supported on the top external flanges of the bed. Observations were then made of the fluidized solids of zircon sand between the model fins. Two faults were immediately apparent with this system. Firstly, the eight pilot bulbs provided insufficient illumination and secondly, sand adhered to the surface of the perspex making observation difficult.

The lighting problem was overcome by dispensing with the eight bulb rosette arrangement and filling the opposing box section volume with as many bulbs as possible. By careful soldering, fifty-four

bulbs were located in position to provide adequate illumination. An anti-static perspex polish was applied to the optical fin flanks to prevent sand adhering to the surfaces. However, after a few seconds the scouring action of the particles removed the polish and the problem returned. It was decided at this stage to abandon perspex for the two opposing surfaces and replace them with 1 mm thick optical glass sheet. The model was reassembled and placed in the bed and observations were successfully made of particle/bubble movement between the central adjacent fins for various superficial fluidizing velocities and fin spacings.

6.3 Experimental Observations

All experiments were carried out using a static bed height of approximately 50 mm, the model being placed directly on the distributor. When fluidized, bed expansion was such that the extended surface was completely submerged in the sand. At spacings of 3 mm, 6 mm and 9 mm observations were made at four different fluidizing velocities.

Ambient Air Conditions

Temperature - 19°C

Relative Humidity - 0.61

Atmospheric Pressure - 760 mm Hg absolute

Bed Temperature - 32°C to 38°C

6.3.1 Observation Number 1 - 3 mm Spacing

Very Low Flow (fixed bed fully expanded)

Bubbles were observed over the whole flank surface of the fin with the exception of the area immediately above the central basic tube. Bubbles were noticeably smaller at the lower flank position. Mean bubble sizes of 3 to 5 mm across at the bottom and 10 to 15 mm across at the top fin positions were estimated. When the bubbles came into contact with the lower regions of the basic tube, they dispersed evenly on each side and joined up with other bubbles which had not made contact with the tube. The coalescence of bubbles was initiated by the basic tube. Particle movement was minimal and no pattern could be established.

Low Flow (68 m^3/h at inlet air conditions - superficial fluidizing velocity 0.084 m/s)

. At this flow the bubbles were observed to be larger than in the previous case with a stagnation area still occuring above the basic tube. However, at this velocity the bubbles were enveloping more of the basic tube surface and being carried into the upper fin flank region. For approximately 25% of the bubbles it was found that images of the light bulbs could be clearly seen, indicating opposite flanks to be scoured at the same time. Again no distinct particle movement was established.

Medium Flow (150 m^3/h at inlet air conditions - superficial fluidizing velocity 0.186 m/s)

The behaviour of the bubbles became more random in nature and irregular in shape. Coalescence was rapid in the higher flank regions, towards the fin side edges. Particle movement could be detected although bubble movement tended to obscure any intelligent interpretation of the observations. Approximately 60% of the bubbles gave light source images.

High Flow (370 m^3/h at inlet air conditions - superficial fluidizing velocity 0.456 m/s)

At this high fluidizing velocity bubble formation was not clearly defined; bubbles were not individually apparent, but rather the fin surface was undergoing a continual scouring action by random "flames" of air and sand. The total flank surface area subjected to the bubbles was in the order of 75% at any given instant of time.

For all these different superficial fluidizing velocities the mean bubble velocities appeared to remain constant.

6.3.2 Observation Number 2 - 6 mm Spacing

Very Low Flow (fixed bed fully expanded)

Bubble size for this condition was observed to be similar to that for observation number 1. However, the bubble growth towards the top of the fin was not so apparent. This was expected since with the wider fin spacing the larger bubbles would not be so restricted. Also it was observed that for this low flow the number of bubbles was reduced by comparison with the 3 mm spacing. As with the previous spacing a

stagnant area was observed immediately above the central tube. Particle movement could not be detected.

Low Flow (68 m^3/h at inlet air conditions - superficial fluidizing velocity 0.084 m/s)

Larger bubbles than at the very low flow but a significant stagnant area above the basic tube. Only a small proportion of the bubbles appeared to be sufficiently large to scour both fin flanks simultaneously.

Medium Flow (150 m^3/h at inlet air conditions - superficial fluidizing velocity 0.186 m/s)

Bubbles larger than at low flow condition being random in shape and distribution. Growth due to coalescence not very apparent, but a higher percentage scoured both surfaces simultaneously. Stagnant area above basic tube reduced to a small triangular area immediately above the tube. The net particle movement tended to be in from the fin edges at the position between distributor and the basic tube and out from the fin edges in the region above the basic tube. More movement of particles was observed from the side rather than the top fin edges. Figure 6.6 shows the net particle movement paths.

High Flow (370 m^3/h at inlet air conditions - superficial fluidizing velocity 0.456 m/s)

Very difficult to make any intelligent interpretation other than that the whole fin flank surfaces were completely scoured by sand and air bubbles. Since the extended surface model was situated close to the porous tile distributor, it appeared that sand was excluded from the area between the fins in the lower central region by the high air flow rate.

6.3.3 Observation Number 3 - 9 mm Spacing

Very Low Flow (fixed bed fully expanded)

Very few bubbles were observed, virtually none towards the bottom of the extended surface, and only infrequently towards the top. This is consistent with the previous results and it appears that with this spacing the bubbles were small enough and the intervening sand layer thick enough, for the bubbles to pass between the surfaces

unobserved. Bubbles were noted in the area immediately below the basic tube, being forced to spread when coming into contact with the tube.

Low Flow (68 m^3/h at inlet air conditions - superficial fluidizing velocity 0.084 m/s)

Observations comparable to 6 mm spacing. No discernible differences could be noticed.

Medium Flow (150 m^3/h at inlet air conditions - superficial fluidizing velocity 0.186 m/s)

Observations comparable to 6 mm spacing. No discernible differences could be noticed.

High Flow (370 m^3/h at inlet air conditions - superficial fluidizing velocity 0.456 m/s)

Observations comparable to 6 mm spacing. No discernible differences could be noticed.

At this spacing the light source was diffused, making observation more difficult compared with the smaller fin spacings.

6.4 Interpretation of Results

It appears, from the observations made, that the small fin spacing of 3 mm will be detrimental to good heat transfer. This is not solely due to lack of particle mobility in the restricted space betwee fin flanks but due to blanketing of the surfaces with bubbles. Higher bubble frequencies were observed even at the very low flow rates. The condition is impaired in the upper fin flank regions where bubble coalescence is taking place. At higher fluidizing velocities where the scouring action of the bubbles is more predominant, this effect will be more pronounced.

At the 6 mm spacing, less bubbles were noted at the low to mediu flow rates, this being probably due to the bubbles passing between th adjacent fins without making physical contact with the surfaces. Furthermore, at the medium to high flow rates a net particle movement was observed as shown in figure 6.6. It is interesting to note that the main particle movements appear to be in and out of the fin side

edges. This may be extremely immportant when considering the bed configuration and the particular arrangement of such surfaces in tube bundles. The influence of a constraining wall close to the fin edge could have an effect on the surface heat transfer performance. The main heat transfer experimental work, that follows, substantiates this point The defluidized cap above the basic tube is apparent at all spacings up to medium flow rates, the random scouring action at high flow rates tending to remove this "dead zone" barrier.

No apparent differences were noted between the 6 mm and 9 mm spacing positions although the quality of the light source was reduced at the 9 mm spacing. It is therefore implied that the particle/bubble movements and therefore the heat transfer performance will be relativel unaffected as the spacing is increased beyond a particular value.

The authors observations are opposite to those of Hager and Thomson[30], 1973, who concluded that "the particles appeared to be actually packed within the finned structure". They suggested that the impinging bubbles were diverted around the fin tip edges with few bein able to penetrate into the fins, leaving a large defluidized area. However, Hager and Thomson used a spine type of extended surface where it would be expected that this type of flow pattern occurred. Furtherm as indicated in the introduction, they were viewing the patterns externally in a two-dimensional bed and cannot conclusively offer evidence to indicate the motion between adjacent fins.

6.5 Recommendations for Further Work

The observations made, apply primarily to a rather large extended surface model. Although fin spacing was a variable the basic size and configuration of the fin remained constant. The work carried out, has proved that the visual optical system adopted is suitable for studying this difficult problem. Further work could be directed to the miniaturisation of such a system, which would be more representative to an actual extended surface working in a practical application. A miniature periscope arrangement should present no practical problems, although it may be difficult to obtain a sufficiently small light source at the opposing surface. It is suggested another periscope arrangement could be employed to project light from an external source to the opposing fin flank surface.

Experimentation with reflected light may also yield valuable information. The investigations carried out so far have been by transmitted light and this suffers from the disadvantage that bubbles scouring one surface are only visible if they are sufficiently large to render the sand at that point in the bed translucent. In the case or certain bed materials which do not expand greatly, difficulties may arise. Reflected light would allow any bubble in contact with the viewed face to be seen clearly, irrespective of size.

The development of photographic techniques such as cinematic or video tape recording would be ideal since apart from conclusive evidence, the slowing down or freezing of particle/bubble motion could be used with advantage. Finally, the use of introscope or fibre optic systems could be utilised to establish more conclusive scientific evidence.

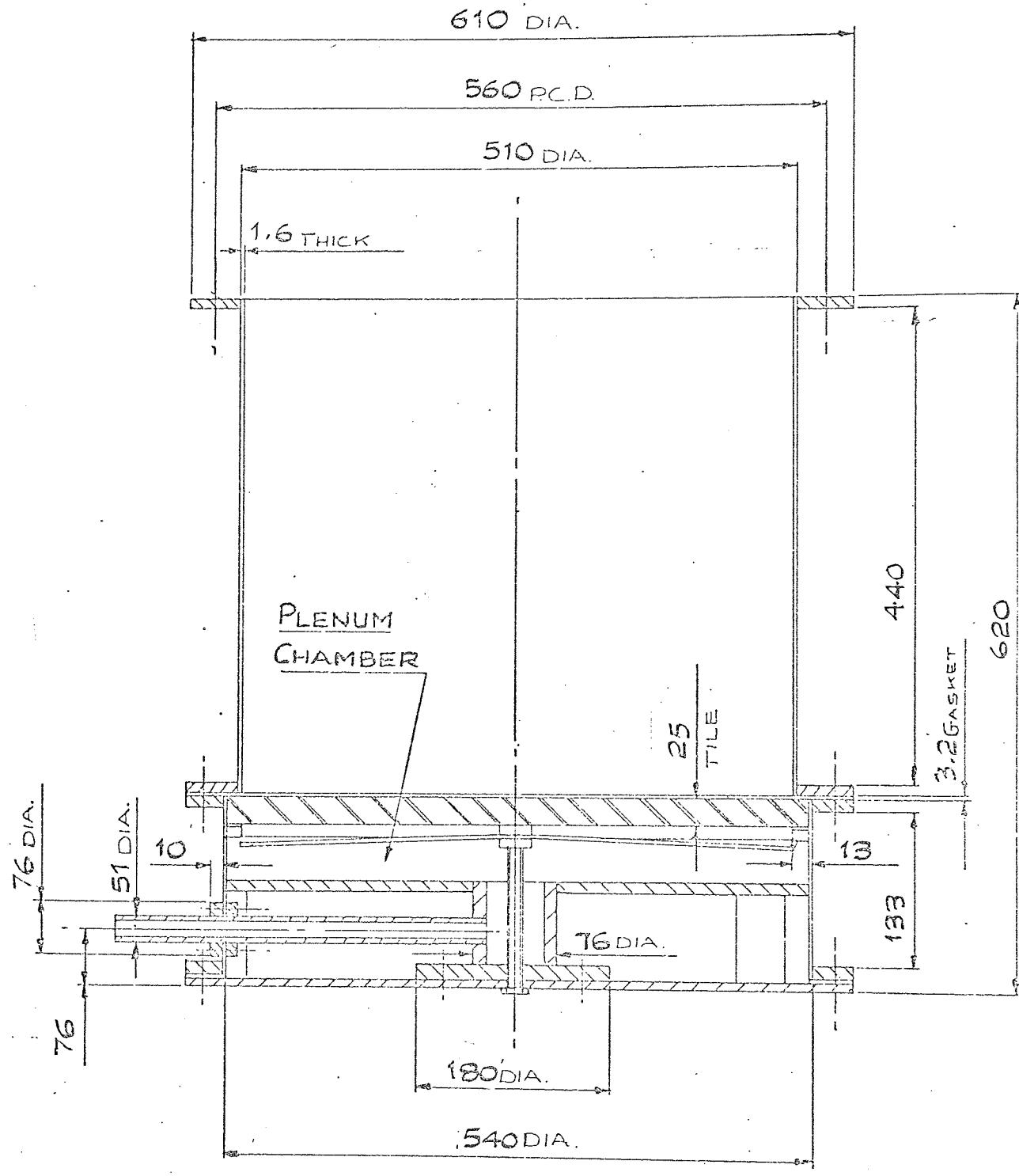

ALL DIMENSIONS IN MILLIMETRES

Figure 6.1 Sectional Elevation of Bed and Plenum Chamber

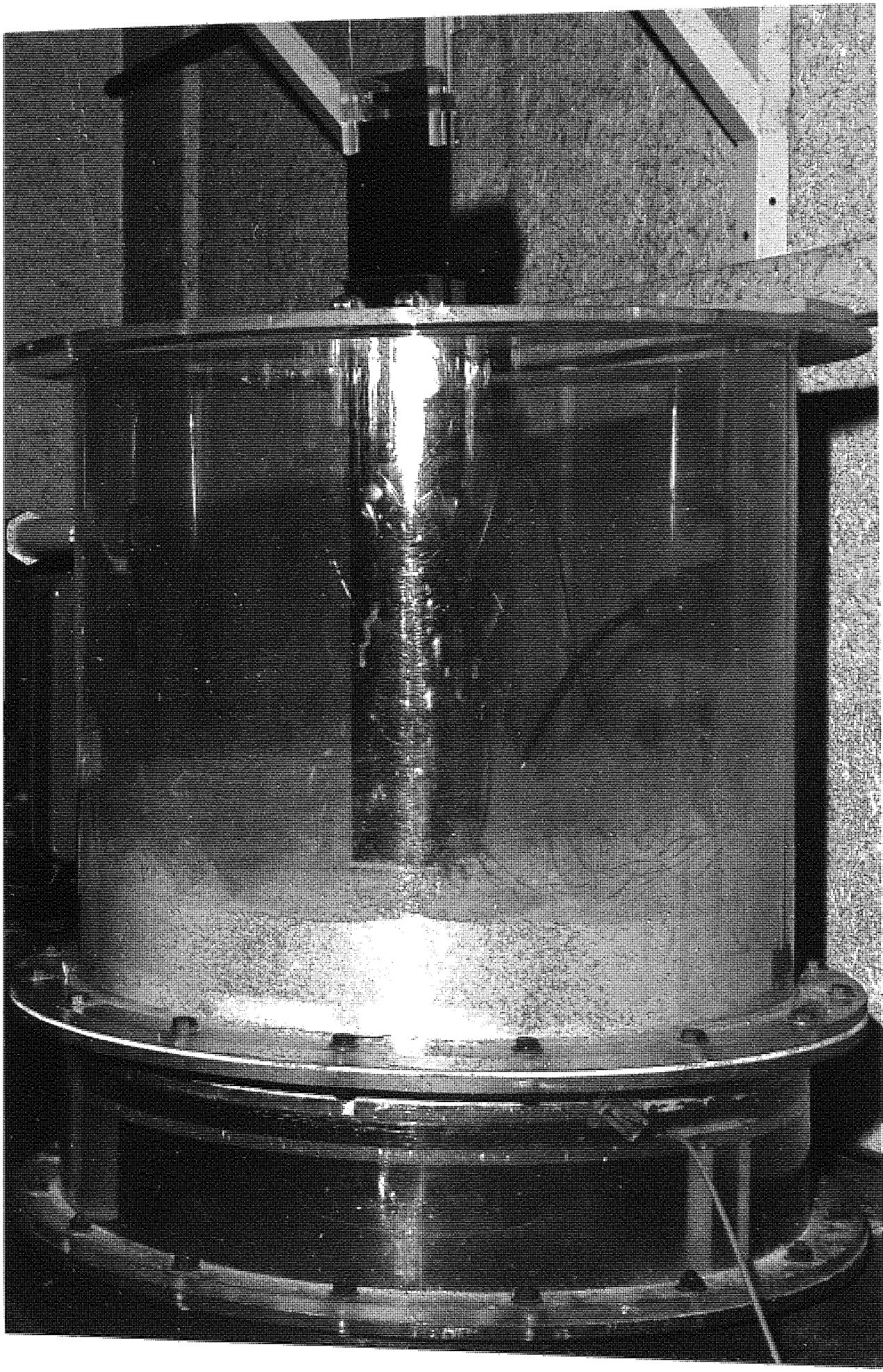

Figure 6.2 Flow Visualisation Rig - Bed View

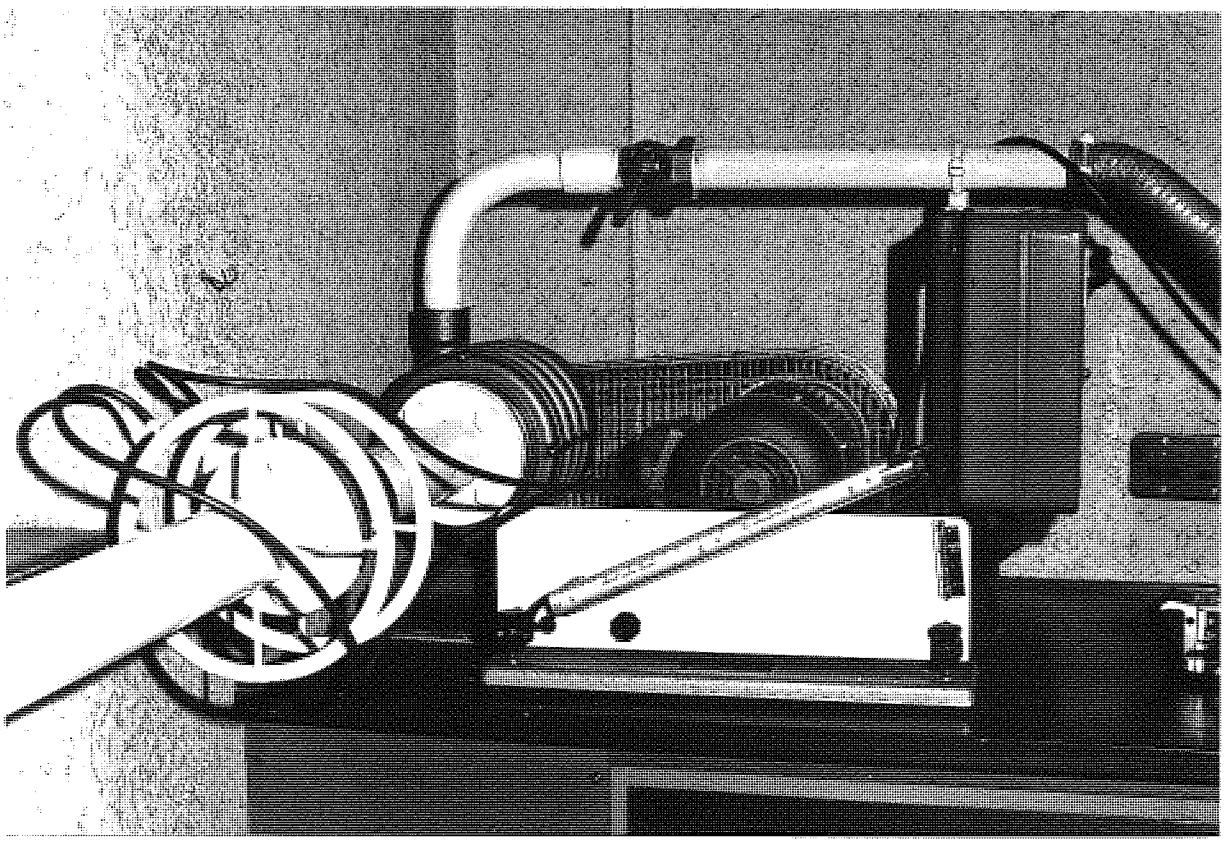

Figure 6.3 Flow Visualisation Rig – Compressor

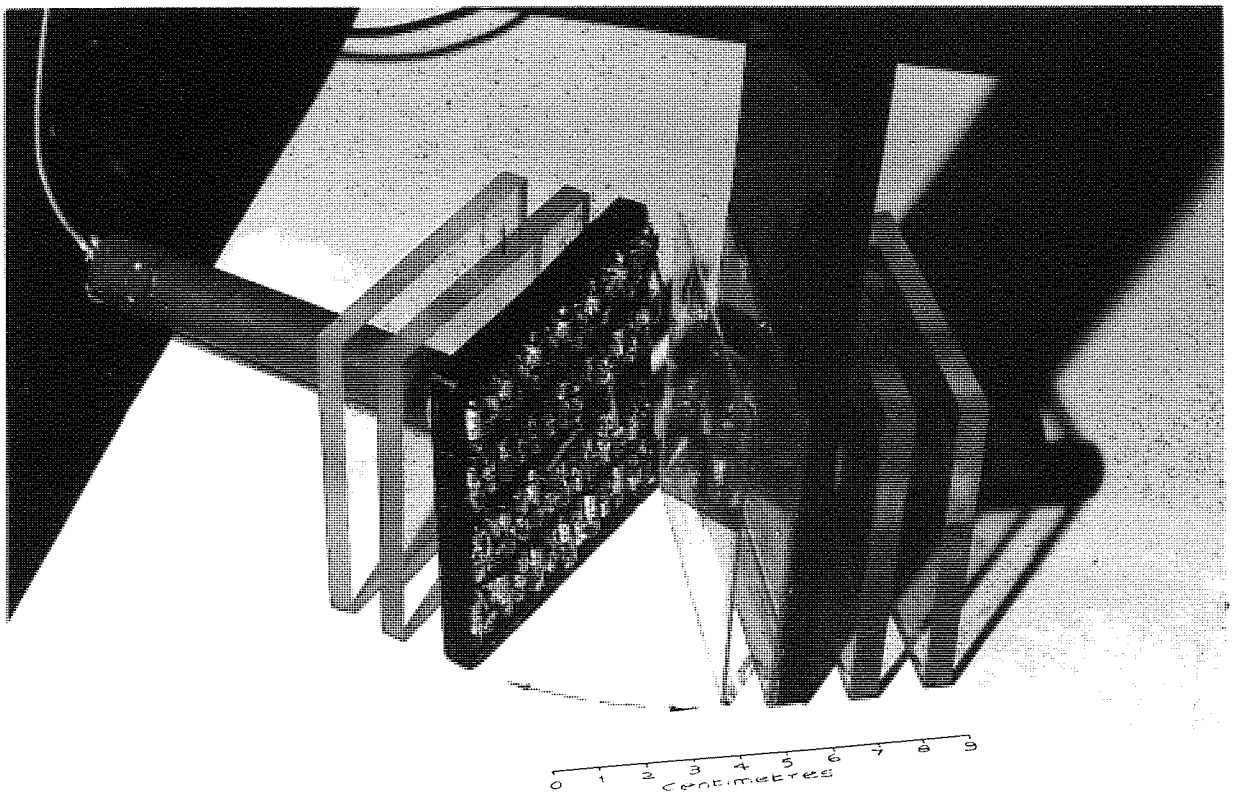

Figure 6.4 Extended Surface Model

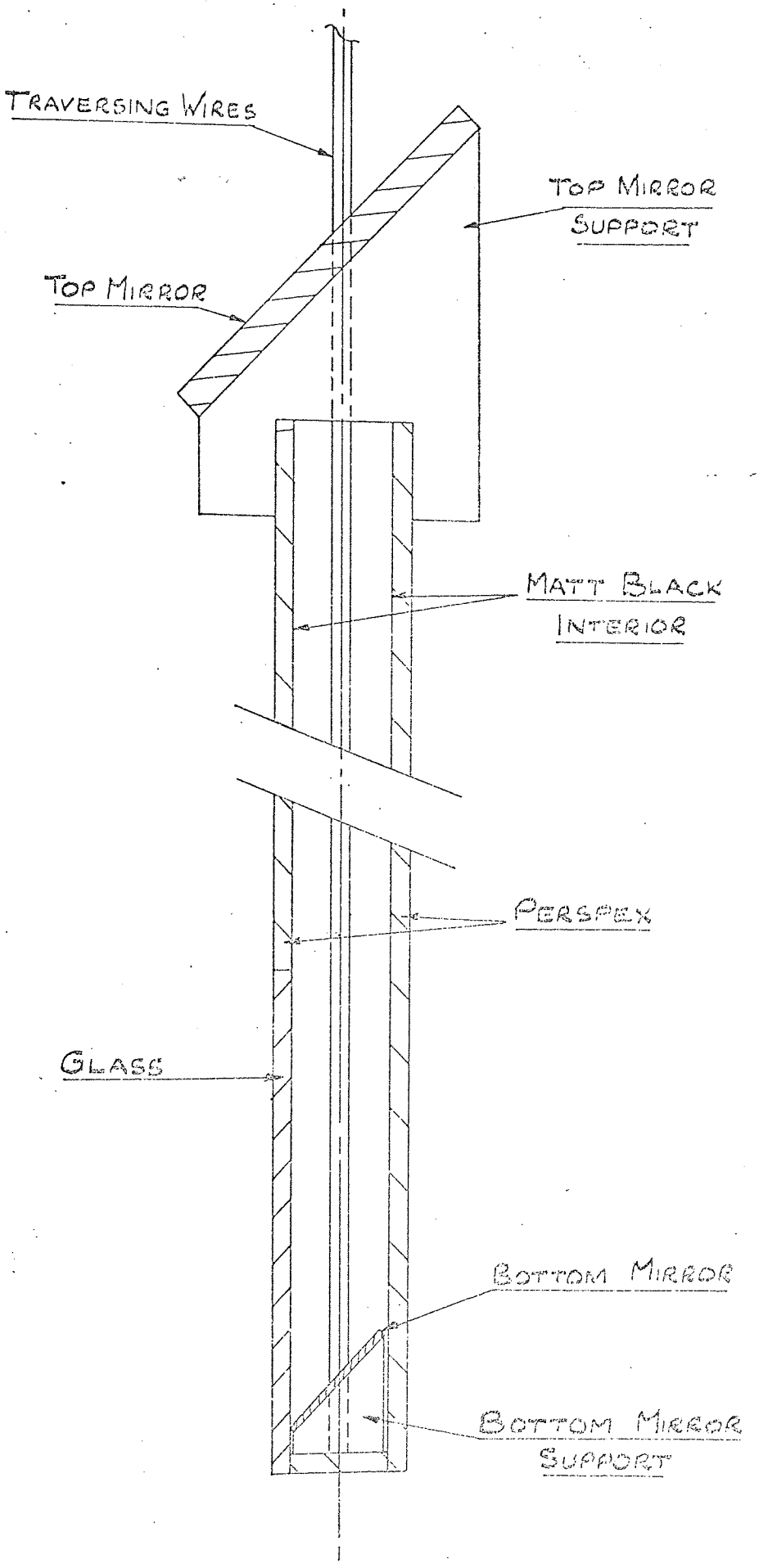

Figure 6.5 Sectional Elevation of Periscope Fin

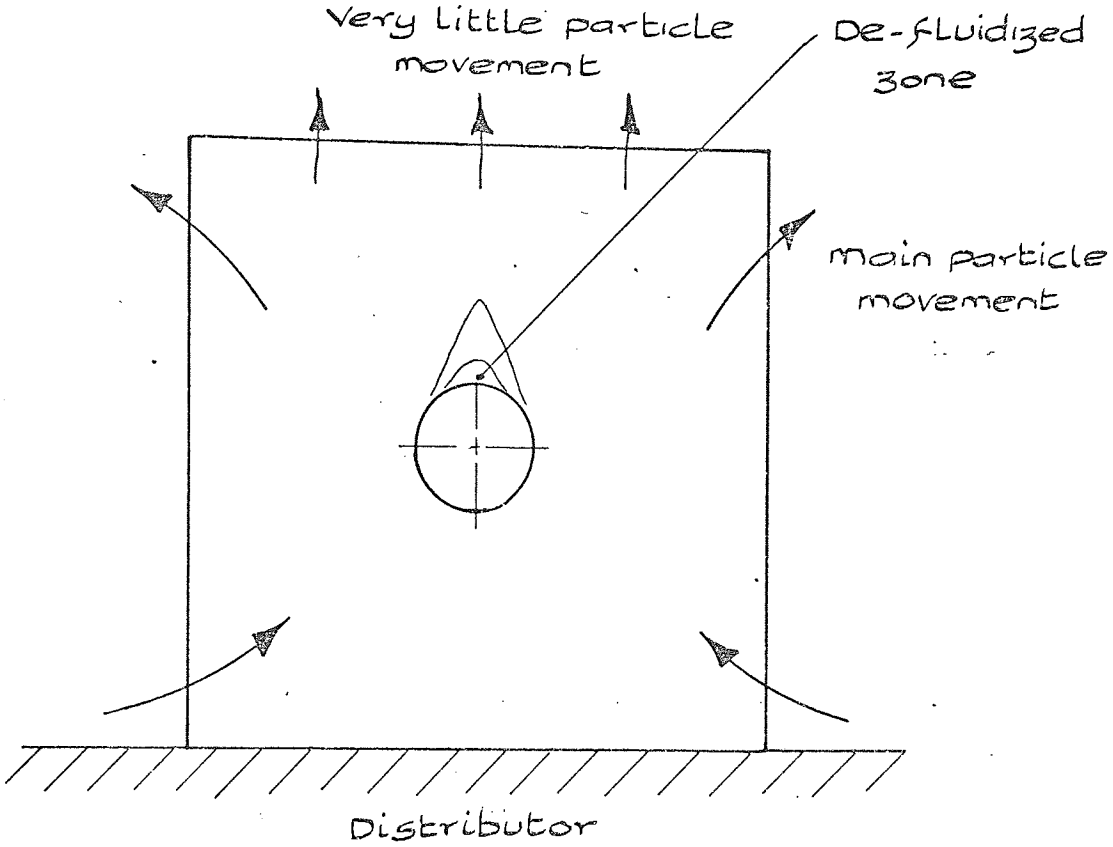

Figure 6.6 Net Particle Movement Between Adjacent Fins - Medium Flow - 6 mm Spacing.

CHAPTER VII

THE EXPERIMENTAL INVESTIGATIONS

7.1 Experimental Procedure

The particular heat exchanger surface to be tested was accurately located in the fluidized bed. For tests conducted in the Mk 1 bed, a depth gauge was used for the positioning of surfaces above the distributor plate. The grub screws in the top plate support were tightened to hold the surface at the desired height. In the case of the Mk 2 and Mk 3 bed tests the "Sindanyo" end supports were accurately machined to achieve the exact positioning. When required, thermocouples recording the extended surface fin temperatures were connected to the terminal block adjacent to the fluidized bed. The bed material used for the test was sieved to the required static height and checked using the depth gauge. To achieve uniformity of height the bed was momentarily fluidized and solids added or removed. Water pipe connections between the heat exchanger and the rig were effected before water circulation was established.

Referring to figure 5.14, showing the schematic diagram of the water circuit, the following operation was carried out for each test. With all valves except A,C, and I, in the open position, the feed pump was started and water pumped around the circuit to expel most of the entrained air. After a few minutes valve C was cracked open and the circulation pump started to flush any air from this part of the water system. All air was then expelled from the orifice pressure tappings by opening a vent valve on the manometer and allowing the limbs to fill with water. Valves A and I were then cracked open and valves D and J and finally valve E were closed. The water system was ready for tests to commence. This procedure was adopted to ensure expulsion of all air from the water circuit since it was found that the presence of air caused cavitation at the impeller of the circulating pump and, more important, false readings on the manometer connected across the orifice plate. The rate of water circulation was controlled by valve C and the feed water flow rate by valve A, within the capacity ranges of the two water pumps.

When the water system was in operation, the air fan was started and the gas burner ignited to raise the bed temperature to operating

levels using the preheated flow of fluidizing air. As the bed temperature rose above about 100°C the air flow through the bed was adjusted to give minimum uniform fluidization of the bed material, and the gas flow altered to the minimum value which ensured stable combustion with the air flow. Once the minimum gas and air flow rates were determined, the circulatory and feed water flow rates were adjusted to maintain a minimum feed water differential temperature of about 10 K for a high circulatory water flow rate. This ensured a reasonable experimental accuracy in the determination of the heat transfer rate from the bed to the water. Furthermore, the high flow rate through the heat exchanger limited the temperature differential to less than 3 K and provided a high inside heat transfer coefficient at the basic tube surface. When testing surfaces C/1/MS and C/2/MS the flow rate was controlled by the restriction offered by the heat exchanger basic tube cross-section, which resulted in a slightly higher temperature differential. These water flow rates were maintained for the remainder of each test.

The three bed thermocouple temperatures were continually recorded and once steady conditions were achieved the following readings noted:-

(1) Feed water inlet temperature
(2) Water outlet temperature
(3) Feed water rotameter reading
(4) Pressure difference across circulation water orifice plate
(5) Pressure difference across air orifice plate
(6) Air pressure at orifice plate
(7) Air temperature at orifice plate
(8) Gas rotameter reading at 750 mm Hg gauge pressure
(9) Ambient temperature
(10) Barometric pressure

Tho bed temperatures, and fin metal temperatures when required, were noted from the Leeds and Northrup 24 point recorder.

Sets of readings were taken at various levels of fluidizing air flow rates allowing some fifteen to twenty minutes between each, to allow steady conditions to prevail. The flow rate was increased progressively until excessive elutriation of the bed material was

observed. With each increase in air velocity, the gas flow rate was adjusted as necessary to maintain stable combustion.

This procedure, with the exception of certain specialized tests, was repeated for the remaining heat exchangers. Thus for each surface a complete set of results covering a wide range of fluidizing conditions was obtained. The results were then processed as indicated in the following sections.

7.2 Experimental Results

A total of twenty-nine surfaces were tested, the relevant dimensions being presented in tables 7.1 and 7.2. Table 7.3 lists the individual surface areas and geometric ratios.

Fifty-five tests were conducted in three different bed configurations and three bed materials; zircon sand, silica sand and steel shot. Static bed height and surface positions were changed. During each test superficial fluidizing velocity and bed temperature were varied. The results of these tests are presented in Appendix A3 in tabular form. For clarity of presentation the observed and calculated results are presented together, for the majority of tests. The tables of calculated results are extracts from a standard computer programme, a print-out being given in the appendix.

Graphs are presented from the experimental results in Chapter VIII together with relevant figures from the work of other investigators. Where required, figures indicating the surface fin thermocouple positions are given.

TABLE 7.1 Plain, Oval and Manufactured Surface Dimensions

SURFACE DESIGNATION	d_i mm	d_o mm	D mm	W mm	t mm	l mm	b mm	n fins	L mm	N fins/m	X mm
C/1/Plain	9.02	15.82	-	-	-	-	-	-	-	-	-
C/2/Plain	13.70	15.10	-	-	-	-	-	-	-	-	305
C/3/Plain	8.60	10.00	-	-	-	-	-	-	-	-	305
C/4/Plain	13.60	15.00	-	-	-	-	-	-	-	-	305
AB/1/Oval	-	-	27.56	12.00	1.200	-	-	-	-	-	305
C/1/MS	5.00	6.35	50.80	50.80	1.590	-	3.270	48	233	206	1514
C/2/MS	5.22	6.35	50.80	50.80	1.590	-	6.150	31	240	129	1240
C/3/MS	13.70	15.10	50.80	50.80	1.590	-	3.140	47	222	212	285
C/1/MR	13.70	15.10	50.80	-	1.590	17.85	3.702	48	254	189	304
C/2/MR	13.70	15.10	50.80	-	1.590	17.85	2.550	57	236	242	Variable
C/3/MR	19.80	21.40	50.80	-	1.590	14.70	2.428	57	229	249	279
C/4/MR	13.70	15.10	Variable	-	0.795	Variable	2.591	70	237	295	Variable

TABLE 7.2 Commercially Produced Surface Dimensions

SURFACE DESIGNATION	d_i mm	d_o mm	D mm	t mm	l mm	b mm	n fins	L mm	N fins/m	X mm
C/1/CR	8.00	10.00	26.00	0.254	8.00	2.286	100	254	394	305
C/2/CR	13.70	15.10	31.10	0.254	8.00	1.642	135	256	527	305
C/3/CR	20.20	22.00	38.00	0.254	8.00	1.658	136	260	523	305
C/4/CR	26.20	28.00	44.00	0.254	8.00	1.628	136	256	531	305
C/5/CR	13.60	15.00	29.20	0.254	7.10	3.567	67	256	262	305
C/1/ER	15.88	18.31	35.94	0.460	8.82	3.043	87	305	285	355
C/2/ER	13.46	15.49	22.23	0.410	3.37	1.926	121	283	428	333
C/3/ER	13.46	16.08	18.80	0.410	1.36	0.933	208	279	744	329
C/4/ER	11.18	12.57	19.05	0.510	3.24	1.738	125	281	445	331
C/5/ER	13.97	15.95	18.80	0.380	1.43	0.994	204	280	728	330
C/6/ER	25.40	29.08	45.72	0.610	8.32	3.065	75	276	272	326
C/7/ER	19.05	22.23	40.00	0.610	8.89	2.952	77	274	281	324
MS/1/ER	11.38	16.30	24.20	1.015	3.95	1.235	180	405	444	455
MS/2/ER	20.80	25.40	30.50	0.508	2.55	0.986	271	405	669	455
MS/1/WR	20.30	25.40	50.80	1.270	12.70	2.346	112	405	277	455
MS/2/WR	20.30	25.40	35.60	1.270	5.10	3.439	86	405	212	455
MS/1/Spine	20.20	25.40	50.80	0.794	12.70	3.306	100	410	244	460

Surface consists of 21 spines in every 360° of angular rotation of basic tube, each being rectangular 3.3 mm wide by 0.794 mm thick.

SURFACE DESIGNATION	$\frac{d_o}{d_i}$	$\frac{D}{d_o}$	$\frac{b}{l}$	$A_i \times 10^3$ m^2	$A_o \times 10^3$ m^2	$A_1 \times 10^3$ m^2	$A_2 \times 10^3$ m^2	$\frac{A_1+A_2}{A_o}$	$V_2 \times 10^6$ m^3	
C/1/Plain	1.754	—	—	16.85	27.76	—	—	—	—	
C/2/Plain	1.102	—	—	13.13	14.47	—	—	—	—	
C/3/Plain	1.163	—	—	8.24	9.58	—	—	—	—	
C/4/Plain	1.103	—	—	13.03	14.37	—	—	—	—	
AB/1/Oval	—	—	—	17.23	19.95	—	—	—	—	
C/1/MS	1.270	8.000	—	23.78	30.20	24.11	251.09	9.11	198.50	
C/2/MS	1.216	8.000	—	20.33	24.73	20.80	162.16	7.34	130.82	
C/3/MS	1.102	3.364	—	12.27	13.52	9.98	240.92	18.56	186.50	
C/1/MR	1.102	3.364	0.207	13.08	14.42	10.80	189.56	13.90	149.06	*
C/2/MR	1.102	3.364	0.143	20.44	22.53	18.23	225.11	10.80	174.94	**
				12.31	13.57	9.27	225.11	17.27	174.94	***
				13.13	14.47	10.17	225.11	16.26	174.94	
C/3/MR	1.081	2.374	0.165	17.35	18.76	12.66	204.52	11.58	162.95	+
C/4/MR	1.102	3.364	0.145	12.65	13.95	11.31	267.57	19.99	110.33	++
				13.13	14.47	11.83	267.57	19.31	110.33	+++
				13.13	14.47	11.83	157.85	11.73	67.47	=
				13.13	14.47	11.83	81.86	6.47	37.93	
				13.13	14.47	11.83	31.99	3.03	18.69	

* Test Number 20 ** Test Numbers 21 and 22 *** Test Numbers 23 and 24

\+ Test Number 26 ++ Test Numbers 27 and 28 +++ Test Numbers 29 and 30

= Test Numbers 31 and 32 == Test Numbers 33 and 34

TABLE 7.3 Individual Surface Areas and Geometric Ratios

TABLE 7.3 Individual Surface Areas and Geometric Ratios

SURFACE DESIGNATION	$\frac{d_o}{d_i}$	$\frac{D}{d_o}$	$\frac{b}{l}$	$A_i \times 10^3$ m^2	$A_o \times 10^3$ m^2	$A_1 \times 10^3$ m^2	$A_2 \times 10^3$ m^2	$\frac{A_1+A_2}{A_o}$	$V_2 \times 10^6$ m^3
C/1/CR	1.250	2.600	0.286	7.66	9.58	8.78	92.55	10.58	18.67
C/2/CR	1.102	2.060	0.205	13.13	14.47	12.84	160.10	11.95	28.01
C/3/CR	1.089	1.727	0.207	19.36	21.08	18.69	209.21	10.81	41.56
C/4/CR	1.069	1.571	0.204	25.10	26.83	23.79	250.87	10.24	50.87
C/5/CR	1.103	1.947	0.502	13.03	14.37	13.57	67.62	5.65	16.44
C/1/ER	1.153	1.963	0.345	17.70	20.41	18.11	135.22	7.51	49.95
C/2/ER	1.151	1.435	0.571	14.06	16.19	13.77	51.79	4.05	22.95
C/3/ER	1.195	1.169	0.686	13.93	16.64	12.33	36.03	2.91	23.34
C/4/ER	1.124	1.516	0.536	11.63	13.07	10.55	44.05	4.18	17.54
C/5/ER	1.142	1.179	0.697	14.49	16.55	12.66	36.31	2.96	19.07
C/6/ER	1.145	1.572	0.368	25.98	29.75	25.57	153.21	6.01	88.12
C/7/ER	1.167	1.799	0.332	19.41	22.65	19.37	139.65	7.02	69.07
MS/1/ER	1.432	1.485	0.313	16.27	23.30	13.94	104.35	5.08	89.23
MS/2/ER	1.221	1.201	0.387	29.73	36.31	25.32	134.55	4.40	98.42
MS/1/WR	1.251	2.000	0.185	29.02	36.31	24.96	363.21	10.69	290.36
MS/2/WR	1.251	1.401	0.674	29.02	36.31	27.59	96.27	3.41	127.51
MS/1/Spine	1.257	2.000	0.260	29.19	36.71	-	-	-	-

CHAPTER VIII

COMPARISON OF EXPERIMENTAL RESULTS

8.1 Introduction

This chapter presents the experimental results of the author's work, in a suitable graphical form enabling a logical analysis of the research programme to be undertaken. The combined results from the plain tube and radial fin surface tests are analysed, using a linear multiple regression model as outlined in Appendices A1 and A2. The computer print output is suitably arranged and detailed in Appendix A6. Using the graph plotter presentation programme given in Appendix A2 a selection of these analysed results are represented by a series of graphs, showing the influence of the main variables on the surface heat transfer performance. The results derived from the theoretical work on radial finned surfaces given in Chapter IV and Appendix A4 is summarised and presented. Finally, a collection of relevant graphs from the work of other research investigators is reproduced for comparison purposes.

8.2 Plain and Oval Tube Results

8.2.1 Experimental Results

Figure 8,1

EFFECT OF STATIC BED HEIGHT ON HEAT TRANSFER COEFFICIENT (Bed to Tube) FOR VARYING FLUIDIZING VELOCITY – BED MATERIAL : ZIRCON SAND ($\bar{d}_p$ = 138 μm)

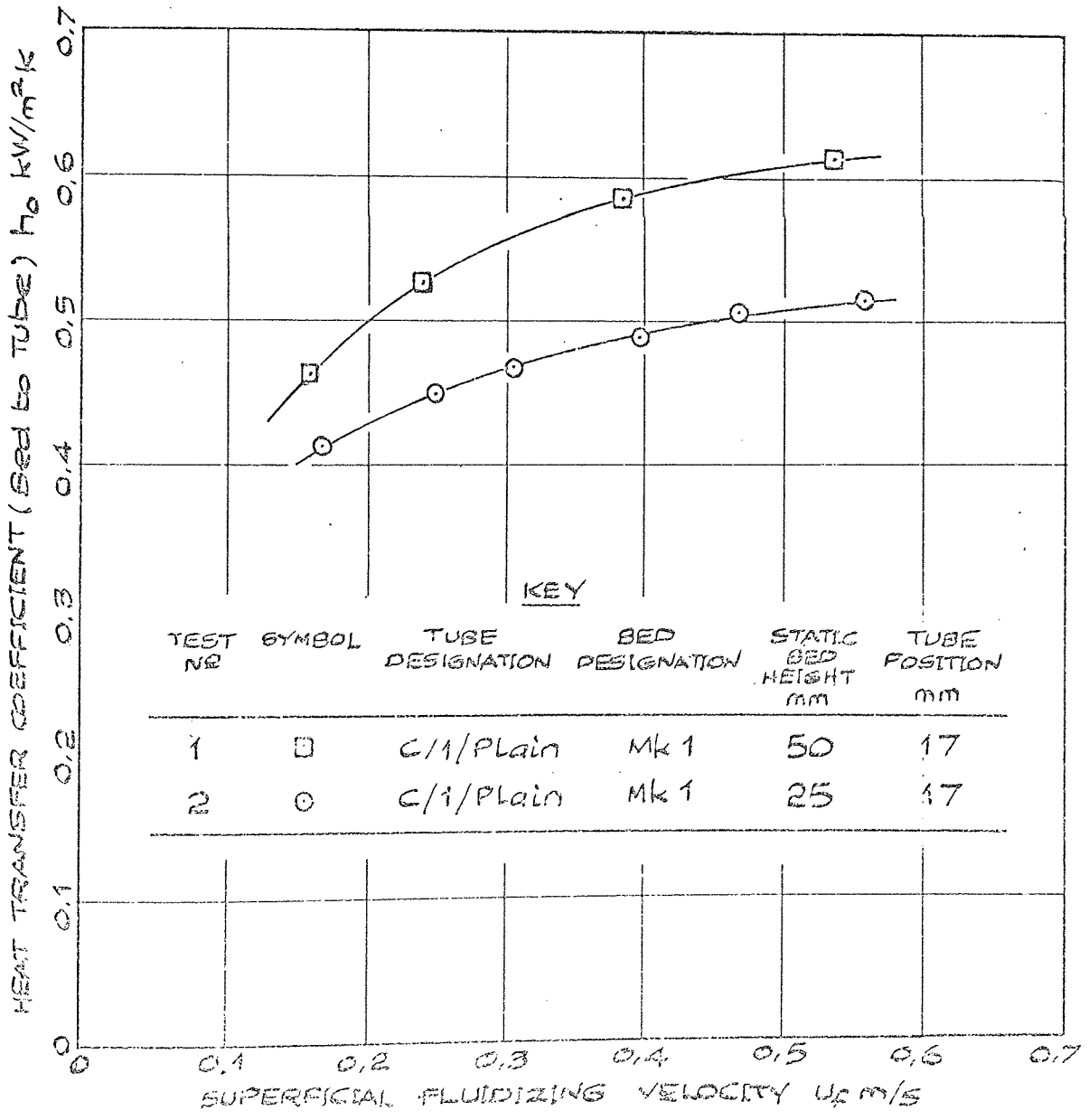

Figure 8.2

EFFECT OF BED MATERIAL ON HEAT TRANSFER COEFFICIENT (Bed to Tube) FOR VARYING FLUIDIZING VELOCITY - HORIZONTAL TUBE IN Mk 3 BED.

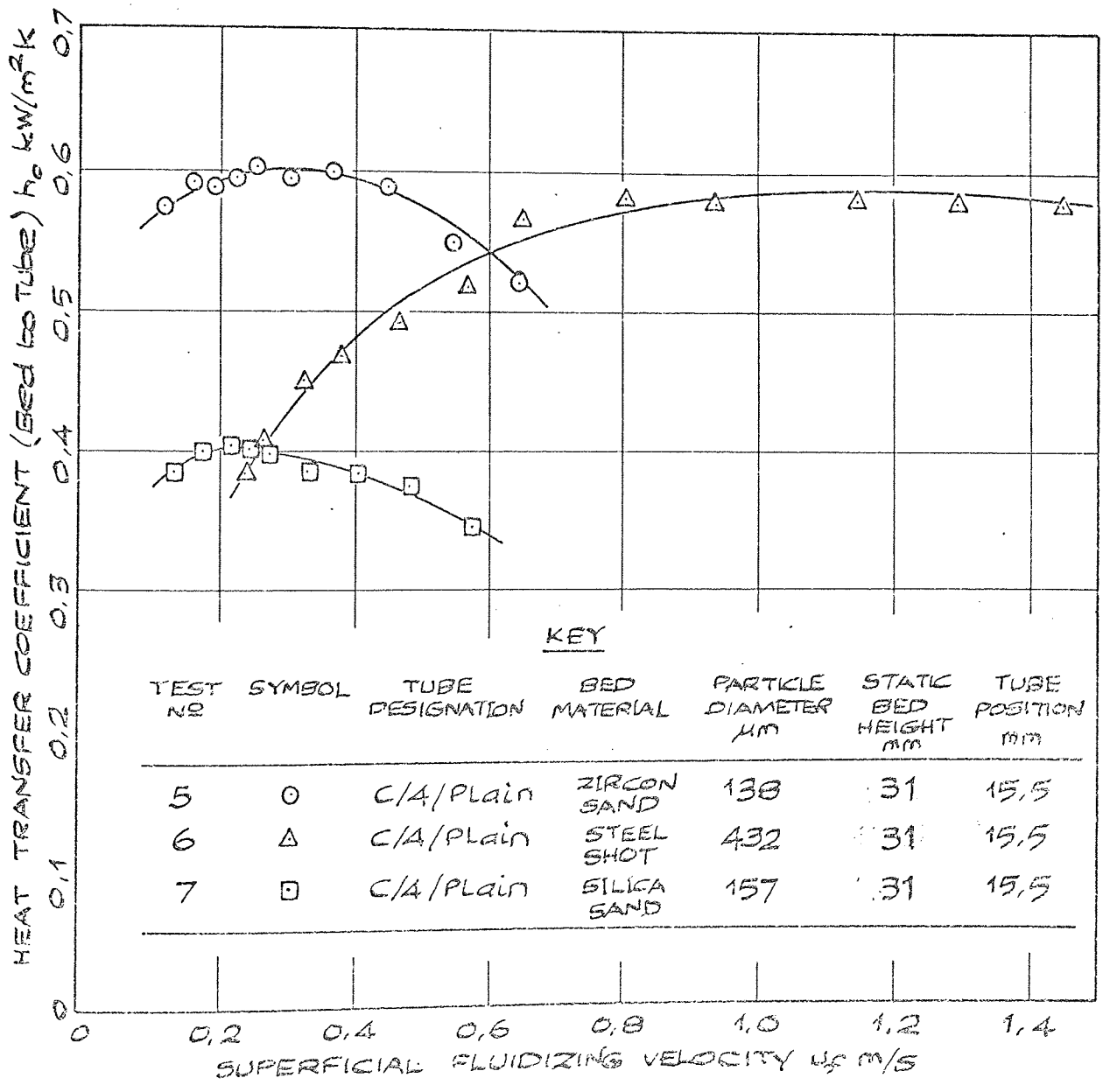

KEY

TEST Nº	SYMBOL	TUBE DESIGNATION	BED MATERIAL	PARTICLE DIAMETER μm	STATIC BED HEIGHT mm	TUBE POSITION mm
5	○	C/4/Plain	ZIRCON SAND	138	31	15,5
6	△	C/4/Plain	STEEL SHOT	432	31	15,5
7	□	C/4/Plain	SILICA SAND	157	31	15,5

Figure 8,3

EFFECT OF BED SIZE ON HEAT TRANSFER COEFFICIENT (Bed to Tube) FOR VARYING FLUIDIZING VELOCITY - HORIZONTAL TUBE IN ZIRCON SAND ($\bar{d}_p$ = 133 μm)

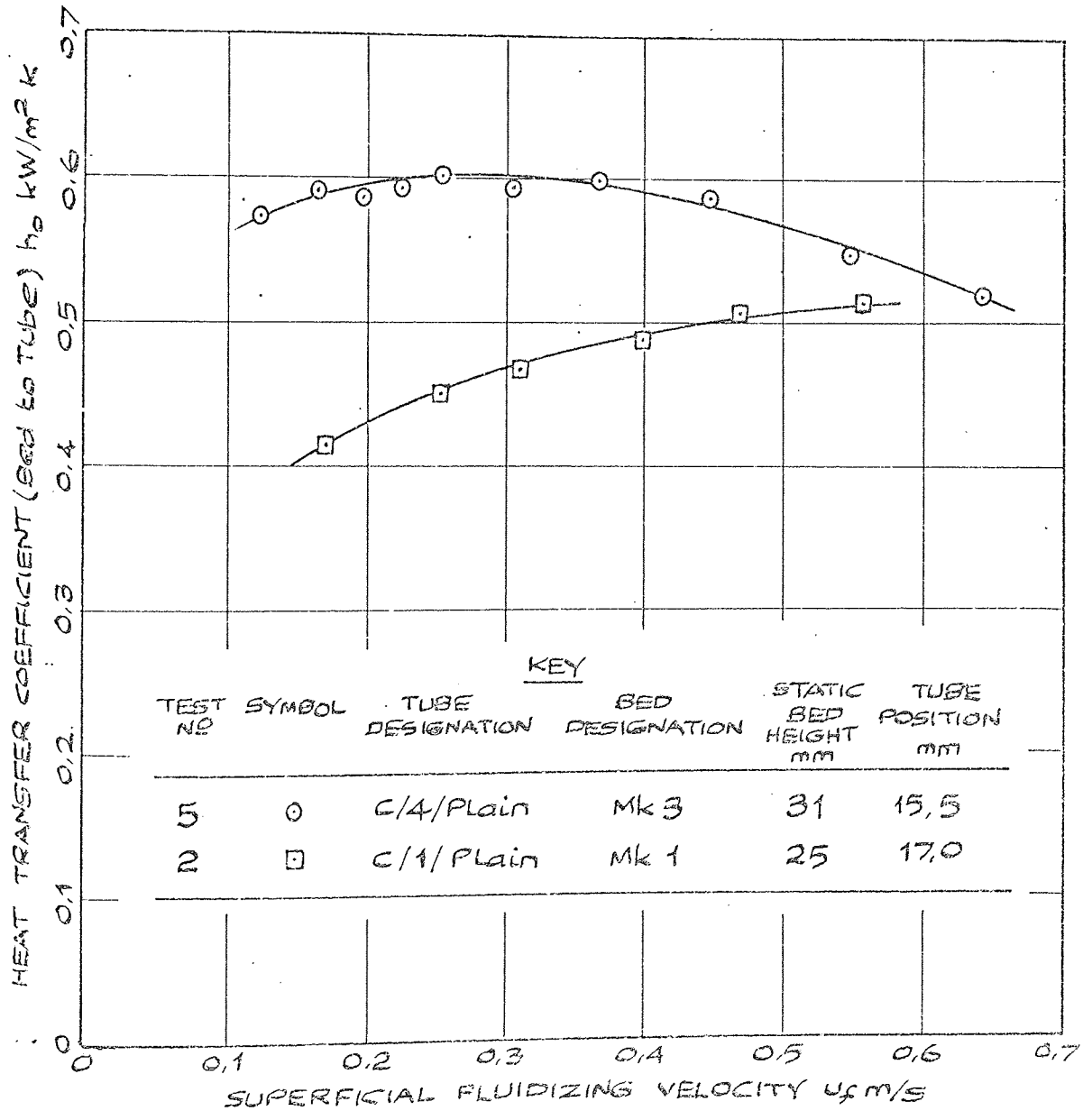

Figure 8,4

EFFECT OF TUBE DIAMETER ON HEAT TRANSFER COEFFICIENT (Bed to Tube) FOR VARYING FLUIDIZING VELOCITY - HORIZONTAL TUBE IN ZIRCON SAND ($\bar{d}_p$ = 138 μm) IN Mk 3 BED.

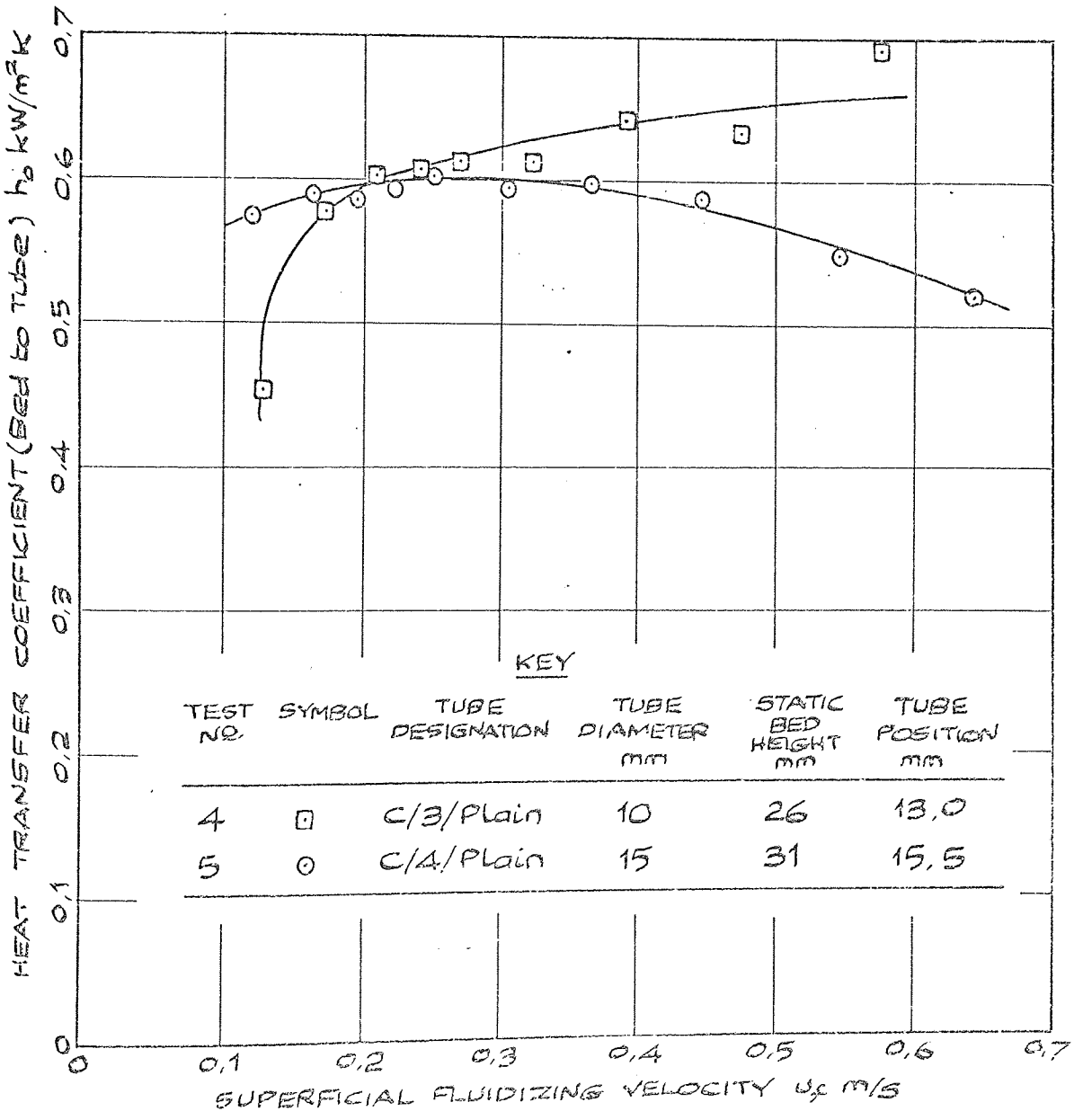

Figure 8.5

EFFECT OF BED SIZE AND TUBE POSITION ON HEAT TRANSFER COEFFICIENT (Bed to Tube) FOR VARYING FLUIDIZING VELOCITY - HORIZONTAL TUBE IN ZIRCON SAND (d_p = 138 μm)

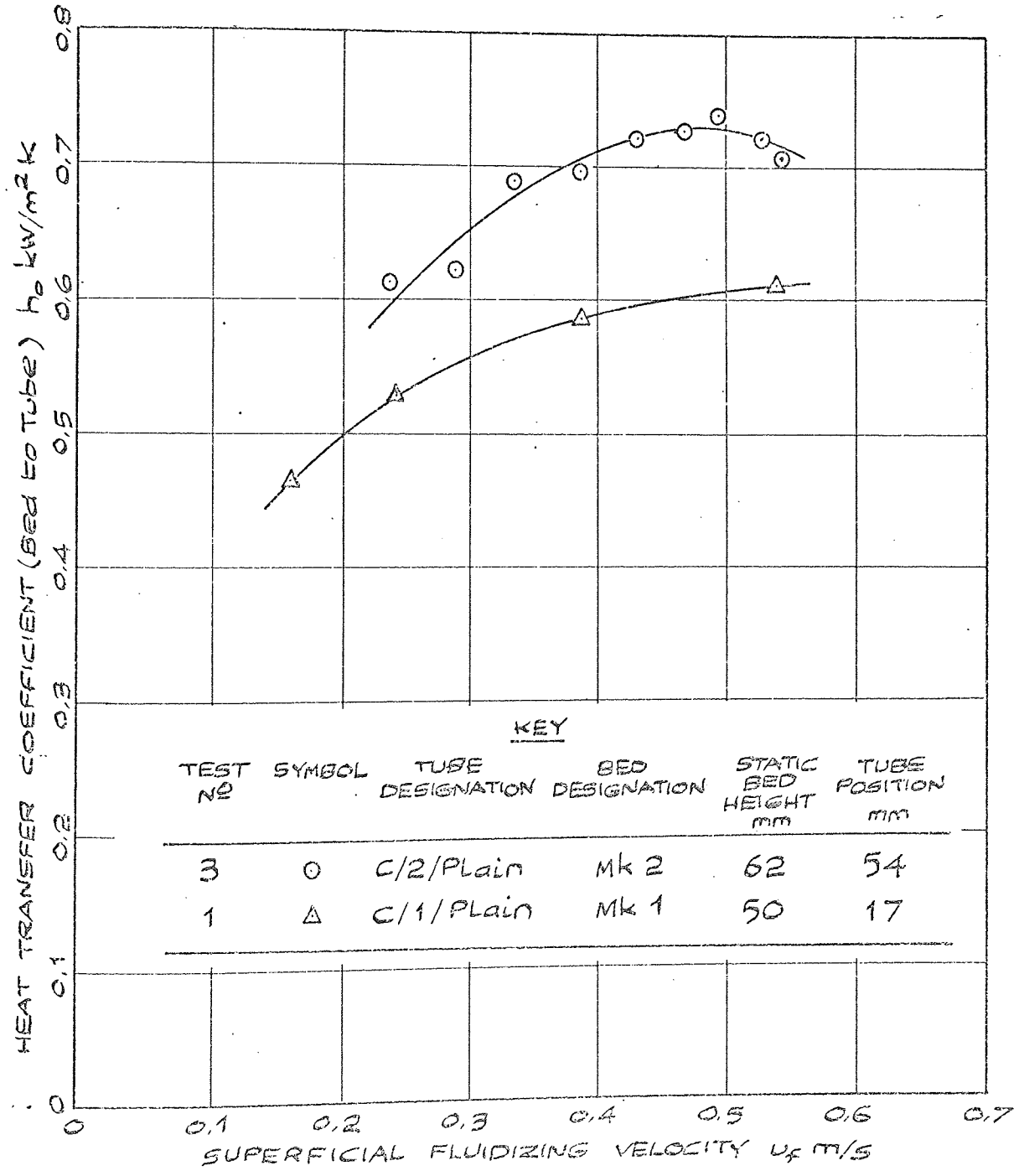

Figure 8.6

COMPARISON OF HEAT TRANSFER COEFFICIENT (Bed to Tube) BETWEEN PLAIN AND OVAL HORIZONTAL TUBE FOR VARYING FLUIDIZING VELOCITY – BED MATERIAL: ZIRCON SAND ($\bar{d}_p$ = 138 μm).

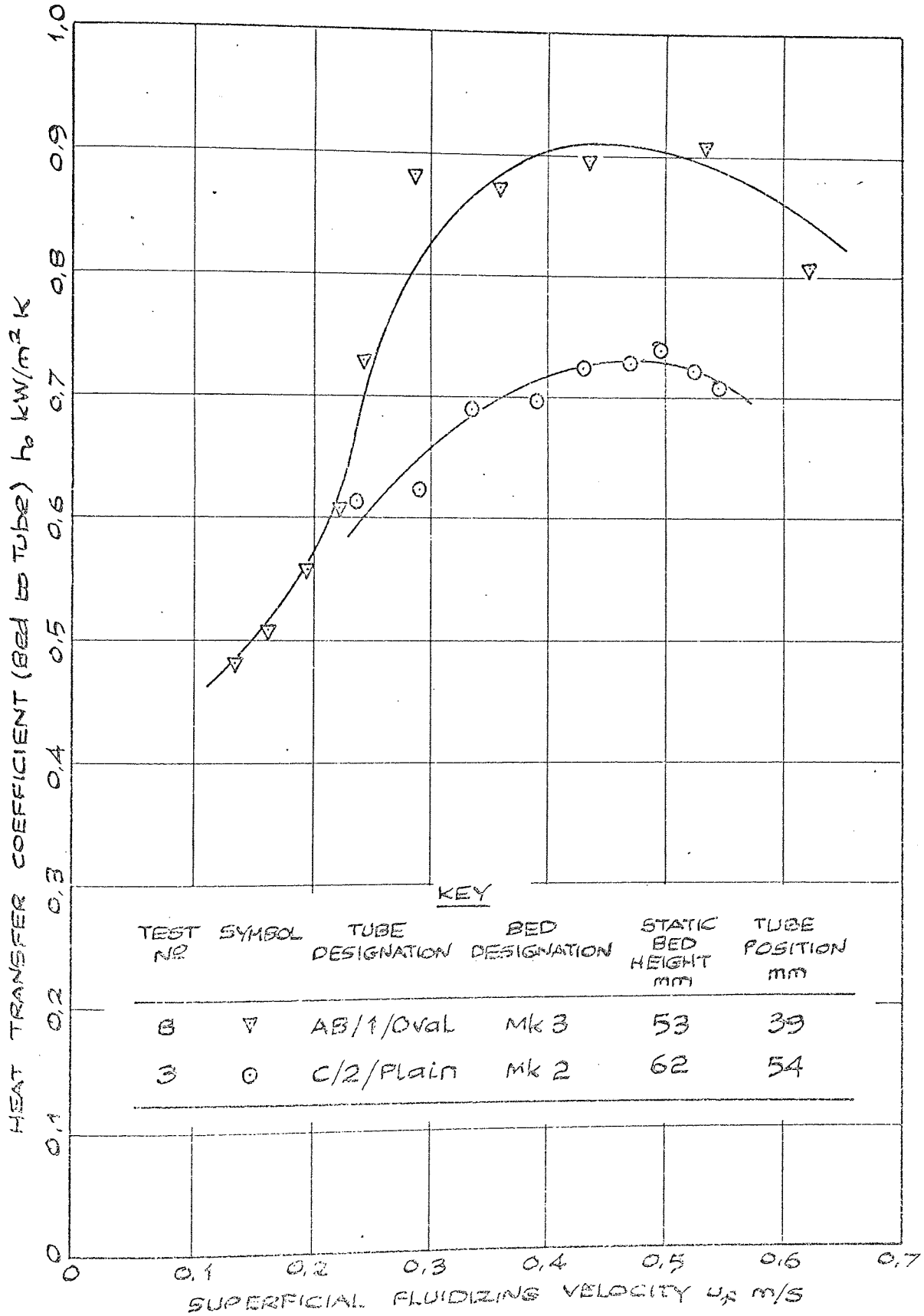

Figure 8.7 EFFECT OF TUBE ORIENTATION ON HEAT TRANSFER COEFFICIENT (Bed to Tube) FOR VARYING FLUIDIZING VELOCITY - HORIZONTAL OVAL TUBE AB/1/Oval IN ZIRCON SAND ($\bar{d}_p$ = 138 μm) IN Mk 3 BED.

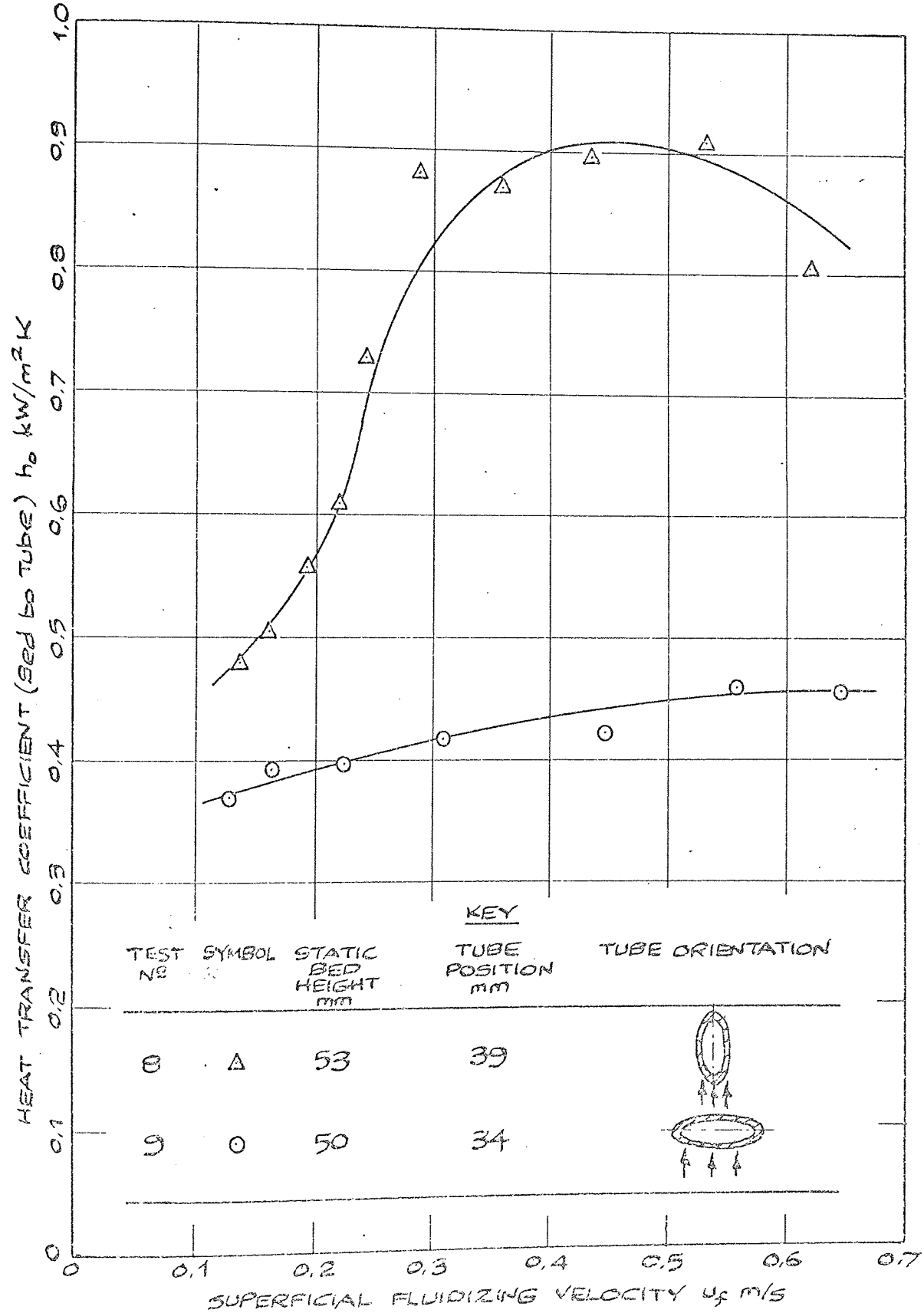

Figure 8.8 EFFECT OF TUBE ORIENTATION ON OVERALL HEAT TRANSFER COEFFICIENT FOR VARYING FLUIDIZING VELOCITY - HORIZONTAL OVAL TUBE AB/1/Oval IN ZIRCON SAND ($\bar{d}_p$ = 138 μm) IN Mk 3 BED

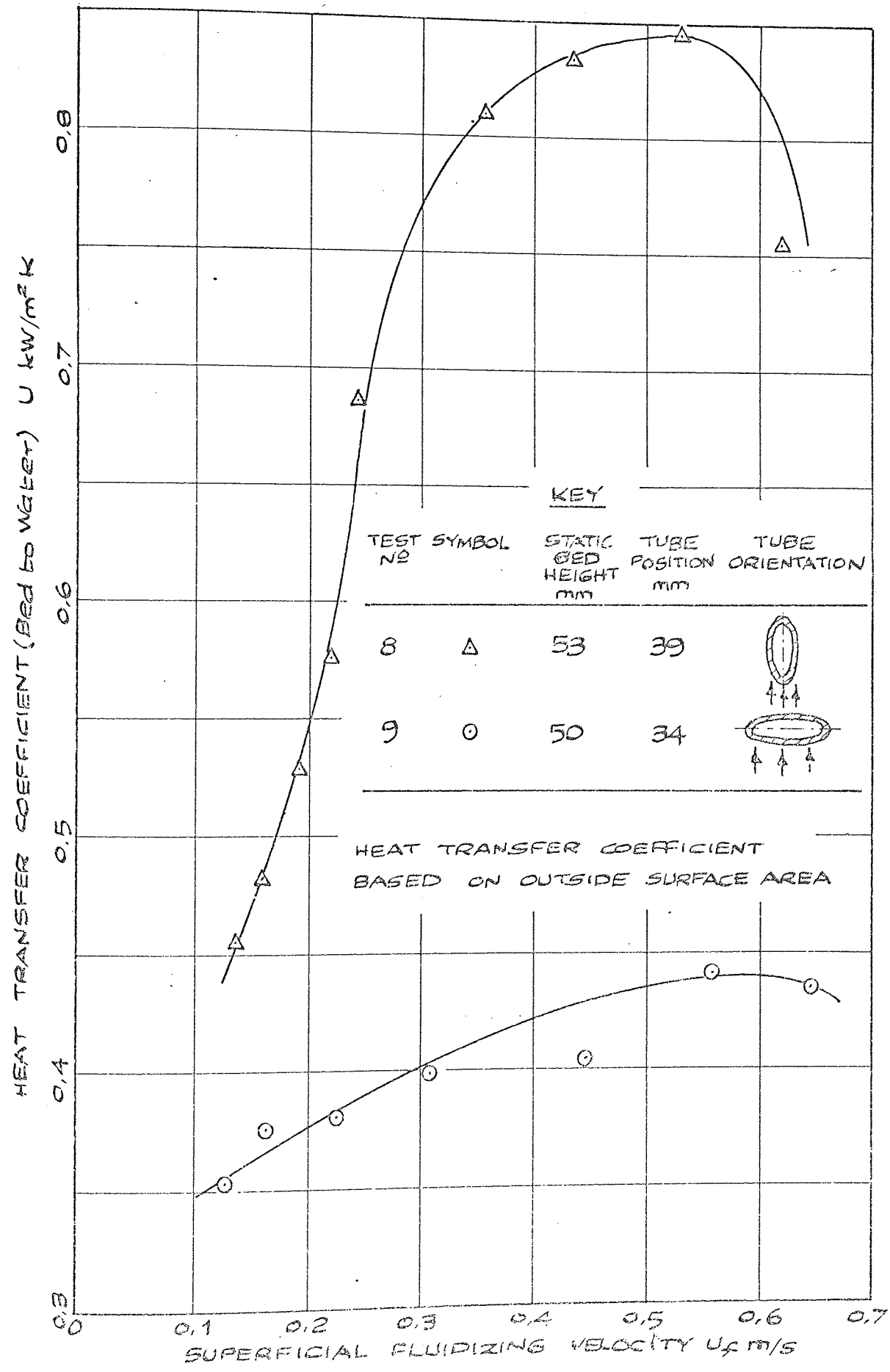

8.2.2 Graph Plotter Results for Plain Tube Surfaces

The following figures 8.9 to 8.11 inclusive are the graph plotter results using the presentation programme outlined in Appendix A2. The regression equation given in Appendix A6, section A6.2 was used, together with the following typical values:-

BEDMK2 = 1 MASHOT = 1 MASICA = 1
STATHT = 50 mm POSITN = 17.5 mm
TUBDIA = 15 mm VELOTY = 0.5 m/s
VELSQU = 0.25 m^2/s^2 TEMBED = 250°C
PRODUD = 7.5 mm x m/s PROUUD = 3.75 mm x m^2/s^2
VELSHT = 0.5 m/s VELSIC = 0.5 m/s

It will be noted from section A6.2 that BEDMK3 is not included in the regression set and therefore does not require a typical value. The graphs that follow are "typical" for plain tube surfaces in BEDMK1 or BEDMK3 configurations using zircon sand as the bed material.

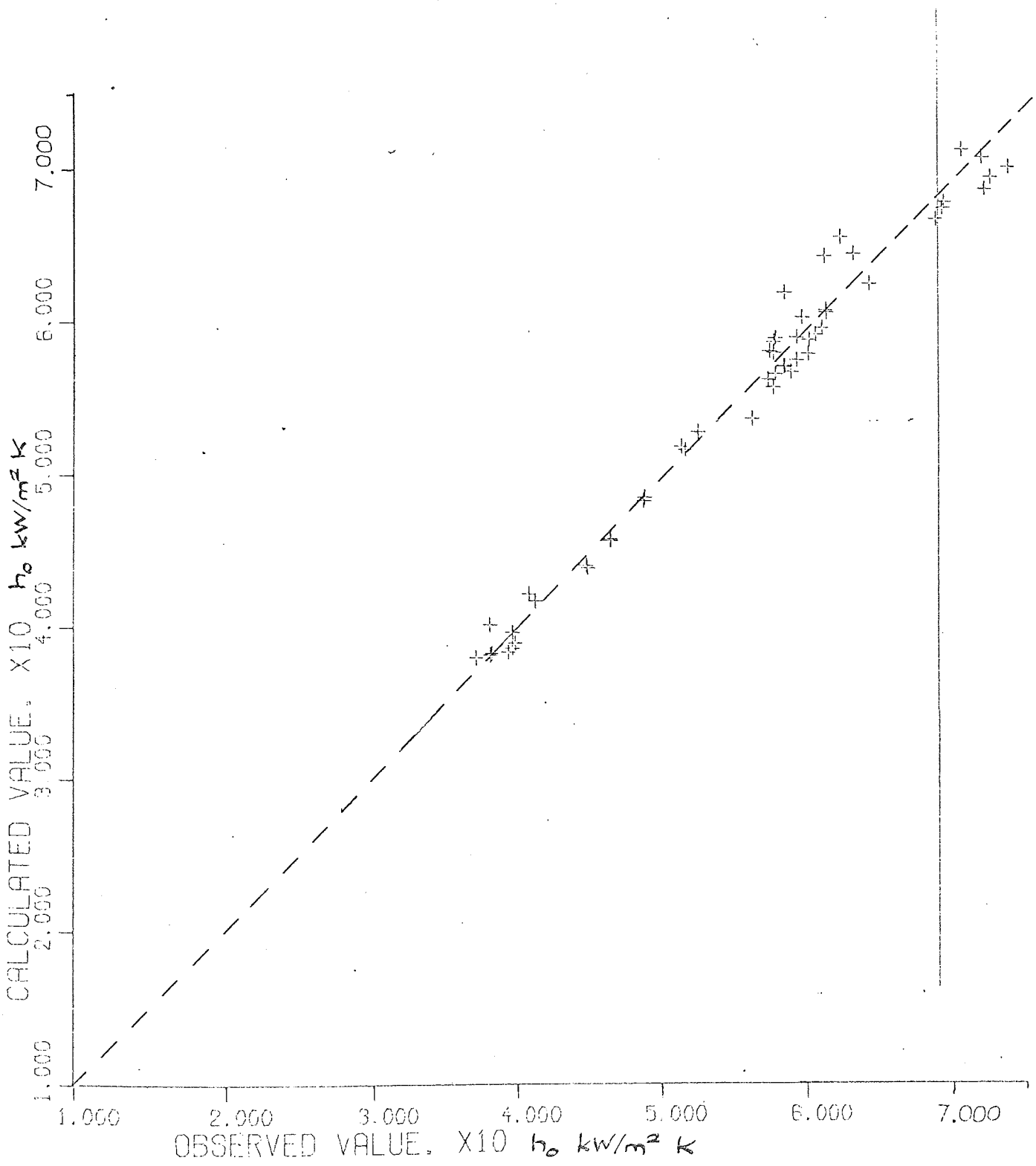

Figure 8.9

OBSERVED V. CALCULATED.

Statistical Analysis of Plain Tube Results

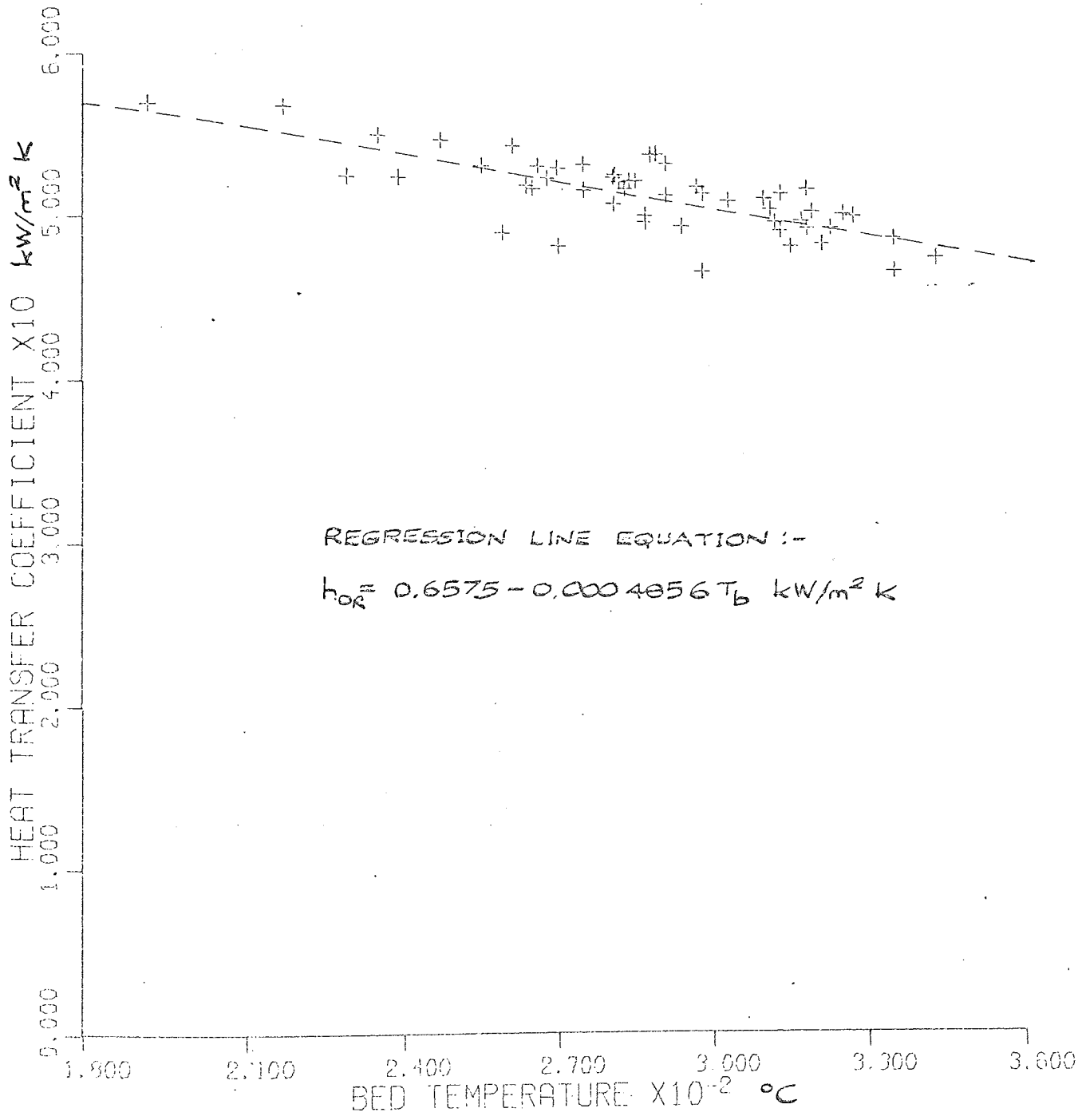

Figure 8,10

HO VERSUS BED TEMPERATURE

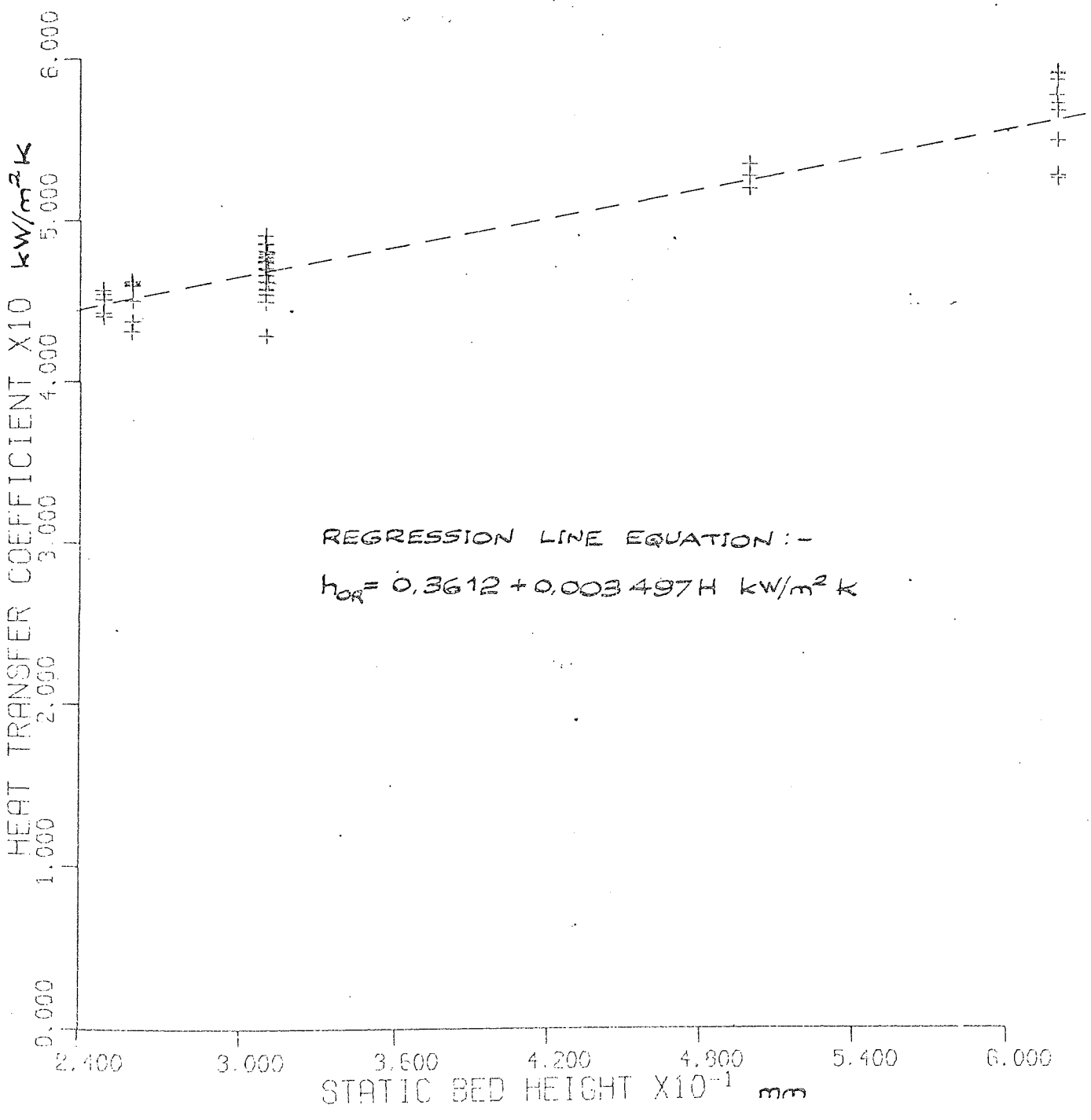

Figure 8.11

HO VERSUS STATIC BED HEIGHT

Statistical Analysis of Plain Tube Results

8.3 Square Fin Tube Results

Figure 8.12

VARIATION OF BED TO METAL HEAT TRANSFER COEFFICIENT FOR EXTENDED SURFACE C/1/MS IN MK 1 BED — MATERIAL ZIRCON SAND TO STATIC HEIGHT OF 75 mm. ($\bar{d}_p$ = 138 μm)

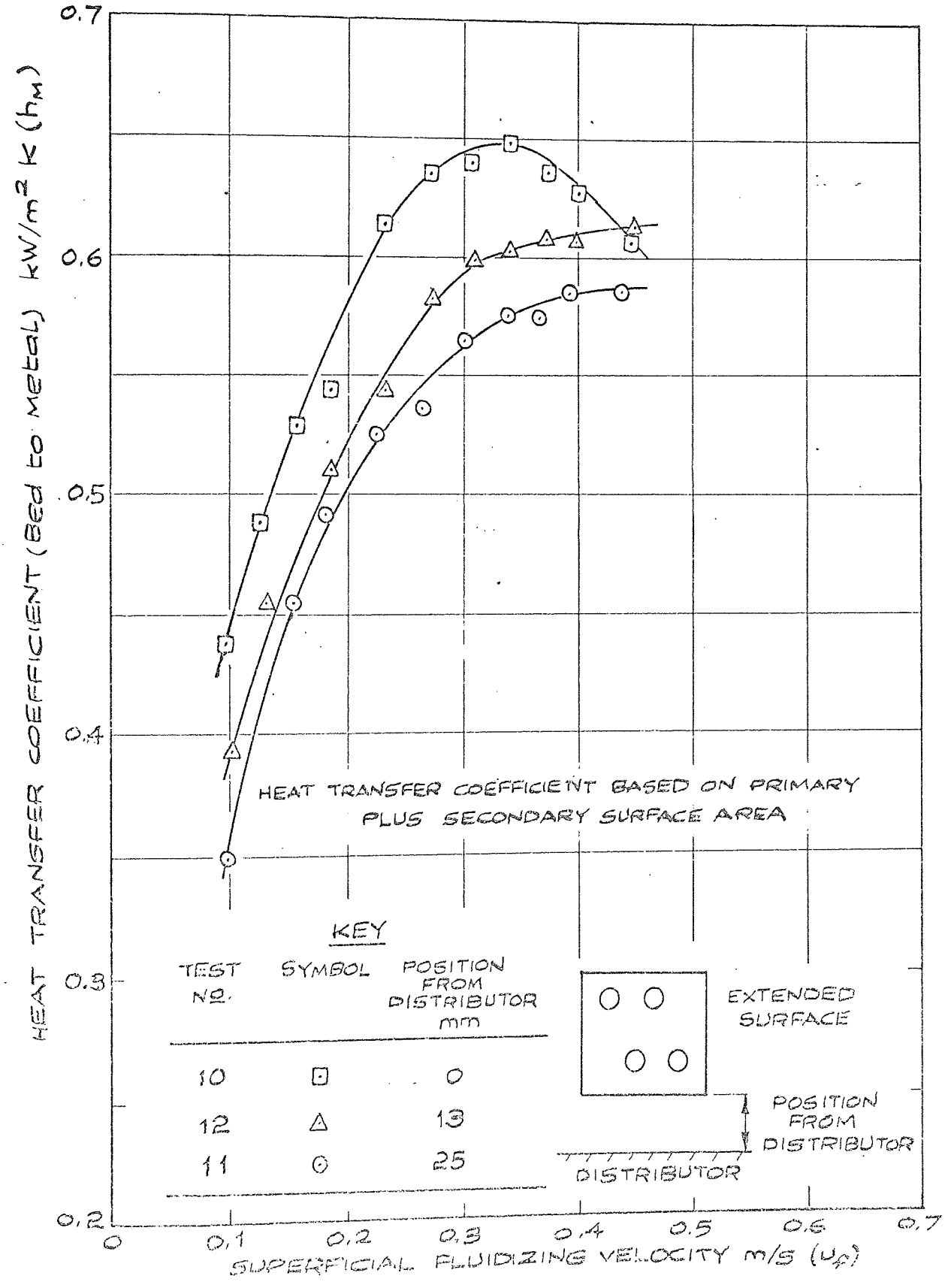

Figure 8.13

EFFECT OF SURFACE POSITION ON OVERALL HEAT TRANSFER COEFFICIENT FOR VARYING FLUIDIZING VELOCITY - EXTENDED SURFACE C/1/MS IN ZIRCON SAND ($\bar{d}_p$ = 138 μm) IN MK 1 BED.

STATIC BED HEIGHT 75 mm

HEAT TRANSFER COEFFICIENT BASED ON BASIC TUBE OUTSIDE SURFACE AREA

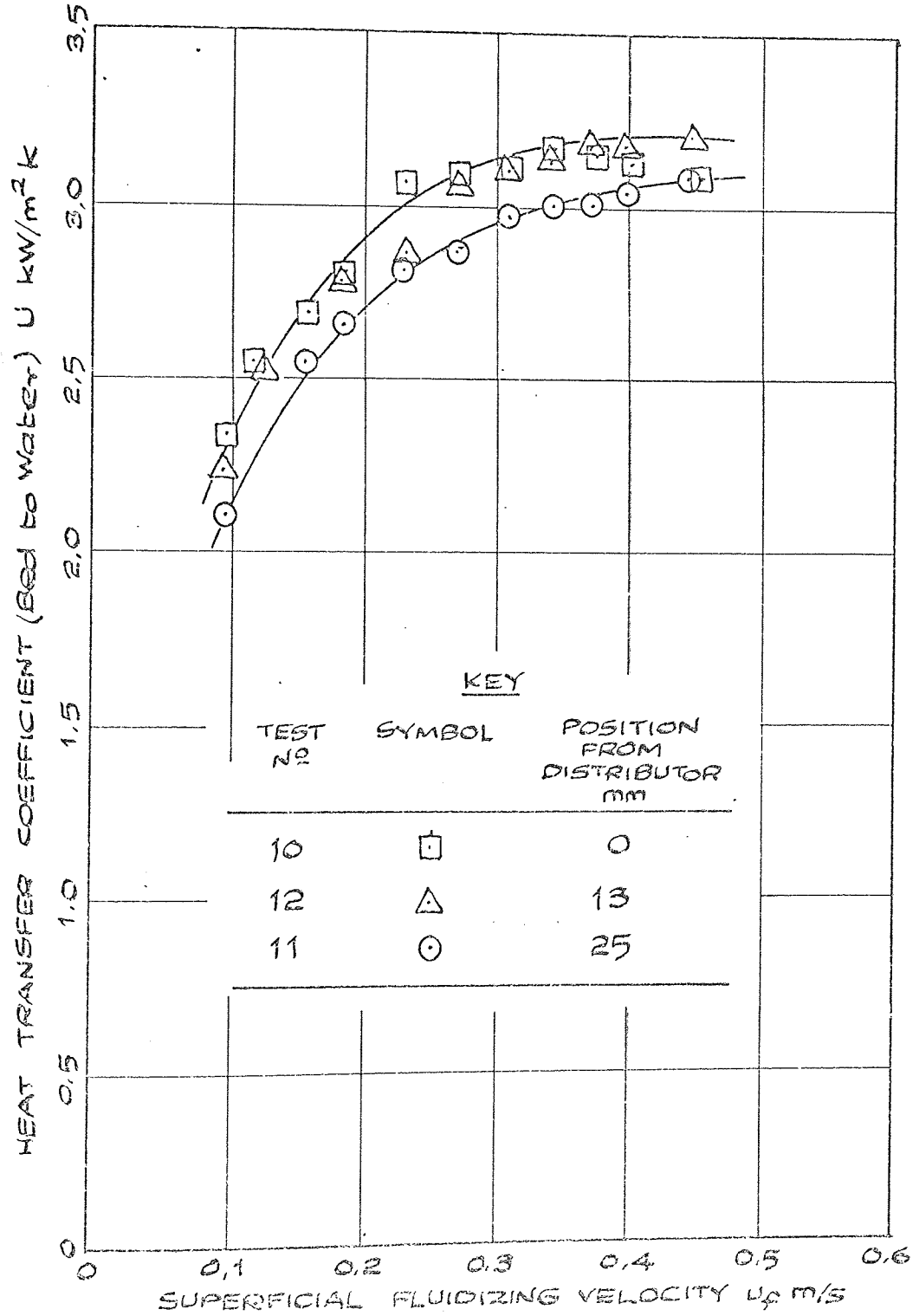

Figure 8.14

EFFECT OF STATIC BED HEIGHT ON BED TO METAL HEAT TRANSFER COEFFICIENT FOR EXTENDED SURFACE C/1/MS IN Mk 1 BED - MATERIAL ZIRCON SAND HEAT TRANSFER COEFFICIENT BASED ON PRIMARY PLUS SECONDARY SURFACE AREA

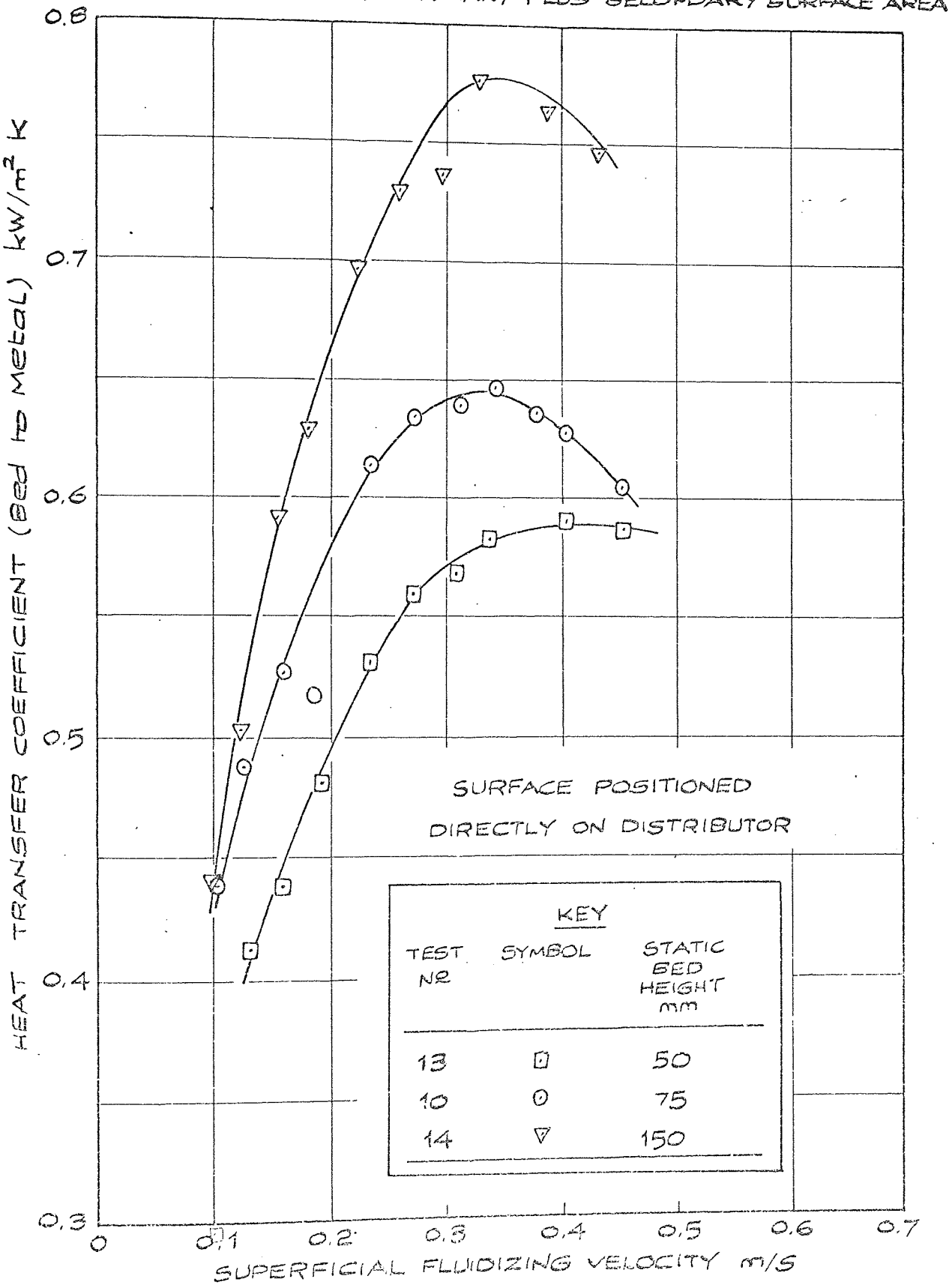

Figure 8.15

EFFECT OF STATIC BED HEIGHT ON OVERALL HEAT TRANSFER COEFFICIENT FOR VARYING FLUIDIZING VELOCITY - EXTENDED SURFACE C/1/MS IN ZIRCON SAND ($\bar{d}_p$ = 138 μm) IN MK 1 BED.

HEAT TRANSFER COEFFICIENT BASED ON BASIC TUBE OUTSIDE SURFACE AREA.

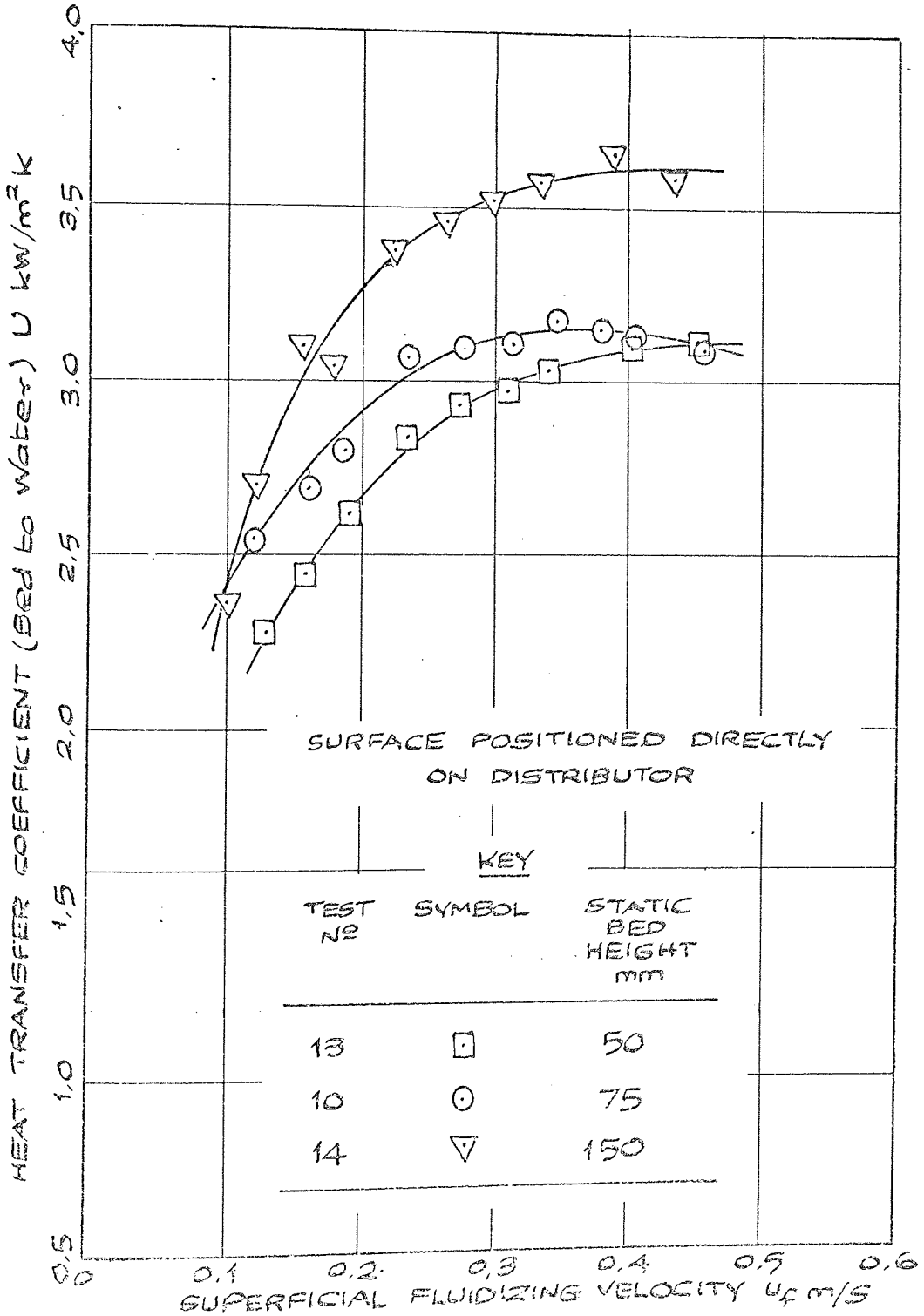

Figure 8.16

YARIATION OF BED TO METAL HEAT TRANSFER COEFFICIENT FOR EXTENDED SURFACE C/1/MS IN Mk1 BED — MATERIAL ZIRCON SAND TO STATIC HEIGHT OF 150 mm ($\bar{d}_p$ = 138 μm).

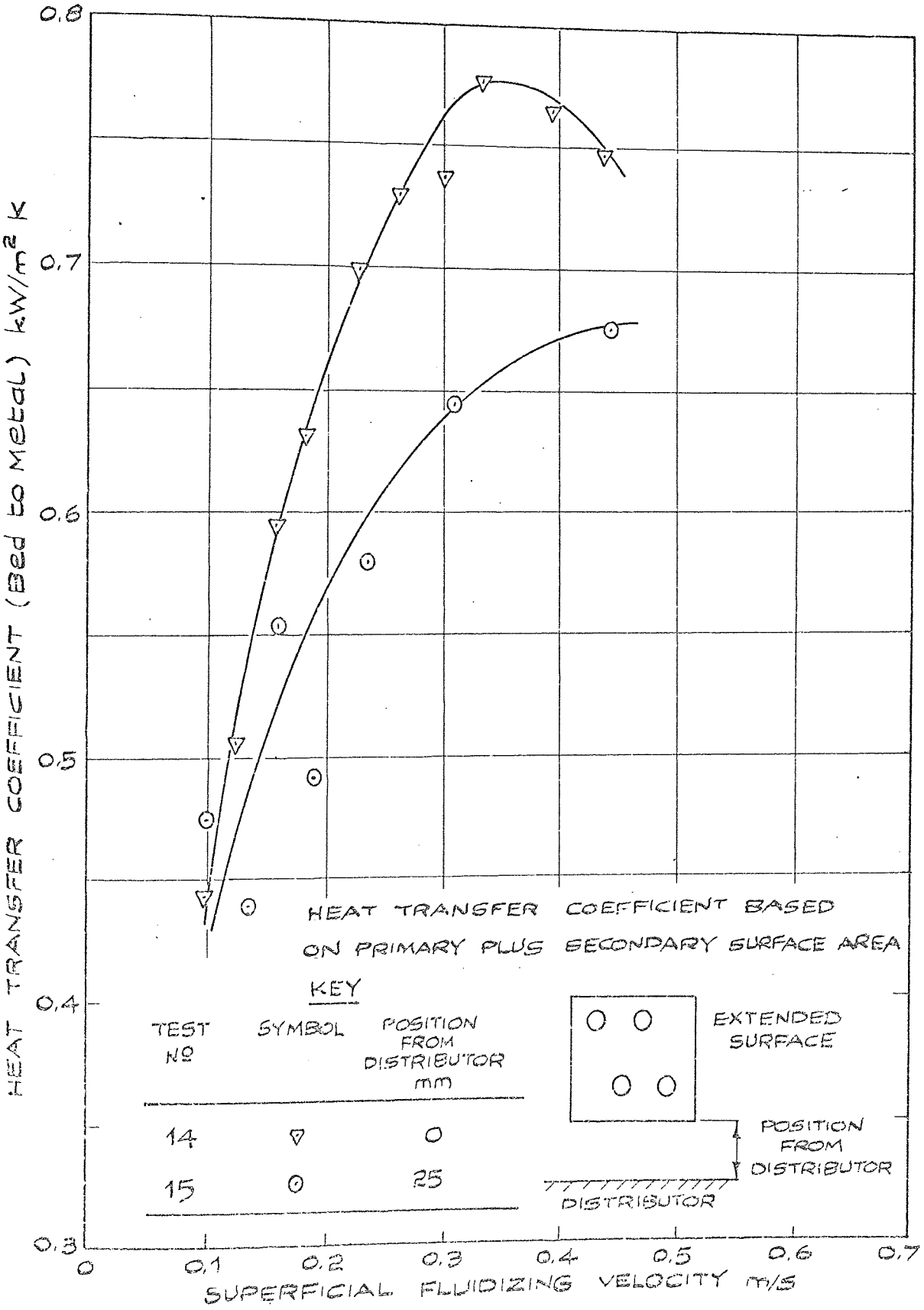

Figure 8.17 EFFECT OF SURFACE POSITION ON OVERALL HEAT TRANSFER COEFFICIENT FOR VARYING FLUIDIZING VELOCITY - EXTENDED SURFACE C/1/MS IN ZIRCON SAND (d_p = 138 μm) IN Mk 1 BED.

STATIC BED HEIGHT 150 mm

HEAT TRANSFER COEFFICIENT BASED ON BASIC TUBE OUTSIDE SURFACE AREA.

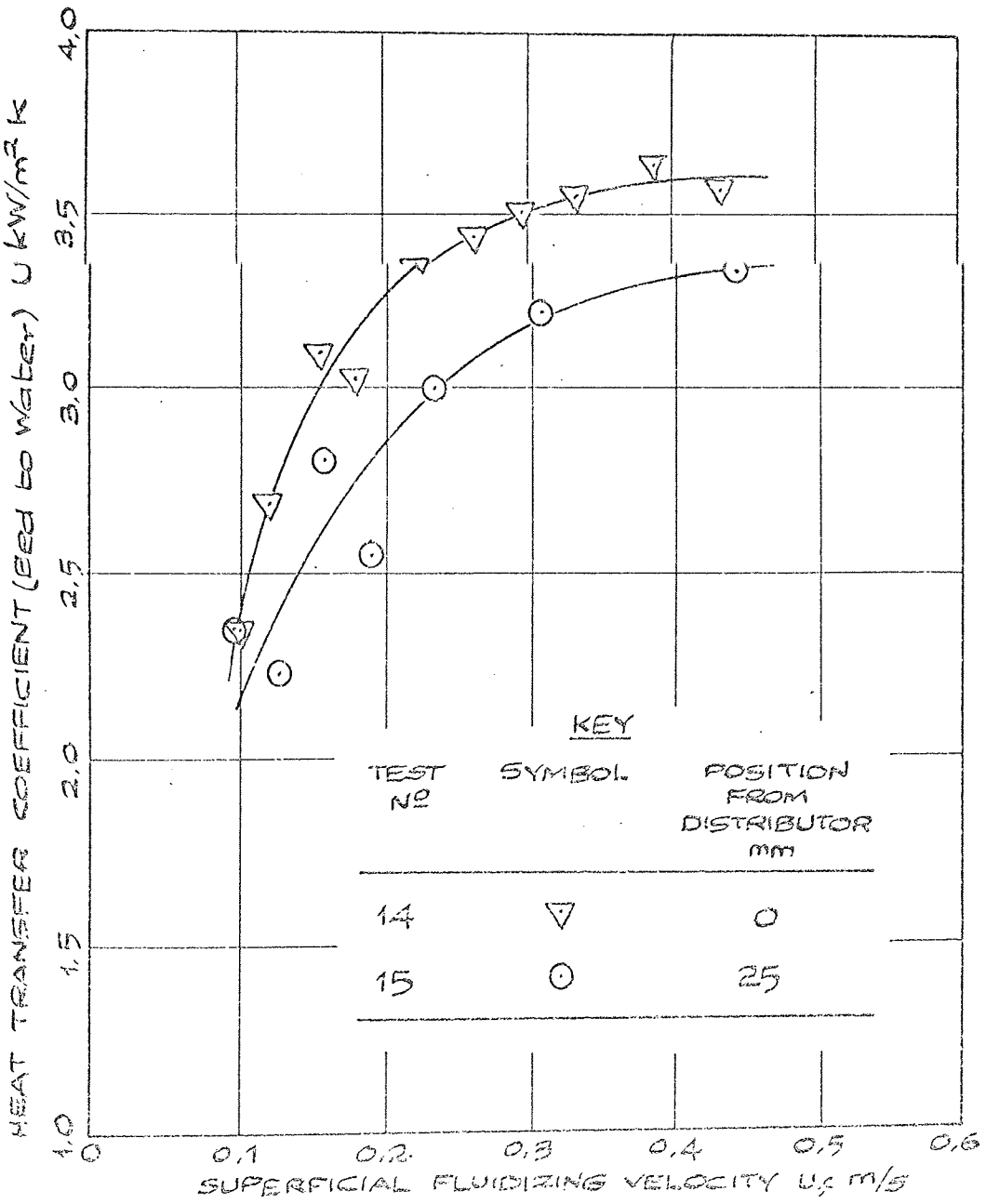

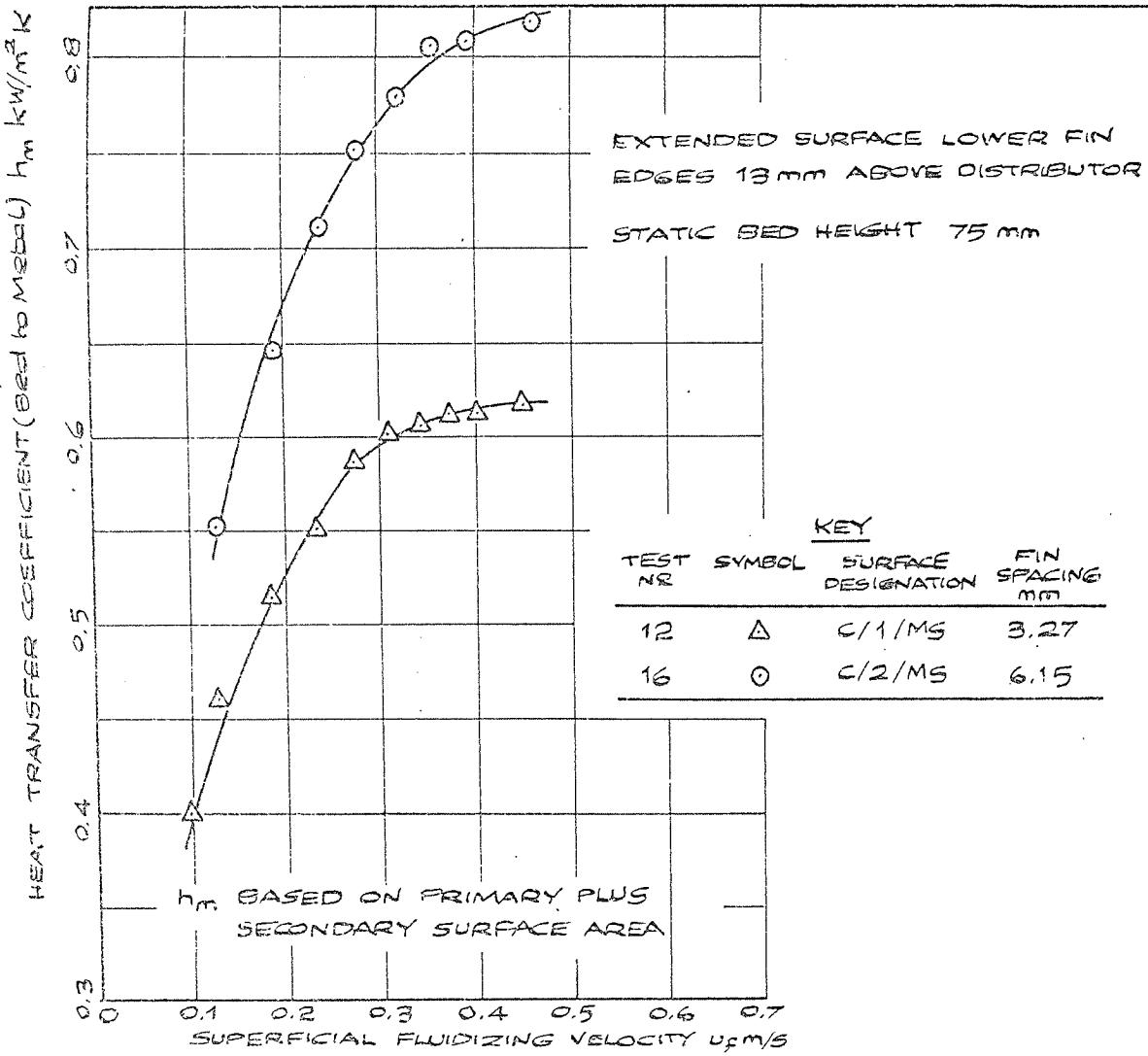

FIGURE 8.18

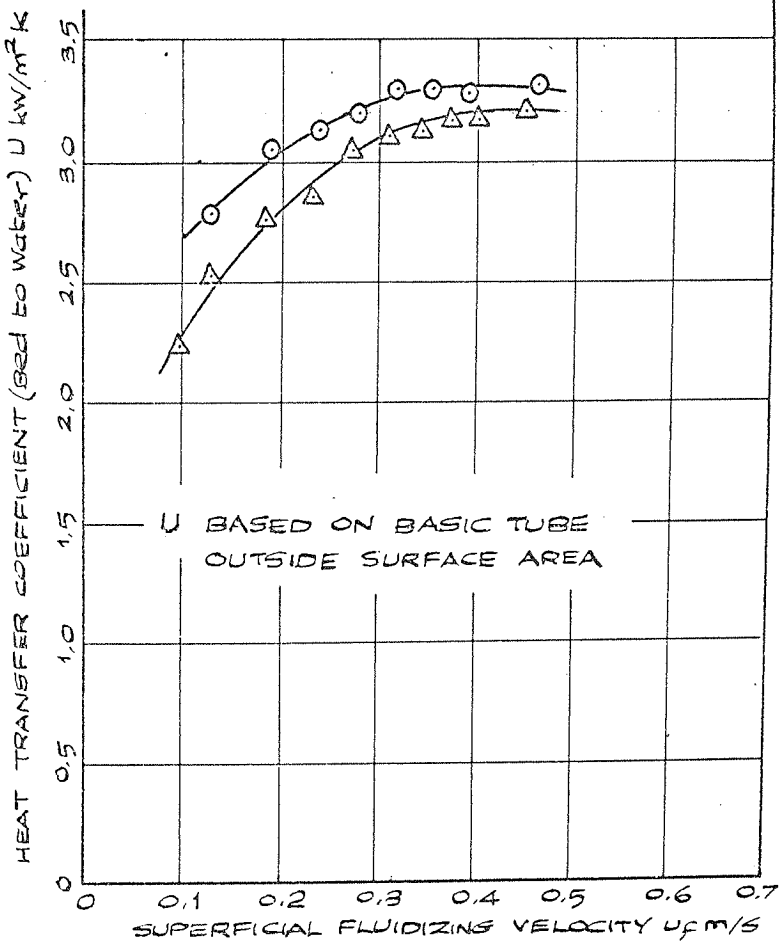

FIGURE 8.19

EFFECT OF FIN SPACING ON HEAT TRANSFER COEFFICIENTS FOR VARYING FLUIDIZING VELOCITY - SQUARE FIN EXTENDED SURFACE IN ZIRCON SAND ($\bar{d}_p$ = 138 μm) IN Mk 1 BED

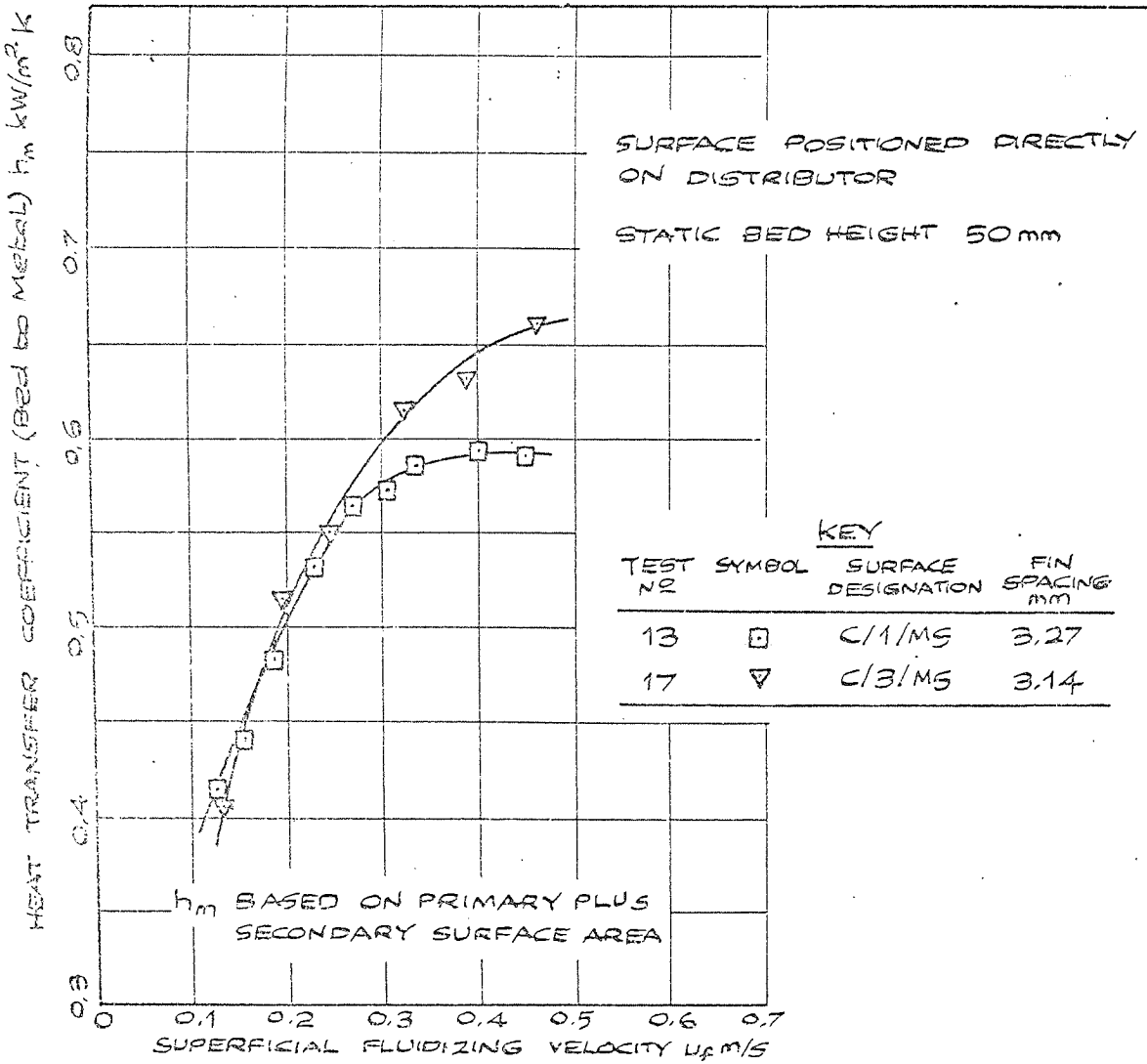

FIGURE 8.20

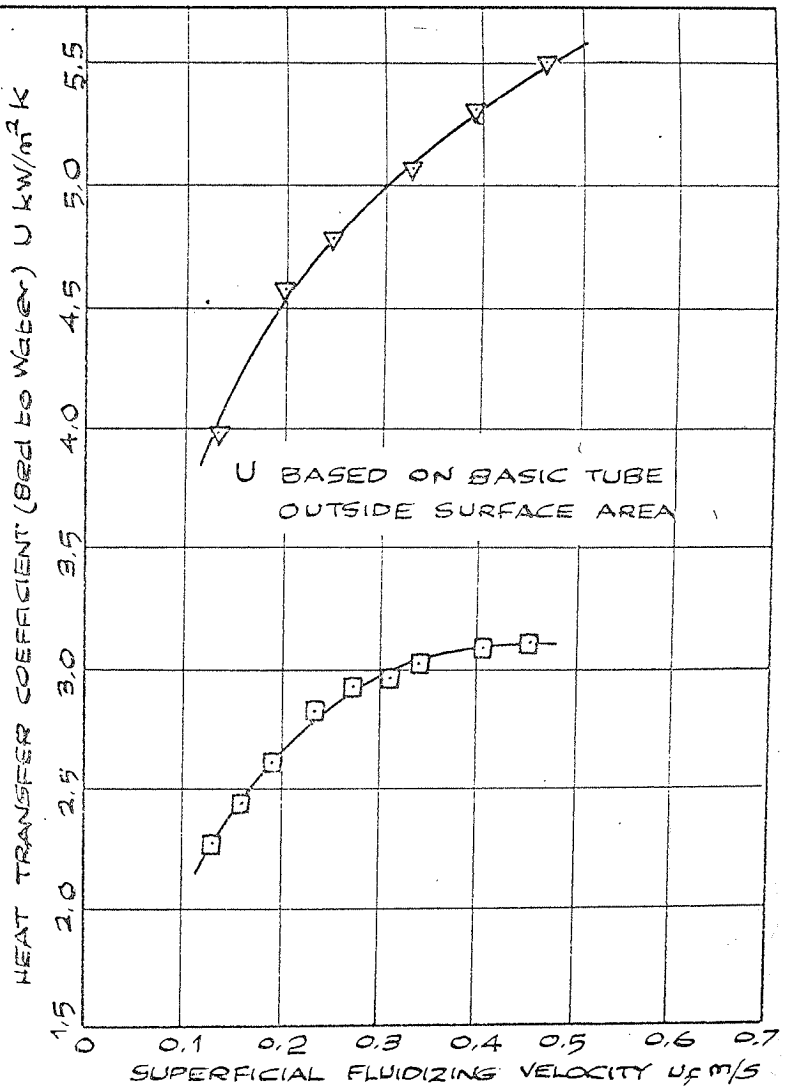

FIGURE 8.21

COMPARISON OF HEAT TRANSFER COEFFICIENTS FOR MANUFACTURED SQUARE FIN EXTENDED SURFACE IN ZIRCON SAND ($\bar{d}_p$ = 138 μm) IN Mk 1 BED

Figure 8.22

EXPERIMENTALLY DETERMINED FIN EFFICIENCIES FOR EXTENDED SURFACE C/1/MS AND C/2/MS IN ZIRCON SAND ($\bar{d}_p$ = 138 μm) IN Mk 1 BED.

STATIC BED HEIGHT 75 mm

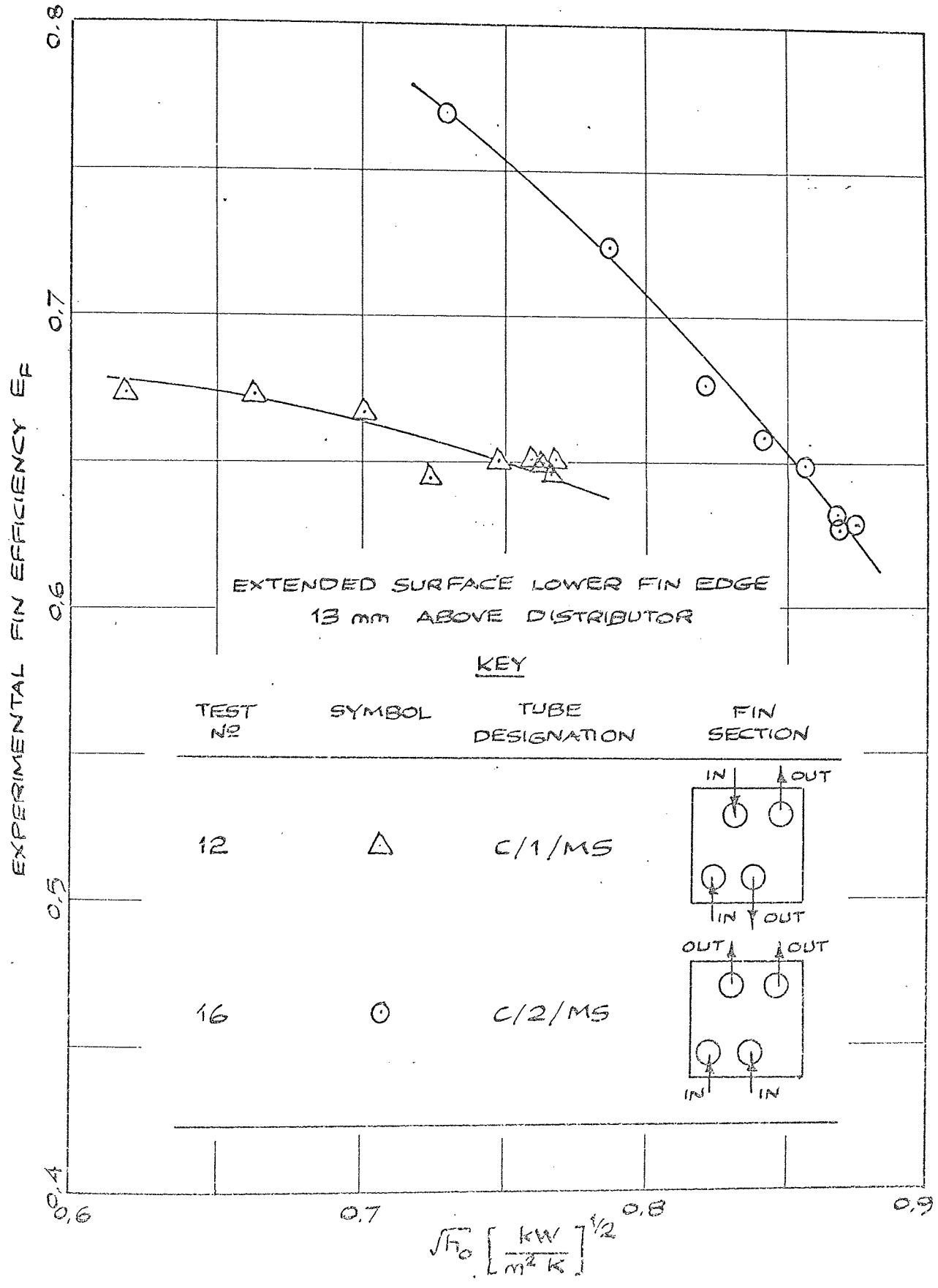

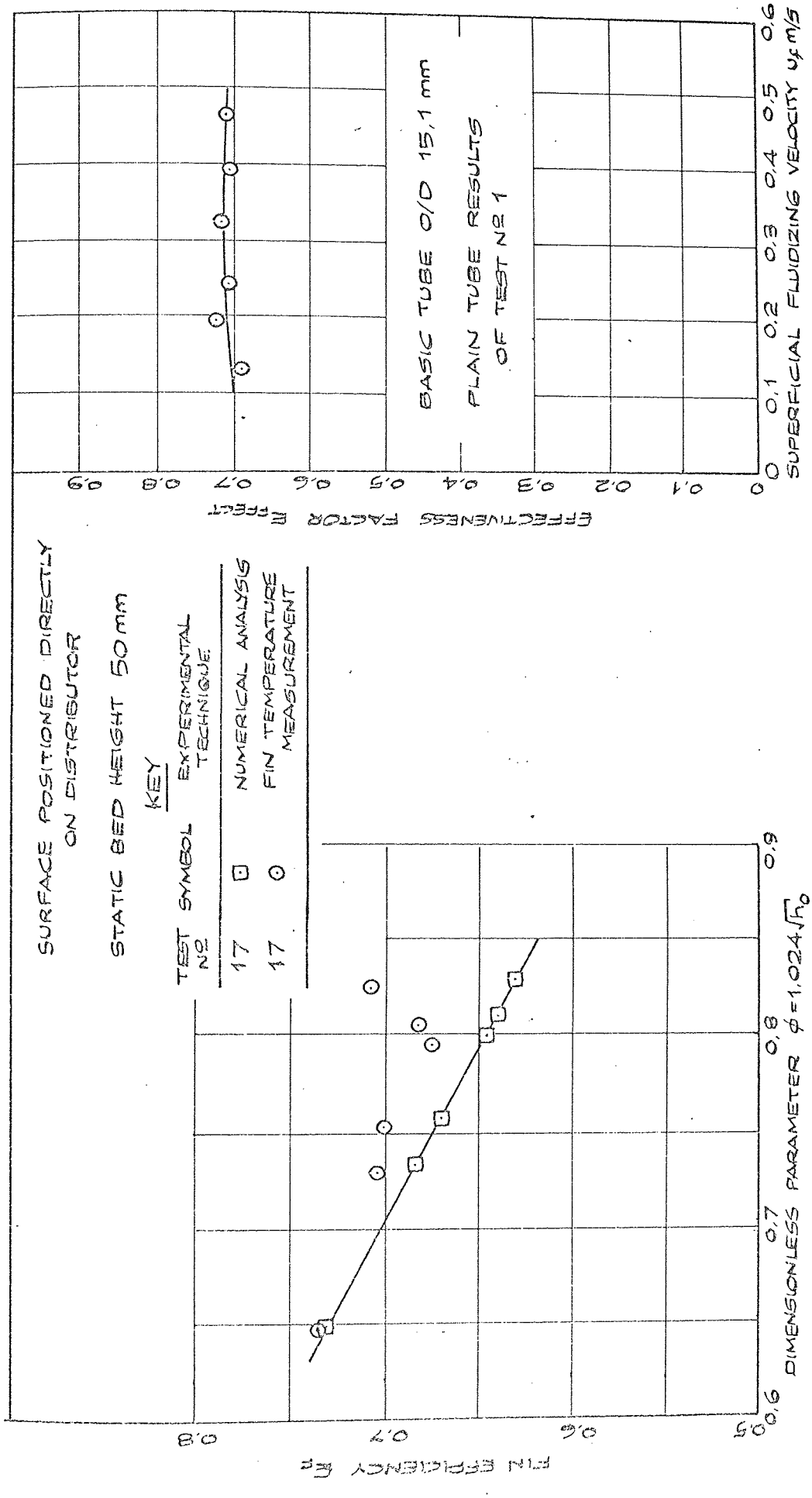

FIGURE 8.24

FIGURE 8.23

COMPARISON OF EXPERIMENTALLY DETERMINED FIN EFFICIENCIES AND EFFECTIVENESS FACTOR FOR SQUARE FIN EXTENDED SURFACE C/3/MS IN ZIRCON SAND ($\bar{d}_p$=138 μm) IN MK 1 BED

8.4 Radial Fin Tube Results

8.4.1 Manufactured Tube Experimental Results

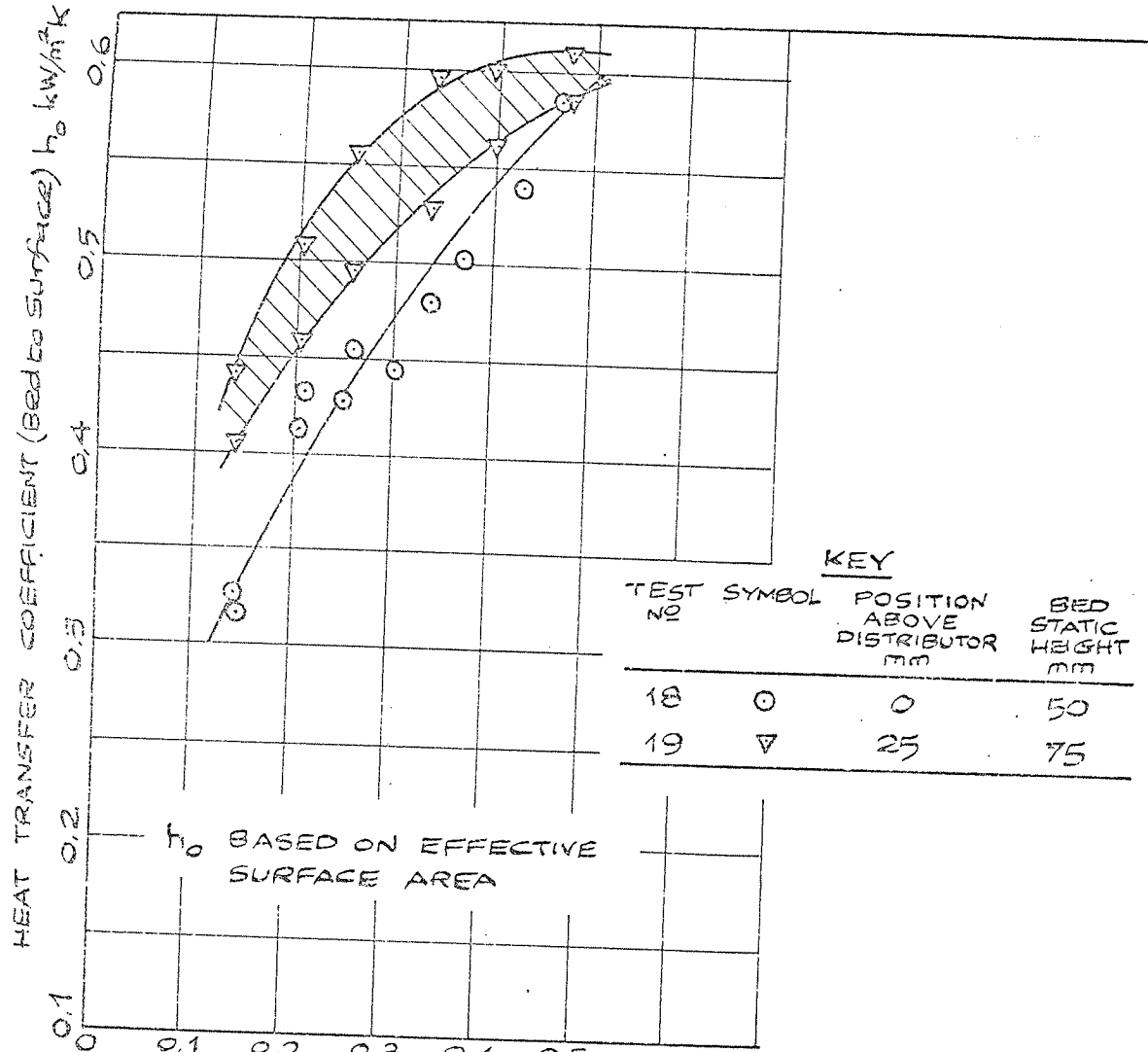

FIGURE 8.25

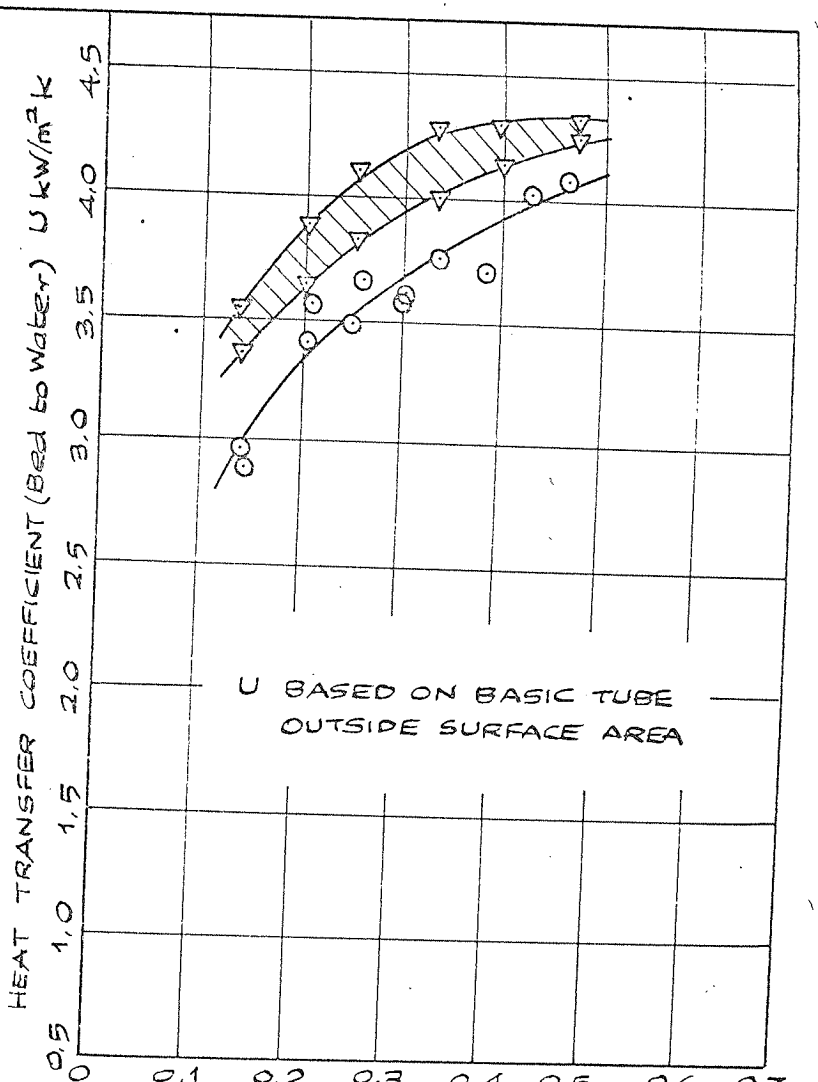

FIGURE 8.26

EFFECT OF SURFACE POSITION AND BED STATIC HEIGHT ON HEAT TRANSFER COEFFICIENTS FOR RADIAL FIN EXTENDED SURFACE C/1/MR IN ZIRCON SAND ($\bar{d}_p$ = 138 μm) IN MK 1 BED.

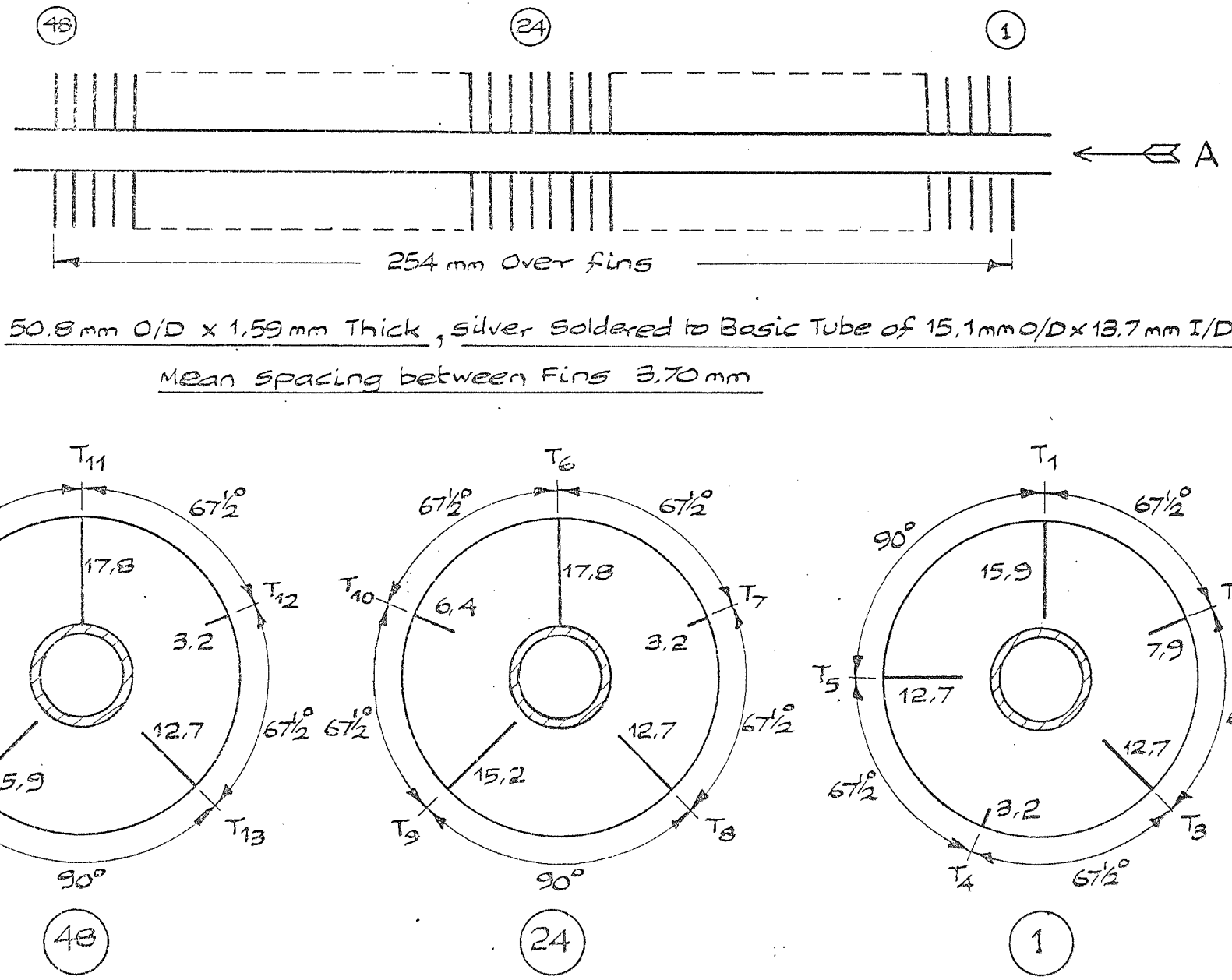

48 Fins, 50.8 mm O/D x 1,59 mm Thick, Silver Soldered to Basic Tube of 15,1 mm O/D x 13,7 mm I/D

Mean Spacing between Fins 3,70 mm

View of Numbered Fins in the Direction of Arrow "A", Thermocouple Packets Drilled to depths shown in mm, each being 1 mm Diameter Central to Fin Thickness.

Figure 8.27 Arrangement of Thermocouples for Surface C/1/M2

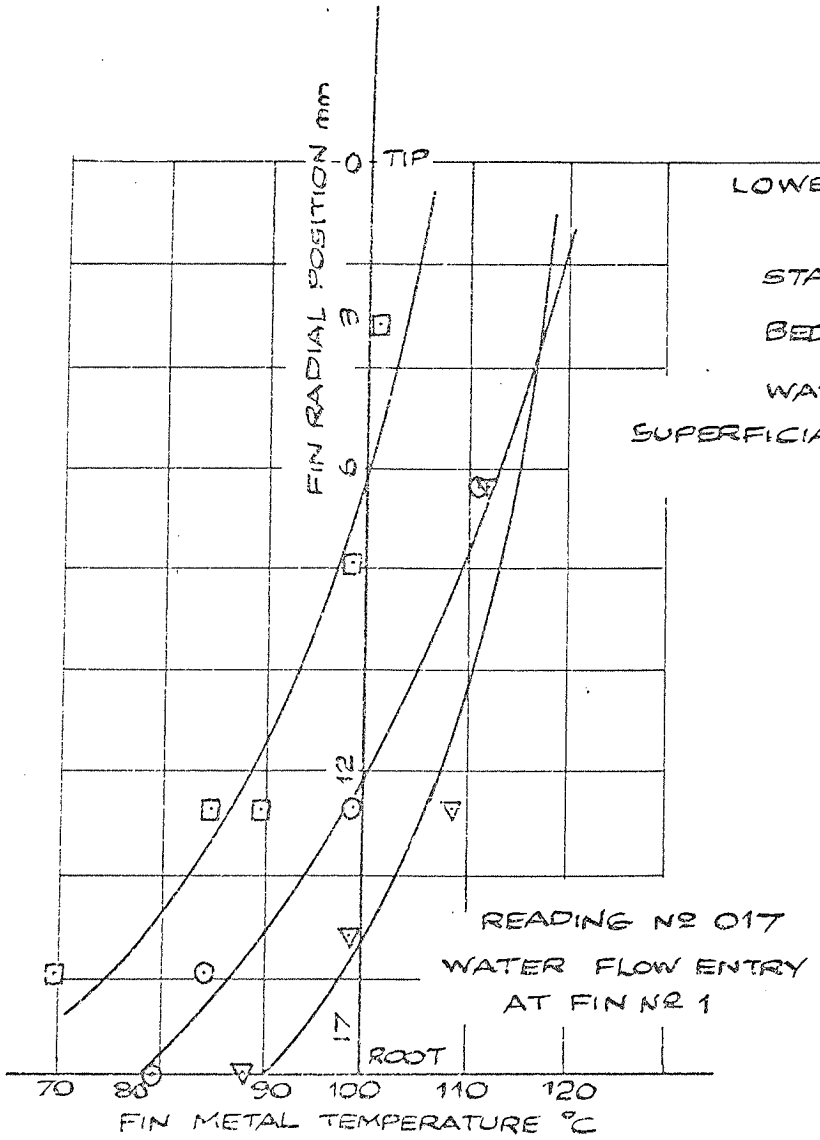

FIGURE 8,28

LOWER FIN EDGE 25 mm ABOVE DISTRIBUTOR

STATIC BED HEIGHT 75 mm

BED TEMPERATURE 204 - 207 °C

WATER TEMPERATURE 29,4 °C

SUPERFICIAL FLUIDIZING VELOCITY 0,4 m/s

KEY

SYMBOL	FIN Nº
⊡	1
▽	24
⊙	48

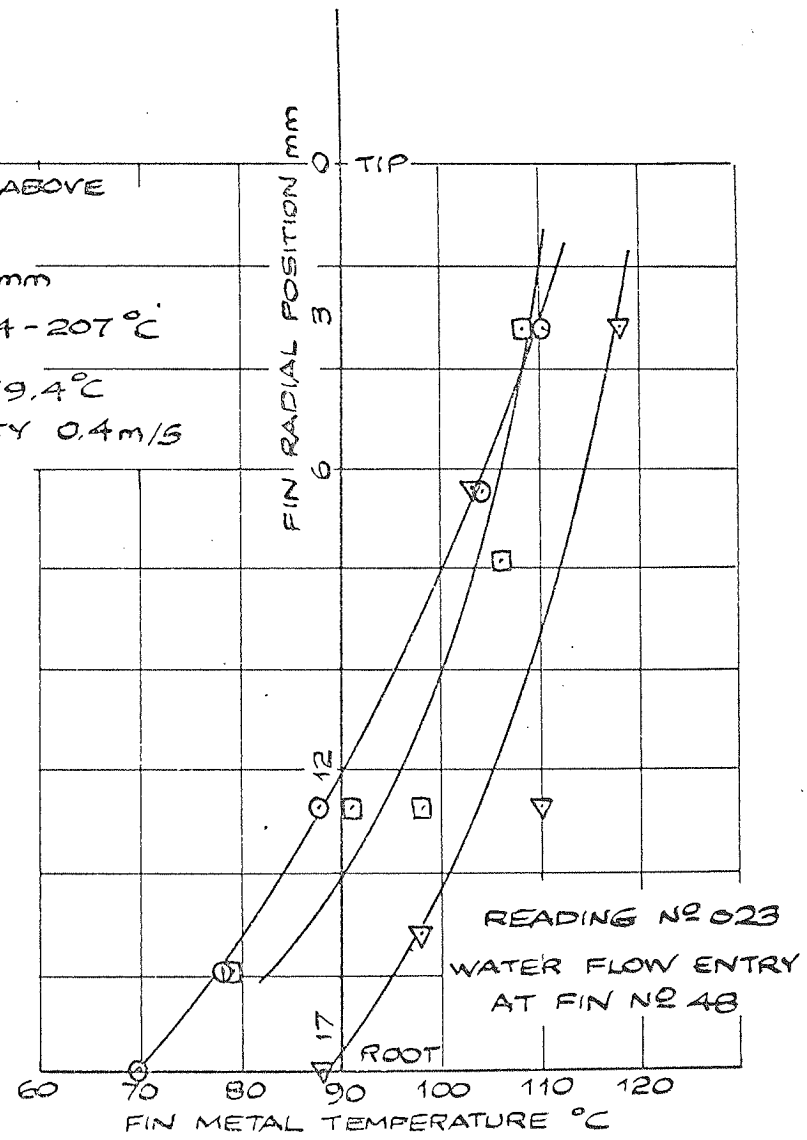

FIGURE 8,29

TEMPERATURE PROFILES FOR RADIAL FIN EXTENDED SURFACE C/1/MR IN ZIRCON SAND ($\bar{d}_p$ = 138 μm)

IN MK 1 BED — RESULTS OF TEST NUMBER 19

Figure 8.30

VARIATION OF FIN TEMPERATURE PROFILE FOR EXTENDED SURFACE C/1/MR IN ZIRCON SAND (d_p = 138 μm) IN MK1 BED.

BED STATIC HEIGHT 75 mm

LOWER FIN EDGE 25 mm ABOVE DISTRIBUTOR

BED TEMPERATURE 204°C ; SUPERFICIAL FLUIDIZING VELOCITY 0.399 m/s

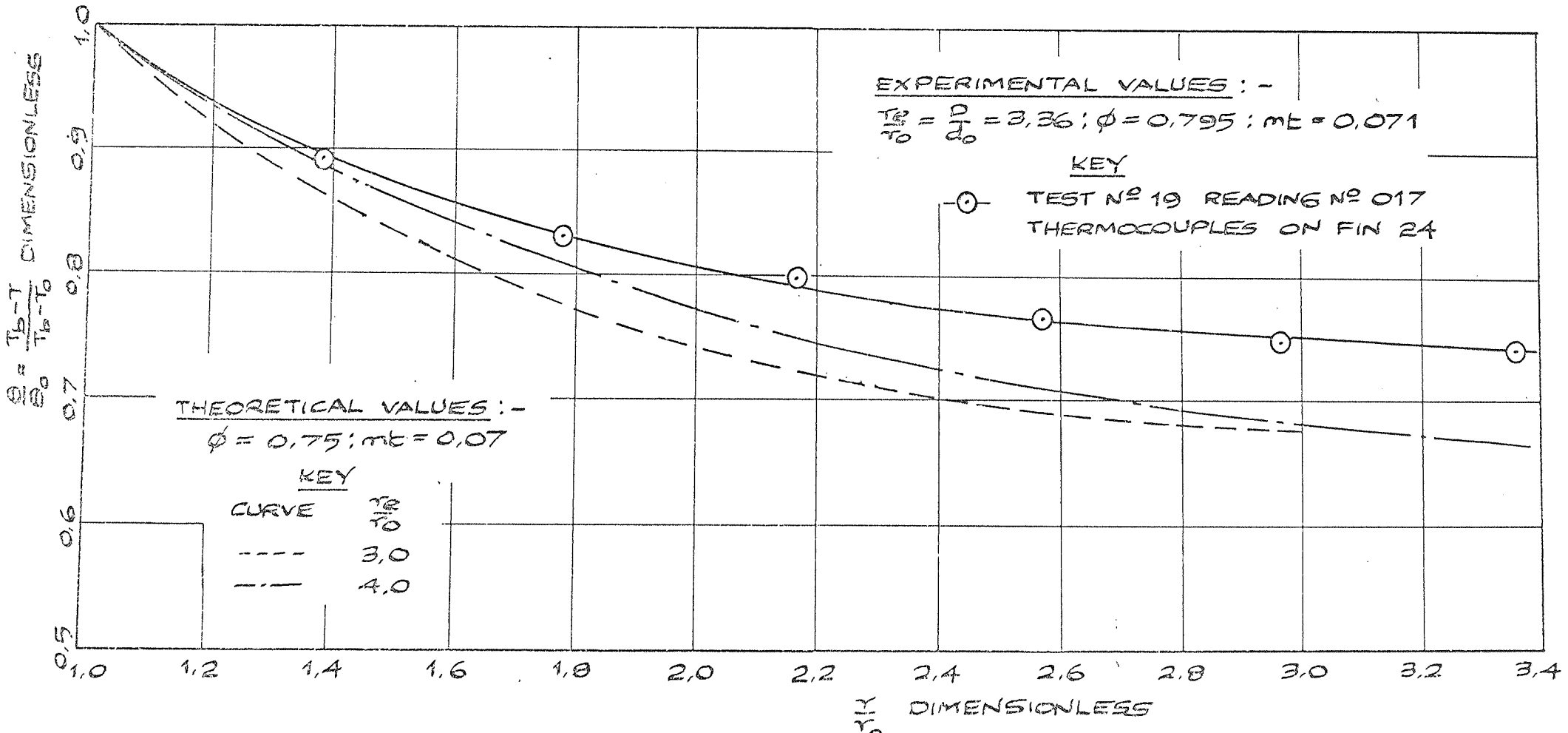

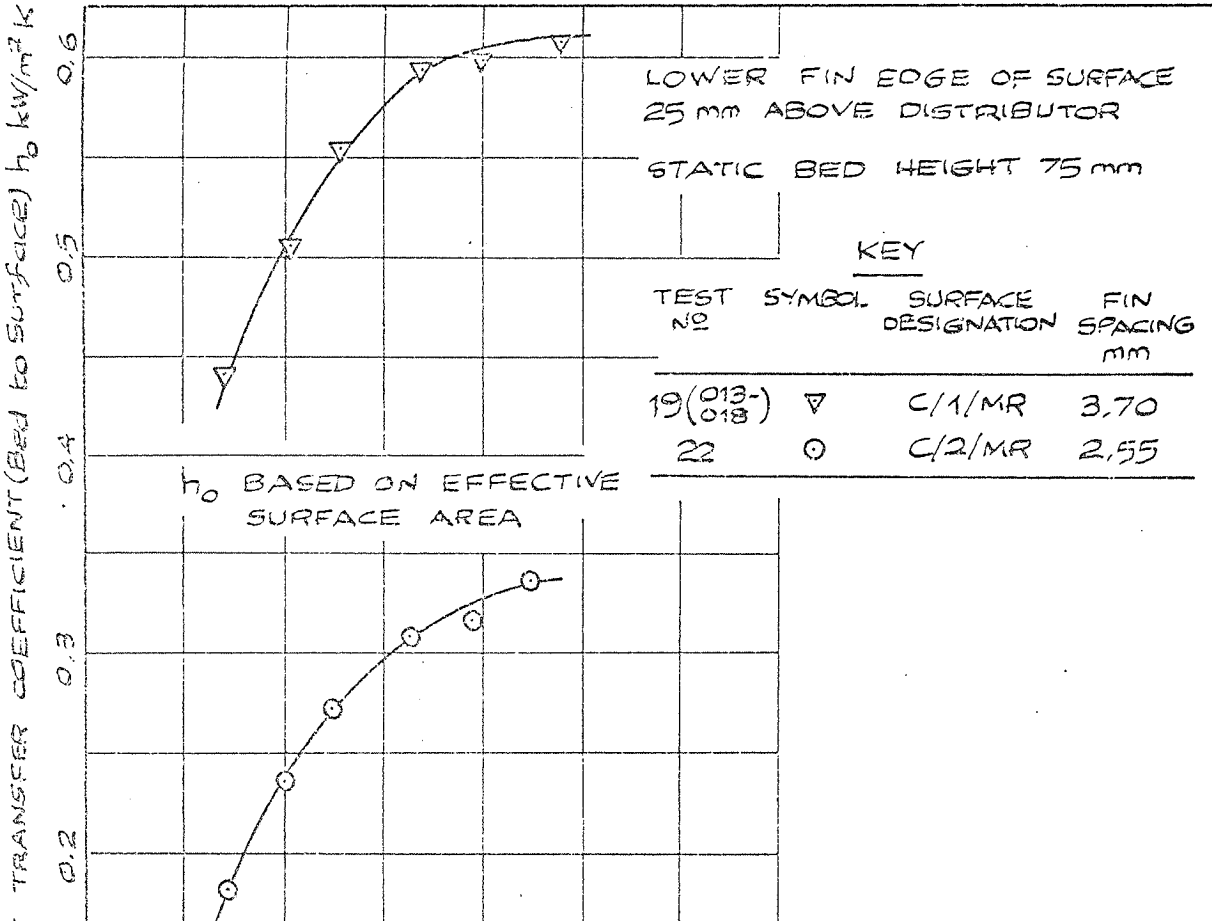

FIGURE 8.31

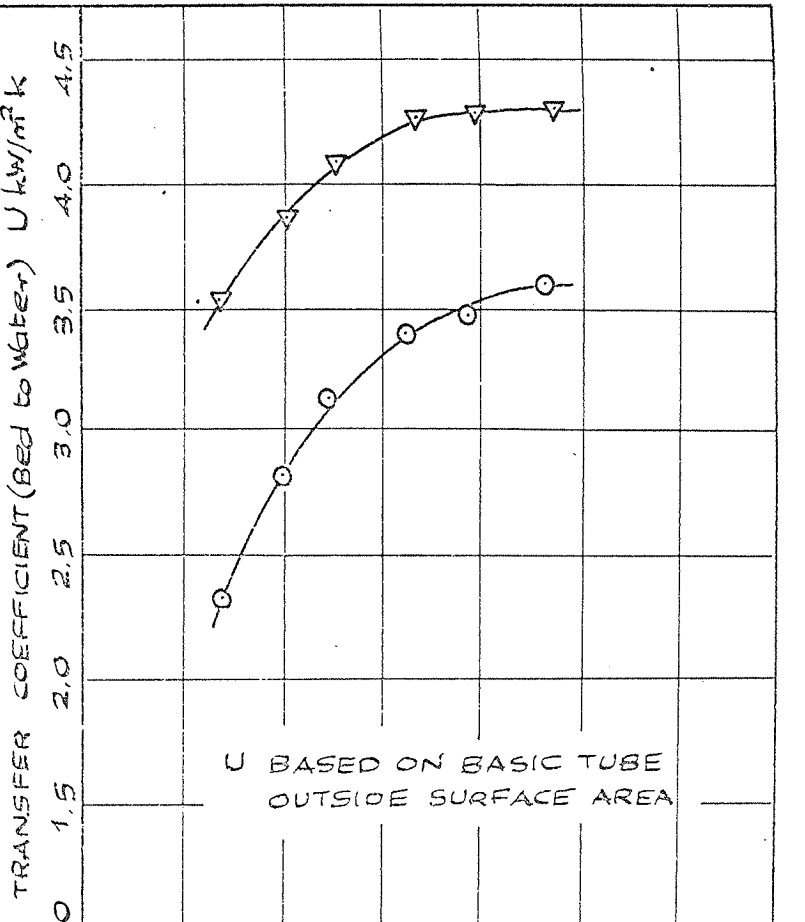

FIGURE 8.32

EFFECT OF FIN SPACING ON HEAT TRANSFER COEFFICIENTS FOR RADIAL FIN EXTENDED SURFACE IN ZIRCON SAND ($\bar{d}_p$ = 138 μm) IN MK 1 BED.

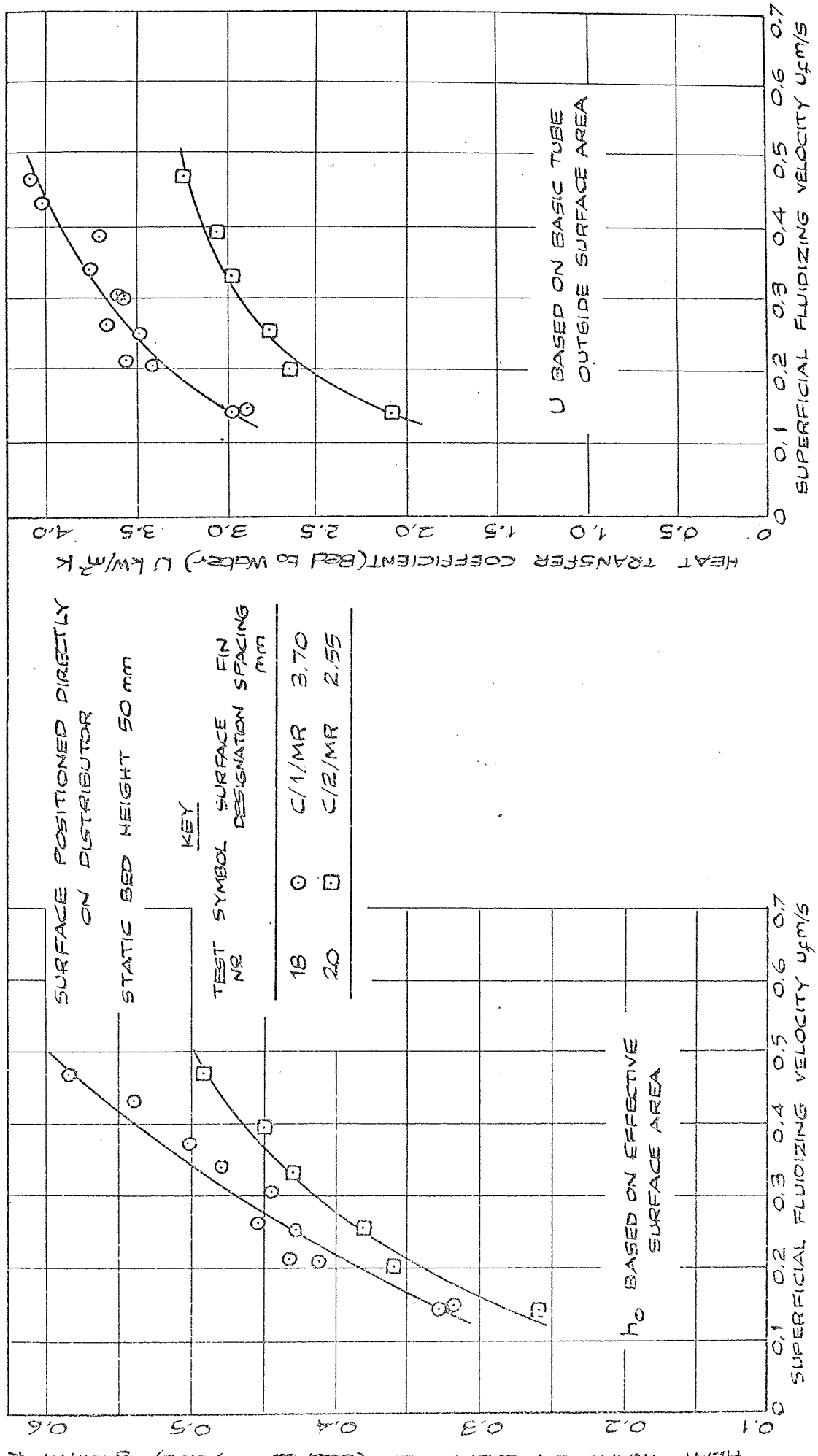

FIGURE 8.33

FIGURE 8.34

EFFECT OF FIN SPACING ON HEAT TRANSFER COEFFICIENTS FOR RADIAL FIN EXTENDED SURFACE IN ZIRCON SAND ($\bar{d}_p$ = 138 μm) IN Mk1 BED.

Figure 8,35 REPEATABILITY OF EXPERIMENTAL READINGS FOR SURFACE C/2/MR IN ZIRCON SAND ($\bar{d}_p$ = 138 μm) IN Mk 1 BED.

STATIC BED HEIGHT 75 mm

HEAT TRANSFER COEFFICIENT BASED ON EFFECTIVE SURFACE AREA.

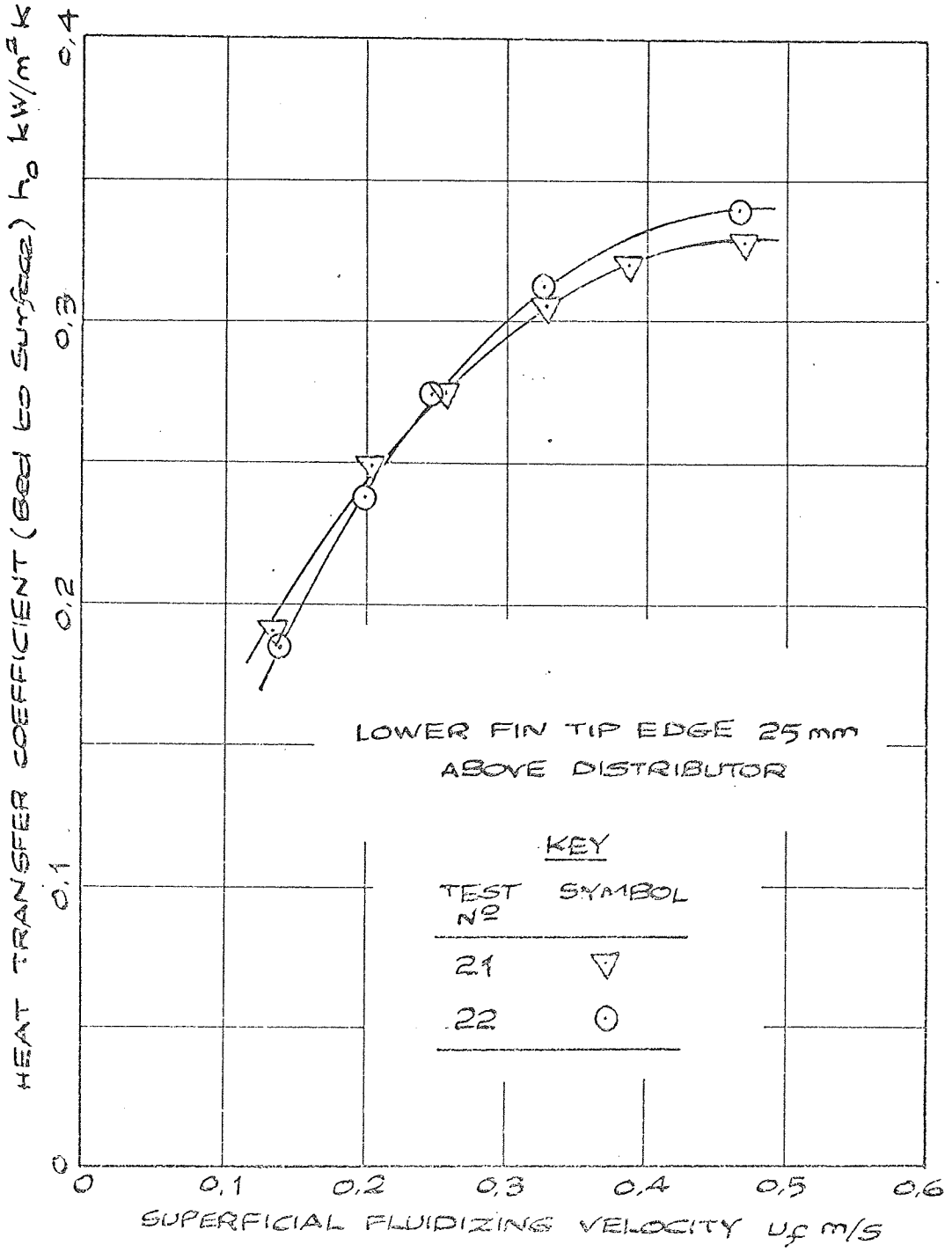

Figure 8.36

EFFECT OF BED SIZE ON BED TO METAL HEAT TRANSFER COEFFICIENT FOR EXTENDED SURFACE C/2/MR – MATERIAL ZIRCON SAND ($\bar{d}_p$ = 138 μm).

HEAT TRANSFER COEFFICIENT BASED ON EFFECTIVE AREA.

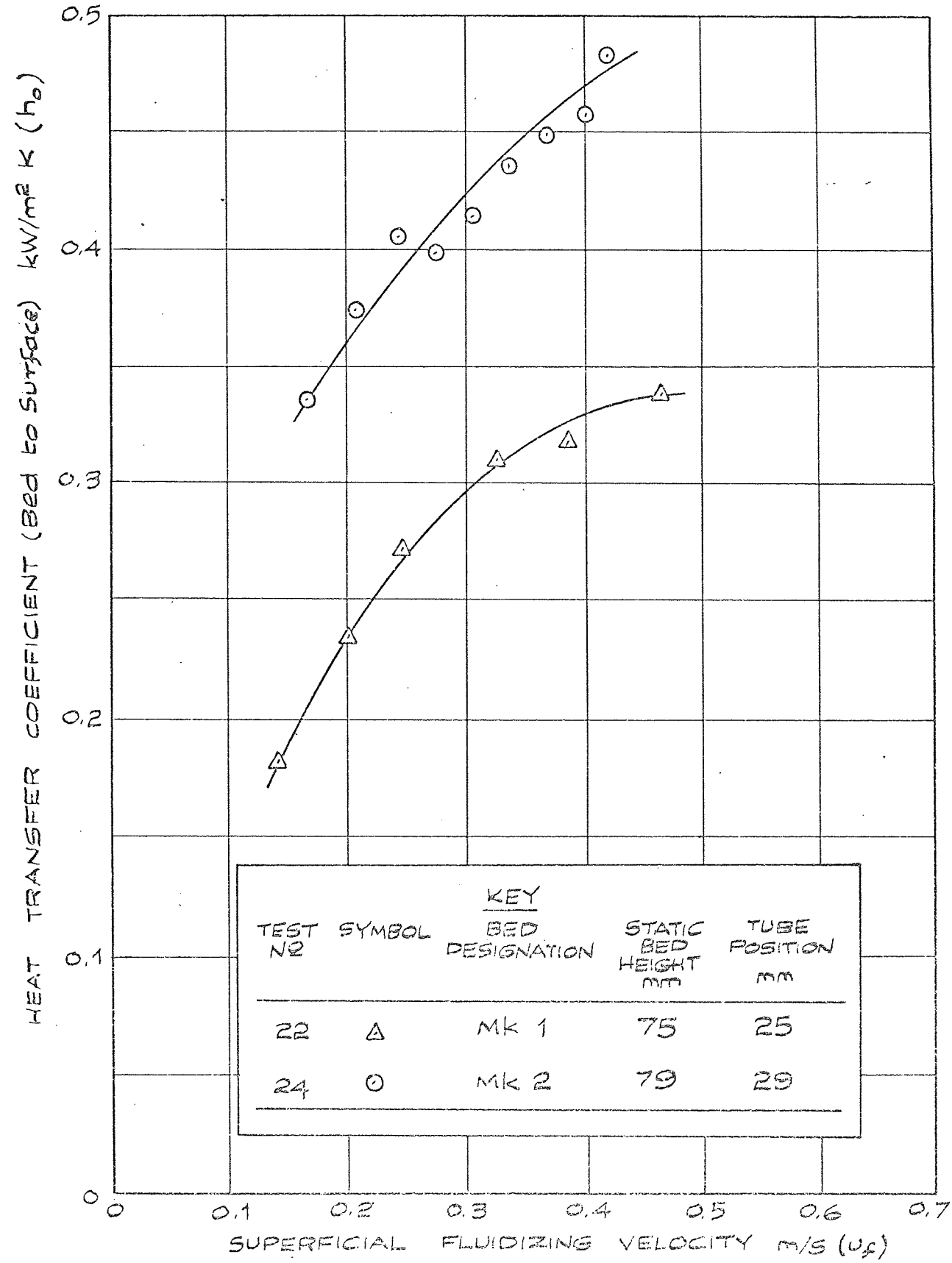

Figure 8.37 EFFECT OF BED SIZE ON OVERALL HEAT TRANSFER COEFFICIENT FOR VARYING FLUIDIZING VELOCITY - EXTENDED SURFACE C/2/MR IN ZIRCON SAND ($\bar{d}_p$ = 138 μm)

HEAT TRANSFER COEFFICIENT BASED ON BASIC TUBE OUTSIDE SURFACE AREA.

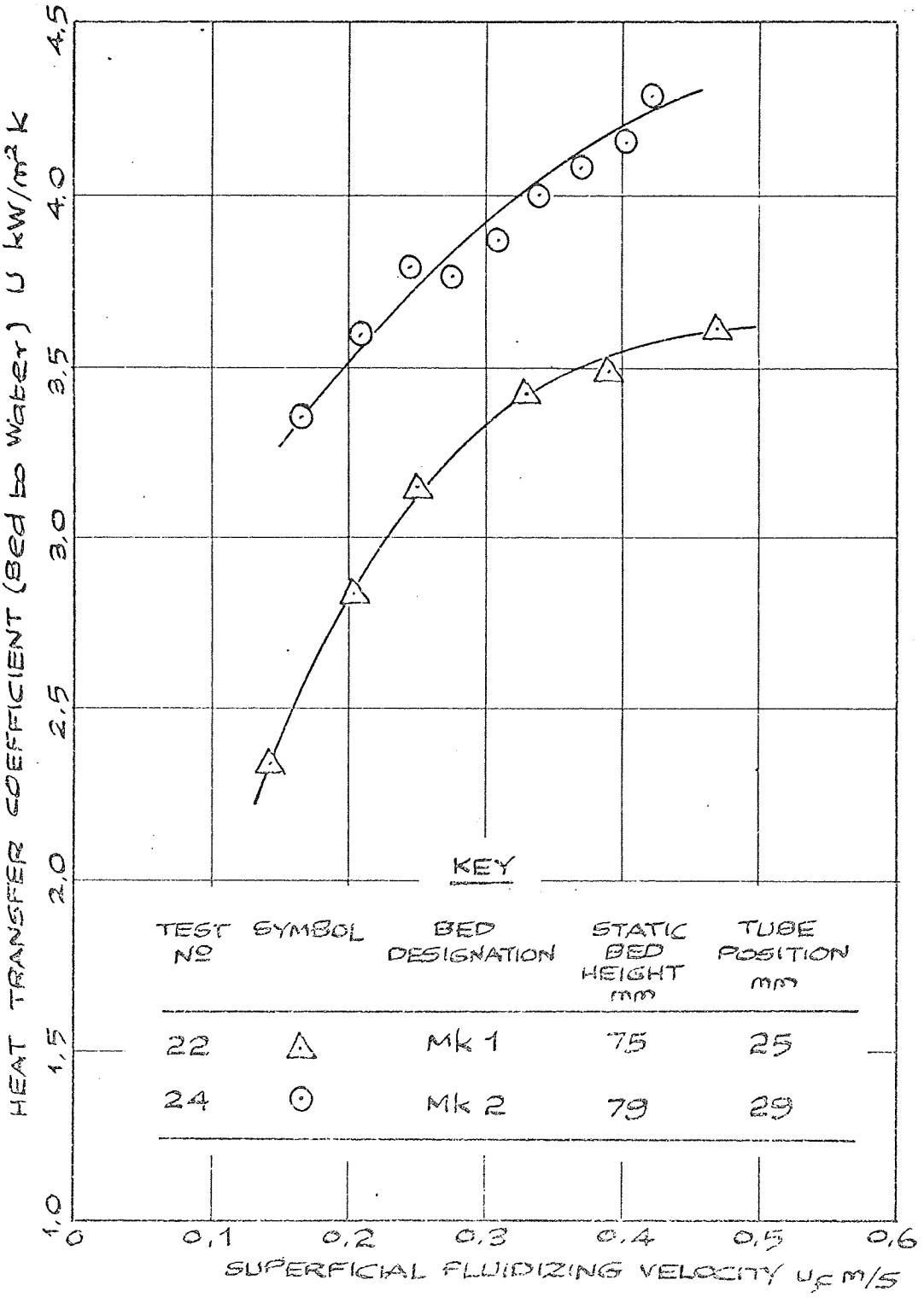

Test number 23, which follows, was devised in order to determine the temperature profile through radial fins of rectangular section. Fourteen thermocouples were located on seven fins of surface C/2/MR according to the positions given in figure 8.39. The depth of each thermocouple from the fin edge was as follows:-

Thermocouple	Position mm	Thermocouple	Position mm
T_1	17.8	T_8	12.8
T_2	12.0	T_9	3.2
T_3	11.7	T_{10}	17.0
T_4	17.8	T_{11}	12.0
T_5	6.5	T_{12}	11.8
T_6	14.5	T_{13}	17.8
T_7	17.8	T_{14}	12.1

The surface was carefully mounted in bed Mk 2 with thermocouple T_6 on fin number 29 in the top vertical position of the bed. The index mechanism shown in figure 8.38 was assembled, the spur gear (40 teeth on a 38 mm P.C.D.) being fixed to the basic tube outside the bed by means of a grub screw. Rotating the tube 90° in a clockwise direction when viewed on "A" in figure 8.39 the first test position (reading number 280) was set up. A ratchet finger modified from a grinding machine gear cutter attachment was used to hold the surface at the desired position and to provide accurate angular location of the heat exchanger for subsequent readings to be taken.

A series of thirteen readings were noted, allowing some 10 to 15 minutes between each, the gas, air and water flows being maintained constant throughout. Surface angular positions were designated positive or negative depending upon the respective clockwise or anti-clockwise direction of rotation when viewed on "A" in figure 8.39. The complete temperature profiles are shown in figures 8.40 and 8.41.

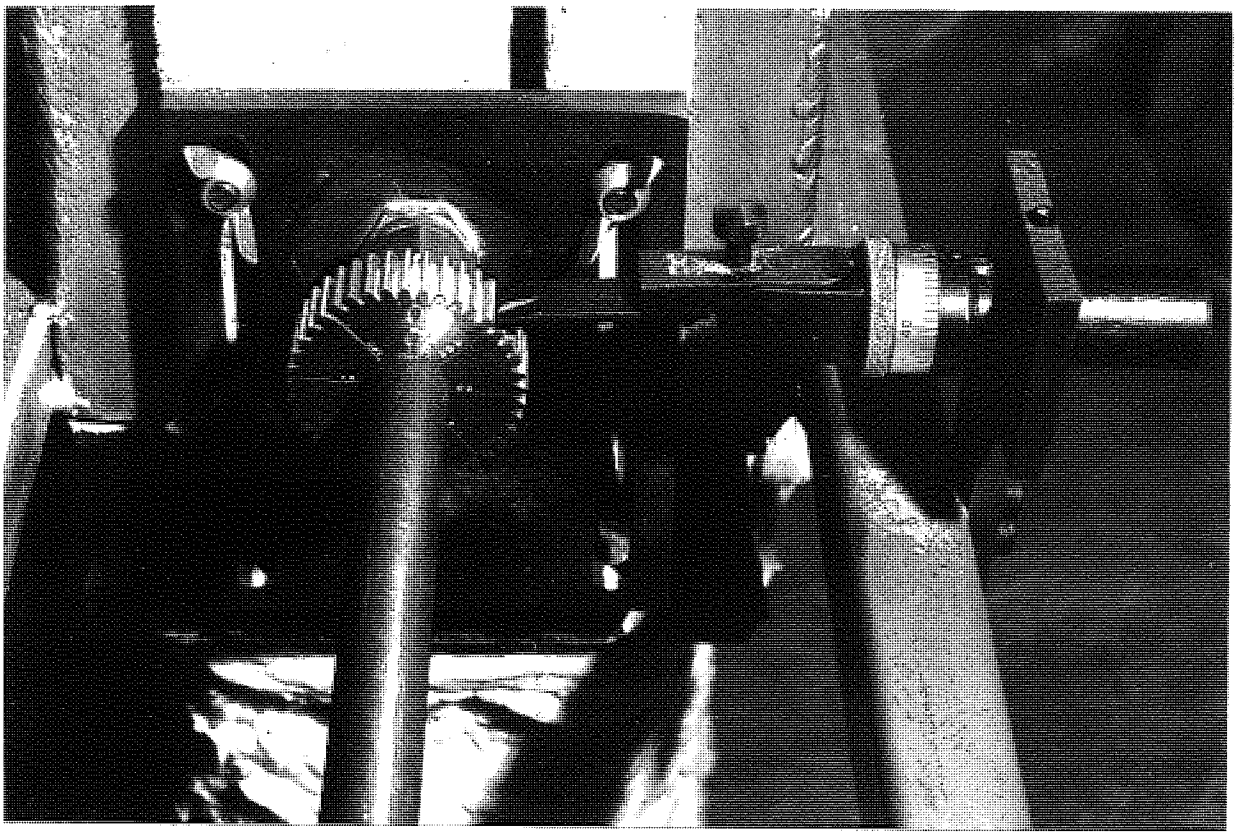

Figure 8.38 Index Mechanism for Fin Temperature Measurement

Figure 8.39

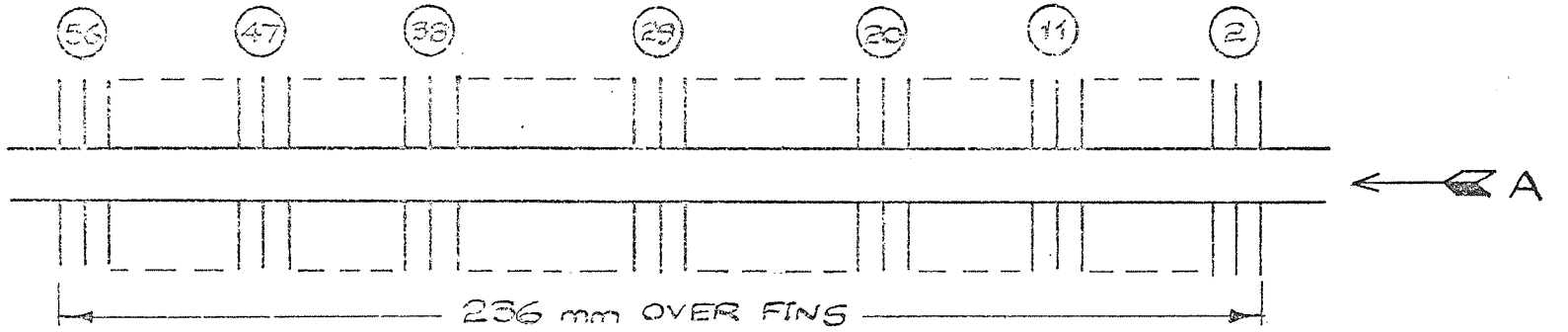

57 FINS, 50,8 mm O/D × 1,59 mm THICK, BRAZED TO BASIC TUBE OF 15,1 mm O/D × 13,7mm I/D

MEAN SPACING BETWEEN FINS 2,45 mm

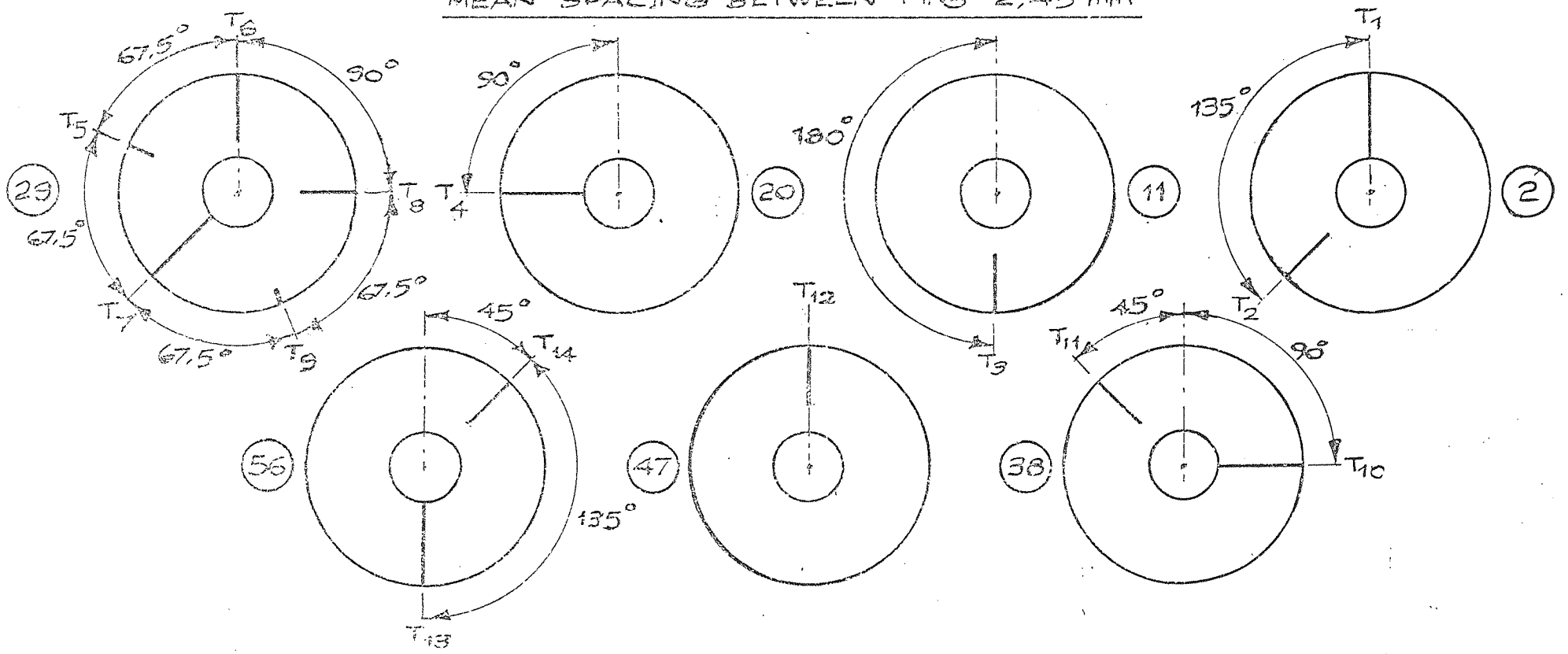

VIEW OF NUMBERED FINS ON ARROW "A". THERMOCOUPLE POCKETS DRILLED

1 mm DIAMETER CENTRAL TO FIN THICKNESS IN POSITIONS INDICATED

Arrangement of Thermocouples on Test Surface C/2/MR

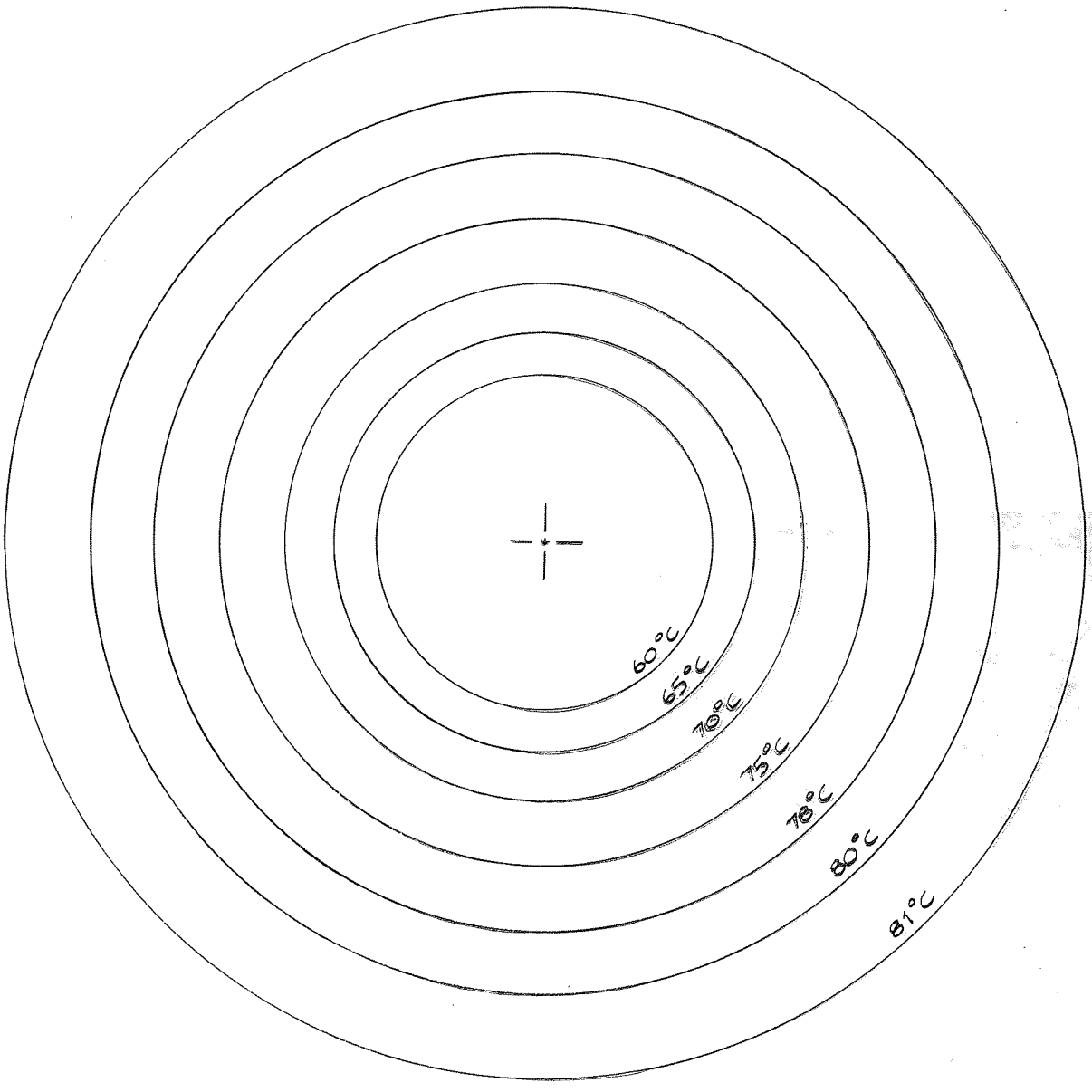

Figure 8.40 THEORETICAL TEMPERATURE PROFILE ON THE ASSUMPTION OF CONSTANT BED TO FIN HEAT TRANSFER COEFFICIENT (h_o=0.421 kW/m^2 K) - TEST Nº 23

Figure 8.41 ACTUAL TEMPERATURE PROFILE THROUGH FIN Nº 29 OF EXTENDED SURFACE C/2/MR IN ZIRCON SAND ($\bar{d}_p$ = 138 μm) IN MK 2 BED - TEST Nº 23.

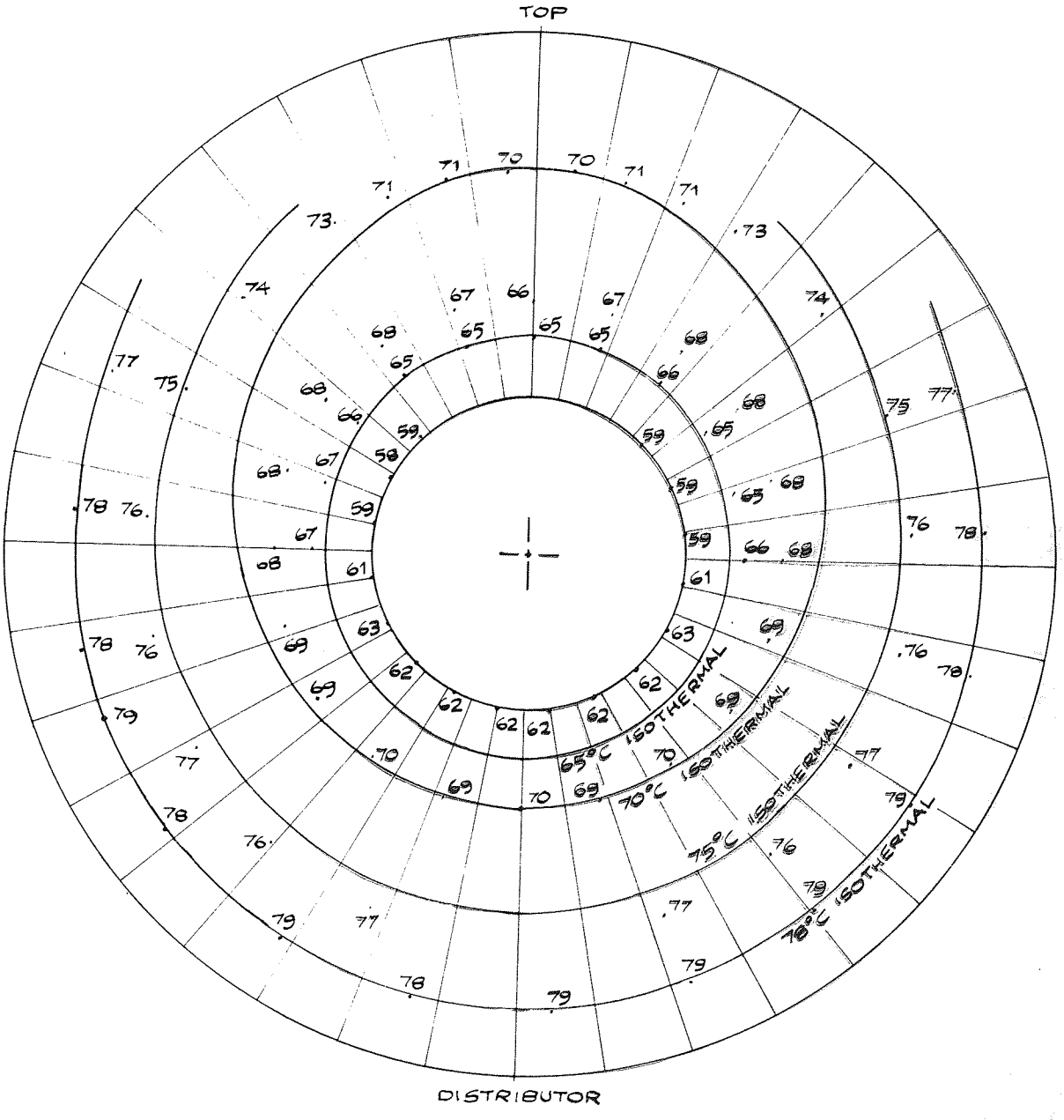

DATA: LOWER FIN EDGE 29 mm ABOVE DISTRIBUTOR
STATIC BED HEIGHT 75 mm
WATER TEMPERATURE 30.3 °C
BED TEMPERATURE 136 °C
SUPERFICIAL FLUIDIZING VELOCITY 0.327 m/s

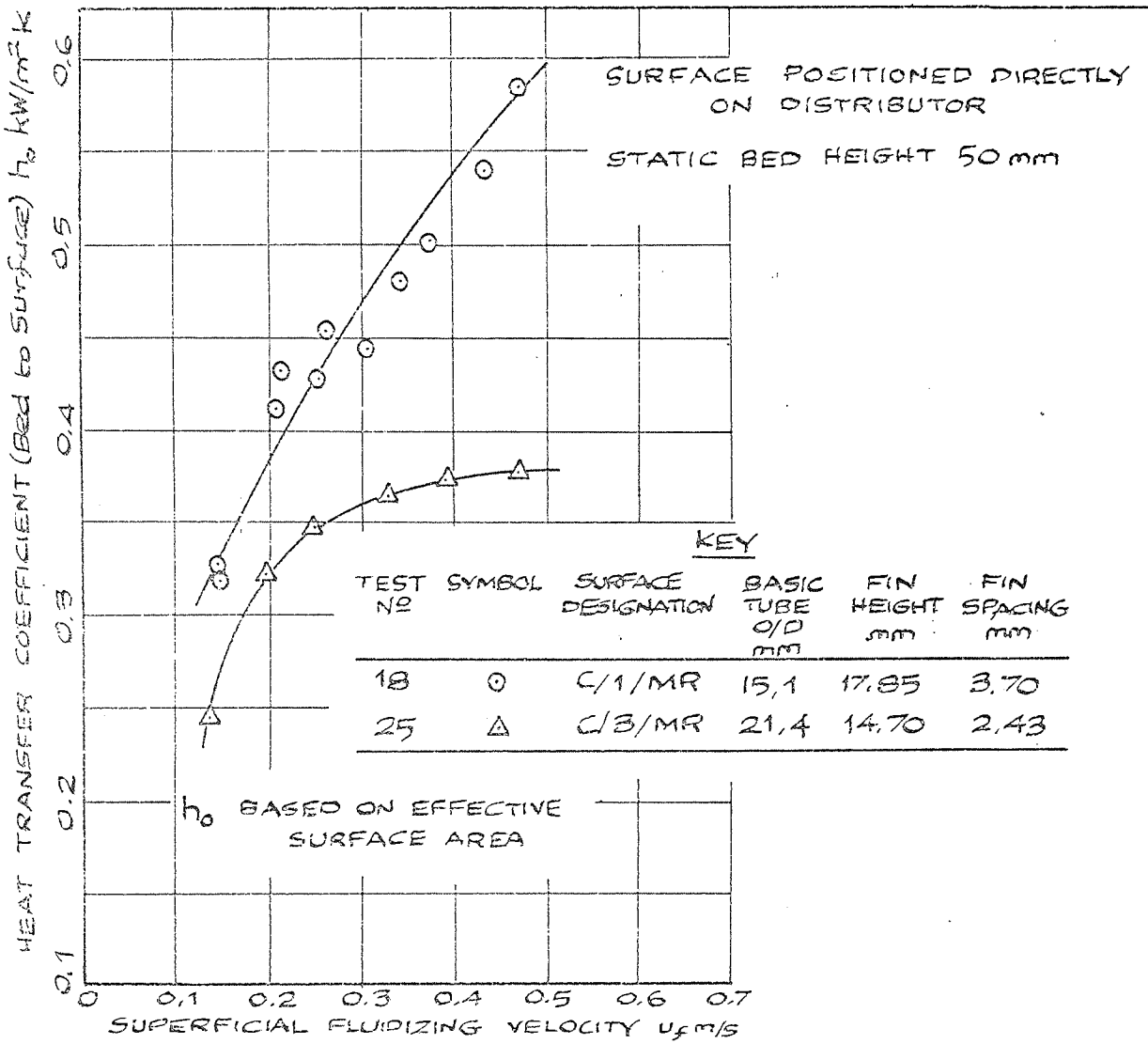

TEST Nº	SYMBOL	SURFACE DESIGNATION	BASIC TUBE O/D mm	FIN HEIGHT mm	FIN SPACING mm
18	⊙	C/1/MR	15,1	17.85	3.70
25	△	C/3/MR	21,4	14.70	2,43

FIGURE 8.42

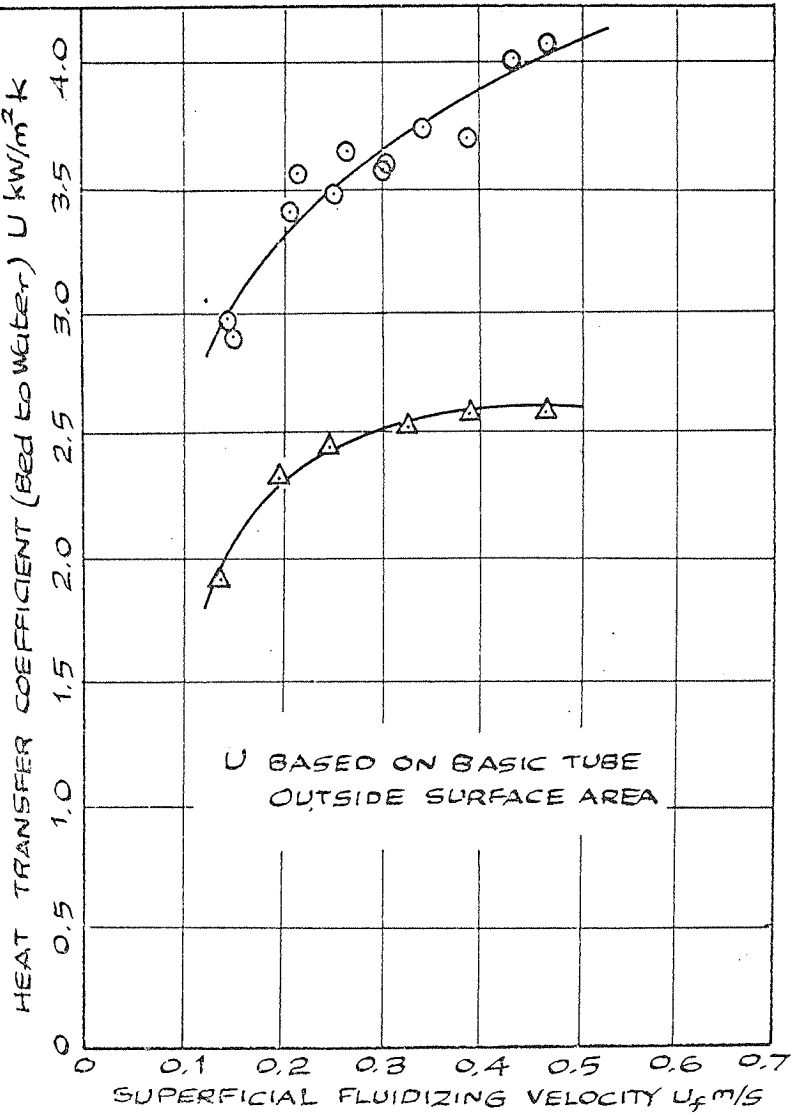

FIGURE 8.43

EFFECT OF MAIN GEOMETRIC VARIABLES ON HEAT TRANSFER COEFFICIENTS FOR RADIAL FIN EXTENDED SURFACE IN ZIRCON SAND ($\bar{d}_p$ = 138 μm) IN Mk 1 BED.

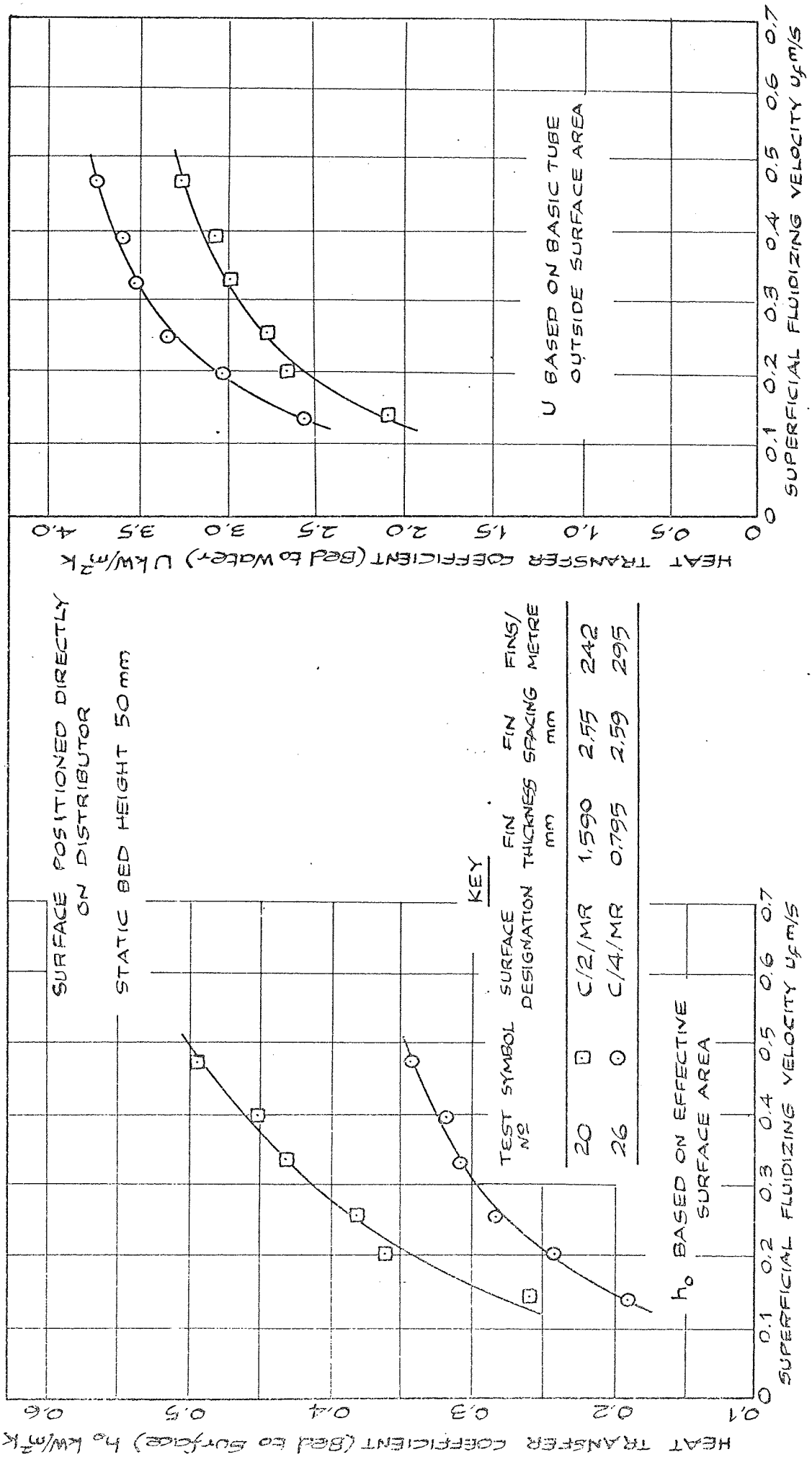

FIGURE 8.44

FIGURE 8.45

EFFECT OF FIN THICKNESS AND FIN SPACING ON HEAT TRANSFER COEFFICIENTS FOR RADIAL FIN EXTENDED SURFACE IN ZIRCON SAND ($\bar{d}_p$ = 138 μm) IN Mk 1 BED.

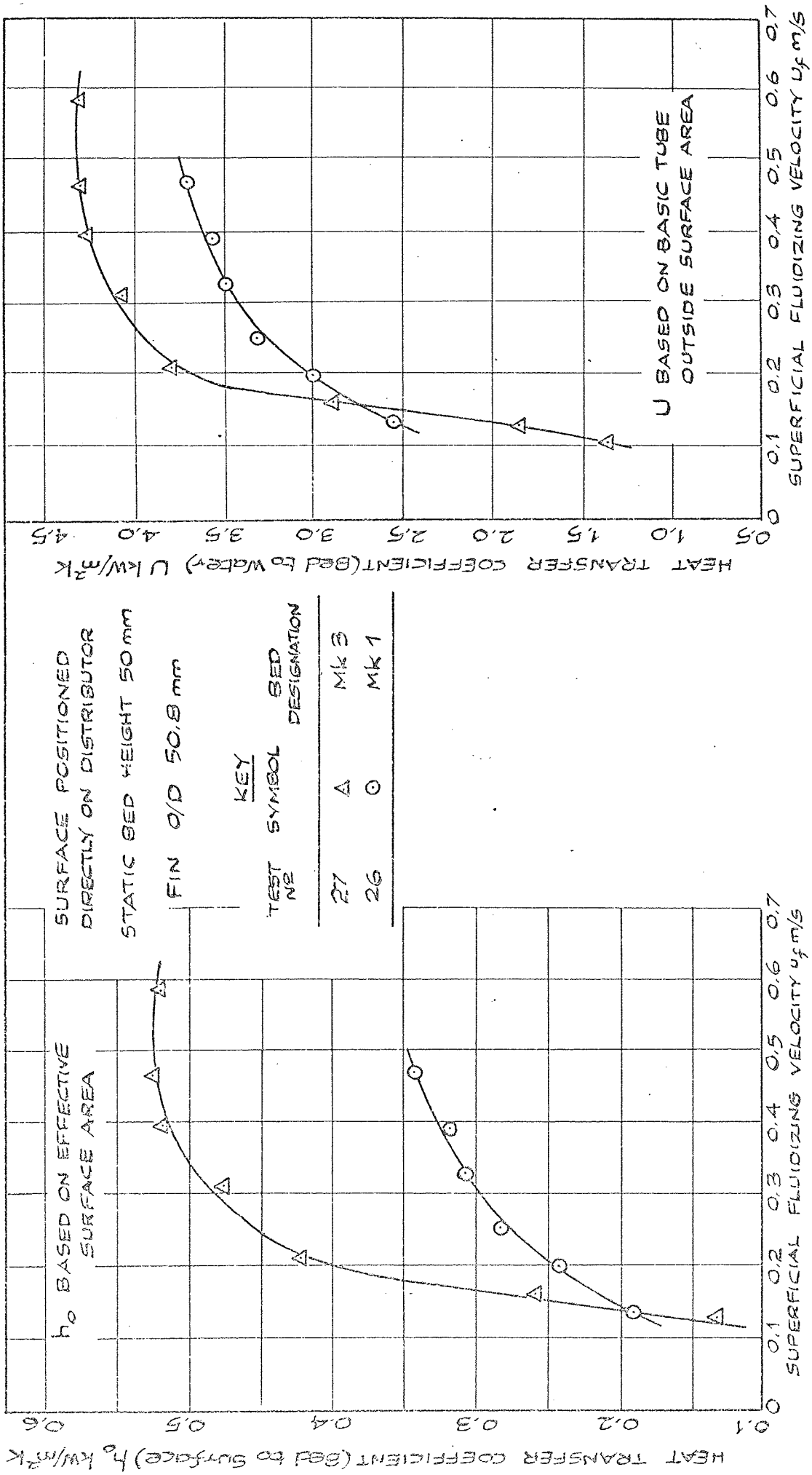

FIGURE 8.46

FIGURE 8.47

EFFECT OF BED SIZE ON HEAT TRANSFER COEFFICIENTS FOR MANUFACTURED RADIAL FIN EXTENDED SURFACE C/4/MR IN ZIRCON SAND (d_p = 138 μm).

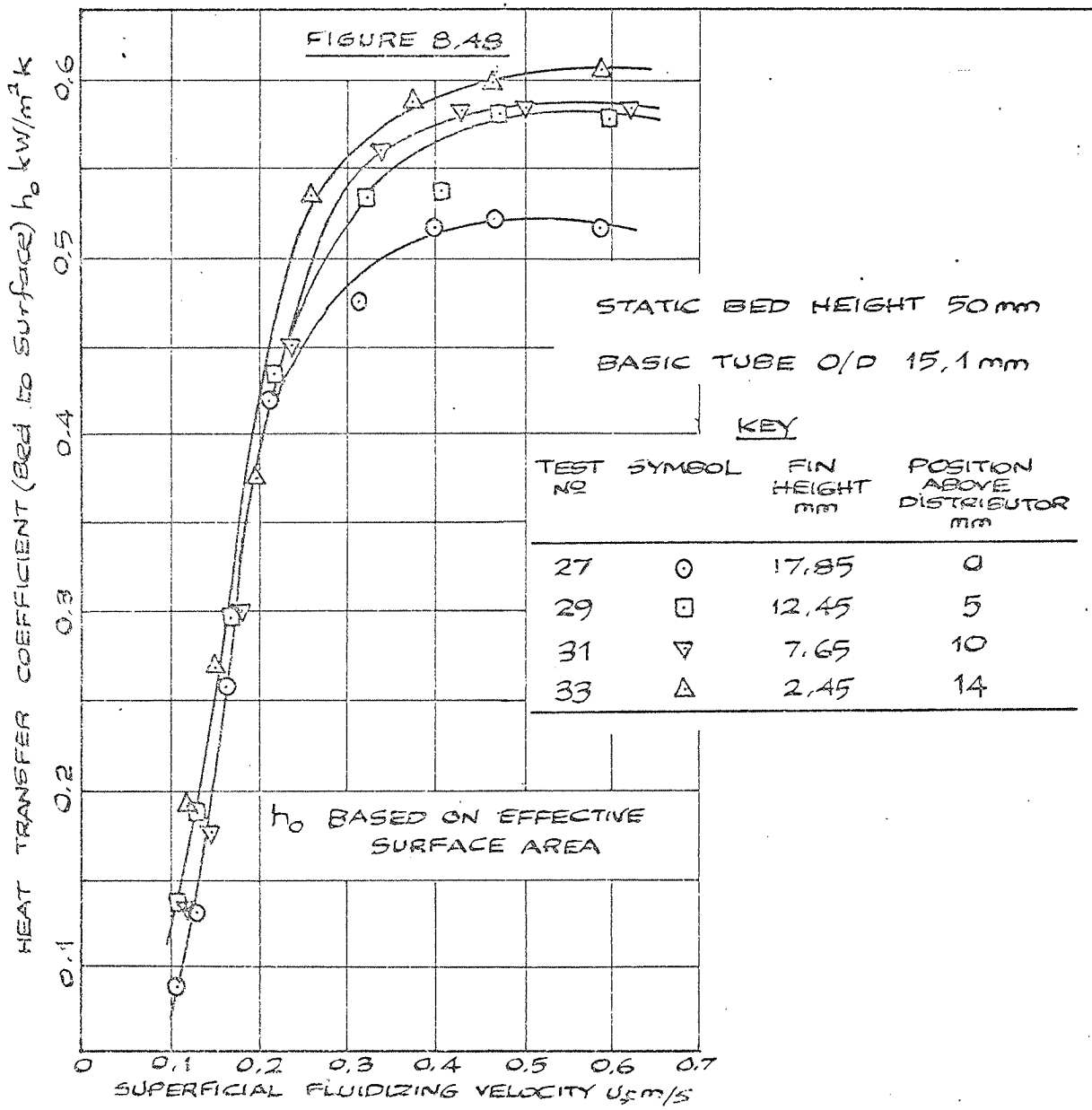

TEST NO	SYMBOL	FIN HEIGHT mm	POSITION ABOVE DISTRIBUTOR mm
27	⊙	17,85	0
29	⊡	12,45	5
31	▽	7,65	10
33	△	2,45	14

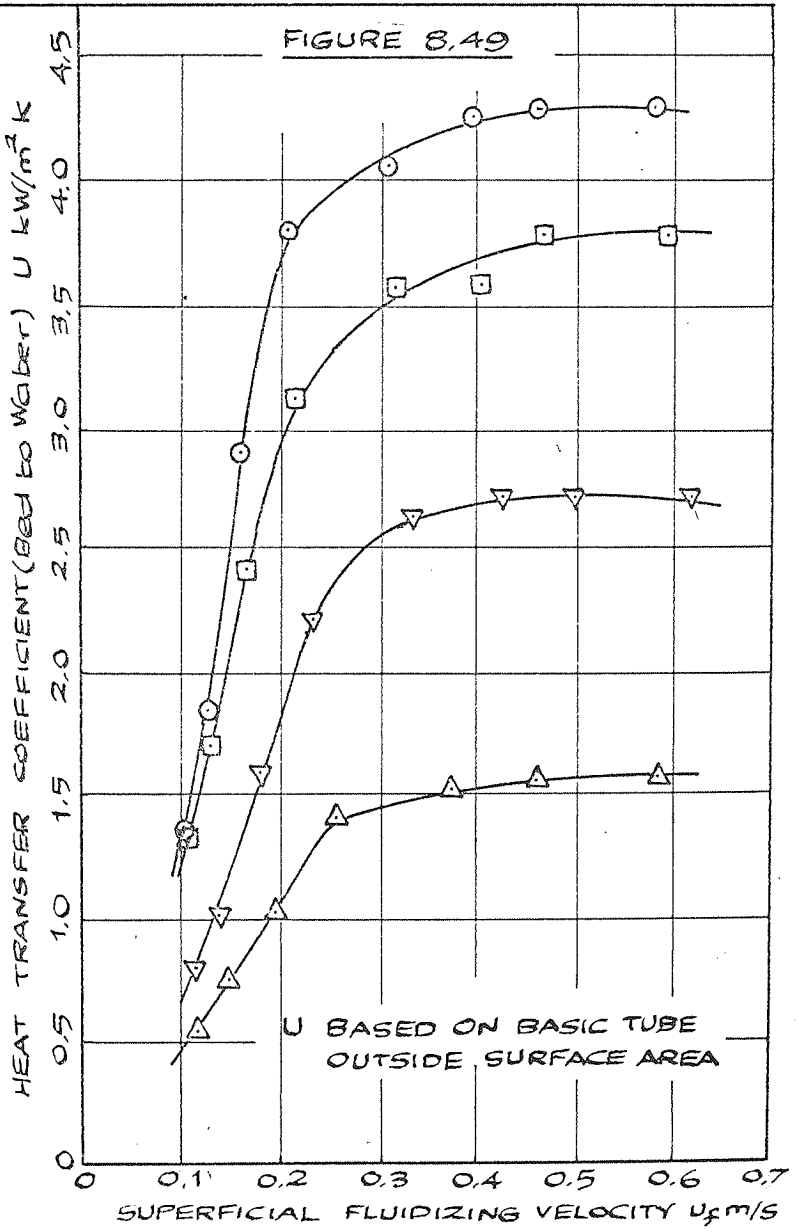

EFFECT OF FIN HEIGHT ON HEAT TRANSFER COEFFICIENTS FOR MANUFACTURED RADIAL FIN EXTENDED SURFACE C/A/MR IN ZIRCON SAND ($\bar{d}_p$ = 138 μm) IN Mk 3 BED.

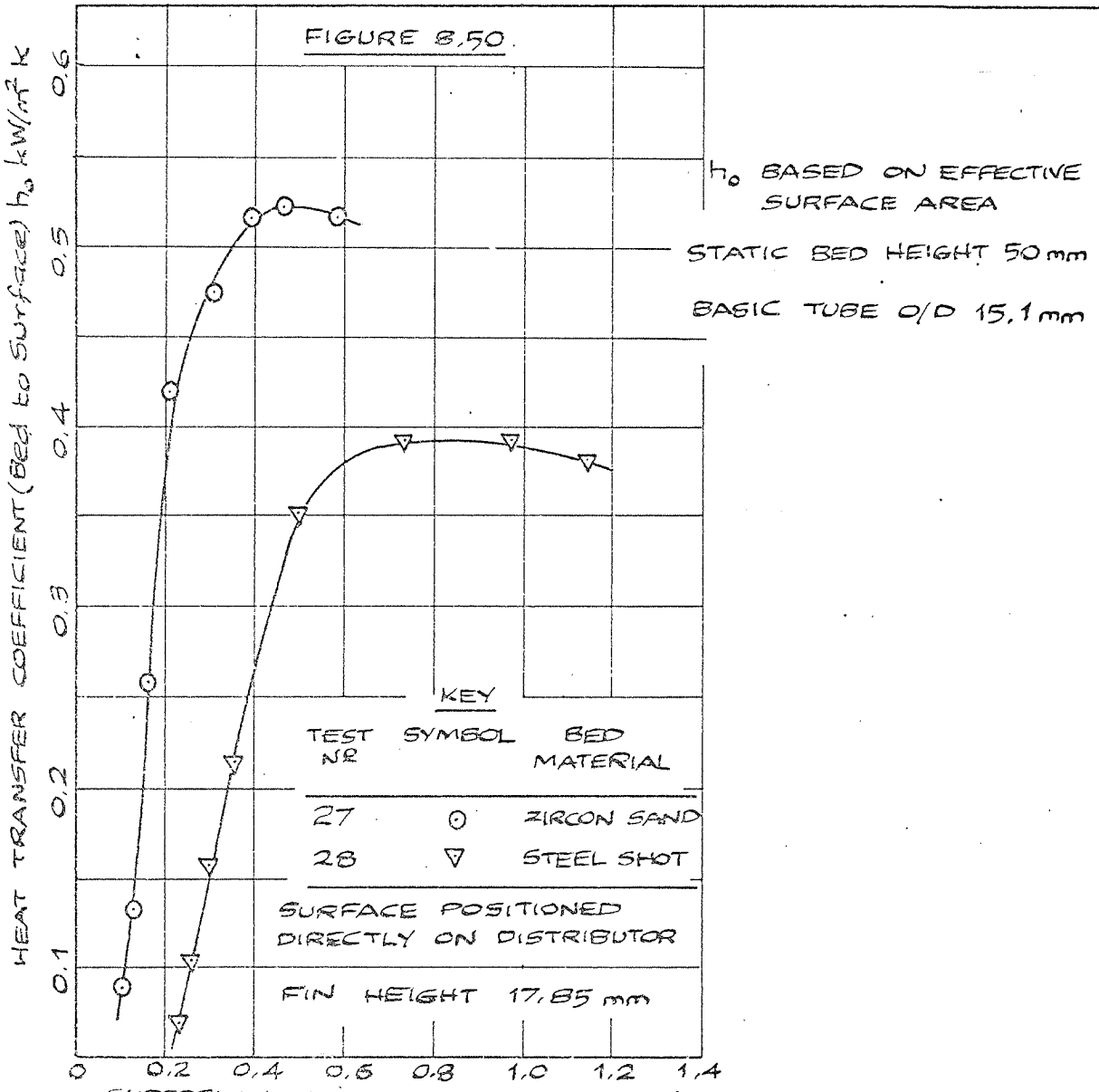

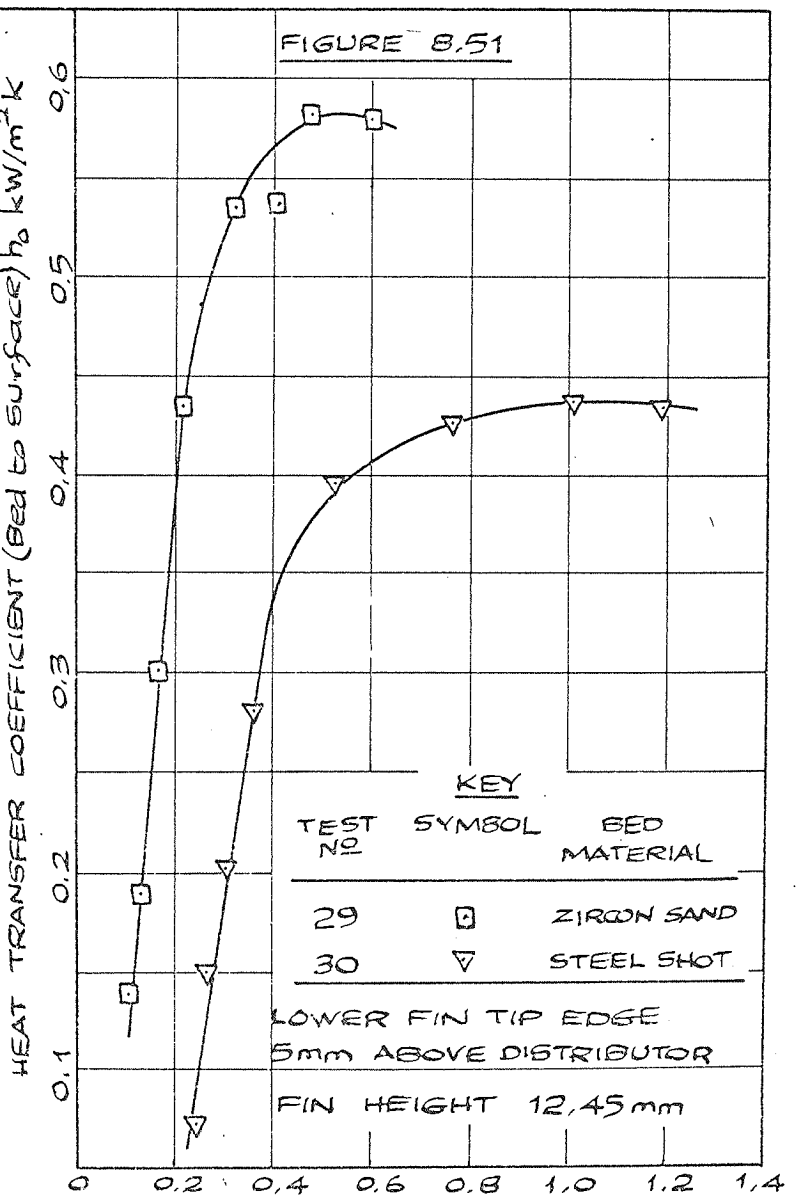

EFFECT OF BED MATERIAL AND FIN HEIGHT ON BED TO SURFACE HEAT TRANSFER COEFFICIENT FOR MANUFACTURED RADIAL FIN EXTENDED SURFACE C/4/MR IN Mk3 BED.

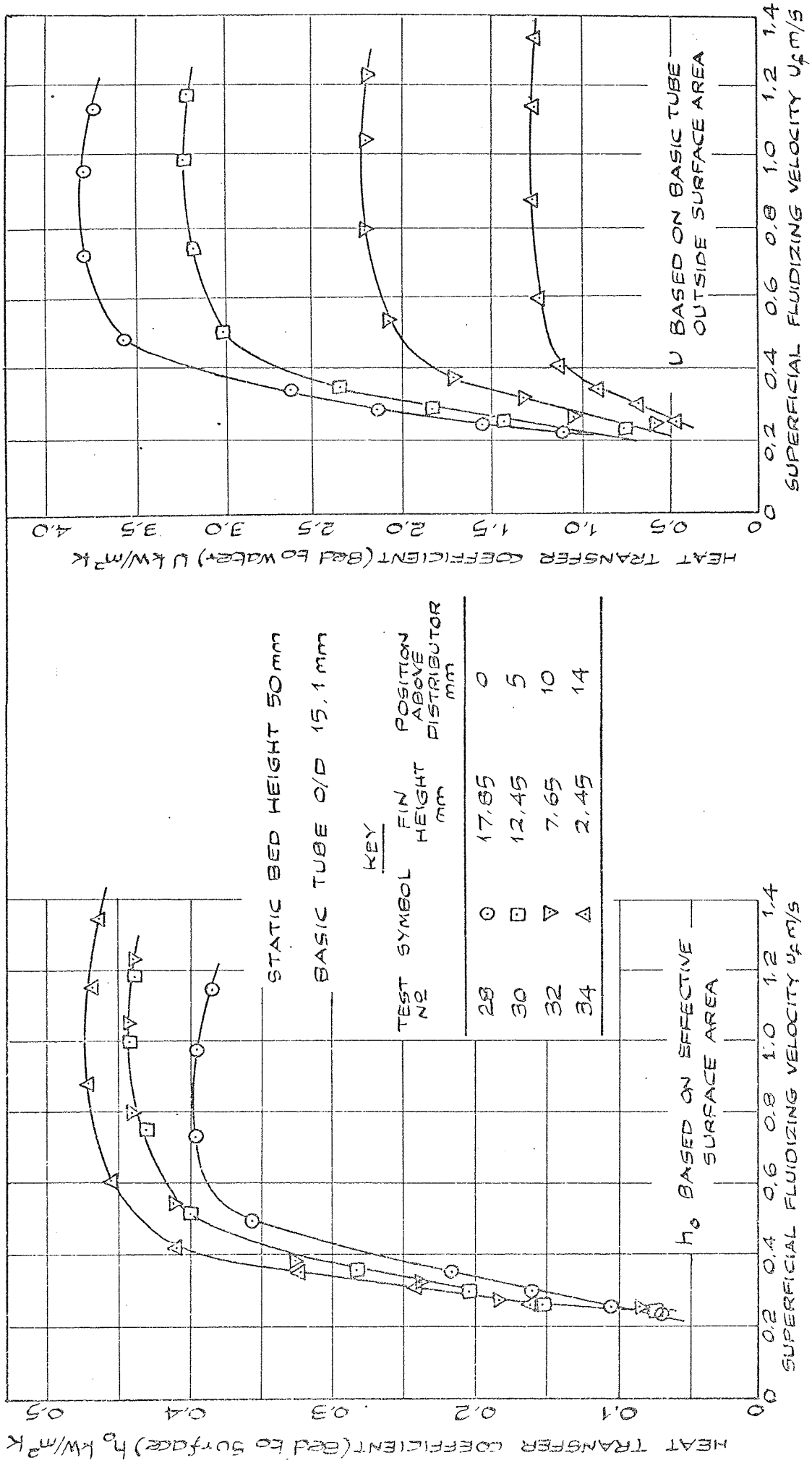

FIGURE 8.52

FIGURE 8.53

EFFECT OF FIN HEIGHT ON HEAT TRANSFER COEFFICIENTS FOR MANUFACTURED RADIAL FIN EXTENDED SURFACE C/4/MR IN STEEL SHOT (d_p = 432 μm) IN MK 3 BED.

FIGURE 8.54

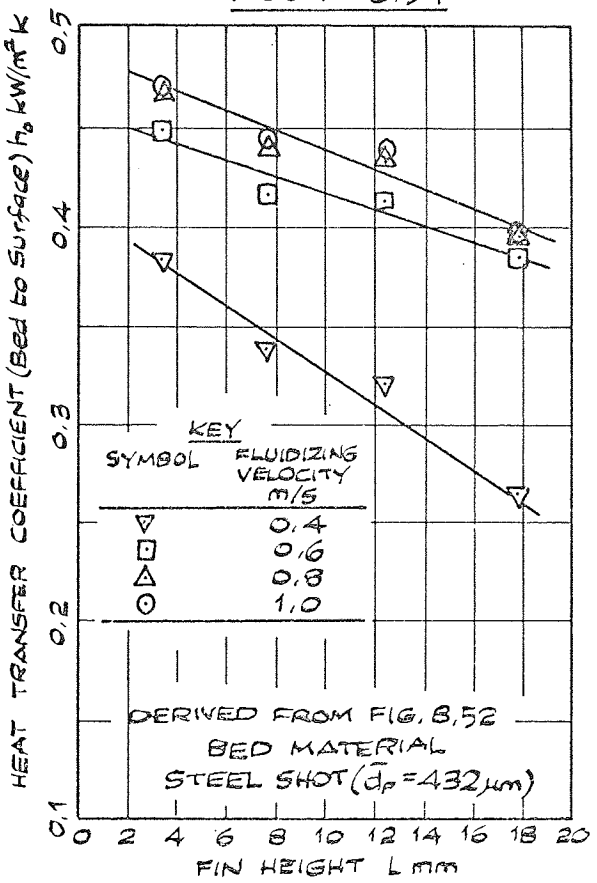

h_o BASED ON EFFECTIVE SURFACE AREA

STATIC BED HEIGHT 50 mm

BASIC TUBE O/D 15,1 mm

FIN SPACING 2,59 mm

SURFACE POSITION ABOVE DISTRIBUTOR VARYING SLIGHTLY WITH FIN HEIGHT.

FIGURE 8.55

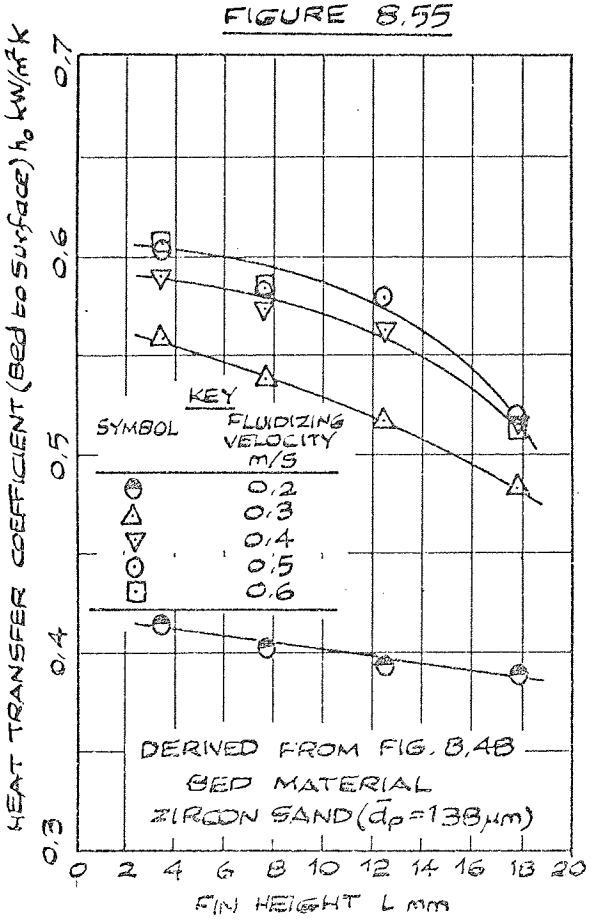

EFFECT OF FIN HEIGHT ON BED TO SURFACE HEAT TRANSFER COEFFICIENT FOR MANUFACTURED RADIAL FIN EXTENDED SURFACE C/4/MR IN MK3 BED.

Figure 8.56

VARIATION IN EFFECTIVENESS FACTOR FOR MANUFACTURED RADIAL SURFACES IN ZIRCON SAND ($\bar{d}_p = 138\,\mu m$) IN Mk 1 BED

EXTENDED SURFACE POSITIONED DIRECTLY ON DISTRIBUTOR.

STATIC BED HEIGHT 50 mm

PLAIN TUBE RESULTS OF TEST NUMBER 1

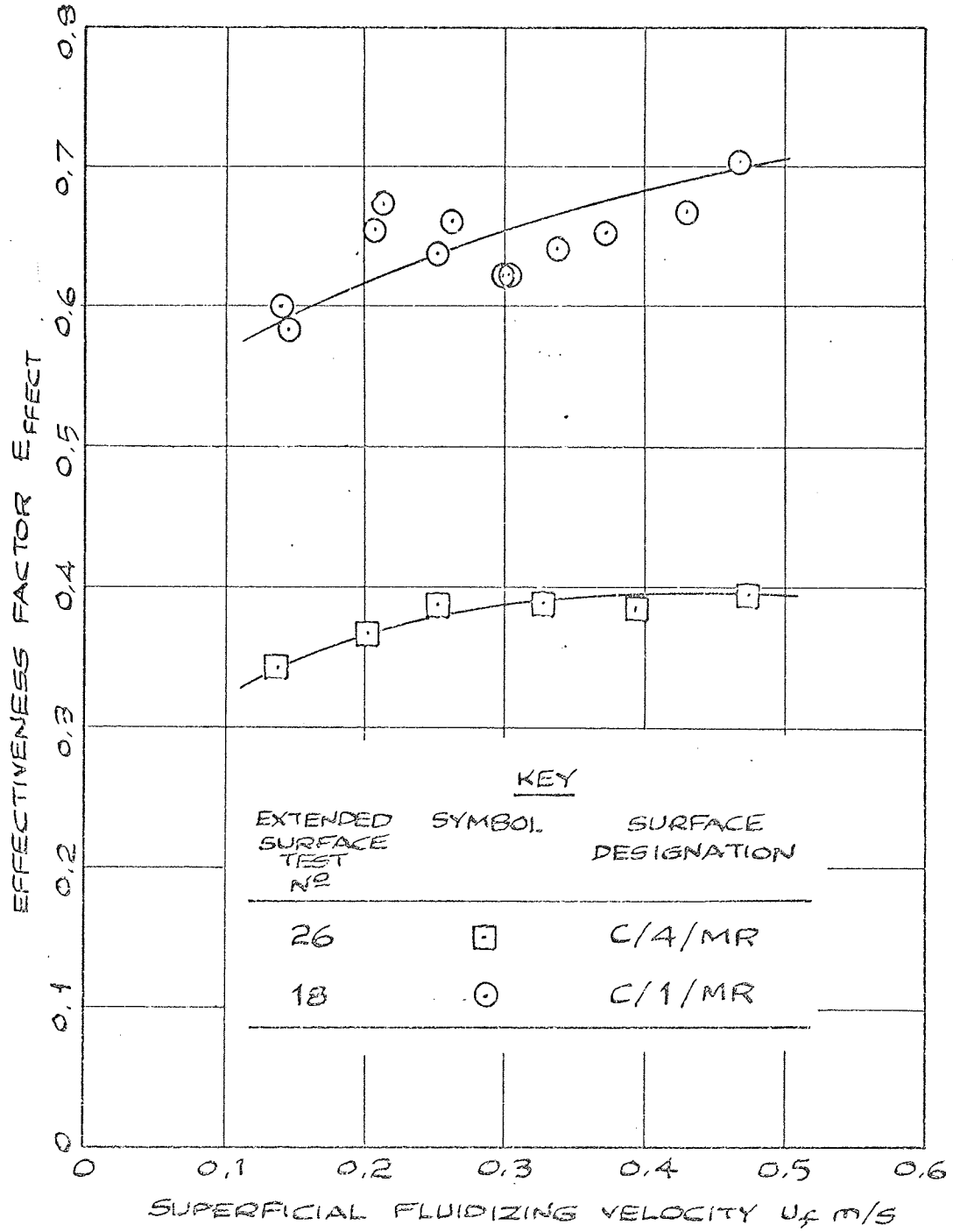

Figure 8.57 EFFECT OF FIN HEIGHT ON EFFECTIVENESS FACTOR FOR MANUFACTURED RADIAL EXTENDED SURFACE C/4/MR IN ZIRCON SAND ($\bar{d}_p$ = 138 μm) IN MK 3 BED.

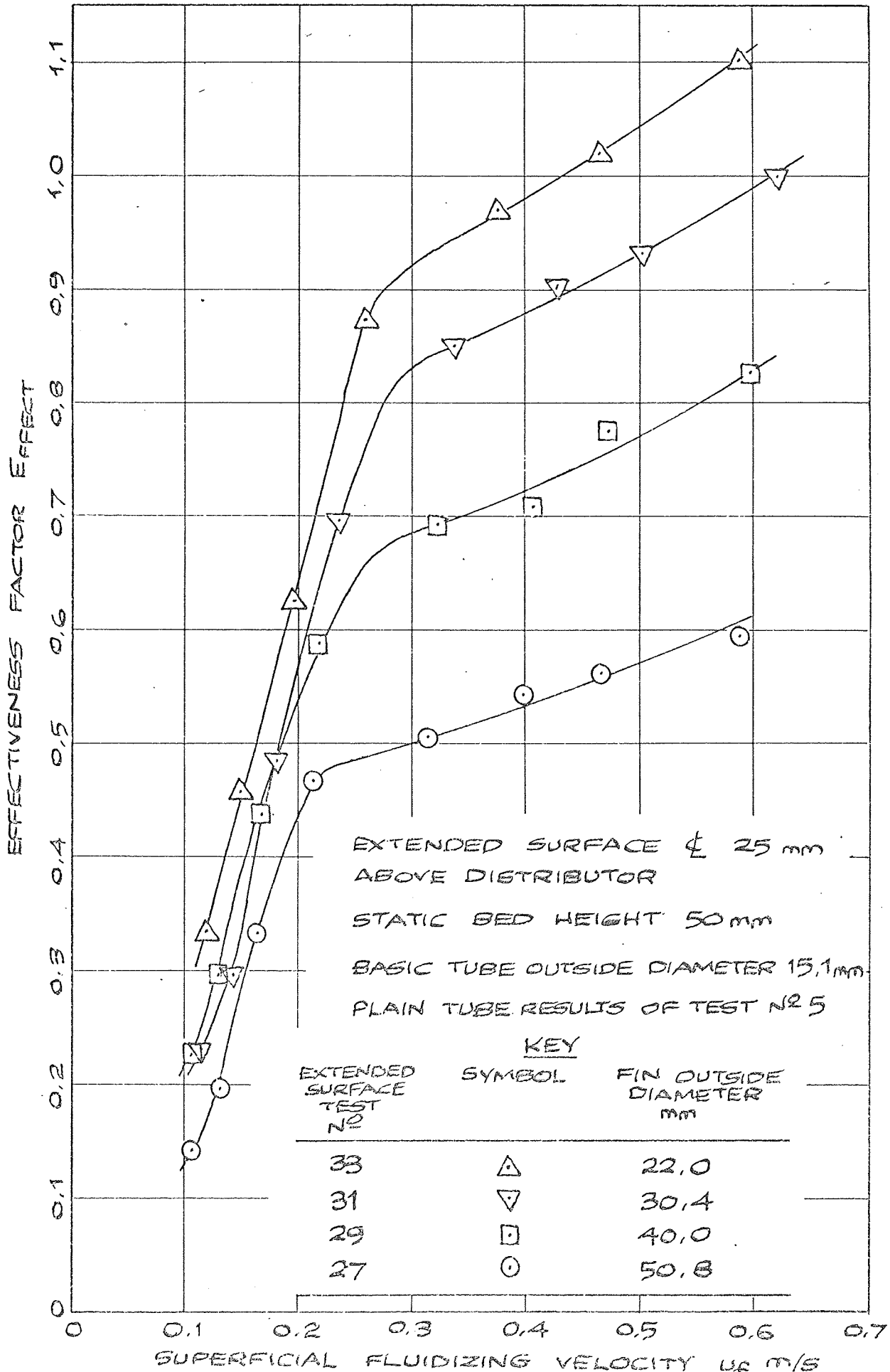

Figure 8.58 EFFECT OF FIN HEIGHT ON EFFECTIVENESS FACTOR FOR MANUFACTURED RADIAL EXTENDED SURFACE C/4/MR IN STEEL SHOT ($\bar{d}_p$ = 432 μm) IN MK 3 BED.

EXTENDED SURFACE ℄ 25 mm ABOVE DISTRIBUTOR

STATIC BED HEIGHT 50 mm

BASIC TUBE OUTSIDE DIAMETER 15,1 mm

PLAIN TUBE RESULTS OF TEST NUMBER 6

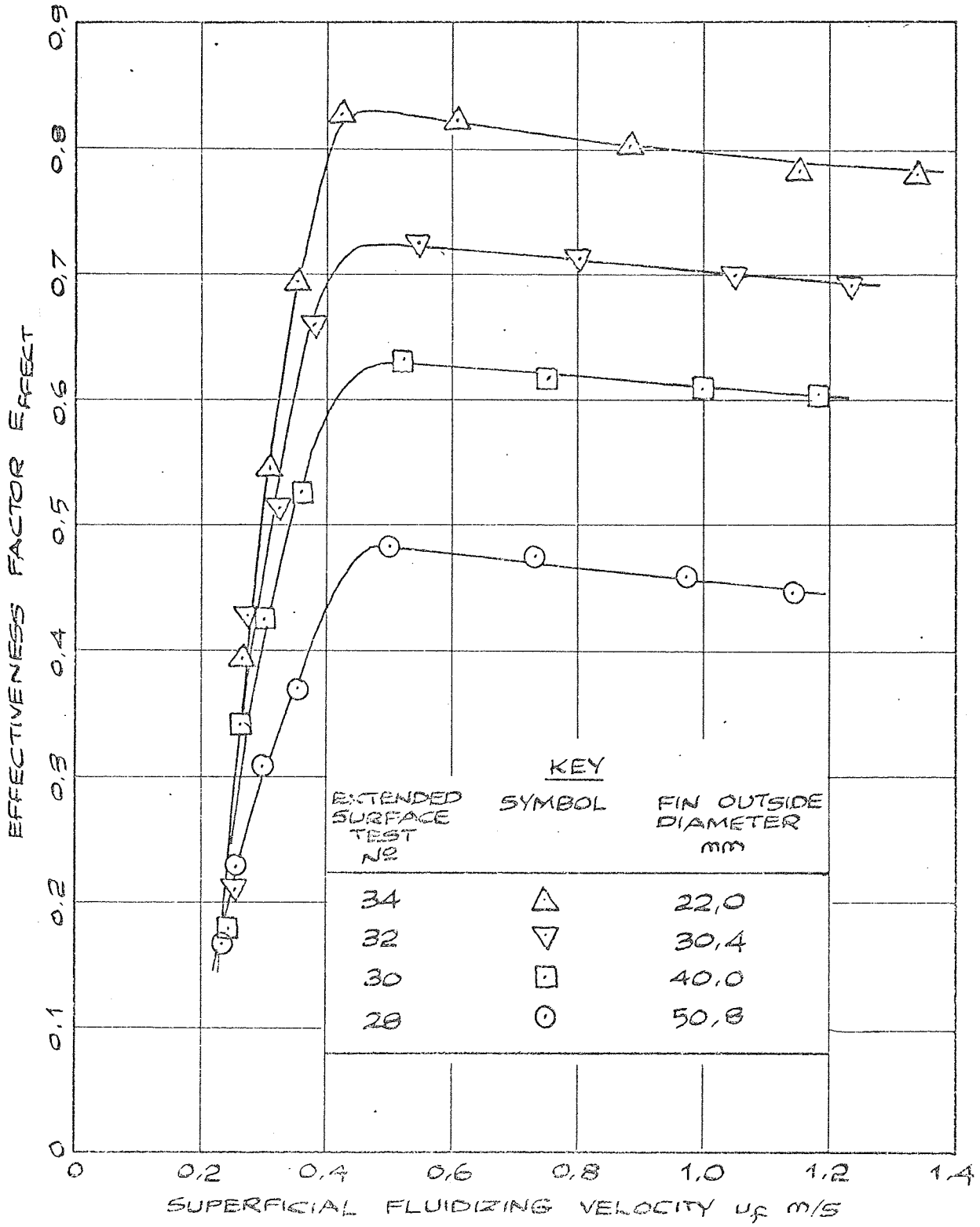

Figure 8.59

INFLUENCE OF BED SIZE ON EFFECTIVENESS FACTOR FOR MANUFACTURED RADIAL EXTENDED SURFACE C/4/MR (D = 50.8 mm) IN ZIRCON SAND ($\bar{d}_p$ = 138 mm).

EXTENDED SURFACE POSITIONED DIRECTLY ON DISTRIBUTOR.

STATIC BED HEIGHT 50 mm

PLAIN TUBE RESULTS OF TEST NUMBERS 1 AND 6

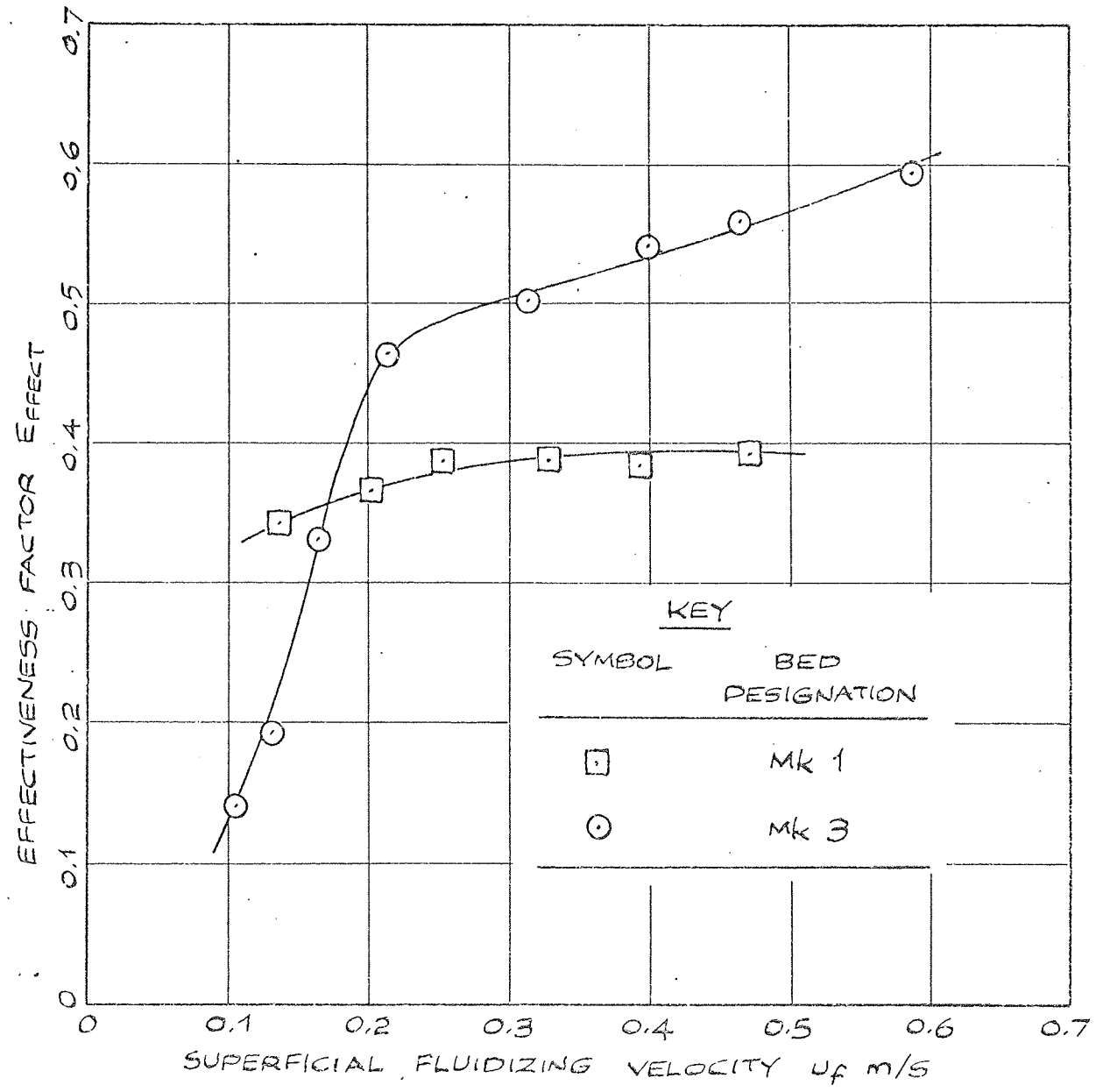

8.4.2 Crimped Radial Fin Experimental Results

Figure 8.60

EFFECT OF BASIC TUBE DIAMETER ON BED TO METAL HEAT TRANSFER COEFFICIENT FOR EXTENDED SURFACE IN Mk 3 BED - MATERIAL ZIRCON SAND ($\bar{d}_p$ = 138 μm)

HEAT TRANSFER COEFFICIENT BASED ON EFFECTIVE AREA.

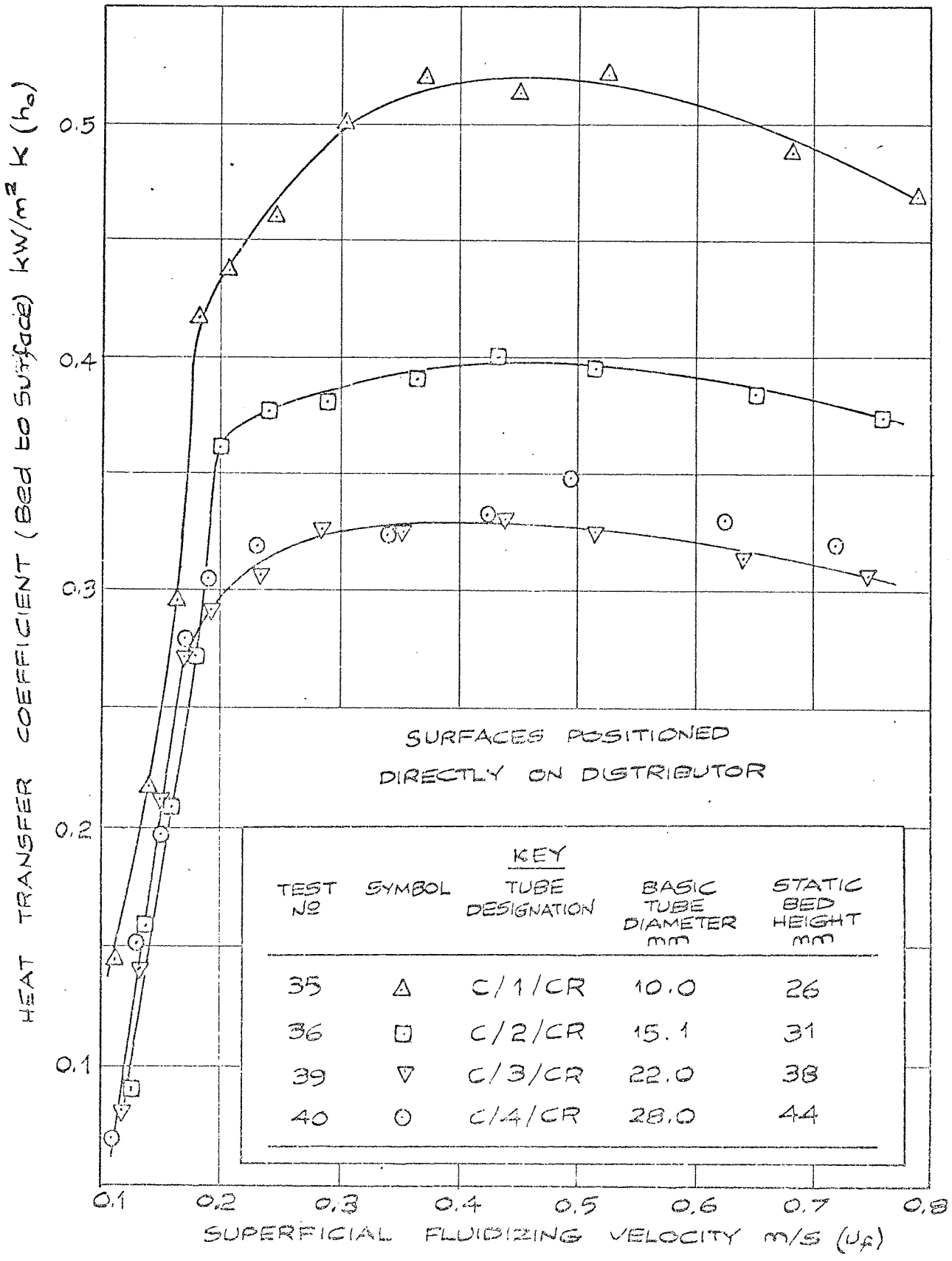

Figure 8.61 EFFECT OF BASIC TUBE OUTSIDE DIAMETER ON OVERALL HEAT TRANSFER COEFFICIENT FOR VARYING FLUIDIZING VELOCITY - CRIMPED RADIAL SURFACE IN ZIRCON SAND ($\bar{d}_p$ = 138 μm) IN Mk 3 BED.

HEAT TRANSFER COEFFICIENT BASED ON BASIC TUBE OUTSIDE SURFACE AREA.

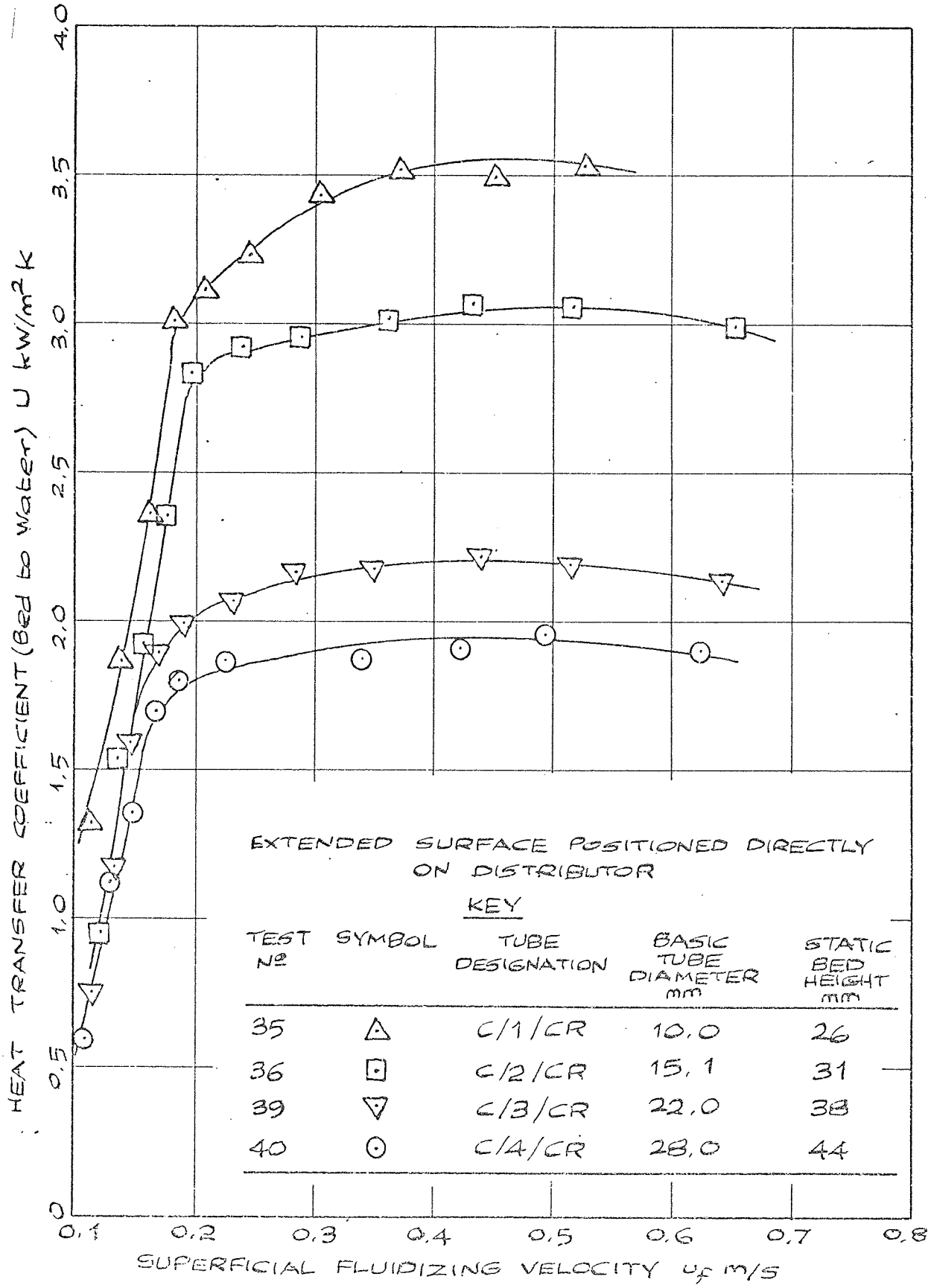

TEST Nº	SYMBOL	TUBE DESIGNATION	BASIC TUBE DIAMETER mm	STATIC BED HEIGHT mm
35	△	C/1/CR	10,0	26
36	□	C/2/CR	15,1	31
39	▽	C/3/CR	22,0	38
40	○	C/4/CR	28,0	44

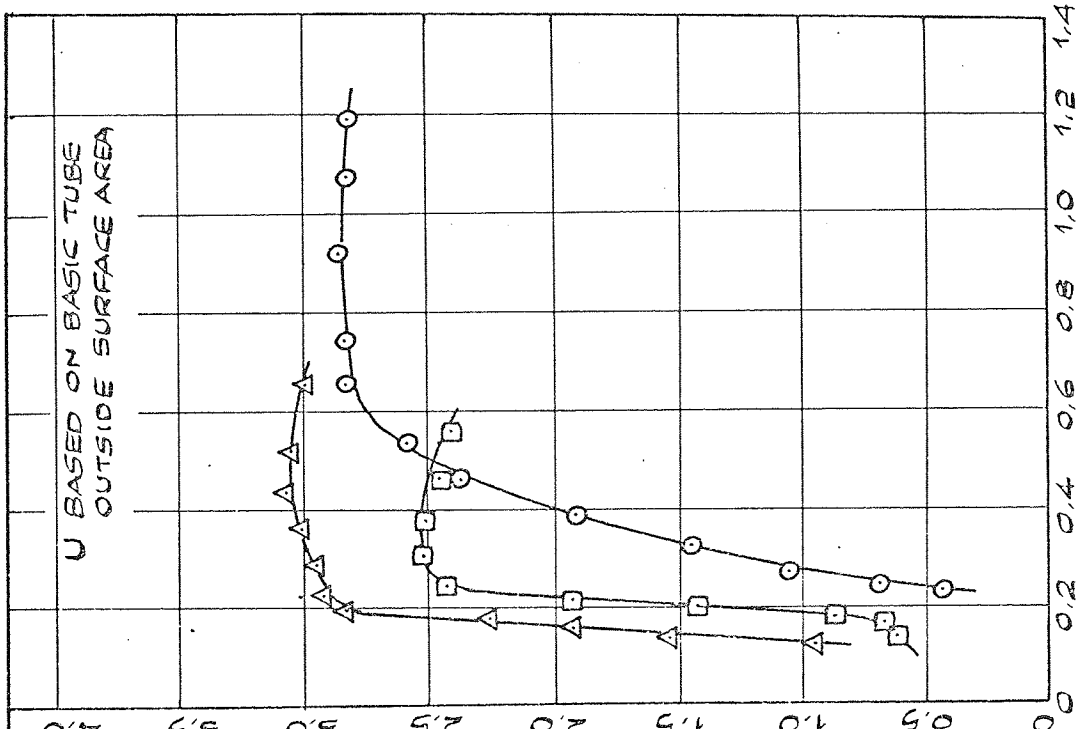

FIGURE 8.63

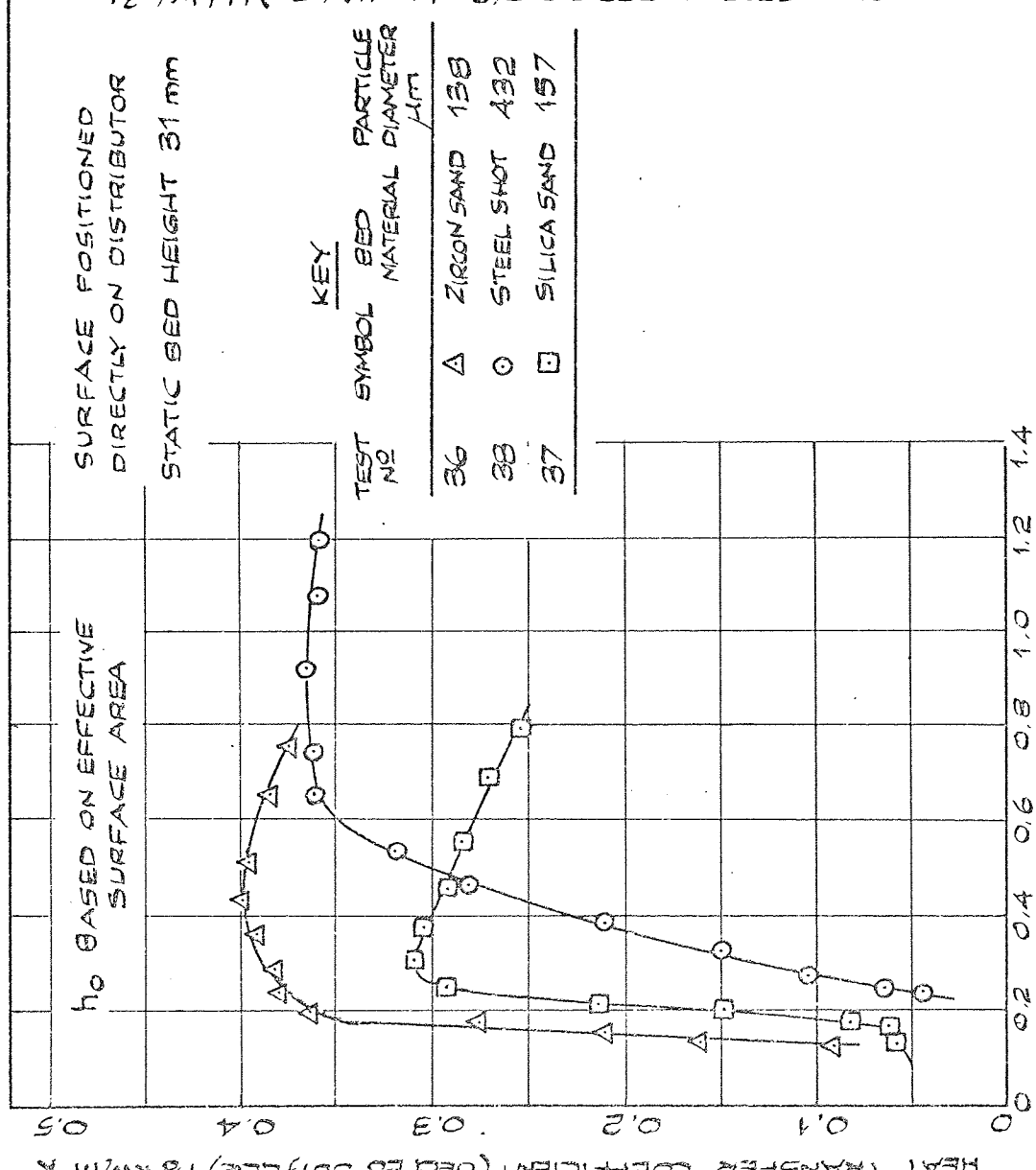

FIGURE 8.62

EFFECT OF BED MATERIAL ON HEAT TRANSFER COEFFICIENTS FOR CRIMPED RADIAL FIN EXTENDED SURFACE C/A1/SR IN Mk 3 BED.

Figure 8.64 EFFECT OF BED MATERIAL ON HEAT TRANSFER COEFFICIENT (Bed to Surface) FOR VARYING FLUIDIZING VELOCITY - CRIMPED RADIAL FIN SURFACE C/5/CR IN Mk 3 BED.

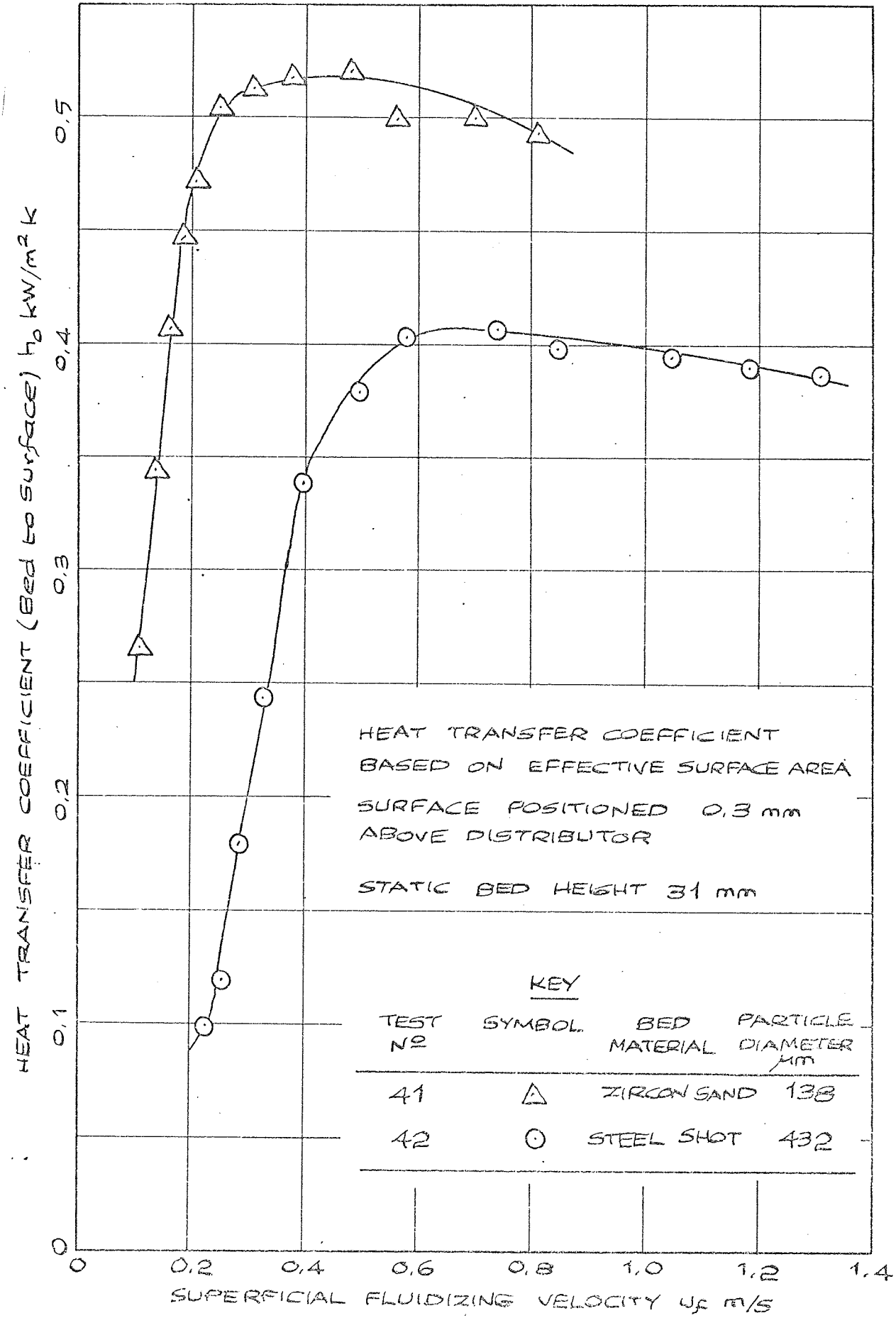

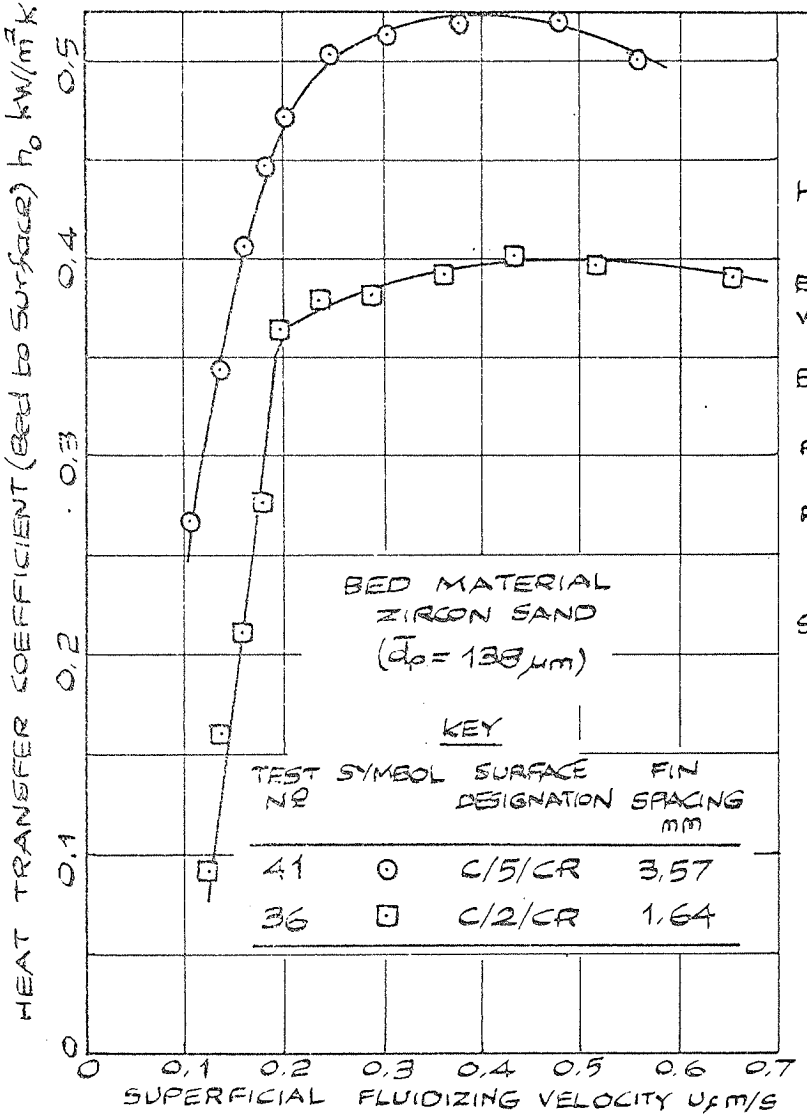

FIGURE 8.65

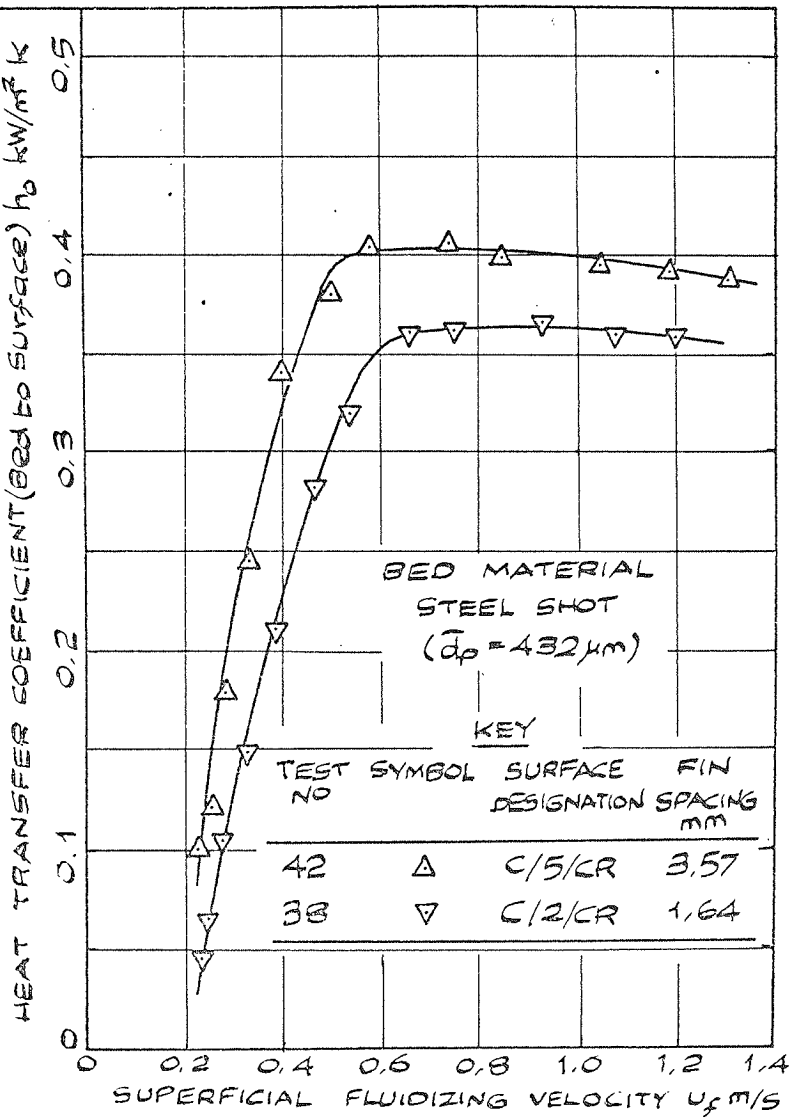

FIGURE 8.66

EFFECT OF FIN SPACING ON BED TO SURFACE HEAT TRANSFER COEFFICIENT FOR CRIMPED RADIAL FIN EXTENDED SURFACE IN MK 3 BED - VARIATION WITH BED MATERIAL.

Figure 8,67 EFFECT OF BED MATERIAL ON EFFECTIVENESS FACTOR FOR CRIMPED RADIAL EXTENDED SURFACE C/2/CR IN Mk3 BED

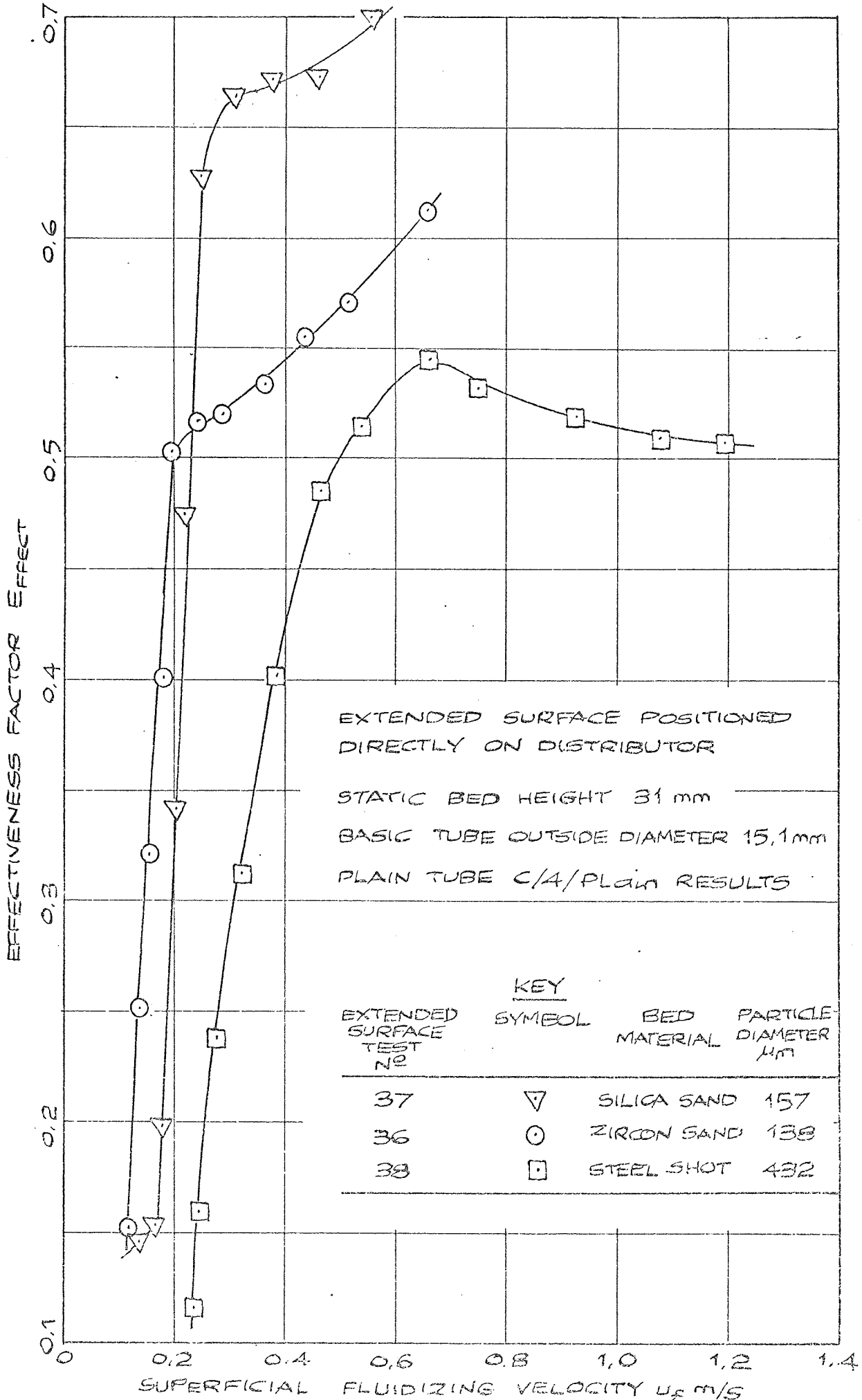

Figure 8.68 EFFECT OF BED MATERIAL ON EFFECTIVENESS FACTOR FOR CRIMPED RADIAL EXTENDED SURFACE C/5/CR IN MK 3 BED

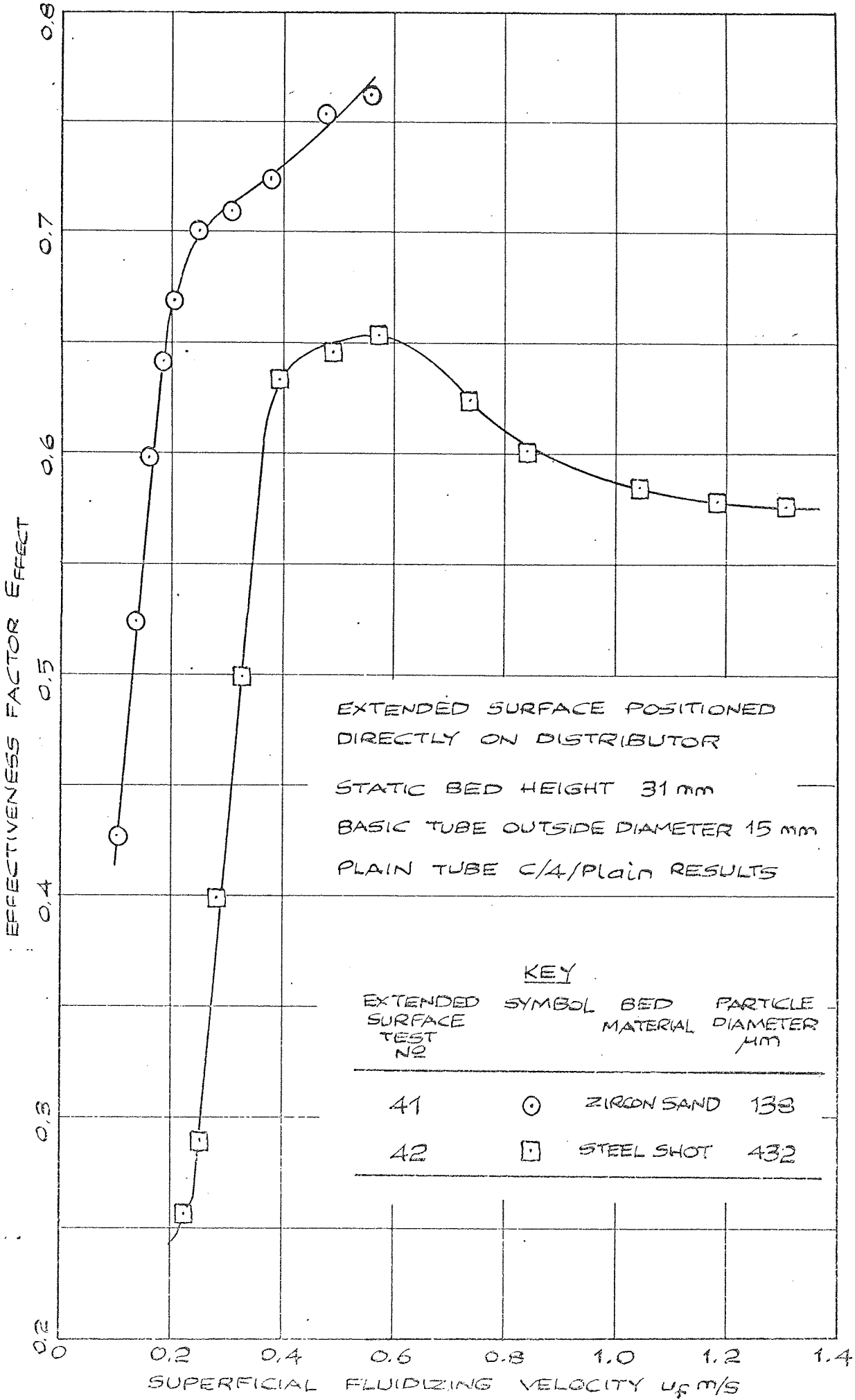

Thermocouple Probes to Establish Variation in Temperature between Adjacent Fins and Bulk of Bed

In order to investigate the possibility of a temperature difference existing between adjacent fins and the bulk of the bed a simple test was carried out.

An extended surface consisting of four fins, each 50.8 mm O/D by 15.0 mm I/D by 1.59 mm thick, was produced by brazing the fins onto a 15.0 mm diameter basic tube at a spacing of 5.0 mm. The lower fin tip edge was then located 29 mm above the distributor of the Mk 2 bed and thermocouple probes arranged as shown in figures 8.69 and 8.70. Four thermocouples were made from 40 S.W.G. chromel/alumel wire and connected to form the circuit as shown in figure 8.69. The output of thermocouples 1 and 3 combined and 2 and 4 combined produced trace 1 and trace 2 respectively on a Solartron oscilloscope. The resolution of the instrument was 1 mV/cm which approximated to 1 mm/2.5 K temperature difference. Thus temperature changes of this magnitude could be detected.

Before tests commenced, zircon sand was sieved into the bed to a static height of 79 mm. The surface was subjected to a range of superficial fluidizing velocities (0.1 - 0.5 m/s) with the bed temperature varying from 250°C to 300°C. During the test thermocouple 3 was positioned between the central adjacent fins, above, to the side and below the basic tube at approximately 9 mm from the fin tip edge. No temperature difference was observed on the oscilloscope at each test condition.

The test was repeated using a second surface of four fins with a spacing of 2.5 mm. A small temperature difference in the order of 3 K was detected at all readings.

It was concluded that at typical representative experimental conditions the temperature between adjacent fins is for all intents and purposes the bed temperature. Thus the assumption made in Section 3.3.1 of Chapter III is valid.

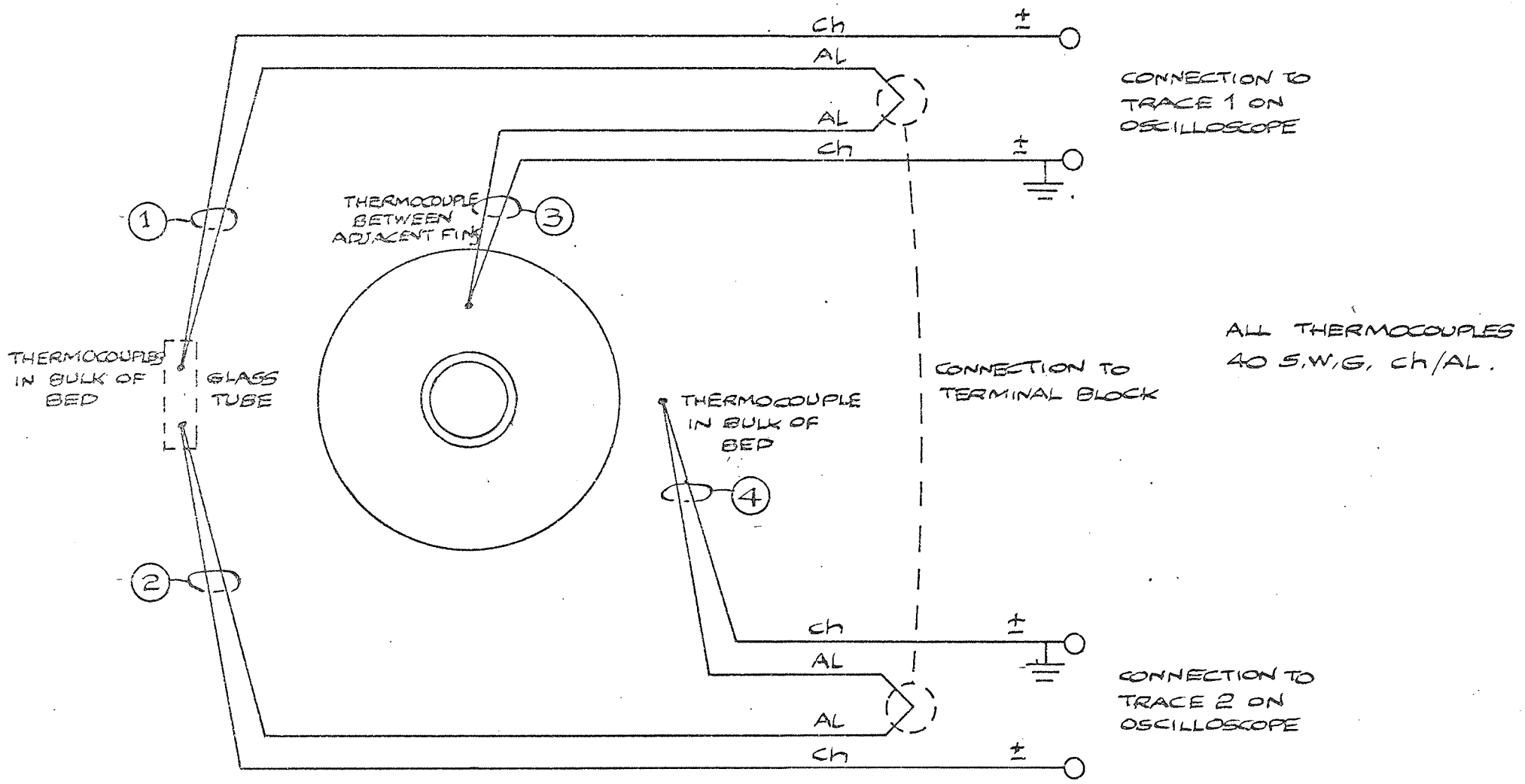

Figure 8.69 Thermocouple Circuit for Measurement of Temperature Difference between Adjacent Fins and Bulk of Bed

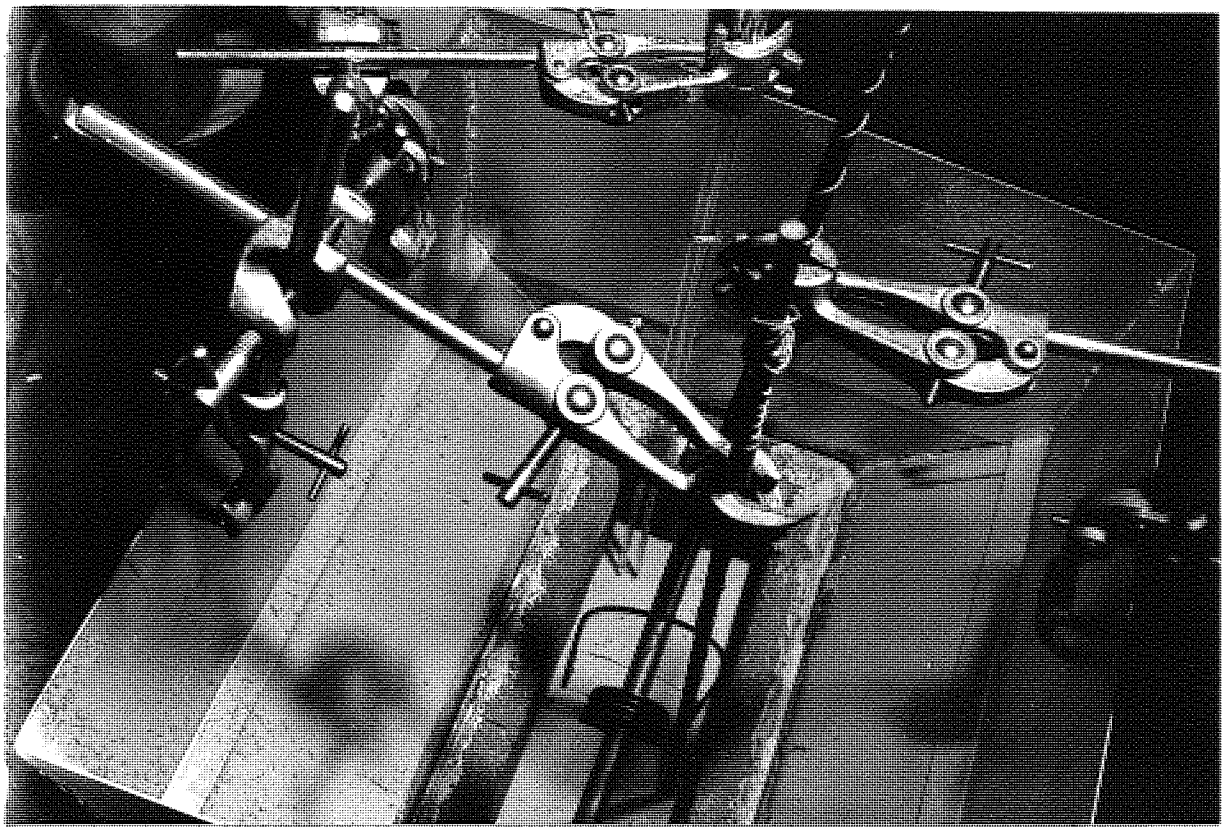

Figure 8.70 Thermocouple Probes for Measurement of Bed Temperature between Adjacent Fins

8.4.3 Graph Plotter Results for Manufactured and Crimped Surfaces in Mk 3 Bed in Zircon Sand

The following figures 8.71 to 8.76 inclusive are the graph plotter results using the presentation programme outlined in Appendix A2. The regression equation given in Appendix A6, section A6.4.1 was used, together with the following typical values:-

VELOTY = 0.5 m/s	VELSQU = 0.25 m^2/s^2
TEMBED = 175°C	SQTSPA = 1.5 $mm^{\frac{1}{2}}$ (SPACNG = 2.25 mm)
TUBDIA = 15 mm	HEIGHT = 8 mm

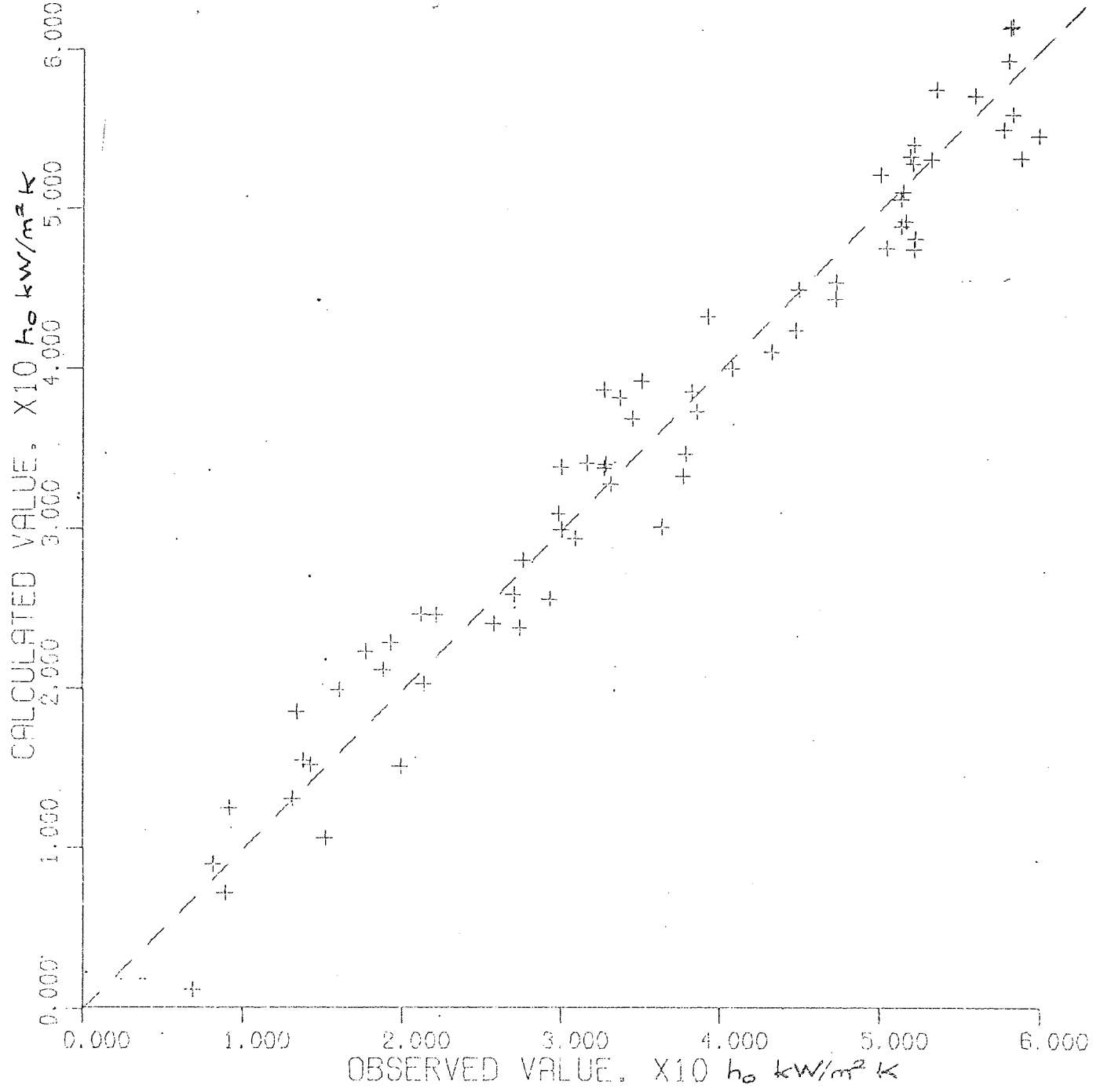

Figure 8.71

Manufactured and Crimped Radial Fin Surface Analysis in Zircon Sand in Mk 3 Bed.

OBSERVED V CALCULATED.

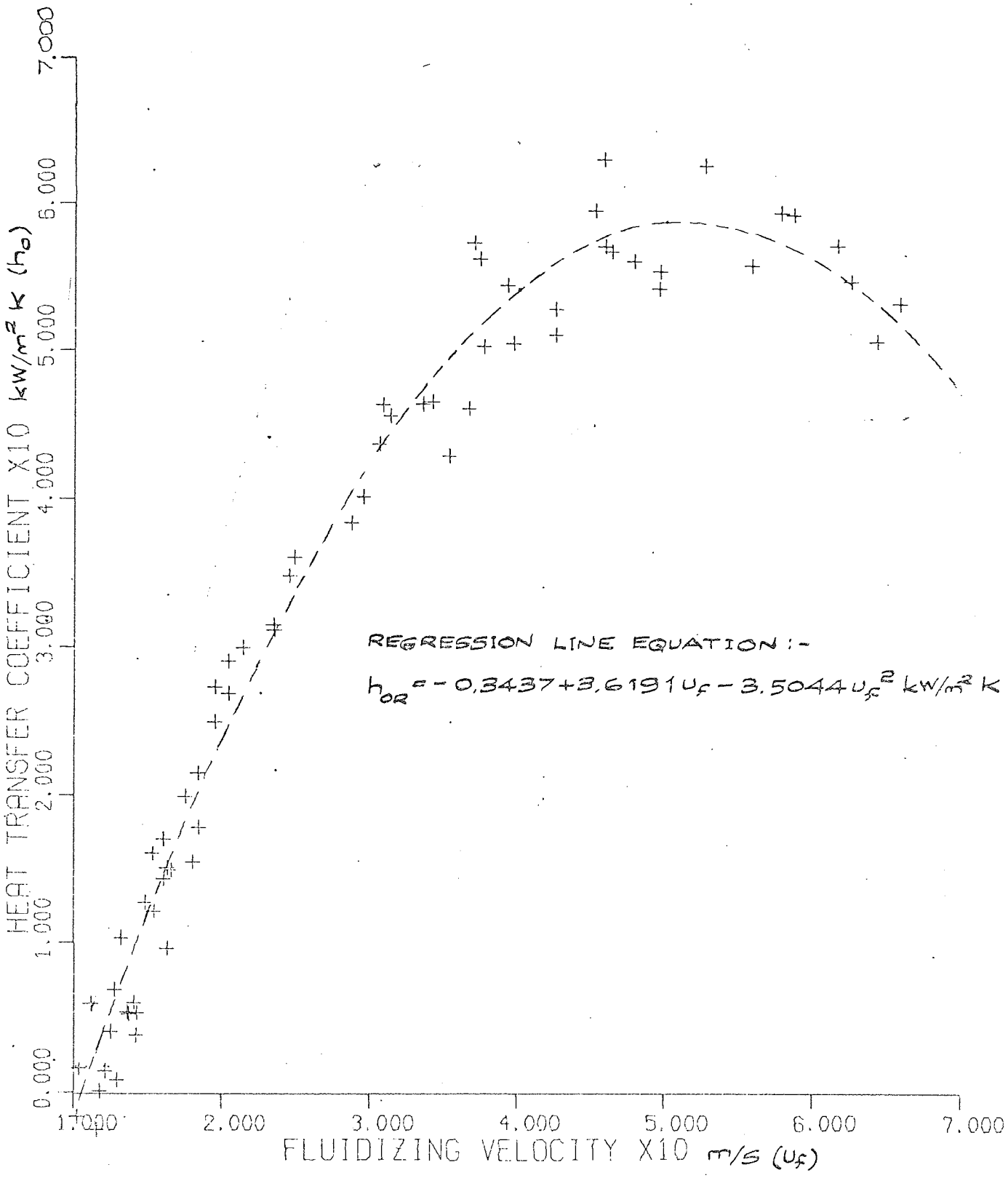

Figure 8.72

Manufactured and Crimped Radial Fin Surface Analysis in Zircon Sand in Mk 3 Bed

HO VERSUS VELOCITY

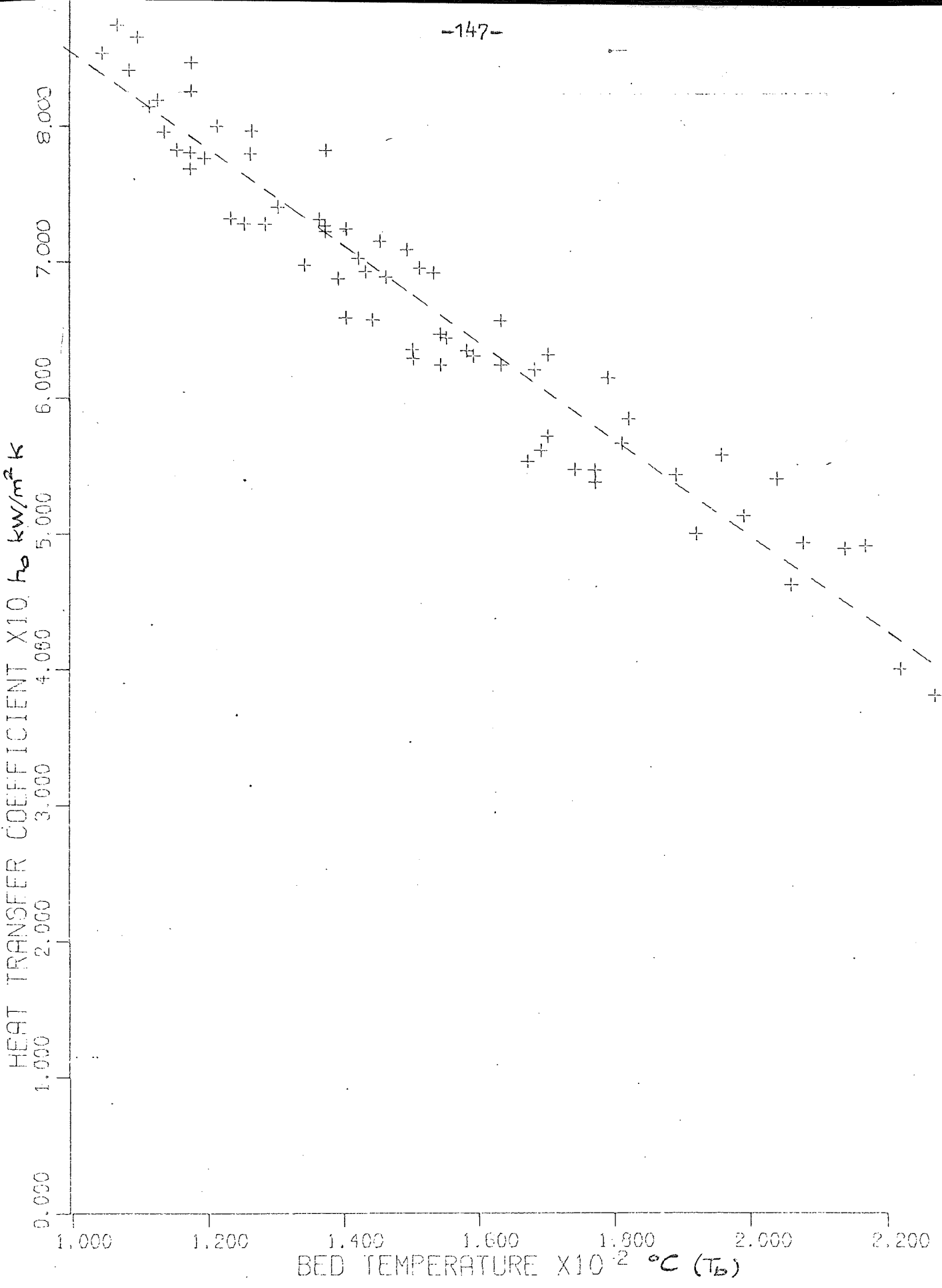

Figure 8.73

HO VERSUS BED TEMPERATURE

Manufactured and Crimped Radial Fin Surface Analysis in Zircon Sand in Mk 3 Bed

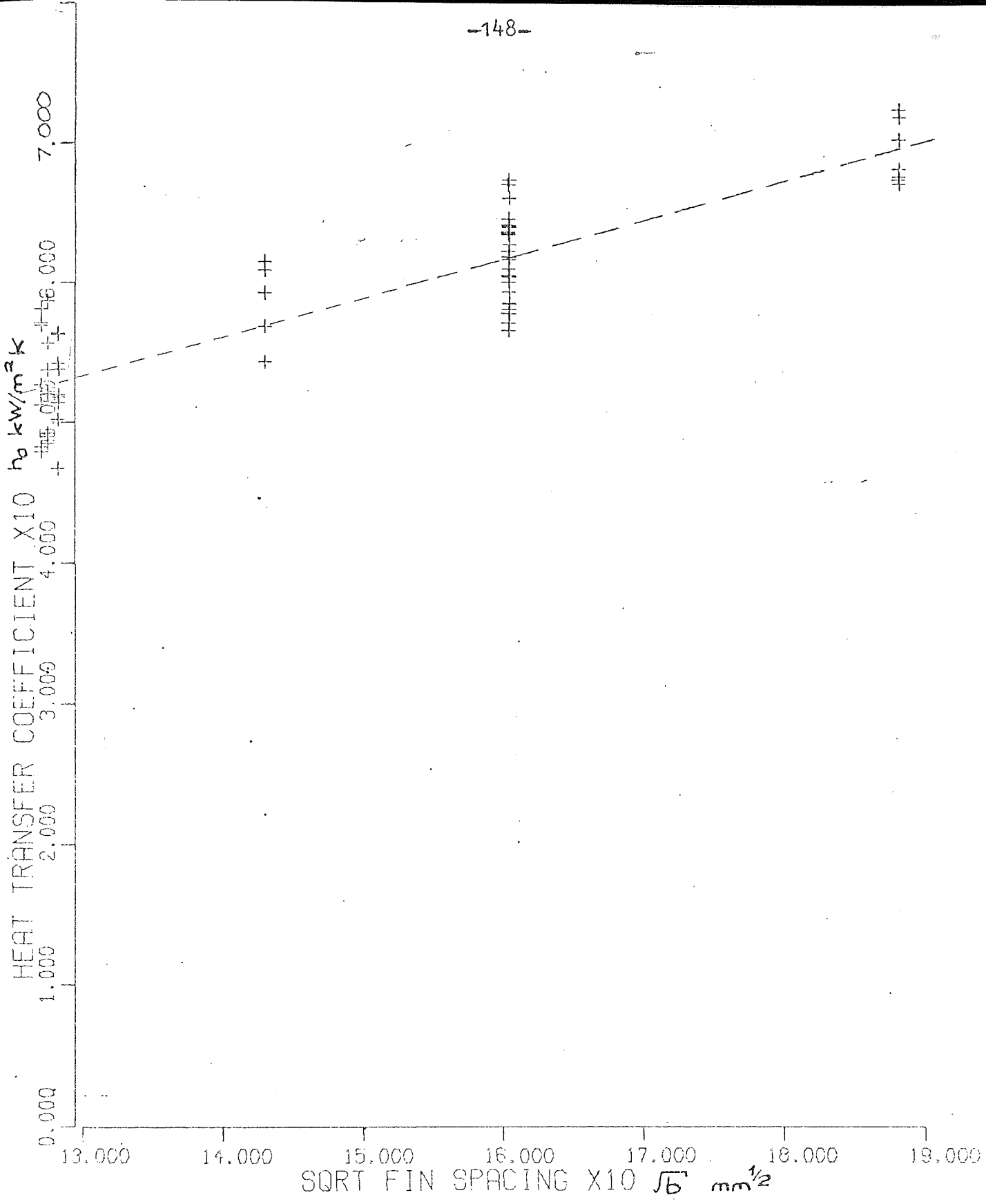

Figure 8.74

Manufactured and Crimped Radial Fin Surface Analysis in Zircon Sand in Mk 3 Bed

HO VERSUS SQTSPA

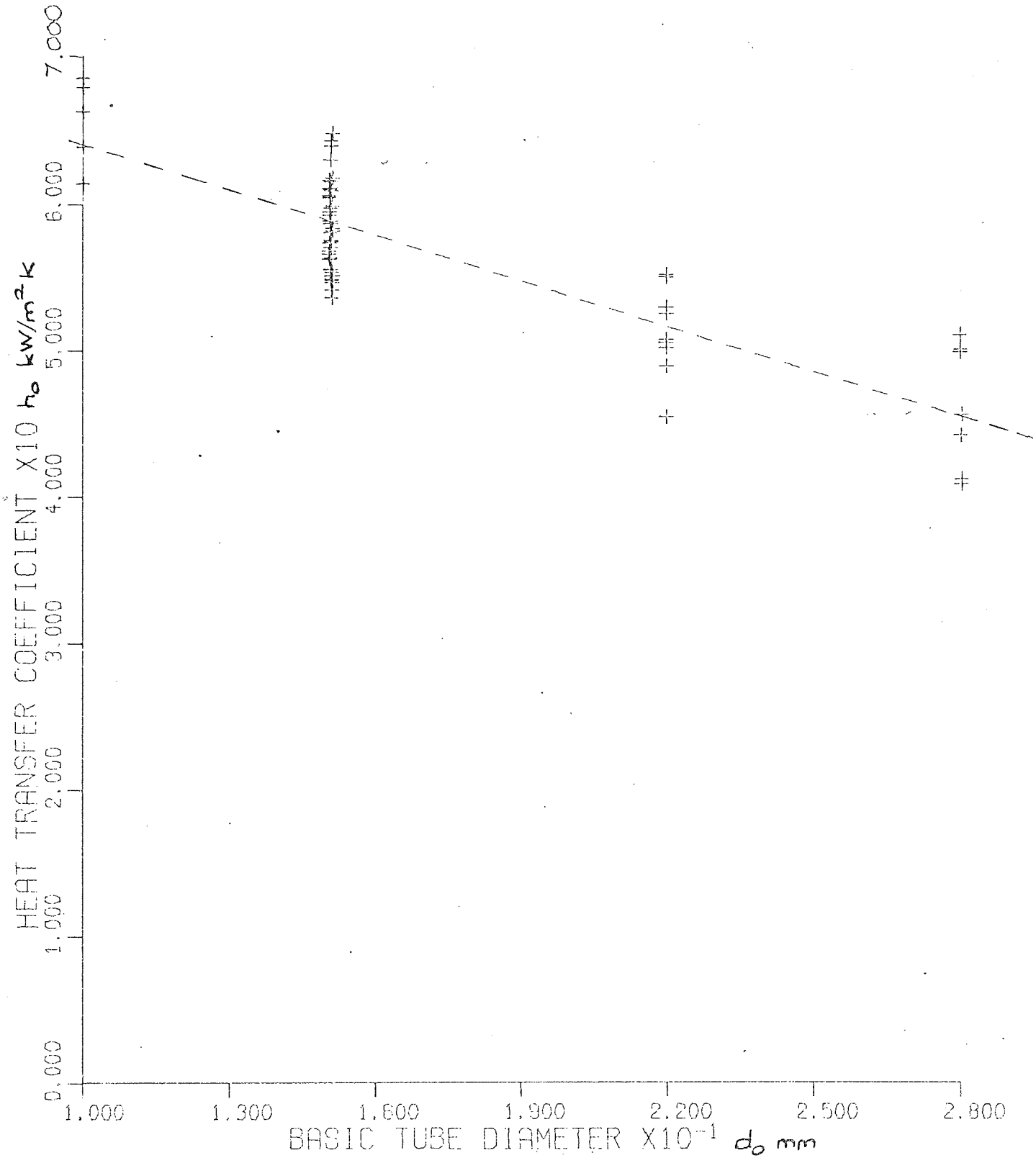

Figure 8.75

Manufactured and Crimped Radial Fin Surface Analysis in Zircon Sand in Mk 3 Bed

HO VERSUS TUBE DIAMETER

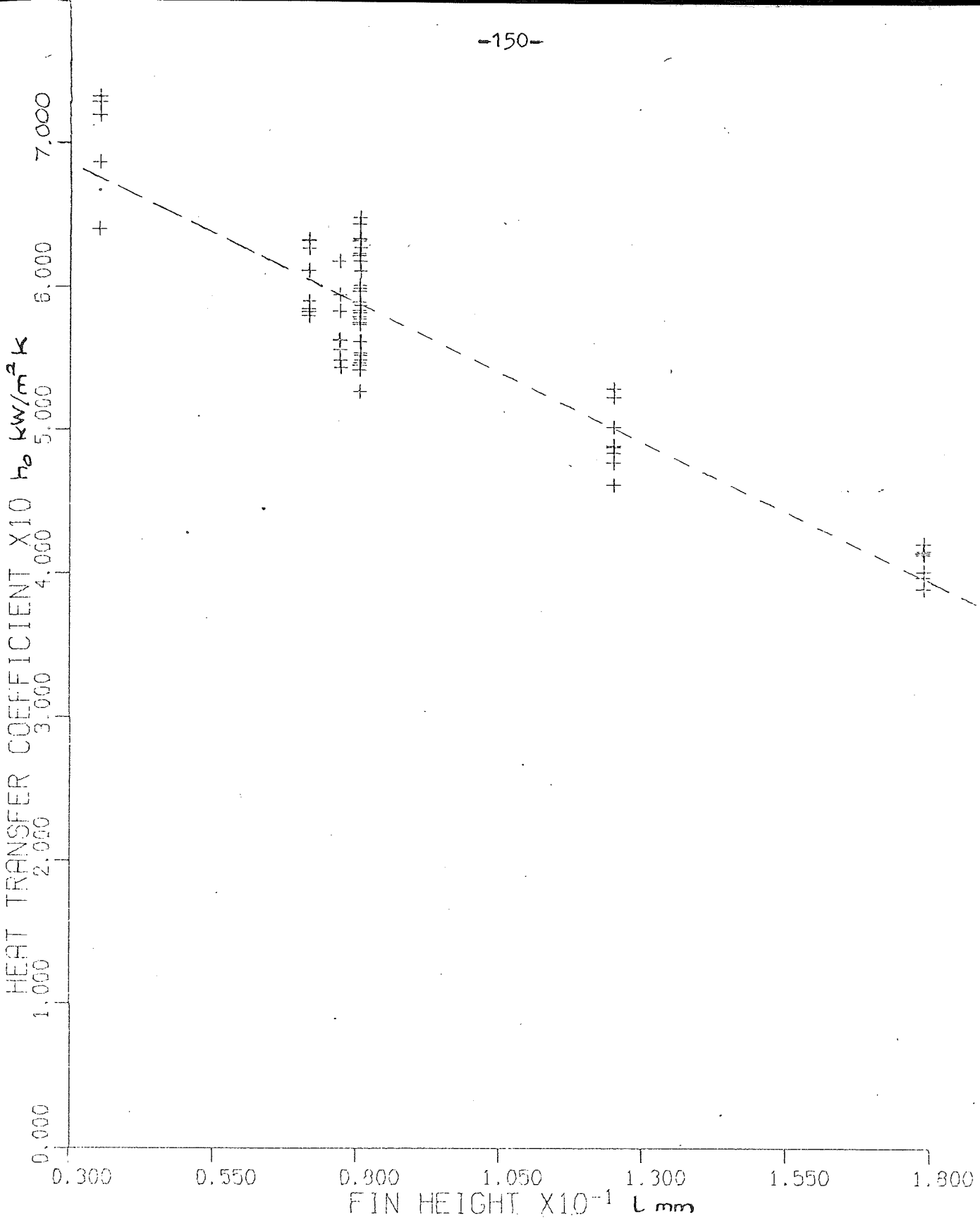

Figure 8.76

Manufactured and Crimped Radial Fin Surface Analysis in Zircon Sand in Mk 3 Bed

HO VERSUS FIN HEIGHT

8.4.4 Extruded Surface Experimental Results

Figure 8.77 VARIATION IN BED TO SURFACE HEAT TRANSFER COEFFICIENT FOR COPPER HIGH-FIN EXTRUDED SURFACES IN ZIRCON SAND ($\bar{d}_p$ = 138 μm) IN Mk 1 BED.

HEAT TRANSFER COEFFICIENT BASED ON EFFECTIVE SURFACE AREA.

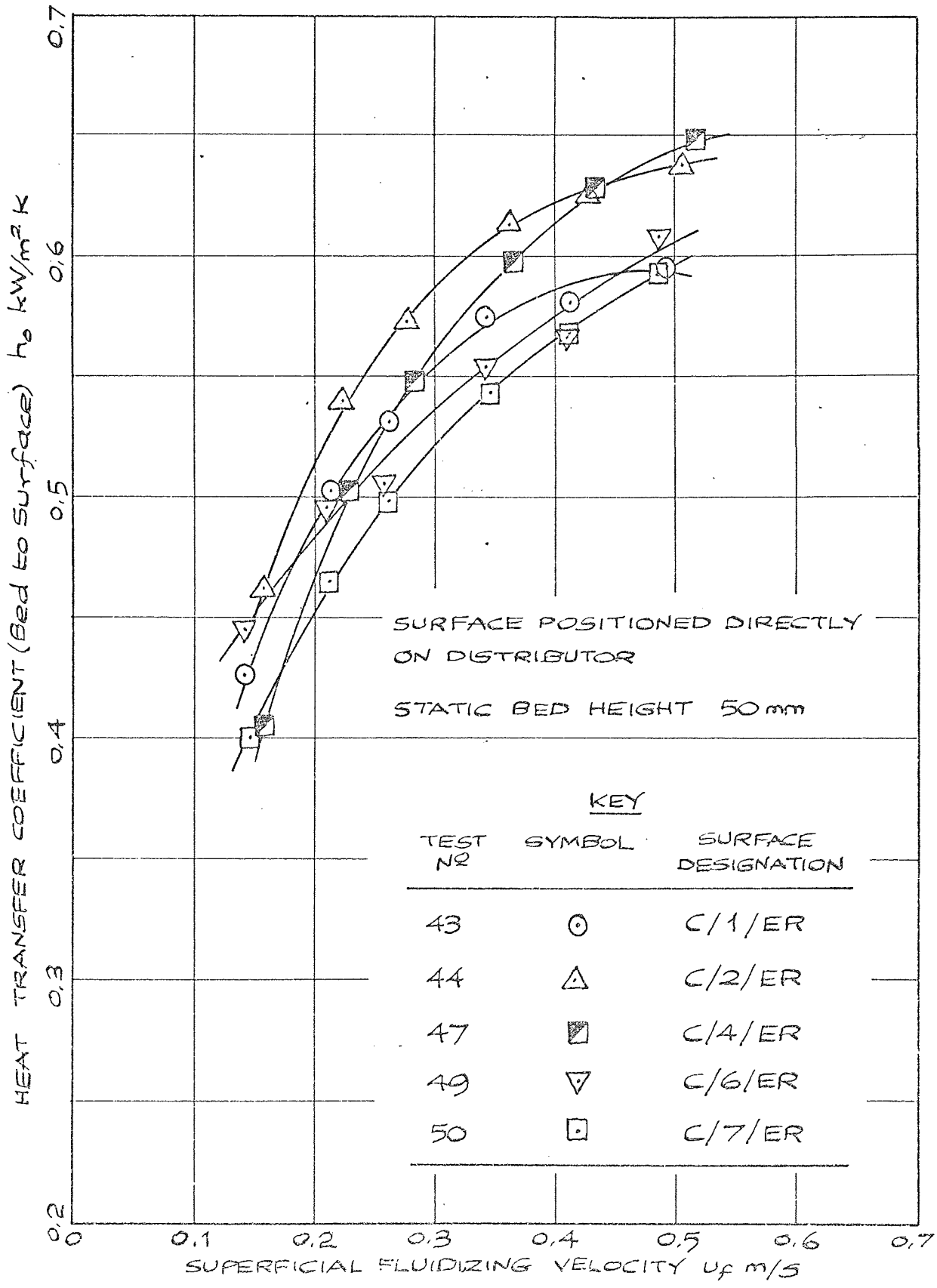

Figure 8.78 VARIATION IN BED TO SURFACE HEAT TRANSFER COEFFICIENT FOR MILD STEEL EXTRUDED SURFACES IN ZIRCON SAND (d_p = 138 μm) IN Mk 1 BED.

HEAT TRANSFER COEFFICIENT BASED ON EFFECTIVE SURFACE AREA.

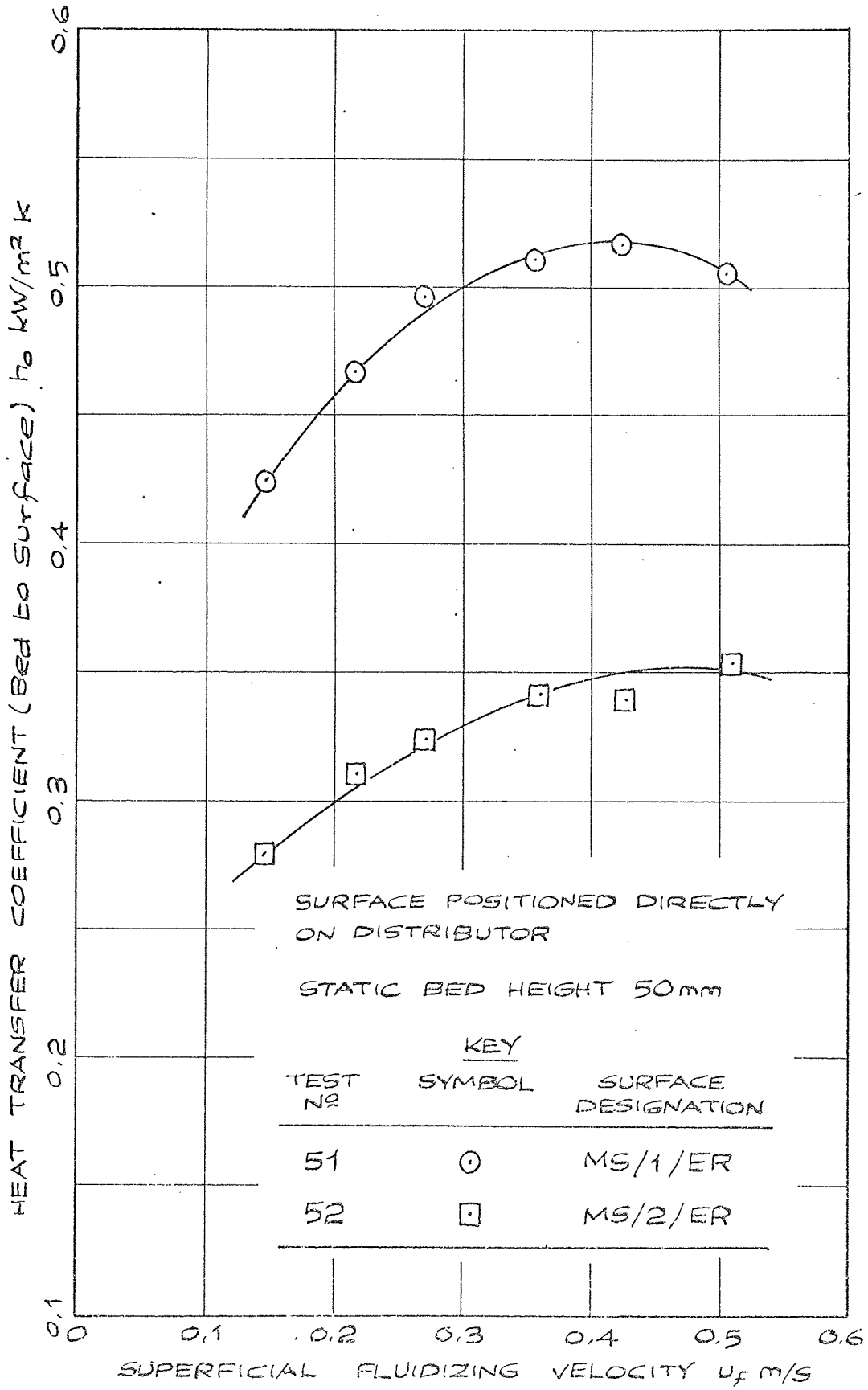

Figure 8,79

OVERALL HEAT TRANSFER COEFFICIENT FOR ALL HIGH FIN EXTRUDED SURFACES IN ZIRCON SAND ($\bar{d}_p = 138\,\mu m$) IN Mk1 BED.

HEAT TRANSFER COEFFICIENT BASED ON BASIC TUBE OUTSIDE SURFACE AREA.

KEY

TEST Nº	SYMBOL	SURFACE DESIGNATION
43	⊙	C/1/ER
44	△	C/2/ER
47	⊡	C/4/ER
49	▽	C/6/ER
50	▨	C/7/ER
51	◐	MS/1/ER
52	▲	MS/2/ER

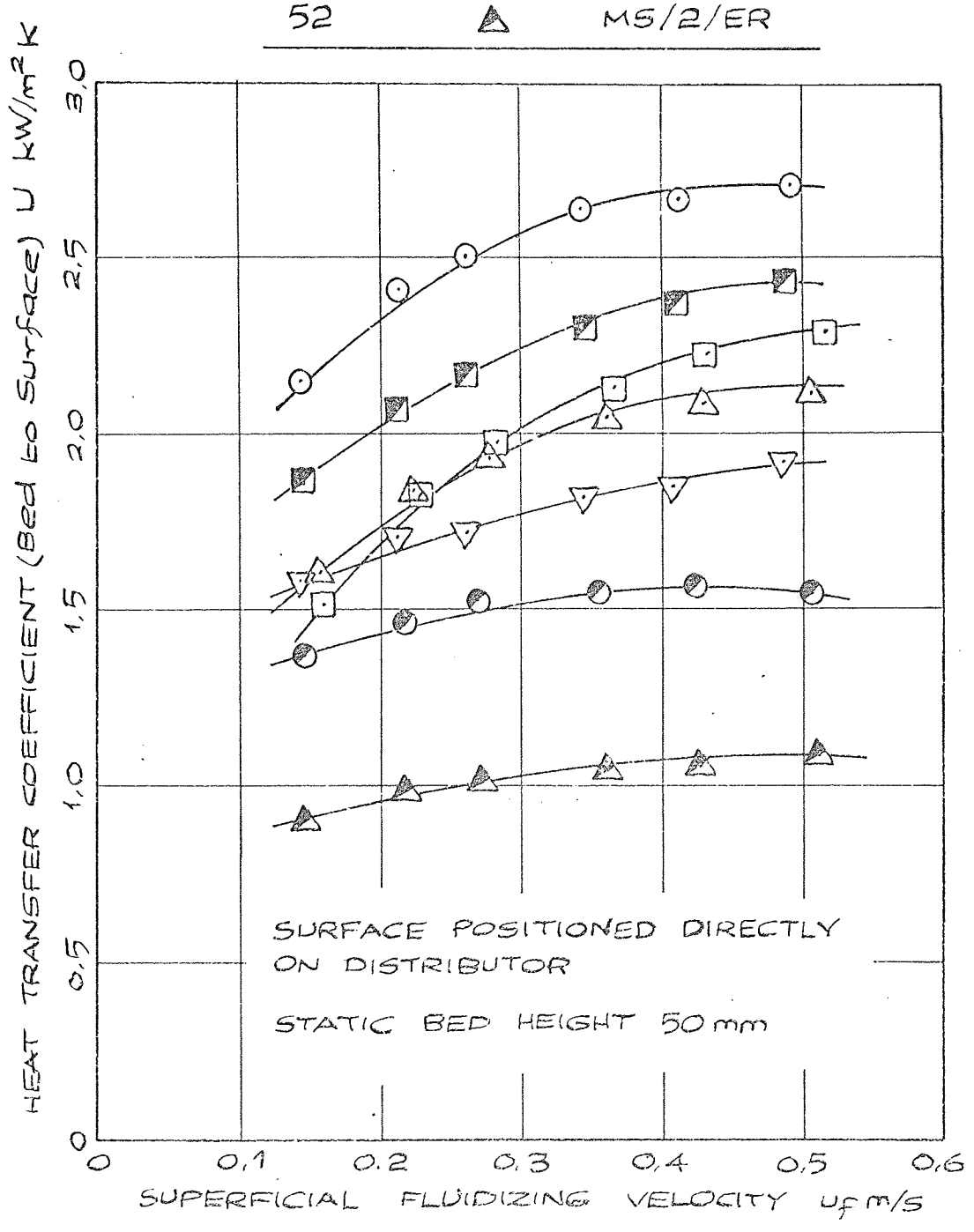

Figure 8,80 HEAT TRANSFER COEFFICIENTS FOR LOW-FIN COPPER EXTRUDED SURFACES IN ZIRCON SAND (d_p = 138 μm) IN Mk 1 BED

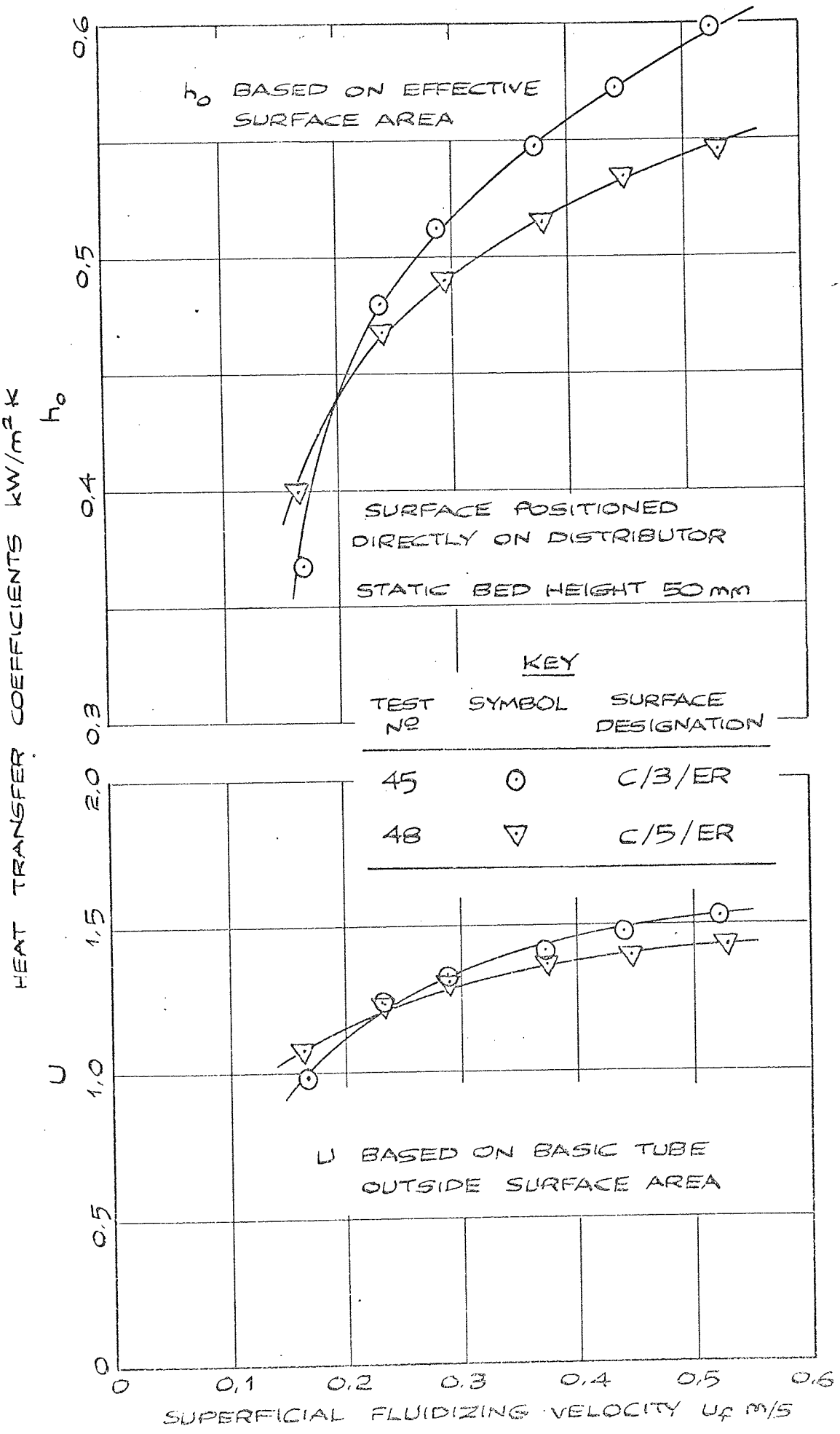

Consideration of Geometric Variables Affecting Heat Transfer Coefficient (Bed to Surface) h_o

TABLE POSITION	SURFACE DESIGNATION	FIN HEIGHT mm	POINTS AWARDED
1	C/4/ER	3.24	5
2	C/2/ER	3.37	4
3	C/6/ER	8.32	3
4	C/1/ER	8.82	2
5	C/7/ER	8.89	1

TABLE POSITION	SURFACE DESIGNATION	FIN SPACING mm	POINTS AWARDED
1	C/6/ER	3.07	5
2	C/1/ER	3.04	4
3	C/7/ER	2.95	3
4	C/2/ER	1.93	2
5	C/4/ER	1.74	1

TABLE POSITION	SURFACE DESIGNATION	BASIC TUBE O/D mm	POINTS AWARDED
1	C/4/ER	12.57	5
2	C/2/ER	15.49	4
3	C/1/ER	18.31	3
4	C/7/ER	22.23	2
5	C/6/ER	29.08	1

OVERALL POSITION	SURFACE DESIGNATION	TOTAL POINTS
1	C/4/ER	11
2	C/2/ER	10
3	C/6/ER	9
3	C/1/ER	9
5	C/7/ER	6

TABLE 8.1 League Tables for High Fin Copper Extruded Surfaces

Figure 8.81

EFFECT OF SURFACE POSITION ON THE BED TO SURFACE HEAT TRANSFER COEFFICIENT FOR LOW-FIN COPPER EXTRUDED SURFACE C/3/ER IN ZIRCON SAND ($\bar{d}_p$ = 138 μm) IN Mk 1 BED.

HEAT TRANSFER COEFFICIENT BASED ON EFFECTIVE SURFACE AREA

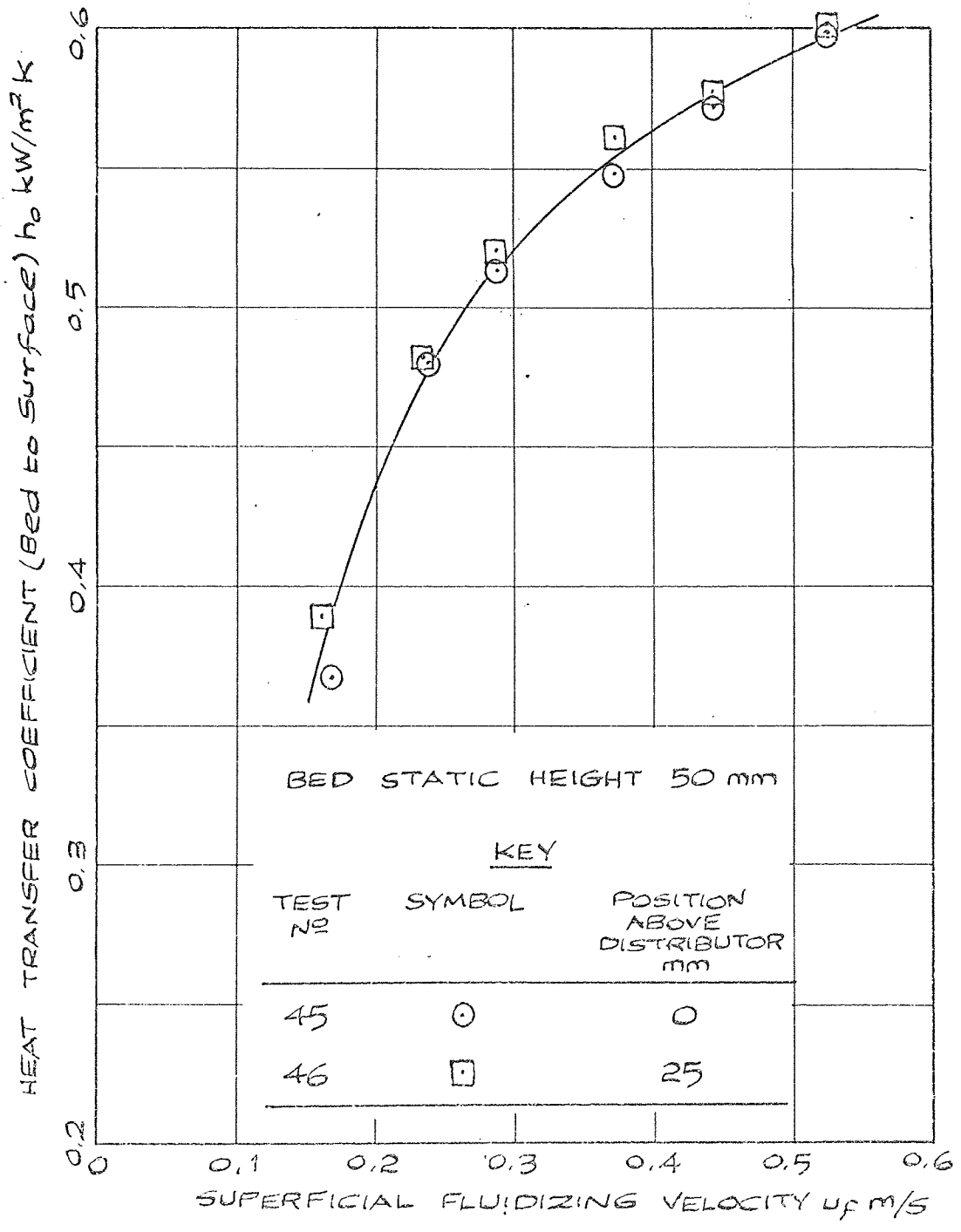

Figure 8.82 EFFECTIVENESS FACTORS FOR EXTRUDED EXTENDED SURFACE IN ZIRCON SAND ($\bar{d}_p$ = 138 μm) IN MK 1 BED.

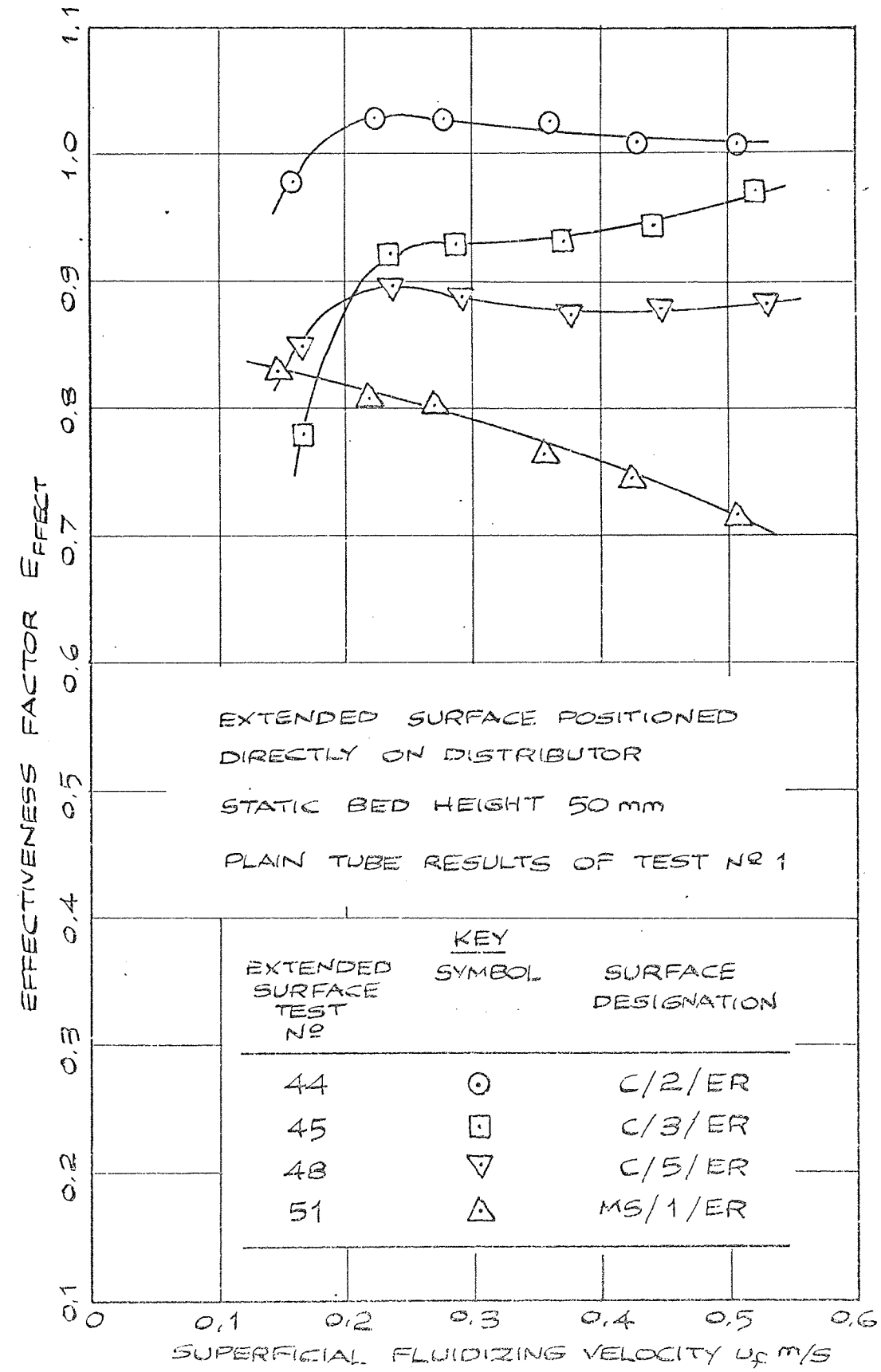

8.4.5 Statistical Analysis of All Results

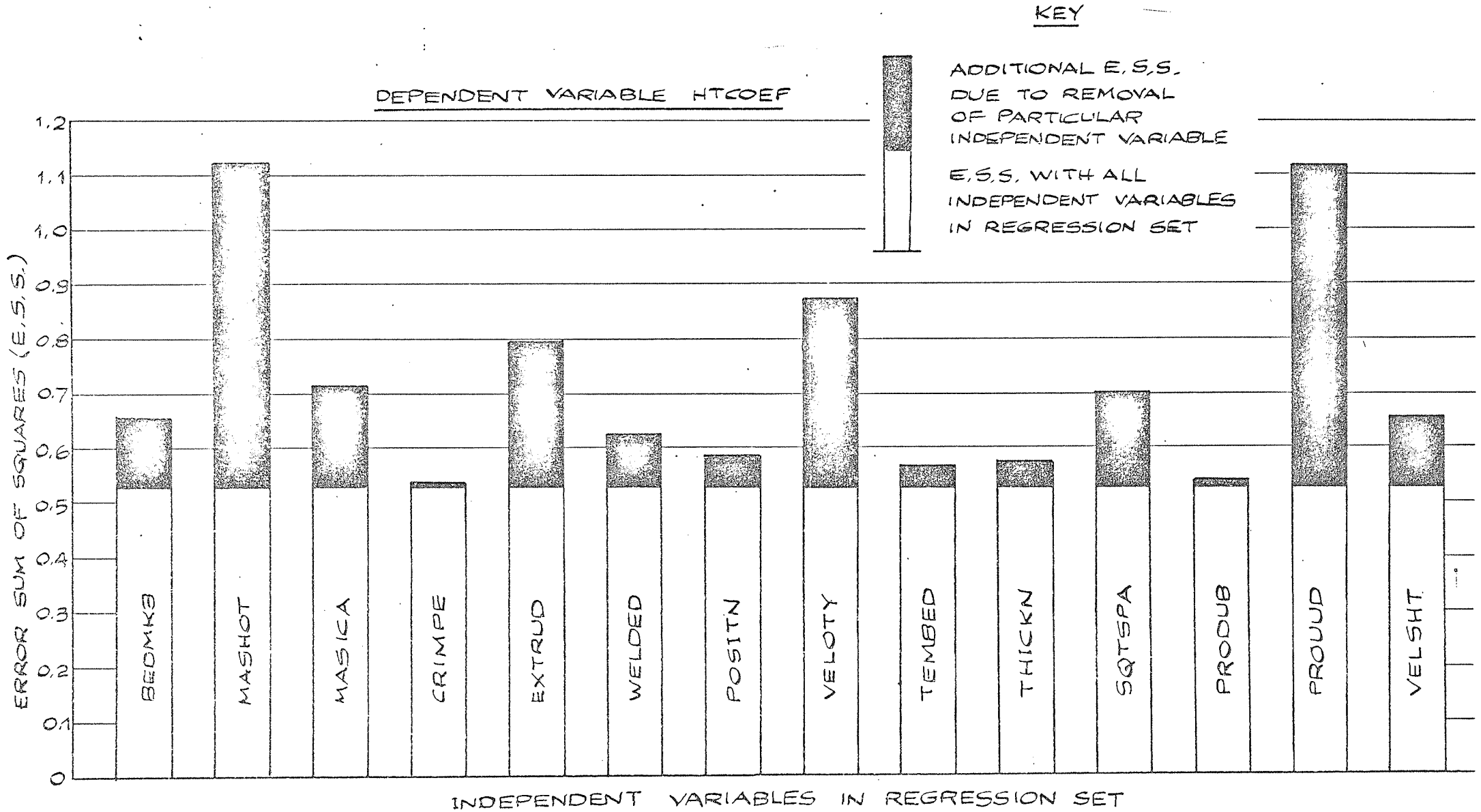

Figure 8.83 BAR CHART INDICATING SIGNIFICANCE OF INDEPENDENT VARIABLES – RADIAL EXTENDED SURFACE STATISTICAL ANALYSIS OF EXPERIMENTAL RESULTS

Figure 8.84 INFLUENCE OF BASIC TUBE OUTSIDE DIAMETER ON BED TO SURFACE HEAT TRANSFER COEFFICIENT DETERMINED FROM REGRESSION EQUATION.

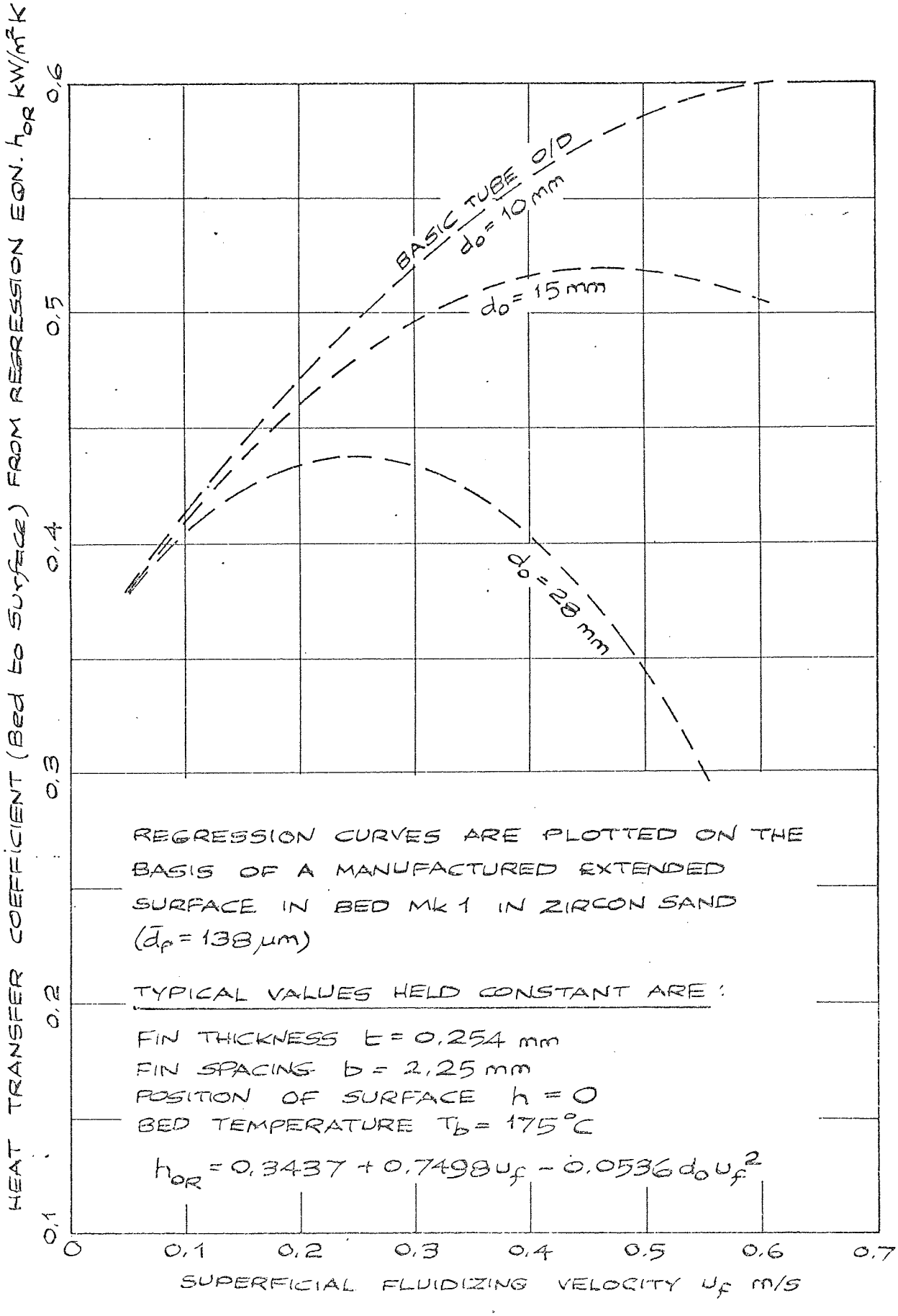

8.5 Welded Radial Fin and Spine Experimental Results

Figure 8.85 HEAT TRANSFER COEFFICIENTS FOR WELDED RADIAL FIN AND SPINE SURFACES IN ZIRCON SAND (d_p = 138 μm) IN Mk1 BED

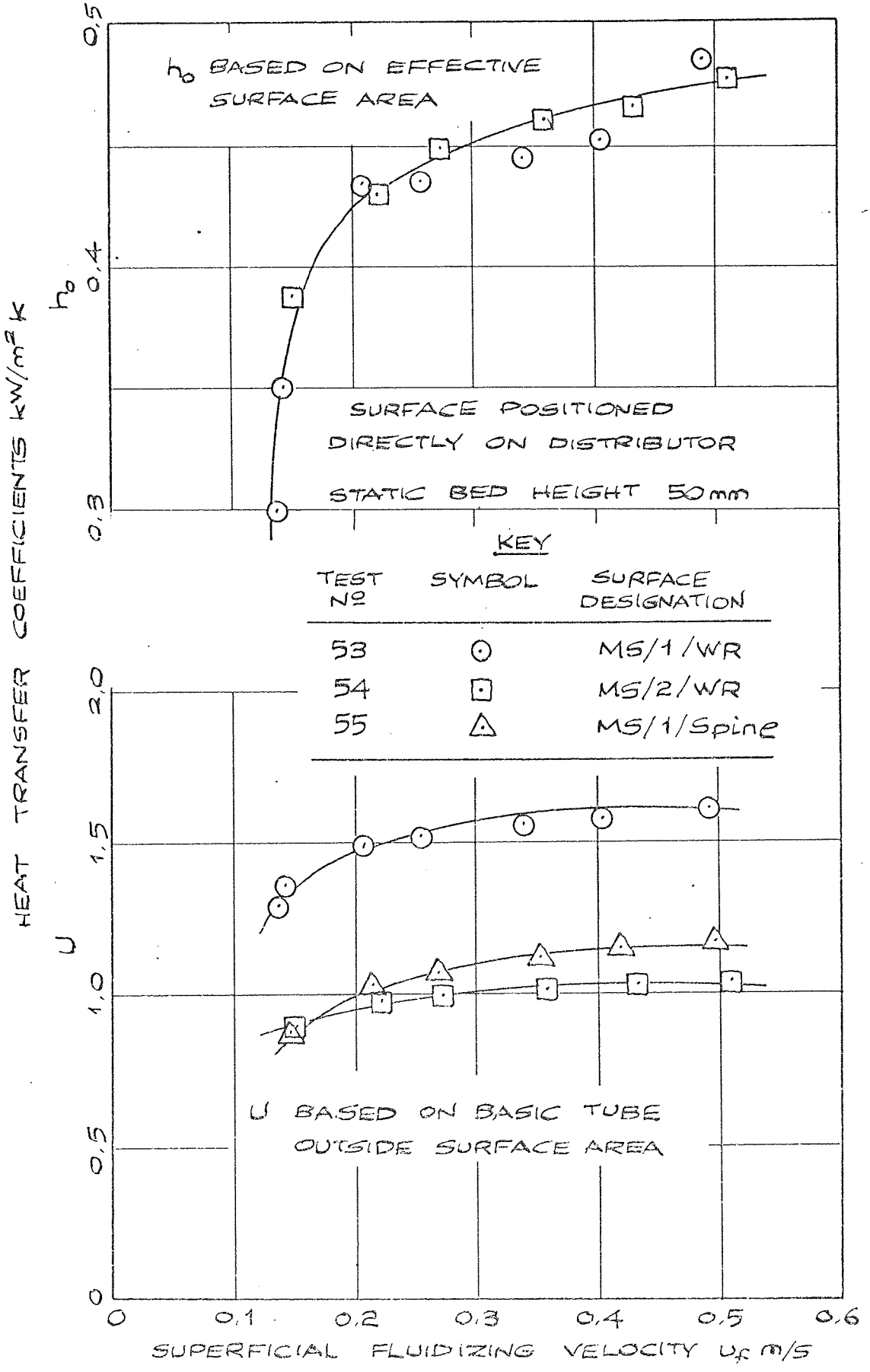

8.6 Results of the Theoretical Analysis - Radial Fins of Rectangular Section

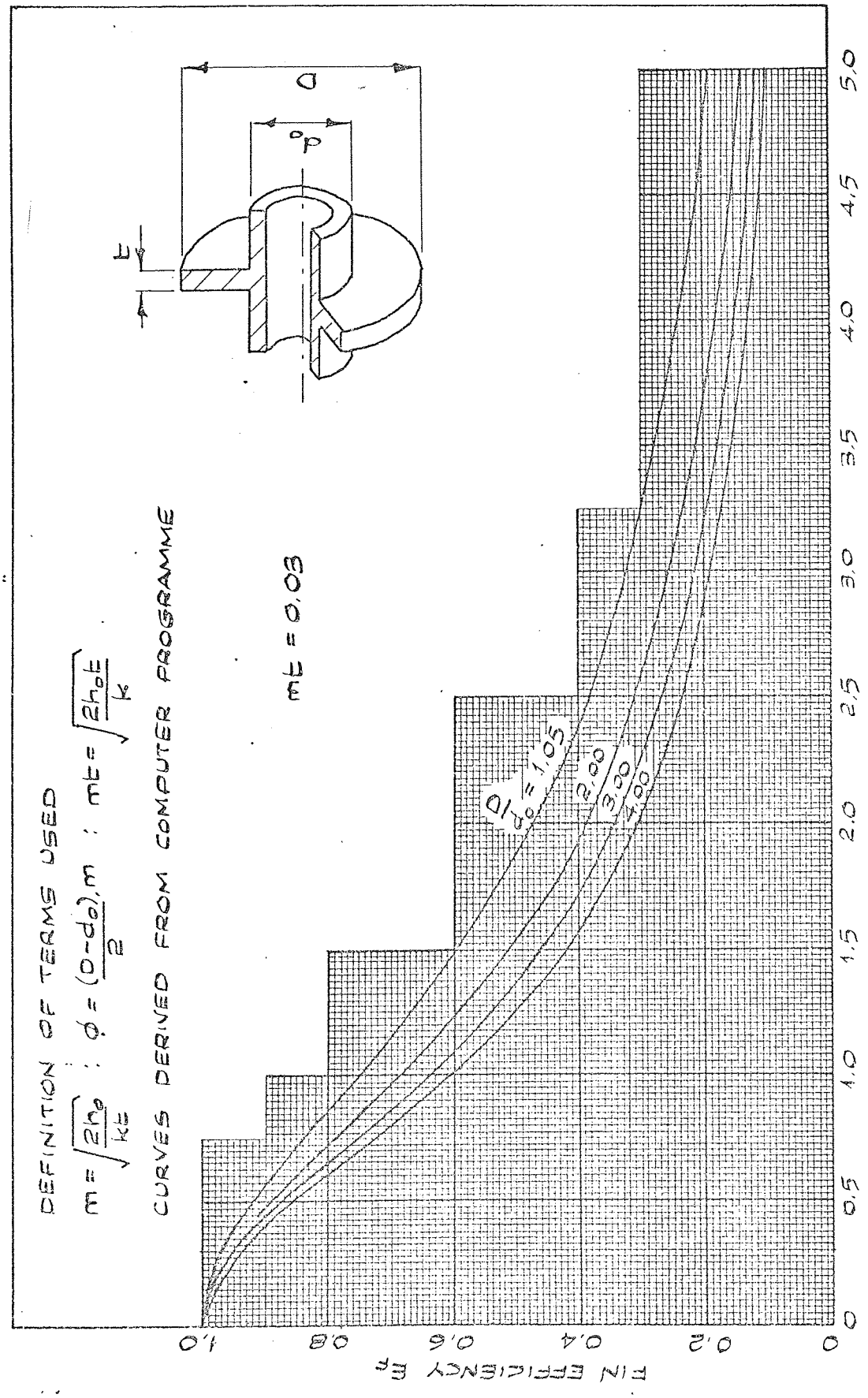

Figure 6.86 FIN EFFICIENCY CURVES FOR RADIAL FIN OF RECTANGULAR SECTION

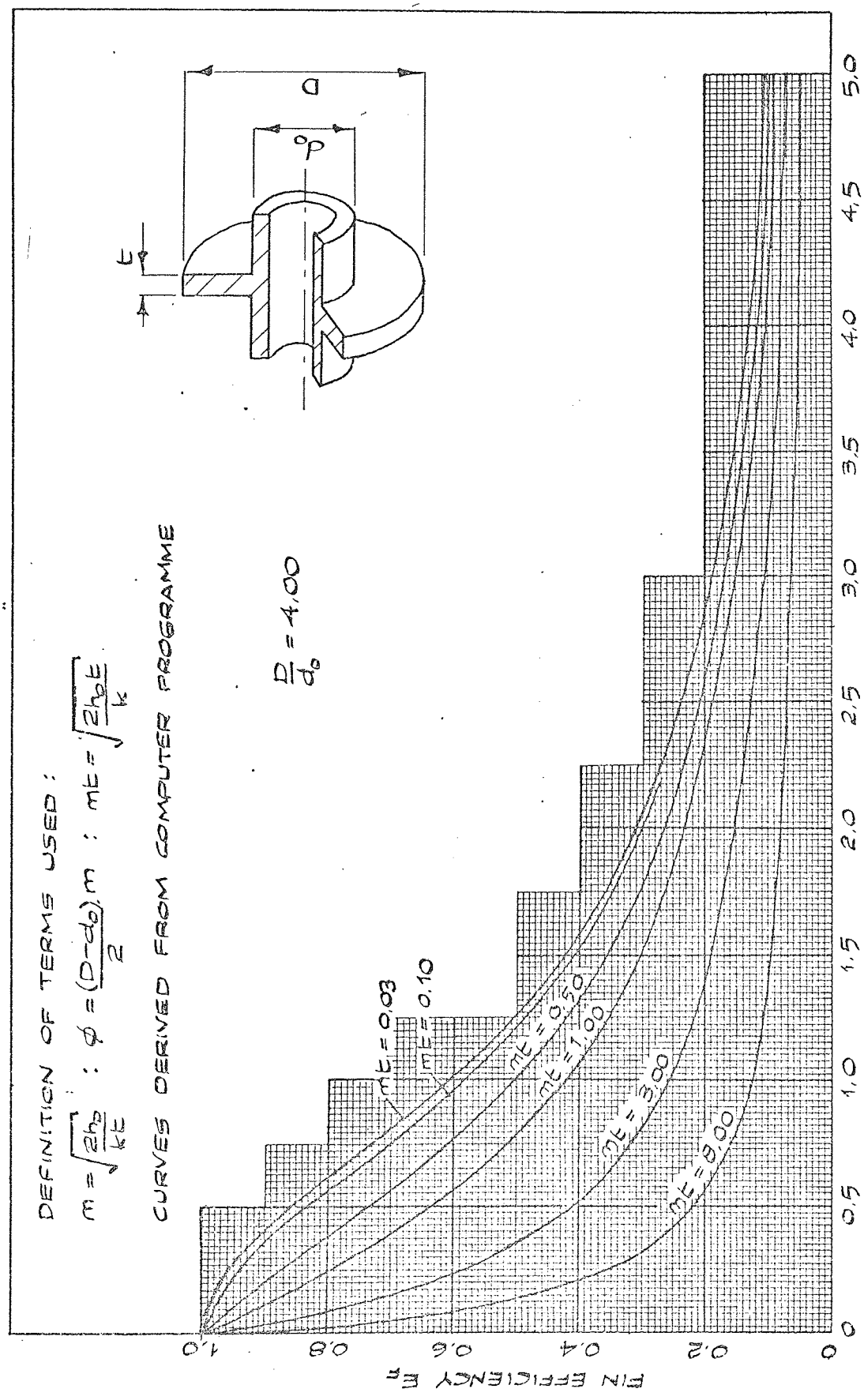

Figure 8.87 INFLUENCE OF DIMENSIONLESS PARAMETERS ON FIN EFFICIENCY FOR RADIAL FIN OF RECTANGULAR SECTION

Table 8, 2 RADIAL FINS OF RECTANGULAR SECTION - VARIATION OF FIN EFFICIENCY WITH BED TO SURFACE HEAT TRANSFER COEFFICIENT.

HEAT TRANSFER COEFFICIENT h_o $\frac{kW}{m^2 K}$	RADIAL FIN EFFICIENCIES FOR L = 12,7mm t = 1,02 mm and d_o = 25,4 mm			
	MILD STEEL k = 0,045 kW/m K	ALUMINIUM BRASS k = 0,100 kW/m K	ALUMINIUM k = 0,200 kW/m K	COPPER k = 0,380 kW/m K
0,050	0,858	0,930	0,960	0,970
0,150	0,692	0,830	0,900	0,945
0,350	0,488	0,640	0,790	0,880
0,825	0,323	0,490	0,650	0,760
1,28	0,270	0,399	0,545	0,680

CALCULATION : FROM FIGURE 8,86

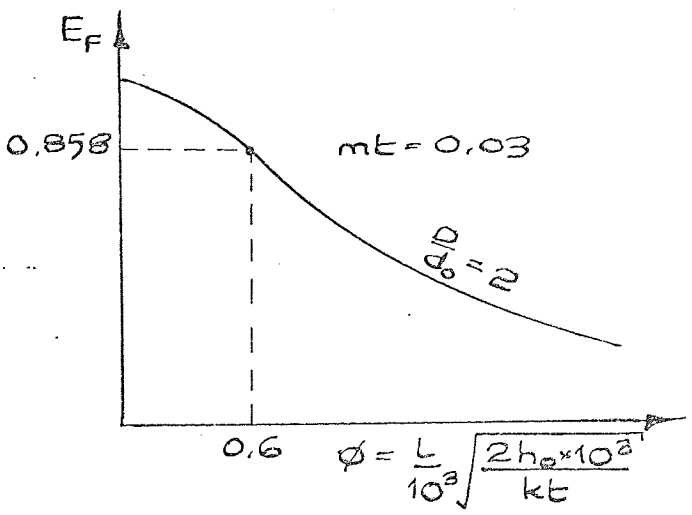

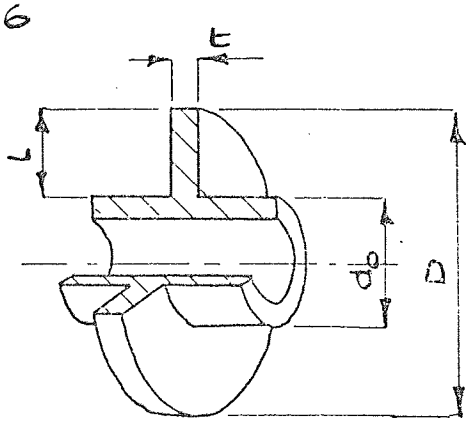

FOR STEEL : $h_o = 0,050$ kW/m² K , $k = 0,045$ kW/m K
$t = 1,02$ mm , $L = 12,7$ mm

$$\phi = \frac{12,7}{10^3}\sqrt{\frac{2 \times 0,050 \times 10^3}{0,045 \times 1,02}} = 0,6 \text{ (DIMENSIONLESS)}$$

$$mt = \sqrt{\frac{2h_o t}{k \times 10^3}} = \phi \cdot \frac{t}{L} = 0,048$$

FROM THE CURVE $E_F = 0,858$

Figure 8.88 **Variation of Maximum Heat Transferred for Extended Surface with Fin Thickness**

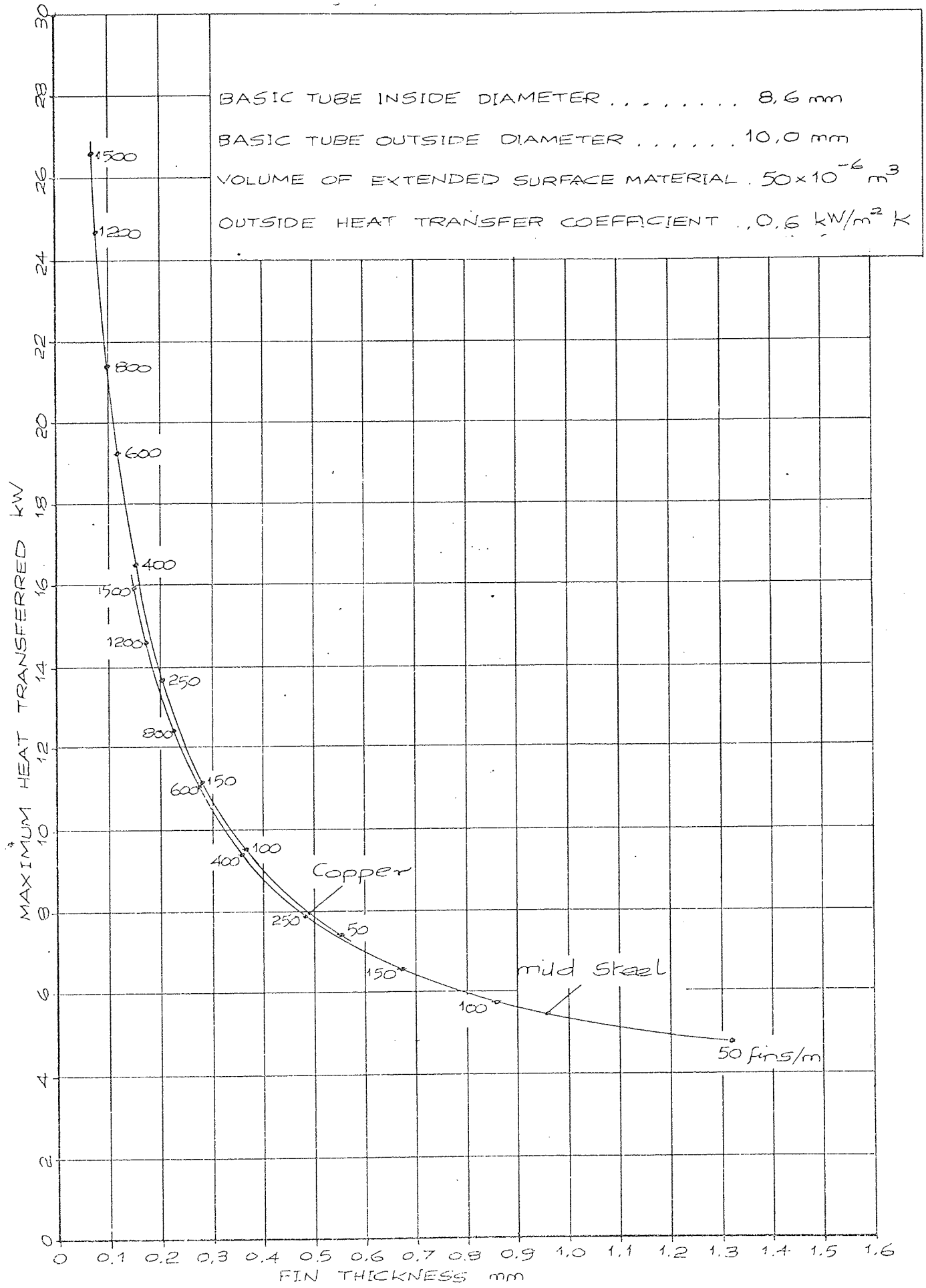

Figure 8.89

Variation of Maximum Heat Transferred for Extended Surface with Fin Thickness

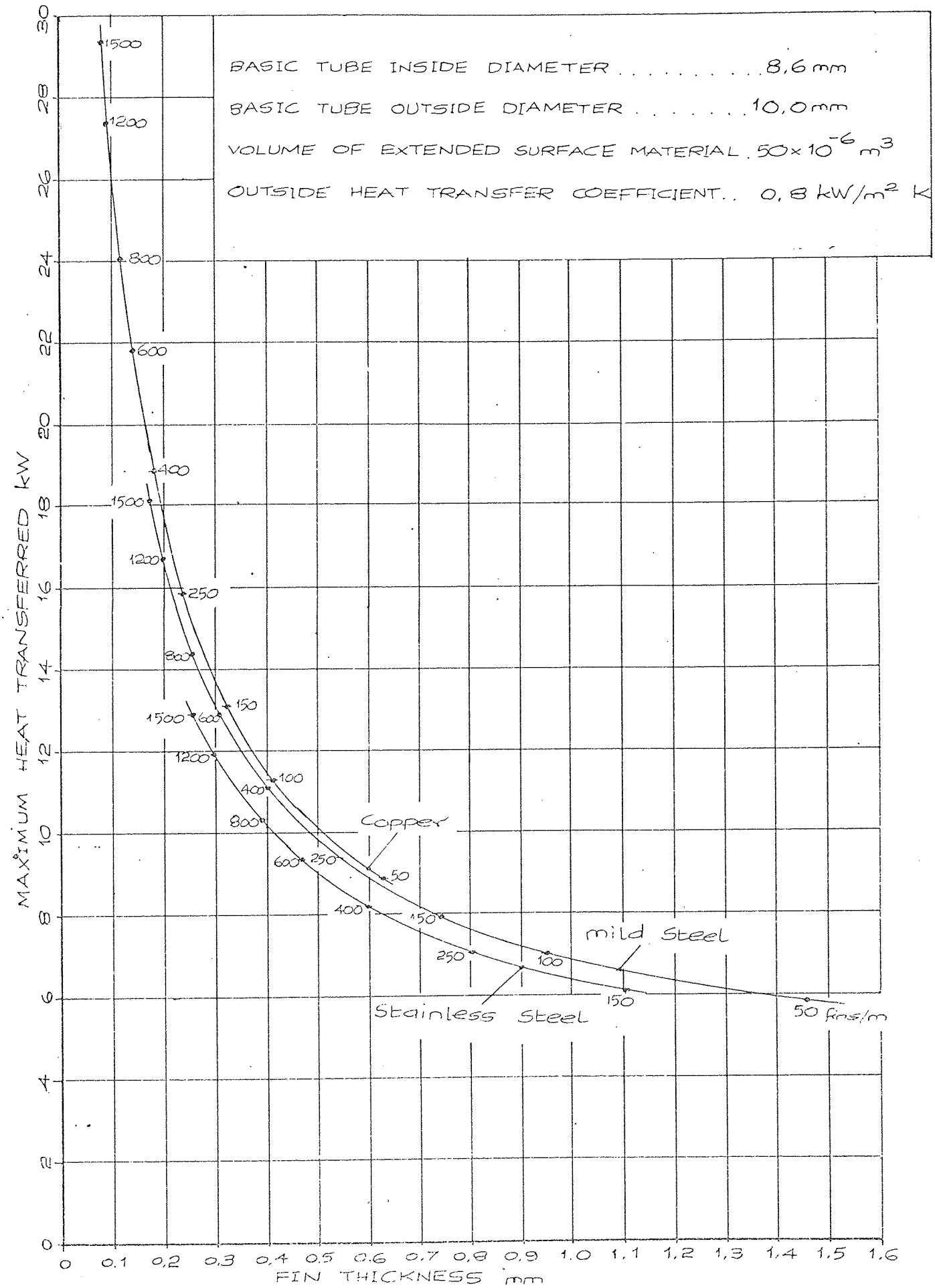

Figure 8,90

Variation of Maximum Heat Transferred for Extended Surface with Fin Thickness

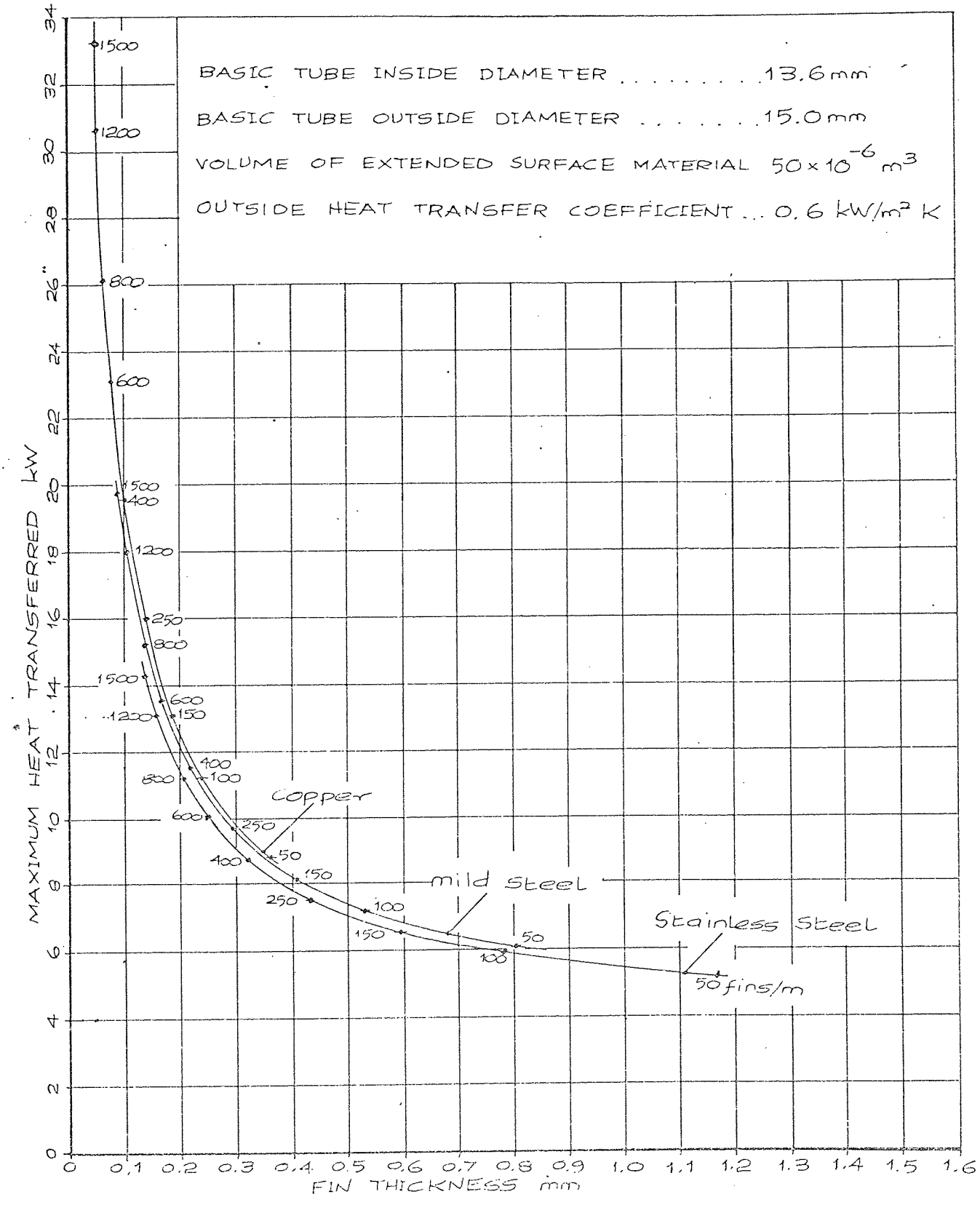

Figure 8.91

Variation of Maximum Heat Transferred per Volume of Extended Surface Material with Number of Fins.

BASIC TUBE INSIDE DIAMETER . . . . . 8.6 mm

BASIC TUBE OUTSIDE DIAMETER . . . . . 10.0 mm

FIN THICKNESS . . . . . 0,2 mm

OUTSIDE HEAT TRANSFER COEFFICIENT . . . 0,6 kW/m² K

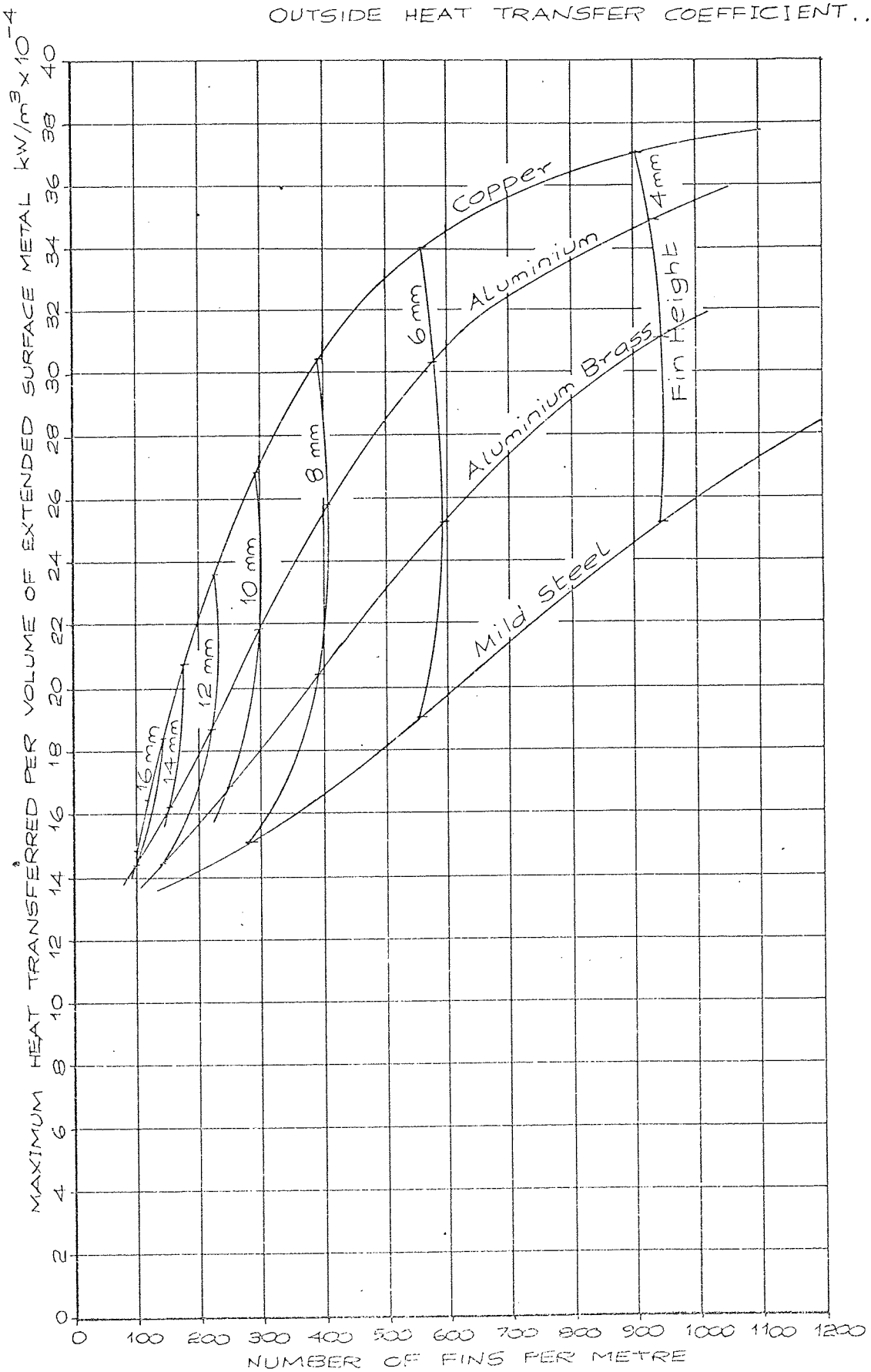

Figure 8.92

Variation of Maximum Heat Transferred per Volume of Extended Surface Material with Number of Fins.

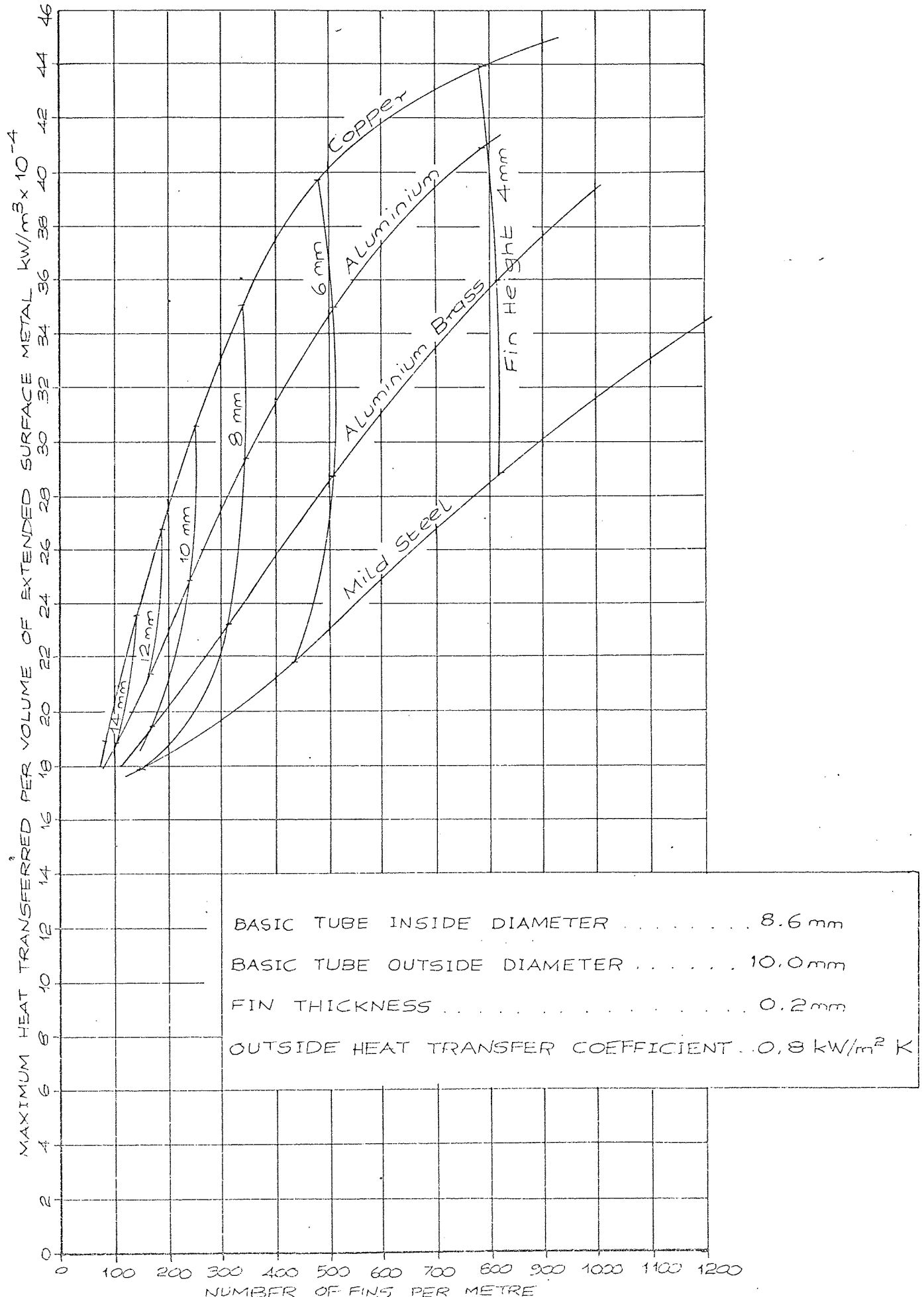

Figure 8.93

VARIATION IN TOTAL HEAT TRANSFERRED FOR A RADIAL FIN EXTENDED SURFACE WITH FIN SPACING AND FIN HEIGHT.

Figure 8.94

CONSTANTS

d_i = 13.7 mm d_o = 15.1 mm

t = 0.79 mm h_i = 12 kW/m² K

h_o = 0.75 kW/m² K $T_b - T_w$ = 125 K

k_{Cu} = 0.380 kW/m K

k_{MS} = 0.045 kW/m K

D = 50.8 mm

L = 17.85 mm

N = 210 fins/m

b = 3.97 mm

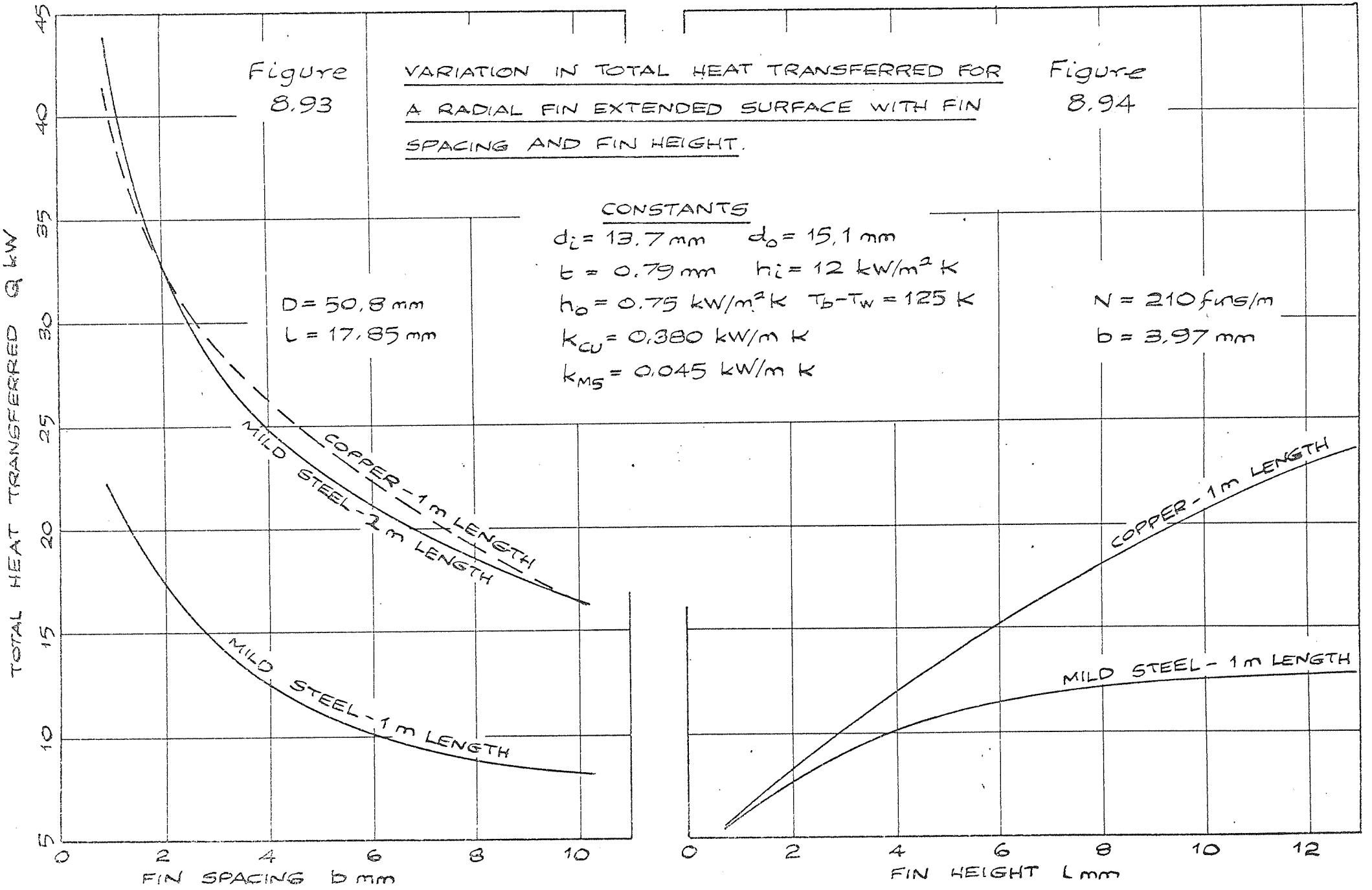

Figure 8.95 VARIATION IN TOTAL HEAT TRANSFERRED FOR A RADIAL FIN COPPER EXTENDED SURFACE WITH FIN THICKNESS.

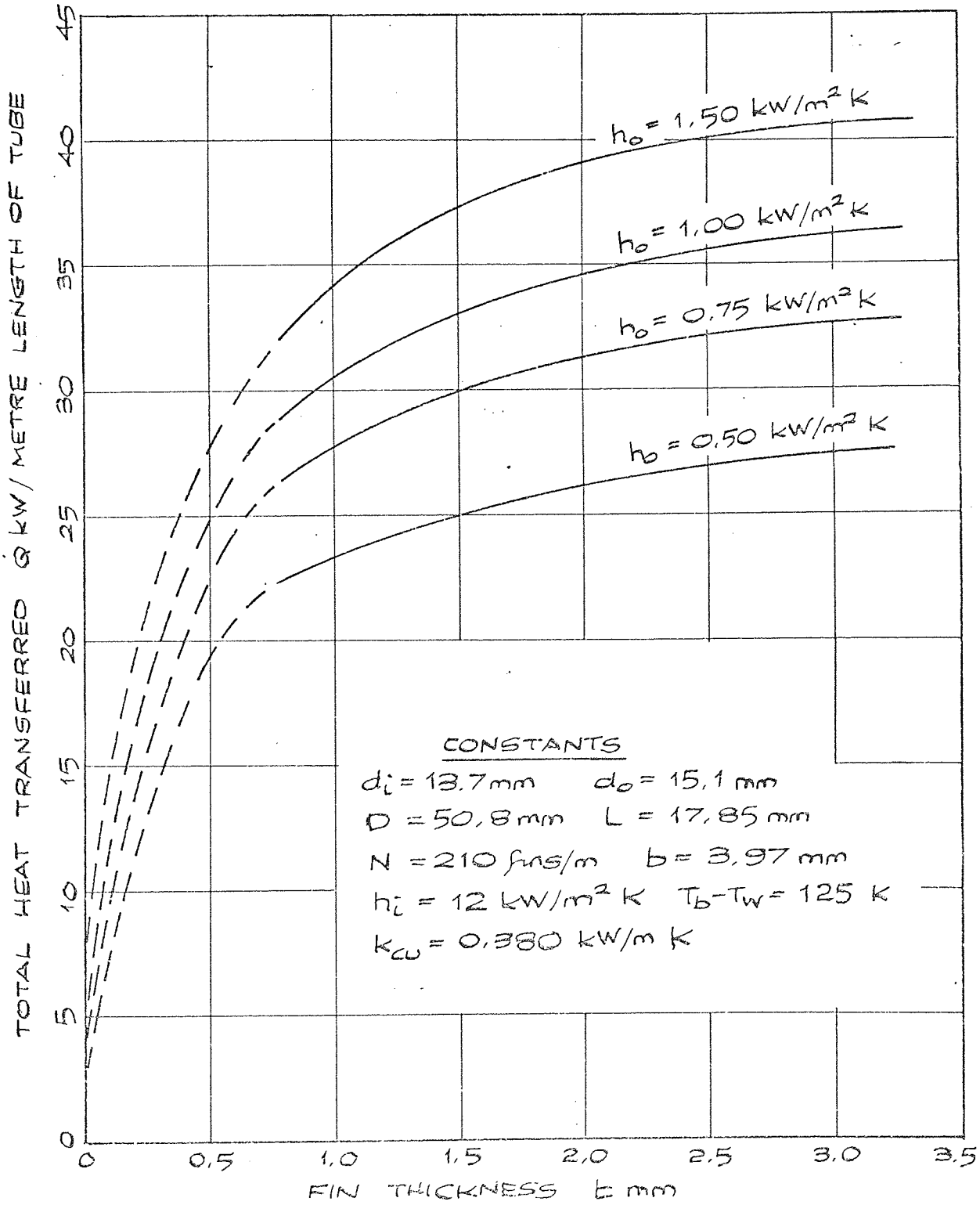

Figures 8.96 and 8.97 are sample graph plotter performance curves and are included inside the back cover pocket of the thesis.

8.7 Other Investigators Experimental Results

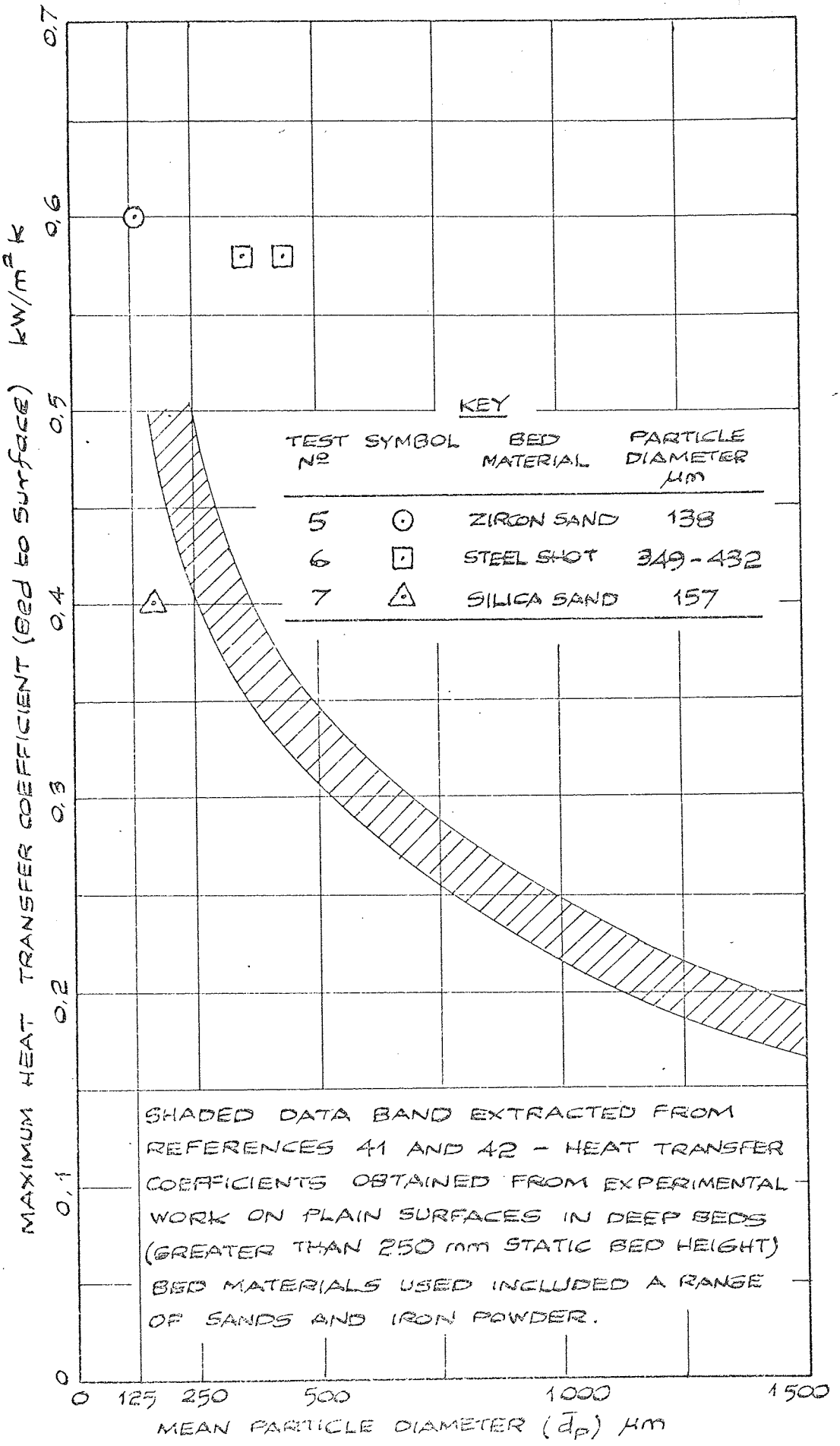

Figure 8.96 CORRELATION BETWEEN HEAT TRANSFER COEFFICIENT AND PARTICLE SIZE

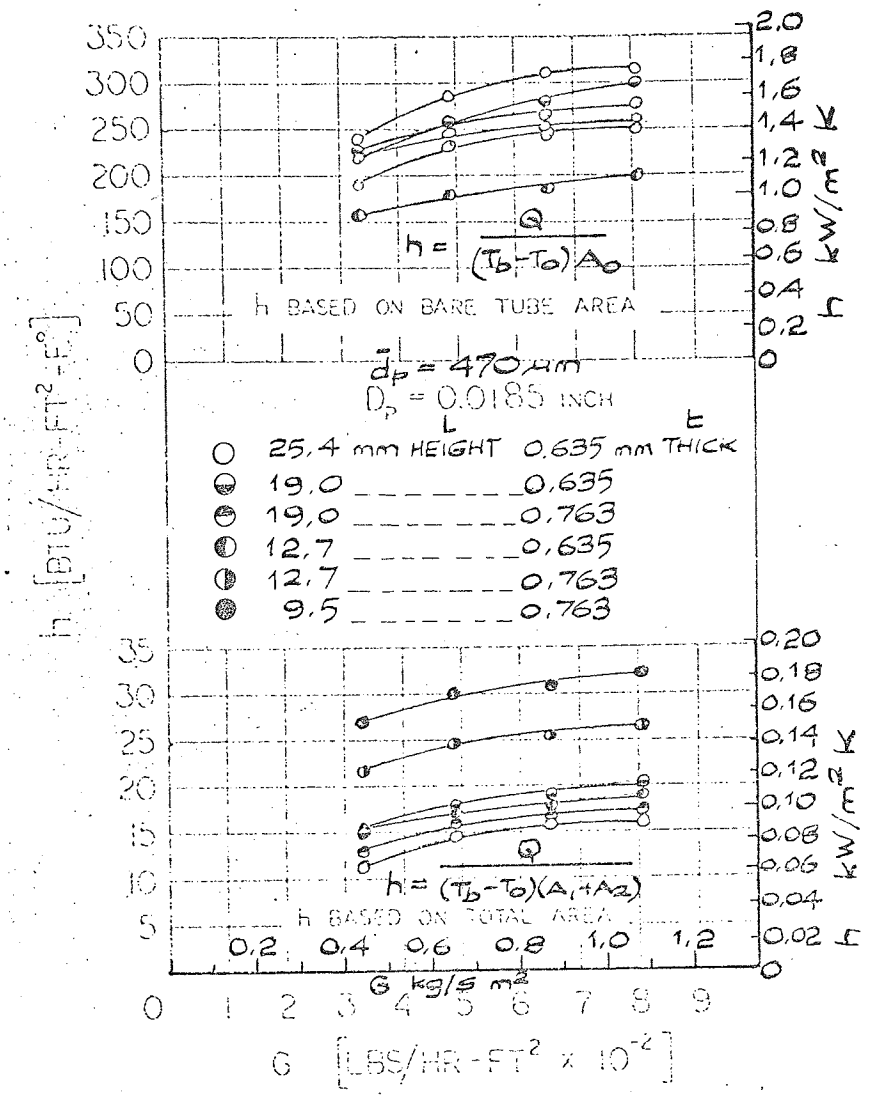

Fig. 5. Heat transfer coefficients for a single horizontal finned tube in a fluidized bed.

Figure 8.99 Extract from Bartel et al[27], p88 - Heat Transfer Coefficients for Extended Surface.

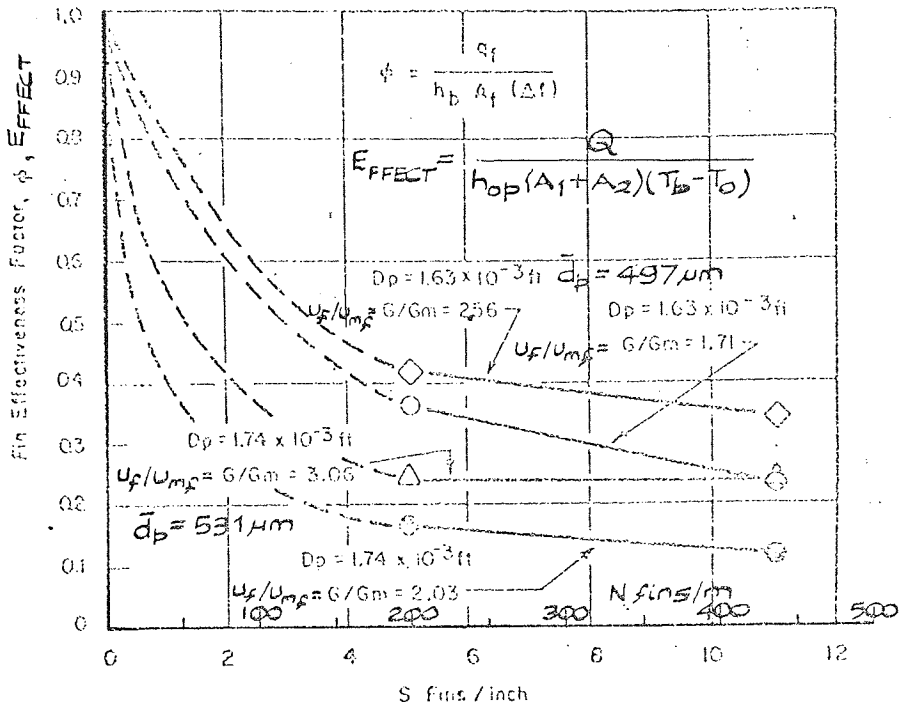

Figure 7. Effectiveness factor for finned tube heat exchangers in fluidized beds.

Figure 8,100 — Extract from Petrie et al[20], p49 — Effectiveness Factor for Extended Surface.

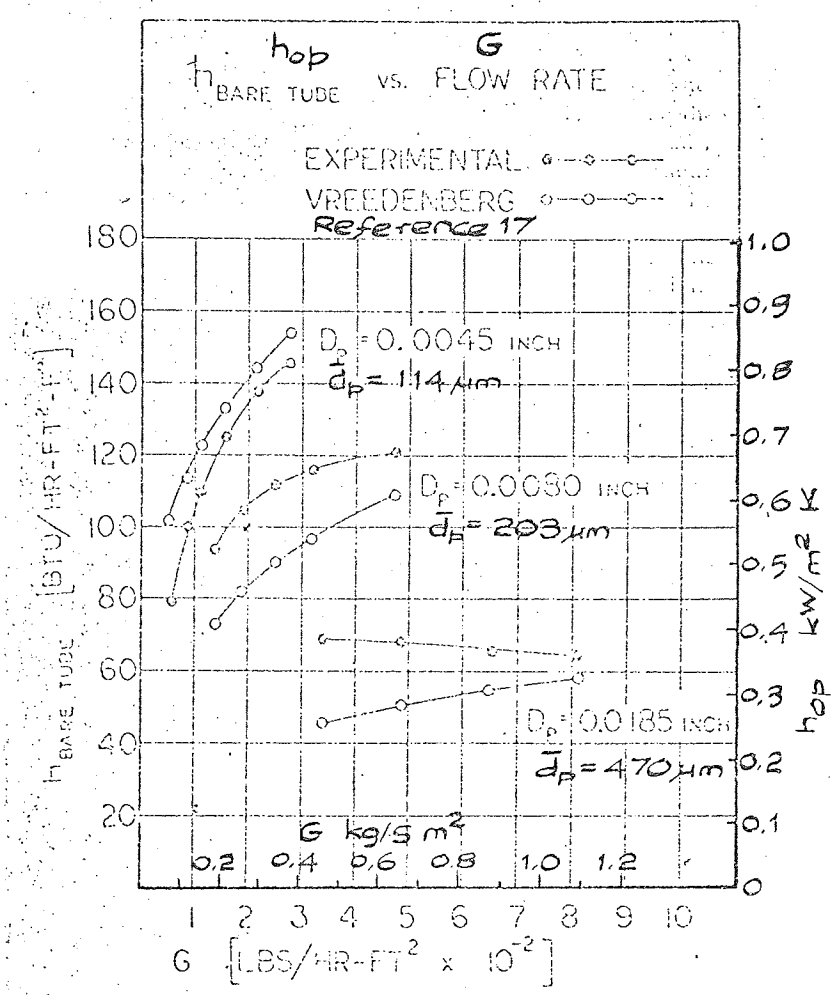

Fig. 3. Comparison of experimental data with Vreedenberg correlation for single horizontal bare tube.

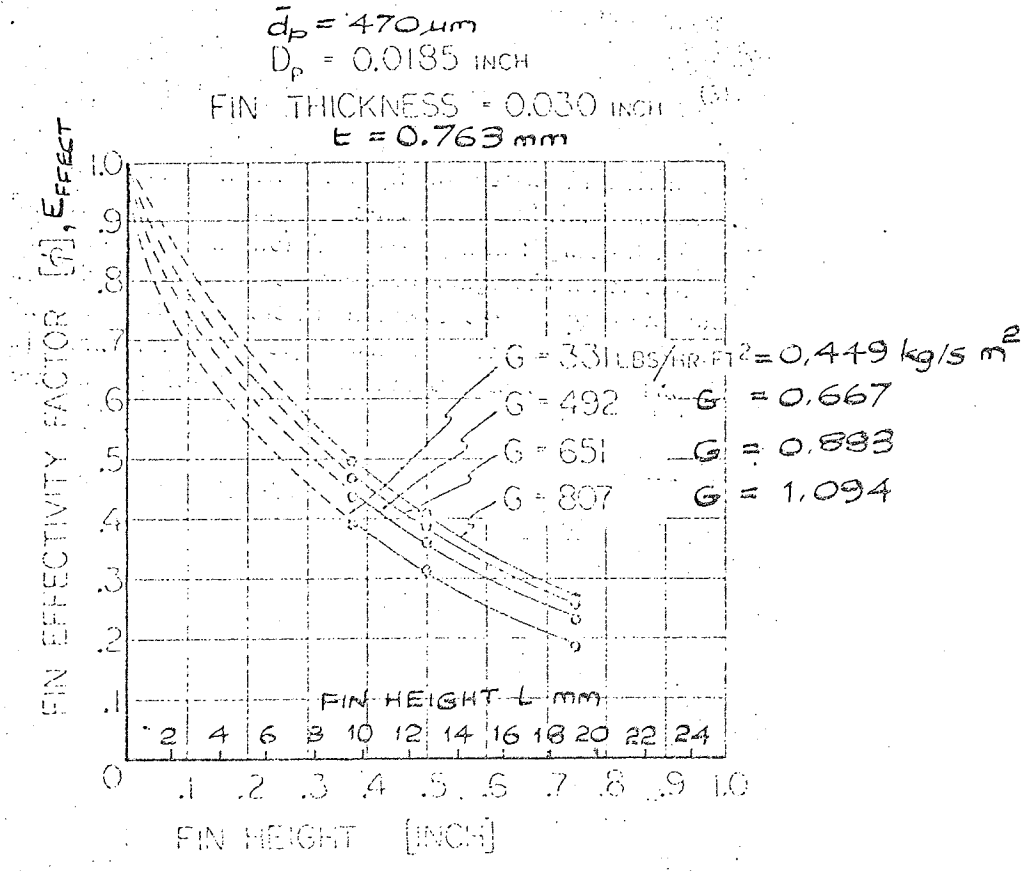

Fig. 4. Effectiveness factor for single horizontal finned tube in a fluidized bed.

Figure 8.101 Extract from Bartel et al[27], p87 - Comparison of Plain Tube and Extended Surface Data

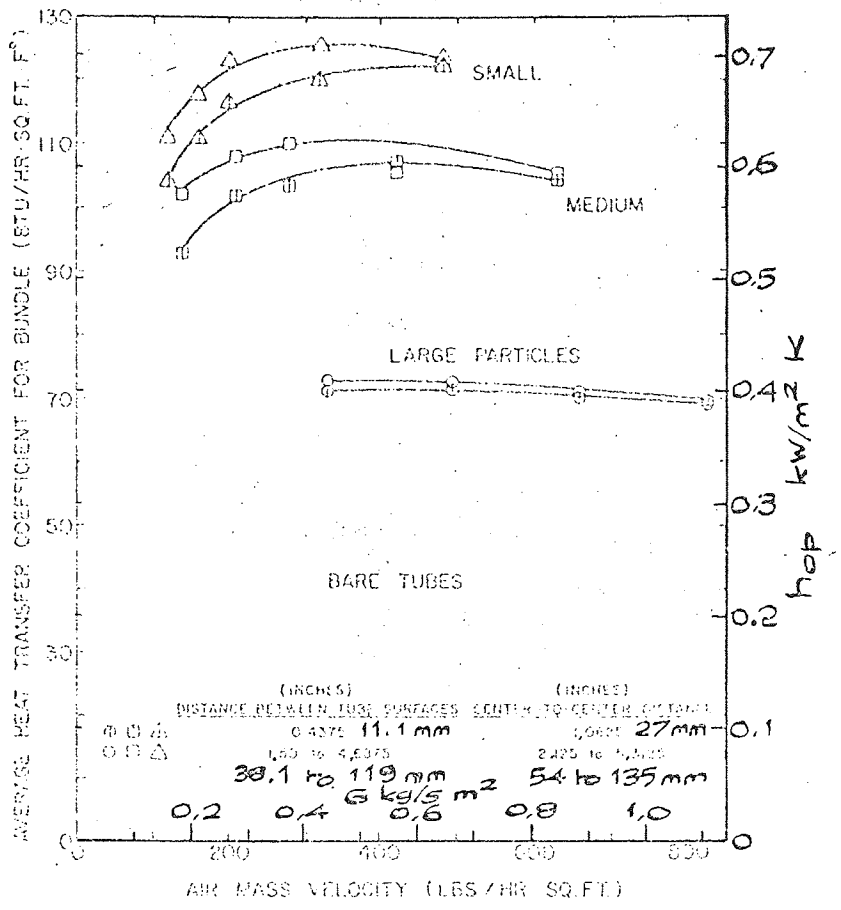

Fig. 7. Performance of bare tubes.

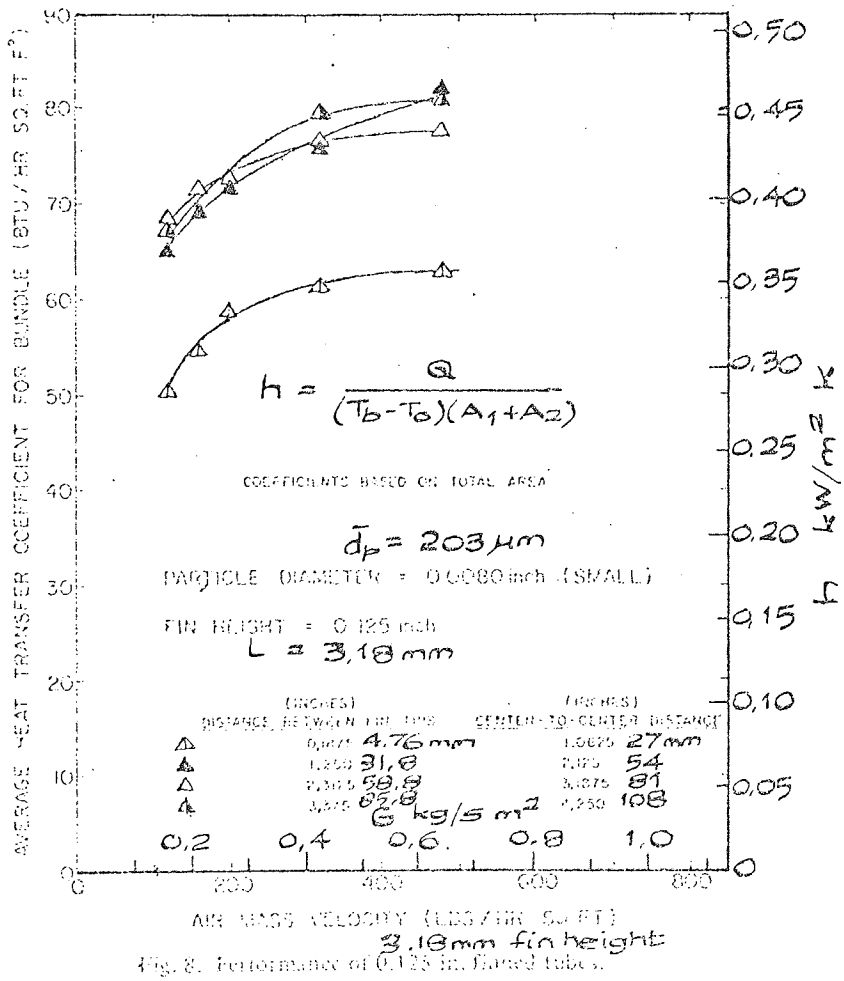

Fig. 8. Performance of 0.125 in. finned tubes.

Figure 8.102 Extract from Bartel and Genetti[29], p88 and p89 - Performance of Plain Tube and Extended Surface

CHAPTER IX
DISCUSSION OF RESULTS

9.1 Plain and Oval Tube Results

9.1.1 Introduction

A series of tests were performed using plain and oval tubes in shallow fluidized bed configurations to complement the extended surface work. Although not extensive in nature, the results obtained are compared with the extended surface heat transfer coefficient characteristic curves and the research data of other investigators using deep fluidized beds.

9.1.2 The Influence of Particle Properties

Particle size has an influence on the bed to surface heat transfer coefficient. Research has shown that most of the heat transfer takes place by conduction through the thin gas film between the particles and the surface, rather than by direct conduction at the particle/surface contact points. However, this gas conduction is not the limiting factor and the residence time of particles near the surface is of prime importance since their heat capacity is small and they soon assume the surface temperature. As might be expected from theory, reducing the particle size reduces the effective gas path to the emulsion phase, and increases the number of contacts at the surface. The effect is illustrated in figure 8.98 which is based on the experimental results of Baerg, et al[41], 1950 and Kim et al[42], 1968, who carried out experiments using different materials in contact with plain surfaces in deep beds - greater than 250 mm. Superimposed on this graph are the maximum heat transfer coefficients obtained from figure 8.2 which represent the $h_o - u_f$ characteristics for a 15 mm diameter horizontal tube in a shallow bed of approximately 30 mm static height. Extrapolation of the experimental results band of figure 8.98, to smaller values of mean particle diameter, shows the zircon sand results to lie within the range. However, the silica sand indicates a lower value and the steel shot a higher value than would be anticipated from the results of deep fluidized beds. It appears that the other particle physical properties such as density, thermal conductivity and specific heat have more of an influence on the bed to surface heat transfer coefficient in shallow beds than particle

size. Furthermore, the shape and surface state of the solid particles may affect the value; heat transfer coefficients will be higher for the rounded and smoother zircon sand and steel shot. This will be observed from figure A5.1 which shows projection microscope photographs of the materials used. Table A5.1 lists the particle properties and examination reveals the steel shot to be high in the "league" table of desirable values. It has the highest density and thermal diffusivity and a thermal capacity comparable to the zircon sand. As well as providing a high heat transfer coefficient, figure 8.2 shows that the fluidizing velocity range for steel shot is more than doubled compared with the sands. This may be an important consideration when designing a system, because a smaller bed area can be utilized to pass a given volumetric flow rate of gas, thereby reducing the bed containment costs.

9.1.3 The Effect of Bed Height

Figure 8.1 shows the effect of a variation in static bed height of zircon sand maintaining the same tube position. At the operating fluidizing velocities of 0.4 to 0.5 m/s the deeper bed produces a 20% increase in h_o. This may be attributed to two possible causes. Firstly, the 50 mm bed will expand less than the 25 mm bed resulting in a lower porosity in the deeper bed. The effect is to increase the particle/surface contacts in the deeper bed, particularly at the higher fluidizing velocities. Secondly, bubble coalescence in the upper zone of the deeper bed could be improving particle mobility in the lower zone, close to the surface. Both these effects may be contributory factors in producing higher heat transfer coefficients. It would be more beneficial from the thermal performance aspect to employ a two-stage bed arrangement, each with a static bed height of 25 mm, instead of a single bed with 50 mm of sand.

9.1.4 Effect of Bed Size and Configuration

It is a well established fact in deep beds that for large scale equipment, the simple circulation patterns of a small scale bed, where bubbles tend to rise up through the centre drawing particles after them before returning the solids downwards along the bed walls, will be absent. The degree of interaction between adjacent bubble streams and the effect on particle circulation cannot be predicted. The overall effect is to produce lower bed to surface heat transfer coefficients in the larger beds. This trend is also apparent from the experimental work and figure 8.3 shows

the influence of both size and configuration on the performance curves. A plain tube immersed in the small rectangular Mk 2 bed produces coefficients 20% to 30% higher at the lower fluidizing velocities than a comparable surface in the large circular Mk 1 bed. This increase will be reduced by about 5% if an allowance is made for the bed static height, such that at the high fluidizing velocities there will be little difference. It may also be noted for all experiments in the Mk 1 bed that no maximum heat transfer coefficient was attained, before elutriation of the bed material - again suggesting that the particle circulation patterns play an important part in the mechanism of heat transfer.

9.1.5 The Effect of Tube Diameter

The results of tests carried out with plain surfaces of 10 mm and 15 mm diameter are given in figure 8.4. The predicted increase in h_o at the small diameter being apparent although to a lesser degree than the other variables. The same trend is exhibited with the extended surface results, which will be discussed later, the decrease in h_o only becoming significant at diameters in the order of 22 mm and 28 mm.

9.1.6 The Influence of Tube Position

Figure 8.5 signifies the result of a change in tube position as well as bed size and configuration. From figure 8.3 it was shown that the higher coefficients were obtained in the rectangular Mk 3 bed. It is expected that higher performances would be achieved in the smaller rectangular Mk 2 bed as a result of the increased motion of the solids. On the basis of the same differences predicted between Mk 1 and Mk 3 bed results it appears that the position has little significance on the heat transfer coefficient. Similar conclusions were suggested by Gelperin and Einstein[52], who summarised the deep bed work of other investigators.

9.1.7 Statistical Analysis of Plain Tube Results

To establish the influence of bed temperature on the heat transfer coefficient and to correlate the limited experimental results a statistical analysis was performed. The regression equation is summarised in section A6.2 and three graphs from the presentation programme outline in Appendix A2 are shown in figures 8.9 to 8.11 inclusive.

Section A6.2 shows that the dependent variable - the heat transfer coefficient is a function of several independent variables, some being more important than others. The degree of significance is measured by the size of the t statistic (T STAT on the computer print out). Inspection shows the bed Mk 2 results and the tube position to be highly significant. This contradicts the previous remarks where it was suggested that tube position was insignificant. The reason is that only one test was carried out in the Mk 2 bed where the tube position was significantly different from all the other tests. Thus with a limited amount of data the relative importance between the two cannot be established using the regression technique. This effect has also resulted in Mk 3 bed variations being eliminated from the equation. However, the equation does correlate the results to a high degree of accuracy, the residual errors between the observed and calculated h_o values being given in the section and figure 8.9.

An interesting feature of the regression technique is that it allows information to be readily determined for all the independent variables. For instance, the influence of bed temperature variation on the heat transfer coefficient cannot be easily established unless controlled experimental conditions are maintained. Figure 8.10 shows the significance of this variable for the range of typical values given in section 8.2.2. Although the heat transfer coefficient is not affected to a great extent, the value decreases with increase in bed temperature which is against the expected trend. It has been established by numerous authors from their deep bed work that a high gas thermal conductivity is conducive to good heat transfer. This results from an increase in bed temperature. The discrepancy cannot be readily explained, although it must be emphasised that the average change in h_o is less than 10% over a wide bed temperature range ($192^{\circ}C$ to $343^{\circ}C$). Whilst it is possible that small temperature gradients exist in the lower regions of the shallow fluidized bed and could therefore lead to erroneous bed temperature readings, experimental evidence suggests that the thermal gradient zone is restricted to a few millimetres above the distributor plate.

The maximum heat transfer coefficient of 0.74 kW/m^2 K was

obtained from the results of test number 3 in the Mk 2 bed using zircon sand ($\bar{d}_p$ = 138 μm), which appears to be comparable with the values given by Bartel, et al[27], 1970 and extracted to form figure 8.101. They were working with glass spherical particles in 550 mm deep beds the 15.8 mm diameter electrically heated tube being located some 200 mm above a perforated plate distributor. It is therefore suggested that very little benefit in heat transfer performance is to be derived by employing plain horizontal tubes in shallow fluidized beds. However, since pressure drop is a direct function of bed height, benefits will be obtained by designing shallow bed heat transfer systems.

9.1.8 Assessment of Oval Tube Performance

It is a well established fact that under normal forced convection applications an oval tube, with its minor axis normal to the gas flow, offers no benefit to the heat transfer performance but is employed solely to reduce the overall pressure drop across the surface. In fluidized bed applications it is desirable to reduce the surface area normal to the gas/particle direction in order to prevent "dead zoning" and "cap" effects at the periphery of the tube. With this point in mind, an oval tube was tested in its most favourable position - major axis normal to the distributor, the results being shown in figure 8.6. For comparison purposes the plain tube results of test 3 are superimposed onto the graph. Considering the oval tube has a minor diameter of 12 mm and the plain tube a diameter of 15.1 mm, the increased performance is very substantial. At a fluidizing velocity of 0.45 m/s the bed to surface heat transfer coefficient is increased by approximately 30%. It suggests that the curvature of the surface is contributing to improved particle agitation in the vicinity of the surface periphery since Sinclair, et al[19], 1964, working with flat vertical plates in deep beds, did not experience heat transfer coefficients of this magnitude. A further test was carried out on the oval tube with its minor axis normal to the distributor, the results being represented in figures 8.7 and 8.8. The major diameter was 27.56 mm.
As expected the performance was comparable with that for a large diameter plain tube, the particles in the lower and upper regions becoming immobile, even at high fluidizing velocities, thereby creating a "heat insulation barrier".

It appears that after only two tests the results are most encouraging and that further work should be carried out to determine the factors influencing the heat transfer performance of oval tubes. Extended surface using basic tubes of the oval type rather than the plain type may be more beneficial in providing higher bed to surface heat transfer coefficients.

9.2 Square Fin Tube Results

9.2.1 Introduction

At the commencement of the research programme on extended surface heat transfer the decision as to which was the best arrangement to utilize in shallow fluidized beds could not be made. It was therefore decided to use the knowledge gained from previous investigators working with plain surfaces and design a suitable finned tube for shallow bed applications. Small basic tubes were utilized to extract the energy, and were distributed across the flank face of vertical fins in a staggered fashion. This would prevent the possibility of interactions occurring between tubes. The choice of a rectangular or square fin compared with a radial fin was made on the basis of obtaining the maximum surface area for a given occupied volume of the heat exchanger.

9.2.2 The Effect of Surface Position

The effect, on the heat transfer performance, of varying the distance between the lower fin edge and the distributor was investigated for a constant static bed height. Inspection of figures 8.12 and 8.13 show that the best position is obtained by placing the surface directly on the distributor. By providing a surface with a straight lower edge, the coalescence of rising bubbles is prevented, for this position, before they enter the space between adjacent fins. The immediate effect is to improve the performance providing the fin spacing is large enough to prevent "blanketing" of the surface with bubbles in the upper fin flank regions. It must also be pointed out that the thermal gradients existing adjacent to the distributor may be assisting the performance of the heat exchanger under these conditions. Surface C/1/MS has a spacing of 3.27 mm which is over twenty times the mean particle diameter of the sand. Maximum bed to metal heat transfer coefficients of 0.65 kW/m^2 K were experienced.

9.2.3 The Effect of Bed Height

Having established that the best performance is obtained when the surface is positioned directly on the distributor the effect of increasing the static bed height was investigated. Figures 8.14 and 8.15 show that the improvement is almost directly proportional to the sand height - an increase in the bed to metal heat transfer coefficient of 35% for a three-fold increase in height from 50 mm. The trends are identical to those experienced in the plain tube tests, the increased particle mobility at the larger heights being attributed to increased bubble activity. From a flow visualisation study it was observed that the net particle movement was in at the lower side edges of the fins and out at the top side edges. With the associated increased bubble activity in the deeper beds the coalescence of bubbles in the upper regions may be inducing improved circulation in the vicinity of the upper fin flank area, thereby improving the heat transfer rate.

Figures 8.16 and 8.17 show the variation in the bed to metal and overall heat transfer coefficients for a movement of 25 mm above the distributor, at a bed height of 150 mm. Again the better performance is experienced when the surface is positioned directly on the distributor. However, the reduction in heat transfer rate is more marked at the deeper bed conditions - a reduction of 15% compared with 10% at a height of 75 mm.

9.2.4 The Influence of Fin Spacing

Results for surface C/2/MS (b = 6.15 mm) are compared with surface C/1/MS (b = 3.27 mm) under identical fluidizing conditions and shown in figures 8.18 and 8.19. The effect of increasing fin spacing appears to be quite marked, with the bed to metal heat transfer coefficients being some 35% higher at an operating fluidizing velocity of 0.4 m/s. However, this increase is misleading since the heat transfer coefficient is based on the primary plus secondary surface areas. Extended surface C/1/MS has 1.5 times more heat exchange area than tube C/2/MS. The combined effect is to reduce the actual bed to surface heat transfer coefficients accordingly. Thus, for this type of square fin tubing the spacing has little effect on the bed to surface resistance, the performance being marginally better at the smaller spacing. This is contrary to the expected trend, although it must be emphasised

that the spacing of 6.15 mm is very large. The coalescence of bubbles between adjacent fins at this spacing may be unrestricted to the extent that the solid circulation could be impaired. Since only two surfaces were tested it is difficult to offer any substantial conclusions. The work on radial finned surfaces, which will be reviewed shortly, has indicated an increase in performance with an increase in fin spacing, but over a smaller range of spacings (0.93 mm to 3.7 mm). It may therefore be possible that an optimum spacing exists. The overall heat transfer coefficient of tube C/2/MS is better than C/1/MS because of the difference in the fin conduction efficiency. A greater resistance to heat transfer is offered to surface C/1/MS due to differences in the direction of the coolant flow. This is explained by reference to figure 8.22 which shows the fin sections. For tests conducted on these surfaces no water circulatory flow was used. As a consequence the overall temperature difference across the heat exchanger ranged from 10 K to 20 K. This resulted in an additional temperature gradient across the fin flanks, the temperature profile being very complex, particularly for surface C/1/MS. These differences are highlighted by the calculated experimental fin efficiency curves. It is therefore important, when high energy transferences are taking place, to ensure that the energy sink points are correctly located within the fin section.

9.2.5 Comparison of Different Fin Sections

In order to establish the effect on performance of size and position of the basic coolant tube or tubes passing through the square fin section a further extended surface was manufactured - namely C/3/MS. This consisted of square fins identical to the previous surface, but with a single central 15.1 mm diameter tube. Figure 8.20 shows a slight increase in the bed to metal heat transfer coefficient for the surface, only at the higher fluidizing velocities, when compared with tube C/1/MS. The primary plus secondary areas are comparable for both surfaces and so the $h_m - u_f$ curve is representative of the relative performances. The effect of a divergence in the characteristic curve indicates the possibility of the downstream basic tubes of surface C/1/MS interfering with the particle movement, at the higher fluidizing velocities.

The overall heat transfer coefficient curves shown in figure

8.21 should be corrected for the variation in basic tube outside surface area. Surface C/1/MS has just over twice that of tube C/3/MS. However, accounting for this, the performance of the latter surface is slightly better due to the reduction in the fin conduction resistance. This may not be the case if surface C/1/MS was modified to give parallel water flow paths through the basic tube.

Fin efficiencies and effectiveness factors are represented in figures 8.23 and 8.24 for surface C/3/MS. Experimentally determined fin efficiencies are compared with those obtained using a numerical method based on a knowledge of the bed to surface heat transfer coefficients. The agreement between the efficiency values using both methods is extremely good. The effectiveness factor is substantially constant at a value of 0.71 for all fluidizing velocities and is much higher than any of the reported values in the literature. Reference to figures 8.100 and 8.101 shows the results of Petrie et al[20] and Bartel et al[27] to be limited to a maximum value of 0.5 or less. The improved performance is attributed to a more efficient extended surface working in a shallow fluidized bed.

The experiments have indicated the great potential, in terms of specific outputs, of square fin extended surface heat exchangers. The best output of 14.1 kW was achieved by tube C/1/MS when placed directly on the distributor, in zircon sand, with a static bed height of 150 mm. It is worthy of note that the best results obtained represent a heat flow intensity of 2.39×10^4 kW/m^3. This is quite remarkable compared with the heat release rate in a conventional oil fired boiler furnace of only about 2×10^3 kW/m^3, and is of the same order as a typical figure for a gas turbine combustion chamber of about 5×10^4 kW/m^3.

9.3 Radial Fin Tube Results

9.3.1 Statistical Analysis of All Results

Before discussing the influence of variations in the surface geometric variables, bed configurations and fluidized materials on the heat transfer performance of radial fin tubes, it is pertinent to look at the overall picture in order to establish the significance of each independent variable. A statistical analysis was carried

out based on the simple model proposed in Appendices A1 and A2, and the results presented in section A6.3. The data matrix (MATRX1) lists the dependent and independent variables used in the analysis together with their minimum and maximum experimental values. The second matrix (MATRX2) includes the range of transformed variables used in the model. The cross-product, covariance and correlation matrices, as defined in Appendix A1, are reproduced from the line-printer output.

It will be appreciated that the degree of correlation depends upon a number of factors, the most important being the type of model used. The assumptions on which the model is based should be determined from a physical understanding of the particular problem. However, there is an unjustified tendency to generalize experimental data extensively in the form of a power relationship of dimensionless groups based on the classical forced convection heat transfer theory. In generalizing the results of systematic experiments this device makes it necessary to introduce a number of other dimensionless expressions, in order that the experimental points may be approximated by a single relationship. The equation usually becomes unwieldy and ill-suited to engineering calculations. It is evident that correct generalization of experimental data over a wide range of variables, should be based on reliable physical concepts concerning the mechanism of heat transfer in shallow fluidized beds. At this point in time, due to the lack of research data and because of the multiplicity of variables and the complexity of their influence on heat transfer, empirical formulae are proposed. They are valid within the limits of the experimental conditions on which they are based.

Due to the wide range of experimental conditions, the analysis of all results has produced an unacceptable correlation, using the multiple linear regression technique. The final regression equation given in section A6.3 was determined after many attempts at correlation, using a variety of transformed independent variables. As a consequence, it was decided to analyse selected results and provide the designer with a series of empirical equations which could be guaranteed to a high degree of accuracy. Hence, whilst the equation developed using all the results should not be used for

design purposes, conclusive evidence regarding the significance of the independent variables may be ascertained.

The bar chart shown in figure 8.83 gives a visual indication of the significance of the independent variables. Bed configuration, type of radial extended surface and bed material are compared with a standard of bed Mk 1 results for the manufactured extended surface in zircon sand. The degree of importance of the other results are therefore relative to the standard. If an individual independent variable - including all transformed products, is removed from the regression set then the total sum of squares (S.O.S.) remains constant and only the error sum of squares (E.S.S.) changes. On the assumption that the experimental error is not affected by the removal of a single variable, then the E.S.S. variation is due solely to the lack of model fit. The magnitude of the resulting E.S.S. is a measure of the contribution made by that variable to the correlation of the experimental results. It is appreciated that the E.S.S. using all the variables is quite high and could be distributed in an unknown fashion amongst the other variables, or indeed further transformed variables, in order to obtain a perfect correlation. Nevertheless, making the further assumption of a uniform distribution, the general trends are apparent.

The most significant variables influencing the bed to surface heat transfer coefficient, apart from the superficial fluidizing velocity, are the steel shot and the basic tube outside diameter. The steel shot is very significant since it is also related in the regression set with the velocity. To highlight the importance of the basic tube diameter, reference must be made to the regression equation. Figure 8.84 shows that the basic tube size only influences h_o at the high superficial fluidizing velocities, the discrepancies increasing as the diameter increases. Selected experimental results substantiate this point. Bed Mk 3 results give higher h_o values compared with the bed Mk 1 values, as indicated by the positive regression coefficient. The apparent rejection of the significance of bed Mk 2 results is not surprising since only 3% of all the results were taken in the bed. Silica sand bed material also affects the heat transfer performance, the negative regression coefficient suggesting a reduction in h_o compared with

zircon sand for constant conditions.

Of the four extended surface tested the extruded type produces the largest variation, compared with the manufactured type. Inspection of the regression equation shows the coefficient for the extruded type to be positive, which indicates that a higher heat transfer coefficient is obtained. It appears that bonding of the fin to the parent tube is of paramount importance, particularly for these fluidized bed applications where high heat fluxes are present. Since the crimped and manufactured surfaces compare very favourably it suggests that a correlating equation may be based on these selected tube results.

The effects of fin spacing are highly significant, the h_o value increasing as the spacing is increased. It will be noted that fin height is not included in the regression set. The reason for this is that the terms $u_f \times 1$ and $u_f^2 \times 1$, which each contain a proportion of the fin height effect, have also been rejected. Since the variables have high "t" values when considered alone, it suggests that when combined together, in the form of a new transformed variable, they would be included in the correlating equation. A discussion of the finalized correlating equations suitable for particular operating conditions will be undertaken at a later stage.

9.3.2 Manufactured Surface Results

In a similar fashion to the square fin surface tests the effects of surface position and bed height were investigated. Figures 8.25 and 8.26 show the variations in the heat transfer coefficients for changes in both position and static bed height. After conducting test number 19 (readings 019 to 024) it was discovered that a large amount of solder was deposited in the entry elbow to surface C/1/MR. It was thought that this protuberance could have caused water flow separation thereby disturbing the steady turbulent flow conditions, and contributing to an adverse overall heat transfer performance. After removal of the obstruction the test was repeated (readings 013 to 018). The effect is shown by the shaded experimental band, the upper limiting curve being used for comparison purposes. It appears that moving the surface off the distributor has little effect compared with increasing the bed static height. In the light of the previous comments made in section

9.1.3 about overall system pressure drop; the majority of the rests were conducted with bed static heights in the order of 50 mm or less. This means that the surfaces are in close proximity to the distributor to ensure that the solids when fluidized, cover the heat exchanger.

To examine the assumption made in the theory that the bed to surface heat transfer coefficient was substantially constant over the complete surface area, two tests were carried out. From the first test, number 19, temperatures were recorded at fixed positions within the fin as shown in figure 8.27. The measured fin temperature distributions are shown in figures 8.28 and 8.29, and compared with the theoretical profiles in figure 8.30. When plotting these curves the measured temperatures were assumed to lie on the same radius. Accepting the profiles given in figure 8.28 to be correct then it appears that the central fin (number 24) temperatures are higher. This would be expected since the end fins were completely exposed on one side to the freshly fluidized particles, culminating in a higher rate of heat transfer from these fins. The theoretical temperature profile is in close agreement with the actual curve obtained from the central fin.

A more sophisticated test (number 23) was carried out on surface C/2/MR in the Mk 2 bed. The complete surface was rotated at 18^{o} intervals and the temperatures recorded, for constant fluidizing conditions. Figure 8.41 shows the actual profile obtained. On the assumption of a constant heat transfer coefficient, concentric isothermal temperatures result. For comparison purposes these isotherms have been plotted in figure 8.40 to form an overlay to figure 8.41. The profiles compare favourably in the lower flank regions but diverge in the upper areas, particularly above the basic tube. This highlights the significance of the basic tube. Clearly, more energy is being transferred in the lower regions where the radial temperature gradients are greater. More experimentation is required to determine the effects at different superficial fluidizing velocities.

The effect of spacing is indicated in figures 8.31, 8.32, 8.33 and 8.34 the trends being similar to those experienced with the

square fin surfaces. Mobility of particles appears to be severely restricted when the spacing is reduced, if the surface has a large fin height and is positioned a distance away from the distributor. This is the case with these surfaces, the fin height being 17.85 mm. The performance of these radial fin tubes is almost certainly impaired by the influence of the size of the bubbles coming into contact with the fins. It has already been pointed out in section 9.2.2 that the best performances are obtained when the bubble coalescence is restricted before entry into the space between adjacent fins. Coalescence cannot be prevented with radial fin surfaces, even when they are positioned on the distributor plate. It is clearly evident that better overall heat transfer performances are achieved from the manufactured square fin tubes even accounting for the greater surface area and the reduced conduction efficiency.

The influence of bed size and configuration is evident from figures 8.36 and 8.37, the small rectangular Mk 2 bed offering a better performance for the radial fin tube C/2/MR than the large circular Mk 1 bed. It has already been mentioned in section 9.1.4 that increased circulation of the solids results from the smaller bed. Increases in h_o are more substantial than those experienced by the plain tube surfaces working under similar conditions - an improvement of some 45% compared with 20% at fluidizing velocities in the order of 0.4 m/s. It will be noticed that the surface is some 25 mm to 30 mm above the distributor with static bed heights in the range 75 mm to 80 mm. If the increase is now compared with the results of surface C/4/MR placed directly on the distributor in both the Mk 1 and Mk 3 beds (figures 8.46 and 8.47) an additional improvement will be realised. The Mk 3 bed results offer just over a 50% increase, for approximately the same fin spacing and fin height. Differences in fin thickness could marginally modify the percentages.

Effective changes in fin thickness are illustrated in figures 8.44 and 8.45 where the fin spacing and fin height is identical for both surfaces. The indications are that the particle movement is affected by the edge of the fins - the greater the thickness the more the circulation. It may well be that thick fins are acting as turbulence promoters in an identical way to that experienced in

forced convection systems. However, when designing a surface for a specific application, fin thicknesses in the order of 1.6 mm would not be employed and therefore the benefits offered would almost certainly not materialize. While it appears that the overall performance of surface C/4/MR is better than C/2/MR as shown in figure 8.45 it must be pointed out that surface C/2/MR has a basic tube outside surface area of some 60% more than C/4/MR. With an improved conduction efficiency and comparable effective area the specific output of C/2/MR is some 45% higher at a fluidizing velocity of 0.45 m/s.

The effects of the main geometric variables such as basic tube outside diameter, fin height and fin spacing on the heat transfer coefficients are shown in figures 8.42 and 8.43. With basic tube size and spacing in favour of surface C/1/MR the increased performance is clearly shown.

Since it appeared that fin height was an important variable, surface C/4/MR was tested in the Mk 3 bed in both zircon sand and steel shot materials. The fin outside diameter was progressively reduced, on a lathe, after each set of readings. The results using the zircon sand are shown in figures 8.48 and 8.49 and the steel shot in figures 8.52 and 8.53. A marked improvement in h_o may be seen as the height is reduced from 17.85 mm to 12.45 mm and thereafter to 2.45 mm the improvement is marginal. This is due to the lower fin edge position above the distributor increasing as the fin height is decreased, and resulted from having to maintain a constant tube centre-line to distributor dimension. The actual dependence of h_o on the fin height is deduced from the statistical analysis. Figures 8.50 and 8.51 show the comparisons between the sand and the steel shot. Plots of h_o against the fin height derived from the above figures are shown in figures 8.54 and 8.55.

Effectiveness factor curves for a range of manufactured surfaces are represented in figures 8.56, 8.57, 8.58 and 8.59. Values are highest in the rectangular bed when using zircon sand, particularly when the fin height is small and at high fluidizing velocities. The influence of fin height is identical to that shown by Bartel et al[27] (figure 8.101) but the effectiveness factors are much larger.

9.3.3 Crimped Surface Results

Figures 8.60 and 8.61 show the influence of basic outside tube diameter on the heat transfer coefficients when working in the Mk 3 bed in zircon sand. Surface C/1/CR has a spacing of 2.3 mm whereas the remaining surfaces have a nominal spacing of 1.6 mm. Therefore surface C/1/CR has the assistance of both tube diameter and fin spacing in promoting high h_o values. Similarly, the bed height helps the remaining tubes as the diameter is increased. It is apparent from these and previous results that the combined influence of several independent variables has necessitated the use of a statistical analysis.

The effect of bed material, including silica sand, is given in figures 8.62 and 8.63, the form of both h_o and U curves with fluidizing velocity, being of a similar form to the plain tube results. The convective component of heat transfer will increase at the higher steel shot fluidizing velocities. However, accounting for this, it appears that the mobility of the particles between adjacent fins of surface C/2/CR is being slightly impeded. This is not surprising since the fin spacing is in the order of only four times the steel shot mean particle diameter. It is interesting to note that the relative difference in performance between zircon sand and steel shot is higher for surface C/5/CR, as shown in figure 8.64, which has a fin spacing twice that of C/2/CR. All other geometric variables are comparable. The indications are that restricted spacings affect the zircon sand more than the steel shot. Figures 8.65 and 8.66 confirm this.

Surface effectiveness factors may be determined from figures 8.68 and 8.69 being of the same order as the manufactured surfaces in the Mk 3 bed.

9.3.4 Statistical Analysis of Manufactured and Crimped Surface Results

It has already been pointed out in the statistical analysis discussion of all the results that there was a need to be selective in order to establish equations which a designer could use. Section A6.5.2 gives a regression equation for the manufactured surfaces in zircon sand in Mk 1 or Mk 3 beds together with the range of experimental variables used in its derivation. From the previous analysis of all the results it was noted that the manufactured and crimped surfaces gave similar performances and could be suitably

analysed together. Section A6.5.1 provides a correlating equation for all such results in zircon sand in the Mk 3 bed.

Before employing these sophisticated regression techniques, to correlate a series of results, one must initially check the magnitude of the experimental repeatibility error. This error must be less than the standard or residual error estimate, of the dependent variable h_o, using the regression equation. If this were not the case it would have been pointless to introduce a complicated model in order to reduce the regression residual error. A series of tests were carried out, the results of one being shown in figure 8.35. The degree of experimental error was determined to be 0.008, which is over one half less than the model residual error produced from the analysis of the manufactured extended surface in the Mk 1 bed at the 99% significant level.

In section 8.4.3 a series of graph plotter curves are derived from the analysis, and show the effects of variations in selected independent variables. The degree of fit, using the regression equation, is indicated by figure 8.71. By suitably modifying the presentation programme it was possible to represent the non-linear variation in h_o with the superficial fluidizing velocity for the range of constant typical values. The scatter of points appears to be less at velocities up to 0.4 m/s. It must be remembered that the magnitude of h_o depends on the typical values chosen. The curve form remains the same and is displaced in the ordinate direction when values are changed. This applies to all the graphs which follow. Figure 8.73, which illustrates the effect of a change in bed temperature, indicates a bed to surface heat transfer coefficient in the order of 0.85 kW/m^2 K at a temperature of 100°C. The reason for this high value is that the overall combination of typical values were not experienced during the experimental work. It does not automatically mean that by employing this typical data the value of h_o can be achieved. The reason for such a marked decrease in h_o as the bed temperature is increased is not very apparent. It has previously been pointed out that a similar trend was observed from the plain tube analysis, although to a lesser extent. To investigate the possibility of thermal gradients existing between the gas/solid particles passing between adjacent fins and that within

the bulk of the bed, a simple test was devised. Details of the test are summarised on page141 and in figures 8.69 and 8.70. A maximum differential temperature in the order of 3 K was detected, the lowest point of the thermocouple probe being 9 mm above the distributor. Probe positions less than this were not used due to the uncertainty of thermocouple location and the variations in bed temperature in the distributor zone. It cannot therefore be reasoned that substantial temperature differential effects influence the negative slope of figure 8.73. Future research could well be directed at determining comprehensive bed temperature profiles between and around extended surface located on the distributor of shallow bed systems.

The variations in h_o due to changes in spacing (figure 8.74) and basic tube outside diameter (figure 8.75) are as expected. Figure 8.76 indicates the influence of fin height which is highly significant over the wide experimental range (3.45 mm to 17.85 mm). The scatter of points about the regression line shows that six different fin heights were used to obtain the correlation.

9.3.5 Extruded Surface Results

High fin extruded surface performance curves ($l > 2.5$ mm) are shown in figures 8.77,8.78 and 8.79. It is difficult to compare these experimental readings with the previous surface results because the geometry and test conditions are not identical. However, similar conditions exist between test number 41 for tube C/5/CR and test number 43 for tube C/1/ER, both sets of results being taken in zircon sand with the surfaces at the distributor. If the relevant independent variables are compared, the advantages offered to the crimped surface are; a smaller rectangular bed, and a smaller basic tube diameter. The fin thickness, fin height and fin spacing are similar and the static bed height slightly favours the extruded surface. The combined effect is to show a 13% improvement in the maximum bed to surface heat transfer coefficient for the extruded surface. The statistical analysis for all extended surface results has also indicated that under identical conditions the extruded tube performances are slightly better. This has been attributed to the fact that the fin and basic tube are integral with one another.

From figure 8.77 it is difficult to assess the merits of individual surfaces, since all the geometric variables are different. In order to establish the relative performances table 8.1 was produced. From previous knowledge, a series of "league" tables were constructed based on the fact that small fin heights, large fin spacings and small basic tube diameters are conducive to good heat transfer performances. The overall positions compare favourably with the curves given in figure 8.77. It is evident that the effects of individual geometric variables are influencing h_o differently as the fluidizing velocity is increased.

The mild steel extruded tube results shown in figure 8.78 illustrate the effects of differences in the main geometric variables. The reduction in performance of surface MS/2/ER is due mainly to its large basic tube size and small fin spacing.

Figure 8.79 shows the overall heat transfer coefficients for both copper and mild steel extruded surfaces. Their relative positions are influenced by a number of factors the most important being due to changes in h_o, A_o and A_E. With the mild steel tubes the resistance to heat transfer by conduction through the radial fins is increased due to the reduced metal thermal conductivity; providing the h_o, t and l values are comparable. Thus, the fin conduction efficiency may be greatly reduced resulting in a lower A_E value for the same total surface area, and a reduced overall heat transfer coefficient.

The copper low fin extruded surfaces heat transfer coefficients are plotted in figure 8.80. A test to determine the influence of tube position, for a constant static bed height, was carried out on tube C/3/ER the results being presented in figure 8.81. It is interesting to note that with low fins (l = 1.36 mm) there is little variation in h_o as the surface is moved to a height of 25 mm above the distributor.

Increased bed to surface heat transfer coefficients for the extruded surfaces, have resulted in higher effectiveness factors and these are shown for selected tubes in figure 8.82. Surface C/2/ER has values in the order of unity. Allowing for the fin

conduction efficiency, the implication is that the heat transfer coefficient is slightly better than that obtained using a plain tube. The mild steel tube MS/1/ER, has lower values due to lower fin efficiencies.

9.3.6 Statistical Analysis of Extruded Surface Results

The regression equation using selected experimental results is given in section A6.6. The range of variables, upon which the equation is based, are listed and the residual errors indicated on the computer line-printer output. Again it is pertinent to mention that the bed temperature is a significant variable, with the h_o values decreasing as T_b increases.

9.4 Other Fin Tube Results

The remaining two mild steel welded radial fin tubes are compared together with the mild steel spine surface in figure 8.85. Performances of the radial tubes are comparable with the extruded type although the h_o values are slightly less due to the inferior bonding between fin and basic tube. Comparison of overall heat transfer coefficients between tube MS/2/WR and tube MS/1/Spine results show the spine surface to have a slight improvement. This is surprizing since the basic tube surface areas are similar and the spine height is 12.7 mm compared with the radial fin height of only 5.1 mm. It would be expected that the U values obtained for the spine would be less on account of the adverse height condition and the poor conduction efficiency. The suggestions are that this type of surface should be more fully investigated for possible shallow fluidized bed heat transfer applications.

9.5 Aspects of Theoretical Analysis

Efficiency curves for radial fins are represented in figure 8.86. These are identical to those published by Gardner[25], and have been derived by solving the relevant equation (3.20) given in Chapter III. The curves have been deduced on the basis of a small mt value (mt = 0.03). This dimensionless parameter may be regarded as a measure of the fin tip heat contribution-the greater the value the larger the heat transfer rate. The effect of variations of fin efficiency, as mt increases, is illustrated in figure 8.87 for a constant D/d_o ratio of 4.0. In fluidized bed applications where

h_o is large, this effect is significant particularly if thick, small fin height, large D/d_o ratio stainless steel tubes are used. As ϕ increases the differences in E_F for changes in mt are reduced. Similarly, the greatest differences in E_F, as mt is varied, are experienced when the D/d_o ratio is large - values greater than 4.0 are not usually employed. Under certain conditions mt values in the order of 0.5 could be obtained, with the resulting reduction in E_F. Hand calculations to determine the fin efficiency may be carried out and table 8.2 shows the results obtained for a range of h_o values. The influence of fin material is clearly shown as the h_o value is increased.

Before dealing with suggested heat transfer design procedures it is interesting to make a few observations regarding the effects of changes in fin spacing, fin height and fin thickness on the extended surface thermal performance. Figure 8.93 shows the variation in Q as the fin spacing is increased for constant conditions. If the copper tube is considered, when b is reduced from 4 mm to 1 mm, Q only increases by 1.55 times even though the secondary surface area is increased by 2.67 times. The reason for this is that for a constant fin efficiency Q is inversely proportional to $(h_i A_i/A_E + h_o)$ and not directly proportional to A_E.

Suppose that it is required to transfer approximately 17 kW of energy using a metre length of tube. From figure 8.93 it is apparent that mild steel tubing could be used with a fin spacing of 2 mm or copper tubing with a fin spacing of approximately 9 mm, providing the constant conditions could be maintained. Even though the volume of metal used to produce the steel surface is nearly 4 times that of the copper, present day raw material prices suggest copper tubing could cost some 4 to 5 times that of the steel. The mild steel would therefore be the best proposition. However, if higher heat transfer rates are required, then it is necessary to increase the length of the tubing. For two metres of mild steel tubing the Q - b characteristic is similar to one metre of copper tubing. The cost of mild steel surface is now approximately one-half that of the copper but it may be better to use copper, since less volume of bed will be occupied by the tubing. Thus the complete analysis, of a shallow fluidized bed system, should consider the

bed containment costs as well as the costs associated with the production of the heat transfer surface.

The effects of increasing fin height on the heat transfer rate is indicated in figure 8.94. Comparisons between copper and mild steel tubing shows that, for the constant conditions, very little benefit is to be derived from using steel fins above fin heights of about 6 mm. Similarly, figure 8.95 suggests that fin thickness variations in the region of 0.1 mm to 0.8 mm have the greatest influence on heat transfer performance, the improvements being marginal as the bed to surface heat transfer coefficient is increased.

Sample performance charts, derived from the theoretical analysis outlined in Chapter IV, are presented in figures 8.96 and 8.97. The curves are obtained directly from the computer programmes specified in Appendix A4, the output being from the graph plotter. Figure 8.96 shows a series of Q - t curves under constant conditions. The problem is one of establishing, for a given volume of metal, the necessary geometric dimensions. The locus of maximum heat transfer points is clearly in evidence, extracts being shown in figures 8.88, 8.89 and 8.90. Figure 8.88 indicates that the locus curve is substantially the same for thermal conductivities in the range 0.045 kW/m K to 0.38 kW/m K. As the thermal conductivity is reduced to 0.015 kW/m K (stainless steel) then the maximum heat transfer rate is reduced, the fin efficiency being critical to the overall performance. These curves are plotted in figures 8.89 and 8.90. The effect is less marked as the basic tube diameter is increased and the heat transfer coefficient is decreased. Figure 8.97 shows the changes in Q/V_2 with the number of fins per metre, for a series of physical constant conditions. Maximum values are obtained indicating the heat transfer rate available for the minimum amount of metal. As a consequence, they are effectively a direct function of the cost required to produce a given surface. Under certain conditions it is possible that no locus of maximum Q/V_2 points exist in the useful range of fin spacing. The curves for stainless steel material shown in figure 8.97 indicate that for fin heights greater than 4 mm, maximum values are only experienced at maximum fin spacings. Maximum Q/V_2 values are summarised in figures 8.91

and 8.92 for specific conditions.

It is appreciated that with the multiplicity of variables, several curves are required to provide a comprehensive set of data which may be utilized by the designer. The computer programme given in Appendix A4 may be used for this purpose. To complete the work a procedure is specified which may be of use to the designer of a heat recovery system.

9.6 Thermal Design Procedure - Heat Recovery System

On the assumption that an extended surface is required to be designed to produce maximum heat transfer for the minimum amount of metal, then the following procedure is recommended.

1. From a knowledge of the fluid to be heated - say water, determine the desirable temperature range and therefore the mean value T_w.
2. From a knowledge of Q the heat transfer rate required, decide on a tube length L. To utilize an extended surface, values in the range of 10 kW/m to 50 kW/m are necessary.
3. Determine the mass flow rate of water through the surface from Q and the temperature difference.
4. Decide on the basic tube inside/outside diameters d_i and d_o, based on the pumping power available. The thermal performance will be improved as the tube size is reduced.
5. Determine the inside surface heat transfer coefficient h_i from the Dittus-Boelter equation

$$Nu = 0.023Re^{0.8}Pr^{0.4}$$

In most cases a value greater than 5 kW/m^2 K will be obtained.

6. Decide on the tube material and type of fin to be employed. Since we are concerned with reducing the overall cost a radial fin of the extruded or crimped type could be employed. A copper tube may be required if the overall heat transfer rate is high.
7. From a knowledge of the fluidizing gas temperature decide on T_b.
8. Assume a bed to surface heat transfer coefficient h_o - say 0.6 kW/m^2 K.
9. Assume a fin height l - say 6 mm initially.
10. From figure 8.91 or equivalent, determine Q/V_2 and the fins/metre N.

11. Determine the metal volume required V_2.
12. Using equations A4.5, A4.9 and A4.10 determine the fin thickness t.
13. Compare the t value with the one specified in figure 8.91 or equivalent. Adjust the fin height accordingly and repeat steps 9. to 13. until the same t value is obtained.
14. Decide on the bed material, surface position and static bed height. The choice of material will be governed by the exhaust gas throughput and bed containment costs. Best thermal performances are achieved when the surface is located at the distributor. To reduce gas pumping power the static bed height should be a minimum providing the surface is submerged.
15. Determine h_o using the regression equations specified in Appendix A6.
16. Compare the h_o value obtained with the assumed value. If substantially different repeat steps 8. to 16.

CHAPTER X
CONCLUSIONS

The experimental work has provided useful information concerning the levels of performance of plain and oval tube and manufactured and commercially produced extended surface in shallow gas fluidized beds.

No significant advantage in heat transfer performance is to be offered by utilizing plain tubes in shallow gas fluidized beds compared with other investigators results in deep gas fluidized beds. However, since pressure drop is a direct function of bed height, benefits will accrue from shallow bed systems and this can be further accentuated by utilizing extended surface.

Performances of oval tubes are far superior to plain tubes when the major axis is placed normal to the distributor. Extended surface using basic tubes of the oval type are worthy of future investigation.

Maximum heat transfers in the order of 14 kW were obtained from an extended surface of overall dimensions 233 mm long by 50.8 mm by 50.8 mm, containing 48 vertical plates, each 1.59 mm thick and silver soldered onto four 6.35 mm outside diameter basic tubes. This corresponds to a heat flow intensity of about 20 MW/m^3, for a temperature difference of 100 K and contrasts with a conventional boiler where the value is an order of magnitude lower at a temperature difference of 1000 K.

Surface position plays an important part in the heat transfer process. The highest performances were achieved when the square fin heat exchanger was placed directly on the porous distributor. This is attributed to the restriction of bubble coalescence before entry between adjacent fins and is confirmed from the results of comparable size radial finned surfaces.

Heat transfer coefficients are higher than those reported in earlier published work using finned tubes in deeper fluidized beds - greater than 250 mm. The improved performance is suggested to be due to the absence of large bubbles in the shallow bed and the improved circulation of the solids when constrained in the narrow passages between adjacent fins.

The bed to surface heat transfer coefficient for radial finned surfaces is influenced by many independent variables. Apart from superficial fluidizing velocity, bed configuration and size, bed material and type of surface are highly significant. The small rectangular Mk 2 (102 mm by 305 mm) and Mk 3 (127 mm by 305 mm) beds produced higher coefficients than the large circular Mk 1 (534 mm diameter) bed. Of the three bed materials used the best performances were given by the zircon sand ($\bar{d}_p$ = 138 μm), followed closely by the steel shot ($\bar{d}_p$ = 432 μm). Silica sand ($\bar{d}_p$ = 157 μm) was not suited to such applications. The fluidizing velocity range for steel shot is more than doubled compared with the sands. This may be an important consideration when designing a system, since smaller bed areas can be utilized to pass a given volumetric flow rate of gas, thereby reducing the bed containment costs. Extruded surfaces provide the best performances, the integral fin bonding with the basic tube, offering less resistance to the high heat fluxes involved.

Of the main geometric variables, basic tube outside diameter, fin height and fin spacing influence the mechanism of heat transfer. The variation due to fin thickness is less significant for the experimental values used.

Variations in the bed temperature, when the surface is positioned on the distributor, is important, the bed to surface heat transfer coefficients decreasing as the temperature increases. This is contrary to the general trend and is attributed to the high energy interaction effects in the vicinity of the distributor. Further research aimed at determining bed temperature profiles and bed porosity in these regions and between adjacent fins is advised.

Flow visualisation studies have suggested that too small a spacing is detrimental to good heat transfer because of impaired particle mobility and the scouring action of the rising bubbles.

The assumptions on which the theoretical model of heat flow for a radial finned surface was derived have been shown to be sound and provided data to assist the designer of shallow fluidized bed systems.

APPENDICES

APPENDIX A1

BACKGROUND THEORY TO MULTIPLE REGRESSION ANALYSIS

A1.1 Introduction

This appendix is concerned with the theory associated with the multiple regression section of the statistical analysis package[51], 1972. In order to develop this theory, a brief description of basic statistical terms is dealt with.

A1.2 The Normal (Gaussian) Distribution

A1.2.1 Estimation

If a continuous random variable x, is such that the probability of its taking values between x_1 and x_2, is the area under the standard normal probability density curve, as shown in figure A1.1(A), then x is said to be normally distributed with mean μ and variance σ^2. This is usually abbreviated by saying that x is distributed as $N(u,\sigma^2)$.

In practical situations, μ and σ^2 will not usually be known. If m independent observations of the variable x are available, then the mean μ, can be estimated by the

$$\text{sample mean,} \quad \bar{x} = \frac{1}{m}\sum_{i=1}^{m} x_i \qquad \text{(A1.1)}$$

and the variance, σ^2, by the

$$\text{sample variance,} \quad s^2 = \frac{1}{m-1}\sum_{i=1}^{m}(x_i - \bar{x})^2 \qquad \text{(A1.2)}$$

The positive square root of s^2 is the sample standard deviation, s. These statistics provide unbiased estimates of μ and σ^2, that is to say

$$E[\bar{x}] = \mu \quad \text{and} \quad E(s^2) = \sigma^2 \qquad \text{(A1.3)}$$

If the original variable x, is distributed as $N(u,\sigma^2)$, then it can be shown that $\bar{x}$ is distributed as $N(u,\frac{\sigma^2}{m})$, so that substituting $\bar{x}$ for x and $\sigma/\sqrt{m}$ for σ, leaving μ unchanged then the term $u = \frac{x-\mu}{\sigma}$ becomes $u = \frac{\bar{x}-u}{\sigma/\sqrt{m}}$ and is distributed as N(0,1). However, if we replace σ by the estimate, s, the quantity $t = \frac{\bar{x}-\mu}{s/\sqrt{m}}$ is not distributed as N(0,1); instead it is said to be distributed as t with γ degrees of freedom, where γ in this case is one less than the sample size, $\gamma = m - 1$.

For a given value of γ, tables will show a value of $t_{\alpha/2}$ such that the probability of t being numerically greater than $t_{\alpha/2}$, that is $t < -t_{\alpha/2}$ or $t > t_{\alpha/2}$, is exactly α. This is equivalent to saying that $100\alpha\%$ of the total area under the probability density curve f(t), as shown in figure A1.1(B), lies in the two tails of the distribution beyond $\pm t_{\alpha/2}$. The total area under f(t) is 1, so the area between $\pm t_{\alpha/2}$ is $(1-\alpha)$, which is the probability of t taking values between $-t_{\alpha/2}$ and $+t_{\alpha/2}$.

Now $\left[-t_{\alpha/2} < t < t_{\alpha/2}\right]$ is equivalent to $\left[-t_{\alpha/2} < \frac{\bar{x}-\mu}{s/\sqrt{m}} < t_{\alpha/2}\right]$. Rearranging terms in the inequality it may be shown that the original statement is also equivalent to $\left[\bar{x} - t_{\alpha/2}\, s/\sqrt{m} < \mu < \bar{x} + t_{\alpha/2}\, s/\sqrt{m}\right]$ so that because $P\left[-t_{\alpha/2} < t < t_{\alpha/2}\right]$ is set equal to $1-\alpha$ then

$$P\left[\bar{x} - t_{\alpha/2}\cdot\frac{s}{\sqrt{m}} < \mu < \bar{x} + t_{\alpha/2}\cdot\frac{s}{\sqrt{m}}\right] = 1-\alpha \qquad \text{(A1.4)}$$

The values $\bar{x} \pm t_{\alpha/2}\, s/\sqrt{m}$ are called the $100(1-\alpha)\%$ <u>confidence limits</u> for the unknown parameter, μ. For statistical work a value of $\alpha = 0.05$ is common, so that 95% confidence levels are specified. The interval between the confidence limits is called the <u>confidence interval</u>. The quantity $s/\sqrt{m}$ which arises in the formula for confidence limits of μ is often called the <u>standard error of the mean</u>; it is an estimate of $\sigma/\sqrt{m}$ which is the standard deviation of the statistic $\bar{x}$ used to estimate the theoretical mean, μ.

A1.2.2 <u>Hypothesis Testing</u>

In most practical work we may have a sample mean $\bar{x}$ and standard deviation s, and we wish to use them to test a <u>null hypothesis</u>, that is an assumption, that μ has some particular value, say $\mu = \mu_o$, against the alternative hypothesis that $\mu \neq \mu_o$. The test is performed by specifying a probability α, called the <u>significant level</u> (expressed as $100\alpha\%$), which determines the two critical values, $\pm t_{\alpha/2}$, such that the combined probability of t being less than $-t_{\alpha/2}$ or greater than $t_{\alpha/2}$ is exactly α. If the calculated t lies between the critical values, we accept that $\mu = \mu_o$, however, if $|t| > t_{\alpha/2}$ we say that μ is significantly different from μ_o at the $100\alpha\%$ significant level. This implies that the probability of obtaining this sort of sample would be unacceptably small ($<\alpha$) if the null hypothesis were true - so we conclude that it is false and reject it in favour of the alternative

that $\mu = \mu_0$.

The ideas of confidence limits and hypothesis tests extend to other parameters (besides normal μ) in different statistical models. In particular they apply to parameters in models for regression and correlation.

A.1.3 Regression and Correlation with Several Dependent Variables

A1.3.1 The Model

It is assumed there is a relationship of the form

$$y_i = b_o x_{io} + b_1 x_{i1} + b_2 x_{i2} + \ldots + b_j x_{ij} + u_i \qquad (A1.5)$$

where y_i is the dependent variable; in this case the bed to metal heat transfer coefficient h_{oi}, and x_{ij} are the i th observations of the j th independent variable. x_{io} is a dummy variable such that $x_{io} = 1$ for all observations. The parameters b_o, b_1, b_2, ... b_j are the unknown population regression coefficients, and u_i is the unobservable random error with zero mean and variance σ_j^2 which is independent of the x_{ij} value; that is to say the probability distribution of μ is normal. Furthermore, it is also assumed that the number of sets of observations is greater than the number of regression coefficients. No restriction is placed on the type of independent variable. Mathematicians usually like each variable to be unrelated and at the most to be of a limited polynomial nature. This enables orthoganal polynomials to be set up which eases the computational procedure and greatly simplifies the analysis of variance. However, the problem is usually one of determining the best correlating equation to fit all the experimental data. To this end, it is necessary to provide independent variables which are a linear combination of one or more of the remaining independent variables as well as incorporating polynomial terms.

Initially we assume that the independent variables can be measured without error. Because of u_i, we find that h_{oi} is a random variable and taking expected values we obtain

$$E(h_{oi}) = b_o + b_1 x_{i1} + b_2 x_{i2} + \ldots + b_j x_{ij} \qquad (A1.6)$$

because $E(u_i) = 0$.

We require to determine values $\beta_o, \beta_1, \beta_2, \ldots\ldots \beta_j$, which are the best estimates of $b_o, b_1, b_2, \ldots\ldots b_j$ respectively. When these values have been found, the discrepancies between the observed and calculated values give an indication of the error which is called the residual.

The values of $\beta_o, \beta_1, \beta_2, \ldots\ldots \beta_j$ are found by minimising the error sum of squares (E.S.S.).

$$E.S.S. = \sum_{i=1}^{m} (h_{oi} - b_o - b_1 x_{i1} - b_2 x_{i2} - \ldots\ldots - b_j x_{ij})^2 \qquad (A1.7)$$

By determining the partial derivatives of E.S.S. with respect to $b_o, b_1, b_2, \ldots\ldots b_j$ and equating to zero a set of (p+1) simultaneous equations can be derived. After algebraic manipulation these equations, known as the normal equations, become

$$\left.\begin{array}{l} \beta_1 S^{11} + \beta_2 S^{12} + \ldots\ldots + \beta_p S^{1p} = S^{h_o 1} \\ \beta_1 S^{21} + \beta_2 S^{22} + \ldots\ldots + \beta_p S^{2p} = S^{h_o 2} \\ \vdots \qquad\quad \vdots \qquad\quad \vdots \qquad\quad \vdots \\ \beta_1 S^{p1} + \beta_2 S^{p2} + \ldots\ldots + \beta_p S^{pp} = S^{h_o p} \\ \text{and} \quad \beta_o = \bar{h}_{oi} - \beta_1 \bar{x}_{i1} - \beta_2 \bar{x}_{i2} - \ldots\ldots - \beta_p \bar{x}_{ip} \end{array}\right\} \qquad (A1.8)$$

($1 \le j \le p$; $1 \le k \le p$)

where $$S^{jk} = \sum_{i=1}^{m} (x_{ij} - \bar{x}_{ij})(x_{ik} - \bar{x}_{ik}) \qquad (A1.9)$$

and is the sum of cross-products of the two variables x_{ij} and x_{ik}, each about its mean. In the case of the dependent variable

$$S^{h_o k} = \sum_{i=1}^{m} (x_{ik} - \bar{x}_{ik})(h_{oi} - \bar{h}_{oi}) \qquad (A1.10)$$

The arithmetic mean of the j th and k th variable are

$$\bar{x}_{ij} = \frac{1}{m}\sum_{i=1}^{m} x_{ij}\ , \quad \bar{x}_{ik} = \frac{1}{m}\sum_{i=1}^{m} x_{ik} \quad \text{and} \quad \bar{h}_{oi} = \frac{1}{m}\sum_{i=1}^{m} h_{oi} \qquad (A1.11)$$

It will be observed that all the values of x_i and h_{oi} variables enter the analysis as deviations from their mean values; data in this form are described as centred. The final equation in (A1.8) shows that the fitted model can also be written in centred form as

$$h_{oi} - \bar{h}_{oi} = \beta_1(x_{i1} - \bar{x}_{i1}) + \beta_2(x_{i2} - \bar{x}_{i2}) + \ldots + \beta_p(x_{ip} - \bar{x}_{ip}) \qquad (A1.12)$$

A1.3.2 Matrix Notation for Least-Squares Estimation

Using matrix notation, the theory and equations of multiple regression analysis can be written in a very concise form. The procedure is to measure the dependent variable and each of the independent variables relative to their respective mean values. Denote the set of m centred observed values of the dependent variable h_o by the m x 1 column matrix $\{h_o\}$ and the set of p unknown parameters $b_1, b_2, \ldots\ldots b_p$ by the p x 1 column matrix $\{b\}$. Also let the set of mp centred values of the independent variables be denoted by the m x p matrix $[X]$. This is often referred to as the Design Matrix, since it describes the combinations of the levels of the independent variables which have been included in the experimental design. Then the centred model under consideration can be written as

$$\{h_o\} = [X]\{b\} + \{U\} \qquad \text{(A1.13)}$$

where $\{U\}$ is an m x 1 column vector of errors in the determination of $\{h_o\}$.

The p least-squares equations for the parameter estimates may then be expressed as

$$[X]'[X]\{\beta\} = [X]'\{h_o\} \qquad \text{(A1.14)}$$

where $[X]'$ is the matrix transpose of $[X]$. The p x p symmetric matrix $[X]'[X]$, consisting of the corrected sums of squares and products S^{jk}, given by (A1.9), is often referred to as the Information Matrix.

The package will print a modified form of this matrix by including $S^{h_o k}$ values given by (A1.10). This n x n matrix is known as the Covariance Matrix $[S]$, where n is the number of observation variables in the original matrix.

$$[S] = \begin{bmatrix} s_{11} & s_{12} & \ldots\ldots & s_{1n} \\ s_{21} & \ldots\ldots\ldots & \vdots \\ \vdots & & \vdots \\ s_{n1} & \ldots\ldots\ldots & s_{nn} \end{bmatrix} \qquad \begin{matrix} 1 \le k \le n \\ \downarrow \\ 1 \le j \le n \end{matrix} \qquad \text{(A1.15)}$$

where

$$s_{jk} = \frac{1}{m-1} \sum_{i=1}^{m} (x_{ij} - \bar{x}_{ij})(x_{ik} - \bar{x}_{ik}) \qquad \text{(A1.16)}$$

The solution to the least-squares equations is simply the p x 1 column vector

$$\{\beta\} = \left[[X]'[X]\right]^{-1}[X]'\{h_o\} \qquad \text{(A1.17)}$$

where $\left[[X]'[X]\right]^{-1}$ is the inverse matrix of $[X]'[X]$. Predicted values of the response are then given by

$$\{h_{op}\} = [X]\{\beta\} \qquad \text{(A1.18)}$$

A1.3.3 The Correlation Matrix

Despite the centring of the original data, the elements S^{jk} of the information matrix or S_{jk} of the covariance matrix, can be of quite different sizes, which may lead to appreciable round-off errors in the computation when the variables cover widely differing ranges and particularly when there are a large number of variables in the model. This difficulty can be overcome by working with standardized deviates. The information matrix then takes the form

$$[R] = (m-1)\begin{bmatrix} 1 & r_{12} & \cdots & r_{1p} \\ r_{21} & 1 & & \vdots \\ \vdots & & \ddots & \\ r_{p1} & \cdots & & 1 \end{bmatrix} \qquad 1 < k \leq p \;\rightarrow,\quad 1 \leq j < p \;\downarrow \qquad \text{(A1.19)}$$

where

$$r_{jk} = r_{kj} = \frac{S_{jk}}{\sqrt{S_{jj} \cdot S_{kk}}} \qquad k \neq j \qquad \text{(A1.20)}$$

r_{jk} is the simple correlation coefficient between x_j and x_k, and similarly for each pair of the independent variables. This array, apart from the (m-1) multiplying factor, contains the correlation coefficients for all possible pairs of variables and is termed the Correlation Matrix [R]. All elements have values between -1 and +1. In practice, the correlation matrix is obtained directly from the information matrix $[X]'[X]$, rather than standardizing all the original individual observations.

A1.3.4 Variances and Covariances of the Coefficients

From (A1.17) we see that each estimated regression coefficient

can be regarded as a weighted linear sum of the observed values of the dependent variable h_o; the weights being rather complicated functions of the values of the independent variables. Since each of the coefficients $\beta_1, \beta_2, \ldots\ldots \beta_p$ depends on the same set of observed h_o values, they cannot normally be estimated independently of each other. The degree of inter-dependence of the estimates is measured by the covariance between each pair of coefficients.

The variances and covariances of the regression coefficients can be set out in a single p x p matrix array, with the variances forming the elements in the leading diagonal and the covariances the off-diagonal elements. This is termed the Variance-Covariance Matrix[C]. It can be shown from (A1.17) that

$$[C] = \left[\left[[X]'[X]\right]^{-1}[X]'\right]\left[\left[[X]'[X]\right]^{-1}[X]'\right]' \sigma^2$$

$$[C] = \left[[X]'[X]\right]^{-1}[X]'[X]\left[[X]'[X]\right]^{-1}\sigma^2 \quad \text{since } [X]'[X] \text{ is symmetrical}$$

$$[C] = \left[[X]'[X]\right]^{-1}\sigma^2 \qquad \text{(A1.21)}$$

Thus the variances and covariances of the coefficients are simply the elements of the inverse of the information matrix multiplied by the error variance of the dependent variable.

The best estimate of b_j for each $j = 0,1,2, \ldots\ldots, p$ is β_j. For $p \geq 1$ an unbiased estimate of σ^2 (the error variance) is provided by

$$\sigma^2 = \frac{E.S.S.}{m-p-1} \qquad \text{(A1.22)}$$

and the standard error of β_j, denoted by S.E.(β_j) is

$$S.E.(\beta_j) = \sigma\sqrt{C_{jj}} \qquad \text{(A1.23)}$$

where C_{jj} is the j th diagonal element of the $\left[[X]'[X]\right]^{-1}$ matrix.

The standard errors give a measure of the uncertainties associated with the separate estimates, while the covariances show how chance errors in the estimation of any one coefficient will affect the estimates of the other coefficients. Both variances and covariances are required in assessing the accuracy of prediction using the regression equation. It is a fortunate fact that their enumeration by

means of (A1.21) is a bi-product of the matrix inversion which is required anyway to estimate the coefficients by means of (A1.17).

The statistic

$$t = \frac{\beta_j - b_j}{S.E.(\beta_j)} \qquad (A1.24)$$

is distributed as t with $\gamma = m - p - 1$, and it can be used to construct confidence intervals or test hypothesis about b_j. The statistical package uses this piece of theory to decide which x - variables should be included in the regression by testing the null hypothesis that $b_j=0$ against the alternative that $b_j=0$ at the $100\alpha\%$ significant level for $j = 0,1,2, \ldots\ldots, p$.

The x - variables are thus divided into two sets: P_1, the regression set, for which the hypothesis that $b_j=0$ has been rejected at the $100\alpha\%$ level for each x_{ij} in the set, and P_2, the set excluded from the regression, for which the hypothesis that $b_j=0$ has been accepted. The package outputs the correct number of degrees of freedom ($\gamma = m - p - 1$), and automatically sets $\alpha=0.99$ unless the user specifies another value. This has the effect of almost certainly including every x - variable which the user has provisionally put in P_1 because even the smallest b_j will lead to t exceeding the 0.99 critical value and hence rejection of the hypothesis that $b_j=0$. It is therefore advisable to specify a small initial value of α, say 0.02 or 0.1, to discover those x-variables which are more important in the regression.

A1.3.5 Partial and Multiple Correlation Coefficients

The simple partial correlation coefficients given in the correlation matrix [R] in section A1.3.3 may give a very false impression of the relationship between the two variables. For example, the correlation coefficient may have a positive value significantly different from zero either because an increase in one variable produces an increase in the other variable or because increases in both variables are due to increases in one or more additional variables. Therefore, it is of interest to be able to calculate the correlation coefficient between two variables with the effect of one or more other variables removed. Such a coefficient is known as a partial correlation coefficient.

These coefficients are most easily explained if we now think of an Observation Matrix[Y], which can be line-printed from the package, and includes the dependent variable vector as well as the (p + 1) x - vectors. The observation matrix is then an m x (p + 2) matrix or an m x l matrix where l = p + 2.

$$[Y] = \begin{bmatrix} h_{01} & x_{10} & \cdots & x_{1p} \\ h_{02} & x_{20} & \cdots & x_{2p} \\ \vdots & \vdots & & \vdots \\ h_{0m} & x_{m0} & \cdots & x_{mp} \end{bmatrix} = \begin{bmatrix} x_{11} & x_{12} & \cdots & x_{1L} \\ x_{21} & x_{22} & \cdots & x_{2L} \\ \vdots & \vdots & & \vdots \\ x_{m1} & x_{m2} & \cdots & x_{mL} \end{bmatrix} \qquad x_{ij},\ 1 \le j \le L,\ 1 \le i \le m \qquad \text{(A1.25)}$$

Column x_{i1} values are set at unity and given the name CONST. The line printer output shows the columns and rows interchanged; that is the Transpose Matrix$[Y]'$.

$$[Y]' = \begin{bmatrix} x_{11} & x_{21} & \cdots & x_{m1} \\ x_{12} & x_{22} & \cdots & \vdots \\ \vdots & \vdots & & \vdots \\ x_{1L} & x_{2L} & \cdots & x_{mL} \end{bmatrix} \qquad x_{ik},\ 1 \le i \le m,\ 1 \le k \le L \qquad \text{(A1.26)}$$

Column j of $[Y]$ then shows all observations of variable x_j, and we define the partial correlation of x_j with x_k (i.e. row k of $[Y]'$) where $j \neq k$ as the correlation between these two variables when all other x - variables are held constant.

The usual notation for a sample partial correlation is an r with the numbers of the two variables suffixed and followed by a dot and the numbers of the variables held constant. For example, the sample partial correlation of x_1 with x_2 holding x_3, x_4, x_5 constant is written $r_{12.345}$. The value of $r^2_{jk.etc.}$ can be found by using elements of the $\left[[Y]'[Y]\right]^{-1}$ matrix. If C^{jk} is the element in row j and column k of this matrix, then it can be shown that

$$r^2_{jk.etc.} = \frac{(C^{jk})^2}{C^{JJ} \cdot C^{kk}} \qquad \text{(A1.27)}$$

The product of the observation transpose matrix and the observation matrix $[Y]'[Y]$ is given by the statistical package as the Cross-Product Matrix[P].

$$[P] = \begin{bmatrix} P_{11} & P_{12} & \cdots & P_{1L} \\ P_{21} & P_{22} & \cdots & \vdots \\ \vdots & & & \vdots \\ P_{l1} & \cdots & \cdots & P_{LL} \end{bmatrix} \qquad 1 \le k \le L,\ 1 \le j \le L \qquad \text{(A1.28)}$$

In general each

$$P_{jk} = \sum_{i=1}^{m} x_{ij} . x_{ik} \qquad \text{(A1.29)}$$

Since all the x_{i1} values are set at unity then term $P_{11} = \sum_{i=1}^{m} 1^2 = m$, the total number of observations. The principal diagonal values represent the sum of squares (S.O.S.) of each data variable in turn. Also the conjugates are the same.

If all the variables are normally distributed then it may also be shown that

$$t = \sqrt{\frac{(m-b-1).r_{jk,etc,}^{2}}{1 - r_{jk,etc,}^{2}}} \qquad \text{(A1.30)}$$

This statistic is used to examine the partial correlations of h_o with each of the x-variables in the excluded set P_2. If any x-variable in P_2 has a partial correlation which is significantly different from zero, then that variable is transferred to P_1 and so included in the regression set.

The sample multiple correlation between the dependent variable h_o and the independent variable x_j is denoted by R_j. R_j^2 can be interpreted as the reduction in the variance of the dependent variable which is caused by including x_j as an independent variable in the regression set. The package outputs a value of R_j for each of the independent variables and also (below E.S.S. and residual error on print out) shows the multiple correlation between the dependent variable h_o and the regression estimate h_{oc}. It may be shown that

$$R_j^2 = 1 - \frac{E.S.S.}{\sum_{i=1}^{m} (h_{oi} - \bar{h}_{oi})^2} \qquad \text{(A1.31)}$$

which may be interpreted as:-

$$R_j^2 = 1 - \frac{\text{Variance of dependent variable not explained by regression}}{\text{Total variance of dependent variable}}$$

$$R_j^2 = \frac{\text{Variance of dependent variable explained by regression}}{\text{Total variance of dependent variable}}$$

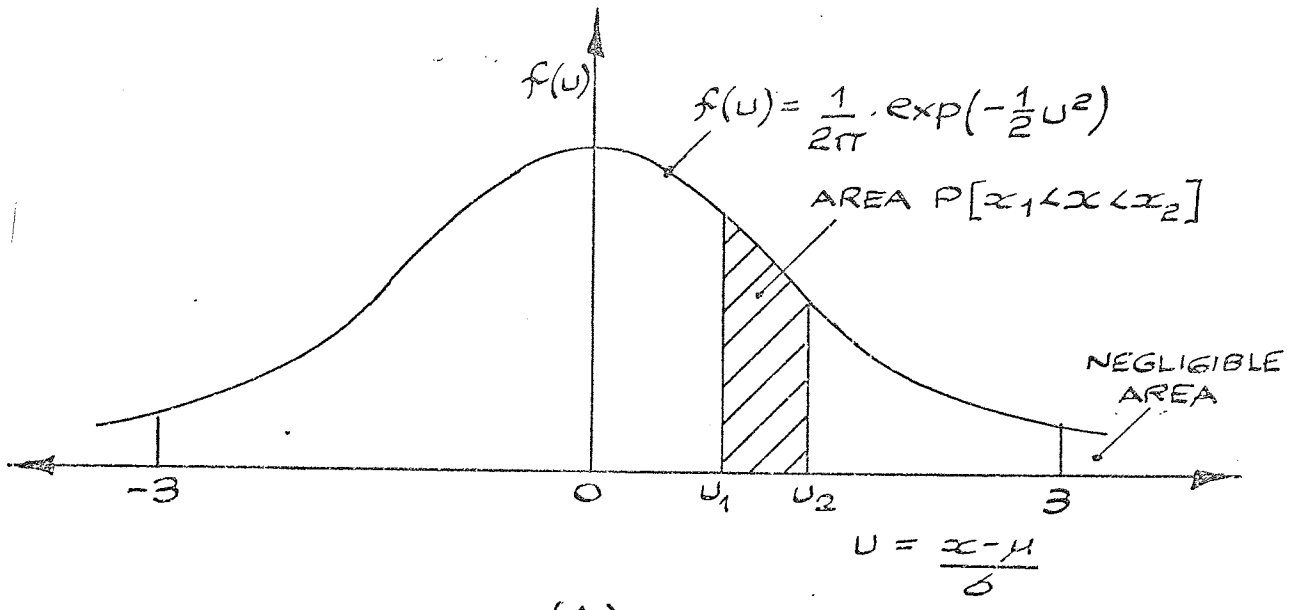

(A)

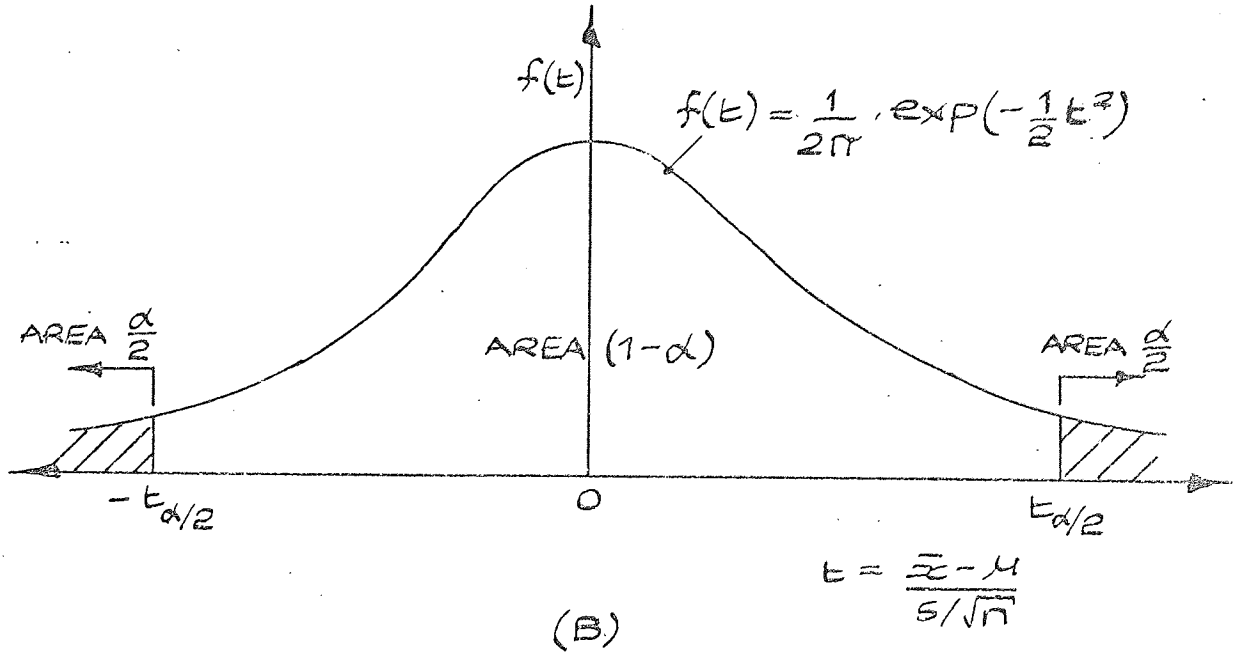

(B)

Figure A1.1 Normal Distribution Curves

APPENDIX A2

MULTIPLE REGRESSION PRESENTATION PROGRAMME

A2.1 Introduction

A computer application programme is available to users of the ICL 1900 Statistical Analysis Multiple Regression Programme[46], at the University of Aston in Birmingham Computer Centre, to enable results from the regression analysis to be presented in the form of a graphical output. A series of graphs may be plotted to indicate the significance of the important independent variables in the regression equation, and to illustrate their influence on the dependent variable. A scatter diagram showing the observed dependent variable compared with the dependent variable calculated from the regression equation may also be represented.

A2.2 General Theory

As specified in Appendix A1 the analysis is concerned with establishing the relationships between the dependent variable h_o and the independent variables $x_1, x_2, x_3, \ldots\ldots x_n$, including those formed by transformation and cross-product. For an observation value the observed h_o value is denoted by h_{oo} and that calculated from the regression equation:-

$$h_{oc} = \beta_o + \beta_1 x_1 + \beta_2 x_2 + \beta_3 x_3 + \ldots\ldots + \beta_n x_n \qquad (A2.1)$$

If the "typical values" of the independent variables are given by $t_1, t_2, t_3, \ldots\ldots t_n$, then

$$h_{oct} = \beta_o + \beta_1 t_1 + \beta_2 t_2 + \beta_3 t_3 + \ldots\ldots + \beta_n t_n \qquad (A2.2)$$

h_{oct} being the calculated value of h_o using the typical values. Since we are concerned with several variables then a fully corrected value for the dependent variable h_o may be defined by

$$h_{ofc} = h_{oo} - (h_{oc} - h_{oct}) \qquad (A2.3)$$

Substituting for h_{oc} and h_{oct} from (A2.1) and (A2.2) gives

$$h_{ofc} = h_{oo} - \beta_1(x_1 - t_1) - \beta_2(x_2 - t_2) - \beta_3(x_3 - t_3) - \ldots\ldots - \beta_n(x_n - t_n) \qquad (A2.4)$$

$\beta_1(x_1 - t_1)$, $\beta_2(x_2 - t_2)$,....., $\beta_n(x_n - t_n)$ are the correction terms corresponding to each of the independent variables $x_1, x_2, x_3, \ldots\ldots x_n$. If the individual correction terms are omitted from (A2.4) then we obtain a partially corrected h_o value, namely h_{opc}. For the second independent variable

$$h_{opc2} = h_{oo} - \beta_1(x_1 - t_1) - \beta_3(x_3 - t_3) - \ldots\ldots - \beta_n(x_n - t_n) \quad \text{(A2.5)}$$

A series of h_{opc2} values may be obtained by declaring typical values $t_1, t_3, \ldots\ldots t_n$, which are held constant, and using each of the observed data values of $h_{oo}, x_1, x_3, \ldots\ldots x_n$. By plotting these h_{opc2} values against their respective observed x_2 values a graph is obtained as shown in figure A2.1(A). It is customary to superimpose on these plotted points the regression line equation given from (A2.1) with the remaining corresponding independent variables assuming their constant typical values, such that h_{or2} the linear regression equation for independent variable x_2 is denoted by

$$h_{or2} = \beta_o + \beta_1 t_1 + \beta_2 t_2 + \beta_3 t_3 + \ldots\ldots + \beta_n t_n \quad \text{(A2.6)}$$

from which

$$h_{or2} = \alpha_2 + \beta_2 x_2 \quad \text{(A2.7)}$$

where α_2 is the constant intercept term

$$\alpha_2 = \beta_o + \beta_1 t_1 + \beta_3 t_3 + \ldots\ldots + \beta_n t_n \quad \text{(A2.8)}$$

In practice it may be necessary, in order to improve the correlation, to introduce polynomial terms of an existing independent variable or indeed cross-product terms of a combination of existing independent variables. This greatly complicates the analysis and cannot be dealt with directly using the graphplotter presentation programme, which was devised for linear unrelated independent variables. However, this difficulty may be partially overcome by surpressing the plotting of particular graphs and/or modifying the form of the regression equation. Equation (A2.7) will then be a modified expression in terms of x_2.

A plot, for each of the independent variables, against its

partially corrected value of h_o provides for the multiple regression user the sort of advice that a simple plot provides for the simple regression user. In particular, it may save him from making wrong assumptions from the regression equation. If the points lie on a curved line, rather than the straight, calculated line, then a further transformation of variable may be tried. For points that are not evenly distributed along both axes care must be taken in interpretation.

These "partially corrected" graphs are equivalent to looking at a plot of the observations and the regression equation in "n dimensional space". An individual graph shows what you would see if you looked through this space from a side corresponding to the independent variable and looking in such a direction that the regression plane appeared as a single line. Perfect correlation will be obtained when all points lie exactly on this line.

Finally, by plotting h_{oc} against h_{oo} values and superimposing a 45 degrees line to both variable axes as shown in figure A2.1(B) it is possible to determine those points which show the largest discrepancy between the observed and calculated dependent variable. Useful information can then be established for enquiring further into the source of these observations. Alternatively, the maximum discrepancies can be picked out from the columns of the analysis residual columns produced by the ICL Statistical Package[51]. The difference between points is given in the form of the percentage ratio h_{oc}/h_{oo}. The nearer to 100 for each point, the better will be the correlation.

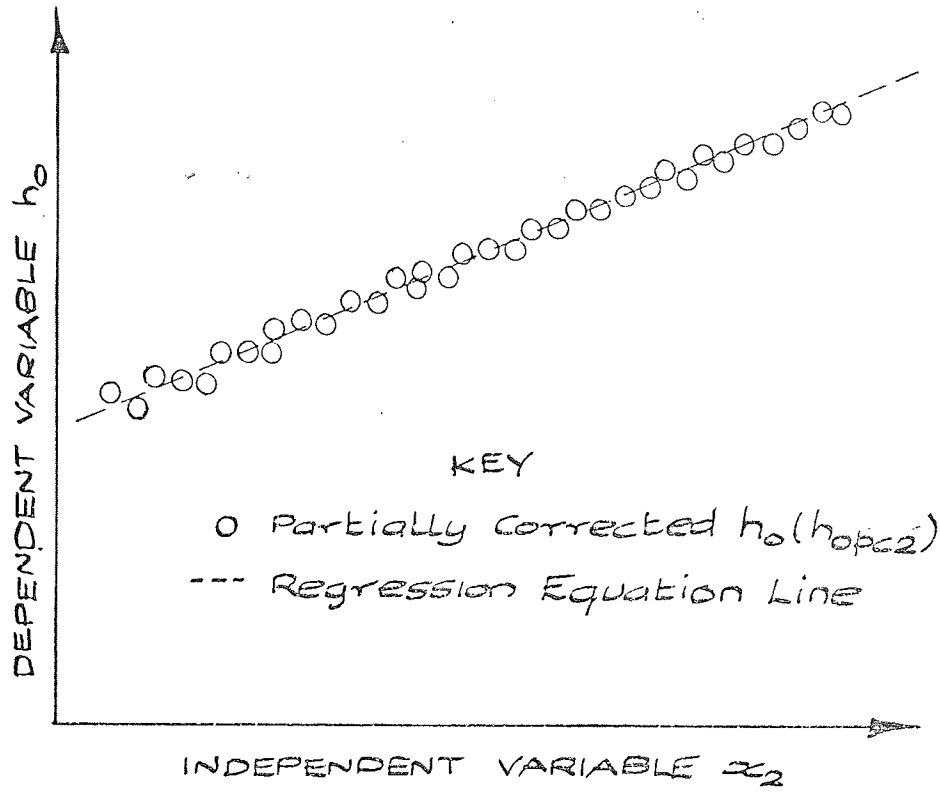

(A)

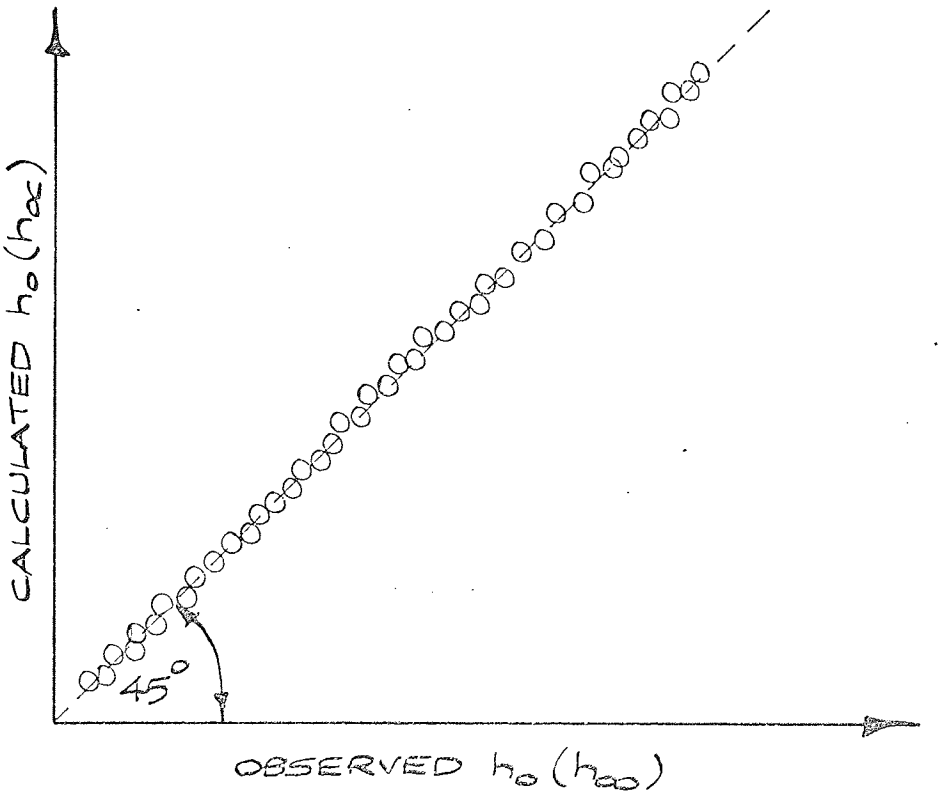

(B)

Figure A2.1 Graphplotter Results from Presentation Programme

APPENDIX A3

EXPERIMENTAL RESULT TABLES

A3.1 Introduction

All observed experimental results, together with those derived, are given in this appendix. The calculated results were evaluated from a standard programme which is also listed - radial fin surfaces.

The thermophysical properties of water equations were extracted from the following references:

(1) thermal conductivity k_w(XK) kW/m K - reference 53

(2) dynamic viscosity μ(XMU) kg/m s - reference 54, p F-36

(3) specific heat c_p(CP) kJ/kg K - reference 54, p D-122 (numerical data only)

In the case of c_p a series of linear and quadratic equations were fitted to the numerical data, over a range of temperatures, using a least-squares curve fitting technique.

Depending on the bed configuration, the constants in the equations for V_a(VA) and u_f(UF) require changing. The following summary indicates the alterations necessary.

Circular Mk 1 Bed - 534 mm diameter $A_b = 0.2240\ m^2$

Air orifice plate diameter 38.1 mm

$$\dot{V}_a = \frac{1}{562}\sqrt{\frac{(P_a+P_{at})H_a}{(T_a+273.15)}}\ m^3/s \qquad @\ 760\ mm\ Hg\ abs\ and\ 15°C$$

$$u_f = \frac{1}{64.2}\cdot V_a(T_b+273.15)\ m/s \qquad based\ on\ bed\ conditions\ of\ T_b\ and\ P_{at}$$

Rectangular Mk 2 Bed - 102 mm by 305 mm $A_b = 0.0311\ m^2$

Air orifice plate diameter 25.4 mm

$$\dot{V}_a = \frac{1}{1310}\sqrt{\frac{(P_a+P_{at})H_a}{(T_a+273.15)}}\ m^3/s$$

$$u_f = \frac{1}{8.91}\cdot V_a(T_b+273.15)\ m/s$$

Rectangular Mk 3 Bed - 127 mm by 305 mm $A_b = 0.0387\ m^2$

Air orifice plate diameter 25.4 mm

$$\dot{V}_a = \frac{1}{1310}\sqrt{\frac{(P_a+P_{at})H_a}{(T_a+273.15)}}\ m^3/s$$

$$u_f = \frac{1}{11.10}\cdot V_a(T_b+273.15)\ m/s$$

EVALUATION OF CALCULATED EXPERIMENTAL RESULTS - Master Computer Programme Listing.

```
      MASTER
C     EVALUATION OF FLUIDIZED BED RESULTS OF 8/6/72 FOR C/2/MR TUBE
C     IN ZIRCON SAND-MK1 BED
      DIMENSION R(10)
      WRITE(2,10)
   10 FORMAT(1H1,70HFLUIDIZED BED RESULTS OF 8/6/72 FOR C/2/MR TUBE IN Z
     1IRCON SAND-MK1 BED)
      READ(1,35)N
   35 FORMAT(I2)
      READ(1,40)DI,DO,D,T,XN,XL,XKM
   40 FORMAT(7F0.0)
      READ(1,168)(R(J),J=1,10)
  168 FORMAT(10F0.0)
      WRITE(2,45)DI,DO,D,T,XN,XL,XKM
   45 FORMAT(/,6H DI = ,F5.2,3X,5HDO = ,F5.2,3X,4HD = ,F5.2,3X,4HT = ,
     1F5.3,3X,5HXN = ,F5.1,3X,5HXL = ,F5.1,3X,6HXKM = ,F6.4)
   20 FORMAT(//,3X,2HXM,10X,2HTW,11X,2HQ,11X,3HXHI,11X,3HXHO,10X,2HUO,
     111X,2HUF,10X,2HEF,10X,2HTB,10X,3HXMT)
   30 FORMAT(1H0,    F5.4,8X,F5.2,7X,F6.3,7X,F6.3,7X,F5.3,8X,F5.3,7X,
     1F4.3,7X,F6.4,7X,F5.1,7X,F6.4)
      I=0
   50 I=I+1
      IF(I.GT.N) GO TO 160
      READ(1,60)TWI,TWO,XMDOT1,HW,HA,PA,TA,PAA,TB
   60 FORMAT(9F0.0)
      AI=3.1416*DI*XL/1.0E 6
      AO=3.1416*DO*XL/1.0E 6
      A1=3.1416*DO*(XL-XN*T)/1.0E 6
      A2=((D**2-DO**2)/2.0+D*T)*3.1416*XN/1.0E 6
      XMDOT2=0.05*SQRT(HW)
      XM=XMDOT1+XMDOT2
      TW=TWO-0.5*XMDOT1*(TWO-TWI)/XM+0.39/(2.0*XM*4.18)
      IF(TW-20.0)70,70,80
   70 CP=10.8014-12.3942*(TW+273.15)/273.15+5.75*((TW+273.15)/273.15)**2
      GO TO 110
   80 IF(TW-33.0)90,90,100
   90 CP=6.2256-7.2917*(TW+273.15)/273.15+3.2857*((TW+273.15)/273.15)**2
      GO TO 110
  100 CP=4.1202+0.04324*(TW+273.15)/273.15
  110 Q=CP*XMDOT1*(TWO-TWI)-0.39
      UO=Q/(AO*(TB-TW))
      X=(PA+PAA)*HA/(TA+273.15)
      VA=SQRT(X)/562.0
      UF=VA*(TB+273.15)/64.2
      XK=(-922.47+2839.5*(TW+273.15)/273.15-1800.7*((TW+273.15)/273.15)
     1**2+525.77*((TW+273.15)/273.15)**3-73.44*((TW+273.15)/273.15)**4)/
     210**6
      IF(TW-20.0)120,120,130
  120 XLMU=((1301.0/(998.333+8.1855*(TW-20.0)+0.00585*(TW-20.0)**2))-
     13.30233)*2.30258
      XMU=EXP(XLMU)/10.0
      GO TO 140
  130 XLMU=((1.3272*(20.0-TW)-0.001053*(TW-20.0)**2)/(TW+105.0))+1301.0
     1/998.333-3.30233)*2.30258
      XMU=EXP(XLMU)/10.0
```

```
140 PRANDTL=CP*XMU/XK
    XHI=((2.0*XK)/DI)*(4000.0*XM/(3.1416*DI*XMU))**0.8*PRANDTL**0.4
    EF=0.8
150 EFX=EF
    AE=A1+EF*A2
    RECXHO=AE/(AO*UO)-AE*DO*ALOG(DO/DI)/(2.0*AO*XKM*10**3)-AE/(AI*XHI)
    XHO=1.0/RECXHO
    X=2.0*T*XHO/(XKM*10**3)
    XMT=SQRT(X)
    X=2.0*XHO*10**3/(XKM*T)
    PHI=(D-DO)*SQRT(X)/(2.0*10**3)
    XMRO=PHI/(D/DO-1.0)
    XMR=XMRO*D/DO
    XHOXKM=XMT/2.0
    X=XMRE
    CALL F4I0(X,VALUE)
    VALUE1=VALUE*EXP(X)
    CALL F4I1(X,VALUE)
    VALUE2=VALUE*EXP(X)
    CALL F4K0(X,VALUE)
    VALUE3=VALUE/EXP(X)
    CALL F4K1(X,VALUE)
    VALUE4=VALUE/EXP(X)
    A=XHOXKM*VALUE1+VALUE2
    B=VALUE4-XHOXKM*VALUE3
    X=XMRO
    CALL F4I0(X,VALUE)
    VALUE5=VALUE*EXP(X)
    CALL F4I1(X,VALUE)
    VALUE6=VALUE*EXP(X)
    CALL F4K0(X,VALUE)
    VALUE7=VALUE/EXP(X)
    CALL F4K1(X,VALUE)
    VALUE8=VALUE/EXP(X)
    Z=((A*VALUE8)/B-VALUE6)/(VALUE5+(A*VALUE7)/B)
    EF=2.0*Z/((PHI+XMT)*D/DO+PHI)
    IF(ABS(EF-EFX).GT.0.000001) GO TO 150
    WRITE(2,20)
    WRITE(2,30)XM,TW,Q,XHI,XHO,UO,UF,EF,TB,XMT
    TDIFF=Q/(XHO*AE)
    J=0
170 J=J+1
    RATIO=R(J)/R(1)
    XMR=XMRO*RATIO
    X=XMR
    CALL F4I0(X,VALUE)
    VALUE9=VALUE*EXP(X)
    CALL F4K0(X,VALUE)
    VALUE10=VALUE/EXP(X)
    THETA=(VALUE9+A*VALUE10/B)/(A*VALUE7/B+VALUE5)
    TEMP=TB-THETA*TDIFF
    WRITE(2,167)R(J),TEMP
167 FORMAT(/,10H RADIUS = ,F5.2,2X,7HTEMP = ,F7.3)
    IF(J-10)170,50,50
160 STOP
    END
```

Plain and Oval Tube Results

Tests 1 - 9

TEST NUMBER 1

SURFACE: C/1/Plain TEST BED: Mk 1 POSITION: 17.0 mm between tube ℄ and distributor plate
BED MATERIAL: Zircon sand, size range 63 - 210 μm; static height 50 mm

OBSERVED RESULTS

READING NUMBER	BED			WATER				GAS	AIR			AMBIENT	
	T_{16} °C	T_{17} °C	T_{18} °C	T_{wi} °C	T_{wo} °C	ROT. READ	H_w mm H_2O	ROT. READ	H_a mm H_2O	T_a °C	P_a mm Hg	P_{at} mm Hg	T_{at} °C
P01	250	251	249	10.5	24.4	9.7	68	18.1	48	48	77	755	23.5
P02	265	267	263	10.5	26.8	9.8	68	20.4	101	48	77	755	24.0
P03	270	273	268	10.5	28.6	9.8	68	24.9	254	46	75	755	25.0
P04	270	268	265	10.5	29.2	9.9	68	29.9	495	44	73	755	25.5

CALCULATED RESULTS

READING NUMBER	$\dot{m}$ kg/s	$\dot{M}$ kg/s	T_w °C	T_b °C	Q kW	$\dot{V}_a$ m^3/s $x10^3$	$\dot{V}_g$ m^3/s $x10^3$	u_f m/s	U kW/m^2K	h_i kW/m^2K	h_o kW/m^2K
P01	0.055	0.421	23.7	250	2.81	19.8	0.184	0.162	0.447	25.25	0.463
P02	0.055	0.421	26.0	265	3.36	28.8	0.203	0.241	0.506	25.86	0.526
P03	0.055	0.421	27.7	270	3.77	45.7	0.242	0.387	0.560	26.31	0.585
P04	0.055	0.421	28.2	268	3.91	64.0	0.288	0.539	0.587	26.47	0.614

TEST NUMBER 2

SURFACE: C/1/Plain TEST BED: Mk 1 POSITION: 17.0 mm between tube ℄ and distributor plate
BED MATERIAL: Zircon sand, size range 63 - 210 μm; static height 25 mm

OBSERVED RESULTS

READING NUMBER	BED			WATER				GAS	AIR			AMBIENT	
	T_{16} °C	T_{17} °C	T_{18} °C	T_{wi} °C	T_{wo} °C	ROT. READ	H_w mm H_2O	ROT. READ	H_a mm H_2O	T_a °C	P_a mm Hg	P_{at} mm Hg	T_{at} °C
P05	263	267	263	11.9	25.2	9.6	78	17.3	49	48	80	774	22.0
P06	284	282	275	11.9	27.0	9.7	77	20.2	100	48	80	774	23.0
P07	284	285	277	11.8	27.4	9.7	78	21.7	151	48	80	774	24.0
P08	282	286	280	11.8	28.1	9.7	78	25.0	252	47	79	774	24.0
P09	280	284	280	11.8	28.2	9.8	78	27.4	349	46	78	774	25.0
P10	280	284	278	11.8	28.4	9.8	78	30.2	494	46	76	774	25.0

CALCULATED RESULTS

READING NUMBER	$\dot{m}$ kg/s	$\dot{M}$ kg/s	T_w °C	T_b °C	Q kW	$\dot{V}_a$ m^3/s $x10^3$	$\dot{V}_g$ m^3/s $x10^3$	u_f m/s	U kW/m^2K	h_i kW/m^2K	h_o kW/m^2K
P05	0.055	0.450	24.6	264	2.67	20.3	0.177	0.170	0.401	26.76	0.413
P06	0.055	0.448	26.3	281	3.08	29.0	0.201	0.251	0.436	27.11	0.450
P07	0.055	0.450	26.6	282	3.20	35.7	0.215	0.308	0.451	27.34	0.466
P08	0.055	0.450	27.3	283	3.36	46.1	0.243	0.399	0.473	27.53	0.489
P09	0.056	0.450	27.4	281	3.45	54.3	0.264	0.469	0.490	27.60	0.507
P10	0.056	0.450	27.6	281	3.50	64.5	0.290	0.557	0.497	27.65	0.515

TEST NUMBER 3

SURFACE: C/2/Plain TEST BED: Mk 2 POSITION: 54.0 mm between tube ℄ and distributor plate
BED MATERIAL: Zircon sand, size range 63 - 210 μm; static height 62 mm

OBSERVED RESULTS

READING NUMBER	BED			WATER				GAS	AIR			AMBIENT	
	T_{16} °C	T_{17} °C	T_{18} °C	T_{wi} °C	T_{wo} °C	ROT. READ	H_w mm H_2O	ROT. READ	H_a mm H_2O	T_a °C	P_a mm Hg	P_{at} mm Hg	T_{at} °C
P11	274	278	275	10.7	24.0	8.2	147	13.0	19.0	48	78	781	25.5
P12	283	287	282	10.4	24.2	8.2	142	11.7	24.9	49	78	781	26.0
P13	287	291	286	10.0	24.3	8.3	141	11.2	30.1	50	78	781	27.0
P14	290	294	289	9.9	24.4	8.3	137	10.5	35.3	50	78	781	27.0
P15	288	292	287	9.8	24.4	8.3	138	9.8	39.7	51	78	781	27.0
P16	290	294	289	9.8	24.2	8.3	137	9.8	45.2	51	78	781	27.0
P17	286	290	285	9.7	23.7	8.3	133	9.8	48.4	51	78	781	27.0
P18	269	273	268	9.6	21.6	8.3	133	15.6	14.3	48	78	781	25.5
P19	258	262	257	9.5	20.9	8.3	132	14.2	9.9	47	78	781	25.5

CALCULATED RESULTS

READING NUMBER	$\dot{m}$ kg/s	$\dot{M}$ kg/s	T_w °C	T_b °C	Q kW	$\dot{V}_a$ m^3/s x10^3	$\dot{V}_g$ m^3/s x10^3	u_f m/s	U kW/m^2K	h_i kW/m^2K	h_o kW/m^2K
P11	0.050	0.618	23.6	275	2.39	5.44	0.142	0.335	0.657	15.60	0.690
P12	0.050	0.608	23.8	284	2.49	6.22	0.132	0.389	0.662	15.43	0.696
P13	0.051	0.605	23.8	288	2.63	6.82	0.127	0.430	0.688	15.41	0.724
P14	0.051	0.596	23.9	291	2.67	7.39	0.122	0.468	0.691	15.27	0.728
P15	0.051	0.599	23.9	289	2.69	7.82	0.117	0.494	0.702	15.31	0.740
P16	0.051	0.596	23.7	291	2.65	8.35	0.117	0.529	0.685	15.23	0.722
P17	0.051	0.588	23.2	287	2.57	8.64	0.117	0.544	0.672	14.99	0.708
P18	0.051	0.588	21.2	270	2.14	4.72	0.163	0.288	0.596	14.66	0.624
P19	0.051	0.585	20.5	259	2.02	3.93	0.151	0.235	0.585	14.51	0.613

TEST NUMBER 4

SURFACE: C/3/Plain TEST BED: Mk 3 POSITION: 13.0 mm between tube ℄ and distributor plate
BED MATERIAL: Zircon sand, size range 63 - 210 μm; static height 26 mm

OBSERVED RESULTS

READING NUMBER	BED			WATER				GAS	AIR			AMBIENT	
	T_{16} °C	T_{17} °C	T_{18} °C	T_{wi} °C	T_{wo} °C	ROT. READ	H_w mm H_2O	ROT. READ	H_a mm H_2O	T_a °C	P_a mm Hg	P_{at} mm Hg	T_{at} °C
P20	206	200	207	21.0	27.8	5.7	30	9.1	5.9	40	76	762	22.5
P21	240	236	242	15.9	25.1	5.7	29	9.5	8.9	44	76	762	23.0
P22	268	269	262	13.6	24.0	5.7	29	9.5	12.0	46	76	762	24.0
P23	286	288	282	12.9	24.0	5.7	29	9.5	15.1	47	76	762	25.0
P24	300	300	294	12.4	24.0	5.7	28	9.5	18.1	48	76	762	25.0
P25	314	314	308	12.0	24.1	5.7	28	9.5	24.6	48	76	762	25.0
P26	326	326	322	11.8	24.8	5.7	28	9.5	35.1	49	76	762	25.0
P27	336	336	332	11.7	25.2	5.6	28	9.5	49.5	50	76	761	25.0
P28	328	328	324	11.8	26.0	5.5	28	9.5	76.0	52	76	759	25.0

CALCULATED RESULTS

READING NUMBER	$\dot{m}$ kg/s	$\dot{M}$ kg/s	T_w °C	T_b °C	Q kW	$\dot{V}_a$ m^3/s x10^3	$\dot{V}_g$ m^3/s x10^3	u_f m/s	U kW/m^2K	h_i kW/m^2K	h_o kW/m^2K
P20	0.040	0.279	27.5	204	0.75	3.03	0.110	0.130	0.441	20.82	0.453
P21	0.040	0.275	24.7	239	1.15	3.70	0.114	0.171	0.559	19.98	0.578
P22	0.040	0.275	23.5	266	1.35	4.28	0.114	0.208	0.580	19.73	0.602
P23	0.040	0.275	23.4	285	1.47	4.80	0.114	0.241	0.585	19.72	0.607
P24	0.040	0.270	23.4	298	1.55	5.25	0.114	0.270	0.589	19.47	0.611
P25	0.040	0.270	23.5	312	1.63	6.12	0.114	0.322	0.591	19.48	0.613
P26	0.040	0.270	24.1	325	1.78	7.29	0.114	0.393	0.619	19.62	0.643
P27	0.039	0.270	24.5	335	1.81	8.64	0.114	0.474	0.609	19.65	0.632
P28	0.039	0.270	25.3	327	1.92	10.66	0.114	0.577	0.666	19.81	0.694

TEST NUMBER 5

SURFACE: C/4/Plain TEST BED: Mk 3 POSITION: 15.5 mm between tube ℄ and distributor plate
BED MATERIAL: Zircon sand, size range 63 - 210 μm; static height 31 mm

OBSERVED RESULTS

READING NUMBER	BED			WATER				GAS	AIR			AMBIENT	
	T_{16} °C	T_{17} °C	T_{18} °C	T_{wi} °C	T_{wo} °C	ROT. READ	H_w mm H_2O	ROT. READ	H_a mm H_2O	T_a °C	P_a mm Hg	P_{at} mm Hg	T_{at} °C
P29	192	188	196	10.4	17.3	10.8	85	9.0	5.5	46	75	763	27.0
P30	218	214	220	9.7	17.4	10.9	85	9.0	9.0	47	75	763	25.0
P31	236	232	238	9.3	18.7	9.0	86	8.9	12.0	47	76	763	25.0
P32	248	244	250	9.1	19.2	8.9	87	8.9	14.8	47	76	763	24.5
P33	262	256	264	9.0	19.9	8.7	86	8.9	18.0	47	76	763	24.0
P34	276	272	278	9.0	20.3	8.6	87	8.9	25.1	48	76	763	24.0
P35	288	284	290	9.0	20.8	8.7	87	8.9	34.9	49	76	763	24.0
P36	300	298	294	9.0	21.0	8.6	87	8.9	49.9	50	76	763	24.0
P37	304	300	300	9.0	20.5	8.6	88	8.9	74.0	51	77	763	24.0
P38	310	306	310	9.1	20.6	8.5	88	9.5	99.0	51	77	763	24.0

CALCULATED RESULTS

READING NUMBER	$\dot{m}$ kg/s	$\dot{M}$ kg/s	T_w °C	T_b °C	Q kW	$\dot{V}_a$ $m^3/s \times 10^3$	$\dot{V}_g$ $m^3/s \times 10^3$	u_f m/s	U kW/m^2K	h_i kW/m^2K	h_o kW/m^2K
P29	0.061	0.470	17.0	192	1.37	2.90	0.110	0.122	0.545	12.22	0.574
P30	0.062	0.470	17.0	217	1.61	3.70	0.110	0.164	0.559	12.24	0.590
P31	0.054	0.473	18.3	235	1.73	4.28	0.109	0.196	0.557	12.33	0.586
P32	0.053	0.476	18.8	247	1.85	4.75	0.109	0.223	0.564	12.43	0.594
P33	0.052	0.473	19.5	261	1.98	5.24	0.109	0.252	0.571	12.45	0.602
P34	0.052	0.476	19.8	275	2.07	6.18	0.109	0.305	0.564	12.56	0.594
P35	0.052	0.476	20.3	287	2.18	7.28	0.109	0.367	0.568	12.63	0.598
P36	0.052	0.476	20.5	298	2.22	8.69	0.109	0.447	0.557	12.65	0.586
P37	0.052	0.478	20.0	301	2.11	10.57	0.109	0.547	0.523	12.64	0.548
P38	0.051	0.478	20.1	309	2.06	12.23	0.113	0.641	0.497	12.64	0.520

TEST NUMBER 6

SURFACE: C/4/Plain TEST BED: Mk 3 POSITION: 15.5 mm between tube ℄ and distributor plate
BED MATERIAL: Steel shot, size range 75 - 500 μm; static height 31 mm

OBSERVED RESULTS

READING NUMBER	BED			WATER				GAS	AIR			AMBIENT	
	T_{16} °C	T_{17} °C	T_{18} °C	T_{wi} °C	T_{wo} °C	ROT. READ	H_w mm H_2O	ROT. READ	H_a mm H_2O	T_a °C	P_a mm Hg	P_{at} mm Hg	T_{at} °C
P39	286	-	288	11.1	19.3	9.0	85	8.9	15.0	44	76	762	23.0
P40	294	-	294	10.4	19.2	9.0	85	9.2	17.9	46	76	762	23.0
P41	304	-	302	10.1	19.8	9.0	85	9.2	25.2	47	76	762	23.5
P42	312	-	310	9.9	20.1	9.0	85	9.2	33.7	48	76	762	23.5
P43	318	312	316	9.8	20.6	9.0	85	9.1	49.9	49	76	762	24.0
P44	318	314	318	9.7	21.0	9.0	85	9.1	75.0	50	76	762	24.0
P45	318	316	318	9.7	21.8	9.0	85	10.0	98.4	51	76	762	24.0
P46	320	318	320	9.6	22.0	9.0	85	11.0	150.0	51	76	762	24.0
P47	322	320	322	9.6	22.0	8.8	85	12.0	202.0	51	76	762	24.0
P48	316	312	316	9.6	22.1	8.7	86	13.0	310.0	50	76	762	24.0
P49	316	312	316	9.6	22.0	8.7	86	14.4	399.0	50	76	762	24.0
P50	314	314	312	9.6	22.0	8.7	86	15.4	498.0	50	76	762	24.0

CALCULATED RESULTS

READING NUMBER	$\dot{m}$ kg/s	$\dot{M}$ kg/s	T_w °C	T_b °C	Q kW	$\dot{V}_a$ $m^3/s \times 10^3$	$\dot{V}_g$ $m^3/s \times 10^3$	u_f m/s	U kW/m^2K	h_i kW/m^2K	h_o kW/m^2K
P39	0.053	0.470	19.0	287	1.43	4.81	0.109	0.243	0.371	12.35	0.384
P40	0.053	0.470	18.8	294	1.56	5.23	0.111	0.267	0.395	12.33	0.409
P41	0.053	0.470	19.4	303	1.76	6.20	0.111	0.322	0.432	12.41	0.449
P42	0.053	0.470	19.7	311	1.87	7.16	0.111	0.377	0.447	12.45	0.466
P43	0.053	0.470	20.1	317	2.00	8.70	0.110	0.462	0.470	12.52	0.490
P44	0.053	0.470	20.5	318	2.12	10.65	0.110	0.567	0.495	12.57	0.518
P45	0.053	0.470	21.3	318	2.29	12.18	0.118	0.648	0.537	12.68	0.564
P46	0.053	0.470	21.5	319	2.36	15.05	0.125	0.802	0.551	12.70	0.580
P47	0.053	0.470	21.5	321	2.36	17.44	0.133	0.934	0.548	12.70	0.576
P48	0.052	0.473	21.6	315	2.33	21.64	0.141	1.147	0.552	12.75	0.580
P49	0.052	0.473	21.5	313	2.31	24.55	0.153	1.297	0.550	12.74	0.579
P50	0.052	0.473	21.5	313	2.31	27.43	0.161	1.449	0.550	12.74	0.579

TEST NUMBER 7

SURFACE: C/4/Plain TEST BED: Mk 3 POSITION: 15.5 mm between tube ℄ and distributor plate
BED MATERIAL: Silica sand, size range 90 - 355 μm; static height 31 mm

OBSERVED RESULTS

READING NUMBER	BED			WATER				GAS	AIR			AMBIENT	
	T_{16} °C	T_{17} °C	T_{18} °C	T_{wi} °C	T_{wo} °C	ROT. READ	H_w mm H_2O	ROT. READ	H_a mm H_2O	T_a °C	P_a mm Hg	P_{at} mm Hg	T_{at} °C
P51	230	226	232	10.2	17.6	8.0	92	9.0	5.8	42	76	771	23.5
P52	256	252	257	10.0	18.3	7.9	92	9.0	9.0	44	76	771	24.0
P53	282	276	284	10.2	19.4	7.7	92	9.0	12.1	46	76	771	24.0
P54	298	294	298	10.4	20.0	7.6	93	8.9	15.0	47	76	771	24.5
P55	312	306	311	10.5	20.6	7.5	93	8.9	18.1	48	77	771	24.5
P56	324	320	325	10.5	20.7	7.5	95	8.9	24.7	48	77	771	25.0
P57	338	332	336	10.5	21.0	7.5	95	9.1	35.2	49	77	771	25.0
P58	340	344	344	10.5	21.0	7.5	94	9.0	49.5	49	77	771	24.5
P59	346	340	346	10.6	20.5	7.5	94	9.0	70.2	49	77	771	24.5

CALCULATED RESULTS

READING NUMBER	$\dot{m}$ kg/s	$\dot{M}$ kg/s	T_w °C	T_b °C	Q kW	$\dot{V}_a$ m^3/s x10^3	$\dot{V}_g$ m^3/s x10^3	u_f m/s	U kW/m^2K	h_i kW/m^2K	h_o kW/m^2K
P51	0.049	0.489	17.4	229	1.13	3.01	0.110	0.136	0.370	12.40	0.383
P52	0.049	0.489	18.0	255	1.31	3.74	0.110	0.178	0.385	12.49	0.399
P53	0.048	0.489	19.1	281	1.46	4.33	0.110	0.216	0.387	12.63	0.401
P54	0.048	0.492	19.7	297	1.54	4.81	0.109	0.247	0.386	12.76	0.399
P55	0.047	0.492	20.3	310	1.60	5.28	0.109	0.277	0.383	12.83	0.396
P56	0.047	0.497	20.4	323	1.62	6.16	0.109	0.331	0.371	12.95	0.384
P57	0.047	0.497	20.6	335	1.67	7.35	0.111	0.403	0.370	12.99	0.383
P58	0.047	0.495	20.6	343	1.67	8.71	0.110	0.484	0.361	12.94	0.373
P59	0.047	0.495	20.2	344	1.56	10.38	0.110	0.577	0.334	12.87	0.344

TEST NUMBER 8

SURFACE: AB/1/Oval TEST BED: Mk 3 POSITION: 39.0 mm between tube minor axis ℄ and distributor plate
BED MATERIAL: Zircon sand, size range 63 - 210 μm; static height 53 mm

OBSERVED RESULTS

READING NUMBER	BED			WATER				GAS	AIR			AMBIENT	
	T_{16} °C	T_{17} °C	T_{18} °C	T_{wi} °C	T_{wo} °C	ROT. READ	H_w mm H_2O	ROT. READ	H_a mm H_2O	T_a °C	P_a mm Hg	P_{at} mm Hg	T_{at} °C
Ø01	186	186	184	19.9	28.6	8.2	86	8.7	6.9	43	77	775	25.0
Ø02	199	200	202	20.3	30.0	8.2	87	10.0	9.0	44	77	775	25.0
Ø03	220	218	217	20.6	31.9	8.2	88	10.9	12.0	45	77	775	26.0
Ø04	234	233	231	21.1	33.7	8.3	88	11.4	15.0	46	77	775	26.0
Ø05	235	234	230	21.6	36.1	8.4	88	12.2	18.2	47	77	775	26.5
Ø06	268	266	260	22.8	41.3	8.7	90	14.5	35.6	49	77	775	27.0
Ø07	285	282	276	23.1	42.8	8.9	90	14.6	49.5	50	77	775	27.0
Ø08	296	294	288	23.4	43.8	9.0	90	14.5	71.0	50	77	775	27.0
Ø09	306	305	300	23.8	43.0	9.0	90	14.0	93.2	51	77	775	27.0

CALCULATED RESULTS

READING NUMBER	$\dot{m}$ kg/s	$\dot{M}$ kg/s	T_w °C	T_b °C	Q kW	$\dot{V}_a$ m^3/s x10^3	$\dot{V}_g$ m^3/s x10^3	u_f m/s	U kW/m^2K	h_i kW/m^2K	h_o kW/m^2K
Ø01	0.050	0.473	28.3	185	1.43	3.29	0.108	0.136	0.457	15.19	0.476
Ø02	0.050	0.476	29.6	200	1.64	3.75	0.118	0.160	0.482	15.46	0.503
Ø03	0.050	0.478	31.5	218	1.97	4.33	0.125	0.192	0.530	15.80	0.555
Ø04	0.051	0.478	33.2	233	2.30	4.83	0.128	0.220	0.576	16.09	0.606
Ø05	0.051	0.478	35.5	233	2.70	5.31	0.135	0.242	0.686	16.44	0.727
Ø06	0.052	0.484	40.5	265	3.63	7.41	0.154	0.359	0.812	17.37	0.868
Ø07	0.053	0.484	41.9	281	3.97	8.72	0.155	0.435	0.834	17.61	0.893
Ø08	0.054	0.484	42.9	293	4.21	10.44	0.154	0.533	0.846	17.78	0.906
Ø09	0.054	0.484	42.1	304	3.94	11.95	0.150	0.621	0.756	17.67	0.804

TEST NUMBER 6

SURFACE: AB/1/Oval TEST BED: Mk 3 POSITION: 34.0 mm between tube major axis ℄ and distributor plate

BED MATERIAL: Zircon sand, size range 63 - 210 μm; static height 50 mm

OBSERVED RESULTS

READING NUMBER	BED			WATER				GAS	AIR			AMBIENT	
	T_{16} °C	T_{17} °C	T_{18} °C	T_{wi} °C	T_{wo} °C	ROT. READ	H_w mm H_2O	ROT. READ	H_a mm H_2O	T_a °C	P_a mm Hg	P_{at} mm Hg	T_{at} °C
Ø10	187	188	189	12.3	19.3	9.0	90	8.8	5.9	40	78	777	23.0
Ø11	212	215	213	11.0	19.2	9.0	90	9.3	8.8	43	78	777	23.0
Ø12	241	244	241	10.8	20.0	9.0	90	9.6	15.0	45	78	777	23.0
Ø13	271	275	270	10.6	21.2	9.0	90	9.6	25.3	47	78	777	23.0
Ø14	295	298	293	10.5	22.0	9.0	90	9.6	49.3	49	78	777	23.0
Ø15	299	302	297	10.5	23.0	9.0	90	9.6	76.0	50	78	777	24.0
Ø16	303	306	301	10.5	23.0	9.0	90	9.6	101.0	51	78	777	24.0

CALCULATED RESULTS

READING NUMBER	$\dot{m}$ kg/s	$\dot{M}$ kg/s	T_w °C	T_b °C	Q kW	$\dot{V}_a$ m^3/s x10^3	$\dot{V}_g$ m^3/s x10^3	u_f m/s	U kW/m^2K	h_i kW/m^2K	h_o kW/m^2K
Ø10	0.054	0.484	19.0	188	1.19	3.06	0.108	0.127	0.353	14.06	0.366
Ø11	0.054	0.484	18.9	214	1.46	3.72	0.112	0.163	0.376	14.04	0.390
Ø12	0.054	0.484	19.6	242	1.69	4.85	0.114	0.225	0.381	14.16	0.395
Ø13	0.054	0.484	20.8	272	2.00	6.27	0.114	0.308	0.400	14.34	0.415
Ø14	0.054	0.484	21.5	295	2.21	8.73	0.114	0.447	0.405	14.46	0.420
Ø15	0.054	0.484	22.5	299	2.43	10.82	0.114	0.558	0.441	14.61	0.460
Ø16	0.054	0.484	22.5	303	2.43	12.45	0.114	0.646	0.435	14.61	0.453

Square Fin Tube Results

Tests 10 - 17

C/1/MS

VIEW IN DIRECTION OF WATER ENTRY AND EXIT PIPE CONNECTIONS

CENTRAL FIN 24

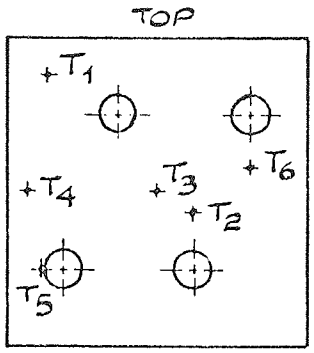

C/2/MS

VIEW IN DIRECTION OF WATER ENTRY AND EXIT PIPE CONNECTIONS

WATER ENTRY AND EXIT AT FIN 1

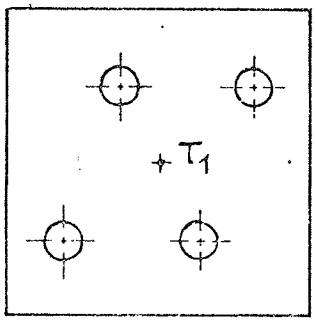

CENTRAL FIN 15

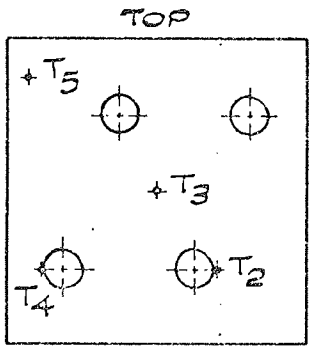

END FIN 31

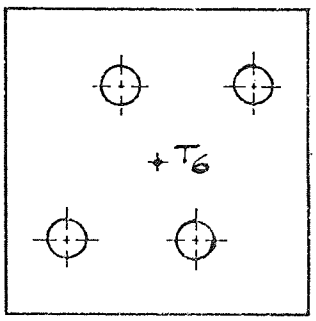

C/3/MS

WATER EXIT AT FIN 1

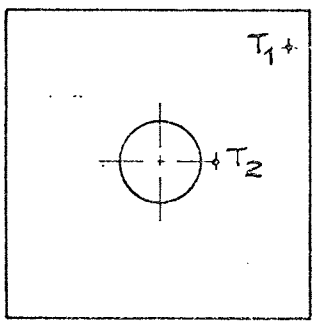

CENTRAL FIN 24

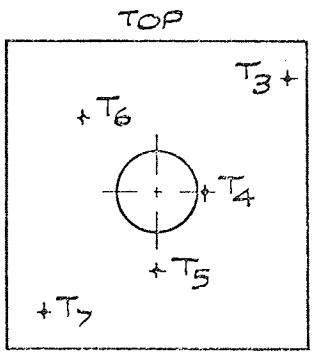

WATER ENTRY AT FIN 47

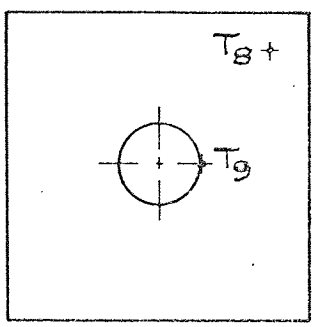

SCALE : 3/4 ACTUAL SIZE

Figure A3.1 Location of Thermocouples in Square Fin Extended Surface

SURFACE: C/1/MS TEST BED: Mk 1 POSITION: Placed directly on distributor plate

BED MATERIAL: Zircon sand, size range 63 - 210 μm; static height 75 mm

OBSERVED RESULTS

READING NUMBER	BED			FIN METAL TEMPERATURES						WATER			GAS	AIR			AMBIENT	
	T_{16} °C	T_{17} °C	T_{18} °C	T_1 °C	T_2 °C	T_3 °C	T_4 °C	T_5 °C	T_6 °C	T_{wi} °C	T_{wo} °C	ROT. READ	ROT. READ	H_a mmH_2O	T_a °C	P_a mm Hg	P_{at} mm Hg	T_{at} °C
S001	138	129	133	81	82	72	-	64	63	19.0	31.5	31.9	20.2	48	49	79	767	23.0
S002	146	136	142	85	84	77	-	69	68	19.0	33.5	32.0	21.3	100	49	79	767	23.0
S003	151	141	146	91	91	80	-	72	71	18.5	35.0	32.0	24.1	150	48	79	767	23.5
S004	160	150	155	97	96	87	-	78	78	18.5	36.3	32.0	26.5	201	47	79	767	23.5
S005	167	158	163	102	101	90	-	82	82	18.5	37.5	32.0	28.8	250	47	79	767	24.0
S006	172	163	167	103	103	91	-	83	83	18.5	38.3	32.0	30.0	300	46	78	767	24.0
S007	177	170	173	105	105	93	-	85	86	18.5	39.0	32.0	31.3	351	46	78	767	24.0
S008	178	170	173	106	105	93	-	85	84	18.5	39.0	32.0	31.3	400	46	77	767	24.5
S009	178	170	174	103	103	92	-	82	85	18.5	38.8	32.0	31.3	501	45	76	767	25.0
S010	138	133	135	82	82	73	-	67	68	18.5	32.0	31.9	20.9	74	49	79	767	23.5
S011	129	124	126	75	73	68	-	60	60	18.5	29.5	31.8	18.7	30	49	79	767	23.5

CALCULATED RESULTS

READING NUMBER	$\dot{m}$ kg/s	T_w °C	T_b °C	T_m °C	Q kW	$\dot{V}_a$ m^3/s x10^3	$\dot{V}_g$ m^3/s x10^3	u_f m/s	U kW/m^2K	h_m kW/m^2K
S001	0.158	25.3	133	72	8.26	19.98	0.202	0.126	2.538	0.492
S002	0.160	26.3	141	77	9.70	28.83	0.210	0.186	2.800	0.551
S003	0.160	26.8	146	81	11.04	35.37	0.235	0.231	3.065	0.617
S004	0.160	27.4	155	87	11.90	41.01	0.257	0.273	3.089	0.636
S005	0.160	28.0	163	91	12.71	45.73	0.278	0.311	3.117	0.641
S006	0.160	28.4	167	93	13.24	50.15	0.288	0.344	3.164	0.650
S007	0.160	28.8	173	95	13.71	54.24	0.300	0.377	3.148	0.639
S008	0.160	28.8	174	95	13.71	57.87	0.300	0.403	3.127	0.631
S009	0.160	28.6	174	93	13.58	64.83	0.300	0.452	3.092	0.609
S010	0.158	25.3	135	74	8.92	24.80	0.207	0.158	2.691	0.531
S011	0.156	24.0	126	67	7.17	15.79	0.190	0.098	2.329	0.442

SURFACE: C/1/MS TEST BED: Mk 1 POSITION: Lower fin edge 25 mm above distributor plate

BED MATERIAL: Zircon sand, size range 63 - 210 μm; static height 75 mm

OBSERVED RESULTS

READING NUMBER	BED			FIN METAL TEMPERATURES						WATER			GAS	AIR			AMBIENT	
	T_{16} °C	T_{17} °C	T_{18} °C	T_1 °C	T_2 °C	T_3 °C	T_4 °C	T_5 °C	T_6 °C	T_{wi} °C	T_{wo} °C	ROT. READ	ROT. READ	H_a mmH_2O	T_a °C	P_a mm Hg	P_{at} mm Hg	T_{at} °C
S012	144	140	138	82	72	76	-	69	69	19.0	32.8	31.9	21.3	100	48	79	755	23.0
S013	151	145	147	88	76	78	-	72	71	19.0	34.4	32.0	24.3	150	48	78	755	23.0
S014	159	154	155	92	80	82	-	76	76	19.0	35.6	32.0	26.5	200	48	78	755	23.5
S015	168	160	164	98	86	86	-	80	80	19.0	37.2	32.0	28.7	251	47	78	755	23.5
S016	172	167	168	101	88	88	-	83	83	19.0	38.0	32.0	30.0	301	47	78	755	24.0
S017	179	170	174	105	90	90	-	84	84	19.0	38.7	32.0	31.2	350	47	76	755	24.0
S018	179	170	174	105	90	90	-	85	85	19.0	38.9	32.0	31.2	401	47	75	755	24.5
S019	176	169	169	101	87	88	-	83	85	19.0	38.8	32.0	31.2	502	46	74	755	25.0
S020	139	135	136	78	70	71	-	65	63	19.0	31.8	31.9	20.9	74	49	78	755	24.0
S021	132	128	128	70	58	62	-	56	54	19.0	29.0	31.7	18.8	30	49	78	755	23.5

CALCULATED RESULTS

READING NUMBER	$\dot{m}$ kg/s	T_w °C	T_b °C	T_m °C	Q kW	$\dot{V}_a$ m^3/s x10^3	$\dot{V}_g$ m^3/s x10^3	u_f m/s	U kW/m^2K	h_m kW/m^2K
S012	0.160	25.9	141	74	9.23	28.67	0.210	0.185	2.655	0.501
S013	0.160	26.7	148	77	10.30	35.10	0.238	0.230	2.812	0.527
S014	0.160	27.3	156	81	11.10	40.53	0.257	0.271	2.856	0.538
S015	0.160	28.1	164	86	12.17	45.47	0.276	0.310	2.966	0.567
S016	0.160	28.5	169	89	12.71	49.80	0.288	0.343	2.995	0.577
S017	0.160	28.9	174	91	13.18	53.63	0.300	0.374	3.007	0.577
S018	0.160	29.0	174	91	13.31	57.37	0.300	0.400	3.039	0.583
S019	0.160	28.9	171	89	13.24	64.25	0.300	0.445	3.086	0.587
S020	0.160	25.4	137	69	8.56	24.61	0.207	0.157	2.540	0.457
S021	0.159	24.0	129	60	6.65	15.67	0.190	0.098	2.096	0.350

SURFACE: C/1/MS TEST BED: Mk 1 POSITION: Lower fin edge 13 mm above distributor plate

BED MATERIAL: Zircon sand, size range 63 - 210 μm; static height 75 mm

OBSERVED RESULTS

READING NUMBER	BED			FIN METAL TEMPERATURES						WATER			GAS	AIR			AMBIENT	
	T_{16} °C	T_{17} °C	T_{18} °C	T_1 °C	T_2 °C	T_3 °C	T_4 °C	T_5 °C	T_6 °C	T_{wi} °C	T_{wo} °C	ROT. READ	ROT. READ	H_a mm H_2O	T_a °C	P_a mm Hg	P_{at} mm Hg	T_{at} °C
S022	133	128	126	71	68	66	-	61	63	18.5	30.4	31.9	20.5	50	49	79	763	23.0
S023	143	138	138	80	74	73	-	69	71	18.5	32.8	31.9	21.3	100	48	78	763	23.0
S024	155	147	146	88	80	80	-	72	74	18.4	34.2	31.9	24.3	150	47	78	763	23.5
S025	158	152	154	90	82	82	-	76	78	18.4	36.0	31.9	26.5	201	47	78	763	23.5
S026	166	160	160	97	86	87	-	80	81	18.4	37.2	32.0	28.8	250	46	78	763	24.0
S027	170	164	163	98	85	87	-	80	84	18.4	37.8	32.0	30.0	300	45	77	763	24.0
S028	175	170	170	102	90	90	-	83	86	18.4	38.8	32.0	31.2	350	45	76	763	24.5
S029	175	170	170	102	88	90	-	84	86	18.4	38.8	32.0	31.2	400	44	76	763	25.0
S030	172	167	167	100	88	90	-	82	86	18.3	38.6	32.0	31.2	505	43	75	763	25.0
S031	130	128	125	71	66	64	-	59	60	18.3	28.8	31.9	19.0	29	48	78	763	23.5

CALCULATED RESULTS

READING NUMBER	$\dot{m}$ kg/s	T_w °C	T_b °C	T_m °C	Q kW	$\dot{V}^a$ m^3/s x10^3	$\dot{V}^g$ m^3/s x10^3	u_f m/s	U kW/m^2K	h_{m_2} kW/m^2K	h_{i_2} kW/m^2K	E_f	h_{o_2} kW/m^2K
S022	0.160	24.5	129	66	7.96	20.34	0.203	0.127	2.522	0.459	30.77	0.672	0.440
S023	0.160	25.6	140	73	9.56	28.79	0.210	0.185	2.768	0.519	31.22	0.666	0.492
S024	0.160	26.3	149	79	10.57	35.32	0.238	0.232	2.852	0.549	31.47	0.644	0.524
S025	0.160	27.2	155	82	11.77	40.89	0.257	0.273	3.050	0.586	31.77	0.650	0.560
S026	0.160	27.8	162	86	12.57	45.67	0.277	0.310	3.102	0.601	31.98	0.646	0.573
S027	0.160	28.1	165	87	12.97	50.08	0.288	0.342	3.138	0.604	32.05	0.650	0.578
S028	0.160	28.6	171	90	13.64	54.06	0.300	0.374	3.173	0.612	32.22	0.650	0.584
S029	0.160	28.6	171	90	13.64	57.88	0.300	0.400	3.173	0.612	32.22	0.650	0.584
S030	0.160	28.5	169	89	13.58	65.10	0.300	0.448	3.200	0.617	32.20	0.650	0.590
S031	0.160	23.6	128	64	7.02	15.51	0.191	0.097	2.227	0.399	30.45	0.673	0.383

SURFACE: C/1/MS TEST BED: Mk 1 POSITION: Placed directly on distributor plate

BED MATERIAL: Zircon sand, size range 63 - 210 μm; static height 50 mm

OBSERVED RESULTS

READING NUMBER	BED			FIN METAL TEMPERATURES						WATER			GAS	AIR			AMBIENT	
	T_{16} °C	T_{17} °C	T_{18} °C	T_1 °C	T_2 °C	T_3 °C	T_4 °C	T_5 °C	T_6 °C	T_{wi} °C	T_{wo} °C	ROT. READ	ROT. READ	H_a mm H_2O	T_a °C	P_a mm Hg	P_{at} mm Hg	T_{at} °C
S032	140	134	136	81	67	72	-	63	62	18.0	29.6	31.9	20.0	49	48	79	769	23.0
S033	148	142	148	85	73	73	-	69	68	17.5	31.8	31.9	21.5	101	48	78	769	23.0
S034	152	146	150	87	75	78	-	71	73	17.4	33.2	32.0	23.4	150	48	78	769	23.5
S035	158	150	155	90	80	81	-	75	77	17.4	34.3	32.0	25.3	201	48	78	769	23.5
S036	167	160	165	97	85	86	-	81	79	17.3	35.7	32.0	28.0	248	47	78	769	24.0
S037	173	163	168	99	89	89	-	80	83	17.3	36.6	32.0	29.6	290	46	77	769	24.0
S038	177	170	175	101	90	90	-	82	85	17.3	37.8	32.0	31.2	401	46	76	769	24.5
S039	177	168	173	100	90	89	-	80	86	17.3	37.7	32.0	31.2	502	45	75	769	24.5
S040	145	135	137	78	68	70	-	65	64	17.3	30.0	31.9	20.6	74	49	78	769	23.5

CALCULATED RESULTS

READING NUMBER	$\dot{m}$ kg/s	T_w °C	T_b °C	T_m °C	Q kW	$\dot{V}^a$ m^3/s x10^3	$\dot{V}^g$ m^3/s x10^3	u_f m/s	U kW/m^2K	h_{m_2} kW/m^2K
S032	0.160	23.8	137	69	7.76	20.24	0.200	0.129	2.269	0.415
S033	0.160	24.7	145	74	9.56	29.04	0.212	0.190	2.611	0.483
S034	0.160	25.3	149	77	10.57	35.39	0.229	0.233	2.829	0.533
S035	0.160	25.9	154	81	11.30	40.97	0.245	0.273	2.922	0.563
S036	0.160	26.5	164	86	12.31	45.58	0.270	0.310	2.963	0.573
S037	0.160	27.0	168	88	12.91	49.33	0.285	0.339	3.031	0.586
S038	0.160	27.6	174	90	13.71	57.98	0.300	0.404	3.101	0.593
S039	0.160	27.5	173	89	13.64	64.93	0.300	0.451	3.105	0.590
S040	0.160	23.7	139	69	8.49	24.82	0.205	0.159	2.439	0.441

SURFACE: C/1/MS TEST BED: Mk 1 POSITION: Placed directly on distributor plate

BED MATERIAL: Zircon sand, size range 63 - 210 μm; static height 150 mm

OBSERVED RESULTS

READING NUMBER	BED			FIN METAL TEMPERATURES						WATER			GAS	AIR			AMBIENT	
	T_{16} °C	T_{17} °C	T_{18} °C	T_1 °C	T_2 °C	T_3 °C	T_4 °C	T_5 °C	T_6 °C	T_{wi} °C	T_{wo} °C	ROT. READ	ROT. READ	H_a mmH_2O	T_a °C	P_a mm Hg	P_{at} mm Hg	T_{at} °C
S041	109	108	108	67	53	56	–	55	57	17.2	27.6	31.9	19.9	49	46	79	768	23.0
S042	120	118	119	77	65	67	–	64	65	16.4	29.4	32.0	21.7	100	46	79	768	23.0
S043	130	128	128	83	71	73	–	70	70	16.2	32.0	32.0	23.7	152	46	79	768	23.5
S044	137	134	134	88	76	80	–	73	74	16.2	33.4	32.0	25.5	200	45	78	768	23.5
S045	142	142	142	91	80	83	–	76	77	16.1	34.6	32.0	26.0	250	45	78	768	24.0
S046	150	150	150	97	83	88	–	81	81	16.1	36.0	32.0	30.1	302	44	77	768	24.0
S047	158	153	154	100	86	90	–	83	82	16.1	37.2	32.1	31.2	402	44	76	768	24.5
S048	160	154	154	100	85	90	–	82	83	16.1	37.0	32.1	31.2	498	43	75	768	25.0
S049	128	126	126	78	63	67	–	65	66	16.1	30.6	32.0	20.6	72	46	79	768	23.5
S050	120	120	120	72	57	65	–	88	60	16.1	26.6	31.9	19.0	31	48	79	768	23.0

CALCULATED RESULTS

READING NUMBER	$\dot{m}$ kg/s	T_w °C	T_b °C	T_m °C	Q kW	$\dot{V}^a$ m^3/s x10^3	$\dot{V}^{38}$ m^3/s x10^3	u_f m/s	U kW/m^2K	h_m kW/m^2K
S041	0.160	22.4	108	58	6.96	20.29	0.198	0.120	2.691	0.505
S042	0.160	22.9	118	68	8.69	28.99	0.215	0.177	3.027	0.632
S043	0.160	24.1	128	73	10.57	35.74	0.232	0.223	3.368	0.698
S044	0.160	24.8	135	78	11.50	41.03	0.248	0.261	3.456	0.733
S045	0.160	25.4	142	81	12.37	45.88	0.270	0.297	3.514	0.737
S046	0.160	26.1	150	88	13.31	50.47	0.290	0.333	3.557	0.780
S047	0.160	26.7	155	88	14.11	58.20	0.300	0.388	3.642	0.765
S048	0.160	26.6	156	88	13.98	64.84	0.300	0.433	3.577	0.747
S049	0.160	23.4	127	68	9.70	24.60	0.205	0.153	3.099	0.597
S050	0.160	21.4	120	62	7.02	16.09	0.192	0.099	2.358	0.440

SURFACE: C/1/MS TEST BED: Mk 1 POSITION: Lower fin edge 25 mm above distributor plate

BED MATERIAL: Zircon sand, size range 63 - 210 μm; static height 150 mm

OBSERVED RESULTS

READING NUMBER	BED			FIN METAL TEMPERATURES						WATER			GAS	AIR			AMBIENT	
	T_{16} °C	T_{17} °C	T_{18} °C	T_1 °C	T_2 °C	T_3 °C	T_4 °C	T_5 °C	T_6 °C	T_{wi} °C	T_{wo} °C	ROT. READ	ROT. READ	H_a mmH_2O	T_a °C	P_a mm Hg	P_{at} mm Hg	T_{at} °C
S051	130	130	130	79	69	74	–	63	63	16.5	27.4	31.9	20.2	49	39	79	774	23.0
S052	142	139	141	84	71	75	–	69	69	16.4	30.0	32.0	22.1	101	39	79	774	23.0
S053	143	140	141	87	75	75	–	69	71	16.4	32.4	32.0	24.0	151	38	78	774	23.5
S054	153	151	152	93	81	82	–	79	79	16.4	34.7	32.0	28.1	250	37	77	774	24.0
S055	163	158	159	100	87	90	–	82	83	16.4	36.5	32.1	31.2	492	35	75	774	25.0
S056	132	130	131	80	69	73	–	66	65	16.3	30.0	32.0	21.0	73	38	79	774	23.5
S057	125	122	122	76	66	72	–	63	62	16.3	27.1	31.9	19.0	30	39	79	774	23.0

CALCULATED RESULTS

READING NUMBER	$\dot{m}$ kg/s	T_w °C	T_b °C	T_m °C	Q kW	$\dot{V}^a$ m^3/s x10^3	$\dot{V}^{38}$ m^3/s x10^3	u_f m/s	U kW/m^2K	h_m kW/m^2K
S051	0.160	22.0	130	70	7.29	20.59	0.202	0.129	2.235	0.441
S052	0.160	23.2	141	74	9.10	29.56	0.217	0.191	2.557	0.493
S053	0.160	24.4	142	75	10.70	36.18	0.234	0.234	3.013	0.580
S054	0.160	25.6	152	83	12.24	46.60	0.270	0.309	3.206	0.645
S055	0.160	26.5	160	88	13.44	65.51	0.300	0.442	3.334	0.678
S056	0.160	23.2	131	71	9.16	25.17	0.208	0.158	2.814	0.555
S057	0.160	21.7	123	68	7.22	16.11	0.192	0.099	2.361	0.477

SURFACE: C/2/MS TEST BED: Mk 1 POSITION: Lower fin edge 13 mm above distributor plate

BED MATERIAL: Zircon sand, size range 63 – 210 μm; static height 75 mm

OBSERVED RESULTS

READING NUMBER	BED			FIN METAL TEMPERATURES						WATER			GAS	AIR			AMBIENT	
	T_{16} °C	T_{17} °C	T_{18} °C	T_1 °C	T_2 °C	T_3 °C	T_4 °C	T_5 °C	T_6 °C	T_{wi} °C	T_{wo} °C	ROT. READ	ROT. READ	H_a mmH_2O	T_a °C	P_a mm Hg	P_{at} mm Hg	T_{at} °C
S058	131	131	133	–	48	55	48	74	69	19.5	30.5	32.0	19.6	50	46	79	768	23.0
S059	147	147	145	–	60	67	58	68	76	19.5	33.0	32.0	21.0	101	46	79	768	23.0
S060	158	157	155	–	72	79	65	100	84	19.5	34.5	32.0	24.5	151	46	79	768	23.5
S061	163	163	163	–	76	83	70	107	90	19.5	35.5	32.0	26.4	201	45	78	768	23.5
S062	173	171	172	–	82	91	74	112	94	19.5	37.0	32.0	28.8	250	45	78	768	24.0
S063	177	177	177	–	89	95	77	117	98	19.5	37.5	32.0	30.0	300	44	77	768	24.0
S064	182	182	182	–	92	98	80	122	100	19.5	38.0	32.0	31.3	350	44	76	768	24.5
S065	180	180	180	–	92	97	78	122	98	19.5	38.0	32.0	31.2	501	43	75	768	25.0

CALCULATED RESULTS

READING NUMBER	$\dot{m}$ kg/s	T_w °C	T_b °C	T_m °C	Q kW	$\dot{V}_a$ m^3/s x10^3	$\dot{V}_g$ m^3/s x10^3	u_f m/s	U kW/m^2K	h_m kW/m^2K	h_i kW/m^2K	E_f	h_o kW/m^2K
S058	0.160	25.0	132	59	7.36	20.50	0.196	0.129	2.780	0.551	29.94	0.769	0.533
S059	0.160	26.3	146	70	9.03	29.13	0.208	0.190	3.050	0.649	30.41	0.723	0.622
S060	0.160	27.0	157	80	10.03	35.62	0.238	0.239	3.120	0.712	30.67	0.676	0.675
S061	0.160	27.5	163	85	10.70	41.14	0.256	0.279	3.193	0.750	30.81	0.659	0.708
S062	0.160	28.3	172	91	11.70	45.88	0.277	0.318	3.293	0.790	31.06	0.647	0.744
S063	0.160	28.5	177	95	12.04	50.31	0.288	0.353	3.278	0.802	31.11	0.633	0.753
S064	0.160	28.8	182	98	12.37	54.30	0.300	0.385	3.266	0.805	31.18	0.628	0.754
S065	0.160	28.8	180	97	12.37	65.04	0.300	0.459	3.309	0.815	31.18	0.630	0.764

TEST NUMBER 16

NUMERICAL ANALYSIS OF RESULTS FOR C/3/MS SURFACE - TEST NUMBER 17

Master Computer Programme Listing - Fortran II

```
100C    NUMERICAL METHOD TO DETERMINE TEMPERATURE DISTRIBUTION AND
105C    EFFICIENCY OF A HEAT EXCHANGER USING SQUARE FINS ON
110C    ROUND TUBES.
115     DIMENSION T(11,11),M(11,11)
120     READ,TIN,HO,A,XT,TKM,TB
125     DO=6.0*A
130     W=20.0*A
135     PRINT 10,TIN,HO,A,XT,TKM,TB,DO,W
140 10  FORMAT(8F9.4)
145     DO 24 J=3,4
150     DO 24 I=1,3
155 24  M(J,I)=1
160     DO 25 J=1,2
165     DO 25 I=1,4
170 25  M(J,I)=1
175     DO 26 J=5,10
180     DO 26 I=2,10
185 26  M(J,I)=2
190     DO 27 J=2,4
195     DO 27 I=5,10
200 27  M(J,I)=2
205     DO 28 J=3,4
210 28  M(J,4)=2
215     DO 19 J=5,10
220 19  M(J,1)=3
225     DO 21 I=5,10
230 21  M(1,I)=4
235     M(11,1)=5
240     M(1,11)=6
245     DO 22 I=2,10
250 22  M(11,I)=7
255     DO 23 J=2,10
260 23  M(J,11)=8
265     M(11,11)=9
270     AB=HO*A/(TKM*10↑3)
275     AC=2.0*AB*A/XT
280     AD=4.0+AC
285     AE=AB*(A/XT+1.0)
290     AF=2.0+AE
295     AG=AB*(A/XT+2.0)
300     AH=2.0+AG
305     DO 20 J= 1,11
310     DO 20 I= 1,11
315 20  T(J,I)=100.0
320     ITER=0
325 30  L=0
330     DO 60 J= 1,11
335     DO 60 I= 1,11
340     K=M(J,I)
345     GO TO (1,2,3,4,5,6,7,8,9),K
350   1 X=TIN
355     GO TO 40
360   2 X=(T(J,I+1)+T(J+1,I)+T(J,I-1)+T(J-1,I)+AC*TB)/AD
365     GO TO 40
370   3 X=(2.0*T(J,I+1)+T(J+1,I)+T(J-1,I)+AC*TB)/AD
375     GO TO 40
```

```
380    4 X=(T(J,I+1)+2.0*T(J+1,I)+T(J,I-1)+AC*TB)/AD
385      GO TO 40
390    5 X=(T(J,I+1)+T(J-1,I)+AE*TB)/AF
395      GO TO 40
400    6 X=(T(J+1,I)+T(J,I-1)+AE*TB)/AF
405      GO TO 40
410    7 X=(0.5*(T(J,I+1)+T(J,I-1))+T(J-1,I)+AE*TB)/AF
415      GO TO 40
420    8 X=(0.5*(T(J+1,I)+T(J-1,I))+T(J,I-1)+AE*TB)/AF
425      GO TO 40
430    9 X=(T(J,I-1)+T(J-1,I)+AG*TB)/AH
435   40 Z=0.0
440      Z=Z+ABS(T(J,I)-X)
445      IF(Z-0.0005)50,50,60
450   50 L=L+1
455   60 T(J,I)=T(J,I)+1.9*(X-T(J,I))
460      ITER=ITER+1
465      IF(ITER-750)70,70,80
470   70 IF(121-L)80,80,30
475   80 PRINT 90,((T(J,I),I=1,11),J=1,11)
480   90 FORMAT(//11F6.1)
485      PRINT 11,ITER,L
490   11 FORMAT(//2I5)
495      AJ=TKL*XT/10↑3
500      AK=HO*A↑2*(TB-TIN)/10↑6
505      QIN=0.0
510      QIN=QIN+0.5*(AJ*(T(5,1)-TIN)+AK)
515      QIN=QIN+AJ*(T(5,2)-TIN)+AK
520      QIN=QIN+AJ*(T(4,4)-TIN)+AJ*(T(5,3)-TIN)+1.5*AK
525      QIN=QIN+AJ*(T(3,4)-TIN)+AK
530      QIN=QIN+0.5*AK
535      QIN=QIN+AJ*(T(2,5)-TIN)+AJ*(T(3,4)-TIN)+1.5*AK
540      QIN=QIN+0.5*(AJ*(T(1,5)-TIN)+AK)
545      QINT=4.0*QIN
550      QIDEAL=(2.0*((20*A)↑2-3.14159*(3*A)↑2)+4.0*20*A*XT)*HO*(TB-
555     +TIN)/10↑6
560      EF=QINT/QIDEAL
565      X=2.0*XT*HO/(TKL*10↑3)
570      XNT=SQRT(X)
575      X=2.0*HO*10↑3/(TKL*XT)
580      PHI=(W-P0)*SQRT(X)/(2.0*10↑3)
585      PRINT 99,EF,QINT,QIDEAL,XNT,PHI
590   99 FORMAT(4HEF =,F6.4,2X,6HQINT =,F6.5,2X,8HQIDEAL =,F6.5,2X,
595     +5HXNT =,F6.4,2X,5HPHI =,F6.4)
600      END
605      &DATA
610      S1.31,0.405,2.54,1.59,0.382,146.0
```

Data given for reading number S066

SAMPLE RESULTS FOR SURFACE C/3/MS - Reading Number S066

T_o TIN °C	h_o kW/m^{2}K	a mm	t mm	k kW/mK	T_b °C	d_o mm	W mm
61.3100	.4050	2.5400	1.5900	.3820	146.0000	15.2400	50.800

TEMPERATURES AT NODAL POINTS

61.3	61.3	61.3	61.3	69.2	75.3	79.8	83.1	85.4	86.7	87.3
61.3	61.3	61.3	61.3	69.7	75.7	80.1	83.3	85.5	86.9	87.4
61.3	61.3	61.3	66.2	72.1	77.2	81.1	84.0	86.1	87.3	87.9
61.3	61.3	61.3	69.3	74.8	79.1	82.5	85.1	86.9	88.0	88.5
68.6	69.0	70.4	74.2	78.0	81.4	84.1	86.3	87.9	88.9	89.3
74.6	75.0	76.3	78.6	81.2	83.7	85.9	87.6	89.0	89.8	90.2
79.2	79.5	80.5	82.1	83.9	85.8	87.5	88.9	90.0	90.7	91.1
82.6	82.8	83.6	84.7	86.1	87.5	88.8	90.0	90.9	91.6	91.9
84.9	85.1	85.7	86.6	87.6	88.8	89.9	90.9	91.7	92.2	92.5
86.3	86.5	87.0	87.7	88.7	89.7	90.6	91.5	92.2	92.7	93.0
86.9	87.1	87.5	88.2	89.1	90.0	91.0	91.8	92.5	93.0	93.2

ITER L(Counter)
126 121

EF = .7315 QINT = .12844 kW QIDEAL = .17560 kW XLT = .0581 PHI = .6493

SURFACE: C/3/MS TEST BED: Mk 1 POSITION: Placed directly on distributor plate

BED MATERIAL: Zircon sand, size range 63 – 210 μm; static height 50 mm

OBSERVED RESULTS

READING NUMBER	BED			FIN METAL TEMPERATURES									WATER				GAS	AIR			AMBIENT	
	T_{16} °C	T_{17} °C	T_{18} °C	T_1 °C	T_2 °C	T_3 °C	T_4 °C	T_5 °C	T_6 °C	T_7 °C	T_8 °C	T_9 °C	T_{wi} °C	T_{wo} °C	ROT. READ	H_w mmH$_2$O	ROT. READ	H_a mmH$_2$O	T_a °C	P_a mm Hg	P_{at} mm Hg	T_{at} °C
S066	147	142	149	97	76	86	65	83	84	100	95	60	11.4	27.8	19.4	455	20.5	49	49	79	764	23.0
S067	165	166	169	117	87	112	83	97	111	120	112	70	11.0	30.6	21.8	430	22.5	101	49	79	764	23.5
S068	173	171	177	127	94	121	87	101	112	128	119	74	11.0	32.2	21.8	423	24.5	151	49	79	764	24.0
S069	183	181	188	137	101	134	96	111	122	140	128	80	11.0	34.2	21.9	423	27.5	253	48	77	764	24.0
S070	195	190	196	145	107	142	100	117	127	146	135	85	11.0	35.5	22.0	420	30.0	352	48	76	764	24.5
S071	195	194	197	147	107	143	100	116	128	145	137	86	11.0	36.2	22.1	423	31.3	494	47	74	764	25.0

CALCULATED RESULTS

READING NUMBER	$\dot{m}$ kg/s	$\dot{M}$ kg/s	T_w °C	T_b °C	T_m °C	Q kW	$\dot{V}_a$ m^3/s x10^3	$\dot{V}_g$ m^3/s x10^3	u_f m/s	U kW/m^{2}K	h_m kW/m^{2}K	h_i kW/m^{2}K	E_f EXP.	h_o kW/m^{2}K EXP.	E_f NUM.	T_o °C NUM.
S066	0.099	0.533	26.6	146	83	6.40	20.15	0.204	0.134	3.965	0.405	15.43	0.736	0.399	0.732	61.31
S067	0.109	0.518	29.0	167	101	8.53	28.93	0.221	0.198	4.571	0.515	15.72	0.704	0.507	0.684	74.44
S068	0.109	0.514	30.4	174	107	9.26	35.37	0.239	0.246	4.769	0.550	15.80	0.700	0.541	0.670	79.49
S069	0.111	0.514	32.2	184	117	10.36	45.80	0.265	0.326	5.048	0.616	16.07	0.675	0.604	0.646	86.20
S070	0.114	0.512	33.4	194	123	11.27	53.99	0.288	0.393	5.187	0.632	16.24	0.682	0.621	0.641	91.56
S071	0.117	0.514	33.9	195	123	11.94	63.98	0.300	0.465	5.481	0.661	16.41	0.707	0.650	0.631	94.88

TEST NUMBER 17

Manufactured Radial Fin Tube Results

Tests 18 - 34

SURFACE: C/1/MR TEST BED: Mk 1 POSITION: Placed directly on distributor plate

BED MATERIAL: Zircon sand, size range 63 - 210 μm; static height 50 mm

OBSERVED RESULTS

READING NUMBER	BED			WATER				GAS	AIR			AMBIENT	
	T_{16} °C	T_{17} °C	T_{18} °C	T_{wi} °C	T_{wo} °C	ROT. READ	H_w mm H_2O	ROT. READ	H_a mm H_2O	T_a °C	P_a mm Hg	P_{at} mm Hg	T_{at} °C
001	180	185	185	13.4	34.3	14.5	475	21.0	47	45	79	770	27.5
002	184	199	190	13.5	38.1	15.2	470	22.3	102	44	79	770	27.5
003	187	201	199	13.4	39.0	15.5	455	24.0	151	44	79	770	27.5
004	189	205	205	13.4	39.2	15.5	435	25.5	200	43	78	770	28.0
005	183	200	200	13.3	32.5	22.0	430	25.0	200	43	79	770	29.0
006	190	203	203	13.2	33.4	22.1	430	26.6	250	43	78	770	28.5
007	193	200	208	13.2	34.0	22.2	430	28.0	298	42	78	770	29.0
008	192	200	206	13.2	34.3	22.5	430	28.0	400	41	77	770	28.5
009	183	187	191	13.2	33.7	22.5	430	27.9	495	39	76	770	28.0
010	181	188	188	13.1	30.8	22.2	435	24.0	144	42	79	770	28.0
011	178	191	189	13.1	30.3	22.3	435	22.6	99	43	79	770	28.0
012	175	189	181	13.1	28.0	22.0	440	21.0	50	43	80	770	27.5

CALCULATED RESULTS

READING NUMBER	$\dot{m}$ kg/s	$\dot{M}$ kg/s	T_w °C	T_b °C	Q kW	$\dot{V}_a$ m^3/s x10^3	$\dot{V}_g$ m^3/s x10^3	u_f m/s	U kW/m^2K	h_i kW/m^2K	E_f	h_o kW/m^2K
001	0.078	0.545	33.1	183	6.42	19.93	0.208	0.142	2.969	16.23	0.815	0.327
002	0.081	0.542	36.6	191	7.94	29.40	0.220	0.213	3.563	16.77	0.771	0.431
003	0.082	0.533	37.4	196	8.38	35.77	0.234	0.261	3.664	16.73	0.763	0.453
004	0.082	0.521	37.5	200	8.45	41.21	0.248	0.304	3.606	16.49	0.766	0.443
005	0.111	0.518	30.9	196	8.51	41.24	0.243	0.301	3.576	16.03	0.767	0.442
006	0.112	0.518	31.7	199	9.06	46.08	0.257	0.339	3.756	16.17	0.752	0.479
007	0.112	0.518	32.2	200	9.34	50.39	0.270	0.371	3.862	16.26	0.744	0.502
008	0.114	0.518	32.5	199	9.66	58.43	0.270	0.430	4.023	16.34	0.730	0.539
009	0.114	0.518	31.9	187	9.38	65.17	0.268	0.467	4.192	16.25	0.715	0.584
010	0.112	0.521	29.3	186	7.89	35.05	0.234	0.251	3.493	15.86	0.773	0.427
011	0.113	0.521	28.8	186	7.73	29.01	0.222	0.207	3.411	15.81	0.779	0.411
012	0.111	0.523	26.8	182	6.46	20.63	0.208	0.146	2.885	15.48	0.820	0.317

SURFACE: C/1/MR TEST BED: Mk 1 POSITION: Lower fin tip edge 25 mm above distributor plate
BED MATERIAL: Zircon sand, size range 63 - 210 μm; static height 75 mm

OBSERVED RESULTS

READING NUMBER	BED			WATER				GAS	AIR			AMBIENT	
	T_{16} °C	T_{17} °C	T_{18} °C	T_{wi} °C	T_{wo} °C	ROT. READ	H_w mm H_2O	ROT. READ	H_a mm H_2O	T_a °C	P_a mm Hg	P_{at} mm Hg	T_{at} °C
013	174	175	172	8.2	25.2	22.5	120	21.0	49	49	78	760	27.0
014	190	189	188	8.2	28.1	22.7	120	23.1	100	49	78	760	27.0
015	198	196	195	8.2	29.7	22.9	123	24.5	151	49	78	760	27.0
016	208	204	201	8.2	31.4	23.0	123	27.6	252	49	77	760	27.5
017	208	203	201	8.2	31.5	23.0	123	30.0	350	48	76	760	28.0
018	207	200	200	8.2	31.4	23.0	123	31.1	505	47	74	760	28.0
019	179	175	174	8.2	24.7	22.5	120	20.5	50	49	79	762	28.0
020	191	187	185	8.2	27.1	22.5	120	23.0	100	49	78	762	28.0
021	195	191	190	8.2	28.2	22.7	123	24.5	151	49	78	762	28.5
022	205	200	199	8.2	29.9	22.9	123	27.5	252	49	77	762	28.5
023	210	206	204	8.1	31.0	22.9	123	30.0	351	49	76	762	29.0
024	209	203	201	8.2	31.2	22.9	123	31.1	505	48	74	762	29.0

READING NUMBER	FIN METAL TEMPERATURES °C														
	T_1	T_2	T_3	T_4	T_5	T_6	T_7	T_8	T_9	T_{10}	T_{11}	T_{12}	T_{13}	T_{14}	T_{15}
013	52	75	72	80	68	75	100	93	86	97	61	92	77	69	89
014	58	86	81	93	75	83	111	102	91	106	70	106	86	75	98
015	63	92	82	95	79	82	114	107	94	110	73	110	89	80	103
016	69	98	89	101	87	86	118	110	98	113	80	119	93	84	110
017	70	99	90	101	85	89	119	109	99	112	80	119	99	85	111
018	70	98	89	99	83	88	120	109	99	115	80	116	97	84	111
019	59	81	72	81	71	72	98	89	83	97	52	86	68	59	79
020	64	90	81	91	78	79	105	99	88	101	60	93	75	66	89
021	69	93	84	99	64	80	109	100	90	104	63	100	80	70	94
022	73	99	92	105	89	85	115	105	93	110	68	103	82	73	100
023	79	106	98	108	91	88	118	110	98	103	70	110	88	78	104
024	79	106	98	108	92	85	118	108	99	101	70	109	87	77	102

TEST NUMBER 19

SURFACE: C/1/MR TEST BED: Mk 1 POSITION: Lower fin tip edge 25 mm above distributor
BED MATERIAL: Zircon sand, size range 63 - 210 μm; static height 75 mm

CALCULATED RESULTS

READING NUMBER	$\dot{m}$ kg/s	$\dot{M}$ kg/s	T_w °C	T_b °C	Q kW	$\dot{V}_a$ m^3/s x10^3	$\dot{V}_g$ m^3/s x10^3	u_f m/s	U kW/m^2K	h_i kW/m^2K	E_f	h_o kW/m^2K
013	0.113	0.559	23.8	173	7.64	20.09	0.208	0.140	3.551	15.71	0.767	0.441
014	0.114	0.559	26.5	189	9.09	28.70	0.226	0.207	3.878	16.17	0.742	0.507
015	0.115	0.566	28.0	196	9.94	35.27	0.238	0.258	4.102	16.57	0.725	0.555
016	0.115	0.566	29.5	204	10.76	45.53	0.266	0.338	4.275	16.83	0.711	0.595
017	0.115	0.566	29.6	204	10.81	53.71	0.288	0.399	4.296	16.85	0.710	0.600
018	0.115	0.566	29.5	202	10.76	64.54	0.299	0.478	4.324	16.83	0.707	0.608
019	0.113	0.559	23.4	176	7.40	20.33	0.204	0.142	3.364	15.63	0.782	0.403
020	0.113	0.559	25.6	188	8.54	28.73	0.225	0.206	3.644	16.00	0.761	0.457
021	0.114	0.566	26.6	192	9.14	35.31	0.238	0.256	3.830	16.32	0.747	0.494
022	0.114	0.566	28.1	202	9.99	45.58	0.265	0.337	3.986	16.58	0.735	0.526
023	0.115	0.566	29.1	207	10.61	53.77	0.288	0.402	4.138	16.77	0.723	0.560
024	0.115	0.566	29.3	204	10.66	64.51	0.299	0.479	4.232	16.80	0.715	0.584

TEST NUMBER 19

TEST NUMBER 20

SURFACE: C/2/MR TEST BED: Mk 1 POSITION: Placed directly on distributor plate
BED MATERIAL: Zircon sand, size range 63 - 210 μm; static height 50 mm

OBSERVED RESULTS

READING NUMBER	BED			WATER				GAS	AIR			AMBIENT	
	T_{16} °C	T_{17} °C	T_{18} °C	T_{wi} °C	T_{wo} °C	ROT. READ	H_w mm H_2O	ROT. READ	H_a mm H_2O	T_a °C	P_a mm Hg	P_{at} mm Hg	T_{at} °C
025	174	173	175	13.5	32.3	17.5	145	20.5	49	46	80	767	21.0
026	182	179	179	13.5	36.9	17.8	145	23.0	99	46	79	767	21.5
027	189	188	186	13.5	38.8	18.0	145	24.7	151	45	79	767	22.0
028	190	190	190	13.4	31.8	28.6	132	27.4	252	44	78	767	22.5
029	188	193	189	13.3	32.2	28.7	134	29.5	354	42	77	767	22.5
030	189	195	190	13.3	33.2	28.9	134	31.1	498	41	76	767	22.5

CALCULATED RESULTS

READING NUMBER	$\dot{m}$ kg/s	$\dot{M}$ kg/s	T_w °C	T_b °C	Q kW	$\dot{V}^a$ m^3/s x10^3	$\dot{V}^g$ m^3/s x10^3	u_f m/s	U kW/m^2K	h_i kW/m^2K	E_f	h_o kW/m^2K
025	0.090	0.614	31.2	174	6.68	20.29	0.204	0.141	2.075	17.58	0.848	0.258
026	0.092	0.614	35.4	180	8.61	28.82	0.226	0.203	2.642	18.35	0.801	0.358
027	0.092	0.614	37.2	188	9.34	35.66	0.240	0.256	2.748	18.65	0.793	0.378
028	0.144	0.586	30.1	190	10.68	46.11	0.264	0.333	2.963	17.90	0.772	0.428
029	0.144	0.590	30.4	190	10.98	54.79	0.283	0.395	3.054	18.05	0.764	0.448
030	0.145	0.590	31.3	191	11.67	65.05	0.299	0.470	3.242	18.23	0.748	0.491

TEST NUMBER 21

SURFACE: C/2/MR TEST BED: Mk 1 POSITION: Lower fin tip edge 25 mm above distributor plate
BED MATERIAL: Zircon sand, size range 63 - 210 μm; static height 75 mm

OBSERVED RESULTS

READING NUMBER	BED			WATER				GAS	AIR			AMBIENT	
	T_{16} °C	T_{17} °C	T_{18} °C	T_{wi} °C	T_{wo} °C	ROT. READ	H_w mm H_2O	ROT. READ	H_a mm H_2O	T_a °C	P_a mm Hg	P_{at} mm Hg	T_{at} °C
274	167	167	167	15.3	26.0	22.2	135	19.5	48	48	80	776	23.0
275	178	176	174	15.3	28.9	22.0	135	22.1	101	46	80	776	22.0
276	184	181	179	15.3	30.0	22.3	135	24.2	155	46	80	776	22.5
277	183	181	180	15.3	30.8	22.5	135	25.9	254	45	79	776	23.0
278	188	185	184	15.3	31.5	22.5	135	28.0	350	44	78	776	23.0
279	190	187	187	15.3	32.0	22.7	135	30.6	501	43	76	776	23.5

CALCULATED RESULTS

READING NUMBER	$\dot{m}$ kg/s	$\dot{M}$ kg/s	T_w °C	T_b °C	Q kW	$\dot{V}^a$ m^3/s x10^3	$\dot{V}^g$ m^3/s x10^3	u_f m/s	U kW/m^2K	h_i kW/m^2K	E_f	h_o kW/m^2K
274	0.112	0.593	25.2	167	4.62	20.13	0.196	0.138	2.401	16.56	0.874	0.189
275	0.110	0.593	27.9	176	5.86	29.29	0.217	0.205	2.917	16.99	0.844	0.247
276	0.112	0.593	28.9	181	6.49	36.28	0.236	0.257	3.144	17.20	0.831	0.274
277	0.113	0.593	29.6	181	6.93	46.49	0.252	0.329	3.373	17.34	0.817	0.304
278	0.113	0.593	30.3	186	7.26	54.63	0.270	0.391	3.435	17.46	0.813	0.312
279	0.114	0.593	30.7	188	7.56	65.38	0.293	0.470	3.545	17.55	0.806	0.327

SURFACE: C/2/MR TEST BED: Mk 1 POSITION: Lower fin tip edge 25 mm above distributor plate

BED MATERIAL: Zircon sand, size range 63 – 210 μm; static height 75 mm

OBSERVED RESULTS

READING NUMBER	BED			WATER				GAS	AIR			AMBIENT	
	T_{16} °C	T_{17} °C	T_{18} °C	T_{wi} °C	T_{wo} °C	ROT. READ	H_w mm H_2O	ROT. READ	H_a mm H_2O	T_a °C	P_a mm Hg	P_{at} mm Hg	T_{at} °C
031	168	168	168	15.2	27.0	19.4	134	19.4	50	48	79	774	24.0
032	171	169	169	15.3	29.4	19.3	134	22.1	100	46	80	774	21.5
033	178	174	173	15.3	31.0	19.6	135	23.7	150	46	79	774	22.5
034	181	177	176	15.2	32.4	19.7	135	25.6	255	45	78	774	23.5
035	185	183	182	15.2	33.2	19.7	135	28.2	352	44	77	774	24.0
036	186	185	184	15.2	34.0	19.7	135	30.4	501	43	76	774	24.0

CALCULATED RESULTS

READING NUMBER	$\dot{m}$ kg/s	$\dot{M}$ kg/s	T_w °C	T_b °C	Q kW	$\dot{V}_a$ m^3/s $\times 10^3$	$\dot{V}_g$ m^3/s $\times 10^3$	u_f m/s	U kW/m^2K	h_i kW/m^2K	E_f	h_o kW/m^2K
031	0.099	0.590	26.2	168	4.49	20.51	0.195	0.141	2.335	16.45	0.877	0.183
032	0.099	0.590	28.5	170	5.44	29.11	0.217	0.201	2.834	16.83	0.849	0.237
033	0.100	0.593	29.9	175	6.17	35.63	0.232	0.249	3.135	17.14	0.831	0.273
034	0.100	0.593	31.2	178	6.80	46.50	0.248	0.327	3.413	17.36	0.814	0.310
035	0.100	0.593	32.0	183	7.13	54.68	0.271	0.389	3.480	17.49	0.810	0.318
036	0.100	0.594	32.7	185	7.47	65.30	0.292	0.466	3.613	17.61	0.799	0.338

TEST NUMBER 22

SURFACE: C/2/MR TEST BED: Mk 2 POSITION: Lower fin tip edge 29 mm above distributor
BED MATERIAL: Zircon sand, size range 63 - 210 μm; static height 79 mm

OBSERVED RESULTS

BED			WATER				GAS	AIR			AMBIENT	
T_{16} °C	T_{17} °C	T_{18} °C	T_{wi} °C	T_{wo} °C	ROT. READ	H_w mm H_2O	ROT. READ	H_a mm H_2O	T_a °C	P_a mm Hg	P_{at} mm Hg	T_{at} °C
138	136	135	9.1	31.4	12.5	122	15.9	33.0	48	76	776	24.5

READING NUMBER	SURFACE ANGULAR POSITION	FIN METAL TEMPERATURES °C												
		T_1	T_2	T_3	T_4	T_5	T_6	T_7	T_8	T_9	T_{10}	T_{11}	T_{12}	T_{13}	T_{14}
280	+90°	54	68	69	57	71	66	59	70	79	65	68	72	62	72
281	+72°	54	74	70	56	70	65	59	69	78	65	68	71	60	71
282	+54°	53	76	71	56	71	65	59	70	79	64	68	72	63	71
283	+36°	53	76	71	57	73	66	61	69	78	63	68	70	62	71
284	+18°	53	75	69	58	74	65	63	69	79	63	68	73	63	71
285	0°	52	75	71	59	75	65	62	68	79	63	71	72	63	70
286	-18°	52	73	70	60	76	65	62	68	79	64	73	73	61	68
287	-36°	53	74	71	60	76	65	62	68	79	63	72	74	62	70
288	-54°	55	73	70	60	77	66	62	68	78	63	73	74	63	69
289	-72°	55	73	70	60	76	67	62	67	78	62	73	74	61	70
290	-90°	55	72	70	62	77	67	62	66	77	62	73	75	61	71
291	0°	53	73	71	59	75	65	62	68	80	63	70	72	63	71
292	+72°	55	71	71	56	73	68	60	71	78	65	68	73	62	73

TEST NUMBER 23

SURFACE: C/2/MR TEST BED: Mk 2 POSITION: Lower fin tip edge 29 mm above distributor
BED MATERIAL: Zircon sand, size range 63 - 210 μm; static height 79 mm

CALCULATED RESULTS

$\dot{m}$ kg/s	$\dot{M}$ kg/s	T_w °C	T_b °C	Q kW	$\dot{V}_a$ m^3/s x10^3	$\dot{V}_g$ m^3/s x10^3	u_f m/s	U kW/m^2K	h_i kW/m^2K	E_f	h_o kW/m^2K	
0.069	0.560	30.3	136	5.95	7.14	0.165	0.327	3.887	15.92	0.775	0.421	

FIN RADIUS mm	METAL TEMPERATURE °C
7.55	59.5
10.10	66.7
12.65	71.7
15.20	75.3
17.75	77.8
20.30	79.5
22.85	80.5
25.40	80.9

TEST NUMBER 24

SURFACE: C/2/MR TEST BED: Mk 2 POSITION: Lower fin tip edge 29 mm above distributor plate
BED MATERIAL: Zircon sand, size range 63 - 210 μm; static height 79 mm

OBSERVED RESULTS

READING NUMBER	BED			WATER				GAS	AIR			AMBIENT	
	T_{16} °C	T_{17} °C	T_{18} °C	T_{wi} °C	T_{wo} °C	ROT. READ	H_w mm H_2O	ROT. READ	H_a mm H_2O	T_a °C	P_a mm Hg	P_{at} mm Hg	T_{at} °C
037	123	123	124	7.6	33.5	8.1	117	15.3	24.7	45	78	773	22.0
038	119	117	118	7.6	32.2	8.5	117	14.3	20.0	46	78	773	23.0
039	112	110	111	7.6	30.2	8.2	117	13.4	15.0	46	78	773	24.0
040	101	102	103	7.7	27.4	8.1	117	12.0	10.0	45	78	773	25.0
041	134	132	133	7.7	35.4	8.6	116	16.3	29.6	47	78	773	25.0
042	141	139	140	7.8	37.7	8.6	116	16.9	34.7	48	78	773	25.5
043	150	148	149	8.0	39.8	8.8	117	17.7	39.7	49	78	773	26.0
044	157	156	156	8.1	41.8	8.8	117	18.5	45.8	49	78	773	26.0
045	161	159	160	8.1	43.0	9.0	117	18.9	48.8	50	78	773	26.5

CALCULATED RESULTS

READING NUMBER	$\dot{m}$ kg/s	$\dot{M}$ kg/s	T_w °C	T_b °C	Q kW	$\dot{V}_a$ m^3/s x10^3	$\dot{V}_g$ m^3/s x10^3	u_f m/s	U kW/m^2K	h_i kW/m^2K	E_f	h_o kW/m^2K
037	0.049	0.552	32.5	123	4.91	6.20	0.160	0.276	3.753	15.67	0.784	0.399
038	0.050	0.552	31.3	118	4.75	5.57	0.152	0.245	3.784	15.52	0.781	0.407
039	0.049	0.552	29.4	111	4.24	4.83	0.145	0.208	3.587	15.21	0.794	0.375
040	0.049	0.552	26.7	102	3.64	3.95	0.133	0.166	3.343	14.80	0.811	0.337
041	0.051	0.549	34.3	133	5.51	6.77	0.169	0.309	3.860	15.94	0.777	0.416
042	0.051	0.549	36.5	140	5.98	7.32	0.173	0.339	3.995	16.27	0.769	0.437
043	0.052	0.552	38.5	149	6.52	7.82	0.181	0.370	4.078	16.64	0.764	0.449
044	0.052	0.552	40.4	156	6.93	8.40	0.188	0.404	4.146	16.92	0.760	0.458
045	0.053	0.552	41.6	160	7.34	8.65	0.190	0.421	4.283	17.11	0.751	0.483

TEST NUMBER 24

SURFACE: C/3/MR TEST BED: Mk 1 POSITION: Placed directly on distributor plate
BED MATERIAL: Zircon sand, size range 63 - 210 μm; static height 50 mm

OBSERVED RESULTS

READING NUMBER	BED			WATER				GAS	AIR			AMBIENT	
	T_{16} °C	T_{17} °C	T_{18} °C	T_{wi} °C	T_{wo} °C	ROT. READ	H_w mm H_2O	ROT. READ	H_a mm H_2O	T_a °C	P_a mm Hg	P_{at} mm Hg	T_{at} °C
046	163	155	158	15.0	28.4	17.6	135	20.1	48	48	79	771	25.5
047	172	157	164	15.0	31.2	17.8	135	21.3	99	48	78	771	23.5
048	183	170	176	15.0	33.2	17.8	135	24.2	149	48	78	771	24.5
049	189	178	183	15.0	34.5	17.8	135	26.1	252	48	77	771	25.0
050	192	183	186	15.0	35.3	17.9	136	28.2	354	47	76	771	25.5
051	195	186	190	15.0	35.7	17.9	135	30.7	501	47	75	771	26.0

CALCULATED RESULTS

READING NUMBER	$\dot{m}$ kg/s	$\dot{M}$ kg/s	T_w °C	T_b °C	Q kW	$\dot{V}_a$ m^3/s x10^3	$\dot{V}_g$ m^3/s x10^3	u_f m/s	U kW/m^2K	h_i kW/m^2K	E_f	h_o kW/m^2K
046	0.091	0.593	27.6	159	4.71	20.06	0.200	0.135	1.909	8.54	0.899	0.242
047	0.092	0.593	30.2	164	5.84	28.79	0.211	0.196	2.325	8.77	0.878	0.320
048	0.092	0.593	32.1	176	6.61	35.31	0.236	0.247	2.447	8.93	0.871	0.344
049	0.092	0.593	33.3	183	7.11	45.90	0.253	0.326	2.530	9.04	0.865	0.362
050	0.092	0.595	34.0	187	7.41	54.45	0.272	0.390	2.583	9.13	0.862	0.372
051	0.092	0.593	34.4	190	7.57	64.74	0.295	0.467	2.592	9.13	0.861	0.374

TEST NUMBER 25

SURFACE: C/4/MR TEST BED: Mk 1 POSITION: Placed directly on distributor plate
BED MATERIAL: Zircon sand, size range 63 - 210 μm; static height 50 mm

OBSERVED RESULTS

READING NUMBER	BED			WATER				GAS	AIR			AMBIENT	
	T_{16} °C	T_{17} °C	T_{18} °C	T_{wi} °C	T_{wo} °C	ROT. READ	H_w mm H_2O	ROT. READ	H_a mm H_2O	T_a °C	P_a mm Hg	P_{at} mm Hg	T_{at} °C
052	160	160	160	15.6	27.2	20.7	142	19.8	49	47	80	773	23.0
053	171	170	170	15.6	29.7	20.9	143	22.1	101	47	80	773	23.5
054	182	178	180	15.6	31.6	21.2	142	24.2	151	47	79	773	24.0
055	187	180	184	15.6	32.7	21.3	142	26.2	252	45	78	773	24.0
056	191	183	187	15.5	33.2	21.3	141	28.0	355	44	77	773	24.5
057	193	187	189	15.5	34.0	21.4	140	30.6	502	43	76	773	24.5

TEST NUMBER 26

CALCULATED RESULTS

READING NUMBER	$\dot{m}$ kg/s	$\dot{M}$ kg/s	T_w °C	T_b °C	Q kW	$\dot{V}_a$ m^3/s $\times 10^3$	$\dot{V}_g$ m^3/s $\times 10^3$	u_f m/s	U kW/m^2K	h_i kW/m^2K	E_f	h_o kW/m^2K
052	0.104	0.608	26.4	160	4.65	20.33	0.198	0.137	2.557	16.91	0.790	0.189
053	0.105	0.610	28.7	170	5.80	29.19	0.217	0.201	3.013	17.37	0.750	0.241
054	0.107	0.608	30.5	180	6.76	35.67	0.237	0.252	3.322	17.67	0.722	0.282
055	0.107	0.608	31.5	184	7.26	46.20	0.253	0.329	3.494	17.85	0.707	0.306
056	0.107	0.606	31.9	187	7.52	54.89	0.270	0.393	3.564	17.88	0.700	0.316
057	0.108	0.603	32.7	190	7.96	65.33	0.294	0.471	3.715	17.98	0.686	0.340

SURFACE: C/4/MR (D=50.8 mm) TEST BED Mk 3 POSITION: Placed directly on distributor plate
BED MATERIAL: Zircon sand, size range 63 - 210 μm; static height 50 mm

OBSERVED RESULTS

READING NUMBER	BED			WATER				GAS	AIR			AMBIENT	
	T_{16} °C	T_{17} °C	T_{18} °C	T_{wi} °C	T_{wo} °C	ROT. READ	H_w mm H_2O	ROT. READ	H_a mm H_2O	T_a °C	P_a mm Hg	P_{at} mm Hg	T_{at} °C
058	110	114	104	10.0	16.9	14.4	100	9.6	6.0	39	78	775	21.5
059	110	116	109	9.7	19.4	13.0	102	10.3	9.0	42	78	775	21.5
060	103	110	101	9.6	22.6	13.0	102	10.6	14.8	44	78	775	21.5
061	105	116	102	9.5	26.1	13.0	103	11.6	24.7	46	78	775	21.5
062	125	135	120	9.5	30.2	13.0	104	12.6	49.0	48	78	775	22.0
063	137	146	131	9.4	32.8	13.0	105	13.2	75.2	49	78	775	22.0
064	144	152	136	9.4	34.0	13.0	105	13.2	99.8	50	78	775	22.0
065	151	160	145	9.4	35.4	13.0	105	13.6	152.0	50	78	775	22.0

TEST NUMBER 27

CALCULATED RESULTS

READING NUMBER	$\dot{m}$ kg/s	$\dot{M}$ kg/s	T_w C	T_b C	Q kW	$\dot{V}_a$ m^3/s $\times 10^3$	$\dot{V}_g$ m^3/s $\times 10^3$	u_f m/s	U kW/m^2K	h_i kW/m^2K	E_f	h_o kW/m^2K
058	0.077	0.510	16.5	109	1.83	3.09	0.115	0.106	1.370	12.99	0.893	0.090
059	0.071	0.515	18.9	112	2.49	3.77	0.120	0.131	1.849	13.34	0.851	0.132
060	0.071	0.515	21.9	105	3.47	4.82	0.122	0.164	2.885	13.79	0.748	0.258
061	0.071	0.515	25.2	108	4.54	6.20	0.130	0.213	3.785	14.34	0.650	0.420
062	0.071	0.520	29.0	127	5.75	8.71	0.138	0.314	4.057	14.97	0.623	0.474
063	0.071	0.523	31.5	138	6.55	10.77	0.143	0.399	4.251	15.38	0.604	0.516
064	0.071	0.523	32.6	144	6.91	12.39	0.143	0.466	4.286	15.55	0.602	0.522
065	0.071	0.523	33.9	152	7.32	15.29	0.147	0.586	4.286	15.75	0.604	0.517

SURFACE: C/4/MR (D=50.8 mm) TEST BED: Mk 3 POSITION: Placed directly on distributor plate
BED MATERIAL: Steel shot, size range 75 - 500 μm; static height 50 mm

OBSERVED RESULTS

READING NUMBER	BED			WATER				GAS	AIR			AMBIENT	
	T_{16} °C	T_{17} °C	T_{18} °C	T_{wi} °C	T_{wo} °C	ROT. READ	H_w mm H_2O	ROT. READ	H_a mm H_2O	T_a °C	P_a mm Hg	P_{at} mm Hg	T_{at} °C
066	195	200	193	9.1	20.0	12.7	103	12.0	19.0	44	78	775	22.0
067	191	183	187	9.1	23.0	12.7	103	12.0	24.7	46	78	775	22.0
068	175	180	178	9.1	26.4	12.8	105	13.1	34.9	48	78	775	22.0
069	170	177	185	9.1	29.6	12.8	105	13.7	49.2	49	78	775	22.0
070	168	177	171	9.2	34.5	12.9	105	14.5	101.0	50	78	775	22.5
071	176	185	175	9.2	36.9	13.0	105	15.0	210.0	51	78	775	22.5
072	180	179	188	9.2	37.4	13.0	106	15.4	364.0	50	79	775	22.5
073	183	180	190	9.2	37.4	13.0	106	16.1	501.0	50	79	775	23.0

CALCULATED RESULTS

READING NUMBER	$\dot{m}$ kg/s	$\dot{M}$ kg/s	T_w °C	T_b °C	Q kW	$\dot{V}_a$ m^3/s x10^3	$\dot{V}_g$ m^3/s x10^3	u_f m/s	U kW/m^2K	h_i kW/m^2K	E_f	h_o kW/m^2K
066	0.070	0.518	19.4	196	2.80	5.46	0.133	0.231	1.097	13.45	0.917	0.068
067	0.070	0.518	22.3	187	3.68	6.20	0.133	0.257	1.543	13.88	0.879	0.103
068	0.070	0.523	25.5	178	4.67	7.35	0.142	0.299	2.116	14.46	0.828	0.157
069	0.070	0.523	28.5	177	5.61	8.71	0.147	0.353	2.608	14.91	0.781	0.213
070	0.071	0.523	33.1	172	7.11	12.46	0.153	0.500	3.539	15.62	0.687	0.352
071	0.071	0.523	35.3	179	7.83	17.94	0.157	0.731	3.765	15.95	0.665	0.392
072	0.071	0.525	35.8	182	7.98	23.68	0.161	0.971	3.770	16.08	0.665	0.392
073	0.071	0.525	35.8	184	7.98	27.78	0.168	1.144	3.719	16.08	0.671	0.381

SURFACE: C/4/MR (D=40.0 mm) TEST BED: Mk 3 POSITION: Lower fin tip edge 5 mm above distributor plate
BED MATERIAL: Zircon sand, size range 63 - 210 μm; static height 50 mm

OBSERVED RESULTS

READING NUMBER	BED			WATER				GAS	AIR			AMBIENT	
	T_{16} °C	T_{17} °C	T_{18} °C	T_{wi} °C	T_{wo} °C	ROT. READ	H_w mm H_2O	ROT. READ	H_a mm H_2O	T_a °C	P_a mm Hg	P_{at} mm Hg	T_{at} °C
074	116	120	113	10.5	18.0	13.4	99	9.6	6.0	41	76	760	23.0
075	117	122	115	10.1	19.4	13.4	100	10.1	8.9	43	76	760	23.0
076	115	120	118	10.0	22.3	13.5	100	10.6	14.8	45	76	760	23.0
077	120	127	119	10.0	25.6	13.5	100	11.6	24.9	47	76	760	23.0
078	137	145	134	9.9	29.4	13.6	100	12.5	49.8	48	76	760	23.5
079	150	157	145	9.9	31.4	13.6	100	13.2	74.6	49	76	760	23.5
080	155	164	151	9.9	32.8	13.8	101	13.2	99.4	50	76	760	23.5
081	164	170	159	9.9	34.0	13.8	101	13.7	152.0	50	76	760	24.0

CALCULATED RESULTS

READING NUMBER	$\dot{m}$ kg/s	$\dot{M}$ kg/s	T_w °C	T_b °C	Q kW	$\dot{V}_a$ m^3/s x10^3	$\dot{V}_g$ m^3/s x10^3	u_f m/s	U kW/m^2K	h_i kW/m^2K	E_f	h_o kW/m^2K
074	0.073	0.507	17.6	116	1.90	3.05	0.115	0.107	1.335	13.04	0.924	0.138
075	0.073	0.510	18.9	118	2.45	3.70	0.118	0.130	1.708	13.28	0.900	0.188
076	0.073	0.510	21.6	118	3.36	4.76	0.122	0.168	2.412	13.69	0.852	0.298
077	0.073	0.510	24.7	122	4.37	6.16	0.130	0.219	3.104	14.16	0.799	0.433
078	0.074	0.510	28.2	138	5.64	8.69	0.137	0.322	3.551	14.71	0.765	0.533
079	0.074	0.510	30.1	151	6.26	10.62	0.143	0.406	3.578	14.98	0.764	0.536
080	0.075	0.513	31.4	156	6.79	12.24	0.143	0.473	3.765	15.25	0.750	0.581
081	0.075	0.513	32.5	164	7.16	15.14	0.147	0.596	3.766	15.41	0.750	0.578

SURFACE: C/4/MR (D=40.0 mm) TEST BED: Mk 3 POSITION: Lower fin tip edge 5 mm above distributor plate

BED MATERIAL: Steel shot, size range 75 - 500 μm; static height 50 mm

OBSERVED RESULTS

READING NUMBER	BED			WATER				GAS	AIR			AMBIENT	
	T_{16} °C	T_{17} °C	T_{18} °C	T_{wi} °C	T_{wo} °C	ROT. READ	H_w mm H_2O	ROT. READ	H_a mm H_2O	T_a °C	P_a mm Hg	P_{at} mm Hg	T_{at} °C
082	235	231	233	9.6	18.8	12.9	101	12.1	18.4	45	76	760	23.0
083	200	194	197	9.6	23.0	12.9	101	12.4	24.9	47	76	760	23.0
084	195	191	193	9.6	25.8	12.9	102	13.1	34.1	48	76	760	23.0
085	184	190	195	9.6	29.3	13.0	102	14.2	49.1	49	76	760	23.0
086	189	189	195	9.6	34.0	13.0	102	14.9	102.6	50	76	760	23.5
087	197	195	204	9.6	36.0	13.0	103	15.4	208.0	50	76	760	23.5
088	202	200	208	9.6	36.8	13.1	104	15.9	360.0	50	77	760	23.5
089	203	200	209	9.5	36.7	13.1	104	16.4	502.0	50	77	760	24.0

CALCULATED RESULTS

READING NUMBER	$\dot{m}$ kg/s	$\dot{M}$ kg/s	T_w °C	T_b °C	Q kW	$\dot{V}_a$ m^3/s x10^3	$\dot{V}_g$ m^3/s x10^3	u_f m/s	U kW/m^2K	h_i kW/m^2K	E_f	h_o kW/m^2K
082	0.071	0.513	18.3	233	2.34	5.31	0.134	0.242	0.754	13.20	0.959	0.071
083	0.071	0.513	22.3	197	3.59	6.16	0.137	0.261	1.419	13.80	0.920	0.148
084	0.071	0.515	24.9	193	4.42	7.19	0.142	0.302	1.816	14.25	0.894	0.201
085	0.071	0.515	28.2	190	5.45	8.62	0.151	0.360	2.330	14.74	0.860	0.278
086	0.071	0.515	32.6	191	6.85	12.44	0.157	0.520	2.988	15.39	0.813	0.395
087	0.071	0.518	34.5	198	7.44	17.71	0.161	0.752	3.145	15.72	0.802	0.425
088	0.072	0.520	35.2	203	7.79	23.31	0.165	1.000	3.210	15.91	0.798	0.437
089	0.072	0.520	35.1	204	7.79	27.53	0.170	1.183	3.189	15.89	0.799	0.433

SURFACE: C/4/MR (D=30.4 mm) TEST BED: Mk 3 POSITION: Lower fin tip edge 10 mm above distributor plate

BED MATERIAL: Zircon sand, size range 63 - 210 μm; static height 50 mm

OBSERVED RESULTS

READING NUMBER	BED			WATER				GAS	AIR			AMBIENT	
	T_{16} °C	T_{17} °C	T_{18} °C	T_{wi} °C	T_{wo} °C	ROT. READ	H_w mm H_2O	ROT. READ	H_a mm H_2O	T_a °C	P_a mm Hg	P_{at} mm Hg	T_{at} °C
090	141	144	139	12.2	18.0	13.6	100	9.8	6.1	38	77	768	21.5
091	151	153	149	10.0	17.6	13.6	100	10.1	9.0	42	77	768	22.0
092	144	145	147	9.5	20.0	13.9	100	10.5	14.8	44	77	768	22.0
093	145	150	144	9.2	23.0	14.0	100	11.2	25.1	46	77	768	23.0
094	158	165	155	9.1	26.3	14.1	101	11.9	49.3	49	77	768	23.5
095	170	176	167	9.0	28.0	14.1	101	12.2	75.4	50	77	768	23.5
096	176	184	174	9.1	28.9	14.1	101	12.2	99.8	50	77	768	23.5
097	182	190	179	9.0	29.4	14.1	101	12.2	150.0	51	78	768	23.5

CALCULATED RESULTS

READING NUMBER	$\dot{m}$ kg/s	$\dot{M}$ kg/s	T_w °C	T_b °C	Q kW	$\dot{V}_a$ m^3/s x10^3	$\dot{V}_g$ m^3/s x10^3	u_f m/s	U kW/m^2K	h_i kW/m^2K	E_f	h_o kW/m^2K
090	0.074	0.510	17.7	141	1.41	3.11	0.116	0.116	0.788	13.12	0.973	0.134
091	0.074	0.510	17.2	151	1.96	3.75	0.118	0.143	1.014	13.04	0.965	0.177
092	0.075	0.510	19.4	145	2.90	4.79	0.122	0.181	1.598	13.40	0.943	0.300
093	0.076	0.510	22.2	147	4.00	6.22	0.127	0.236	2.212	13.84	0.917	0.450
094	0.076	0.513	25.3	159	5.07	8.68	0.132	0.338	2.622	14.35	0.898	0.560
095	0.076	0.513	26.9	171	5.64	10.72	0.135	0.429	2.706	14.59	0.895	0.582
096	0.076	0.513	27.7	178	5.90	12.33	0.135	0.501	2.712	14.72	0.895	0.583
097	0.076	0.513	28.2	183	6.09	15.10	0.135	0.621	2.717	14.78	0.895	0.583

SURFACE: C/4/MR (D=30.4 mm) TEST BED: Mk 3 POSITION: Lower fin tip edge 10 mm above distributor plate

BED MATERIAL: Steel shot, size range 75 - 500 μm; static height 50 mm

OBSERVED RESULTS

READING NUMBER	BED			WATER				GAS	AIR			AMBIENT	
	T_{16} °C	T_{17} °C	T_{18} °C	T_{wi} °C	T_{wo} °C	ROT. READ	H_w mm H_2O	ROT. READ	H_a mm H_2O	T_a °C	P_a mm Hg	P_{at} mm Hg	T_{at} °C
098	260	263	260	9.0	16.0	13.8	100	11.5	18.4	47	77	770	24.0
099	222	225	223	9.0	20.0	13.9	100	11.5	24.8	48	77	770	24.0
100	219	225	222	9.0	22.2	14.0	101	12.1	35.0	49	77	770	24.0
101	208	216	220	9.0	25.1	14.0	101	12.8	49.2	50	77	770	24.5
102	216	216	225	9.0	28.3	14.1	101	13.4	100.0	51	77	770	24.5
103	226	231	223	9.0	30.0	14.1	102	14.0	208.0	51	77	770	24.5
104	224	224	230	9.0	30.0	14.1	102	14.4	359.0	51	77	770	24.5
105	219	219	224	9.0	29.4	14.1	102	14.4	503.0	50	77	770	25.0

CALCULATED RESULTS

READING NUMBER	$\dot{m}$ kg/s	$\dot{M}$ kg/s	T_w °C	T_b °C	Q kW	$\dot{V}_a$ m^3/s x10^3	$\dot{V}_g$ m^3/s x10^3	u_f m/s	U kW/m^2K	h_i kW/m^2K	E_f	h_o kW/m^2K
098	0.075	0.510	15.6	261	1.81	5.33	0.130	0.256	0.509	12.81	0.983	0.084
099	0.075	0.510	19.4	223	3.06	6.17	0.130	0.276	1.039	13.39	0.964	0.181
100	0.076	0.513	21.4	222	3.81	7.32	0.134	0.327	1.311	13.77	0.954	0.236
101	0.076	0.513	24.1	215	4.72	8.67	0.140	0.381	1.711	14.18	0.938	0.323
102	0.076	0.513	27.1	219	5.74	12.34	0.145	0.547	2.067	14.63	0.924	0.407
103	0.076	0.515	28.7	227	6.28	17.80	0.150	0.802	2.189	14.92	0.919	0.436
104	0.076	0.515	28.7	226	6.28	23.38	0.153	1.051	2.200	14.92	0.918	0.439
105	0.076	0.515	28.2	221	6.09	27.72	0.153	1.234	2.182	14.84	0.919	0.435

SURFACE: C/4/MR (D=22.0 mm) TEST BED: Mk 3 POSITION: Lower fin tip edge 14 mm above distributor plate

BED MATERIAL: Zircon sand, size range 63 - 210 μm; static height 50 mm

OBSERVED RESULTS

READING NUMBER	BED			WATER				GAS	AIR			AMBIENT	
	T_{16} °C	T_{17} °C	T_{18} °C	T_{wi} °C	T_{wo} °C	ROT. READ	H_w mm H_2O	ROT. READ	H_a mm H_2O	T_a °C	P_a mm Hg	P_{at} mm Hg	T_{at} °C
106	154	157	153	11.4	16.8	11.9	102	9.2	6.0	37	78	776	21.0
107	168	171	166	10.6	18.0	11.9	103	9.2	9.0	41	78	776	21.0
108	180	184	176	10.4	20.3	12.0	104	9.7	14.9	44	78	776	21.5
109	185	190	184	10.1	23.4	12.0	104	10.1	25.3	46	78	776	22.0
110	205	209	201	10.1	25.8	12.2	104	10.6	48.9	48	78	776	22.0
111	217	222	215	10.0	26.7	12.3	105	11.2	71.2	49	78	776	22.0
112	224	234	225	10.0	27.5	12.3	105	12.0	110.0	50	78	776	22.0

CALCULATED RESULTS

READING NUMBER	$\dot{m}$ kg/s	$\dot{M}$ kg/s	T_w °C	T_b °C	Q kW	$\dot{V}_a$ m^3/s x10^3	$\dot{V}_g$ m^3/s x10^3	u_f m/s	U kW/m^2K	h_i kW/m^2K	E_f	h_o kW/m^2K
106	0.066	0.515	16.6	155	1.10	3.10	0.112	0.120	0.550	12.89	0.992	0.192
107	0.066	0.518	17.7	169	1.65	3.78	0.112	0.150	0.755	13.10	0.989	0.269
108	0.067	0.520	19.8	180	2.38	4.84	0.115	0.197	1.029	13.50	0.985	0.376
109	0.067	0.520	22.7	186	3.34	6.28	0.118	0.260	1.412	13.94	0.979	0.534
110	0.067	0.520	25.0	205	4.01	8.70	0.122	0.375	1.538	14.28	0.977	0.588
111	0.068	0.523	25.8	218	4.36	10.49	0.127	0.464	1.566	14.47	0.977	0.599
112	0.068	0.523	26.6	227	4.58	13.02	0.133	0.586	1.580	14.59	0.977	0.605

SURFACE: C/4/MR (D=22.0 mm) TEST BED: Mk 3 POSITION: Lower fin tip edge 14 mm above distributor plate

BED MATERIAL: Steel shot, size range 75 – 500 μm; static height 50 mm

OBSERVED RESULTS

READING NUMBER	BED			WATER				GAS	AIR			AMBIENT	
	T_{16} °C	T_{17} °C	T_{18} °C	T_{wi} °C	T_{wo} °C	ROT. READ	H_w mm H_2O	ROT. READ	H_a mm H_2O	T_a °C	P_a mm Hg	P_{at} mm Hg	T_{at} °C
113	289	293	288	8.9	16.8	12.2	103	10.8	17.5	46	78	776	23.5
114	283	284	275	9.2	19.7	12.2	103	10.8	24.9	47	78	776	23.5
115	266	273	275	9.3	22.0	12.3	104	11.1	33.6	48	78	776	24.0
116	258	265	259	9.4	24.2	12.3	105	11.4	49.8	49	78	776	24.0
117	270	275	269	9.4	26.0	12.3	105	12.3	100.6	50	78	776	24.0
118	270	273	268	9.4	26.2	12.4	105	13.0	211.0	50	78	776	24.0
119	270	273	268	9.5	26.2	12.4	105	14.0	360.0	50	78	776	24.0
120	264	266	263	9.5	25.7	12.4	105	14.9	501.0	50	78	776	24.0

CALCULATED RESULTS

READING NUMBER	$\dot{m}$ kg/s	$\dot{M}$ kg/s	T_w °C	T_b °C	Q kW	$\dot{V}_a$ m^3/s x10^3	$\dot{V}_g$ m^3/s x10^3	u_f m/s	U kW/m^2K	h_i kW/m^2K	E_f	h_o kW/m^2K
113	0.067	0.518	16.4	290	1.83	5.22	0.124	0.265	0.461	12.93	0.994	0.159
114	0.067	0.518	19.2	281	2.55	6.22	0.124	0.311	0.674	13.35	0.991	0.238
115	0.068	0.520	21.4	272	3.22	7.22	0.126	0.354	0.888	13.75	0.988	0.319
116	0.068	0.523	23.4	261	3.82	8.77	0.128	0.422	1.110	14.11	0.984	0.407
117	0.068	0.523	25.1	271	4.33	12.45	0.136	0.610	1.216	14.37	0.982	0.450
118	0.069	0.523	25.3	270	4.45	18.03	0.142	0.882	1.258	14.41	0.982	0.467
119	0.069	0.523	25.3	270	4.43	23.55	0.150	1.152	1.250	14.41	0.982	0.464
120	0.069	0.523	24.8	264	4.28	27.78	0.157	1.344	1.237	14.34	0.982	0.459

TEST NUMBER 34

Crimped Radial Fin Surface Results

Tests 35 - 42

TEST NUMBER 35

SURFACE: C/1/CR TEST BED: Mk 3 POSITION: Placed directly on distributor plate

BED MATERIAL: Zircon sand, size range 63 - 210 μm; static height 26 mm

OBSERVED RESULTS

READING NUMBER	BED			WATER				GAS	AIR			AMBIENT	
	T_{16} °C	T_{17} °C	T_{18} °C	T_{wi} °C	T_{wo} °C	ROT. READ	H_w mm H_2O	ROT. READ	H_a mm H_2O	T_a °C	P_a mm Hg	P_{at} mm Hg	T_{at} °C
121	130	130	132	20.2	27.0	10.6	45	9.5	6.0	42	78	781	23.0
122	138	140	142	20.2	29.5	10.7	44	10.2	8.7	44	78	781	25.0
123	140	144	144	20.1	31.6	10.8	42	11.0	12.0	44	78	781	25.0
124	140	141	142	20.0	33.6	11.0	41	11.7	15.0	46	78	781	25.0
125	152	152	154	20.0	35.2	11.0	40	12.4	18.5	46	78	781	25.0
126	166	168	170	20.0	37.3	11.0	40	13.4	24.7	47	78	781	25.0
127	180	186	188	20.0	39.8	11.1	40	14.6	35.1	48	78	781	25.0
128	192	198	202	20.0	41.6	11.2	39	14.7	50.3	49	78	781	25.0
129	204	210	212	20.0	42.8	11.2	39	14.6	70.2	50	78	781	25.0
130	210	216	218	20.0	43.4	11.3	39	14.6	93.0	50	78	781	26.0

CALCULATED RESULTS

READING NUMBER	$\dot{m}$ kg/s	$\dot{M}$ kg/s	T_w °C	T_b °C	Q kW	$\dot{V}_a$ m^3/s x10^3	$\dot{V}_g$ m^3/s x10^3	u_f m/s	U kW/m^2K	h_i kW/m^2K	E_f	h_o kW/m^2K
121	0.060	0.342	26.6	131	1.32	3.09	0.114	0.112	1.315	28.25	0.904	0.145
122	0.061	0.338	28.9	140	1.98	3.71	0.119	0.138	1.860	28.76	0.862	0.220
123	0.061	0.331	30.8	143	2.54	4.35	0.125	0.163	2.364	28.85	0.823	0.299
124	0.062	0.327	32.6	141	3.13	4.85	0.131	0.181	3.018	29.19	0.770	0.419
125	0.062	0.323	34.1	153	3.55	5.39	0.137	0.207	3.113	29.35	0.762	0.438
126	0.062	0.323	36.0	168	4.09	6.21	0.145	0.247	3.236	29.88	0.753	0.462
127	0.063	0.323	38.3	185	4.82	7.40	0.154	0.305	3.431	30.56	0.737	0.502
128	0.063	0.319	39.9	197	5.30	8.84	0.156	0.374	3.519	30.74	0.730	0.521
129	0.063	0.319	41.0	209	5.61	10.43	0.154	0.453	3.487	31.04	0.733	0.513
130	0.064	0.319	41.6	215	5.89	12.00	0.154	0.528	3.531	31.24	0.730	0.522

TEST NUMBER 36

SURFACE: C/2/CR TEST BED: Mk 3 POSITION: Placed directly on distributor plate

BED MATERIAL: Zircon sand, size range 63 - 210 μm; static height 31 mm

OBSERVED RESULTS

READING NUMBER	BED			WATER				GAS	AIR			AMBIENT	
	T_{16} °C	T_{17} °C	T_{18} °C	T_{wi} °C	T_{wo} °C	ROT. READ	H_w mm H_2O	ROT. READ	H_a mm H_2O	T_a °C	P_a mm Hg	P_{at} mm Hg	T_{at} °C
131	134	138	132	23.3	31.5	8.9	87	10.0	7.0	41	78	776	22.5
132	124	126	122	24.9	35.6	8.9	89	10.7	9.0	42	78	776	23.0
133	127	128	122	25.6	38.4	8.9	90	11.1	12.0	44	78	776	24.0
134	128	132	133	27.9	43.0	9.0	90	12.1	15.1	45	78	776	24.0
135	140	140	134	22.5	41.9	9.0	90	13.1	18.2	46	78	776	25.0
136	152	152	144	21.3	42.9	9.4	90	14.0	25.2	47	78	776	25.0
137	166	166	158	20.5	44.6	9.4	90	15.0	34.7	48	78	776	25.5
138	180	180	172	20.2	47.0	9.4	90	15.0	51.0	49	78	776	25.5
139	188	188	180	20.0	48.5	9.4	90	15.0	70.6	49	78	776	25.5
140	194	196	188	20.0	49.5	9.3	91	15.0	98.0	50	78	776	26.0
141	200	202	196	20.0	50.2	9.4	90	15.0	153.0	50	78	776	26.0

CALCULATED RESULTS

READING NUMBER	$\dot{m}$ kg/s	$\dot{M}$ kg/s	T_w °C	T_b °C	Q kW	$\dot{V}_a$ m^3/s x10^3	$\dot{V}_g$ m^3/s x10^3	u_f m/s	U kW/m^2K	h_i kW/m^2K	E_f	h_o kW/m^2K
131	0.053	0.476	31.2	135	1.43	3.33	0.117	0.122	0.949	13.98	0.944	0.091
132	0.053	0.481	35.2	124	1.98	3.77	0.123	0.135	1.540	14.64	0.906	0.160
133	0.053	0.484	37.9	126	2.45	4.34	0.127	0.156	1.917	15.06	0.880	0.211
134	0.054	0.484	42.3	131	3.02	4.86	0.134	0.177	2.352	15.68	0.850	0.275
135	0.054	0.484	41.0	138	3.99	5.33	0.142	0.197	2.842	15.51	0.812	0.363
136	0.055	0.484	41.9	150	4.58	6.26	0.150	0.239	2.924	15.65	0.806	0.378
137	0.055	0.484	43.5	164	5.15	7.33	0.157	0.289	2.953	15.86	0.804	0.382
138	0.055	0.484	45.7	178	5.77	8.88	0.157	0.361	3.015	16.16	0.800	0.392
139	0.055	0.484	47.1	186	6.16	10.44	0.157	0.432	3.067	16.34	0.797	0.401
140	0.055	0.487	48.1	193	6.39	12.28	0.157	0.516	3.049	16.53	0.799	0.396
141	0.055	0.484	48.8	200	6.55	15.35	0.157	0.654	2.994	16.55	0.803	0.385

TEST NUMBER 37

SURFACE: C/2/CR TEST BED: Mk 3 POSITION: Placed directly on distributor plate

BED MATERIAL: Silica sand, size range 90 – 355 μm; static height 31 mm

OBSERVED RESULTS

READING NUMBER	BED			WATER				GAS	AIR			AMBIENT	
	T_{16} °C	T_{17} °C	T_{18} °C	T_{wi} °C	T_{wo} °C	ROT. READ	H_w mm H_2O	ROT. READ	H_a mm H_2O	T_a °C	P_a mm Hg	P_{at} mm Hg	T_{at} °C
142	177	180	178	11.0	19.2	9.3	94.0	10.0	6.9	40	78	775	18.0
143	196	200	200	10.6	20.0	9.3	94.0	10.7	9.0	40	78	775	18.0
144	200	200	202	10.3	22.0	9.3	94.0	10.9	11.1	40	78	775	21.0
145	180	180	180	10.1	26.0	9.3	95.0	12.1	15.2	42	78	775	21.0
146	168	168	168	10.3	29.5	9.2	95.0	13.1	18.1	45	78	775	22.0
147	168	168	160	10.3	33.2	9.2	94.0	14.2	24.9	46	78	775	22.0
148	185	186	176	10.2	36.2	9.1	94.0	15.2	35.1	47	78	775	22.5
149	200	202	192	10.2	38.8	8.9	94.0	15.2	49.8	48	78	775	23.0
150	214	212	204	10.0	40.2	8.8	94.0	15.1	70.6	49	77	775	23.0
151	214	223	214	9.8	41.0	8.8	94.0	15.2	100.8	50	77	775	23.5

CALCULATED RESULTS

READING NUMBER	$\dot{m}$ kg/s	$\dot{M}$ kg/s	T_w °C	T_b °C	Q kW	$\dot{V}^a$ m^3/s x10^3	$\dot{V}^g$ m^3/s x10^3	u_f m/s	U kW/m^2K	h_i kW/m^2K	E_f	h_{o_2} kW/m^2K
142	0.054	0.495	18.9	179	1.46	3.31	0.117	0.135	0.631	12.64	0.964	0.058
143	0.054	0.495	19.6	199	1.73	3.78	0.123	0.161	0.668	12.75	0.961	0.062
144	0.054	0.495	21.5	201	2.25	4.20	0.125	0.179	0.867	13.03	0.949	0.082
145	0.054	0.497	25.3	180	3.20	4.90	0.134	0.200	1.429	13.62	0.913	0.148
146	0.053	0.497	28.7	168	3.86	5.32	0.142	0.211	1.915	14.08	0.879	0.213
147	0.053	0.495	32.2	166	4.68	6.23	0.151	0.246	2.418	14.52	0.843	0.292
148	0.053	0.495	35.0	182	5.37	7.38	0.159	0.303	2.524	14.91	0.835	0.308
149	0.052	0.495	37.5	198	5.82	8.78	0.159	0.373	2.508	15.23	0.837	0.304
150	0.051	0.495	38.9	210	6.05	10.43	0.158	0.454	2.442	15.40	0.843	0.291
151	0.051	0.495	39.6	220	6.26	12.44	0.159	0.553	2.398	15.50	0.846	0.284

TEST NUMBER 38

SURFACE: C/2/CR TEST BED: Mk 3 POSITION: Placed directly on distributor plate

BED MATERIAL: Steel shot, size range 75 – 500 μm; static height 31 mm

OBSERVED RESULTS

READING NUMBER	BED			WATER				GAS	AIR			AMBIENT	
	T_{16} °C	T_{17} °C	T_{18} °C	T_{wi} °C	T_{wo} °C	ROT. READ	H_w mm H_2O	ROT. READ	H_a mm H_2O	T_a °C	P_a mm Hg	P_{at} mm Hg	T_{at} °C
152	264	260	262	13.7	23.0	9.1	93	9.0	14.7	43	78	773	22.5
153	252	240	240	11.6	23.2	9.1	92	10.1	17.8	46	77	773	23.5
154	224	224	220	11.2	26.3	9.1	92	12.0	24.0	47	77	773	24.0
155	216	216	212	11.0	30.0	9.1	93	13.0	35.0	48	77	773	23.5
156	202	216	204	11.0	34.4	9.1	92	13.9	49.9	50	77	773	23.5
157	200	204	204	11.0	38.0	9.1	93	14.4	75.4	50	77	773	24.0
158	202	204	206	11.0	40.2	9.1	93	14.7	100.8	51	77	773	24.0
159	204	196	196	10.3	40.8	9.1	93	14.6	155.0	51	77	773	24.0
160	204	196	196	9.7	40.3	9.1	93	14.6	204.0	51	77	773	24.0
161	206	198	198	9.5	41.0	9.1	93	14.6	303.0	51	78	773	24.0
162	208	202	200	9.5	41.0	9.1	94	15.3	407.0	50	78	773	24.0
163	208	200	202	9.4	40.9	9.1	94	15.7	501.0	50	78	773	24.0

CALCULATED RESULTS

READING NUMBER	$\dot{m}$ kg/s	$\dot{M}$ kg/s	T_w °C	T_b °C	Q kW	$\dot{V}^a$ m^3/s x10^3	$\dot{V}^g$ m^3/s x10^3	u_f m/s	U kW/m^2K	h_i kW/m^2K	E_f	h_{o_2} kW/m^2K
152	0.054	0.492	22.6	262	1.71	4.80	0.112	0.232	0.494	13.13	0.972	0.044
153	0.054	0.489	22.7	244	2.23	5.26	0.118	0.245	0.696	13.10	0.960	0.064
154	0.054	0.489	25.6	223	3.02	6.09	0.133	0.272	1.057	13.51	0.937	0.103
155	0.054	0.492	29.2	215	3.90	7.35	0.141	0.323	1.449	14.06	0.912	0.149
156	0.054	0.489	33.3	210	4.89	8.75	0.148	0.381	1.913	14.58	0.880	0.211
157	0.054	0.492	36.8	203	5.70	10.75	0.153	0.461	2.370	15.11	0.847	0.281
158	0.054	0.492	38.8	204	6.20	12.41	0.156	0.533	2.594	15.40	0.831	0.318
159	0.054	0.492	39.4	198	6.49	15.39	0.155	0.653	2.829	15.47	0.813	0.361
160	0.054	0.492	38.9	198	6.52	17.66	0.155	0.749	2.830	15.40	0.813	0.362
161	0.054	0.492	39.5	202	6.72	21.53	0.155	0.922	2.858	15.49	0.811	0.366
162	0.054	0.495	39.5	204	6.72	24.99	0.160	1.074	2.823	15.55	0.814	0.359
163	0.054	0.495	39.4	204	6.72	27.73	0.164	1.192	2.821	15.54	0.814	0.359

TEST NUMBER 39

SURFACE: C/3/CR TEST BED: Mk 3 POSITION: Placed directly on distributor plate

BED MATERIAL: Zircon sand, size range 63 - 210 μm; static height 38 mm

OBSERVED RESULTS

READING NUMBER	BED			WATER				GAS	AIR			AMBIENT	
	T_{16} °C	T_{17} °C	T_{18} °C	T_{wi} °C	T_{wo} °C	ROT. READ	H_w mm H_2O	ROT. READ	H_a mm H_2O	T_a °C	P_a mm Hg	P_{at} mm Hg	T_{at} °C
164	118	122	119	19.9	27.8	9.7	110	9.2	6.9	45	77	761	20.0
165	112	116	114	19.4	30.0	9.7	110	10.3	9.1	47	77	761	21.0
166	112	114	112	19.1	32.2	9.8	111	11.0	11.9	47	76	761	21.0
167	120	120	114	19.1	35.0	9.7	111	12.1	15.2	48	76	761	21.0
168	128	129	122	19.1	37.0	9.5	112	13.0	18.0	43	76	761	21.0
169	142	144	136	19.1	39.8	9.5	114	14.2	25.0	44	76	761	21.0
170	158	156	150	19.1	42.8	9.5	114	15.0	35.2	44	77	762	22.0
171	168	172	164	19.1	45.4	9.4	114	15.0	50.3	44	77	762	22.0
172	180	182	176	19.1	47.6	9.4	114	15.0	75.6	44	76	763	23.0
173	186	188	182	19.1	48.0	9.6	114	15.0	101.0	44	77	763	23.0
174	192	196	190	19.1	48.8	9.7	114	15.0	153.0	48	77	763	23.0

CALCULATED RESULTS

READING NUMBER	$\dot{m}$ kg/s	$\dot{M}$ kg/s	T_w °C	T_b °C	Q kW	$\dot{V}_a$ m^3/s x10^3	$\dot{V}_g$ m^3/s x10^3	u_f m/s	U kW/m^2K	h_i kW/m^2K	E_f	h_o kW/m^2K
164	0.056	0.535	27.5	120	1.46	3.25	0.112	0.115	0.748	7.32	0.954	0.081
165	0.056	0.535	29.6	114	2.09	3.73	0.120	0.130	1.174	7.48	0.923	0.142
166	0.057	0.537	31.7	113	2.73	4.26	0.125	0.148	1.592	7.67	0.888	0.213
167	0.056	0.537	34.3	118	3.33	4.80	0.134	0.169	1.888	7.85	0.862	0.273
168	0.056	0.540	36.2	127	3.80	5.27	0.142	0.190	1.985	8.02	0.854	0.292
169	0.056	0.545	38.9	141	4.45	6.20	0.151	0.231	2.070	8.27	0.847	0.308
170	0.056	0.545	41.8	155	5.16	7.37	0.157	0.284	2.160	8.48	0.840	0.327
171	0.055	0.545	44.3	168	5.66	8.81	0.157	0.350	2.168	8.64	0.840	0.326
172	0.055	0.545	46.4	179	6.16	10.80	0.157	0.440	2.204	8.79	0.838	0.332
173	0.056	0.545	46.7	185	6.38	12.49	0.157	0.515	2.187	8.83	0.840	0.327
174	0.056	0.545	47.5	193	6.56	15.27	0.157	0.641	2.139	8.89	0.844	0.315

TEST NUMBER 40

SURFACE: C/4/CR TEST BED: Mk 3 POSITION: Placed directly on distributor plate

BED MATERIAL: Zircon sand, size range 63 - 210 μm; static height 44 mm

OBSERVED RESULTS

READING NUMBER	BED			WATER				GAS	AIR			AMBIENT	
	T_{16} °C	T_{17} °C	T_{18} °C	T_{wi} °C	T_{wo} °C	ROT. READ	H_w mm H_2O	ROT. READ	H_a mm H_2O	T_a °C	P_a mm Hg	P_{at} mm Hg	T_{at} °C
175	120	120	115	19.8	26.6	11.7	163	9.5	6.0	39	77	764	20.0
176	108	106	106	19.3	29.2	11.9	163	10.0	9.0	41	77	764	20.5
177	110	112	109	19.1	31.0	11.9	164	11.3	12.0	43	77	764	21.0
178	112	114	110	19.0	33.3	12.0	164	12.0	15.0	45	77	764	22.5
179	120	120	116	19.0	35.0	12.0	164	13.0	18.0	46	77	764	23.0
180	134	134	128	19.0	37.4	12.0	164	14.0	25.1	47	77	764	23.5
181	162	162	156	19.3	42.3	11.9	143	14.9	49.8	48	77	764	24.0
182	172	172	164	19.0	44.0	11.9	142	14.8	74.2	49	77	764	24.0
183	176	176	172	19.0	45.0	12.0	142	14.8	99.0	49	77	764	24.0
184	184	184	179	19.0	45.8	11.9	143	14.8	153.0	50	77	764	24.0

CALCULATED RESULTS

READING NUMBER	$\dot{m}$ kg/s	$\dot{M}$ kg/s	T_w °C	T_b °C	Q kW	$\dot{V}_a$ m^3/s x10^3	$\dot{V}_g$ m^3/s x10^3	u_f m/s	U kW/m^2K	h_i kW/m^2K	E_f	h_o kW/m^2K
175	0.065	0.651	26.4	118	1.46	3.07	0.114	0.108	0.593	5.29	0.963	0.068
176	0.066	0.651	28.8	107	2.34	3.75	0.117	0.128	1.115	5.43	0.922	0.151
177	0.066	0.653	30.5	110	2.89	4.31	0.128	0.149	1.356	5.53	0.900	0.198
178	0.067	0.653	32.7	112	3.61	4.81	0.133	0.167	1.698	5.66	0.865	0.281
179	0.067	0.653	34.3	119	4.09	5.26	0.142	0.186	1.800	5.74	0.854	0.307
180	0.067	0.653	36.6	132	4.76	6.20	0.150	0.226	1.860	5.86	0.848	0.321
181	0.066	0.610	41.3	160	5.95	8.72	0.157	0.340	1.869	5.81	0.847	0.326
182	0.066	0.608	42.8	170	6.51	10.62	0.156	0.424	1.907	5.87	0.843	0.336
183	0.067	0.608	43.8	175	6.89	12.27	0.156	0.495	1.957	5.93	0.838	0.350
184	0.066	0.610	44.6	182	7.00	15.23	0.156	0.625	1.899	5.97	0.845	0.330

TEST NUMBER 41

SURFACE: C/5/CR TEST BED: Mk 3 POSITION: Lower fin tip edge 1 mm above distributor plate

BED MATERIAL: Zircon sand, size range 63 – 210 μm; static height 31 mm

OBSERVED RESULTS

READING NUMBER	BED			WATER				GAS	AIR			AMBIENT	
	T_{16} °C	T_{17} °C	T_{18} °C	T_{wi} °C	T_{wo} °C	ROT. READ	H_w mm H_2O	ROT. READ	H_a mm H_2O	T_a °C	P_a mm Hg	P_{at} mm Hg	T_{at} °C
185	116	120	122	13.5	22.8	9.1	88	8.9	5.5	40	76	764	22.0
186	127	127	132	11.4	23.2	9.1	88	10.2	8.9	42	76	764	22.5
187	135	141	135	10.8	24.7	9.1	88	11.0	11.8	44	76	764	22.5
188	143	145	150	10.6	26.3	9.2	89	12.0	15.0	45	76	764	22.5
189	150	153	160	10.5	27.6	9.2	89	12.6	18.0	46	76	764	23.0
190	167	170	177	10.0	29.8	9.2	89	13.2	24.9	47	76	764	23.0
191	185	189	196	9.4	31.7	9.2	90	14.4	35.0	47	76	764	23.0
192	203	205	213	9.3	33.8	9.2	90	14.8	49.7	48	76	764	23.0
193	218	220	230	9.1	35.6	9.2	90	14.8	75.6	49	76	764	23.0
194	226	224	234	8.5	35.0	9.2	91	14.8	100.6	49	77	764	23.0

CALCULATED RESULTS

READING NUMBER	$\dot{m}$ kg/s	$\dot{M}$ kg/s	T_w °C	T_b °C	Q kW	$\dot{V}_a$ m^3/s x10^3	$\dot{V}_g$ m^3/s x10^3	u_f m/s	U kW/m^2K	h_i kW/m^2K	E_f	h_o kW/m^2K
185	0.054	0.478	22.4	120	1.71	2.93	0.109	0.104	1.219	13.02	0.883	0.267
186	0.054	0.478	22.7	129	2.27	3.72	0.119	0.135	1.488	13.06	0.855	0.344
187	0.054	0.478	24.1	137	2.75	4.27	0.125	0.156	1.693	13.25	0.834	0.407
188	0.054	0.481	25.6	146	3.15	4.80	0.133	0.181	1.822	13.52	0.820	0.447
189	0.054	0.481	26.8	154	3.47	5.25	0.138	0.202	1.898	13.69	0.812	0.472
190	0.054	0.481	28.9	171	4.08	6.17	0.143	0.247	1.996	13.98	0.802	0.504
191	0.054	0.484	30.7	190	4.64	7.32	0.153	0.305	2.027	14.29	0.800	0.513
192	0.054	0.484	32.7	207	5.14	8.70	0.157	0.376	2.050	14.57	0.798	0.519
193	0.054	0.484	34.4	223	5.59	10.72	0.157	0.479	2.061	14.80	0.797	0.521
194	0.054	0.487	33.8	228	5.59	12.37	0.157	0.559	2.002	14.78	0.804	0.500

TEST NUMBER 42

SURFACE: C/5/CR TEST BED: Mk 3 POSITION: Lower fin tip edge 1 mm above distributor plate

BED MATERIAL: Steel shot, size range 75 – 500 μm; static height 31 mm

OBSERVED RESULTS

READING NUMBER	BED			WATER				GAS	AIR			AMBIENT	
	T_{16} °C	T_{17} °C	T_{18} °C	T_{wi} °C	T_{wo} °C	ROT. READ	H_w mm H_2O	ROT. READ	H_a mm H_2O	T_a °C	P_a mm Hg	P_{at} mm Hg	T_{at} °C
195	240	246	238	14.4	23.0	9.5	92	8.8	15.2	39	77	755	17.5
196	248	248	248	11.9	22.0	9.6	92	9.6	18.4	40	77	755	17.5
197	235	230	225	11.0	23.7	9.5	92	10.4	25.1	42	77	755	17.5
198	235	220	221	10.6	26.2	9.5	92	11.9	34.7	42	77	755	17.5
199	229	220	222	10.4	29.9	9.5	93	13.2	49.9	44	77	755	17.5
200	240	232	233	10.3	32.3	9.5	93	14.0	75.8	45	77	755	18.5
201	250	242	243	10.2	34.1	9.6	93	14.9	99.2	46	77	755	19.0
202	261	255	253	10.1	35.2	9.6	93	15.5	157.0	47	77	755	19.0
203	265	257	258	10.1	35.3	9.6	94	15.7	202.0	47	77	755	19.0
204	264	257	258	10.2	35.2	9.7	95	15.8	311.0	47	77	755	19.0
205	257	252	250	10.2	34.4	9.7	95	15.8	410.0	47	77	755	19.0
206	251	246	244	10.1	33.6	9.7	95	15.8	509.0	46	77	755	19.0

CALCULATED RESULTS

READING NUMBER	$\dot{m}$ kg/s	$\dot{M}$ kg/s	T_w °C	T_b °C	Q kW	$\dot{V}_a$ m^3/s x10^3	$\dot{V}_g$ m^3/s x10^3	u_f m/s	U kW/m^2K	h_i kW/m^2K	E_f	h_o kW/m^2K
195	0.056	0.489	22.6	242	1.62	4.86	0.108	0.225	0.515	13.30	0.953	0.099
196	0.056	0.489	21.6	248	1.98	5.34	0.114	0.251	0.607	13.14	0.944	0.119
197	0.056	0.489	23.1	230	2.58	6.21	0.121	0.282	0.869	13.37	0.918	0.178
198	0.056	0.489	25.5	225	3.26	7.31	0.133	0.328	1.137	13.71	0.892	0.244
199	0.056	0.492	29.0	224	4.17	8.73	0.143	0.391	1.489	14.26	0.857	0.339
200	0.056	0.492	31.3	235	4.76	10.75	0.150	0.492	1.625	14.59	0.843	0.379
201	0.056	0.492	33.0	245	5.20	12.28	0.157	0.573	1.707	14.83	0.835	0.403
202	0.056	0.492	34.0	256	5.48	15.42	0.162	0.735	1.718	14.97	0.834	0.406
203	0.056	0.495	34.1	260	5.51	17.49	0.164	0.840	1.696	15.05	0.836	0.398
204	0.056	0.497	34.0	260	5.46	21.70	0.164	1.042	1.681	15.09	0.838	0.394
205	0.056	0.497	33.3	253	5.27	24.92	0.164	1.181	1.669	14.98	0.839	0.391
206	0.056	0.497	32.5	247	5.11	27.81	0.164	1.303	1.657	14.88	0.840	0.387

Extruded Surface Results

Tests 43 - 52

TEST NUMBER 43

SURFACE: C/1/ER TEST BED: Mk 1 POSITION: Placed directly on distributor plate
BED MATERIAL: Zircon sand, size range 63 – 210 μm; static height 50 mm

OBSERVED RESULTS

READING NUMBER	BED			WATER				GAS	AIR			AMBIENT	
	T_{16} °C	T_{17} °C	T_{18} °C	T_{wi} °C	T_{wo} °C	ROT. READ	H_w mm H_2O	ROT. READ	H_a mm H_2O	T_a °C	P_a mm Hg	P_{at} mm Hg	T_{at} °C
207	189	186	190	9.3	25.6	22.0	103	20.4	48	49	78	767	30.0
208	201	198	200	9.3	28.5	22.2	103	23.1	101	49	79	767	30.0
209	206	201	205	9.3	29.4	22.3	103	24.6	150	49	78	767	30.0
210	214	208	211	9.3	30.9	22.4	105	27.5	251	49	77	767	30.5
211	220	215	218	9.3	31.8	22.5	105	30.1	352	49	77	767	30.5
212	219	213	215	9.2	31.8	22.5	105	31.2	504	49	75	767	31.0

CALCULATED RESULTS

READING NUMBER	$\dot{m}$ kg/s	$\dot{M}$ kg/s	T_w °C	T_b °C	Q kW	$\dot{V}_a$ m^3/s	$\dot{V}_g$ m^3/s $\times 10^3$	u_f m/s $\times 10^3$	U kW/m^2K	h_i kW/m^2K	E_f	h_o kW/m^2K
207	0.111	0.518	24.2	188	7.17	19.97	0.203	0.143	2.146	11.47	0.846	0.426
208	0.111	0.518	26.9	200	8.52	28.98	0.226	0.214	2.410	11.79	0.823	0.503
209	0.112	0.518	27.7	204	9.02	35.29	0.239	0.262	2.506	11.90	0.815	0.532
210	0.113	0.523	29.1	211	9.81	45.63	0.265	0.344	2.641	12.16	0.804	0.574
211	0.113	0.523	29.9	218	10.23	54.04	0.289	0.413	2.665	12.26	0.802	0.581
212	0.113	0.523	29.9	216	10.28	64.58	0.300	0.492	2.706	12.26	0.798	0.595

TEST NUMBER 44

SURFACE: C/2/ER TEST BED: Mk 1 POSITION: Placed directly on distributor plate
BED MATERIAL: Zircon sand, size range 63 - 210 μm; static height 50 mm

OBSERVED RESULTS

READING NUMBER	BED			WATER				GAS	AIR			AMBIENT	
	T_{16} °C	T_{17} °C	T_{18} °C	T_{wi} °C	T_{wo} °C	ROT. READ	H_w mm H_2O	ROT. READ	H_a mm H_2O	T_a °C	P_a mm Hg	P_{at} mm Hg	T_{at} °C
213	231	225	229	7.5	22.6	17.8	125	20.5	50	49	76	742	25.0
214	238	235	236	7.6	25.0	17.9	125	23.0	99	49	75	742	26.0
215	242	240	240	7.6	26.0	18.0	125	24.5	150	49	75	741	27.0
216	245	244	243	7.8	27.4	18.0	125	27.5	251	49	74	741	28.0
217	250	249	248	7.9	28.2	18.0	125	30.0	350	49	73	741	29.0
218	242	242	241	8.0	28.0	18.0	125	31.2	500	49	71	741	30.0

CALCULATED RESULTS

READING NUMBER	$\dot{m}$ kg/s	$\dot{M}$ kg/s	T_w °C	T_b °C	Q kW	$\dot{V}_a$ m^3/s	$\dot{V}_g$ m^3/s $\times 10^3$	u_f m/s $\times 10^3$	U kW/m^2K	h_i kW/m^2K	E_f	h_o kW/m^2K
213	0.091	0.570	21.6	228	5.36	20.05	0.204	0.157	1.603	15.64	0.971	0.462
214	0.092	0.570	23.9	236	6.30	28.19	0.226	0.224	1.835	16.04	0.966	0.539
215	0.093	0.570	24.8	241	6.76	34.68	0.238	0.278	1.932	16.22	0.964	0.573
216	0.093	0.570	26.1	244	7.23	44.84	0.265	0.361	2.049	16.44	0.961	0.613
217	0.093	0.570	26.9	249	7.50	52.92	0.288	0.430	2.085	16.57	0.961	0.626
218	0.093	0.570	26.7	242	7.38	63.17	0.300	0.507	2.118	16.54	0.960	0.638

TEST NUMBER 45

SURFACE: C/3/ER TEST BED: Mk 1 POSITION: Placed directly on distributor plate
BED MATERIAL: Zircon sand, size range 63 - 210 μm; static height 50 mm

OBSERVED RESULTS

READING NUMBER	BED			WATER				GAS	AIR			AMBIENT	
	T_{16} °C	T_{17} °C	T_{18} °C	T_{wi} °C	T_{wo} °C	ROT. READ	H_w mm H_2O	ROT. READ	H_a mm H_2O	T_a °C	P_a mm Hg	P_{at} mm Hg	T_{at} °C
219	265	262	260	8.0	21.8	14.2	148	18.6	50	49	76	741	29.0
220	262	259	259	7.9	24.8	14.0	130	20.8	100	49	76	741	28.5
221	263	260	258	7.9	25.7	14.0	130	22.3	150	49	76	740	29.0
222	265	263	261	7.9	26.9	14.0	130	25.5	251	49	75	740	29.0
223	262	263	260	8.0	27.6	14.0	130	28.0	350	49	73	740	29.0
224	259	260	255	8.0	28.0	14.1	130	30.0	503	49	72	740	29.0

CALCULATED RESULTS

READING NUMBER	$\dot{m}$ kg/s	$\dot{M}$ kg/s	T_w °C	T_b °C	Q kW	$\dot{V}_a$ m^3/s x10^3	$\dot{V}_g$ m^3/s x10^3	u_f m/s	U kW/m^2K	h_i kW/m^2K	E_f	h_o kW/m^2K
219	0.075	0.620	21.1	262	3.94	20.04	0.188	0.167	0.982	16.19	0.996	0.367
220	0.075	0.582	23.9	260	4.91	28.34	0.207	0.235	1.249	15.94	0.995	0.479
221	0.075	0.582	24.8	260	5.19	34.68	0.219	0.288	1.326	16.08	0.994	0.511
222	0.075	0.582	25.9	263	5.57	44.84	0.248	0.374	1.410	16.27	0.994	0.547
223	0.075	0.582	26.6	262	5.75	52.88	0.270	0.441	1.468	16.38	0.994	0.572
224	0.075	0.582	26.9	258	5.88	63.36	0.288	0.524	1.529	16.45	0.993	0.598

TEST NUMBER 46

SURFACE: C/3/ER TEST BED: Mk 1 POSITION: Lower fin tip edge 25 mm above distributor
BED MATERIAL: Zircon sand, size range 63 - 210 μm; static height 50 mm

OBSERVED RESULTS

READING NUMBER	BED			WATER				GAS	AIR			AMBIENT	
	T_{16} °C	T_{17} °C	T_{18} °C	T_{wi} °C	T_{wo} °C	ROT. READ	H_w mm H_2O	ROT. READ	H_a mm H_2O	T_a °C	P_a mm Hg	P_{at} mm Hg	T_{at} °C
225	246	245	243	7.9	21.6	13.9	130	18.6	50	49	76	740	29.0
226	262	261	258	8.0	25.0	14.0	130	20.9	98	49	76	740	29.0
227	263	264	259	7.9	26.1	14.0	130	22.3	150	49	75	740	29.0
228	262	265	259	7.9	27.2	14.1	130	25.5	251	49	74	740	29.0
229	265	265	260	8.0	27.8	14.1	130	28.1	352	49	73	740	29.5
230	258	260	255	8.1	28.2	14.2	130	30.1	505	49	72	740	29.0

CALCULATED RESULTS

READING NUMBER	$\dot{m}$ kg/s	$\dot{M}$ kg/s	T_w °C	T_b °C	Q kW	$\dot{V}_a$ m^3/s x10^3	$\dot{V}_g$ m^3/s x10^3	u_f m/s	U kW/m^2K	h_i kW/m^2K	E_f	h_o kW/m^2K
225	0.074	0.582	20.9	245	3.85	20.02	0.188	0.162	1.032	15.40	0.996	0.389
226	0.075	0.582	24.1	260	4.94	28.03	0.208	0.233	1.258	15.97	0.995	0.482
227	0.075	0.582	25.1	262	5.32	34.66	0.219	0.289	1.348	16.14	0.994	0.520
228	0.075	0.582	26.2	262	5.66	44.81	0.248	0.374	1.442	16.32	0.994	0.561
229	0.075	0.582	26.7	263	5.82	53.03	0.271	0.443	1.479	16.42	0.994	0.577
230	0.075	0.582	27.1	258	5.91	63.48	0.289	0.525	1.538	16.48	0.993	0.602

TEST NUMBER 47

SURFACE: C/4/ER TEST BED: Mk 1 POSITION: Placed directly on distributor plate
BED MATERIAL: Zircon sand, size range 63 - 210 μm; static height 50 mm

OBSERVED RESULTS

READING NUMBER	BED			WATER				GAS	AIR			AMBIENT	
	T_{16} °C	T_{17} °C	T_{18} °C	T_{wi} °C	T_{wo} °C	ROT. READ	H_w mm H_2O	ROT. READ	H_a mm H_2O	T_a °C	P_a mm Hg	P_{at} mm Hg	T_{at} °C
231	239	235	237	7.8	21.9	15.0	88	18.6	50	49	77	752	25.0
232	245	245	245	7.9	24.9	15.1	88	21.0	99	49	76	752	26.0
233	245	245	245	7.8	26.0	15.1	89	22.5	150	49	76	752	27.0
234	246	245	246	7.8	27.3	15.1	89	25.5	253	49	75	752	27.0
235	249	248	247	7.8	28.0	15.3	88	28.0	352	49	74	752	28.0
236	249	249	248	7.8	28.6	15.4	88	30.5	499	49	73	752	28.0

CALCULATED RESULTS

READING NUMBER	$\dot{m}$ kg/s	$\dot{M}$ kg/s	T_w °C	T_b °C	Q kW	$\dot{V}^a$ m^3/s x10^3	$\dot{V}^g$ m^3/s x10^3	u_f m/s	U kW/m^2K	h_i kW/m^2K	E_f	h_o kW/m^2K
231	0.079	0.478	21.0	237	4.27	20.18	0.188	0.160	1.512	18.91	0.979	0.406
232	0.080	0.478	23.8	245	5.30	28.38	0.208	0.229	1.831	19.52	0.975	0.502
233	0.080	0.481	24.8	245	5.70	34.94	0.221	0.282	1.979	19.81	0.972	0.548
234	0.080	0.481	26.0	246	6.13	45.35	0.248	0.367	2.131	20.07	0.970	0.597
235	0.081	0.478	26.6	248	6.45	53.46	0.270	0.434	2.228	20.15	0.968	0.628
236	0.081	0.478	27.2	249	6.65	63.61	0.293	0.517	2.293	20.26	0.967	0.649

TEST NUMBER 48

SURFACE: C/5/ER TEST BED: Mk 1 POSITION: Placed directly on distributor plate
BED MATERIAL: Zircon sand, size range 63 - 210 μm; static height 50 mm

OBSERVED RESULTS

READING NUMBER	BED			WATER				GAS	AIR			AMBIENT	
	T_{16} °C	T_{17} °C	T_{18} °C	T_{wi} °C	T_{wo} °C	ROT. READ	H_w mm H_2O	ROT. READ	H_a mm H_2O	T_a °C	P_a mm Hg	P_{at} mm Hg	T_{at} °C
237	254	250	251	7.9	22.4	13.8	130	18.5	50	49	77	752	28.5
238	262	259	259	7.9	24.6	14.0	131	21.0	100	49	77	752	28.5
239	264	261	260	7.9	25.4	14.0	131	22.5	150	49	77	752	28.5
240	265	265	261	7.9	26.2	14.0	130	25.5	250	49	76	752	28.5
241	265	266	262	7.9	26.8	14.0	131	28.0	351	49	75	752	29.5
242	262	263	260	7.9	26.9	14.1	132	30.5	500	49	72	752	30.0

CALCULATED RESULTS

READING NUMBER	$\dot{m}$ kg/s	$\dot{M}$ kg/s	T_w °C	T_b °C	Q kW	$\dot{V}^a$ m^3/s x10^3	$\dot{V}^g$ m^3/s x10^3	u_f m/s	U kW/m^2K	h_i kW/m^2K	E_f	h_o kW/m^2K
237	0.074	0.582	21.7	252	4.10	20.18	0.187	0.165	1.075	14.53	0.995	0.399
238	0.075	0.584	23.7	260	4.85	28.54	0.208	0.237	1.239	14.91	0.994	0.466
239	0.075	0.584	24.5	262	5.10	34.96	0.221	0.291	1.297	15.03	0.994	0.490
240	0.075	0.582	25.2	264	5.35	45.10	0.248	0.377	1.353	15.11	0.993	0.514
241	0.075	0.584	25.8	265	5.53	53.41	0.270	0.448	1.398	15.24	0.993	0.533
242	0.075	0.586	25.9	262	5.57	63.63	0.293	0.530	1.424	15.30	0.993	0.544

TEST NUMBER 49

SURFACE: C/6/ER TEST BED: Mk 1 POSITION: Placed directly on distributor plate

BED MATERIAL: Zircon sand, size range 63 – 210 μm; static height 50 mm

OBSERVED RESULTS

READING NUMBER	BED			WATER				GAS	AIR			AMBIENT	
	T_{16} °C	T_{17} °C	T_{18} °C	T_{wi} °C	T_{wo} °C	ROT. READ	H_w mm H_2O	ROT. READ	H_a mm H_2O	T_a °C	P_a mm Hg	P_{at} mm Hg	T_{at} °C
243	187	189	188	7.6	25.1	22.1	130	20.5	49	49	77	752	29.0
244	207	202	204	7.5	27.4	22.4	130	23.0	100	49	76	752	29.0
245	207	208	205	7.5	27.9	22.4	130	24.5	146	49	76	752	29.0
246	212	215	212	7.5	29.6	22.5	132	27.5	254	49	75	752	29.0
247	218	219	219	7.5	30.5	22.5	130	30.0	350	49	74	752	29.0
248	218	212	218	7.5	30.8	22.6	130	31.2	502	49	72	752	29.5

CALCULATED RESULTS

READING NUMBER	$\dot{m}$ kg/s	$\dot{M}$ kg/s	T_w °C	T_b °C	Q kW	$\dot{V}_a$ m^3/s x10^3	$\dot{V}_g$ m^3/s x10^3	u_f m/s	U kW/m^2K	h_i kW/m^2K	E_f	h_o kW/m^2K
243	0.111	0.582	23.8	188	7.73	19.98	0.204	0.144	1.582	5.29	0.895	0.445
244	0.113	0.582	25.9	204	9.01	28.53	0.226	0.212	1.700	5.43	0.884	0.496
245	0.113	0.582	26.3	207	9.24	34.47	0.238	0.258	1.720	5.45	0.882	0.505
246	0.113	0.586	27.9	213	10.04	45.44	0.265	0.344	1.824	5.57	0.873	0.553
247	0.113	0.582	28.7	219	10.47	53.30	0.288	0.409	1.849	5.59	0.870	0.566
248	0.113	0.582	29.0	216	10.71	63.76	0.300	0.486	1.925	5.61	0.862	0.608

TEST NUMBER 50

SURFACE: C/7/ER TEST BED: Mk 1 POSITION: Placed directly on distributor plate

BED MATERIAL: Zircon sand, size range 63 – 210 μm; static height 50 mm

OBSERVED RESULTS

READING NUMBER	BED			WATER				GAS	AIR			AMBIENT	
	T_{16} °C	T_{17} °C	T_{18} °C	T_{wi} °C	T_{wo} °C	ROT. READ	H_w mm H_2O	ROT. READ	H_a mm H_2O	T_a °C	P_a mm Hg	P_{at} mm Hg	T_{at} °C
249	200	192	200	7.5	23.9	23.0	125	20.6	50	49	77	752	27.5
250	208	207	205	7.5	26.0	23.1	125	23.0	100	49	77	752	27.0
251	211	214	210	7.4	27.0	23.3	125	24.5	147	49	77	753	27.5
252	218	221	216	7.4	28.6	23.4	125	27.5	253	49	76	754	28.0
253	222	224	221	7.4	29.6	23.4	125	30.0	350	49	75	754	28.0
254	216	220	219	7.3	29.6	23.4	125	31.3	502	49	73	754	28.0

CALCULATED RESULTS

READING NUMBER	$\dot{m}$ kg/s	$\dot{M}$ kg/s	T_w °C	T_b °C	Q kW	$\dot{V}_a$ m^3/s x10^3	$\dot{V}_g$ m^3/s x10^3	u_f m/s	U kW/m^2K	h_i kW/m^2K	E_f	h_o kW/m^2K
249	0.115	0.570	22.6	199	7.49	20.18	0.205	0.148	1.876	8.70	0.886	0.401
250	0.116	0.570	24.5	207	8.58	28.54	0.226	0.213	2.076	8.89	0.870	0.464
251	0.117	0.570	25.4	212	9.19	34.63	0.238	0.262	2.175	8.99	0.862	0.498
252	0.117	0.570	26.9	218	9.97	45.43	0.265	0.347	2.304	9.12	0.852	0.543
253	0.117	0.570	27.8	222	10.46	53.40	0.288	0.411	2.379	9.21	0.846	0.569
254	0.117	0.570	27.8	218	10.51	63.88	0.301	0.488	2.440	9.21	0.841	0.594

TEST NUMBER 51

SURFACE: MS/1/ER TEST BED: Mk 1 POSITION: Placed directly on distributor plate
BED MATERIAL: Zircon sand, size range 63 - 210 μm; static height 50 mm

OBSERVED RESULTS

READING NUMBER	BED			WATER				GAS	AIR			AMBIENT	
	T_{16} °C	T_{17} °C	T_{18} °C	T_{wi} °C	T_{wo} °C	ROT. READ	H_w mm H_2O	ROT. READ	H_a mm H_2O	T_a °C	P_a mm Hg	P_{at} mm Hg	T_{at} °C
255	198	196	195	11.4	25.6	19.8	45	20.5	49	49	78	754	26.0
256	215	213	212	11.5	27.8	19.8	45	23.0	101	49	78	754	26.5
257	221	219	220	11.3	28.8	19.7	45	24.5	151	49	78	754	27.0
258	230	228	229	11.3	29.8	19.7	45	27.5	253	48	77	754	27.0
259	237	236	234	11.4	30.6	19.7	45	30.0	350	47	76	754	27.0
260	233	231	233	11.3	31.2	19.6	45	31.2	503	46	74	754	27.5

CALCULATED RESULTS

READING NUMBER	$\dot{m}$ kg/s	$\dot{M}$ kg/s	T_w °C	T_b °C	Q kW	$\dot{V}_a$ m^3/s x10^3	$\dot{V}_g$ m^3/s x10^3	u_f m/s	U kW/m^2K	h_i kW/m^2K	E_f	h_g kW/m^2K
255	0.100	0.168	23.1	196	5.55	20.02	0.204	0.146	1.377	10.43	0.871	0.424
256	0.100	0.168	24.9	213	6.42	28.74	0.225	0.218	1.466	10.63	0.860	0.466
257	0.100	0.168	25.7	220	6.92	35.14	0.239	0.270	1.529	10.72	0.852	0.497
258	0.100	0.168	26.5	229	7.34	45.53	0.265	0.356	1.556	10.81	0.849	0.510
259	0.100	0.168	27.2	236	7.63	53.60	0.289	0.425	1.569	10.89	0.848	0.516
260	0.099	0.168	26.9	233	7.43	64.28	0.300	0.507	1.547	10.82	0.850	0.505

TEST NUMBER 52

SURFACE: MS/2/ER TEST BED: Mk 1 POSITION: Placed directly on distributor plate
BED MATERIAL: Zircon sand, size range 63 - 210 μm; static height 50 mm

OBSERVED RESULTS

READING NUMBER	BED			WATER				GAS	AIR			AMBIENT	
	T_{16} °C	T_{17} °C	T_{18} °C	T_{wi} °C	T_{wo} °C	ROT. READ	H_w mm H_2O	ROT. READ	H_a mm H_2O	T_a °C	P_a mm Hg	P_{at} mm Hg	T_{at} °C
261	190	188	190	9.2	27.2	14.6	85	20.5	50	49	79	766	24.0
262	210	209	210	9.3	30.8	14.6	85	23.0	101	49	79	766	25.0
263	219	217	219	9.3	32.2	14.6	85	24.5	152	49	78	766	25.5
264	228	227	229	9.4	34.2	14.6	85	27.5	258	49	78	766	26.0
265	236	234	235	9.4	34.6	14.7	85	30.0	350	48	77	766	26.5
266	232	234	234	9.5	35.0	14.8	85	31.2	502	47	75	766	27.0

CALCULATED RESULTS

READING NUMBER	$\dot{m}$ kg/s	$\dot{M}$ kg/s	T_w °C	T_b °C	Q kW	$\dot{V}_a$ m^3/s x10^3	$\dot{V}_g$ m^3/s x10^3	u_f m/s	U kW/m^2K	h_i kW/m^2K	E_f	h_o kW/m^2K
261	0.076	0.470	26.0	189	5.33	20.38	0.204	0.147	0.900	6.43	0.935	0.278
262	0.076	0.470	29.4	210	6.44	28.96	0.226	0.218	0.982	6.65	0.928	0.310
263	0.076	0.470	30.7	218	6.88	35.51	0.238	0.272	1.012	6.74	0.926	0.323
264	0.076	0.470	32.6	228	7.49	46.26	0.265	0.361	1.055	6.86	0.922	0.341
265	0.077	0.470	32.9	235	7.72	53.93	0.289	0.427	1.052	6.89	0.922	0.339
266	0.078	0.470	33.3	234	7.92	64.62	0.300	0.510	1.087	6.93	0.919	0.354

Welded Radial and Spine Results

Tests 53 - 55

TEST NUMBER 53

SURFACE: MS/1/WR TEST BED: Mk 1 POSITION: Placed directly on distributor plate
BED MATERIAL: Zircon sand, size range 63 – 210 μm; static height 50 mm

OBSERVED RESULTS

READING NUMBER	BED			WATER				GAS	AIR			AMBIENT	
	T_{16} °C	T_{17} °C	T_{18} °C	T_{wi} °C	T_{wo} °C	ROT. READ	H_w mm H_2O	ROT. READ	H_a mm H_2O	T_a °C	P_a mm Hg	P_{at} mm Hg	T_{at} °C
267	177	174	176	9.2	26.0	22.0	75	20.5	50	49	79	766	28.0
268	189	186	190	9.1	28.4	22.3	75	23.1	101	49	79	766	28.0
269	194	193	196	9.1	29.2	22.4	90	24.5	149	49	78	766	28.0
270	205	201	206	9.1	30.7	22.5	105	27.5	253	49	77	766	28.0
271	213	209	211	9.0	31.6	22.5	110	30.0	349	49	76	766	28.0
272	215	209	213	9.1	32.1	22.6	105	31.2	504	49	75	766	28.5
273	171	168	169	9.1	24.6	22.2	95	20.6	48	49	79	766	28.0

CALCULATED RESULTS

READING NUMBER	$\dot{m}$ kg/s	$\dot{M}$ kg/s	T_w °C	T_b °C	Q kW	$\dot{V}^a$ m^3/s x10^3	$\dot{V}^g$ m^3/s x10^3	u_f m/s	U kW/m^2K	h_i kW/m^2K	E_f	h_g kW/m^2K
267	0.112	0.442	24.4	176	7.47	20.38	0.204	0.143	1.358	6.67	0.521	0.349
268	0.113	0.442	26.5	188	8.72	28.96	0.227	0.208	1.488	6.83	0.473	0.433
269	0.114	0.484	27.4	194	9.18	35.16	0.238	0.256	1.518	7.32	0.472	0.435
270	0.114	0.523	28.8	204	9.90	45.78	0.265	0.340	1.556	7.81	0.468	0.445
271	0.114	0.535	29.7	211	10.38	53.74	0.289	0.405	1.576	8.00	0.464	0.452
272	0.115	0.523	30.1	212	10.66	64.54	0.300	0.488	1.614	7.92	0.449	0.485
273	0.112	0.497	23.3	170	6.87	19.97	0.205	0.138	1.289	7.11	0.556	0.298

TEST NUMBER 54

SURFACE: MS/2/WR TEST BED: Mk 1 POSITION: Placed directly on distributor plate
BED MATERIAL: Zircon sand, size range 63 – 210 μm; static height 50 mm

OBSERVED RESULTS

READING NUMBER	BED			WATER				GAS	AIR			AMBIENT	
	T_{16} °C	T_{17} °C	T_{18} °C	T_{wi} °C	T_{wo} °C	ROT. READ	H_w mm H_2O	ROT. READ	H_a mm H_2O	T_a °C	P_a mm Hg	P_{at} mm Hg	T_{at} °C
274	210	208	210	9.1	23.0	22.0	75	19.0	48	49	79	766	29.0
275	221	218	220	9.2	24.8	22.0	75	21.6	101	49	79	766	29.0
276	226	222	225	9.2	25.5	22.0	75	23.1	150	49	78	766	29.5
277	232	229	231	9.3	26.4	22.0	75	26.1	252	49	78	766	29.5
278	237	234	235	9.4	26.9	22.1	75	28.5	358	49	77	766	29.5
279	236	232	233	9.4	27.1	22.1	75	30.5	504	49	75	766	29.5

CALCULATED RESULTS

READING NUMBER	$\dot{m}$ kg/s	$\dot{M}$ kg/s	T_w °C	T_b °C	Q kW	$\dot{V}^a$ m^3/s x10^3	$\dot{V}^g$ m^3/s x10^3	u_f m/s	U kW/m^2K	h_i kW/m^2K	E_f	h_{o_2} kW/m^2K
274	0.112	0.442	21.7	209	6.12	19.97	0.192	0.150	0.900	6.48	0.853	0.387
275	0.112	0.442	23.3	220	6.91	28.96	0.213	0.222	0.968	6.59	0.839	0.429
276	0.112	0.442	23.9	224	7.24	35.27	0.226	0.273	0.997	6.64	0.834	0.448
277	0.112	0.442	24.8	231	7.61	45.72	0.253	0.359	1.017	6.70	0.830	0.460
278	0.112	0.442	25.2	235	7.80	54.46	0.275	0.431	1.024	6.73	0.829	0.465
279	0.112	0.442	25.4	234	7.90	64.54	0.293	0.510	1.042	6.74	0.825	0.477

SURFACE: MS/1/Spine TEST BED: Mk 1 POSITION: Placed directly on distributor plate

BED MATERIAL: Zircon sand, size range 63 – 210 μm; static height 50 mm

OBSERVED RESULTS

READING NUMBER	BED			WATER				GAS	AIR			AMBIENT	
	T_{16} °C	T_{17} °C	T_{18} °C	T_{wi} °C	T_{wo} °C	ROT. READ	H_w mm H_2O	ROT. READ	H_a mm H_2O	T_a °C	P_a mm Hg	P_{at} mm Hg	T_{at} °C
SP1	193	191	193	12.0	25.8	19.8	125	20.8	49	45	80	767	20.0
SP2	206	205	202	12.0	28.6	19.9	126	23.0	100	45	80	767	21.0
SP3	214	214	210	11.8	29.8	19.8	127	24.5	151	44	79	767	21.0
SP4	218	221	217	11.7	31.0	19.8	129	27.3	251	43	79	767	21.0
SP5	220	220	225	11.6	31.8	19.7	130	29.5	350	42	78	767	21.0
SP6	215	221	218	11.4	31.8	19.6	131	31.0	495	41	77	767	21.0

CALCULATED RESULTS

READING NUMBER	$\dot{m}$ kg/s	$\dot{M}$ kg/s	T_w °C	T_b °C	Q kW	$\dot{V}_a$ m^3/s $x10^3$	$\dot{V}_g$ m^3/s $x10^3$	u_f m/s	U kW/m^2K	h_i kW/m^2K	E_f	h_o kW/m^2K
SP1	0.101	0.570	24.8	192	5.44	20.32	0.207	0.147	0.886			
SP2	0.101	0.573	27.4	204	6.62	29.03	0.225	0.216	1.021			
SP3	0.101	0.575	28.5	213	7.21	35.71	0.238	0.270	1.065			
SP4	0.101	0.579	29.6	219	7.76	46.11	0.263	0.353	1.116			
SP5	0.100	0.582	30.4	222	8.05	54.51	0.283	0.420	1.145			
SP6	0.099	0.584	30.4	218	8.05	64.89	0.298	0.496	1.169			

TEST NUMBER 55

APPENDIX A4

RADIAL FIN EXTENDED SURFACE ANALYSIS

A4.1 Basic Equations

A4.1.1 Geometry Variables

Fin spacing

$$b = \frac{10^3}{N} - t \quad mm \tag{A4.1}$$

Fin height

$$L = \frac{(D-d_o)}{2} \quad mm \tag{A4.2}$$

A4.1.2 Surface Areas

Basic tube area

$$A_i = \frac{\pi d_i}{10^3} \quad m^2/m \text{ length tube} \tag{A4.3}$$

$$A_o = A_i \cdot \frac{d_o}{d_i} \quad m^2/m \text{ length tube} \tag{A4.4}$$

Primary surface area

$$A_1 = \frac{\pi d_o}{10^3}\left[1 - \frac{Nt}{10^3}\right] m^2/m \text{ length tube} \tag{A4.5}$$

Secondary surface area

$$A_2 = \left[\frac{2\pi(D^2-d_o^2)}{4} + \pi D t\right]\frac{N}{10^6} \quad m^2/m \text{ length tube} \tag{A4.6}$$

Finned surface area

$$A_1 + A_2 = \frac{\pi}{10^3}\left[\frac{2NL(t+L+d_o)}{10^3} + d_o\right] m^2/m \text{ length tube} \tag{A4.7}$$

Area ratio

$$A_R = \frac{A_1 + A_2}{A_o} \tag{A4.8}$$

Effective surface area

$$A_E = A_1 + E_F A_2 \; m^2/m \text{ length tube} \tag{3.13}$$

A4.1.3 Surface Volumes

Volume occupied by extended surface in bed

$$V_1 \times 10^6 = \frac{\pi D^2}{4} \; m^3/m \text{ length tube} \tag{A4.9}$$

Volume occupied by metal of extended surface

$$V_2 \times 10^6 = V_1 \times 10^6\left[\frac{Nt}{10^3} - \left(\frac{d_i}{D}\right)^2\right] + \frac{A_1 \cdot d_o \cdot 10^3}{4} \tag{A4.10}$$

m^3/m length tube

Volume occupied by metal of fins

$$V_{FIN} \times 10^6 = V_2 \times 10^6 - \frac{\pi(d_o^2 - d_i^2)}{4} \; m^3/m \text{ length tube} \tag{A4.11}$$

A4.1.4 Heat Transfer Calculations

Fin efficiency

$$E_F = \frac{2}{\frac{r_e}{r_o}(\phi + mt) + \phi}\left[\frac{\gamma K_1(mr_o) - I_1(mr_o)}{I_o(mr_o) + \gamma K_o(mr_o)}\right] \qquad (3.20)$$

where $$\gamma = \frac{\frac{h_o}{km} \cdot I_o(mr_e) + I_1(mr_e)}{K_1(mr_e) - \frac{h_o}{km} \cdot K_o(mr_e)}$$

and $$m = \sqrt{\frac{2h_o}{kt}}$$ and $$\phi = m(r_e - r_o)$$

Overall heat transfer coefficient - overall thermal resistance (bed to coolant). Rearranging equation (3.10) gives

$$\frac{1}{UA_o} = \frac{1}{h_o A_E} + \frac{\ln\left(\frac{d_o}{d_i}\right)}{2\pi k} + \frac{1}{h_i A_i} \qquad (A4.12)$$

and

$$Q = UA_o(T_b - T_w) \qquad (3.9)$$

A4.2 Computer Programmes

A4.2.1 Introduction

The University of Aston in Birmingham has an ICL 1905E computer equipped with an ICL 1934/4 graph plotter manufactured by Calcomp Ltd. All programmes are written in FORTRAN language and use is made of the mathematical subroutines contained in the standard ICL library software package[36], together with subroutines from the Nottingham Algorithms Group Library Manual[37]. For information on graph plotter subroutines the reader is referred to the relevant section in the User's Handbook[38].

The programmes produce a print out as well as graphs from the graph plotter. The plotter output is in the form of a series of five graphs, one for each extended surface material - copper, aluminium, aluminium - brass, mild steel and stainless steel. Final output is ten graphs, each set of five being for a constant h_o. Each programme is designed with individual flexibility and variations in the form of output can easily be made. Safety checks are built into the programmes to saveguard against physical dimensions being greater or less than those likely to be met in practice - in the case of the Q - t curves, fin heights in the range 1 mm $\leq l \leq$ 25 mm were used and the minimum fin spacing was limited to values greater than 0.1 mm.

A4.2.2 Nomenclature for Programme Identifiers

Only the main variables are listed in this section and since they eventually assume specific units, they are also stated. The general symbols used in the analysis are enclosed in parenthesis.

MASTER PROGRAMME FORTRAN IDENTIFIER	QUANTITY
DI	Basic tube inside diameter (d_i) mm
DO	Basic tube outside diameter (d_o) mm
D	Fin outside diameter (D) mm
T	Fin thickness (t) mm
L	Fin height (l) mm
B	Fin spacing (b) mm
N	Number of fins per metre length of tube (N) fins/m
TRATIO	Basic tube diameter ratio (d_o/d_i)
FRATIO	Fin/Basic tube outside diameter ratio ($D/d_o = r_e/r_o$)
AI	Basic tube inside surface area (A_i) m^2/m length tube
AO	Basic tube outside surface area (A_o) m^2/m length tube
A1	Primary surface area (A_1) m^2/m length tube
A2	Secondary surface area (A_2) m^2/m length tube
A	Finned surface area ($A_1 + A_2$) m^2/m length tube
ARATIO	Area ratio (A_R) m^2/m length tube
AE	Effective surface area (A_E) m^2/m length tube
V1	Volume occupied by extended surface in bed ($V_1 \times 10^6$) m^3/m length tube
V2	Volume occupied by metal of extended surface ($V_2 \times 10^6$) m^3/m length tube
VFIN	Volume occupied by metal of fins ($V_{FIN} \times 10^6$) m^3/m length tube
EF	Fin efficiency (E_F)
XHI	Inside heat transfer coefficient - basic tube to coolant (h_i) kW/m^2 K
XHO	Outside heat transfer coefficient - bed to extended surface (h_o) kW/m^2 K
U	Overall heat transfer coefficient - bed to coolant (U) kW/m^2 K
CTHERM	Overall thermal resistance - bed to coolant ($1/UA_o$) K/kW/m length tube
TDIFF	Temperature difference between bed and coolant ($T_b - T_w$) K
XKM	Thermal conductivity of extended surface material (k) kW/m K
Q	Heat transferred to extended surface (Q) kW/m length tube.

MASTER PROGRAMME FORTRAN IDENTIFIER	QUANTITY
Q1	Heat transferred per volume occupied by extended surface in bed ($Q/V_1 \times 10^6$) kW/m^3/m length tube
Q2	Heat transferred per volume occupied by metal of extended surface ($Q/V_2 \times 10^6$) kW/m^3/m length tube
XMT	Dimensionless parameter in fin efficiency expression (mt)
XHOXKM	Dimensionless parameter in fin efficiency expression ($h_o/km = mt/2$)
PHI	Dimensionless parameter in fin efficiency expression (ϕ)
XMRO	Dimensionless parameter in fin efficiency expression ($mr_o = \phi/(r_e/r_o - 1)$)
XMRE	Dimensionless parameter in fin efficiency expression ($mr_e = mr_o \cdot r_e/r_o$)
Z	Dimensionless parameter in fin efficiency expression

F4I0(X,VALUE)
F4I1(X,VALUE)
F4K0(X,VALUE)
F4K1(X,VALUE)

These are FORTRAN library subroutines[36], for modified Bessel functions of zero order and first and second kind.

DEFBUF

A library subroutine to enable the heat transfer per volume of metal graph title arrays to be stored. An own programme description is required to provide a new channel.

E02ABF

A Nottingham Algorithm Group Library subroutine[37] enabling a least squares polynomial approximation to be obtained for the loci of maximum Q points.

OPENPLOT
HGPLOT
PLOT
HGPSCURVE
HGPAXISV
HGPSYMBL
HGPNUMBER
HGPRECT
CLOSEPLOT

These are Graph Plotter subroutines[38], enabling the individual graphs to be plotted according to a particular layout.

For the optimum heat transfer programme two subroutines were developed, namely

1. SUBROUTINE PLOT - to allow smooth curves to be plotted. In the maximum Q loci regions, the increments of t were reduced in the master programme before utilizing this subroutine.
2. SUBROUTINE LOCI - to approximate the maximum Q values for each graph curve. This was carried out by extracting three Q values, for each curve, about the maximum position, fitting a quadratic equation and establishing the value of t for which the slope of the curve was zero. The quadratic constants were expressed in determinant form before conversion to FORTRAN programming language. Library subroutine E02ABF in the master programme, was then used to obtain a polynomial approximation to these points.

A4.2.3 Flow Chart and Listing for Maximum Heat Transfer Programme

Figure A4.1 Maximum Heat Transfer – Simplified Overall Flowchart for Master Programme

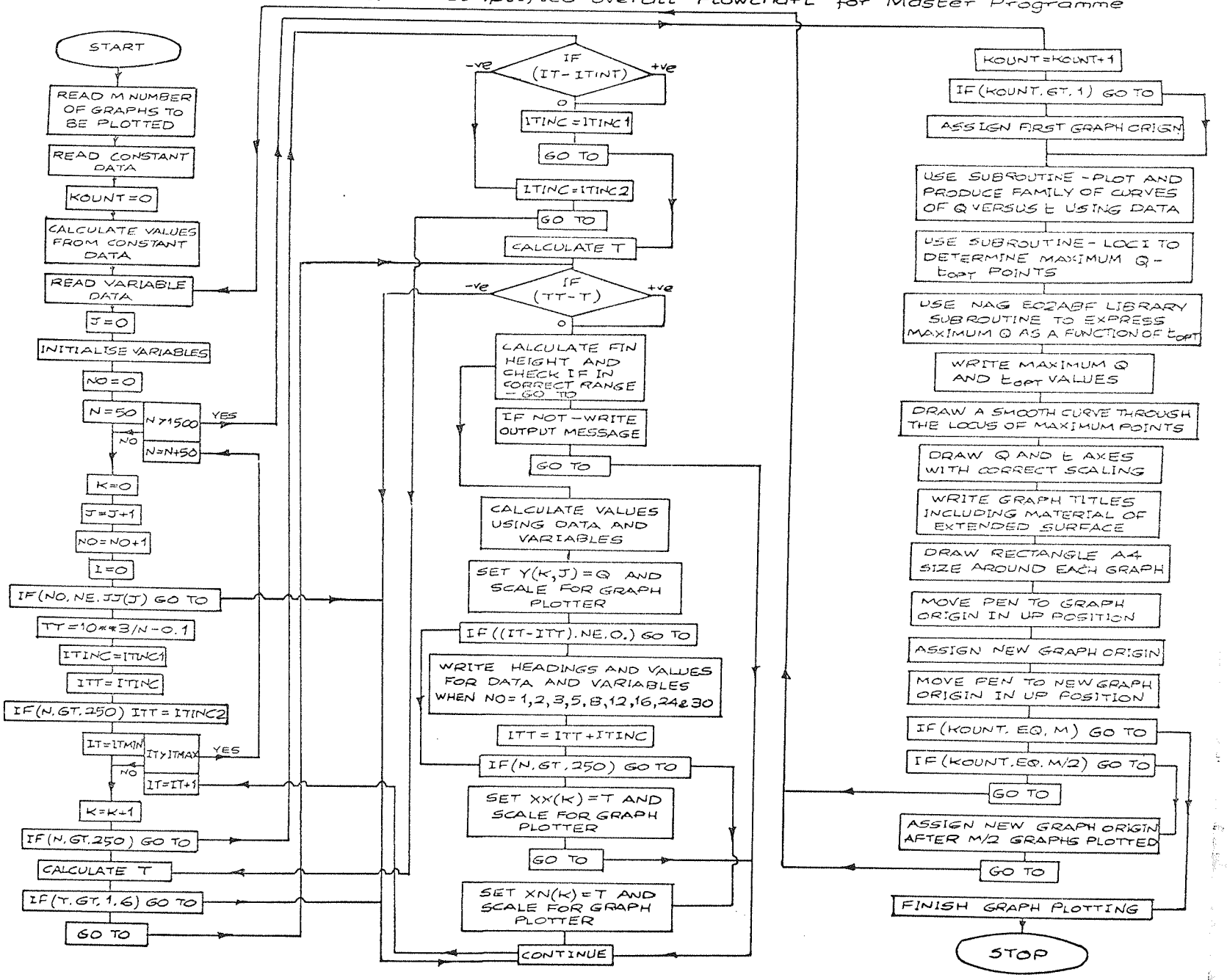

MAXIMUM HEAT TRANSFER PROGRAMME LISTING.

MASTER PROGRAMME

```
      MASTER
C     PERFORMANCE DATA FOR RADIAL FINS OF RECTANGULAR PROFILE-OPTIMUM
C     HEAT TRANSFER FOR EXTENDED SURFACE - GRAPHICAL OUTPUT USING
C     GRAPH PLOTTER
      REAL L
      DIMENSION Y(50,9),XX(50),XCD(2),YCD(2),TCA(5),TCB(5),TCC(3),TCD(3)
     1,TCE(4),TCF(3),TCG(4),TCH(4),TCJ(4),TCK(5),TCL(5),NPTS(9),XN(50)
      DIMENSION XX1(9),YL(9),XXXL(9),YYL(9),W(9),P(7),ST(7)
      LOGICAL LL
      INTEGER JJ(9)
      DATA JJ/1,2,3,5,8,12,16,24,30/
      DATA XCD(1)/13HFIN THICKNESS/
      DATA YCD(1)/15HHEAT TRANSFERRED/
      DATA TCA(1)/34HVARIATION OF HEAT TRANSFERRED FOR /
      DATA TCB(1)/35HEXTENDED SURFACE WITH FIN THICKNESS/
      DATA TCC(1)/17HMATERIAL - COPPER/
      DATA TCD(1)/20HMATERIAL - ALUMINIUM/
      DATA TCL(1)/26HMATERIAL - ALUMINIUM BRASS/
      DATA TCF(1)/21HMATERIAL - MILD STEEL/
      DATA TCG(1)/26HMATERIAL - STAINLESS STEEL/
      DATA TCH(1)/30HBASIC TUBE INSIDE DIAMETER  = /
      DATA TCJ(1)/30HBASIC TUBE OUTSIDE DIAMETER = /
      DATA TCK(1)/38HVOLUME OF EXTENDED SURFACE MATERIAL = /
      DATA TCL(1)/36HOUTSIDE HEAT TRANSFER COEFFICIENT = /
      CALL OPENPLOT
      WRITE(2,1)
    1 FORMAT(1H1,30X,55HPERFORMANCE DATA FOR RADIAL FINS OF RECTANGULAR
     1PROFILE/36X,42HOPTIMUM HEAT TRANSFER FOR EXTENDED SURFACE)
      READ(1,2)M
    2 FORMAT(I0)
      READ(1,3)DI,DO,V2,XHI,TDIFF,YYMAX
    3 FORMAT(6F0.0)
      DY=2.0
      YGAP=0.45
      YLENGTH=YYMAX*YGAP/DY
      KOUNT=0
      TRATIO=DO/DI
      A1=3.1416*DI/1.0E 3
      AO=AI*TRATIO
      VFIN=V2-3.1416/4.0*(DO**2-DI**2)
    4 READ(1,5)XHO,XKM
    5 FORMAT(2F0.0)
      J=0
      ITMIN=1
      ITINT=24
      ITMAX=50
      XGAP=0.375
      ITINC1=2
      ITINC2=8
      KK=(ITMAX-ITINT)+ITINT*ITINC1/ITINC2
      NO=0
      DO 24 N=50,1500,50
      K=0
      J=J+1
      NO=NO+1
      I=0
      IF(NO.NE.JJ(J)) GO TO 41
      YT=1.0E 3/N-0.1
      ITINC=ITINC1
      ITT=ITINC
      IF(N.GT.250) ITT=ITINC2
      DO 20 IT=ITMIN,ITMAX
      K=K+1
      IF(N.GT.250) GO TO 66
   69 T=IT/(10.0*ITINC)
      IF(T.GT.1.6) GO TO 25
      GO TO 67
   66 IF(IT-ITINT)71,68,68
   68 ITINC=ITINC1
      GO TO 70
   71 ITINC=ITINC2
      GO TO 69
   70 T=ITINT/(10.0*ITINC2)+(IT-ITINT)/(10.0*ITINC1)
   67 IF(TT-T)64,6,6
    6 CX=VFIN*1.0E 3/(3.1416*N*T)
      BX=DO
       L=-(BX/2.0)+SQRT((BX/2.0)**2+CX)
      IF(L-1.0) 8,7,7
    7 IF(L-25.0)10,10,15
    8 WRITE(2,9)N,T
    9 FORMAT(1H0,33HFIN HEIGHT LESS THAN 1MM FOR N = ,I4,35H FINS/METR
     1AND ALL T IN THE RANGE ,F6.4,11HMM TO 1.6MM)
      GO TO 17
   64 WRITE(2,65)N,T
   65 FORMAT(1H0,36HFIN SPACING LESS THAN 0.1MM FOR N = ,I4,35H FINS/M
     1RL AND ALL T IN THE RANGE ,F4.2,11HMM TO 1.6MM)
      GO TO 17
   10 X=2.0*T*XHO/(XKM*1.0E 3)
      XHT=SQRT(X)
      XHOXKM=XHT/2.0
      A1=3.1416*DO*(1.0-N*T/1.0E 3)/1.0E 3
      B=1.0E 3/N-T
      PHI=XHT*L/T
      D=DO+2.0*L
      V1=3.1416*D**2/4.0
      FRATIO=D/DO
      XHRO=PHI/(FRATIO-1.0)
      XHRE=XHRO*FRATIO
      X=XHRE
      CALL F4I0(X,VALUE)
      VALUE1=VALUE*EXP(X)
      CALL F4I1(X,VALUE)
      VALUE2=VALUE*EXP(X)
      CALL F4K0(X,VALUE)
      VALUE3=VALUE/EXP(X)
      CALL F4K1(X,VALUE)
      VALUE4=VALUE/EXP(X)
      AA=XHOXKM*VALUE1+VALUE2
      BB=VALUE4-XHOXKM*VALUE3
      X=XHRO
```

```
      CALL F4J0(X,VALUE)
      VALUE5=VALUE*EXP(X)
      CALL F4J1(X,VALUE)
      VALUE6=VALUE*EXP(X)
      CALL F4K0(X,VALUE)
      VALUE7=VALUE/EXP(X)
      CALL F4K1(X,VALUE)
      VALUE8=VALUE/EXP(X)
      Z=((AA*VALUE8)/BB-VALUE6)/(VALUE5+(AA*VALUE7)/BB)
      EF=2.0*Z/((PHI+XMT)*FRATIO+PHI)
      A=3.1416*(2.*N*L*(T*L*DO)/1.0E 3+DO)/1.0E 3
      A2=A-A1
      AE=A1+EF*A2
      ARATIO=A/A0
      V2=V1*(L*T/1.0E 3-(DI/D)**2)+A1*DO*1.0E 3/4.0
      OTHERM=1.0/(AE*XHO)+ALOG(TRATIO)/(2.0*3.1416*XKM)+1.0/(AI*XHI)
      UO=1.0/(OTHERM*AO)
      Q=TDIFF/OTHERM
      Q1=Q*1.0E 6/V1
      Q2=Q*1.0E 6/V2
      Y(K,J)=Q
      Y(K,J)=Y(K,J)/YYMAX*YLENGTH
      IF((IT-ITT) NE.0) GO TO 72
      WRITE(2,11)
   11 FORMAT(//,3X,2HDI,4X,2HDO,4X,1HD,5X,1HT,6X,1HN,6X,1HL,6X,1HB,5X,5H
     1DO/DI,3X,4HD/DO,5X,2HAI,7X,2HAO,7X,2HA1,7X,2HA2,7X,2HAE,6X,6HARATI
     2O)
      WRITE(2,12)DI,DO,D,T,N,L,B,TRATIO,FRATIO,AI,AO,A1,A2,AE,ARATIO
   12 FORMAT(1H ,F5.1,2X,F4.1,1X,F6.3,1X,F3.1,2X,I6,1X,F6.3,1X,F6.3,2X,
     1F6.4,2X,F6.4,2X,F7.5,2X,F7.5,2X,F7.5,2X,F7.5,2X,F7.5,2X,F7.4)
      WRITE(2,13)
   13 FORMAT(1H ,4X,1HK,5X,2HKO,4X,2HKI,5X,2HUO,3X,7H1/UO.AO,2X,5HTB-TW,
     1,4X,2HV1,7X,2HV2,3X,1HQ,7X,4HQ/V1,7X,4HQ/V2,4X,3HPHI,7X,2HMT,7X,2HE
     2F)
      WRITE(2,14)XKM,XHO,XHI,UO,OTHERM,TDIFF,V1,V2,Q,Q1,Q2,PHI,XMT,EF
   14 FORMAT(1H ,F7.3,2X,F4.2,2X,F4.1,2X,F6.4,1X,F7.4,2X,F5.1,1X,F8.3,1X
     1,F8.3,2X,F7.4,1X,F9.3,1X,F10.3,1X,F6.4,2X,F8.6,2X,F6.4)
      ITT=ITT+ITINC
   72 IF(N.GT.250) GO TO 73
      XX(K)=T
      XX(K)=XX(K)*6.0/1.6
      GO TO 20
   73 XN(K)=T
      XN(K)=XN(K)*6.0/1.6
      GO TO 20
   15 WRITE(2,16)N,T
   16 FORMAT(1H0,37HFIN HEIGHT GREATER THAN 25MM FOR N = ,I4,20H FINS/ME
     1TRE AND T = ,F6.4,2HMM)
      I=I+1
      IF((IT-ITT).NE.0) GO TO 72
      ITT=ITT+ITINC
      GO TO 72
   41 J=J-1
      GO TO 24
   17 NPTS(J)=K-1-I
      GO TO 21
   20 CONTINUE
      NPTS(J)=K-I
      GO TO 21
   25 NPTS(J)=K-1-I
   21 IF(NPTS(J)-1)22,24,24
   22 IF(K.EQ.1) GO TO 24
      WRITE(2,23)N
   23 FORMAT(1H0,37HFIN HEIGHT GREATER THAN 25MM FOR N = ,I4,52H FINS/ME
     1TRE AND ALL T IN THE RANGE 0.0125MM TO 1.6MM)
   24 CONTINUE
      WRITE(2,26)(XX(K),(Y(K,J),J=1,4),K=1,KK)
   26 FORMAT(1H0,1X,5E10.6)
      WRITE(2,52)(NPTS(J),J=1,4)
   52 FORMAT(1H0,6X,4I10)
      WRITE(2,19)(XN(K),(Y(K,J),J=5,9),K=1,ITMAX)
   19 FORMAT(1H0,1X,6E10.6)
      WRITE(2,42)(NPTS(J),J=5,9)
   42 FORMAT(1H0,6X,5I10)
      KOUNT=KOUNT+1
      IF(KOUNT.GT.1) GO TO 27
      CALL AGPLOT(-5.0,11.0,0.4)
   27 CALL PLOT(XX,1.4,32,Y,NPTS)
      CALL PLOT(XN,5.9,50,Y,NPTS)
C     TO REDUCE THE MAXIMUM VALUE OF Q AND PLOT A CONTINUOUS CURVE
C     THROUGH THE LOCI OF POINTS AND WRITE VALUES
      MM=0
      NCURVES=4
      CALL LOCI(XX,1,NCURVES,32,Y,XXL,XXXL,YL,YYL,MM,YLENGTH,YYMAX,
     1NOMIT)
      MM=NCURVES
      NCURVES=9
      CALL LOCI(XN,5,NCURVES,50,Y,XXL,XXXL,YL,YYL,MM,YLENGTH,YYMAX,
     1NOMIT)
      NL=NCURVES-NOMIT
      WRITE(2,47)
   47 FORMAT(1H0,20X,19HTOPT MM      QMAX KW)
      WRITE(2,48)((XXXL(MM),YYL(MM)),MM=1,NL)
   48 FORMAT(1H ,15X,2F12.4)
C     NAGF SUBROUTINE E02ABF LEAST SQUARES POLYNOMIAL APPROXIMATION TO
C     LOCI OF POINTS
      LL=.FALSE.
      K1=7
      DO 53 J=1,NL
      W(J)=1.0
   53 CONTINUE
      CALL E02ABF(NL,XXXL,YYL,W,K1,NN,SI,P,LL)
      WRITE(2,54)
   54 FORMAT(1H0,51H LEAST SQUARES FIT BY ORTHOGONAL POLYNOMIALS E02ABF)
      WRITE(2,55)
   55 FORMAT(1H0,5X,15HCOEFFICIENTS OF,10X,8HGOODNESS/5X,15HBEST POLYNOM
     1IAL,11X,6HOF FIT)
      DO 57 J=1,K1
      WRITE(2,56)P(J),SI(J)
   56 FORMAT(4X,E14.6,8X,E14.6)
   57 CONTINUE
      WRITE(2,58)NN
   58 FORMAT(1H0,20H DEGREE OF BEST POLY,I4)
      WRITE(2,59)
   59 FORMAT(1H0,3X,4HTOPT,8X,4HQMAX,12X,3HFIT,9X,8HRESIDUAL)
      DO 62 J=1,NL
      TOPT=XXXL(J)
      N1=NN+1
```

```
      S=P(N1)
      DO 60 II=1,NN
      I11=N1-II
      S=S*TOPT+P(I11)
   60 CONTINUE
      ORESIDUAL=YYL(J)-S
      WRITE(2,61)TOPT,YYL(J),S,ORESIDUAL
   61 FORMAT(1H ,F6.3,3E15.6)
   62 CONTINUE
      CALL HGPSCURVE(XXL,YL,NL,0,0,0,0,0)
      CALL HGPAXISV(0.0,0.0,XCD(1),-13,6.0,0.0,0.0,0.0,1.0,XGAP,-2)
      CALL HGPAXISV(0.0,0.0,YCD(1),16,YLENGTH,90.0,0.0,0.0,DY,YGAP,-2)
      CALL HGPSYMBL(0.5,10.5,0.15,TCA(1),0.0,34)
      CALL HGPSYMBL(0.5,10.15,0.15,TCB(1),0.0,35)
      IF(XKM.EQ.0.38) GO TO 32
      IF(XKM.EQ.0.20) GO TO 33
      IF(XKM.EQ.0.10) GO TO 34
      IF(XKM.EQ.0.045) GO TO 35
      IF(XKM.EQ.0.015) GO TO 36
   32 CALL HGPSYMBL(0.5,9.7,0.1,TCC(1),0.0,17)
      GO TO 37
   33 CALL HGPSYMBL(0.5,9.7,0.1,TCD(1),0.0,20)
      GO TO 37
   34 CALL HGPSYMBL(0.5,9.7,0.1,TCE(1),0.0,26)
      GO TO 37
   35 CALL HGPSYMBL(0.5,9.7,0.1,TCF(1),0.0,21)
      GO TO 37
   36 CALL HGPSYMBL(0.5,9.7,0.1,TCG(1),0.0,26)
   37 CALL HGPSYMBL(0.5,9.5,0.1,TCH(1),0.0,30)
      CALL HGPNUMBER(3.0,9.5,0.1,DI,0.0,0,2,1)
      CALL HGPSYMBL(0.5,9.3,0.1,TCJ(1),0.0,30)
      CALL HGPNUMBER(3.0,9.3,0.1,DO,0.0,0,2,1)
      CALL HGPSYMBL(0.5,9.1,0.1,TCK(1),0.0,38)
      CALL HGPNUMBER(3.8,9.1,0.1,V2,0.0,0,3,0)
      CALL HGPSYMBL(0.5,8.9,0.1,TCL(1),0.0,36)
      CALL HGPNUMBER(3.6,8.9,0.1,XHO,0.0,0,1,1)
      CALL HGPRECT(-1.50,-0.75,11.75,8.25,0.0,3)
      CALL HGPLOT(0.0,0.0,3,0)
      CALL HGPLOT(-9.25,0.0,0,4)
      CALL HGPLOT(0.0,0.0,3,0)
      IF(KOUNT.EQ.M) GO TO 39
      IF(KOUNT.EQ.M/2) GO TO 38
      GO TO 4
   38 DIST=9.25*M/2.0
      CALL HGPLOT(DIST,14.0,0,4)
      GO TO 4
   39 CALL CLOSEPLOT
      STOP
      END
```

SUBROUTINES FOR MAXIMUM HEAT TRANSFER PROGRAMME

```
      SUBROUTINE PLOT(XT,NINITIAL,NCURVES,ITPTS,Y,NPTS)
      DIMENSION XT(50),Y(50,9),NPTS(9)
      DO 6 J=NINITIAL,NCURVES
      IF(NPTS(J)-1)6,1,1
    1 DO 2 K=1,ITPTS
      IF(Y(K,J).NE.0.0) GO TO 3
    2 CONTINUE
    3 IF(NPTS(J)-4)5,4,4
    4 CALL HGPSCURVE(XT(K),Y(K,J),NPTS(J),0,0.0,0.0,0.0)
      GO TO 6
    5 CALL ASTSYMBOL(XT(K),Y(K,J),NPTS(J),3,0.005,0)
    6 CONTINUE
      RETURN
      END
```

```
      SUBROUTINE LOCI(XT,NINITIAL,NCURVES,ITPTS,Y,XXL,XXXL,YL,YYL,MM,
     1YLENGTH,YYMAX,NOMIT)
      DIMENSION XT(50),Y(50,9),XXL(9),XXXL(9),YL(9),YYL(9)
      DO 3 J=NINITIAL,NCURVES
      YMAX=0.0
      DO 1 K=1,ITPTS
      IF(Y(K,J).LT.YMAX) GO TO 1
      YMAX=Y(K,J)
      MK=K
    1 CONTINUE
      NOMIT=0
      IF(MK.EQ.1.OR.MK.EQ.ITPTS) GO TO 2
      IF(Y(MK-1,J) EQ.0.0) GO TO 2
      K=MK
      MM=MM+1
      Z1=Y(K-1,MM)-Y(K,MM)
      Z2=Y(K,MM)-Y(K+1,MM)
      A12=XT(K-1)-XT(K)
      A22=XT(K)-XT(K+1)
      A11=A12*(XT(K-1)+XT(K))
      A21=A22*(XT(K)+XT(K+1))
      AZ=(Z1*A22-Z2*A12)/(A11*A22-A12*A21)
      BZ=(Z2*A11-Z1*A21)/(A11*A22-A12*A21)
      CZ=Y(K,MM)-XT(K)*(AZ*XT(K)+BZ)
      XVAL=-0.5*(A11*Z2-A21*Z1)/(A22*Z1-A12*Z2)
      YMAX=XVAL*(AZ*XVAL+BZ)+CZ
      XXL(MM)=XVAL
      XXXL(MM)=XXL(MM)*1.6/6.0
      YL(MM)=YMAX
      YYL(MM)=YL(MM)*YYMAX/YLENGTH
      GO TO 3
    2 NOMIT=NOMIT+1
    3 CONTINUE
      RETURN
      END
```

A4.2.4 Flow Chart and Listing for Maximum Heat Transfer per Metal Volume Programme

Figure A4.2 Maximum Heat Transfer per Metal Volume – Flowchart for Master Programme

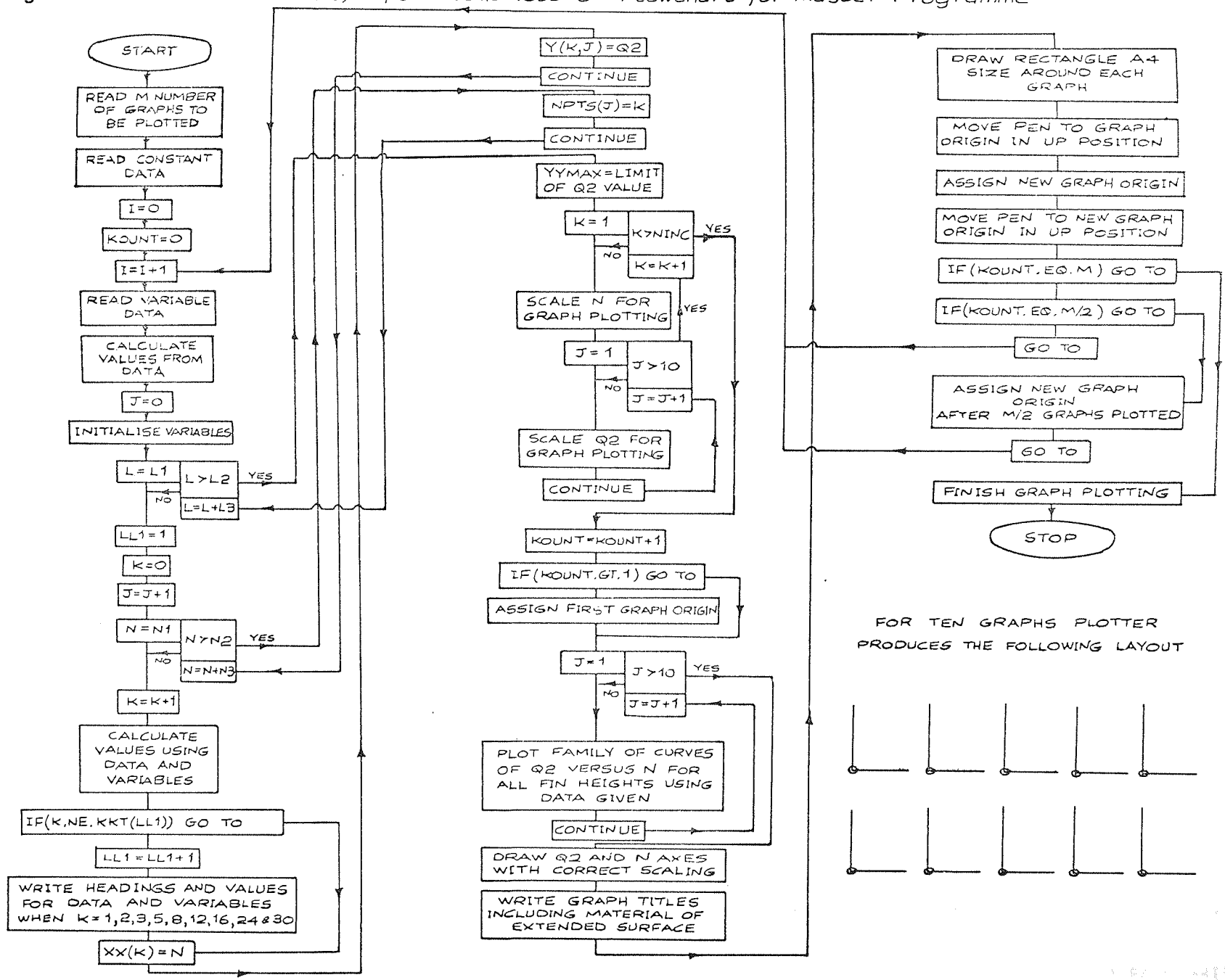

MAXIMUM HEAT TRANSFER PER METAL VOLUME PROGRAMME LISTING

OWN PROGRAMME DESCRIPTION.

```
LIST(LP)
LIBRARY(ED,SUBGROUPONE)
PROGRAM(FXXX)
INPUT 1 =CR0
INPUT 3 =TR0
INPUT 5 =CR1
OUTPUT 2=LP0
OUTPUT 6=LP1
USE 7=/ARRAY
COMPRESS INTEGER AND LOGICAL
COMPACT
NO TRACE
END
```

MASTER PROGRAMME

```
      MASTER
C     PERFORMANCE DATA FOR RADIAL FINS OF RECTANGULAR PROFILE-OPTIMUM
C     HEAT TRANSFER PER VOLUME OF EXTENDED SURFACE MATERIAL - GRAPHICAL
C     OUTPUT USING GRAPH PLOTTER
      DIMENSION Y(30,10),XX(30),XCD(4),YCD(8),TCD(6),TCH(3),TCJ(5),
     1TCE(6),TCF(3),TCG(6),DARR(4),NPTS(10),TCK(5),
     2TCL(3),TCM(4),TCN(3),TCP(6)
      INTEGER KKT(8)
      DATA KKT/1,2,3,5,8,12,16,24,30/
      DATA XCD(1)/26HNUMBER OF FINS PER METRE N/,YCD(1)/58HHEAT TRANSFER
     1RED PER VOLUME OF METAL Q2 KW PER METRE CUBED/,TCD(1)/43HVARIATION
     2 OF HEAT TRANSFERRED PER VOLUME OF/,TCE(1)/45HEXTENDED SURFACE MAT
     3ERIAL WITH NUMBER OF FINS/,TCF(1)/16HFIN THICKNESS = /,TCG(1)/40HO
     4UTSIDE HEAT TRANSFER COEFFICIENT      = /
      DATA TCH(1)/17HMATERIAL - COPPER/
      DATA TCJ(1)/32HBASIC TUBE OUTSIDE DIAMETER    = /
      DATA TCK(1)/32HBASIC TUBE INSIDE DIAMETER     = /
      DATA TCL(1)/20HMATERIAL - ALUMINIUM/
      DATA TCM(1)/26HMATERIAL - ALUMINIUM BRASS/
      DATA TCN(1)/21HMATERIAL - MILD STEEL/
      DATA TCP(1)/26HMATERIAL - STAINLESS STEEL/
      CALL OPENPLOT
      CALL DEFBUF(7,4,DARR)
      WRITE(2,1)
    1 FORMAT(1H1,30X,55HPERFORMANCE DATA FOR RADIAL FINS OF RECTANGULAR
     1PROFILE/27X,61HOPTIMUM HEAT TRANSFER PER VOLUME OF EXTENDED SURFAC
     2E MATERIAL)
      READ(1,2)M
    2 FORMAT(I0)
      READ(1,3)DI,DO,T,XMI,TDIFF,NMAX
    3 FORMAT(5F0.0,I0)
      I=0
      KOUNT=0
    4 I=I+1
      READ(1,5)XHO,XKM
    5 FORMAT(2F0.0)
      TRATIO=DO/DI
      AI=3.1416*DI/1.0E 3
      AO=AI*TRATIO
      XGAP=100.0/NMAX*6.0
      X=2.0*T*XHO/(XKM*1.0E 3)
      XMT=SQRT(X)
      XHOXKM=XMT/2.0
      J=0
      L1=2
      L2=20
      L3=2
      N1=50
      N2=NMAX
      N3=50
      NINC=N2/N3
      DO 120 L=L1,L2,L3
      LL1=1
      K=0
      J=J+1
      DO 12 N=N1,N2,N3
      K=K+1
      A1=3.1416*DO*(1.0-N*T/1.0E 3)/1.0E 3
      B=1.0E 3/N-T
      PHI=XMT*L/T
      D=DO+2.0*L
      V1=3.1416*D**2/4.0
      ERATIO=D/DO
      XMRO=PHI/(ERATIO-1.0)
      XMRE=XMRO*ERATIO
      X=XMRE
      CALL F4I0(X,VALUE)
      VALUE1=VALUE*EXP(X)
      CALL F4I1(X,VALUE)
      VALUE2=VALUE*EXP(X)
      CALL F4K0(X,VALUE)
      VALUE3=VALUE/EXP(X)
      CALL F4K1(X,VALUE)
      VALUE4=VALUE/EXP(X)
      AA=XHOXKM*VALUE1+VALUE2
      BB=VALUE4-XHOXKM*VALUE3
      X=XMRO
      CALL F4I0(X,VALUE)
      VALUE5=VALUE*EXP(X)
      CALL F4I1(X,VALUE)
      VALUE6=VALUE*EXP(X)
      CALL F4K0(X,VALUE)
      VALUE7=VALUE/EXP(X)
      CALL F4K1(X,VALUE)
      VALUE8=VALUE/EXP(X)
      Z=((AA*VALUE8)/BB-VALUE6)/(VALUE5+(AA*VALUE7)/BB)
      EF=2.0*Z/((PHI*XMT)*ERATIO+PHI)
      A=3.1416*(2.0*N*L*(T+L+DO)/1.0E 3+DO)/1.0E 3
      A2=A-A1
      AE=A1+EF*A2
      ARATIO=A/AO
      V2=V1*(N*T/1.0E 3-(DI/D)**2)+A1*DO*1.0E 3/4.0
      OTHERM=1.0/(AE*XHO)+ALOG(TRATIO)/(2.0*3.1416*XKM)+1.0/(AI*XHI)
      UO=1.0/(OTHERM*AO)
      Q=TDIFF/OTHERM
```

```
      Q1=Q*1.0E 6/V1
      Q2=Q*1.0E 6/V2
      IF(K.NE.KKT(LL1)) GO TO 10
      LL1=LL1+1
      WRITE(2,6)
    6 FORMAT(//,3X,2HDI,4X,2HDO,4X,1HD,5X,1HT,6X,1HN,6X,1HL,6X,1HB,5X,5H
     1DO/DI,3X,4HD/DO,5X,2HAI,7X,2HAO,7X,2HA1,7X,2HA2,7X,2HAE,6X,6HARATI
     20)
      WRITE(2,7)DI,DO,D,T,N,L,B,TRATIO,FRATIO,AI,AO,A1,A2,AE,ARATIO
    7 FORMAT(1H ,F6.1,2X,F4.1,2X,F4.1,2X,F3.1,2X,I6,2X,I4,2X,F6.3,2X,F6.
     14,2X,F6.4,2X,F7.5,2X,F7.5,2X,F7.5,2X,F7.5,2X,F7.5,2X,F7.4)
      WRITE(2,8)
    8 FORMAT(1H ,4X,1HK,5X,2HHO,4X,2HHI,5X,2HHO,3X,7H1/HO.AO,2X,5HTB-TW,
     14X,2HV1,7X,2HV2,8X,1HQ,7X,4HQ/V1,7X,4HQ/V2,4X,3HPHI,7X,2HMT,7X,2HE,
     2F)
      WRITE(2,9)XKM,XHO,XHI,UO,OTHERM,TDIFF,V1,V2,Q,Q1,Q2,PHI,XMT,EF
    9 FORMAT(1H ,F7.3,2X,F4.2,2X,F4.1,2X,F6.4,1X,F7.4,2X,F5.1,1X,F8.3,1X,
     1,F8.3,2X,F7.4,1X,F9.3,1X,F10.3,1X,F6.4,2X,F8.6,2X,F6.4)
   10 XX(K)=1.0*N
      Y(K,J)=Q2
   12 CONTINUE
      NPTS(J)=K
  120 CONTINUE
      YYMAX=440000.0
      DO 13 K=1,NINC
      XX(K)=XX(K)/XMAX*6.0
      DO 13 J=1,10
   13 Y(K,J)=Y(K,J)/YYMAX*8.8
      WRITE(2,100)(XX(K),(Y(K,J),J=1,10),K=1,NINC)
  100 FORMAT(1X,11F10.6)
      KOUNT=KOUNT+1
      IF(KOUNT.GT.1) GO TO 14
      CALL HGPLOT(-5.0,11.0,0,4)
   14 DO 15 J=1,10
   15 CALL HGPSCURVE(XX,Y(1,J),NPTS(J),0,0.0,0.0,0.0)
      CALL HGPAXISV(0.0,0.0,XCD(1),-26,6.0,0.0,0.0,0.0,100.0,XGAP,-2)
      DY=2.0
      CALL HGPAXISV(0.0,0.0,YCD(1),58,8.8,90.0,0.0,0.0,DY,0.4,-2)
      CALL HGPSYMBI(0.5,10.50,0.15,TCD(1),0.0,43)
      CALL HGPSYMBI(0.5,10.15,0.15,TCE(1),0.0,45)
      IF(XKM.EQ.0.38) GO TO 26
      IF(XKM.EQ.0.20) GO TO 27
      IF(XKM.EQ.0.10) GO TO 28
      IF(XKM.EQ.0.045) GO TO 29
      IF(XKM.EQ.0.015) GO TO 30
   26 CALL HGPSYMBI(0.5,9.7,0.1,TCH(1),0.0,17)
      GO TO 31
   27 CALL HGPSYMBI(0.5,9.7,0.1,TCL(1),0.0,20)
      GO TO 31
   28 CALL HGPSYMBI(0.5,9.7,0.1,TCM(1),0.0,26)
      GO TO 31
   29 CALL HGPSYMBI(0.5,9.7,0.1,TCN(1),0.0,21)
      GO TO 31
   30 CALL HGPSYMBI(0.5,9.7,0.1,TCP(1),0.0,26)
   31 WRITE(7,24)DI
   24 FORMAT(F4.1)
      READ(7,25)TCK(5)
   25 FORMAT(A4)
      CALL HGPSYMBI(0.5,9.5,0.1,TCK(1),0.0,36)
      WRITE(7,22)DO
   22 FORMAT(F4.1)
      READ(7,23)TCJ(5)
   23 FORMAT(A4)
      CALL HGPSYMBI(0.5,9.3,0.1,TCJ(1),0.0,36)
      WRITE(7,16)T
   16 FORMAT(F3.1)
      READ(7,17)TCF(3)
   17 FORMAT(A3)
      CALL HGPSYMBI(0.5,9.1,0.1,TCF(1),0.0,19)
      WRITE(7,18)XHO
   18 FORMAT(F3.1)
      READ(7,19)TCG(6)
   19 FORMAT(A3)
      CALL HGPSYMBI(0.5,8.9,0.1,TCG(1),0.0,43)
      CALL HGPRECT(-1.50,-0.75,11.75,8.25,0.0,3)
      CALL HGPLOT(0.0,0.0,3,0)
      CALL HGPLOT(-9.25,0.0,0,4)
      CALL HGPLOT(0.0,0.0,3,0)
      IF(KOUNT.EQ.M) GO TO 21
      IF(KOUNT.EQ.M/2) GO TO 20
      GO TO 4
   20 DIST=9.25*M/2.0
      CALL HGPLOT(DIST,14.0,0,4)
      GO TO 4
   21 CALL CLOSEPLOT
      STOP
      END
```

A4.2.5 Sample Results

A set of typical results are given for both maximum heat transfer and maximum heat transfer per metal volume programmes. The graph plotter sample results are given in a pocket inside the back bound cover of the thesis. Results derived from the computer and graph plotter outputs are given in Chapter VIII.

The range of data used was as follows:-

d_i - 8.6, 13.6, 20.2 and 26.2 mm

d_o - 10.0, 15.0, 22.0 and 28.0 mm

$0.05 \leq t \leq 1.60$ mm

$50 \leq N \leq 1500$ fins/m length tube

$20 \leq V_2 \leq 500$ m^3/m length tube

k - 0.380, 0.200, 0.100, 0.045 and 0.015 kW/m K

h_o - 0.2, 0.4, 0.6 and 0.8 kW/m^2 K

h_i = 15.0 kW/m^2 K

$T_b - T_w$ = 150 K

Sample Results for Maximum Heat Transfer Programme

PERFORMANCE DATA FOR RADIAL FINS OF RECTANGULAR PROFILE
OPTIMUM HEAT TRANSFER FOR EXTENDED SURFACE

FIN HEIGHT GREATER THAN 25MM FOR N = 50 FINS/METRE AND T = 0.05 0MM

FIN HEIGHT GREATER THAN 25MM FOR N = 50 FINS/METRE AND T = 0.10 0MM

DI	DO	D	T	N	I	B	DO/DI	D/DO	A1	A0	A1	A2	AF	ARATIO
13.6	15.0	5[illegible].364	[illegible].2	50	17.932	19.800	1.1029	3.3010	0.04273	0.04712	0.04665	[illegible].18712	0.09156	4.0609
K	HO	HI	UO	1/100.00	TR-TU	V1		V2		Q/V1	Q/V2	PHI	MT	EF
0.380	0.80	15.0	[illegible].3912	15.2533	150.0	2031.973		50.000		9.3336	4839.435	196672.064	2.6019	0.029019	0.2400

DI	DO	D	T	N	I	B	DO/DI	D/DO	A1	A0	A1	A2	AF	ARATIO
13.6	15.0	42.424	0.3	50	13.712	19.700	1.1029	2.8283	0.04273	0.04712	0.04642	0.12568	0.10049	3.4521
K	HO	HI	UO	1/100.00	TR-TU	V1		V2		Q/V1	Q/V2	PHI	MT	EF
0.380	0.80	15.0	[illegible].5115	14.041[illegible]	150.0	1413.554		50.000		10.6830	7557.548	213667.035	1.6245	0.035541	[illegible].4302

DI	DO	D	T	N	I	B	DO/DI	D/DO	A1	A0	A1	A2	AF	ARATIO
13.6	15.0	37.498	0.3	50	11.249	19.600	1.1029	2.4999	0.04273	0.04712	0.04618	0.09512	0.10283	2.9985
K	HO	HI	UO	1/100.00	TR-TU	V1		V2		Q/V1	Q/V2	PHI	MT	EF
0.380	0.80	15.0	[illegible].5465	13.7569	150.0	1104.344		50.000		10.6336	9873.384	218072.293	1.1541	0.041039	[illegible].5956

DI	DO	D	T	N	I	B	DO/DI	D/DO	A1	A0	A1	A2	AF	ARATIO
13.6	15.0	34.208	0.3	50	9.402	19.500	1.1029	2.2802	0.04273	0.04712	0.04595	0.07690	0.10101	2.4068
K	HO	HI	UO	1/100.00	TR-TU	V1		V2		Q/V1	Q/V2	PHI	MT	EF
0.380	0.80	15.0	[illegible].5163	13.9764	150.0	918.818		50.000		10.2326	11609.842	214651.442	0.6811	0.045883	[illegible].7161

DI	DO	D	T	N	I	B	DO/DI	D/DO	A1	A0	A1	A2	AF	ARATIO
13.6	15.0	31.816	0.3	50	8.449	19.400	1.1029	2.1212	0.04273	0.04712	0.04571	0.06484	0.09744	2.8460
K	HO	HI	UO	1/100.00	TR-TU	V1		V2		Q/V1	Q/V2	PHI	MT	EF
0.380	0.80	15.0	[illegible].4706	14.4209	150.0	795.134		50.000		10.8951	13073.353	209901.42	0.7044	0.050262	[illegible].7978

DI	DO	D	T	N	I	B	DO/DI	D/DO	A1	A0	A1	A2	AF	ARATIO
13.6	15.0	29.996	0.3	50	7.499	19.300	1.1029	1.9999	0.04273	0.04712	0.04567	0.05631	0.09347	2.9598
K	HO	HI	UO	1/100.00	TR-TU	V1		V2		Q/V1	Q/V2	PHI	MT	EF
0.380	0.80	15.0	[illegible].4170	14.9753	150.0	706.739		50.000		10.[illegible]165	14171.8[illegible]8	2[illegible].329 507	0.5816	0.054209	[illegible].8523

LEAST SQUARES FIT BY ORTHOGONAL POLYNOMIALS FOZABF

DEGREE OF BEST POLY = 5

TOPT	QMAX	FIT	RESIDUAL
0.395	[illegible].1060327E 02	0.1094327E 02	-0.3493665E-04
0.461	[illegible].1563226E 02	0.1563111E 02	0.1103505E-02
0.505	[illegible].1574884E 02	0.1575584E 02	-0.6983904E-02
0.555	[illegible].1948154E 02	0.1949035E 02	-0.8756885E-01
0.[illegible]	[illegible].2259002E 02	0.2260654E 02	-0.7621922E-01
0.965	[illegible].2682805E 02	0.2677846E 02	0.4955968E-01
3.070	[illegible].2965148E 02	0.2965509E 02	-0.3616774E-02
3.095	[illegible].3468571E 02	0.3468705E 02	-0.1348367E-01
3.046	[illegible].3769544E 02	0.3769335E 02	0.5988366E-01

COEFFICIENTS OF BEST POLYNOMIAL	GOODNESS OF FIT
0.[illegible]899E 02	0.8067[illegible]2E 02
-0.[illegible]742E 04	0.2[illegible]097[illegible]E 02
0.[illegible]6468E 05	0.4468[illegible]E 01
-0.4[illegible]020E 05	0.[illegible]538[illegible]E 00
0.[illegible]576E 06	0.[illegible]507216E 00
-0.9[illegible]501E 05	0.[illegible]6345[illegible]E-02
0.[illegible]000E 00	0.1445[illegible]E-01

Sample Results for Maximum Heat Transfer per Metal Volume Programme

PERFORMANCE DATA FOR RADIAL FINS OF RECTANGULAR PROFILE
OPTIMUM HEAT TRANSFER PER VOLUME OF EXTENDED SURFACE MATERIAL

	DO	D	T	N	L	B	DO/DI	D/DO	AI	AO	A1	A2	AE	ARAT
,6	10,0	14,0	0,2	50	2	19,800	1,1628	1,4000	0,02702	0,03142	0,03110	0,00798	0,03887	1,2
K	HO	HI	UO	1/UO,AO	TB-TW	V1		V2	Q	Q/V1	Q/V2	PHI	MT	E
380	0,60	15,0	0,7009	45,4115	150,0	153,938		21,206	3,3031	21457,478	155765,392	0,2513	0,025131	0,9

	DO	D	T	N	I	B	DO/DI	D/DO	AI	AO	A1	A2	AE	ARAT
,6	10,0	14,0	0,2	100	2	9,800	1,1628	1,4000	0,02702	0,03142	0,03079	0,01596	0,04632	1,4
K	HO	HI	UO	1/UO,AO	TB-TW	V1		V2	Q	Q/V1	Q/V2	PHI	MT	E
380	0,60	15,0	0,8265	38,5131	150,0	153,938		21,960	3,8948	25300,870	177359,462	0,2513	0,025131	0,9

	DO	D	T	N	I	B	DO/DI	D/DO	AI	AO	A1	A2	AE	ARAT
,6	10,0	14,0	0,2	150	2	6,467	1,1628	1,4000	0,02702	0,03142	0,03047	0,02394	0,05377	1,7
K	HO	HI	UO	1/UO,AO	TB-TW	V1		V2	Q	Q/V1	Q/V2	PHI	MT	E
380	0,60	15,0	0,9494	33,5267	150,0	153,938		22,714	4,4740	29063,857	196974,964	0,2513	0,025131	0,9

	DO	D	T	N	I	B	DO/DI	D/DO	AI	AO	A1	A2	AE	ARAT
,6	10,0	14,0	0,2	250	2	3,800	1,1628	1,4000	0,02702	0,03142	0,02985	0,03990	0,06867	2,2
K	HO	HI	UO	1/UO,AO	TB-TW	V1		V2	Q	Q/V1	Q/V2	PHI	MT	E
380	0,60	15,0	1,1877	26,8002	150,0	153,938		24,222	5,5970	36358,498	231072,167	0,2513	0,025131	0,9

	DO	D	T	N	I	B	DO/DI	D/DO	AI	AO	A1	A2	AE	ARAT
,6	10,0	14,0	0,2	400	2	2,300	1,1628	1,4000	0,02702	0,03142	0,02890	0,06384	0,09103	2,9
K	HO	HI	UO	1/UO,AO	TB-TW	V1		V2	Q	Q/V1	Q/V2	PHI	MT	E
380	0,60	15,0	1,5274	20,8402	150,0	153,938		26,484	7,1976	46756,623	271776,335	0,2513	0,025131	0,9

	DO	D	T	N	I	B	DO/DI	D/DO	AI	AO	A1	A2	AE	ARAT
,6	10,0	14,0	0,2	600	2	1,467	1,1628	1,4000	0,02702	0,03142	0,02765	0,09576	0,12083	3,9
K	HO	HI	UO	1/UO,AO	TB-TW	V1		V2	Q	Q/V1	Q/V2	PHI	MT	E
380	0,60	15,0	1,9500	16,3238	150,0	153,938		29,500	9,1890	59692,973	311496,875	0,2513	0,025131	0,9

APPENDIX A5

PROPERTIES OF FLUIDIZED SOLIDS

A5.1 Introduction

This appendix gives details of the fluidized material properties, used in the research work. Three bed materials were used, namely, zircon sand, silica sand and steel shot. Figure A5.1 shows photographs of the particle shape and size distribution taken by a Carl Zeiss Optical projection microscope.

Physical properties such as particle and bulk density, thermal conductivity and specific heat were given by the suppliers of the material and are tabulated in table A5.1. The size distribution range and mean particle diameter were obtained by conducting individual sieve analyses according to B.S. 410[39], 1969. The particle diameter was determined by two methods: firstly by a mass fraction averaging technique outlined by Kunii and Levenspiel[56], (p 67-69), of their book and secondly by a probability technique recommended by Dallavalle[55], (p 51-57). The latter method is more representative in establishing a "mean particle diameter" when the size frequency distribution curves are assymetric. In most instances they may be made symmetrical and thus follow the normal probability law if the logarithms of the sizes are substituted for the sizes. This is the case with the steel shot which has a wide frequency range (75-500 μm) and quite a large proportion of particles at the top end of the range. Figure A5.2 gives the logarithmic - probability plots for all materials obtained from the sieve analyses. Using these diameters, table A5.1 lists dimensionless groups of Nusselt and Fourier number for the materials in terms of the particle heat transfer coefficient and residence time at a surface.

A5.2 Sieve Analyses and Particle Diameter Estimation

A5.2.1 Zircon Sand

For a 1000 g sample the sieve analysis was:

+212 μm	0
-212 +180 μm	40.0 g
-180 +125 μm	772.0 g
-125 +106 μm	164.7 g
-106 + 90 μm	58.7 g
- 90 + 63 μm	14.6 g
Total	1000.0 g

Diameter Range μm	d_{pi} μm	Mass Fraction in Interval x_i	$\frac{x_i}{d_{pi}} \times 10^4$
63 - 90	76.5	0.0146	1.908
90 - 106	98.0	0.0587	5.990
106 - 125	115.5	0.1647	14.260
125 - 180	152.5	0.7220	47.344
180 - 212	196.0	0.0400	2.041
			Σ 71.535

Hence, $\bar{d}_p = \frac{10^4}{71.54} = 140$ μm

From figure A5.2 $\bar{d}_p = 138$ μm

A5.2.2 Silica Sand

For a 1000 g sample the sieve analysis was:

	+355 μm	0
-355	+300 μm	4 g
-300	+250 μm	13 g
-250	+212 μm	108 g
-212	+150 μm	469 g
-150	+106 μm	358 g
-106	+ 90 μm	48 g
	Total	1000 g

Diameter Range μm	d_{pi} μm	Mass Fraction in Interval x_i	$\frac{x_i}{d_{pi}} \times 10^4$
90 - 106	98.0	0.048	4.90
106 - 150	128.0	0.358	28.00
150 - 212	181.0	0.469	25.90
212 - 250	231.0	0.108	4.67
250 - 300	275.0	0.013	0.47
300 - 355	327.5	0.004	0.12
			Σ 64.06

Hence, $\overline{d}_p = \frac{10^4}{64.06} = 156$ μm

From figure A5.2 $\overline{d}_p = 157$ μm

A5.2.3 Steel Shot

For a 5000 g sample the seive analysis was:

	+500 μm	0 g
-500	+355 μm	3247 g
-355	+250 μm	1276 g
-250	+212 μm	164 g
-212	+150 μm	274 g
-150	+106 μm	38 g
-106	+ 75 μm	1 g
	Total	5000 g

Diameter Range μm	d_{pi} μm	Mass Fraction in Interval x_i	$\frac{x_i}{d_{pi}} \times 10^4$
75 - 106	90.5	0.0002	0.022
106 - 150	128.0	0.0076	0.594
150 - 212	181.0	0.0548	3.030
212 - 250	231.0	0.0328	1.420
250 - 355	302.5	0.2552	8.430
355 - 500	427.5	0.6494	15.160
			Σ 28.656

Hence, $\bar{d}_p = \frac{10^4}{28.66} = 349$ μm

From figure A5.2 $\bar{d}_p = 432$ um

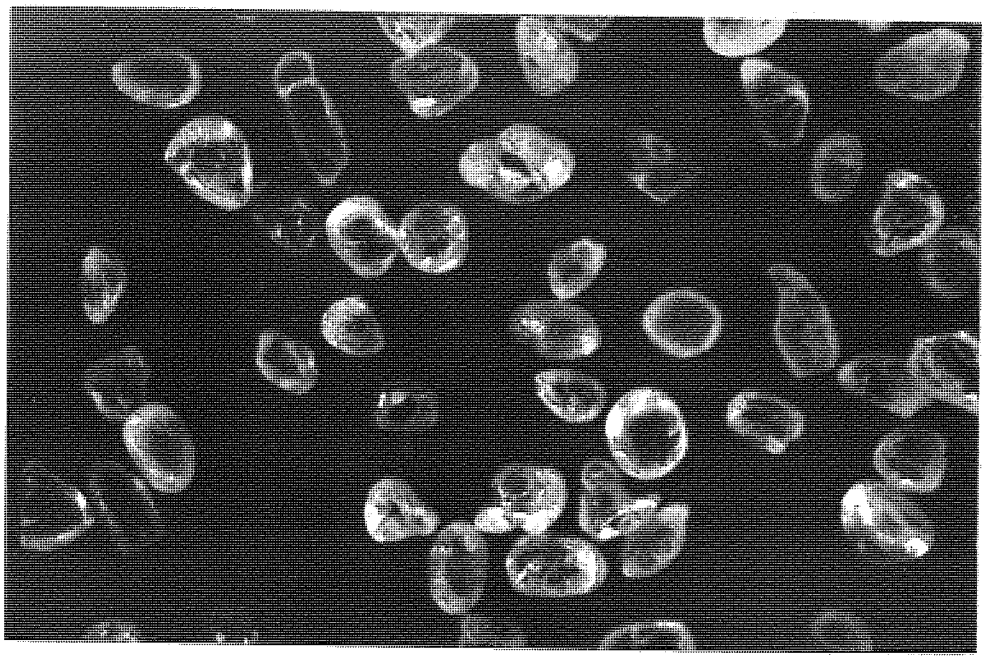

ZIRCON SAND MAGNIFICATION X 56

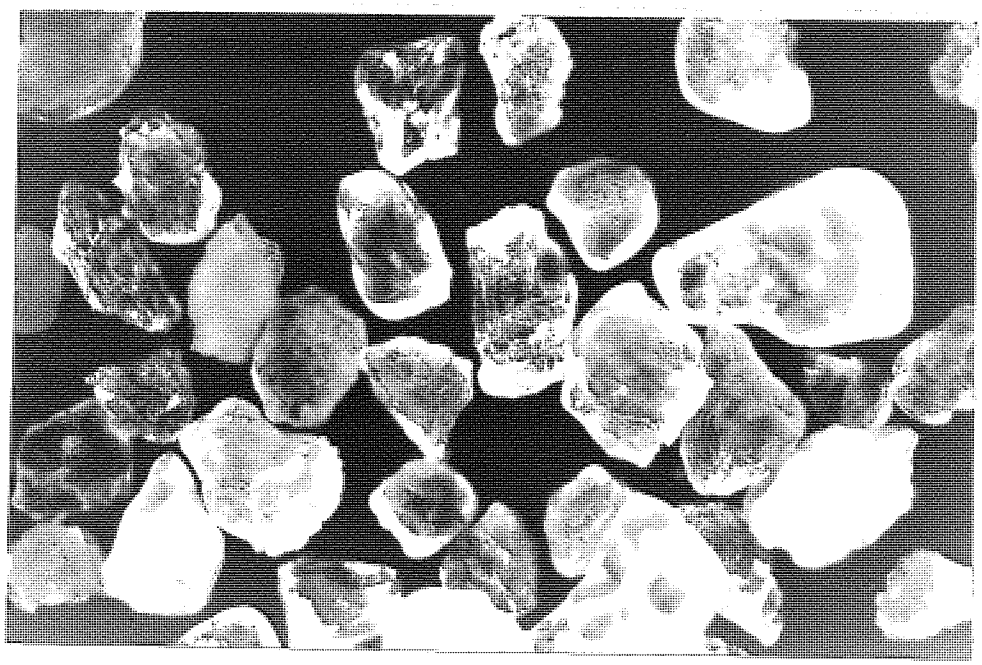

SILICA SAND MAGNIFICATION X 56

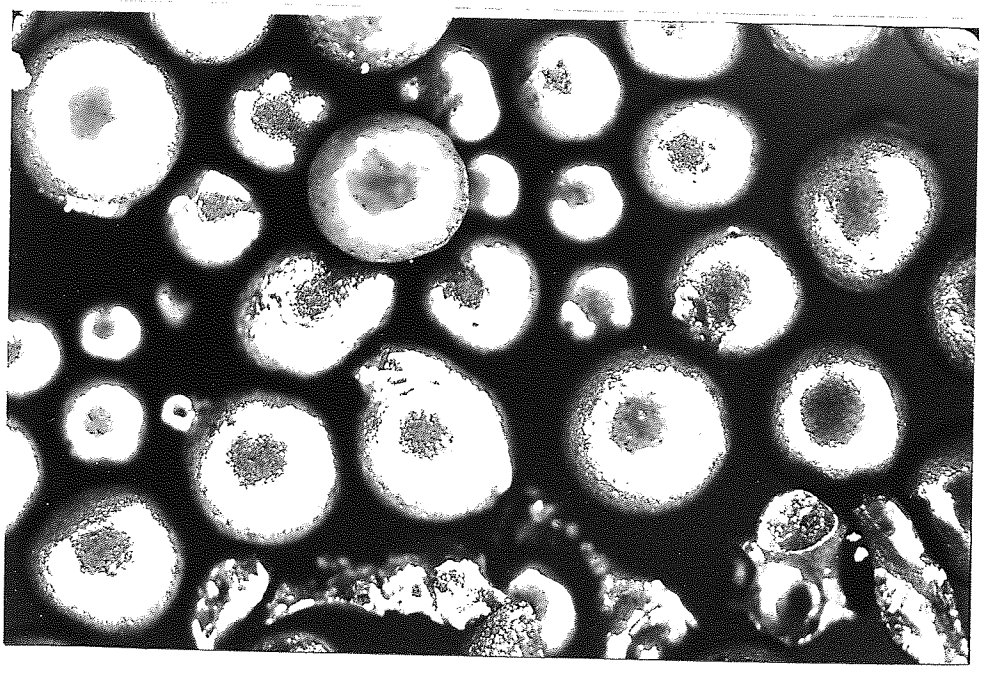

STEEL SHOT MAGNIFICATION X 56

Figure A5.1 Projection Microscope Photographs

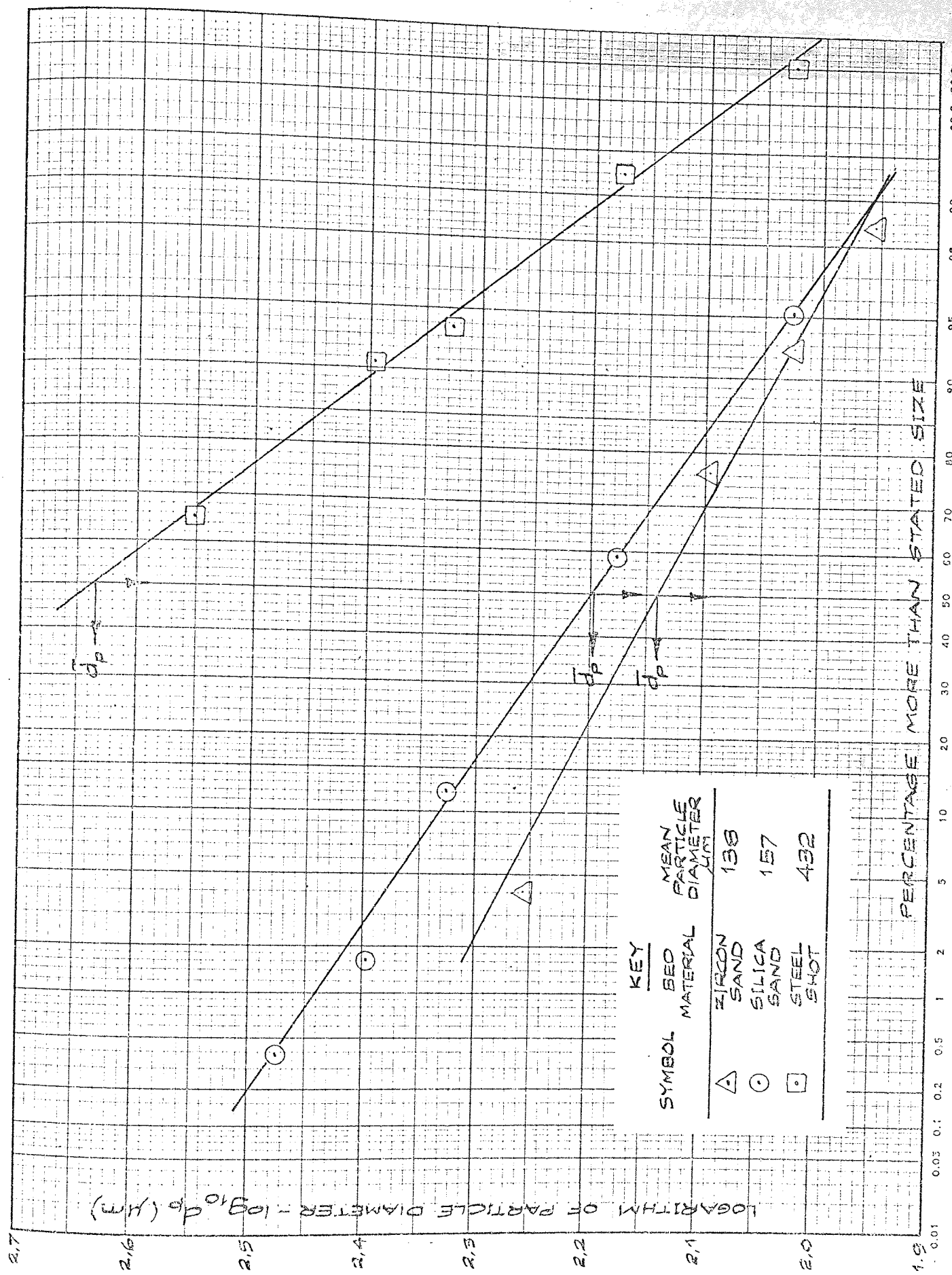

Figure A5.2 Mean Particle Diameter Estimation

Table A5.1 PROPERTIES OF FLUIDIZED PARTICLES

MATERIAL	GRADE	SIZE DISTRIBUTION μm	MEAN PARTICLE DIAMETER μm	PARTICLE DENSITY kg/m^3	BULK DENSITY kg/m^3	THERMAL CONDUCTIVITY $W/m\,K$	SPECIFIC HEAT $kJ/kg\,K$	THERMAL DIFFUSIVITY $m^2/s \times 10^6$
ZIRCON SAND	C.R.Z.	63-212	138	4600	3300	2.32	0.84	0.6
SILICA SAND	50FG	90-355	157	2620	1480	1.32	0.84	0.6
STEEL SHOT	S70	75-500	432	7500	3680	45.00	0.47	12.8

MATERIAL	DIMENSIONLESS GROUPS	
	$\frac{h_0 d_p}{k_f}$	$\frac{\alpha t_r}{d_p^2}$
ZIRCON SAND	0.0600h	0.0316t
SILICA SAND	0.1200h	0.0243t
STEEL SHOT	0.0096h	0.0685t
UNITS:	h_0 kW/m^{2}K ; t_r ms	

APPENDIX A6

STATISTICAL ANALYSIS OF PLAIN AND RADIAL EXTENDED SURFACE RESULTS

A6.1 Introduction

A multiple regression analysis of all plain tube and radial extended surface results was carried out using the model developed in Appendix A2 from the theory derived in Appendix A1. An analysis of all radial extended surface observations produced an unacceptable correlation coefficient. As a result, selected analyses were carried out for the manufactured, crimped and extruded surfaces to improve the degree of correlation. The computer line-printer output is reproduced.

The observations used for analysis purposes are listed in the residual tables, the reading number from the particular test being suffixed by the letters ROW.

When distinguishing between the independent variables relating to the bed configuration, bed material and type of surface, the following system was adopted.

Data : For bed configuration use

BEDMK2	BEDMK3	
1	1	If Mk 1 bed results
2	1	If Mk 2 bed results
1	2	If Mk 3 bed results

Data : For bed materials use

MASHOT	MASICA	
1	1	If zircon sand results
2	1	If steel shot results
1	2	If silica sand results

Data : For type of surface use

CRIMPE	EXTRUD	WELDED	
1	1	1	If manufactured surface results
2	1	1	If crimped tube results
1	2	1	If extruded tube results
1	1	2	If welded tube results

When interpreting the regression equation the same data numbers as listed above must be multiplied by the regression coefficient. This has the effect of modifying the intercept term.

A6.2 Terms Used in the Statistical Analysis

A6.2.1 Data

Bed Configuration:- Standard; Bed Mk 1 results
BEDMK2 - Bed Mk 2 results
BEDMK3 - Bed Mk 3 results

Bed Materials:- Standard; Zircon sand
MASHOT - Steel shot results
MASICA - Silica sand results

Surface Manufacture:- Standard; Manufactured Surface
CRIMPE - Crimped surface results
EXTRUD - Extruded surface results
WELDED - Welded surface results

Surface Position (Lower fin tip edge to distributor)
POSITN - h mm

Bed Static Height
STATHT - H mm

Extended Surface Geometry
Basic tube outside diameter - TUBDIA = d_o mm
Fin height - HEIGHT = l mm
Fin thickness - THICKN = t mm
Fin spacing - SPACNG = b mm

Superficial Fluidizing Velocity

VELOTY = u_f m/s

Temperature of Bed

TEMBED = T_b ^oC

Bed to Surface Heat Transfer Coefficient

HTCOEF = h_o kW/m^2 K

A6.2.2 Transformations

VELSQU = u_f^2 m^2/s^2

PRODUD = u_f x d_o m/s x mm

PROUUD = u_f^2 x d_o m^2/s^2 x mm

VELSHT = u_f x MASHOT m/s

VELSIC = u_f x MASICA m/s

SQTSPA = $\sqrt{b}$ $mm^{\frac{1}{2}}$

PRODUB = u_f x b m/s x mm

PRODUL = u_f x l m/s x mm

PROUUB = u_f^2 x b m^2/s^2 x mm

PROUUL = u_f^2 x l m^2/s^2 x mm

VELEXT = u_f x EXTRUD m/s

ETUDIA = exp(- do/1000)

EHEIHT = exp(l/1000)

A6.3 Plain Tube Results

15/35/34 14/06/74 ICL 1900 STATISTICAL ANALYSIS XDS3/19

MATRIX MATRX2 NUMBER OF OBSERVATIONS IN CROSS PRODUCT IS 52

	MEAN		MINIMUM VALUE		MAXIMUM VALUE		STANDARD DEVIATION	
CONST	.100000E	1						
HTCOEF	.556058E	0	.373000E	0	.740000E	0	.105181E	0
BEDMK2	.117308E	1	.100000E	1	.200000E	1	.384005E	0
BEDMK3	.167308E	1	.100000E	1	.200000E	1	.475665E	0
MASHOT	.121154E	1	.100000E	1	.200000E	1	.414384E	0
MASICA	.115385E	1	.100000E	1	.200000E	1	.364321E	0
STATHT	.561154E	2	.250000E	2	.620000E	2	.130994E	2
POSITN	.220096E	2	.130000E	2	.540000E	2	.148225E	2
TUBDIA	.143742E	2	.100000E	2	.158200E	2	.190514E	1
VELOTY	.420000E	0	.122000E	0	.144900E	1	.275579E	0
VELSQU	.250883E	0	.148840E-	1	.209960E	1	.401467E	0
TEMBED	.287546E	3	.192000E	3	.345000E	3	.315774E	2
PRODUD	.609673E	1	.171000E	1	.217350E	2	.422216E	1
PROUUD	.368658E	1	.223260E	0	.314940E	2	.605997E	1
VELSHT	.579077E	0	.122000E	0	.289800E	1	.614586E	0
VELSIC	.463092E	0	.122000E	0	.144900E	1	.283112E	0

15/42/10 14/06/74 ICL 1900 STATISTICAL ANALYSIS XDS3/19

REGRESSION ANALYSIS COVA MATRX2 CUT OFF PARAMETER .100000E- 5

DEPENDENT VARIABLE HTCOEF DEGREES OF FREEDOM 38

INDEPENDENT VARIABLES AT SIGNIFICANT LEVEL 99.00 %

BEDMK2 BEDMK3 MASHOT MASICA STATHT POSITN TUBDIA VELOTY VELSQU TEMBED PRODUD PROUUD VELSHT VELSIC

VARIABLES NOT IN THE REGRESSION SET

VAR NAME		T STAT	PART CORR	MULTIPLE CORRELATION	E S S
BEDMK3		0.00		0.990	.117731E- 1
E.S.S.	.117731E- 1				
RESIDUAL ERROR	.176017E- 1				
MULT CORR	0.990				
INTERCEPT TERM	- 1.9747061				

VARIABLES IN THE REGRESSION SET

VAR NAME	REGRESSION COEFF	STANDARD ERROR	CONFIDENCE INTERVAL	T STAT	PART CORR	MULTIPLE CORRELATION	E S S
BEDMK2	3.6801093	.379496E 0		9.70	0.84	0.963	.409081E- 1
MASHOT -	0.1771997	.266289E- 1		6.65	-0.73	0.977	.254923E- 1
MASICA -	0.1221089	.201208E- 1		6.07	-0.70	0.979	.231838E- 1
STATHT	0.0034968	.538191E- 3		6.50	0.73	0.978	.248524E- 1
POSITN -	0.0966689	.101042E- 1		9.57	-0.84	0.964	.401312E- 1
TUBDIA	0.0393155	.118966E- 1		3.30	0.47	0.986	.151568E- 1
VELOTY	0.5838930	.104932E 1		0.56	0.09	0.989	.118690E- 1
VELSQU -	0.0530464	.135897E 1		0.04	-0.01	0.990	.117736E- 1
TEMBED -	0.0004856	.222840E- 3		2.18	-0.33	0.988	.132443E- 1
PRODUD	0.0025964	.697826E- 1		0.04	0.01	0.990	.117735E- 1
PROUUD -	0.0144924	.902595E- 1		0.16	-0.03	0.990	.117811E- 1
VELSHT	0.0974374	.528121E- 1		1.84	0.29	0.989	.128277E- 1
VELSIC -	0.2279540	.764738E- 1		2.98	-0.44	0.987	.145259E- 1

RESIDUALS COVA MATRX2

OBS	Y	ESTIMATED Y	Y-ESTY	RATIO
ROWP02	.526000E 0	.533618E 0	-.761833E- 2	101.4484
ROWP03	.585000E 0	.577495E 0	.750479E- 2	98.7171
ROWP04	.614000E 0	.613886E 0	.113549E- 3	99.9815
ROWP05	.413000E 0	.419815E 0	-.681524E- 2	101.6502
ROWP06	.450000E 0	.441983E 0	.801068E- 2	98.2185
ROWP07	.466000E 0	.460686E 0	.531400E- 2	98.8597
ROWP08	.489000E 0	.487032E 0	.196791E- 2	99.5976
ROWP10	.515000E 0	.523483E 0	-.848332E- 2	101.6472
ROWP11	.690000E 0	.677516E 0	.124840E- 1	98.1907
ROWP12	.696000E 0	.689116E 0	.688445E- 2	99.0109
ROWP13	.724000E 0	.698239E 0	.257605E- 1	96.4419
ROWP14	.728000E 0	.706223E 0	.217769E- 1	97.0087
ROWP15	.740000E 0	.713201E 0	.267989E- 1	96.3785
ROWP16	.722000E 0	.719736E 0	.226441E- 2	99.6864
ROWP17	.708000E 0	.724691E 0	-.166908E- 1	102.3575
ROWP18	.624000E 0	.664754E 0	-.407536E- 1	106.5310
ROWP19	.613000E 0	.651525E 0	-.385247E- 1	106.2846
ROWP21	.578000E 0	.593592E 0	-.155919E- 1	102.6976
ROWP22	.602000E 0	.595440E 0	.655985E- 2	98.9105
ROWP23	.607000E 0	.599099E 0	.790136E- 2	98.6985
ROWP24	.611000E 0	.603753E 0	.724702E- 2	98.8159
ROWP25	.613000E 0	.615786E 0	-.278595E- 2	100.4545
ROWP26	.643000E 0	.633456E 0	.954366E- 2	98.5158
ROWP27	.632000E 0	.653524E 0	-.215240E- 1	103.4057
ROWP28	.694000E 0	.685350E 0	.864990E- 2	98.7536
ROWP29	.574000E 0	.568665E 0	.533549E- 2	99.0705
ROWP30	.590000E 0	.573954E 0	.160464E- 1	97.2803
ROWP31	.586000E 0	.577852E 0	.814829E- 2	98.6095

RESIDUALS COVA MATRX2

OBS	Y	ESTIMATED Y	Y-ESTY	RATIO
ROWP32	.594000E 0	.582258E 0	.117422E- 1	98.0252
ROWP33	.602000E 0	.586012E 0	.159085E- 1	97.3441
ROWP34	.594000E 0	.597323E 0	-.332477E- 2	100.5574
ROWP35	.598000E 0	.610752E 0	-.127522E- 1	102.1325
ROWP36	.586000E 0	.627186E 0	-.411859E- 1	107.0285
ROWP40	.409000E 0	.424082E 0	-.150823E- 1	103.6876
ROWP41	.449000E 0	.443388E 0	.561195E- 2	98.7501
ROWP42	.466000E 0	.461543E 0	.445674E- 2	99.0436
ROWP43	.490000E 0	.489473E 0	.526052E- 3	99.8925
ROWP44	.518000E 0	.521694E 0	-.369366E- 2	100.7131
ROWP45	.564000E 0	.542850E 0	.211504E- 1	96.2499
ROWP46	.580000E 0	.572799E 0	.720052E- 2	98.7585
ROWP47	.576000E 0	.587706E 0	-.117065E- 1	102.0324
ROWP48	.580000E 0	.596369E 0	-.163690E- 1	102.8222
ROWP49	.579000E 0	.586664E 0	-.766575E- 2	101.3236
ROWP50	.579000E 0	.563431E 0	.155690E- 1	97.3111
ROWP51	.383000E 0	.403502E 0	-.205024E- 1	105.3551
ROWP52	.399000E 0	.398414E 0	.586453E- 3	99.8551
ROWP53	.401000E 0	.391785E 0	.921479E- 2	97.7020
ROWP54	.399000E 0	.388330E 0	.106705E- 1	97.3257
ROWP55	.396000E 0	.385697E 0	.103035E- 1	97.3981
ROWP56	.384000E 0	.384781E 0	-.780787E- 3	100.2035
ROWP57	.383000E 0	.383696E 0	-.696487E- 3	100.1818
ROWP58	.373000E 0	.381796E 0	-.879656E- 2	102.3581

A6.4 All Extended Surface Results

18/11/13 24/06/74 ICL 1900 STATISTICAL ANALYSIS XDS3/19

MATRIX MATRX1

	MEAN		MINIMUM VALUE		MAXIMUM VALUE		VARIANCE	
CONST	.100000E	1						
HTCOEF	.393433E	0	.440000E-	1	.649000E	0	.196712E-	1
BEDMK2	.103448E	1	.100000E	1	.200000E	1	.334218E-	1
BEDMK3	.152490E	1	.100000E	1	.200000E	1	.250339E	0
MASHOT	.121073E	1	.100000E	1	.200000E	1	.166961E	0
MASICA	.103448E	1	.100000E	1	.200000E	1	.334218E-	1
CRIMPE	.130651E	1	.100000E	1	.200000E	1	.213380E	0
EXTRUD	.121839E	1	.100000E	1	.200000E	1	.171355E	0
WELDED	.104981E	1	.100000E	1	.200000E	1	.473096E-	1
STATHT	.472529E	2	.260000E	2	.790000E	2	.155605E	3
POSITN	.466667E	1	.000000E	0	.290000E	2	.751923E	2
HEIGHT	.966502E	1	.136000E	1	.178500E	2	.294781E	2
SPACNG	.239257E	1	.930000E	0	.570000E	1	.660335E	0
TUBDIA	.171222E	2	.100000E	2	.291000E	2	.187806E	2
THICKN	.739617E	0	.254000E	0	.159000E	1	.257603E	0
VELOTY	.367418E	0	.104000E	0	.134400E	1	.546666E-	1
TEMBED	.195483E	3	.102000E	3	.290000E	3	.176827E	4

MATRIX MATRX2

	MEAN		MINIMUM VALUE		MAXIMUM VALUE		STANDARD DEVIATION	
CONST	.100000E	1						
HTCOEF	.393433E	0	.440000E-	1	.649000E	0	.140254E	0
BEDMK2	.103448E	1	.100000E	1	.200000E	1	.182816E	0
BEDMK3	.152490E	1	.100000E	1	.200000E	1	.500339E	0
MASHOT	.121073E	1	.100000E	1	.200000E	1	.408609E	0
MASICA	.103448E	1	.100000E	1	.200000E	1	.182816E	0
CRIMPE	.130651E	1	.100000E	1	.200000E	1	.461931E	0
EXTRUD	.121839E	1	.100000E	1	.200000E	1	.413948E	0
WELDED	.104981E	1	.100000E	1	.200000E	1	.217967E	0
STATHT	.472529E	2	.260000E	2	.790000E	2	.125938E	2
POSITN	.466667E	1	.000000E	0	.290000E	2	.867135E	1
HEIGHT	.966502E	1	.136000E	1	.178500E	2	.542938E	1
TUBDIA	.171222E	2	.100000E	2	.291000E	2	.433566E	1
THICKN	.739617E	0	.254000E	0	.159000E	1	.487445E	0
VELOTY	.367418E	0	.104000E	0	.134400E	1	.233809E	0
VELSQU	.189453E	0	.108160E-	1	.180634E	1	.295005E	0
TEMBED	.195483E	3	.102000E	3	.290000E	3	.420508E	2
SQTSPA	.152225E	1	.964365E	0	.192354E	1	.274970E	0
PRODUB	.889456E	0	.145530E	0	.465171E	1	.690113E	0
PRODUD	.614168E	1	.112000E	1	.202944E	2	.378100E	1
PRODUL	.545836E	1	.220320E	0	.204204E	2	.289221E	1
PROHUB	.468707E	0	.190125E-	1	.606118E	1	.814925E	0
PROHUL	.172017E	1	.356918E-	1	.233609E	2	.264282E	1
PROHUD	.507225E	1	.125440E	0	.272757E	2	.440344E	1
VELSHT	.494467E	0	.104000E	0	.268800E	1	.503477E	0
VELEXT	.436674E	0	.104000E	0	.134400E	1	.216541E	0

CROSS PRODUCT MATRIX MATRX2

NUMBER OF OBSERVATIONS IN CROSS PRODUCT IS 261

	CONST	HTCOEF	BEDMK2	BEDMK3
CONST	.261000E 3	.102686E 3	.270000E 3	.398000E 3
HTCOEF	.102686E 3	.455146E 2	.106447E 3	.148825E 3
BEDMK2	.270000E 3	.106447E 3	.288000E 3	.407000E 3
BEDMK3	.398000E 3	.148825E 3	.407000E 3	.672000E 3
MASHOT	.316000E 3	.118952E 3	.325000E 3	.508000E 3
MASICA	.270000E 3	.104436E 3	.279000E 3	.416000E 3
CRIMPE	.341000E 3	.126992E 3	.350000E 3	.558000E 3
EXTRUD	.318000E 3	.131482E 3	.327000E 3	.455000E 3
WELDED	.274000E 3	.108249E 3	.283000E 3	.411000E 3
STATHT	.123350E 5	.493645E 4	.130440E 5	.178500E 5
POSITN	.121800E 4	.537493E 3	.147900E 4	.165000E 4
HEIGHT	.252257E 4	.970412E 3	.268322E 4	.373577E 4
TURDIA	.446890E 4	.174752E 4	.460480E 4	.669960E 4
THICKN	.193040E 3	.794096E 2	.207350E 3	.258675E 3
VELOTY	.956960E 2	.401462E 2	.986340E 2	.154048E 3
VELSQU	.494472E 2	.211582E 2	.503420E 2	.857668E 2
TEMBED	.510210E 5	.205104E 5	.522150E 5	.766370E 5
SQTSPA	.397306E 3	.157644E 3	.411395E 3	.605559E 3
PRODUB	.232148E 3	.984160E 2	.238856E 3	.373665E 3
PRODUD	.160298E 4	.667267E 3	.164432E 4	.252719E 4
PRODUL	.902632E 3	.360627E 3	.951505E 3	.1419546 4
PRODUB	.122552E 3	.527555E 2	.124525E 3	.213592E 3
PRODUL	.448965E 3	.188475E 3	.464037E 3	.768431E 3
PRODUD	.801857E 3	.341666E 3	.815388E 3	.136805E 4
VELSHT	.129056E 3	.519078E 2	.131794E 3	.220566E 3
VELEXT	.113972E 3	.494710E 2	.116710E 3	.172124E 3

	MASHOT	MASICA	CRIMPE	EXTRUD
CONST	.316000E 3	.270000E 3	.341000E 3	.318000E 3
HTCOEF	.118954E 3	.104436E 3	.126992E 3	.131482E 3
BEDMK2	.325000E 3	.279000E 3	.350000E 3	.327000E 3
BEDMK3	.508000E 3	.416000E 3	.558000E 3	.455000E 3
MASHOT	.426000E 3	.325000E 3	.419000E 3	.373000E 3
MASICA	.325000E 3	.288000E 3	.359000E 3	.327000E 3
CRIMPE	.419000E 3	.359000E 3	.501000E 3	.398000E 3
EXTRUD	.373000E 3	.327000E 3	.398000E 3	.432000E 3
WELDED	.329000E 3	.283000E 3	.354000E 3	.331000E 3
STATHT	.146460E 5	.126120E 5	.169800E 5	.151850E 5
POSITN	.146100E 4	.121800E 4	.123900E 4	.136800E 4
HEIGHT	.302787E 4	.259457E 4	.514367E 4	.276749E 4
TURDIA	.529830E 4	.460480E 4	.583890E 4	.552370E 4
THICKN	.224322E 3	.193525E 3	.213360E 3	.222845E 3
VELOTY	.129050E 3	.984650E 2	.125934E 3	.113972E 3
VELSQU	.602052E 2	.505508E 2	.664144E 2	.559918E 2
TEMBED	.633100E 5	.527580E 5	.654710E 5	.643280E 5
SQTSPA	.484958E 3	.408833E 3	.513826E 3	.471156E 3
PRODUB	.318014E 3	.256361E 3	.300850E 3	.263807E 3
PRODUD	.210301E 4	.164177E 4	.210267E 4	.193325E 4
PRODUL	.120055E 4	.923184E 3	.113434E 4	.978014E 3
PRODUB	.192185E 3	.123814E 3	.163469E 3	.133603E 3
PRODUL	.688975E 3	.456194E 3	.578666E 3	.475452E 3
PRODUD	.120533E 4	.815500E 3	.107583E 4	.920089E 3
VELSHT	.195376E 3	.151625E 3	.172934E 3	.147132E 3
VELEXT	.147132E 3	.116541E 3	.144010E 3	.150124E 3

	WELDED	STATHT	POSITN	HEIGHT
CONST	.274000E 3	.123350E 5	.121800E 4	.252257E 4
HTCOEF	.108249E 3	.493645E 4	.537493E 3	.970412E 3
BEDMK2	.283000E 3	.130440E 5	.147900E 4	.268322E 4
BEDMK3	.411000E 3	.178500E 5	.165000E 4	.373577E 4
MASHOT	.329000E 3	.146460E 5	.146100E 4	.302787E 4
MASICA	.283000E 3	.126120E 5	.121800E 4	.259457E 4
CRIMPE	.354000E 3	.169800E 5	.123900E 4	.514367E 4
EXTRUD	.331000E 3	.151850E 5	.136800E 4	.276749E 4
WELDED	.300000E 3	.129830E 5	.121800E 4	.264207E 4
STATHT	.129830E 5	.622707E 6	.777450E 5	.127010E 6
POSITN	.121800E 4	.777450E 5	.652340E 5	.143860E 5
HEIGHT	.264207E 4	.127010E 6	.143860E 5	.320450E 5
TURDIA	.479910E 4	.211955E 6	.165397E 5	.424442E 5
THICKN	.209550E 3	.103196E 5	.140482E 4	.233455E 4
VELOTY	.998490E 2	.445722E 4	.455104E 3	.902632E 3
VELSQU	.508345E 2	.222934E 4	.237336E 3	.448965E 3
TEMBED	.537290E 5	.240467E 7	.256884E 6	.464274E 6
SQTSPA	.419167E 3	.189625E 5	.194870E 4	.404844E 4
PRODUB	.245487E 3	.109435E 5	.119180E 4	.250360E 4
PRODUD	.170262E 4	.748670E 5	.692177E 4	.148943E 5
PRODUL	.937672E 3	.444187E 5	.477996E 4	.111673E 5
PRODUB	.126376E 3	.555201E 4	.620084E 3	.119722E 4
PRODUL	.461101E 3	.212156E 5	.208857E 4	.529649E 4
PRODUD	.837082E 3	.383506E 5	.380249E 4	.722565E 4
VELSHT	.132079E 3	.585226E 4	.608507E 3	.120055E 4
VELEXT	.117895E 3	.536102E 4	.505754E 3	.978014E 3

	TURDIA	THICKN	VELOTY	VELSQU
CONST	.446890E 4	.193040E 3	.956960E 2	.494472E 2
HTCOEF	.174752E 4	.794096E 2	.401462E 2	.211582E 2
BEDMK2	.460480E 4	.207350E 3	.986340E 2	.503420E 2
BEDMK3	.669960E 4	.258675E 3	.154048E 3	.857668E 2
MASHOT	.529830E 4	.224322E 3	.129056E 3	.602052E 2
MASICA	.460480E 4	.193526E 3	.984650E 2	.505508E 2
CRIMPE	.583890E 4	.213360E 3	.125934E 3	.664144E 2
EXTRUD	.552370E 4	.222845E 3	.113972E 3	.559918E 2
WELDED	.479910E 4	.209550E 3	.998490E 2	.508345E 2
STATHT	.211955E 6	.103196E 5	.445722E 4	.222934E 4
POSITN	.165397E 5	.140482E 4	.455104E 3	.237336E 3
HEIGHT	.424442E 5	.233455E 4	.902632E 3	.448965E 3
TURDIA	.814004E 5	.329628E 4	.160298E 4	.801857E 3
THICKN	.529628E 4	.206552E 3	.678726E 2	.325431E 2
VELOTY	.160298E 4	.678726E 2	.494472E 2	.351848E 2
VELSQU	.801857E 3	.325431E 2	.351848E 2	.516894E 2
TEMBED	.867765E 6	.370709E 5	.196722E 5	.105647E 5
SQTSPA	.677089E 4	.310112E 3	.147010E 3	.167911E 2
PRODUB	.[illegible]91E 4	.178500E 3	.122332E 3	.895062E 2
PRODUD	.282799E 5	.113785E 4	.801857E 3	.553826E 3
PRODUL	.148945E 5	.784317E 3	.448965E 3	.307831E 3
PRODUB	.196790E 4	.851021E 2	.895062E 2	.826169E 2
PRODUL	.722565E 4	.349539E 3	.307831E 3	.268296E 3
PRODUD	.135619E 5	.578841E 3	.553826E 3	.488440E 3
VELSHT	.210301E 4	.867474E 2	.762052E 2	.610667E 2
VELEXT	.193325E 4	.771657E 2	.559918E 2	.377960E 2

	TEMBED		SQTSPA		PRODUB		PRODUD	
CONST	.510210E	5	.397508E	3	.232148E	3	.160298E	4
HTCOEF	.205104E	5	.157644E	3	.984160E	2	.667267E	3
BEDMK2	.522150E	5	.411395E	3	.238856E	3	.164432E	4
BEDMK3	.760370E	5	.605559E	3	.373665E	3	.252719E	4
MASHOT	.653100E	5	.484958E	5	.318014E	3	.210301E	4
MASICA	.527580E	5	.408855E	3	.256361E	3	.164177E	4
CRIMPE	.654710E	5	.515825E	3	.300850E	3	.210267E	4
EXTRUD	.643260E	5	.471156E	3	.263807E	3	.193325E	4
WELDED	.537290E	5	.419167E	3	.243687E	3	.170262E	4
STATHT	.240467E	7	.189625E	5	.109455E	5	.748670E	5
POSITN	.256884E	6	.194876E	4	.119188E	4	.692177E	4
HEIGHT	.462478E	6	.404844E	4	.236360E	4	.148945E	5
TURBIA	.867765E	6	.677089E	4	.384991E	4	.252799E	5
THICKN	.370709E	5	.310112E	5	.178500E	3	.113783E	4
VELOTY	.196722E	5	.147010E	3	.122352E	3	.801857E	3
VELSQU	.105647E	5	.767911E	2	.895062E	2	.558826E	3
TEMPED	.104335E	8	.772809E	5	.475156E	5	.327001E	6
SQTSPA	.772809E	5	.624460E	3	.375923E	3	.244655E	4
PRODUB	.475156E	5	.375925E	3	.330313E	3	.196790E	4
PRODUD	.327001E	6	.244655E	4	.196790E	4	.135619E	5
PRODUL	.173138E	6	.144737E	4	.116972E	4	.722565E	4
PROUUB	.262690E	5	.199158E	3	.244895E	3	.139910E	4
PROUUL	.898467E	5	.718601E	3	.801963E	3	.482896E	4
PROUUD	.170464E	6	.123961E	4	.139910E	4	.896014E	4
VELSHT	.270850E	5	.199969E	3	.192185E	3	.120533E	4
VELEXT	.239585E	5	.170236E	3	.133603E	3	.920089E	3

	PRODUL		PROUUB		PROUUL		PROUUD	
CONST	.902852E	3	.122556E	3	.448965E	3	.801857E	3
HTCOEF	.369627E	3	.527555E	2	.188475E	3	.341666E	3
BEDMK2	.951505E	3	.124525E	3	.464937E	3	.815560E	3
BEDMK3	.141934E	4	.213592E	3	.768431E	3	.156803E	4
MASHOT	.120055E	4	.192185E	3	.683975E	3	.120555E	4
MASICA	.923184E	3	.123814E	3	.456194E	3	.815500E	3
CRIMPE	.113434E	4	.163469E	3	.578666E	3	.107585E	4
EXTRUD	.978014E	3	.133605E	3	.475452E	3	.920089E	3
WELDED	.937672E	3	.126576E	3	.461101E	3	.857089E	3
STATHT	.444187E	5	.355201E	4	.212156E	5	.365506E	5
POSITN	.477996E	4	.620084E	3	.208837E	4	.360249E	4
HEIGHT	.111675E	5	.116972E	4	.529649E	4	.722565E	4
TURBIA	.148045E	5	.196790E	4	.722565E	4	.135619E	5
THICKN	.784317E	3	.851021E	2	.549539E	3	.550841E	3
VELOTY	.448965E	3	.895062E	2	.307851E	3	.555826E	3
VELSQU	.307831E	3	.626169E	2	.268296E	3	.488440E	3
TEMPED	.175138E	6	.262690E	5	.898467E	5	.170464E	6
SQTSPA	.144737E	4	.199158E	3	.718601E	3	.123961E	4
PRODUB	.116972E	4	.244895E	3	.801965E	3	.139910E	4
PRODUD	.722565E	4	.139910E	4	.482896E	4	.896014E	4
PRODUL	.529649E	4	.801963E	3	.344407E	4	.482896E	4
PROUUB	.801965E	3	.229157E	3	.703099E	3	.126725E	4
PROUUL	.344407E	4	.703099E	3	.287352E	4	.413056E	4
PROUUD	.482896E	4	.126725E	4	.413056E	4	.764330E	4
VELSHT	.683975E	3	.157705E	3	.529998E	3	.944058E	3
VELEXT	.475452E	3	.939265E	2	.518088E	3	.600548E	3

	VELSHT		VELEXT	
CONST	.129056E	3	.113972E	3
HTCOEF	.519078E	2	.694710E	2
BEDMK2	.131794E	3	.114710E	3
BEDMK3	.220368E	3	.192124E	3
MASHOT	.195370E	3	.147152E	3
MASICA	.131625E	3	.114541E	3
CRIMPE	.172954E	3	.144010E	3
EXTRUD	.147152E	3	.150124E	3
WELDED	.132979E	3	.117695E	3
STATHT	.585226E	4	.536102E	4
POSITN	.608507E	3	.506754E	3
HEIGHT	.120055E	4	.976014E	3
TURBIA	.210301E	4	.193325E	4
THICKN	.867474E	2	.771657E	2
VELOTY	.762052E	2	.550018E	2
VELSQU	.610667E	2	.377960E	2
TEMBED	.270850E	5	.239585E	5
SQTSPA	.199969E	3	.170236E	3
PRODUB	.192185E	3	.133603E	3
PRODUD	.120533E	4	.920089E	3
PRODUL	.683975E	3	.475452E	3
PROUUB	.157705E	3	.939265E	2
PROUUL	.529998E	3	.518088E	3
PROUUD	.944058E	3	.600548E	3
VELSHT	.129721E	3	.827498E	2
VELEXT	.827498E	2	.690811E	2

COVARIANCE MATRIX MATRX2

NUMBER OF OBSERVATIONS IS 461

	HTCOEF	BEDMK2	BEDMK3	MASHOT
HTCOEF	.196712E- 1	.846552E- 3	-.298512E- 1	-.206647E- 1
BEDMK2	.846552E- 3	.334216E- 1	-.181696E- 1	-.729443E- 2
BEDMK3	-.298512E- 1	-.181696E- 1	.250339E 0	.100301E 0
MASHOT	-.206647E- 1	-.729443E- 2	.100301E 0	.166961E 0
MASICA	-.688806E- 2	-.119363E- 2	.164456E- 1	-.729443E- 2
CRIMPE	-.275717E- 1	-.106101E- 1	.146185E 0	.236222E- 1
EXTRUD	.245012E- 1	-.755968E- 2	-.115075E 0	-.461981E- 1
WELDED	.172451E- 2	-.172414E- 2	-.262452E- 1	-.105364E- 1
STATHT	.554759E 0	.109894E 1	-.375632E 1	-.109965E 1
POSITN	.224199E 0	.842308E 0	-.797436E 0	-.325641E- 1
HEIGHT	-.848095E- 1	.283326E 0	-.426760E 0	-.101064E 0
TURDIA	-.411100E- 1	-.700000E- 1	-.442479E 0	-.432009E 0
THICKN	.136590E- 1	.294365E- 1	-.137279E 0	-.361420E- 1
VELOTY	.929843E- 2	-.218753E- 2	.300607E- 1	.498155E- 1
VELSQU	.655414E- 2	-.311652E- 2	.398633E- 1	.628385E- 1
TEMBED	.168105E 1	-.218210E 1	-.525055E 1	.391526E 1
SQTSPA	.511598E- 2	.148834E- 2	-.114110E- 2	.151027E- 1
PRODUB	.272359E- 1	-.498847E- 2	.756227E- 1	.142100E 0
PRODUD	.140780E 0	-.535818E- 1	.316491E 0	.624014E 0
PRODUL	.557776E- 1	.683618E- 1	.165051E 0	.414195E 0
PRODUB	.177921E- 1	-.772288E- 2	.104025E 0	.169513E 0
PRODUL	.455268E- 1	.188566E- 2	.322317E 0	.540003E 0
PRODUD	.100729E 0	-.543809E- 1	.558816E 0	.901915E 0
VELSHT	.435747E- 2	-.658541E- 2	.906537E- 1	.150478E 0
VELEXT	.185796E- 1	-.458488E- 2	-.643224E- 2	.351650E- 1

	MASICA	CRIMPE	EXTRUD	WELDED
HTCOEF	-.688806E- 2	-.275717E- 1	.245012E- 1	.172451E- 2
BEDMK2	-.119363E- 2	-.106101E- 1	-.755968E- 2	-.172414E- 2
BEDMK3	.164456E- 1	.146185E 0	-.115075E 0	-.262452E- 1
MASHOT	-.729443E- 2	.236222E- 1	-.461981E- 1	-.105364E- 1
MASICA	.554210E- 1	.240053E- 1	-.755968E- 2	-.172414E- 2
CRIMPE	.240053E- 1	.213380E 0	-.671972E- 1	-.153257E- 1
EXTRUD	-.755968E- 2	-.671972E- 1	.171355E 0	-.109195E- 1
WELDED	-.172414E- 2	-.153257E- 1	-.109195E- 1	.475096E- 1
STATHT	-.562599E 0	-.455858E 1	.602255E 0	.132356E 0
POSITN	-.161556E 0	-.135513E 1	-.446154E 0	-.233353E 0
HEIGHT	-.576355E- 1	-.585000E 0	-.117687E 1	-.236356E- 1
TURDIA	-.700000E- 1	.854704E- 3	.303205E 0	.413889E 0
THICKN	-.168096E- 1	-.149421E 0	-.475122E- 1	.265192E- 1
VELOTY	-.283753E- 2	.247919E- 2	-.110262E- 1	-.329242E- 2
VELSQU	-.308271E- 2	.696510E- 2	-.163622E- 1	-.413758E- 2
TEMBED	-.859410E- 1	-.457162E 1	.832495E 1	.641247E 0
SQTSPA	-.856396E- 2	-.202554E- 1	-.496950E- 1	.796106E- 2
PRODUB	-.145844E- 1	-.943994E- 2	-.732293E- 1	-.860860E- 3
PRODUD	-.633968E- 1	.321607E- 1	-.761672E- 1	.761632E- 1
PRODUL	-.406665E- 1	-.172914E 0	-.468247E 0	-.381485E- 1
PRODUB	-.105250E- 1	.140005E- 1	-.594069E- 1	-.787504E- 2
PRODUL	-.517422E- 1	-.304556E- 1	-.275241E 0	-.393305E- 1
PRODUD	-.538704E- 1	.108420E 0	-.218790E 0	-.181017E- 1
VELSHT	-.723541E- 2	.166117E- 1	-.388794E- 1	-.963491E- 2
VELEXT	-.523488E- 2	-.188306E- 1	.433137E- 1	-.674525E- 2

	STATHT	POSITN	HEIGHT	TURDIA
HTCOEF	.554759E 0	.224199E 0	-.848095E- 1	-.411100E- 1
BEDMK2	.109894E 1	.842308E 0	.283326E 0	-.700000E- 1
BEDMK3	-.375632E 1	-.797436E 0	-.426760E 0	-.442479E 0
MASHOT	-.109965E 1	-.325641E- 1	-.101064E 0	-.432009E 0
MASICA	-.562599E 0	-.161556E 0	-.576355E- 1	-.700000E- 1
CRIMPE	-.455858E 1	-.135513E 1	-.585000E 0	.854704E- 3
EXTRUD	.602255E 0	-.446154E 0	-.117687E 1	.303205E 0
WELDED	.132356E 0	-.233353E 0	-.236356E- 1	.413889E 0
STATHT	.153603E 3	.765038E 2	.300674E 2	.301628E 1
POSITN	.765038E 2	.751925E 2	.100564E 2	-.870449E 1
HEIGHT	.300674E 2	.100564E 2	.294701E 2	-.287699E 1
TURDIA	.301628E 1	-.870449E 1	-.287699E 1	.187405E 1
THICKN	.460724E 1	.193855E 1	.180512E 1	-.545794E- 1
VELOTY	-.285140E 0	-.291897E- 1	-.930959E- 1	-.144905E 0
VELSQU	-.412259E 0	-.253160E- 1	-.111320E 0	-.172267E 0
TEMBED	-.239035E 2	-.466925E 1	-.117851E 3	-.224165E 2
SQTSPA	.724421E 0	.364069E 0	.801757E 0	-.122694E 0
PRODUB	-.100741E 0	.417393E 0	.461116E 0	-.480933E 0
PRODUD	-.337784E 1	-.214921E 1	-.250162E 1	.320507E 1
PRODUL	.679530E 1	.218339E 1	.939756E 1	-.215605E 1
PRODUB	-.879026E 0	.189228E 0	-.485451E- 1	-.487516E 0
PRODUL	.288015E- 2	-.261433E- 1	.568169E 1	-.177351E 1
PRODUD	-.592097E 1	-.536547E 0	-.201659E 1	-.644783E 0
VELSHT	-.946180E 0	.240218E- 1	-.172986E 0	-.410435E 0
VELEXT	-.941712E- 1	-.100444E 0	-.475100E 0	-.700181E- 1

	THICKN	VELOTY	VELSQU	TEMBED
HTCOEF	.136590E- 1	.929843E- 2	.655414E- 2	.168105E 1
BEDMK2	.294365E- 1	-.218755E- 2	-.311652E- 2	-.218210E 1
BEDMK3	-.137279E 0	.300607E- 1	.398633E- 1	-.525055E 1
MASHOT	-.361420E- 1	.498155E- 1	.628385E- 1	.391526E 1
MASICA	-.168096E- 1	-.283753E- 2	-.308271E- 2	-.859410E- 1
CRIMPE	-.149421E 0	.247919E- 2	.696510E- 2	-.457162E 1
EXTRUD	-.475122E- 1	-.110262E- 1	-.163622E- 1	.832495E 1
WELDED	.265192E- 1	-.329242E- 2	-.413758E- 2	.641247E 0
STATHT	.460724E 1	-.285140E 0	-.412259E 0	-.239035E 2
POSITN	.193855E 1	-.291897E- 1	-.253160E- 1	-.466925E 1
HEIGHT	.180512E 1	-.930959E- 1	-.111320E 0	-.117851E 3
TURDIA	-.545794E- 1	-.144905E 0	-.172267E 0	-.224165E 2
THICKN	.237603E 0	-.117449E- 1	-.154956E- 1	-.455817E 1
VELOTY	-.117449E- 1	.544666E- 1	.654501E- 1	.356214E 1
VELSQU	-.154956E- 1	.654501E- 1	.859517E- 1	.345621E 1
TEMBED	-.455817E 1	.356214E 1	.345621E 1	.176827E 4
SQTSPA	.625242E- 1	.327157E- 2	.584635E- 2	-.148410E 1
PRODUB	.261504E- 1	.142451E 0	.175097E 0	.821018E 1
PRODUD	-.183695E 0	.818825E 0	.962068E 0	.524881E 2
PRODUL	.448905E 0	.451239E 0	.526251E 0	-.127345E 2
PRODUB	-.206810E- 1	.171381E 0	.228618E 0	.905812E 1
PRODUL	.672190E- 1	.549514E 0	.704764E 0	.800681E 1
PRODUD	-.239328E 0	.996962E 0	.129436E 1	.527490E 2
VELSHT	-.334792E- 1	.110722E 0	.140835E 0	.714147E 1
VELEXT	-.274227E- 1	.542943E- 1	.623217E- 1	.645740E 1

	SQTSPA	PRODUB	PRODUD	PRODUL
HTCOEF	.511596E- 2	.272559E- 1	.140780E 0	.557776E- 1
BEDMK2	.148834E- 2	-.498847E- 2	-.535818E- 1	.682618E- 1
BEDMK3	-.114110E- 2	.756227E- 1	.518491E 0	.165051E 0
MASHOT	.131027E- 1	.142100E 0	.624014E 0	.414195E 0
MASICA	-.836396E- 2	-.145844E- 1	-.833968E- 1	-.406663E- 1
CRIMPE	-.202354E- 1	-.943994E- 2	.321607E- 1	-.172919E 0
EXTRUD	-.496950E- 1	-.752295E- 1	-.761672E- 1	-.468247E 0
WELDED	.796106E- 2	-.860860E- 3	.761652E- 1	-.381485E- 1
STATHT	.724421E 0	-.100741E 0	-.557784E 1	.670550E 1
POSITN	.564069E 0	.417595E 0	-.214971E 1	.218339E 1
HEIGHT	.801757E 0	.461116E 0	-.230125E 1	.959756E 1
TUBDIA	-.122694E 0	-.480690E 0	.320507E 1	-.215606E 1
THICKN	.625242E- 1	.261504E- 1	-.183695E 0	.448905E 0
VELOTY	.597157E- 2	.142451E 0	.818825E 0	.451239E 0
VELSQU	.584655E- 2	.175097E 0	.962068E 0	.526251E 0
TEMPED	-.148410E 1	.821015E 1	.524881E 2	-.122343E 2
SQTSPA	.756084E- 1	.866764E- 1	.246109E- 1	.282077E 0
PRODUB	.866764E- 1	.476257E 0	.208509E 1	.141105E 1
PRODUD	.246109E- 1	.208509E 1	.142960E 2	.646914E 1
PRODUL	.282077E 0	.141105E 1	.646914E 1	.836486E 1
PRODUB	.497605E- 1	.523407E 0	.249144E 1	.145728E 1
PRODUL	.135476E 0	.154857E 1	.796754E 1	.727457E 1
PRODUD	.730251E- 1	.263801E 1	.155208E 2	.790711E 1
VELSHT	.135116E- 1	.297674E 0	.158754E 1	.914051E 0
VELEXT	-.125326E- 1	.125961E 0	.846577E 0	.312677E 0

	PRODUB	PRODUL	PRODUD	VELSHT
HTCOEF	.177921E- 1	.455288E- 1	.100729E 0	.455747E- 2
BEDMK2	-.779588E- 2	.188566E- 2	-.543809E- 1	-.658541E- 2
BEDMK3	.104625E 0	.522517E 0	.558810E 0	.906537E- 1
MASHOT	.169513E 0	.540005E 0	.901915E 0	.150478E 0
MASICA	-.105250E- 1	-.517422E- 1	-.558704E- 1	-.725541E- 2
CRIMPE	.140005E- 1	-.504356E- 1	.108420E 0	.166177E- 1
EXTRUD	-.594067E- 1	-.275241E 0	-.218790E 0	-.388794E- 1
WELDED	-.787504E- 2	-.593303E- 1	-.181017E- 1	-.963491E- 2
STATHT	-.879028E 0	.288913E- 2	-.592097E 1	-.946180E 0
POSITN	.189228E 0	-.261435E- 1	-.536547E 0	.240218E- 1
HEIGHT	-.485451E- 1	.368169E 1	-.201659E 1	-.179986E 0
TUBDIA	-.487818E 0	-.177551E 1	-.644785E 0	-.410435E 0
THICKN	-.206810E- 1	.672190E- 1	-.239328E 0	-.334792E- 1
VELOTY	.171381E 0	.549514E 0	.996962E 0	.110722E 0
VELSQU	.228618E 0	.704764E 0	.129436E 1	.140635E 0
TEMPED	.905812E 1	.800681E 1	.527490E 2	.714147E 1
SQTSPA	.497605E- 1	.135476E 0	.730251E- 1	.135116E- 1
PRODUB	.523407E 0	.154857E 1	.263801E 1	.297674E 0
PRODUD	.249144E 1	.796754E 1	.155200E 2	.158734E 1
PRODUL	.145728E 1	.727457E 1	.790711E 1	.914051E 0
PRODUB	.660845E 0	.189487E 1	.542851E 1	.375897E 0
PRODUL	.199487E 1	.808165E 1	.105816E 2	.118461E 1
PRODUD	.342851E 1	.105816E 2	.199225E 2	.210602E 1
VELSHT	.375897E 0	.118461E 1	.210602E 1	.255489E 0
VELEXT	.155796E 0	.469372E 0	.963069E 0	.101517E 0

	VELEXT
HTCOEF	.486060E 0
BEDMK2	-.920198E- 1
BEDMK3	-.471700E- 1
MASHOT	.515770E 0
MASICA	-.105066E 0
CRIMPE	-.140573E 0
EXTRUD	.583926E 0
WELDED	-.113547E 0
STATHT	-.278794E- 1
POSITN	-.425014E- 1
HEIGHT	-.321077E 0
TUBDIA	-.592821E- 1
THICKN	-.206420E 0
VELOTY	.852042E 0
VELSQU	.780427E 0
TEMPED	.563445E 0
SQTSPA	-.167254E 0
PRODUB	.659070E 0
PRODUD	.821556E 0
PRODUL	.396675E 0
PRODUB	.703195E 0
PRODUL	.605808E 0
PRODUD	.791691E 0
VELSHT	.739820E 0
VELEXT	.100000E 1

CORRELATION MATRIX MATRX2

NUMBER OF OBSERVATIONS IS 261

	HTCOEF	BEDMK2	BEDMK3	MASHOT
HTCOEF	.100000E 1	.330160E- 1	-.425386E 0	-.360585E 0
BEDMK2	.330160E- 1	.100000E 1	-.198442E 0	-.976492E- 1
BEDMK3	-.425386E 0	-.198442E 0	.100000E 1	.491585E 0
MASHOT	-.360585E 0	-.976492E- 1	.491585E 0	.100000E 1
MASICA	-.268636E 0	-.357143E- 1	.179792E 0	-.976492E- 1
CRIMPE	-.425570E 0	-.125640E 0	.632494E 0	.125151E 0
EXTRUD	.422015E 0	-.998949E- 1	-.555612E 0	-.273130E 0
WELDED	.564104E- 1	-.432680E- 1	-.240655E 0	-.118302E 0
STATHT	.319144E 0	.485016E 0	-.605753E 0	-.217141E 0
POSITN	.184345E 0	.531336E 0	-.183800E 0	-.148552E- 1
HEIGHT	-.111375E 0	.284465E 0	-.157098E 0	-.455542E- 1
TUBDIA	-.676361E- 1	-.883546E- 1	-.204067E 0	-.243966E 0
THICKN	.199792E 0	.330327E 0	-.562878E 0	-.181459E 0
VELOTY	.283553E 0	-.511775E- 1	.256065E 0	.521429E 0
VELSQU	.159487E 0	-.581810E- 1	.271917E 0	.524861E 0
TEMRED	.285028E 0	-.283848E 0	-.249554E 0	.544148E 0
SQTSPA	.132657E 0	.296076E- 1	-.829421E- 2	.134417E 0
PRODUB	.281368E 0	-.398395E- 1	.214011E 0	.503925E 0
PRODUD	.265472E 0	-.775166E- 1	.168355E 0	.403905E 0
PRODUL	.137504E 0	.129102E 0	.114057E 0	.350483E 0
PROUUB	.156049E 0	-.524365E- 1	.255755E 0	.310525E 0
PROUUL	.114188E 0	.362827E- 2	.226605E 0	.466878E 0
PROUUD	.160905E 0	-.666442E- 1	.250228E 0	.494525E 0
VELSHT	.617079E- 1	-.715466E- 1	.359867E 0	.731452E 0
VELEXT	.486060E 0	-.920198E- 1	-.471700E- 1	.515770E 0

	MASICA	CRIMPE	EXTRUD	WELDED
HTCOEF	-.268636E 0	-.425570E 0	.422015E 0	.564104E- 1
BEDMK2	-.357143E- 1	-.125640E 0	-.998949E- 1	-.432680E- 1
BEDMK3	.179792E 0	.632494E 0	-.555612E 0	-.240655E 0
MASHOT	-.976492E- 1	.125151E 0	-.273130E 0	-.118302E 0
MASICA	.100000E 1	.284260E 0	-.998949E- 1	-.432680E- 1
CRIMPE	.284260E 0	.100000E 1	-.351421E 0	-.152213E 0
EXTRUD	-.998949E- 1	-.351421E 0	.100000E 1	-.121023E 0
WELDED	-.432680E- 1	-.152213E 0	-.121023E 0	.100000E 1
STATHT	-.248305E 0	-.761315E 0	.117390E 0	.508458E- 1
POSITN	-.101900E 0	-.338511E 0	-.124295E 0	-.123452E 0
HEIGHT	-.580663E- 1	-.253255E 0	-.523640E 0	-.199722E- 1
TUBDIA	-.883546E- 1	.426957E- 3	.169019E 0	.438166E 0
THICKN	-.188635E 0	-.663602E 0	-.235469E 0	.240599E 0
VELOTY	-.663845E- 1	.229547E- 1	-.113925E 0	-.644084E- 1
VELSQU	-.575498E- 1	.514607E- 1	-.134903E 0	-.647860E- 1
TEMRED	-.111795E- 1	-.253352E 0	.478257E 0	.696618E- 1
SQTSPA	-.166365E 0	-.159312E 0	-.436580E 0	.132830E 0
PRODUB	-.115590E 0	-.296122E- 1	-.256341E 0	-.572296E- 2
PRODUD	-.917162E- 1	.184137E- 1	-.486649E- 1	.924160E- 1
PRODUL	-.769113E- 1	-.129430E 0	-.391111E 0	-.605139E- 1
PROUUB	-.708204E- 1	.372831E- 1	-.176540E 0	-.444440E- 1
PROUUL	-.610764E- 1	-.251769E- 1	-.233893E 0	-.634727E- 1
PROUUD	-.660185E- 1	.525849E- 1	-.118417E 0	-.184063E- 1
VELSHT	-.786085E- 1	.714520E- 1	-.186550E 0	-.877966E- 1
VELEXT	-.105066E 0	-.149575E 0	.383926E 0	-.113547E 0

	STATHT	POSITN	HEIGHT	TUBDIA
HTCOEF	.319144E 0	.184345E 0	-.111375E 0	-.676361E- 1
BEDMK2	.485016E 0	.531336E 0	.284465E 0	-.883546E- 1
BEDMK3	-.605753E 0	-.183800E 0	-.157098E 0	-.204067E 0
MASHOT	-.217141E 0	-.148552E- 1	-.455542E- 1	-.243966E 0
MASICA	-.248305E 0	-.101900E 0	-.580663E- 1	-.883546E- 1
CRIMPE	-.761315E 0	-.338511E 0	-.253255E 0	.426957E- 3
EXTRUD	.117390E 0	-.124295E 0	-.523640E 0	.169019E 0
WELDED	.508458E- 1	-.123452E 0	-.199722E- 1	.438166E 0
STATHT	.100000E 1	.711859E 0	.446831E 0	.561584E- 1
POSITN	.711859E 0	.100000E 1	.213602E 0	-.255955E 0
HEIGHT	.446831E 0	.213602E 0	.100000E 1	-.122256E 0
TUBDIA	.561584E- 1	-.255955E 0	-.122256E 0	.100000E 1
THICKN	.762628E 0	.458580E 0	.681316E 0	-.163696E- 1
VELOTY	-.984067E- 1	.143973E- 1	-.733364E- 1	-.147945E 0
VELSQU	-.113525E 0	.996402E- 2	-.697359E- 1	-.135667E 0
TEMRED	-.458650E- 1	-.128052E- 1	-.516109E 0	-.123010E 0
SQTSPA	.212571E 0	.152690E 0	.337041E 0	-.102964E 0
PRODUB	-.117785E- 1	.697488E- 1	.123066E 0	-.100730E 0
PRODUD	-.720825E- 1	-.655519E- 1	-.112099E 0	.195603E 0
PRODUL	.189575E 0	.870592E- 1	.598460E 0	-.172017E 0
PROUUB	-.872468E- 1	.268441E- 1	-.109988E- 1	-.138327E 0
PROUUL	.820001E- 4	-.106055E- 2	.258552E 0	-.144118E 0
PROUUD	-.107034E 0	-.138628E- 1	-.852141E- 1	-.355541E- 1
VELSHT	-.151632E 0	.350224E- 2	-.658431E- 1	-.106107E 0
VELEXT	-.278794E- 1	-.425014E- 1	-.321077E 0	-.592821E- 1

	THICKN	VELOTY	VELSQU	TEMRED
HTCOEF	.199792E 0	.283553E 0	.159487E 0	.285028E 0
BEDMK2	.330327E 0	-.511775E- 1	-.581810E- 1	-.283848E 0
BEDMK3	-.562878E 0	.256065E 0	.271917E 0	-.249554E 0
MASHOT	-.181459E 0	.521429E 0	.524861E 0	.544148E 0
MASICA	-.188635E 0	-.663845E- 1	-.575498E- 1	-.111795E- 1
CRIMPE	-.663602E 0	.229547E- 1	.514607E- 1	-.235352E 0
EXTRUD	-.235469E 0	-.113925E 0	-.134903E 0	.478257E 0
WELDED	.240599E 0	-.644084E- 1	-.647860E- 1	.696618E- 1
STATHT	.762628E 0	-.984067E- 1	-.113525E 0	-.458650E- 1
POSITN	.458580E 0	.143973E- 1	.996402E- 2	-.128052E- 1
HEIGHT	.681316E 0	-.733364E- 1	-.697359E- 1	-.516109E 0
TUBDIA	-.163696E- 1	-.147946E 0	-.135667E 0	-.123010E 0
THICKN	.100000E 1	-.103055E 0	-.108496E 0	-.124805E 0
VELOTY	-.103055E 0	.100000E 1	.955377E 0	.362306E 0
VELSQU	-.108496E 0	.955377E 0	.100000E 1	.280512E 0
TEMRED	-.124805E 0	.362306E 0	.280512E 0	.100000E 1
SQTSPA	.466485E 0	.617754E- 1	.725645E- 1	-.128556E 0
PRODUB	.777377E- 1	.882859E 0	.865927E 0	.682916E 0
PRODUD	-.996688E- 1	.926258E 0	.886407E 0	.530126E 0
PRODUL	.518419E 0	.667292E 0	.620995E 0	-.104706E 0
PROUUB	-.521911E- 1	.901681E 0	.959815E 0	.664981E 0
PROUUL	.485084E- 1	.824739E 0	.846096E 0	.669787E- 1
PROUUD	-.110001E 0	.955317E 0	.989715E 0	.681042E 0
VELSHT	-.136418E 0	.940575E 0	.954665E 0	.537314E 0
VELEXT	-.206420E 0	.852042E 0	.780427E 0	.563445E 0

	SQTSPA		PRODUB		PRODUD		PRODUL	
HTCOEF	.132657E	0	.261385E	0	.265472E	0	.137504E	0
BEDMK2	.296076E-	1	-.395525E-	1	-.775168E-	1	.129102E	0
BEDMK3	-.829421E-	2	.219011E	0	.168355E	0	.114057E	0
MASHOT	.134419E	0	.503925E	0	.403905E	0	.350488E	0
MASICA	-.166385E	0	-.115598E	0	-.917162E-	1	-.769115E-	1
CRIMPE	-.159512E	0	-.296122E-	1	.184137E-	1	-.129450E	0
EXTRUD	-.436580E	0	-.256341E	0	-.486649E-	1	-.391111E	0
WELDED	.132830E	0	-.572295E-	2	.924960E-	1	-.605159E-	1
STATHT	.212571E	0	-.117785E-	1	-.720823E-	1	.185575E	0
POSITN	.152690E	0	.697488E-	1	-.655519E-	1	.870592E-	1
HEIGHT	.537041E	0	.123066E	0	-.112099E	0	.598460E	0
TURBIA	-.102964E	0	-.160730E	0	.195603E	0	-.172019E	0
THICKN	.466485E	0	.777377E-	1	-.996686E-	1	.318419E	0
VELOTY	.617754E-	1	.882834E	0	.926238E	0	.667292E	0
VELSQU	.725645E-	1	.865927E	0	.868409E	0	.620995E	0
TEMPED	-.128358E	0	.262916E	0	.530126E	0	-.104706E	0
SQTSPA	.100000E	1	.455760E	0	.236720E-	1	.354692E	0
PRODUB	.456760E	0	.100000E	1	.799090E	0	.706955E	0
PRODUD	.236720E-	1	.799090E	0	.100000E	1	.591574E	0
PRODUL	.354692E	0	.706955E	0	.591574E	0	.100000E	1
PROUUB	.222613E	0	.932972E	0	.810575E	0	.619819E	0
PROUUL	.173312E	0	.789333E	0	.741255E	0	.884766E	0
PROUUD	.594984E-	1	.856417E	0	.919679E	0	.612517E	0
VELSHT	.975981E-	1	.856721E	0	.833839E	0	.627713E	0
VELEXT	-.167234E	0	.654070E	0	.821538E	0	.396475E	0

	PROUUB		PROUUL		PROUUD		VELSHT	
HTCOEF	.156049E	0	.114188E	0	.160903E	0	.617079E-	1
BEDMK2	-.524365E-	1	.562827E-	2	-.664442E-	1	-.715465E-	1
BEDMK3	.255755E	0	.426605E	0	.450226E	0	.359867E	0
MASHOT	.510325E	0	.464878E	0	.494523E	0	.751452E	0
MASICA	-.705204E-	1	-.610764E-	1	-.660185E-	1	-.786085E-	1
CRIMPE	.372831E-	1	-.231769E-	1	.525849E-	1	.714520E-	1
EXTRUD	-.176540E	0	-.233895E	0	-.118417E	0	-.186550E	0
WELDED	-.444440E-	1	-.634727E-	1	-.186065E-	1	-.877960E-	1
STATHT	-.872468E-	1	.820001E-	4	-.107054E	0	-.151632E	0
POSITN	.268441E-	1	-.106055E-	2	-.138628E-	1	.550224E-	2
HEIGHT	-.109385E-	1	.238532E	0	-.852141E-	1	-.658431E-	1
TURBIA	-.136327E	0	-.144118E	0	-.533541E-	1	-.186104E	0
THICKN	-.521911E-	1	.485084E-	1	-.110001E	0	-.130418E	0
VELOTY	.901681E	0	.826754E	0	.955317E	0	.940575E	0
VELSQU	.959813E	0	.846096E	0	.989713E	0	.954665E	0
TEMPED	.264981E	0	.669787E-	1	.281042E	0	.357314E	0
SQTSPA	.222613E	0	.173512E	0	.594984E-	1	.975981E-	1
PRODUB	.932972E	0	.789333E	0	.856417E	0	.856721E	0
PRODUD	.810575E	0	.741255E	0	.919679E	0	.833839E	0
PRODUL	.619819E	0	.884766E	0	.612517E	0	.627713E	0
PROUUB	.100000E	1	.819938E	0	.944901E	0	.913531E	0
PROUUL	.819938E	0	.100000E	1	.833939E	0	.827655E	0
PROUUD	.944901E	0	.833939E	0	.100000E	1	.957161E	0
VELSHT	.913531E	0	.827655E	0	.957161E	0	.100000E	1
VELEXT	.703195E	0	.605808E	0	.791691E	0	.739820E	0

	VELEXT	
HTCOEF	.185796E-	1
BEDMK2	-.458488E-	2
BEDMK3	-.643224E-	2
MASHOT	.351650E-	1
MASICA	-.523486E-	2
CRIMPE	-.188306E-	1
EXTRUD	.433137E-	1
WELDED	-.674525E-	2
STATHT	-.941712E-	1
POSITN	-.100444E	0
HEIGHT	-.475106E	0
TURBIA	-.700181E-	1
THICKN	-.774227E-	1
VELOTY	.542945E-	1
VELSQU	.623217E-	1
TEMPED	.645740E	1
SQTSPA	-.125826E-	1
PRODUB	.123961E	0
PRODUD	.846577E	0
PRODUL	.512677E	0
PROUUB	.155796E	0
PROUUL	.469372E	0
PROUUD	.963069E	0
VELSHT	.101517E	0
VELEXT	.742766E-	1

18/13/12 24/06/74 ICL 1900 STATISTICAL ANALYSIS XDS3/19

REGRESSION ANALYSIS COVA MATRX2 CUT OFF PARAMETER .100000E- 5

DEPENDENT VARIABLE HTCOEF DEGREES OF FREEDOM 246

INDEPENDENT VARIABLES AT SIGNIFICANT LEVEL 10.00 %

BEDMK2 BEDMK3 MASHOT MASICA CRIMPE EXTRUD WELDED STATHT POSITN HEIGHT TUBDIA THICKN
TEMBED SQTSPA PRODUB PRODUD PRODUL PROUUB PROUUL PROUUD VELSHT VELEXT VELOTY VELSQU

VARIABLES IN THE REGRESSION SET

VAR NAME	REGRESSION COEFF	STANDARD ERROR	CONFIDENCE INTERVAL	T STAT	PART CORR	MULTIPLE CORRELATION	E S S
BEDMK3	0.1416974	.185032E- 1	.305857E- 1	7.66	0.44	0.934	.655574E 0
MASHOT -	0.4076884	.245175E- 1	.405274E- 1	16.63	-0.73	0.883	.112440E 1
MASICA -	0.1629920	.175145E- 1	.289515E- 1	9.31	-0.51	0.927	.715739E 0
CRIMPE	0.0241766	.142064E- 1	.234832E- 1	1.70	0.11	0.946	.535606E 0
EXTRUD	0.2533843	.228387E- 1	.377523E- 1	11.09	0.58	0.919	.794251E 0
WELDED	0.1085594	.164451E- 1	.271837E- 1	6.60	0.39	0.937	.623150E 0
POSITN	0.0020737	.398214E- 3	.658248E- 3	5.21	0.32	0.941	.587732E 0
THICKN	0.0966165	.213501E- 1	.352917E- 1	4.53	0.28	0.942	.573445E 0
VELOTY	0.8504141	.675415E- 1	.111646E 0	12.59	0.63	0.911	.870525E 0
TEMBED	0.0005245	.125788E- 3	.207928E- 3	4.17	0.26	0.943	.566790E 0
SQTSPA	0.2095042	.234161E- 1	.387068E- 1	8.95	0.50	0.929	.701634E 0
PRODUB -	0.0447034	.182584E- 1	.301811E- 1	2.45	-0.15	0.946	.542274E 0
PROUUD -	0.0536239	.323839E- 2	.535305E- 2	16.56	-0.73	0.884	.111942E 1
VELSHT	0.3584604	.469480E- 1	.776051E- 1	7.64	0.44	0.934	.654825E 0

VARIABLES NOT IN THE REGRESSION SET

VAR NAME	T STAT	PART CORR	MULTIPLE CORRELATION	E S S
BEDMK2	0.18	-0.01	0.947	.529307E 0
STATHT	0.14	0.01	0.947	.529329E 0
HEIGHT	0.91	-0.06	0.947	.527575E 0
TUBDIA	1.14	-0.07	0.947	.526565E 0
VELSQU	0.68	-0.04	0.947	.528390E 0
PRODUD	0.13	-0.01	0.947	.529335E 0
PRODUL	0.85	-0.05	0.947	.527832E 0
PROUUB	0.29	-0.02	0.947	.529191E 0
PROUUL	1.32	-0.08	0.947	.525610E 0
VELEXT	0.69	-0.04	0.947	.528356E 0

E.S.S. .529374E 0

RESIDUAL ERROR .463889E- 1

MULT CORR 0.947

INTERCEPT TERM = 0.4024882

A6.5 Manufactured and Crimped Surface Results

A6.5.1 Manufactured and Crimped Mk 3 Bed Results in Zircon Sand

17/41/02 21/06/74 ICL 1900 STATISTICAL ANALYSIS XDS5/19

NUMBER OF OBSERVATIONS IN CROSS PRODUCT IS 67

MATRIX MATRX1

	MEAN	MINIMUM VALUE	MAXIMUM VALUE	VARIANCE
CONST	.100000E 1			
HTCOEF	.360627E 0	.680000E- 1	.599000E 0	.243092E- 1
CRIMPE	.158209E 1	.100000E 1	.200000E 1	.246947E 0
STATHT	.408657E 2	.260000E 2	.500000E 2	.808455E 2
POSITN	.297015E 1	.000000E 0	.140000E 2	.211809E 2
HEIGHT	.905821E 1	.345000E 1	.178500E 2	.132475E 2
SPACNG	.232925E 1	.165000E 1	.355000E 1	.421980E 0
TUBDIA	.169806E 2	.100000E 2	.280000E 2	.223234E 2
THICKN	.480090E 0	.254000E 0	.795000E 0	.722767E- 1
VELOTY	.292731E 0	.106000E 0	.654000E 0	.270972E- 1
TEMBED	.153403E 3	.105000E 3	.228000E 3	.102709E 4

MATRIX MATRX2

	MEAN	MINIMUM VALUE	MAXIMUM VALUE	STANDARD DEVIATION
CONST	.100000E 1			
HTCOEF	.360627E 0	.680000E- 1	.599000E 0	.155914E 0
CRIMPE	.158209E 1	.100000E 1	.200000E 1	.496938E 0
STATHT	.408657E 2	.260000E 2	.500000E 2	.899140E 1
POSITN	.297015E 1	.000000E 0	.140000E 2	.460227E 1
THICKN	.480090E 0	.254000E 0	.795000E 0	.268843E 0
VELOTY	.292731E 0	.106000E 0	.654000E 0	.154612E 0
VELSQU	.112384E 0	.112360E- 1	.427716E 0	.116810E 0
TEMBED	.153403E 3	.105000E 3	.228000E 3	.320483E 2
SQTSPA	.151196E 1	.127471E 1	.188944E 1	.209481E 0
TUBDIA	.169806E 2	.100000E 2	.280000E 2	.472588E 1
HEIGHT	.905821E 1	.345000E 1	.178500E 2	.365971E 1

REGRESSION ANALYSIS COVA MATRX2 CUT OFF PARAMETER .100000E- 5

DEPENDENT VARIABLE HTCOEF DEGREES OF FREEDOM 60

INDEPENDENT VARIABLES AT SIGNIFICANT LEVEL 10.00 %

CRIMPE STATHT POSITN THICKN VELOTY VELSQU TEMBED SQTSPA TUBDIA HEIGHT

VARIABLES IN THE REGRESSION SET

VAR NAME	REGRESSION COEFF	STANDARD ERROR	CONFIDENCE INTERVAL	T STAT	PART CORR	MULTIPLE CORRELATION	E S S
VELOTY	3.6190471	.158276E 0	264479E 0	22.87	0.95	0.790	.603925E 0
VELSQU -	3.5044292	.184991E 0	309120E 0	18.94	-0.93	0.854	.434029E 0
TEMBED -	0.0033391	.365223E- 3	610288E- 3	9.69	-0.78	0.949	.159474E 0
SQTSPA	0.2780891	.232009E- 1	387688E- 1	11.99	0.84	0.932	.211034E 0
TUBDIA -	0.0109170	.109130E- 2	182356E- 2	9.45	-0.77	0.951	.154786E 0
HEIGHT -	0.0194382	.198426E- 2	331570E- 2	9.80	-0.78	0.948	.161610E 0

VARIABLES NOT IN THE REGRESSION SET

VAR NAME			T STAT	PART CORR	MULTIPLE CORRELATION	E S S
CRIMPE	E.S.S.	.621718E- 1	0.45	0.06	0.981	.619617E- 1
STATHT	RESIDUAL ERROR	.321900E- 1	0.44	-0.06	0.980	.619649E- 1
POSITN	MULT CORR	0.980	0.45	-0.06	0.981	.619572E- 1
THICKN	INTERCEPT TERM	0.1687807	0.45	-0.06	0.981	.619617E- 1

RESIDUALS COVA MATRX2

OBS	Y	ESTIMATED Y	Y-ESTY	RATIO
ROW058	.900000E- 1	.720414E- 1	.179586E- 1	80.0460
ROW059	.132000E 0	.131136E 0	.863018E- 3	99.3462
ROW060	.258000E 0	.241223E 0	.167766E- 1	93.4974
ROW062	.474000E 0	.454952E 0	.190484E- 1	95.9815
ROW063	.516000E 0	.511254E 0	.474000E- 2	99.0812
ROW064	.522000E 0	.529396E 0	-.739607E- 2	101.4159
ROW065	.517000E 0	.492949E 0	.240506E- 1	95.3519
ROW074	.136000E 0	.155106E 0	-.171060E- 1	112.5932
ROW075	.188000E 0	.212143E 0	-.241032E- 1	112.8527
ROW076	.298000E 0	.310003E 0	-.120028E- 1	104.0278
ROW077	.433000E 0	.411251E 0	.217493E- 1	94.9771
ROW078	.533000E 0	.532109E 0	.891167E- 3	99.8328
ROW079	.536000E 0	.575797E 0	-.397970E- 1	107.4248
ROW080	.581000E 0	.594191E 0	-.131911E- 1	102.2704
ROW081	.578000E 0	.550234E 0	.277662E- 1	95.1962
ROW090	.134000E 0	.185468E 0	-.514685E- 1	138.4093
ROW091	.177000E 0	.223285E 0	-.462048E- 1	126.1496
ROW092	.300000E 0	.338807E 0	-.388769E- 1	112.9636
ROW093	.450000E 0	.450492E 0	-.492157E- 3	100.1094
ROW094	.560000E 0	.571988E 0	-.119878E- 1	102.1407
ROW095	.582000E 0	.614253E 0	-.322527E- 1	105.5417
ROW096	.583000E 0	.615393E 0	-.323935E- 1	105.5555
ROW097	.583000E 0	.560147E 0	.228530E- 1	96.0801
ROW106	.192000E 0	.228729E 0	-.367287E- 1	119.1295
ROW107	.269000E 0	.259366E 0	.963387E- 2	96.4186
ROW108	.376000E 0	.333377E 0	.426230E- 1	88.6641
ROW110	.588000E 0	.532282E 0	.557183E- 1	90.5241
ROW111	.599000E 0	.546689E 0	.523113E- 1	91.2694

RESIDUALS COVA MATRX2

OBS	Y	ESTIMATED Y	Y-ESTY	RATIO
ROW122	.220000E 0	.246448E 0	-.264480E- 1	112.0218
ROW123	.299000E 0	.299936E 0	-.935901E- 3	100.3130
ROW128	.521000E 0	.475364E 0	.456356E- 1	91.2406
ROW129	.513000E 0	.489844E 0	.231955E- 1	95.4865
ROW130	.522000E 0	.482200E 0	.398003E- 1	92.3734
ROW131	.910000E- 1	.125196E 0	-.341957E- 1	137.5777
ROW132	.160000E 0	.199466E 0	-.394657E- 1	124.6661
ROW133	.211000E 0	.246972E 0	-.359718E- 1	117.0465
ROW134	.275000E 0	.280770E 0	-.576758E- 2	102.0980
ROW135	.363000E 0	.302163E 0	.608367E- 1	83.2460
ROW136	.338000E 0	.347520E 0	.304796E- 1	91.9350
ROW137	.382000E 0	.386408E 0	-.440877E- 2	101.1559
ROW138	.392000E 0	.433424E 0	-.414238E- 1	110.5673
ROW141	.385000E 0	.373744E 0	.112564E- 1	97.0753
ROW164	.810000E- 1	.897413E- 1	-.874133E- 2	110.7910
ROW165	.142000E 0	.152383E 0	-.103832E- 1	107.3121
ROW166	.213000E 0	.203529E 0	.947101E- 2	95.5555
ROW167	.273000E 0	.238504E 0	.344958E- 1	87.3642
ROW168	.292000E 0	.256232E 0	.357680E- 1	87.7507
ROW169	.308000E 0	.294575E 0	.134251E- 1	95.6412
ROW170	.327000E 0	.341183E 0	-.141829E- 1	104.3375
ROW171	.326000E 0	.387392E 0	-.613917E- 1	118.8318
ROW174	.315000E 0	.341445E 0	-.264449E- 1	108.3952
ROW175	.680000E- 1	.118025E- 1	.561975E- 1	17.3567
ROW176	.151000E 0	.106573E 0	.444268E- 1	70.5783
ROW177	.198000E 0	.151571E 0	.464295E- 1	76.5508
ROW181	.326000E 0	.338541E 0	-.125409E- 1	103.8469
ROW182	.336000E 0	.382249E 0	-.462491E- 1	113.7640

RESIDUALS COVA MATRX2

OBS	Y	ESTIMATED Y	Y-ESTY	RATIO
ROW183	.350000E 0	.392845E 0	-.428452E-1	112.2415
ROW184	.330000E 0	.328302E 0	.169764E-2	99.4856
ROW186	.344000E 0	.369602E 0	-.256021E-1	107.4425
ROW187	.407000E 0	.400911E 0	.608938E-2	98.5058
ROW188	.447000E 0	.424972E 0	.220277E-1	95.0721
ROW189	.472000E 0	.444473E 0	.275270E-1	94.1680
ROW190	.504000E 0	.476358E 0	.276424E-1	94.5154
ROW191	.513000E 0	.506821E 0	.617932E-2	98.7955
ROW192	.519000E 0	.534165E 0	-.151048E-1	102.9219
ROW193	.521000E 0	.541683E 0	-.206827E-1	103.9698
ROW194	.500000E 0	.522503E 0	-.225030E-1	104.5006

A6.5.2 Manufactured Mk 1 and Mk 3 Bed Results in Zircon Sand

MATRIX MATRX1 NUMBER OF OBSERVATIONS IN CROSS PRODUCT IS 61

	MEAN	MINIMUM VALUE	MAXIMUM VALUE	VARIANCE
CONST	.100000E 1			
HTCOEF	.395902E 0	.900000E- 1	.605000E 0	.196662E- 1
BEDMK3	.150820E 1	.100000E 1	.200000E 1	.254098E 0
POSITN	.357377E 1	.000000E 0	.140000E 2	.265486E 2
HEIGHT	.138418E 2	.345000E 1	.178500E 2	.266108E 2
SPACNG	.277885E 1	.243000E 1	.370000E 1	.214680E 0
TURDIA	.157197E 2	.151000E 2	.214000E 2	.337861E 1
THICKN	.110779E 1	.795000E 0	.159000E 1	.155344E 0
VELOTY	.299852E 0	.106000E 0	.621000E 0	.200245E- 1
TEMBED	.167885E 3	.105000E 3	.227000E 3	.854603E 3

MATRIX MATRX2

	MEAN	MINIMUM VALUE	MAXIMUM VALUE	STANDARD DEVIATION
CONST	.100000E 1			
HTCOEF	.395902E 0	.900000E- 1	.605000E 0	.140236E 0
BEDMK3	.150820E 1	.100000E 1	.200000E 1	.504082E 0
POSITN	.357377E 1	.000000E 0	.140000E 2	.515254E 1
THICKN	.110779E 1	.795000E 0	.159000E 1	.371591E 0
VELOTY	.299852E 0	.106000E 0	.621000E 0	.141508E 0
VELSQU	.109608E 0	.112360E- 1	.385641E 0	.965146E- 1
TEMBED	.167885E 3	.105000E 3	.227000E 3	.292336E 2
SQTSPA	.166185E 1	.155885E 1	.192354E 1	.131872E 0
ETUDIA	.984405E 0	.978827E 0	.985015E 0	.185752E- 2
EHEIHT	.101595E 1	.100346E 1	.101801E 1	.521791E- 2
PRODUB	.830523E 0	.274540E 0	.172790E 1	.399171E 0
PRODUD	.470965E 1	.160060E 1	.999380E 1	.226599E 1
PRODUL	.411020E 1	.414000E 0	.104601E 2	.241414E 1
PRODUB	.300921E 0	.291012E- 1	.998810E 0	.258080E 0
PRODUD	.171644E 1	.169664E 0	.582318E 1	.149674E 1
PRODUL	.146584E 1	.496800E- 1	.612962E 1	.134249E 1

REGRESSION ANALYSIS COVA MATRX2 CUT OFF PARAMETER .100000E- 5

DEPENDENT VARIABLE HTCOEF DEGREES OF FREEDOM 47

INDEPENDENT VARIABLES AT SIGNIFICANT LEVEL 99.00 % POSITN THICKN VELOTY BEDMK3 ETUDIA EHEIHT PRODUR PRODUD PRODUL PROUUR PROUUD PROUUL VELSQU TEMBED SQTSPA

VARIABLES IN THE REGRESSION SET

VAR NAME	REGRESSION COEFF	STANDARD ERROR	CONFIDENCE INTERVAL	T STAT	PART CORR	MULTIPLE CORRELATION	E S S
BEDMK3	0.0394204	.492325E- 1		0.80	0.12	0.968	.733403E- 1
POSITN -	0.0088445	.585493E- 2		1.51	-0.22	0.967	.758663E- 1
THICKN	0.1670656	.276704E- 1		6.04	0.66	0.944	.128472E 0
VELOTY	6.8760637	.182269E 1		3.77	0.48	0.959	.942620E- 1
VELSQU -	5.6063238	.319245E 1		1.76	-0.25	0.967	.771009E- 1
TEMBED -	0.0013642	.751685E- 3		1.81	-0.26	0.967	.774240E- 1
SQTSPA	0.6339544	.319071E 0		1.99	0.28	0.966	.784305E- 1
PRODUR -	0.7667454	.651891E 0		1.18	-0.17	0.968	.744830E- 1
PRODUD -	0.0388454	.442741E- 1		0.88	-0.13	0.968	.735384E- 1
PRODUL -	0.1109030	.367812E- 1		3.02	-0.40	0.963	.863491E- 1
PROUUR	0.9993606	.107680E 1		0.93	0.13	0.968	.736794E- 1
PROUUD -	0.0927100	.100054E 0		0.93	-0.13	0.968	.736751E- 1
PROUUL	0.1218427	.538248E- 1		2.26	0.31	0.965	.802419E- 1

VARIABLES NOT IN THE REGRESSION SET

VAR NAME	T STAT	PART CORR	MULTIPLE CORRELATION	E S S
ETUDIA	0.92	-0.13	0.969	.710455E- 1
EHEIHT	1.08	-0.16	0.970	.705516E- 1

E.S.S. .723534E- 1

RESIDUAL ERROR .592356E- 1

MULT CORR 0.969

INTERCEPT TERM - 1.1336002

RESIDUALS COVA MATRXS

OBS	Y	ESTIMATED Y	Y-ESTY	RATIO
ROW058	.900000E- 1	.170753E 0	-.807529E- 1	189.7254
ROW059	.132000E 0	.211471E 0	-.794706E- 1	160.2050
ROW060	.258000E 0	.275877E 0	-.178768E- 1	106.9290
ROW061	.420000E 0	.344225E 0	.757746E- 1	81.9584
ROW062	.474000E 0	.433641E 0	.403585E- 1	91.4855
ROW063	.516000E 0	.480238E 0	.357618E- 1	93.0694
ROW064	.522000E 0	.497768E 0	.242321E- 1	95.3578
ROW065	.517000E 0	.482578E 0	.344222E- 1	93.3419
ROW074	.138000E 0	.175374E 0	-.373737E- 1	127.0844
ROW075	.188000E 0	.224058E 0	-.360585E- 1	119.1800
ROW076	.298000E 0	.302778E 0	-.427764E- 2	101.4355
ROW077	.433000E 0	.388632E 0	.443683E- 1	89.7535
ROW078	.533000E 0	.506211E 0	.267889E- 1	94.9739
ROW079	.536000E 0	.556599E 0	-.205990E- 1	103.8431
ROW080	.581000E 0	.574765E 0	.623499E- 2	98.9269
ROW081	.578000E 0	.541928E 0	.360724E- 1	93.7591
ROW090	.134000E 0	.171410E 0	-.374102E- 1	127.9181
ROW091	.177000E 0	.226683E 0	-.496826E- 1	128.0695
ROW092	.300000E 0	.323249E 0	-.232491E- 1	107.7497
ROW093	.450000E 0	.430611E 0	.193892E- 1	95.6913
ROW094	.560000E 0	.562586E 0	-.258561E- 2	100.4617
ROW095	.582000E 0	.617341E 0	-.353412E- 1	106.0724
ROW096	.583000E 0	.623158E 0	-.401580E- 1	106.8882
ROW097	.583000E 0	.561634E 0	.213655E- 1	96.3352
ROW106	.192000E 0	.175989E 0	.160108E- 1	91.6611
ROW107	.269000E 0	.242140E 0	.268597E- 1	90.0150
ROW108	.376000E 0	.346225E 0	.297745E- 1	92.0812
ROW109	.534000E 0	.469971E 0	.640294E- 1	88.0095
ROW053	.241000E 0	.203478E 0	.375217E- 1	84.4308
ROW054	.282000E 0	.256540E 0	.254598E- 1	90.9717

RESIDUALS COVA MATRXS

OBS	Y	ESTIMATED Y	Y-ESTY	RATIO
ROW110	.588000E 0	.603046E 0	-.150460E- 1	102.5588
ROW111	.599000E 0	.635781E 0	-.367806E- 1	106.1403
ROW112	.605000E 0	.589781E 0	.152194E- 1	97.4844
ROW001	.327000E 0	.327532E 0	-.531649E- 3	100.1626
ROW002	.431000E 0	.392620E 0	.383801E- 1	91.0951
ROW003	.453000E 0	.430705E 0	.222953E- 1	95.0785
ROW004	.443000E 0	.461040E 0	-.180397E- 1	104.0722
ROW005	.442000E 0	.464136E 0	-.221356E- 1	105.0080
ROW006	.479000E 0	.488442E 0	-.944187E- 2	101.9712
ROW007	.502000E 0	.508453E 0	-.645306E- 2	101.2855
ROW008	.539000E 0	.543141E 0	-.414127E- 2	100.7685
ROW009	.584000E 0	.576383E 0	.761091E- 2	98.6957
ROW010	.427000E 0	.435422E 0	-.842235E- 2	101.9724
ROW011	.411000E 0	.393460E 0	.175395E- 1	95.7325
ROW012	.317000E 0	.333482E 0	-.164815E- 1	105.1992
ROW025	.258000E 0	.221821E 0	.361789E- 1	85.9772
ROW026	.358000E 0	.313557E 0	.444433E- 1	87.5857
ROW027	.378000E 0	.373535E 0	.446461E- 2	98.8189
ROW028	.428000E 0	.449949E 0	-.219486E- 1	105.1282
ROW029	.448000E 0	.493137E 0	-.451371E- 1	110.0752
ROW030	.491000E 0	.519533E 0	-.285325E- 1	105.8111
ROW046	.242000E 0	.225774E 0	.162262E- 1	93.2949
ROW047	.520000E 0	.306523E 0	.134772E- 1	95.7884
ROW048	.344000E 0	.344113E 0	-.112658E- 3	100.0327
ROW049	.362000E 0	.383531E 0	-.215510E- 1	105.9478
ROW050	.372000E 0	.386895E 0	-.148949E- 1	104.0040
ROW051	.374000E 0	.356818E 0	.171818E- 1	95.4059
ROW052	.189000E 0	.116905E 0	.720953E- 1	61.8545
ROW055	.306000E 0	.329687E 0	-.236866E- 1	107.7407
ROW056	.316000E 0	.370686E 0	-.546855E- 1	117.3055
ROW057	.340000E 0	.396705E 0	-.567047E- 1	116.6779

A6.6 Copper Extruded Surface Results

MATRIX MATRX1 NUMBER OF OBSERVATIONS IN CROSS PRODUCT IS 42

	MEAN	MINIMUM VALUE	MAXIMUM VALUE	VARIANCE
CONST	.100000E 1			
HTCOEF	.529857E 0	.367000E 0	.649000E 0	.496632E- 2
HEIGHT	.506143E 1	.136000E 1	.889000E 1	.100053E 2
SPACNG	.209143E 1	.930000E 0	.306000E 1	.775661E 0
TURDIA	.185429E 2	.126000E 2	.291000E 2	.200191E 2
THICKN	.484286E 0	.380000E 0	.610000E 0	.801533E- 2
VELOTY	.324119E 0	.143000E 0	.530000E 0	.148817E- 1
TEMBED	.233333E 3	.188000E 3	.265000E 3	.564667E 3

MATRIX MATRX2

	MEAN	MINIMUM VALUE	MAXIMUM VALUE	STANDARD DEVIATION
CONST	.100000E 1			
HTCOEF	.529857E 0	.367000E 0	.649000E 0	.704721E- 1
THICKN	.484286E 0	.380000E 0	.610000E 0	.895284E- 1
TURDIA	.185429E 2	.126000E 2	.291000E 2	.515937E 1
HEIGHT	.506143E 1	.136000E 1	.889000E 1	.325658E 1
SQTSPA	.141116E 1	.964365E 0	.174929E 1	.320171E 0
VELOTY	.324119E 0	.143000E 0	.530000E 0	.121991E 0
VELSQU	.119581E 0	.204490E- 1	.280900E 0	.819085E- 1
TEMBED	.233333E 3	.188000E 3	.265000E 3	.237627E 2
PRODUB	.667019E 0	.155310E 0	.149568E 1	.372259E 0
PRODUD	.596258E 1	.201600E 1	.141426E 2	.276619E 1
PRODUL	.160085E 1	.227120E 0	.433944E 1	.121975E 1
PROUUB	.242539E 0	.259368E- 1	.735875E 0	.197378E 0
PROUUD	.218436E 1	.322560E 0	.687330E 1	.159950E 1
PROUUL	.577685E 0	.379290E- 1	.213500E 1	.570524E 0

15/06/14 14/06/74 ICL 1900 STATISTICAL ANALYSIS XDS3/19

REGRESSION ANALYSIS COVA MATRX2 CUT OFF PARAMETER .100000E- 5

DEPENDENT VARIABLE HTCOEF DEGREES OF FREEDOM 34

INDEPENDENT VARIABLES AT SIGNIFICANT LEVEL 10.00 % THICKN TUBDIA HEIGHT SQTSPA VELOTY VELSQU TEMBED PRODUB PRODUD PRODUL PROUUB PROUUD PROUUL

VARIABLES IN THE REGRESSION SET

VAR NAME	REGRESSION COEFF	STANDARD ERROR	CONFIDENCE INTERVAL	T STAT	PART CORR	MULTIPLE CORRELATION	E S S
HEIGHT -	0.0357451	.418239E- 2	.709752E- 2	8.55	-0.83	0.940	.235692E- 1
SQTSPA	0.1431693	.549432E- 1	.932386E- 1	2.61	0.41	0.978	.898125E- 2
VELOTY	2.0505783	.185410E 0	.314641E 0	11.06	0.88	0.912	.344130E- 1
VELSQU -	2.1117540	.255475E 0	.433541E 0	8.27	-0.82	0.943	.225305E- 1
TEMBED -	0.0032132	.782719E- 3	.132827E- 2	4.11	-0.58	0.972	.111969E- 1
PRODUB	0.0605554	.316764E- 1	.537548E- 1	1.91	0.31	0.979	.829087E- 2
PRODUD -	0.0070765	.201660E- 2	.342217E- 2	3.51	-0.52	0.975	.101975E- 1

VARIABLES NOT IN THE REGRESSION SET

VAR NAME	T STAT	PART CORR	MULTIPLE CORRELATION	E S S
THICKN	1.50	0.25	0.983	.700805E- 2
TUBDIA	0.57	0.10	0.982	.741275E- 2
PRODUL	0.23	-0.04	0.981	.747429E- 2
PROUUB	0.17	0.03	0.981	.747934E- 2
PROUUD	0.11	-0.02	0.981	.748362E- 2
PROUUL	0.10	-0.02	0.981	.748406E- 2

E.S.S. .748620E- 2

RESIDUAL ERROR .148305E- 1

MULT CORR 0.981

INTERCEPT TERM 0.8482569

RESIDUALS COVA MATRX2

OBS	Y	ESTIMATED Y	Y-ESTY	RATIO
ROW207	.426000E 0	.436350E 0	-.103504E-1	102.4297
ROW208	.503000E 0	.493716E 0	.928634E-2	98.1546
ROW209	.532000E 0	.533654E 0	-.165379E-2	100.3109
ROW210	.574000E 0	.578831E 0	-.483118E-2	100.8417
ROW211	.581000E 0	.591278E 0	-.102780E-1	101.7690
ROW212	.595000E 0	.613017E 0	-.180169E-1	103.0281
ROW213	.462000E 0	.465063E 0	-.306338E-2	100.6631
ROW214	.539000E 0	.523308E 0	.156924E-1	97.0886
ROW215	.573000E 0	.561105E 0	.118954E-1	97.9240
ROW216	.613000E 0	.610242E 0	.275840E-2	99.5500
ROW217	.626000E 0	.620890E 0	.511002E-2	99.1837
ROW218	.638000E 0	.649454E 0	-.114540E-1	101.7955
ROW219	.367000E 0	.369744E 0	-.274560E-2	100.7476
ROW220	.479000E 0	.453951E 0	.250490E-1	94.7706
ROW221	.511000E 0	.501032E 0	.996830E-2	98.0493
ROW222	.547000E 0	.542543E 0	.445077E-2	99.1862
ROW223	.572000E 0	.563959E 0	.804078E-2	98.5945
ROW224	.598000E 0	.573070E 0	.249295E-1	95.8312
ROW231	.406000E 0	.436354E 0	-.303544E-1	107.4765
ROW232	.502000E 0	.496561E 0	.543889E-2	98.9166
ROW233	.548000E 0	.548897E 0	-.897431E-3	100.1637
ROW234	.597000E 0	.604848E 0	-.784843E-2	101.3140
ROW235	.628000E 0	.623551E 0	.444864E-2	99.2916
ROW236	.649000E 0	.625177E 0	.238228E-1	96.3295
ROW237	.399000E 0	.401891E 0	-.289079E-2	100.7245
ROW238	.466000E 0	.458854E 0	.714614E-2	98.4665
ROW239	.490000E 0	.500061E 0	-.100607E-1	102.0552
ROW240	.514000E 0	.544069E 0	-.300691E-1	105.8500

RESIDUALS COVA MATRX2

OBS	Y	ESTIMATED Y	Y-ESTY	RATIO
ROW241	.533000E 0	.558954E 0	-.259542E-1	104.8695
ROW242	.544000E 0	.563002E 0	-.190022E-1	103.4930
ROW243	.445000E 0	.445711E 0	-.710564E-3	100.1597
ROW244	.496000E 0	.481201E 0	.147993E-1	97.0165
ROW245	.505000E 0	.519273E 0	-.142735E-1	102.8264
ROW246	.553000E 0	.565223E 0	-.122229E-1	102.2105
ROW247	.566000E 0	.574518E 0	-.851760E-2	101.5049
ROW248	.608000E 0	.594917E 0	.130835E-1	97.8481
ROW249	.401000E 0	.397341E 0	.365904E-2	99.0875
ROW250	.464000E 0	.456758E 0	.724248E-2	98.4391
ROW251	.498000E 0	.493064E 0	.493570E-2	99.0089
ROW252	.543000E 0	.540583E 0	.241699E-2	99.5549
ROW253	.569000E 0	.557887E 0	.111126E-1	98.0470
ROW254	.594000E 0	.584096E 0	.990397E-2	98.3327

BIBLIOGRAPHY

1. ELLIOTT,D.E., Possible Use of Fluidized-Bed Combustion and Heat Transfer, Paper 22, The Total Energy Conference, The Institute of Fuel, Brighton, November 1971, p361 - 372.

2. LEVA,M., WEINTRAUB,M. and GRUMMER,M., Heat Transmission through Fluidized Beds of Fine Particles, Chemical Engineering Progress, Volume 45, Number 9 , 1949, p563 - 572.

3. LEVENSPIEL,O. and WALTON,J.S., Bed-Wall Heat Transfer in Fluidized Systems, Chemical Engineering Progress Symposium Series, Volume 50, Number 9, 1954, p1 - 13.

4. WEN,C.Y. and LEVA,M., Fluidised-Bed Heat Transfer : A Generalized Dense-Phase Correlation, American Institution Chemical Engineers Journal, Volume 2, Number 4, 1956, p482 - 488.

5. MICKLEY,H.S. and TRILLING,C.A., Heat Transfer Characteristics of Fluidized Beds, Industrial and Engineering Chemistry, Volume 41, Number 6, 1949, p1135 - 1147.

6. ZIEGLER,E.N. and BRAZELTON,W.T., Mechanism of Heat Transfer to a Fixed Surface in a Fluidized Bed, Industrial and Engineering Chemistry, Volume 3, Number 2, 1964, p94 - 98.

7. DOW,W.M. and JAKOB,M., Heat Transfer Between a Vertical Tube and a Fluidized Air-Solid Mixture, Chemical Engineering Progress, Volume 47, Number 12, 1951, p637 - 648.

8. ROWE,P.N., PARTRIDGE,B.A., CHENEY,A.G., HENWOOD,G.A. and LYALL,E., The Mechanisms of Solids Mixing in Fluidised Beds, Transactions Institution Chemical Engineers, Volume 43, 1965, pT271 - T286.

9. MICKLEY,H.S. and FAIRBANKS,D.F., Mechanism of Heat Transfer to Fluidized Beds, American Institution Chemical Engineers Journal, Volume 1, Number 3, 1955, p374 - 384.

10. MICKLEY, H.S.,FAIRBANKS, D.F. and HAWTHORNE, R.D., The Relation Between the Transfer Coefficient and Thermal Fluctuations in Fluidized-Bed Heat Transfer, Chemical Engineering Progress Symposium Series, Volume 57, Number 32, 1961, p51 - 60

11. HENWOOD,G.A., Some Aspects of Heat Transfer in a Gas Fluidized Bed, A.E.R.E. report R6027, United Kingdom Atomic Energy Authority, July 1969, 28pp.

12. DRINKENBURG,A.A.H., HUIGE,N.J.J. and RIETEMA,K., Heat Transfer in a Gas-Fluidized Bed, Third International Heat Transfer Conference, Chicago, Paper 147, Part 4, 1966, p271 - 279.

13. BOTTERILL,J.S.M., Heat Transfer to Gas-Fluidized Beds, Powder Technology, Volume 4, 1970/71, p19 - 26.

14. BOTTERILL,J.S.M. and WILLIAMS,J.R., The Mechanism of Heat Transfer to Gas-Fluidized Beds, Transactions Institution Chemical Engineers, Volume 41, 1963, p217 - 230.

15. GABOR,J.D., Wall-to-bed Heat Transfer in Fluidized and Packed Beds, Chemical Engineering Progress Symposium Series, Volume 66, Number 105, 1970, p76 - 86.

16. VREEDENBERG,H.A., Heat Transfer Between Fluidized Beds and Vertically Inserted Tubes, Journal of Applied Chemistry, Volume 2, Supplementary Issue Number 1, 1952, p526 - 533.

17. VREEDENBERG,H.A., Heat Transfer Between a Fluidized Bed and a Horizontal Tube, Chemical Engineering Science, Volume 9, 1958, p52 - 60.

18. VREEDENBERG,H.A., Heat Transfer Between a Fluidized Bed and a Vertical Tube, Chemical Engineering Science, Volume 11, 1960, p274 - 285.

19. SINCLAIR,R., WRIGHT,J.C.J. and THOMAS,C.G., Assessment of Fluidized Beds for the Heat Treatment of Steel, Journal of the Iron and Steel Institute, Volume 203, February 1965, p131 - 137.

20. PETRIE,J.C.,FREEBY,W.A. and BUCKHAM,J.A., In-bed Heat Exchangers, Chemical Engineering Progress, Volume 64, Number 7, 1968. p45 - 51.

21. SPARROW,E.M. and HENNECKE,D.K., Temperature Depression at the Base of a Fin, Journal Heat Transfer, Transactions American Society Mechanical Engineers, Volume 92, Series C, Number 1, February 1970, p204 - 206.

22. KLETT,D.E. and McCULLOCH,J.W., The Effect of Thermal Conductivity and Base-temperature Depression on Fin Effectiveness, Journal Heat Transfer, Transactions American Society Mechanical Engineers, Volume 94, Series C, Number 3, August 1972, p333 - 334.

23. NATUSCH,H.J. and BLENKE,H., Heat Transfer at Finned Tubes in Gas-fluidized Beds, Paper C4.4 presented at 4th International CHISA Congress, Prague, Czechoslovakia, 1972, 29pp.

24. HARPER,D.R. and BROWN,W.B., Mathematical Equations for Heat Conduction in the Fins of Air-cooled Engines, National Advisory Committee for Aeronautics Report 158, Washington, 1922, 32pp.

25. GARDNER,K.A., Efficiency of Extended Surface, Transactions of the American Society Mechanical Engineers, Volume 67, Number 8, 1945, p621 - 631.

26. McADAMS,W.H., Heat Transmission, 3rd Edition, McGraw-Hill Book Company, New York, 1954.

27. BARTEL,W.J.,GENETTI,W.E. and GRIMMETT,E.S., Heat Transfer from a Horizontal Discontinuous Finned Tube in a Fluidized Bed, Paper 15i, American Institution Chemical Engineers Symposium, Chicago, November 29th - December 3rd 1970, p85 - 89.

28. GENETTI, W.E.,SCHMALL,R.A. and GRIMMETT,E.S., The Effect of Tube Orientation on Heat Transfer with Bore and Finned Tubes in a Fluidized Bed, Paper 15h, American Institution Chemical Engineers Symposium, Chicago, November 29th - December 3rd, 1970, p90 - 96.

29. BARTEL,W.J. and GENETTI,W.E., Heat Transfer from a Horizontal Bundle of Bore and Finned Tubes in an Air Fluidized Bed, American Institution Chemical Engineers Symposium Series, Volume 69, Number 128, 1973, p85 - 93.

30. HAGER,W.R. and THOMSON,W.J., Bubble Behavior Around Immersed Tubes in a Fluidized Bed, American Institution Chemical Engineers Symposium Series, Volume 69, Number 128, 1973, p68 - 77.

31. KHASANOV,R.R., ZABRODSKII,S.S., TAMARIN,A.I. and GALERSHTEIN,D.M., Heat Transfer Between Surface and a Fluidized Bed with Packing, Inzhenerno-Fizicheskii Zhurnal, Volume 22, Number 3, 1972, p397 - 402. (In Russian)

32. YOSHIDA,K.D., KUNII,D. and LEVENSPIEL,O., Heat Transfer Mechanism Between Wall Surface and Fluidized Bed, International Journal Heat Mass Transfer, Volume 12, 1969, p529 - 536.

33. WRIGHT,R., Manufacture of Finned Tubing for Economic Heat Transfer in High Pressure Gas Systems, Paper 24, Symposium on High Pressure Gas as a Heat Transport Medium, Institution Mechanical Engineers, London 9 - 10th March 1967, 9pp.

34. WRIGHT,R., Extended Surface Tubes, Joint Symposium on Heat Exchangers, their Specification, Type, Selection and Use, Institution Mechanical Engineers, Manchester, 15th April, 1969, 6pp.

35. BROWN,A., Optimum Dimensions of Uniform Annular Fins, International Journal Heat Mass Transfer, Volume 8, 1965, p655 - 662.

36. ICL 1900 Series Scientific Subroutine Library, Chapter 2, Specifications of the F4 and FP Routines, Issued 26th September 1973.

37. Nottingham Algorithms Group Mini Manual for the N.A.G. ICL 1900 Library, Chapter E04, Curve and Surface Fitting, E02ABF, Issued May 1st 1972.

38. The Graphplotter, Section 0401, The University of Aston in Birmingham Computer Centre User's Handbook, December 1972, 51pp.

39. British Standard 410 : 1969, Specification for Test Sieves, British Standards Institution.

40. British Standard 1042 : Part 1 : 1964, Methods for the Measurement of Fluid Flow in Pipes, British Standards Institution.

41. BAERG,A., KLASSEN,J. and GISHLER,P.E., Heat Transfer in a Fluidized Solids Bed, Canadian Journal of Research, Volume 28, Number 8, 1950, p287 - 307.

42. KIM,K.J.,KIM,D.J.,CHUN,K.S. and CHOO,S.S., Heat and Mass Transfer in Fixed and Fluidized Bed Reactors, International Chemical Engineering, Volume 8, Number 3, 1968, p472 - 490.

43. DAVIDSON,J.F. and HARRISON,D., Fluidized Particles, Cambridge University Press, 1st Edition, 1963.

44. ROWE,P.N., The Effect of Bubbles on Gas-Solid Contacting in Fluidized Beds, Chemical Engineering Progress Symposium Series, Volume 58, Number 38, 1962, p42 - 56.

45. ROWE,P.N. and EVERETT,D,J., Fluidized Bed Bubbles Viewed by X-rays, Transactions Institution Chemical Engineers, Volume 50, Number 1, 1972, p42 - 60.

46. Multiple Regression Application Programme using Graphplotter, UAAP UA13, The University of Aston in Birmingham Computer Centre, July 1974.

47. SMILLIE,K.W., An Introduction to Regression and Correlation, Academic Press, London, 1st Edition, 1966.

48. DRAPER,N.R. and SMITH,H., Applied Regression Analysis, John Wiley and Son, New York, 1st Edition, 1966.

49. DAVIES,O.L. and GOLDSMITH,P.L., Statistical Methods in Research and Production, Oliver and Boyd, Edinburgh, 4th Edition,1972.

50. MOORE,P.G., SHIRLEY,E.A. and EDWARDS,D.E., Standard Statistical Calculations, Pitman, Bath, 2nd Edition, 1972.

51. ICL Statistical Package (XDS3), Section 0301, The University of Aston in Birmingham Computer Centre User's Handbook, August 1972, 20pp.

52. DAVIDSON,J.F. and HARRISON,D., Editors, Fluidization, Academic Press, London, 1st Edition, 1971.

53. "United Kingdom Steam Tables in S.I. Units," Published for the United Kingdom Committee on the Properties of Steam, Edward Arnold, London, 1st Edition, 1970, p155.

54. "Handbook of Chemistry and Physics," Published by The Chemical Rubber Company, Cleveland, Ohio, 50th Edition, 1969 - 1970, pF-36 and pD-122.

55. DALLAVALLE,J.M., Micromeritics - The Technology of Fine Particles, Pitman, London, 2nd Edition, 1948.

56. KUNII,D. and LEVENSPIEL,O., Fluidization Engineering, Wiley, London, 1st Edition, 1969.

57. ZABRODSKY,S.S., Hydrodynamics and Heat Transfer in Fluidized Beds, M.I.T. Press, London, 1st Edition, 1966.

58. BOTTERILL,J.S.M., ELLIOTT,D.E., van der KOLK,M. and McGUIGAN,S., The Flow of Fluidised Solids, Paper presented at Powtech International Powder Technology and Bulk Solids Conference, University of Bradford, 1971.